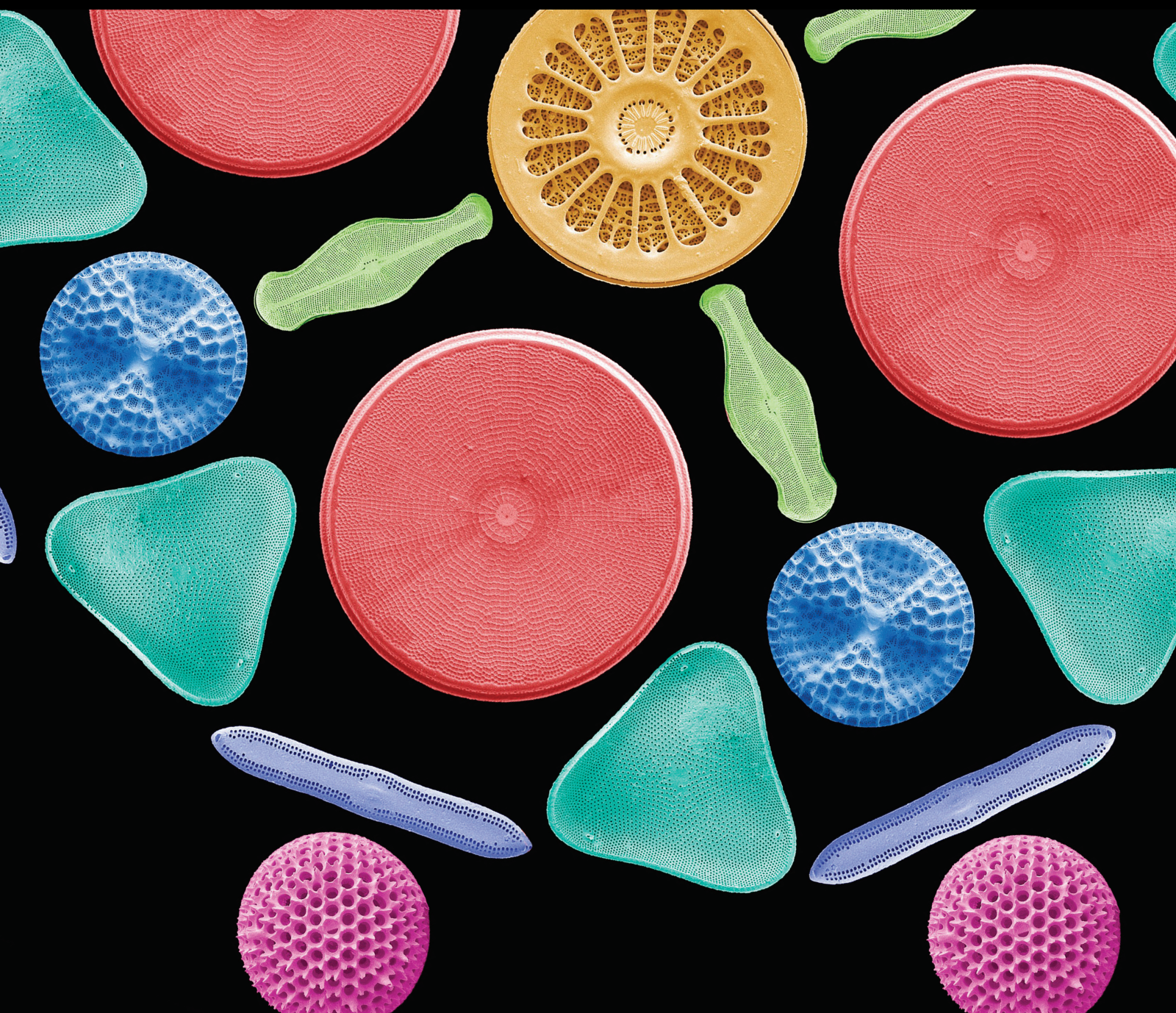


# Laser Scanning Microscopy and its Biomedical Applications

Lead Guest Editor: Balakrishnan Nagaraj

Guest Editors: P Manimegalai and Raffaele Mascella





---

# **Laser Scanning Microscopy and its Biomedical Applications**

Scanning

---

## **Laser Scanning Microscopy and its Biomedical Applications**

Lead Guest Editor: Balakrishnan Nagaraj

Guest Editors: P Manimegalai and Raffaele  
Mascella



---


Copyright © 2023 Hindawi Limited. All rights reserved.


This is a special issue published in "Scanning." All articles are open access articles distributed under the Creative Commons Attribution License, which permits unrestricted use, distribution, and reproduction in any medium, provided the original work is properly cited.

# Chief Editor

Guosong Wu, China

## Associate Editors


Richard Arinero , France

Daniele Passeri , Italy

Andrea Picone , Italy


## Academic Editors

David Alsteens, Belgium


Igor Altfeder , USA

Jose Alvarez , France

Lavinia C. Ardelean , Romania

Renato Buzio , Italy

J. Chen, Canada

Ovidiu Cretu , Japan

Nicolas Delorme , France


Hendrix Demers , Canada

Jonathan R. Felts, USA

Marina I. Giannotti, Spain

Federico Grillo , United Kingdom


Anton V. Ievlev , USA

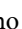
Heng Bo Jiang , China

Berndt Koslowski , Germany

Jessem Landoulsi , France


Jason L. Pitters , Canada

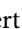
Michela Relucenti , Italy

Francesco Ruffino , Italy

Senthil Kumaran Selvaraj , India

Stefan G. Stanciu, Romania

Andreas Stylianou , Cyprus

Christian Teichert , Austria

Marilena Vivona , United Kingdom

Shuilin Wu, China

# Contents

---

**Retracted: Digital Image Restoration Based on Multicontour Batch Scanning**

Scanning

Retraction (1 page), Article ID 9871470, Volume 2023 (2023)

**Retracted: Application of Ultrasonic Intelligent Imaging in L-Selectin Regulating Embryo Implantation in Mongolian Sheep Endometrium**

Scanning

Retraction (1 page), Article ID 9868943, Volume 2023 (2023)

**Retracted: Construction of Computer Microscope Image Segmentation Model Based on Fourth-Order Partial Differential Equation Smoothing**

Scanning

Retraction (1 page), Article ID 9838407, Volume 2023 (2023)

**Retracted: DSA Image Analysis of Clinical Features and Nursing Care of Cerebral Aneurysm Patients Based on the Deep Learning Algorithm**

Scanning

Retraction (1 page), Article ID 9816025, Volume 2023 (2023)

**Retracted: Application of CT Multimodal Images in Rehabilitation Monitoring of Long-Distance Running**

Scanning

Retraction (1 page), Article ID 9813637, Volume 2023 (2023)

**Retracted: MRI View of Rehabilitation Methods to Relieve Anterior Cruciate Ligament Injury in Dancers**

Scanning

Retraction (1 page), Article ID 9791562, Volume 2023 (2023)

**Retracted: The Application Value of CT Three-Dimensional Microscope Reconstruction Technology in the Diagnosis of Cervical Cancer**

Scanning

Retraction (1 page), Article ID 9786383, Volume 2023 (2023)

**Retracted: Effect of Operation Room Nursing Intervention and Ceramic Prosthesis on Total Hip Arthroplasty**

Scanning

Retraction (1 page), Article ID 9761894, Volume 2023 (2023)

**Retracted: Application of Color Doppler Ultrasound Combined with Magnetic Resonance Imaging in Placenta Accreta**

Scanning

Retraction (1 page), Article ID 9760954, Volume 2023 (2023)

**Retracted: Nursing Methods and Experience of Local Anesthesia Patients under Arthroscope**

Scanning

Retraction (1 page), Article ID 9836460, Volume 2023 (2023)

**Retracted: Analysis of Pathogen Characteristics and Nursing Factors of Tonsil Infection Based on Regression Equation**

Scanning

Retraction (1 page), Article ID 9826924, Volume 2023 (2023)

**Retracted: Visual Dissemination of Intangible Cultural Heritage Information Based on 3D Scanning and Virtual Reality Technology**

Scanning

Retraction (1 page), Article ID 9816725, Volume 2023 (2023)

**Retracted: Magnetic Resonance Imaging Assessment of Fatigue Injury during Exercise**

Scanning

Retraction (1 page), Article ID 9819052, Volume 2023 (2023)

**Retracted: Comparison of Improved Surgical Eight-Step Handwashing Combined with ATP Fluorescence in Detecting the Infection Rate at the Site of Seven-Step Surgical Handwashing and 30-Day Orthopaedic Surgery: A Randomized Study**

Scanning

Retraction (1 page), Article ID 9854789, Volume 2023 (2023)

**Retracted: Injury Prevention Effect of MRI Imaging Technology in Physical Education and Sports Training**

Scanning

Retraction (1 page), Article ID 9852968, Volume 2023 (2023)

**Retracted: Application of CT Scan in Diagnosis of Iliac-Femoral Vein Thrombosis after Hip Replacement**

Scanning

Retraction (1 page), Article ID 9850130, Volume 2023 (2023)

**Retracted: Comparative Study of Macular Vascular Density and Retinal Thickness in Myopia Children with Different Microscope Diopters Based on OCTA**

Scanning

Retraction (1 page), Article ID 9823654, Volume 2023 (2023)

**Retracted: Identification of Sports Athletes' High-Strength Sports Injuries Based on NMR**

Scanning

Retraction (1 page), Article ID 9817542, Volume 2023 (2023)

**Retracted: Observation on the Effect of Rehabilitative Physical Training on Sports Injuries under Ultrasound Image Examination**

Scanning

Retraction (1 page), Article ID 9801674, Volume 2023 (2023)

# Contents

---

**Retracted: Corner Detection of the Computer VR Microscope Image Based on the 3D Reconstruction Algorithm**

Scanning

Retraction (1 page), Article ID 9782473, Volume 2023 (2023)

**Retracted: Construction of Biologic Microscopic Image Segmentation Model Based on Smoothing of Fourth-Order Partial Differential Equation**

Scanning

Retraction (1 page), Article ID 9763981, Volume 2023 (2023)

**Retracted: Effects of Obstructive Sleep Apnea-Hypopnea Syndrome and Cognitive Function in Ischemic Stroke Based on Linear Regression Equation**

Scanning

Retraction (1 page), Article ID 9763714, Volume 2023 (2023)

**Retracted: Effects of Sports Functional Food on Physical Function of Athletes under Ultrasound Observation**

Scanning

Retraction (1 page), Article ID 9760176, Volume 2023 (2023)

**Retracted: Effect of Nursing Intervention on Coronary CT Angiography in Elderly Patients**

Scanning

Retraction (1 page), Article ID 9892328, Volume 2023 (2023)

**Retracted: Nursing Education of Lateral Oblique Complications of Neurosurgery under Microscope**

Scanning

Retraction (1 page), Article ID 9871316, Volume 2023 (2023)

**Retracted: Effect Evaluation of Comfort Nursing Materials Assisted Nursing for Patients with Advanced Malignant Tumor**

Scanning

Retraction (1 page), Article ID 9851262, Volume 2023 (2023)

**Retracted: Application of MRI and CT Images in Surgical Treatment of Early Cervical Cancer**

Scanning

Retraction (1 page), Article ID 9847106, Volume 2023 (2023)

**Retracted: Postoperative Nursing and Functional Rehabilitation of Ultrasound Diagnosis of Lower Rotator Cuff Injury**

Scanning

Retraction (1 page), Article ID 9842603, Volume 2023 (2023)

**Retracted: Effect of Microscope Combined with Wechat Smart Platform on Clinical Efficacy and Gastrointestinal Function of Patients with Cholecystolithiasis Combined with Common Bile Duct Stones**

Scanning

Retraction (1 page), Article ID 9840541, Volume 2023 (2023)



**Retracted: Application of MRI in the Prevention of Sports Injuries in Physical Education Teaching**

Scanning

Retraction (1 page), Article ID 9826025, Volume 2023 (2023)

**Retracted: Preparation and Performance Analysis of Bacterial Cellulose-Based Composite Hydrogel Based on Scanning Electron Microscope**

Scanning

Retraction (1 page), Article ID 9820471, Volume 2023 (2023)

**Retracted: Evaluation of the Effect of Refined Nursing Intervention on Coronary CT Imaging Microscopy**

Scanning

Retraction (1 page), Article ID 9813530, Volume 2023 (2023)

**Retracted: Application of CT Ultrasonography Combined with Microscopic Intraperitoneal Hyperthermic Perfusion Chemotherapy in Postoperative Treatment of Oocyst Carcinoma**

Scanning

Retraction (1 page), Article ID 9808639, Volume 2023 (2023)

**Retracted: Efficacy Evaluation of the Combined Platelet-Rich Plasma and Hyaluronic Acid after Arthroscopic Joint Debridement in Treating Knee Osteoarthritis**

Scanning

Retraction (1 page), Article ID 9801624, Volume 2023 (2023)

**Retracted: Effect of Rehabilitation Physical Training on Basketball Injury under Ultrasound Examination**

Scanning

Retraction (1 page), Article ID 9769547, Volume 2023 (2023)

**Retracted: Application of Multislice Spiral CT and Three-Dimensional Image Reconstruction Technology in the Observation of Ankle Sports Injury under the Microscope**

Scanning

Retraction (1 page), Article ID 9760563, Volume 2023 (2023)

**Retracted: Analysis of Infertility Factors Caused by Gynecological Chronic Pelvic Inflammation Disease Based on Multivariate Regression Analysis of Logistic**

Scanning




Retraction (1 page), Article ID 9757181, Volume 2023 (2023)

**[Retracted] Application of CT Multimodal Images in Rehabilitation Monitoring of Long-Distance Running**

Xufeng Du  and Yaye He 

Research Article (7 pages), Article ID 6425448, Volume 2022 (2022)

**[Retracted] Visual Dissemination of Intangible Cultural Heritage Information Based on 3D Scanning and Virtual Reality Technology**

Wulong Xu , Xijie Sun , and Shihui Pan 

Research Article (7 pages), Article ID 8762504, Volume 2022 (2022)

## Contents

**[Retracted] MRI View of Rehabilitation Methods to Relieve Anterior Cruciate Ligament Injury in Dancers**

Pin Yang 



Research Article (7 pages), Article ID 1544440, Volume 2022 (2022)

**[Retracted] Effects of Sports Functional Food on Physical Function of Athletes under Ultrasound Observation**

Zhao Cheng , Hong Lin , and Zhenmao Zhou 





Research Article (7 pages), Article ID 7769653, Volume 2022 (2022)

**[Retracted] Efficacy Evaluation of the Combined Platelet-Rich Plasma and Hyaluronic Acid after Arthroscopic Joint Debridement in Treating Knee Osteoarthritis**

Min Lu  and Yanquan Jin 


Research Article (5 pages), Article ID 6994017, Volume 2022 (2022)

**[Retracted] Digital Image Restoration Based on Multicontour Batch Scanning**

Yongsheng Ding , Yunbo Wei , Shuisheng Zhang , and Shihang Yu 


Research Article (8 pages), Article ID 8106516, Volume 2022 (2022)

**[Retracted] Injury Prevention Effect of MRI Imaging Technology in Physical Education and Sports Training**

Jianxin Liu 


Research Article (6 pages), Article ID 9991523, Volume 2022 (2022)

**[Retracted] Application of MRI in the Prevention of Sports Injuries in Physical Education Teaching**

Jing Zhao 







Research Article (6 pages), Article ID 7738233, Volume 2022 (2022)

**[Retracted] Postoperative Nursing and Functional Rehabilitation of Ultrasound Diagnosis of Lower Rotator Cuff Injury**

Riying Hou 


Research Article (7 pages), Article ID 8319082, Volume 2022 (2022)

**[Retracted] DSA Image Analysis of Clinical Features and Nursing Care of Cerebral Aneurysm Patients Based on the Deep Learning Algorithm**

Jian Wang , Lin Ti , Xiaorui Sun , Ruping Yang , Nafei Zhang , and Kejuan Sun 

Research Article (6 pages), Article ID 8485651, Volume 2022 (2022)

**[Retracted] Effect of Rehabilitation Physical Training on Basketball Injury under Ultrasound Examination**

Wenjie E.  and Qiufen Yu 


Research Article (8 pages), Article ID 2554581, Volume 2022 (2022)

**[Retracted] Preparation and Performance Analysis of Bacterial Cellulose-Based Composite Hydrogel Based on Scanning Electron Microscope**

Meiling Shao , Zhan Shi , Bin Zhai , Xiangfei Zhang , and Zhongyi Li 

Research Article (7 pages), Article ID 8750394, Volume 2022 (2022)

**[Retracted] Nursing Education of Lateral Oblique Complications of Neurosurgery under Microscope**

Kecui Hu 








Research Article (8 pages), Article ID 2158181, Volume 2022 (2022)

**[Retracted] Application of MRI and CT Images in Surgical Treatment of Early Cervical Cancer**

An Lu  and Guohua Lu 

Research Article (9 pages), Article ID 1592449, Volume 2022 (2022)

**[Retracted] Nursing Methods and Experience of Local Anesthesia Patients under Arthroscope**

Xiaowei Zhang , JingWang , Weixu Gao , Lijuan Li , LiangYu , Kun Liu , and Nan Li 

Research Article (9 pages), Article ID 3689344, Volume 2022 (2022)

**[Retracted] Construction of Biologic Microscopic Image Segmentation Model Based on Smoothing of Fourth-Order Partial Differential Equation**

Ye Ma 

Research Article (8 pages), Article ID 1908644, Volume 2022 (2022)

**[Retracted] Corner Detection of the Computer VR Microscope Image Based on the 3D Reconstruction Algorithm**

Junjun Huang 

Research Article (8 pages), Article ID 8621103, Volume 2022 (2022)

**[Retracted] Comparison of Improved Surgical Eight-Step Handwashing Combined with ATP Fluorescence in Detecting the Infection Rate at the Site of Seven-Step Surgical Handwashing and 30-Day Orthopaedic Surgery: A Randomized Study**

Xiong Chen , Tao Wang , Qinglian Li , Lixia Cheng , Zhimin Xie , Jianping Xu , and Dejian Yang 






Research Article (7 pages), Article ID 3123565, Volume 2022 (2022)

**[Retracted] Identification of Sports Athletes' High-Strength Sports Injuries Based on NMR**

Wenyong Zhou  and Huan Chu 

Research Article (7 pages), Article ID 1016628, Volume 2022 (2022)


**[Retracted] Application of Color Doppler Ultrasound Combined with Magnetic Resonance Imaging in Placenta Accreta**

Xue Sun , Runrun Ren , Xiaoqian Yu , Fang Peng , and Xia Gao 

Research Article (7 pages), Article ID 1050029, Volume 2022 (2022)

## Contents

**[Retracted] Construction of Computer Microscope Image Segmentation Model Based on Fourth-Order Partial Differential Equation Smoothing**

Feng Li 

Research Article (8 pages), Article ID 4355184, Volume 2022 (2022)

**[Retracted] Effect of Microscope Combined with Wechat Smart Platform on Clinical Efficacy and Gastrointestinal Function of Patients with Cholelithiasis Combined with Common Bile Duct Stones**

Xu Xu , Dongmei Guo , Yan Zhang , Dandan Yang , Guangbin Hou , Quanfu Li , Changqing Ge , Zengwang Qie , and Yonggang Zhong 







Research Article (5 pages), Article ID 9661506, Volume 2022 (2022)

**[Retracted] Observation on the Effect of Rehabilitative Physical Training on Sports Injuries under Ultrasound Image Examination**

Lanfeng Wang  and Haoyu Wang 



Research Article (7 pages), Article ID 9998265, Volume 2022 (2022)

**[Retracted] Effects of Obstructive Sleep Apnea-Hypopnea Syndrome and Cognitive Function in Ischemic Stroke Based on Linear Regression Equation**

Peng Ji , Qixing Kou , Xueping Qu , Gen Sun , Songcan Liu , and Jiewen Zhang 

Research Article (8 pages), Article ID 4105169, Volume 2022 (2022)

**[Retracted] Effect of Operation Room Nursing Intervention and Ceramic Prosthesis on Total Hip Arthroplasty**

Ting Xu  and Jie Zhang 

Research Article (8 pages), Article ID 2421723, Volume 2022 (2022)

**[Retracted] Application of CT Scan in Diagnosis of Iliac-Femoral Vein Thrombosis after Hip Replacement**

Dong Li , Lishan Wang , Zhanxin Li , Libin Li , Qingwei Wang , Li Zhang , and Zhigang Guo 


Research Article (9 pages), Article ID 8428963, Volume 2022 (2022)

**[Retracted] Effect Evaluation of Comfort Nursing Materials Assisted Nursing for Patients with Advanced Malignant Tumor**

Mei Zhong , Lanying He , Min Chen , Zhongxiang Lu , Ruyu Li , and Ling Li 

Research Article (6 pages), Article ID 4766252, Volume 2022 (2022)

**[Retracted] Application of Multislice Spiral CT and Three-Dimensional Image Reconstruction Technology in the Observation of Ankle Sports Injury under the Microscope**

Dongxian Zhao 





Research Article (7 pages), Article ID 8174310, Volume 2022 (2022)

**[Retracted] Application of Ultrasonic Intelligent Imaging in L-Selectin Regulating Embryo Implantation in Mongolian Sheep Endometrium**

Changshou Wang , Adong Bao , Qing Hai , Zhengxiang Hu , and Xiaoying Bai 







Research Article (9 pages), Article ID 3323768, Volume 2022 (2022)

**[Retracted] Magnetic Resonance Imaging Assessment of Fatigue Injury during Exercise**

Zhengguo Ai , Na Li , Jing An , and Lei Zhang 



Research Article (7 pages), Article ID 9971966, Volume 2022 (2022)

**[Retracted] Analysis of Infertility Factors Caused by Gynecological Chronic Pelvic Inflammation Disease Based on Multivariate Regression Analysis of Logistic**

Linmei Liu , Gang Yang , Jigang Ren , Limei Zhang , Ting Wu , and Qiao Zheng 



Research Article (7 pages), Article ID 7531190, Volume 2022 (2022)

**[Retracted] Effect of Nursing Intervention on Coronary CT Angiography in Elderly Patients**

Yajuan Yin  and Zhongting Wei 



Research Article (7 pages), Article ID 3663285, Volume 2022 (2022)

**[Retracted] Analysis of Pathogen Characteristics and Nursing Factors of Tonsil Infection Based on Regression Equation**

Longfang Zhang  and Yuanyuan Yang 


Research Article (7 pages), Article ID 3149619, Volume 2022 (2022)

**[Retracted] Comparative Study of Macular Vascular Density and Retinal Thickness in Myopia Children with Different Microscope Diopters Based on OCTA**

Meiling Chen  and Fanning Zhao 




Research Article (6 pages), Article ID 5038918, Volume 2022 (2022)

**[Retracted] Evaluation of the Effect of Refined Nursing Intervention on Coronary CT Imaging Microscopy**

Tao Qian 

Research Article (6 pages), Article ID 4870548, Volume 2022 (2022)

**[Retracted] The Application Value of CT Three-Dimensional Microscope Reconstruction Technology in the Diagnosis of Cervical Cancer**

Shaoliang Sun , Xiye Wang , and Yanjia Chen 

Research Article (6 pages), Article ID 5648195, Volume 2022 (2022)

**[Retracted] Application of CT Ultrasonography Combined with Microscopic Intraperitoneal Hyperthermic Perfusion Chemotherapy in Postoperative Treatment of Oocyst Carcinoma**

Zongbao Xia  and Hong Jin 

Research Article (6 pages), Article ID 5444552, Volume 2022 (2022)

## *Retraction*

# **Retracted: Digital Image Restoration Based on Multicontour Batch Scanning**

### **Scanning**

Received 5 December 2023; Accepted 5 December 2023; Published 6 December 2023

Copyright © 2023 Scanning. This is an open access article distributed under the Creative Commons Attribution License, which permits unrestricted use, distribution, and reproduction in any medium, provided the original work is properly cited.

This article has been retracted by Hindawi, as publisher, following an investigation undertaken by the publisher [1]. This investigation has uncovered evidence of systematic manipulation of the publication and peer-review process. We cannot, therefore, vouch for the reliability or integrity of this article.

Please note that this notice is intended solely to alert readers that the peer-review process of this article has been compromised.

Wiley and Hindawi regret that the usual quality checks did not identify these issues before publication and have since put additional measures in place to safeguard research integrity.

We wish to credit our Research Integrity and Research Publishing teams and anonymous and named external researchers and research integrity experts for contributing to this investigation.

The corresponding author, as the representative of all authors, has been given the opportunity to register their agreement or disagreement to this retraction. We have kept a record of any response received.

### **References**

- [1] Y. Ding, Y. Wei, S. Zhang, and S. Yu, "Digital Image Restoration Based on Multicontour Batch Scanning," *Scanning*, vol. 2022, Article ID 8106516, 8 pages, 2022.

## *Retraction*

# **Retracted: Application of Ultrasonic Intelligent Imaging in L-Selectin Regulating Embryo Implantation in Mongolian Sheep Endometrium**

### **Scanning**

Received 5 December 2023; Accepted 5 December 2023; Published 6 December 2023

Copyright © 2023 Scanning. This is an open access article distributed under the Creative Commons Attribution License, which permits unrestricted use, distribution, and reproduction in any medium, provided the original work is properly cited.

This article has been retracted by Hindawi, as publisher, following an investigation undertaken by the publisher [1]. This investigation has uncovered evidence of systematic manipulation of the publication and peer-review process. We cannot, therefore, vouch for the reliability or integrity of this article.

Please note that this notice is intended solely to alert readers that the peer-review process of this article has been compromised.

Wiley and Hindawi regret that the usual quality checks did not identify these issues before publication and have since put additional measures in place to safeguard research integrity.

We wish to credit our Research Integrity and Research Publishing teams and anonymous and named external researchers and research integrity experts for contributing to this investigation.

The corresponding author, as the representative of all authors, has been given the opportunity to register their agreement or disagreement to this retraction. We have kept a record of any response received.

### **References**

- [1] C. Wang, A. Bao, Q. Hai, Z. Hu, and X. Bai, "Application of Ultrasonic Intelligent Imaging in L-Selectin Regulating Embryo Implantation in Mongolian Sheep Endometrium," *Scanning*, vol. 2022, Article ID 3323768, 9 pages, 2022.

## *Retraction*

# **Retracted: Construction of Computer Microscope Image Segmentation Model Based on Fourth-Order Partial Differential Equation Smoothing**

### **Scanning**

Received 5 December 2023; Accepted 5 December 2023; Published 6 December 2023

Copyright © 2023 Scanning. This is an open access article distributed under the Creative Commons Attribution License, which permits unrestricted use, distribution, and reproduction in any medium, provided the original work is properly cited.

This article has been retracted by Hindawi, as publisher, following an investigation undertaken by the publisher [1]. This investigation has uncovered evidence of systematic manipulation of the publication and peer-review process. We cannot, therefore, vouch for the reliability or integrity of this article.

Please note that this notice is intended solely to alert readers that the peer-review process of this article has been compromised.

Wiley and Hindawi regret that the usual quality checks did not identify these issues before publication and have since put additional measures in place to safeguard research integrity.

We wish to credit our Research Integrity and Research Publishing teams and anonymous and named external researchers and research integrity experts for contributing to this investigation.

The corresponding author, as the representative of all authors, has been given the opportunity to register their agreement or disagreement to this retraction. We have kept a record of any response received.

### **References**

- [1] F. Li, "Construction of Computer Microscope Image Segmentation Model Based on Fourth-Order Partial Differential Equation Smoothing," *Scanning*, vol. 2022, Article ID 4355184, 8 pages, 2022.



## *Retraction*

# **Retracted: DSA Image Analysis of Clinical Features and Nursing Care of Cerebral Aneurysm Patients Based on the Deep Learning Algorithm**

### **Scanning**

Received 5 December 2023; Accepted 5 December 2023; Published 6 December 2023

Copyright © 2023 Scanning. This is an open access article distributed under the Creative Commons Attribution License, which permits unrestricted use, distribution, and reproduction in any medium, provided the original work is properly cited.

This article has been retracted by Hindawi, as publisher, following an investigation undertaken by the publisher [1]. This investigation has uncovered evidence of systematic manipulation of the publication and peer-review process. We cannot, therefore, vouch for the reliability or integrity of this article.

Please note that this notice is intended solely to alert readers that the peer-review process of this article has been compromised.

Wiley and Hindawi regret that the usual quality checks did not identify these issues before publication and have since put additional measures in place to safeguard research integrity.

We wish to credit our Research Integrity and Research Publishing teams and anonymous and named external researchers and research integrity experts for contributing to this investigation.

The corresponding author, as the representative of all authors, has been given the opportunity to register their agreement or disagreement to this retraction. We have kept a record of any response received.

### **References**

- [1] J. Wang, L. Ti, X. Sun, R. Yang, N. Zhang, and K. Sun, "DSA Image Analysis of Clinical Features and Nursing Care of Cerebral Aneurysm Patients Based on the Deep Learning Algorithm," *Scanning*, vol. 2022, Article ID 8485651, 6 pages, 2022.

## *Retraction*

# **Retracted: Application of CT Multimodal Images in Rehabilitation Monitoring of Long-Distance Running**

### **Scanning**

Received 5 December 2023; Accepted 5 December 2023; Published 6 December 2023

Copyright © 2023 Scanning. This is an open access article distributed under the Creative Commons Attribution License, which permits unrestricted use, distribution, and reproduction in any medium, provided the original work is properly cited.

This article has been retracted by Hindawi, as publisher, following an investigation undertaken by the publisher [1]. This investigation has uncovered evidence of systematic manipulation of the publication and peer-review process. We cannot, therefore, vouch for the reliability or integrity of this article.

Please note that this notice is intended solely to alert readers that the peer-review process of this article has been compromised.

Wiley and Hindawi regret that the usual quality checks did not identify these issues before publication and have since put additional measures in place to safeguard research integrity.

We wish to credit our Research Integrity and Research Publishing teams and anonymous and named external researchers and research integrity experts for contributing to this investigation.

The corresponding author, as the representative of all authors, has been given the opportunity to register their agreement or disagreement to this retraction. We have kept a record of any response received.

### **References**

- [1] X. Du and Y. He, "Application of CT Multimodal Images in Rehabilitation Monitoring of Long-Distance Running," *Scanning*, vol. 2022, Article ID 6425448, 7 pages, 2022.

## *Retraction*

# **Retracted: MRI View of Rehabilitation Methods to Relieve Anterior Cruciate Ligament Injury in Dancers**

### **Scanning**

Received 5 December 2023; Accepted 5 December 2023; Published 6 December 2023

Copyright © 2023 Scanning. This is an open access article distributed under the Creative Commons Attribution License, which permits unrestricted use, distribution, and reproduction in any medium, provided the original work is properly cited.

This article has been retracted by Hindawi, as publisher, following an investigation undertaken by the publisher [1]. This investigation has uncovered evidence of systematic manipulation of the publication and peer-review process. We cannot, therefore, vouch for the reliability or integrity of this article.

Please note that this notice is intended solely to alert readers that the peer-review process of this article has been compromised.

Wiley and Hindawi regret that the usual quality checks did not identify these issues before publication and have since put additional measures in place to safeguard research integrity.

We wish to credit our Research Integrity and Research Publishing teams and anonymous and named external researchers and research integrity experts for contributing to this investigation.

The corresponding author, as the representative of all authors, has been given the opportunity to register their agreement or disagreement to this retraction. We have kept a record of any response received.

### **References**

- [1] P. Yang, "MRI View of Rehabilitation Methods to Relieve Anterior Cruciate Ligament Injury in Dancers," *Scanning*, vol. 2022, Article ID 1544440, 7 pages, 2022.

## *Retraction*

# **Retracted: The Application Value of CT Three-Dimensional Microscope Reconstruction Technology in the Diagnosis of Cervical Cancer**

### **Scanning**

Received 5 December 2023; Accepted 5 December 2023; Published 6 December 2023

Copyright © 2023 Scanning. This is an open access article distributed under the Creative Commons Attribution License, which permits unrestricted use, distribution, and reproduction in any medium, provided the original work is properly cited.

This article has been retracted by Hindawi, as publisher, following an investigation undertaken by the publisher [1]. This investigation has uncovered evidence of systematic manipulation of the publication and peer-review process. We cannot, therefore, vouch for the reliability or integrity of this article.

Please note that this notice is intended solely to alert readers that the peer-review process of this article has been compromised.

Wiley and Hindawi regret that the usual quality checks did not identify these issues before publication and have since put additional measures in place to safeguard research integrity.

We wish to credit our Research Integrity and Research Publishing teams and anonymous and named external researchers and research integrity experts for contributing to this investigation.

The corresponding author, as the representative of all authors, has been given the opportunity to register their agreement or disagreement to this retraction. We have kept a record of any response received.

### **References**

- [1] S. Sun, X. Wang, and Y. Chen, "The Application Value of CT Three-Dimensional Microscope Reconstruction Technology in the Diagnosis of Cervical Cancer," *Scanning*, vol. 2022, Article ID 5648195, 6 pages, 2022.

## *Retraction*

# **Retracted: Effect of Operation Room Nursing Intervention and Ceramic Prosthesis on Total Hip Arthroplasty**

### **Scanning**

Received 5 December 2023; Accepted 5 December 2023; Published 6 December 2023

Copyright © 2023 Scanning. This is an open access article distributed under the Creative Commons Attribution License, which permits unrestricted use, distribution, and reproduction in any medium, provided the original work is properly cited.

This article has been retracted by Hindawi, as publisher, following an investigation undertaken by the publisher [1]. This investigation has uncovered evidence of systematic manipulation of the publication and peer-review process. We cannot, therefore, vouch for the reliability or integrity of this article.

Please note that this notice is intended solely to alert readers that the peer-review process of this article has been compromised.

Wiley and Hindawi regret that the usual quality checks did not identify these issues before publication and have since put additional measures in place to safeguard research integrity.

We wish to credit our Research Integrity and Research Publishing teams and anonymous and named external researchers and research integrity experts for contributing to this investigation.

The corresponding author, as the representative of all authors, has been given the opportunity to register their agreement or disagreement to this retraction. We have kept a record of any response received.

### **References**

- [1] T. Xu and J. Zhang, "Effect of Operation Room Nursing Intervention and Ceramic Prosthesis on Total Hip Arthroplasty," *Scanning*, vol. 2022, Article ID 2421723, 8 pages, 2022.

## *Retraction*

# **Retracted: Application of Color Doppler Ultrasound Combined with Magnetic Resonance Imaging in Placenta Accreta**

### **Scanning**

Received 5 December 2023; Accepted 5 December 2023; Published 6 December 2023

Copyright © 2023 Scanning. This is an open access article distributed under the Creative Commons Attribution License, which permits unrestricted use, distribution, and reproduction in any medium, provided the original work is properly cited.

This article has been retracted by Hindawi, as publisher, following an investigation undertaken by the publisher [1]. This investigation has uncovered evidence of systematic manipulation of the publication and peer-review process. We cannot, therefore, vouch for the reliability or integrity of this article.

Please note that this notice is intended solely to alert readers that the peer-review process of this article has been compromised.

Wiley and Hindawi regret that the usual quality checks did not identify these issues before publication and have since put additional measures in place to safeguard research integrity.

We wish to credit our Research Integrity and Research Publishing teams and anonymous and named external researchers and research integrity experts for contributing to this investigation.

The corresponding author, as the representative of all authors, has been given the opportunity to register their agreement or disagreement to this retraction. We have kept a record of any response received.

### **References**

- [1] X. Sun, R. Ren, X. Yu, F. Peng, and X. Gao, "Application of Color Doppler Ultrasound Combined with Magnetic Resonance Imaging in Placenta Accreta," *Scanning*, vol. 2022, Article ID 1050029, 7 pages, 2022.

## Retraction

# Retracted: Nursing Methods and Experience of Local Anesthesia Patients under Arthroscope

### Scanning

Received 26 September 2023; Accepted 26 September 2023; Published 27 September 2023

Copyright © 2023 Scanning. This is an open access article distributed under the Creative Commons Attribution License, which permits unrestricted use, distribution, and reproduction in any medium, provided the original work is properly cited.

This article has been retracted by Hindawi following an investigation undertaken by the publisher [1]. This investigation has uncovered evidence of one or more of the following indicators of systematic manipulation of the publication process:

- (1) Discrepancies in scope
- (2) Discrepancies in the description of the research reported
- (3) Discrepancies between the availability of data and the research described
- (4) Inappropriate citations
- (5) Incoherent, meaningless and/or irrelevant content included in the article
- (6) Peer-review manipulation

The presence of these indicators undermines our confidence in the integrity of the article's content and we cannot, therefore, vouch for its reliability. Please note that this notice is intended solely to alert readers that the content of this article is unreliable. We have not investigated whether authors were aware of or involved in the systematic manipulation of the publication process.

In addition, our investigation has also shown that one or more of the following human-subject reporting requirements has not been met in this article: ethical approval by an Institutional Review Board (IRB) committee or equivalent, patient/participant consent to participate, and/or agreement to publish patient/participant details (where relevant).

Wiley and Hindawi regrets that the usual quality checks did not identify these issues before publication and have since put additional measures in place to safeguard research integrity.

We wish to credit our own Research Integrity and Research Publishing teams and anonymous and named external researchers and research integrity experts for contributing to this investigation.

The corresponding author, as the representative of all authors, has been given the opportunity to register their agreement or disagreement to this retraction. We have kept a record of any response received.

### References

- [1] X. Zhang, J. Wang, W. Gao et al., "Nursing Methods and Experience of Local Anesthesia Patients under Arthroscope," *Scanning*, vol. 2022, Article ID 3689344, 9 pages, 2022.

## Retraction

# Retracted: Analysis of Pathogen Characteristics and Nursing Factors of Tonsil Infection Based on Regression Equation

### Scanning

Received 26 September 2023; Accepted 26 September 2023; Published 27 September 2023

Copyright © 2023 Scanning. This is an open access article distributed under the Creative Commons Attribution License, which permits unrestricted use, distribution, and reproduction in any medium, provided the original work is properly cited.

This article has been retracted by Hindawi following an investigation undertaken by the publisher [1]. This investigation has uncovered evidence of one or more of the following indicators of systematic manipulation of the publication process:

- (1) Discrepancies in scope
- (2) Discrepancies in the description of the research reported
- (3) Discrepancies between the availability of data and the research described
- (4) Inappropriate citations
- (5) Incoherent, meaningless and/or irrelevant content included in the article
- (6) Peer-review manipulation

The presence of these indicators undermines our confidence in the integrity of the article's content and we cannot, therefore, vouch for its reliability. Please note that this notice is intended solely to alert readers that the content of this article is unreliable. We have not investigated whether authors were aware of or involved in the systematic manipulation of the publication process.

In addition, our investigation has also shown that one or more of the following human-subject reporting requirements has not been met in this article: ethical approval by an Institutional Review Board (IRB) committee or equivalent, patient/participant consent to participate, and/or agreement to publish patient/participant details (where relevant).

Wiley and Hindawi regrets that the usual quality checks did not identify these issues before publication and have since put additional measures in place to safeguard research integrity.

We wish to credit our own Research Integrity and Research Publishing teams and anonymous and named external researchers and research integrity experts for contributing to this investigation.

The corresponding author, as the representative of all authors, has been given the opportunity to register their agreement or disagreement to this retraction. We have kept a record of any response received.

### References

- [1] L. Zhang and Y. Yang, "Analysis of Pathogen Characteristics and Nursing Factors of Tonsil Infection Based on Regression Equation," *Scanning*, vol. 2022, Article ID 3149619, 7 pages, 2022.



## *Retraction*

# **Retracted: Visual Dissemination of Intangible Cultural Heritage Information Based on 3D Scanning and Virtual Reality Technology**

### **Scanning**

Received 26 September 2023; Accepted 26 September 2023; Published 27 September 2023

Copyright © 2023 Scanning. This is an open access article distributed under the Creative Commons Attribution License, which permits unrestricted use, distribution, and reproduction in any medium, provided the original work is properly cited.

This article has been retracted by Hindawi following an investigation undertaken by the publisher [1]. This investigation has uncovered evidence of one or more of the following indicators of systematic manipulation of the publication process:

- (1) Discrepancies in scope
- (2) Discrepancies in the description of the research reported
- (3) Discrepancies between the availability of data and the research described
- (4) Inappropriate citations
- (5) Incoherent, meaningless and/or irrelevant content included in the article
- (6) Peer-review manipulation

The presence of these indicators undermines our confidence in the integrity of the article's content and we cannot, therefore, vouch for its reliability. Please note that this notice is intended solely to alert readers that the content of this article is unreliable. We have not investigated whether authors were aware of or involved in the systematic manipulation of the publication process.

Wiley and Hindawi regrets that the usual quality checks did not identify these issues before publication and have since put additional measures in place to safeguard research integrity.

We wish to credit our own Research Integrity and Research Publishing teams and anonymous and named external researchers and research integrity experts for contributing to this investigation.

The corresponding author, as the representative of all authors, has been given the opportunity to register their agreement or disagreement to this retraction. We have kept a record of any response received.

### **References**

- [1] W. Xu, X. Sun, and S. Pan, "Visual Dissemination of Intangible Cultural Heritage Information Based on 3D Scanning and Virtual Reality Technology," *Scanning*, vol. 2022, Article ID 8762504, 7 pages, 2022.

## Retraction

# Retracted: Magnetic Resonance Imaging Assessment of Fatigue Injury during Exercise

### Scanning

Received 18 July 2023; Accepted 18 July 2023; Published 19 July 2023

Copyright © 2023 Scanning. This is an open access article distributed under the Creative Commons Attribution License, which permits unrestricted use, distribution, and reproduction in any medium, provided the original work is properly cited.

This article has been retracted by Hindawi following an investigation undertaken by the publisher [1]. This investigation has uncovered evidence of one or more of the following indicators of systematic manipulation of the publication process:

- (1) Discrepancies in scope
- (2) Discrepancies in the description of the research reported
- (3) Discrepancies between the availability of data and the research described
- (4) Inappropriate citations
- (5) Incoherent, meaningless and/or irrelevant content included in the article
- (6) Peer-review manipulation

The presence of these indicators undermines our confidence in the integrity of the article's content and we cannot, therefore, vouch for its reliability. Please note that this notice is intended solely to alert readers that the content of this article is unreliable. We have not investigated whether authors were aware of or involved in the systematic manipulation of the publication process.

In addition, our investigation has also shown that one or more of the following human-subject reporting requirements has not been met in this article: ethical approval by an Institutional Review Board (IRB) committee or equivalent, patient/participant consent to participate, and/or agreement to publish patient/participant details (where relevant).

Wiley and Hindawi regrets that the usual quality checks did not identify these issues before publication and have since put additional measures in place to safeguard research integrity.

We wish to credit our own Research Integrity and Research Publishing teams and anonymous and named external researchers and research integrity experts for contributing to this investigation.

The corresponding author, as the representative of all authors, has been given the opportunity to register their agreement or disagreement to this retraction. We have kept a record of any response received.

### References

- [1] Z. Ai, N. Li, J. An, and L. Zhang, "Magnetic Resonance Imaging Assessment of Fatigue Injury during Exercise," *Scanning*, vol. 2022, Article ID 9971966, 7 pages, 2022.

## Retraction

# Retracted: Comparison of Improved Surgical Eight-Step Handwashing Combined with ATP Fluorescence in Detecting the Infection Rate at the Site of Seven-Step Surgical Handwashing and 30-Day Orthopaedic Surgery: A Randomized Study

### Scanning

Received 11 July 2023; Accepted 11 July 2023; Published 12 July 2023

Copyright © 2023 Scanning. This is an open access article distributed under the Creative Commons Attribution License, which permits unrestricted use, distribution, and reproduction in any medium, provided the original work is properly cited.

This article has been retracted by Hindawi following an investigation undertaken by the publisher [1]. This investigation has uncovered evidence of one or more of the following indicators of systematic manipulation of the publication process:

- (1) Discrepancies in scope
- (2) Discrepancies in the description of the research reported
- (3) Discrepancies between the availability of data and the research described
- (4) Inappropriate citations
- (5) Incoherent, meaningless and/or irrelevant content included in the article
- (6) Peer-review manipulation

The presence of these indicators undermines our confidence in the integrity of the article's content and we cannot, therefore, vouch for its reliability. Please note that this notice is intended solely to alert readers that the content of this article is unreliable. We have not investigated whether authors were aware of or involved in the systematic manipulation of the publication process.

Wiley and Hindawi regrets that the usual quality checks did not identify these issues before publication and have since put additional measures in place to safeguard research integrity.

We wish to credit our own Research Integrity and Research Publishing teams and anonymous and named

external researchers and research integrity experts for contributing to this investigation.

The corresponding author, as the representative of all authors, has been given the opportunity to register their agreement or disagreement to this retraction. We have kept a record of any response received.

### References

- [1] X. Chen, T. Wang, Q. Li et al., "Comparison of Improved Surgical Eight-Step Handwashing Combined with ATP Fluorescence in Detecting the Infection Rate at the Site of Seven-Step Surgical Handwashing and 30-Day Orthopaedic Surgery: A Randomized Study," *Scanning*, vol. 2022, Article ID 3123565, 7 pages, 2022.

## Retraction

# Retracted: Injury Prevention Effect of MRI Imaging Technology in Physical Education and Sports Training

### Scanning

Received 11 July 2023; Accepted 11 July 2023; Published 12 July 2023

Copyright © 2023 Scanning. This is an open access article distributed under the Creative Commons Attribution License, which permits unrestricted use, distribution, and reproduction in any medium, provided the original work is properly cited.

This article has been retracted by Hindawi following an investigation undertaken by the publisher [1]. This investigation has uncovered evidence of one or more of the following indicators of systematic manipulation of the publication process:

- (1) Discrepancies in scope
- (2) Discrepancies in the description of the research reported
- (3) Discrepancies between the availability of data and the research described
- (4) Inappropriate citations
- (5) Incoherent, meaningless and/or irrelevant content included in the article
- (6) Peer-review manipulation

The presence of these indicators undermines our confidence in the integrity of the article's content and we cannot, therefore, vouch for its reliability. Please note that this notice is intended solely to alert readers that the content of this article is unreliable. We have not investigated whether authors were aware of or involved in the systematic manipulation of the publication process.

In addition, our investigation has also shown that one or more of the following human-subject reporting requirements has not been met in this article: ethical approval by an Institutional Review Board (IRB) committee or equivalent, patient/participant consent to participate, and/or agreement to publish patient/participant details (where relevant).

Wiley and Hindawi regrets that the usual quality checks did not identify these issues before publication and have since put additional measures in place to safeguard research integrity.

We wish to credit our own Research Integrity and Research Publishing teams and anonymous and named external researchers and research integrity experts for contributing to this investigation.

The corresponding author, as the representative of all authors, has been given the opportunity to register their agreement or disagreement to this retraction. We have kept a record of any response received.

### References

- [1] J. Liu, "Injury Prevention Effect of MRI Imaging Technology in Physical Education and Sports Training," *Scanning*, vol. 2022, Article ID 9991523, 6 pages, 2022.

## Retraction

# Retracted: Application of CT Scan in Diagnosis of Iliac-Femoral Vein Thrombosis after Hip Replacement

### Scanning

Received 11 July 2023; Accepted 11 July 2023; Published 12 July 2023

Copyright © 2023 Scanning. This is an open access article distributed under the Creative Commons Attribution License, which permits unrestricted use, distribution, and reproduction in any medium, provided the original work is properly cited.

This article has been retracted by Hindawi following an investigation undertaken by the publisher [1]. This investigation has uncovered evidence of one or more of the following indicators of systematic manipulation of the publication process:

- (1) Discrepancies in scope
- (2) Discrepancies in the description of the research reported
- (3) Discrepancies between the availability of data and the research described
- (4) Inappropriate citations
- (5) Incoherent, meaningless and/or irrelevant content included in the article
- (6) Peer-review manipulation

The presence of these indicators undermines our confidence in the integrity of the article's content and we cannot, therefore, vouch for its reliability. Please note that this notice is intended solely to alert readers that the content of this article is unreliable. We have not investigated whether authors were aware of or involved in the systematic manipulation of the publication process.

In addition, our investigation has also shown that one or more of the following human-subject reporting requirements has not been met in this article: ethical approval by an Institutional Review Board (IRB) committee or equivalent, patient/participant consent to participate, and/or agreement to publish patient/participant details (where relevant).

Wiley and Hindawi regrets that the usual quality checks did not identify these issues before publication and have since put additional measures in place to safeguard research integrity.

We wish to credit our own Research Integrity and Research Publishing teams and anonymous and named external researchers and research integrity experts for contributing to this investigation.

The corresponding author, as the representative of all authors, has been given the opportunity to register their agreement or disagreement to this retraction. We have kept a record of any response received.

### References

- [1] D. Li, L. Wang, Z. Li et al., "Application of CT Scan in Diagnosis of Iliac-Femoral Vein Thrombosis after Hip Replacement," *Scanning*, vol. 2022, Article ID 8428963, 9 pages, 2022.

## Retraction

# Retracted: Comparative Study of Macular Vascular Density and Retinal Thickness in Myopia Children with Different Microscope Diopters Based on OCTA

### Scanning

Received 11 July 2023; Accepted 11 July 2023; Published 12 July 2023

Copyright © 2023 Scanning. This is an open access article distributed under the Creative Commons Attribution License, which permits unrestricted use, distribution, and reproduction in any medium, provided the original work is properly cited.

This article has been retracted by Hindawi following an investigation undertaken by the publisher [1]. This investigation has uncovered evidence of one or more of the following indicators of systematic manipulation of the publication process:

- (1) Discrepancies in scope
- (2) Discrepancies in the description of the research reported
- (3) Discrepancies between the availability of data and the research described
- (4) Inappropriate citations
- (5) Incoherent, meaningless and/or irrelevant content included in the article
- (6) Peer-review manipulation

The presence of these indicators undermines our confidence in the integrity of the article's content and we cannot, therefore, vouch for its reliability. Please note that this notice is intended solely to alert readers that the content of this article is unreliable. We have not investigated whether authors were aware of or involved in the systematic manipulation of the publication process.

In addition, our investigation has also shown that one or more of the following human-subject reporting requirements has not been met in this article: ethical approval by an Institutional Review Board (IRB) committee or equivalent, patient/participant consent to participate, and/or agreement to publish patient/participant details (where relevant).

Wiley and Hindawi regrets that the usual quality checks did not identify these issues before publication and have since put additional measures in place to safeguard research integrity.

We wish to credit our own Research Integrity and Research Publishing teams and anonymous and named external researchers and research integrity experts for contributing to this investigation.

The corresponding author, as the representative of all authors, has been given the opportunity to register their agreement or disagreement to this retraction. We have kept a record of any response received.

### References

- [1] M. Chen and F. Zhao, "Comparative Study of Macular Vascular Density and Retinal Thickness in Myopia Children with Different Microscope Diopters Based on OCTA," *Scanning*, vol. 2022, Article ID 5038918, 6 pages, 2022.

## Retraction

# Retracted: Identification of Sports Athletes' High-Strength Sports Injuries Based on NMR

### Scanning

Received 11 July 2023; Accepted 11 July 2023; Published 12 July 2023

Copyright © 2023 Scanning. This is an open access article distributed under the Creative Commons Attribution License, which permits unrestricted use, distribution, and reproduction in any medium, provided the original work is properly cited.

This article has been retracted by Hindawi following an investigation undertaken by the publisher [1]. This investigation has uncovered evidence of one or more of the following indicators of systematic manipulation of the publication process:

- (1) Discrepancies in scope
- (2) Discrepancies in the description of the research reported
- (3) Discrepancies between the availability of data and the research described
- (4) Inappropriate citations
- (5) Incoherent, meaningless and/or irrelevant content included in the article
- (6) Peer-review manipulation

The presence of these indicators undermines our confidence in the integrity of the article's content and we cannot, therefore, vouch for its reliability. Please note that this notice is intended solely to alert readers that the content of this article is unreliable. We have not investigated whether authors were aware of or involved in the systematic manipulation of the publication process.

In addition, our investigation has also shown that one or more of the following human-subject reporting requirements has not been met in this article: ethical approval by an Institutional Review Board (IRB) committee or equivalent, patient/participant consent to participate, and/or agreement to publish patient/participant details (where relevant).

Wiley and Hindawi regrets that the usual quality checks did not identify these issues before publication and have since put additional measures in place to safeguard research integrity.

We wish to credit our own Research Integrity and Research Publishing teams and anonymous and named external researchers and research integrity experts for contributing to this investigation.

The corresponding author, as the representative of all authors, has been given the opportunity to register their agreement or disagreement to this retraction. We have kept a record of any response received.

### References

- [1] W. Zhou and H. Chu, "Identification of Sports Athletes' High-Strength Sports Injuries Based on NMR," *Scanning*, vol. 2022, Article ID 1016628, 7 pages, 2022.

## Retraction

# Retracted: Observation on the Effect of Rehabilitative Physical Training on Sports Injuries under Ultrasound Image Examination

### Scanning

Received 11 July 2023; Accepted 11 July 2023; Published 12 July 2023

Copyright © 2023 Scanning. This is an open access article distributed under the Creative Commons Attribution License, which permits unrestricted use, distribution, and reproduction in any medium, provided the original work is properly cited.

This article has been retracted by Hindawi following an investigation undertaken by the publisher [1]. This investigation has uncovered evidence of one or more of the following indicators of systematic manipulation of the publication process:

- (1) Discrepancies in scope
- (2) Discrepancies in the description of the research reported
- (3) Discrepancies between the availability of data and the research described
- (4) Inappropriate citations
- (5) Incoherent, meaningless and/or irrelevant content included in the article
- (6) Peer-review manipulation

The presence of these indicators undermines our confidence in the integrity of the article's content and we cannot, therefore, vouch for its reliability. Please note that this notice is intended solely to alert readers that the content of this article is unreliable. We have not investigated whether authors were aware of or involved in the systematic manipulation of the publication process.

In addition, our investigation has also shown that one or more of the following human-subject reporting requirements has not been met in this article: ethical approval by an Institutional Review Board (IRB) committee or equivalent, patient/participant consent to participate, and/or agreement to publish patient/participant details (where relevant).

Wiley and Hindawi regrets that the usual quality checks did not identify these issues before publication and have since put additional measures in place to safeguard research integrity.

We wish to credit our own Research Integrity and Research Publishing teams and anonymous and named external researchers and research integrity experts for contributing to this investigation.

The corresponding author, as the representative of all authors, has been given the opportunity to register their agreement or disagreement to this retraction. We have kept a record of any response received.

### References

- [1] L. Wang and H. Wang, "Observation on the Effect of Rehabilitative Physical Training on Sports Injuries under Ultrasound Image Examination," *Scanning*, vol. 2022, Article ID 9998265, 7 pages, 2022.



## *Retraction*

# **Retracted: Corner Detection of the Computer VR Microscope Image Based on the 3D Reconstruction Algorithm**

### **Scanning**

Received 11 July 2023; Accepted 11 July 2023; Published 12 July 2023

Copyright © 2023 Scanning. This is an open access article distributed under the Creative Commons Attribution License, which permits unrestricted use, distribution, and reproduction in any medium, provided the original work is properly cited.

This article has been retracted by Hindawi following an investigation undertaken by the publisher [1]. This investigation has uncovered evidence of one or more of the following indicators of systematic manipulation of the publication process:

- (1) Discrepancies in scope
- (2) Discrepancies in the description of the research reported
- (3) Discrepancies between the availability of data and the research described
- (4) Inappropriate citations
- (5) Incoherent, meaningless and/or irrelevant content included in the article
- (6) Peer-review manipulation

The presence of these indicators undermines our confidence in the integrity of the article's content and we cannot, therefore, vouch for its reliability. Please note that this notice is intended solely to alert readers that the content of this article is unreliable. We have not investigated whether authors were aware of or involved in the systematic manipulation of the publication process.

Wiley and Hindawi regrets that the usual quality checks did not identify these issues before publication and have since put additional measures in place to safeguard research integrity.

We wish to credit our own Research Integrity and Research Publishing teams and anonymous and named external researchers and research integrity experts for contributing to this investigation.

The corresponding author, as the representative of all authors, has been given the opportunity to register their agreement or disagreement to this retraction. We have kept a record of any response received.

### **References**

- [1] J. Huang, "Corner Detection of the Computer VR Microscope Image Based on the 3D Reconstruction Algorithm," *Scanning*, vol. 2022, Article ID 8621103, 8 pages, 2022.

## Retraction

# Retracted: Construction of Biologic Microscopic Image Segmentation Model Based on Smoothing of Fourth-Order Partial Differential Equation

### Scanning

Received 11 July 2023; Accepted 11 July 2023; Published 12 July 2023

Copyright © 2023 Scanning. This is an open access article distributed under the Creative Commons Attribution License, which permits unrestricted use, distribution, and reproduction in any medium, provided the original work is properly cited.

This article has been retracted by Hindawi following an investigation undertaken by the publisher [1]. This investigation has uncovered evidence of one or more of the following indicators of systematic manipulation of the publication process:

- (1) Discrepancies in scope
- (2) Discrepancies in the description of the research reported
- (3) Discrepancies between the availability of data and the research described
- (4) Inappropriate citations
- (5) Incoherent, meaningless and/or irrelevant content included in the article
- (6) Peer-review manipulation

The presence of these indicators undermines our confidence in the integrity of the article's content and we cannot, therefore, vouch for its reliability. Please note that this notice is intended solely to alert readers that the content of this article is unreliable. We have not investigated whether authors were aware of or involved in the systematic manipulation of the publication process.

Wiley and Hindawi regrets that the usual quality checks did not identify these issues before publication and have since put additional measures in place to safeguard research integrity.

We wish to credit our own Research Integrity and Research Publishing teams and anonymous and named external researchers and research integrity experts for contributing to this investigation.

The corresponding author, as the representative of all authors, has been given the opportunity to register their agreement or disagreement to this retraction. We have kept a record of any response received.

### References

- [1] Y. Ma, "Construction of Biologic Microscopic Image Segmentation Model Based on Smoothing of Fourth-Order Partial Differential Equation," *Scanning*, vol. 2022, Article ID 1908644, 8 pages, 2022.

## Retraction

# Retracted: Effects of Obstructive Sleep Apnea-Hypopnea Syndrome and Cognitive Function in Ischemic Stroke Based on Linear Regression Equation

### Scanning

Received 11 July 2023; Accepted 11 July 2023; Published 12 July 2023

Copyright © 2023 Scanning. This is an open access article distributed under the Creative Commons Attribution License, which permits unrestricted use, distribution, and reproduction in any medium, provided the original work is properly cited.

This article has been retracted by Hindawi following an investigation undertaken by the publisher [1]. This investigation has uncovered evidence of one or more of the following indicators of systematic manipulation of the publication process:

- (1) Discrepancies in scope
- (2) Discrepancies in the description of the research reported
- (3) Discrepancies between the availability of data and the research described
- (4) Inappropriate citations
- (5) Incoherent, meaningless and/or irrelevant content included in the article
- (6) Peer-review manipulation

The presence of these indicators undermines our confidence in the integrity of the article's content and we cannot, therefore, vouch for its reliability. Please note that this notice is intended solely to alert readers that the content of this article is unreliable. We have not investigated whether authors were aware of or involved in the systematic manipulation of the publication process.

In addition, our investigation has also shown that one or more of the following human-subject reporting requirements has not been met in this article: ethical approval by an Institutional Review Board (IRB) committee or equivalent, patient/participant consent to participate, and/or agreement to publish patient/participant details (where relevant).

Wiley and Hindawi regrets that the usual quality checks did not identify these issues before publication and have since put additional measures in place to safeguard research integrity.

We wish to credit our own Research Integrity and Research Publishing teams and anonymous and named external researchers and research integrity experts for contributing to this investigation.

The corresponding author, as the representative of all authors, has been given the opportunity to register their agreement or disagreement to this retraction. We have kept a record of any response received.

### References

- [1] P. Ji, Q. Kou, X. Qu, G. Sun, S. Liu, and J. Zhang, "Effects of Obstructive Sleep Apnea-Hypopnea Syndrome and Cognitive Function in Ischemic Stroke Based on Linear Regression Equation," *Scanning*, vol. 2022, Article ID 4105169, 8 pages, 2022.

## Retraction

# Retracted: Effects of Sports Functional Food on Physical Function of Athletes under Ultrasound Observation

### Scanning

Received 11 July 2023; Accepted 11 July 2023; Published 12 July 2023

Copyright © 2023 Scanning. This is an open access article distributed under the Creative Commons Attribution License, which permits unrestricted use, distribution, and reproduction in any medium, provided the original work is properly cited.

This article has been retracted by Hindawi following an investigation undertaken by the publisher [1]. This investigation has uncovered evidence of one or more of the following indicators of systematic manipulation of the publication process:

- (1) Discrepancies in scope
- (2) Discrepancies in the description of the research reported
- (3) Discrepancies between the availability of data and the research described
- (4) Inappropriate citations
- (5) Incoherent, meaningless and/or irrelevant content included in the article
- (6) Peer-review manipulation

The presence of these indicators undermines our confidence in the integrity of the article's content and we cannot, therefore, vouch for its reliability. Please note that this notice is intended solely to alert readers that the content of this article is unreliable. We have not investigated whether authors were aware of or involved in the systematic manipulation of the publication process.

In addition, our investigation has also shown that one or more of the following human-subject reporting requirements has not been met in this article: ethical approval by an Institutional Review Board (IRB) committee or equivalent, patient/participant consent to participate, and/or agreement to publish patient/participant details (where relevant).

Wiley and Hindawi regrets that the usual quality checks did not identify these issues before publication and have since put additional measures in place to safeguard research integrity.

We wish to credit our own Research Integrity and Research Publishing teams and anonymous and named external researchers and research integrity experts for contributing to this investigation.

The corresponding author, as the representative of all authors, has been given the opportunity to register their agreement or disagreement to this retraction. We have kept a record of any response received.

### References

- [1] Z. Cheng, H. Lin, and Z. Zhou, "Effects of Sports Functional Food on Physical Function of Athletes under Ultrasound Observation," *Scanning*, vol. 2022, Article ID 7769653, 7 pages, 2022.

## Retraction

# Retracted: Effect of Nursing Intervention on Coronary CT Angiography in Elderly Patients

### Scanning

Received 20 June 2023; Accepted 20 June 2023; Published 21 June 2023

Copyright © 2023 Scanning. This is an open access article distributed under the Creative Commons Attribution License, which permits unrestricted use, distribution, and reproduction in any medium, provided the original work is properly cited.

This article has been retracted by Hindawi following an investigation undertaken by the publisher [1]. This investigation has uncovered evidence of one or more of the following indicators of systematic manipulation of the publication process:

- (1) Discrepancies in scope
- (2) Discrepancies in the description of the research reported
- (3) Discrepancies between the availability of data and the research described
- (4) Inappropriate citations
- (5) Incoherent, meaningless and/or irrelevant content included in the article
- (6) Peer-review manipulation

The presence of these indicators undermines our confidence in the integrity of the article's content and we cannot, therefore, vouch for its reliability. Please note that this notice is intended solely to alert readers that the content of this article is unreliable. We have not investigated whether authors were aware of or involved in the systematic manipulation of the publication process.

In addition, our investigation has also shown that one or more of the following human-subject reporting requirements has not been met in this article: ethical approval by an Institutional Review Board (IRB) committee or equivalent, patient/participant consent to participate, and/or agreement to publish patient/participant details (where relevant).

Wiley and Hindawi regrets that the usual quality checks did not identify these issues before publication and have since put additional measures in place to safeguard research integrity.

We wish to credit our own Research Integrity and Research Publishing teams and anonymous and named external researchers and research integrity experts for contributing to this investigation.

The corresponding author, as the representative of all authors, has been given the opportunity to register their agreement or disagreement to this retraction. We have kept a record of any response received.

### References

- [1] Y. Yin and Z. Wei, "Effect of Nursing Intervention on Coronary CT Angiography in Elderly Patients," *Scanning*, vol. 2022, Article ID 3663285, 7 pages, 2022.

## Retraction

# Retracted: Nursing Education of Lateral Oblique Complications of Neurosurgery under Microscope

### Scanning

Received 20 June 2023; Accepted 20 June 2023; Published 21 June 2023

Copyright © 2023 Scanning. This is an open access article distributed under the Creative Commons Attribution License, which permits unrestricted use, distribution, and reproduction in any medium, provided the original work is properly cited.

This article has been retracted by Hindawi following an investigation undertaken by the publisher [1]. This investigation has uncovered evidence of one or more of the following indicators of systematic manipulation of the publication process:

- (1) Discrepancies in scope
- (2) Discrepancies in the description of the research reported
- (3) Discrepancies between the availability of data and the research described
- (4) Inappropriate citations
- (5) Incoherent, meaningless and/or irrelevant content included in the article
- (6) Peer-review manipulation

The presence of these indicators undermines our confidence in the integrity of the article's content and we cannot, therefore, vouch for its reliability. Please note that this notice is intended solely to alert readers that the content of this article is unreliable. We have not investigated whether authors were aware of or involved in the systematic manipulation of the publication process.

In addition, our investigation has also shown that one or more of the following human-subject reporting requirements has not been met in this article: ethical approval by an Institutional Review Board (IRB) committee or equivalent, patient/participant consent to participate, and/or agreement to publish patient/participant details (where relevant).

Wiley and Hindawi regrets that the usual quality checks did not identify these issues before publication and have since put additional measures in place to safeguard research integrity.

We wish to credit our own Research Integrity and Research Publishing teams and anonymous and named exter-

nal researchers and research integrity experts for contributing to this investigation.

The corresponding author, as the representative of all authors, has been given the opportunity to register their agreement or disagreement to this retraction. We have kept a record of any response received.

### References

- [1] K. Hu, "Nursing Education of Lateral Oblique Complications of Neurosurgery under Microscope," *Scanning*, vol. 2022, Article ID 2158181, 8 pages, 2022.

## Retraction

# Retracted: Effect Evaluation of Comfort Nursing Materials Assisted Nursing for Patients with Advanced Malignant Tumor

### Scanning

Received 20 June 2023; Accepted 20 June 2023; Published 21 June 2023

Copyright © 2023 Scanning. This is an open access article distributed under the Creative Commons Attribution License, which permits unrestricted use, distribution, and reproduction in any medium, provided the original work is properly cited.

This article has been retracted by Hindawi following an investigation undertaken by the publisher [1]. This investigation has uncovered evidence of one or more of the following indicators of systematic manipulation of the publication process:

- (1) Discrepancies in scope
- (2) Discrepancies in the description of the research reported
- (3) Discrepancies between the availability of data and the research described
- (4) Inappropriate citations
- (5) Incoherent, meaningless and/or irrelevant content included in the article
- (6) Peer-review manipulation

The presence of these indicators undermines our confidence in the integrity of the article's content and we cannot, therefore, vouch for its reliability. Please note that this notice is intended solely to alert readers that the content of this article is unreliable. We have not investigated whether authors were aware of or involved in the systematic manipulation of the publication process.

In addition, our investigation has also shown that one or more of the following human-subject reporting requirements has not been met in this article: ethical approval by an Institutional Review Board (IRB) committee or equivalent, patient/participant consent to participate, and/or agreement to publish patient/participant details (where relevant).

Wiley and Hindawi regrets that the usual quality checks did not identify these issues before publication and have since put additional measures in place to safeguard research integrity.

We wish to credit our own Research Integrity and Research Publishing teams and anonymous and named external researchers and research integrity experts for contributing to this investigation.

The corresponding author, as the representative of all authors, has been given the opportunity to register their agreement or disagreement to this retraction. We have kept a record of any response received.

### References

- [1] M. Zhong, L. He, M. Chen, Z. Lu, R. Li, and L. Li, "Effect Evaluation of Comfort Nursing Materials Assisted Nursing for Patients with Advanced Malignant Tumor," *Scanning*, vol. 2022, Article ID 4766252, 6 pages, 2022.

## Retraction

# Retracted: Application of MRI and CT Images in Surgical Treatment of Early Cervical Cancer

### Scanning

Received 20 June 2023; Accepted 20 June 2023; Published 21 June 2023

Copyright © 2023 Scanning. This is an open access article distributed under the Creative Commons Attribution License, which permits unrestricted use, distribution, and reproduction in any medium, provided the original work is properly cited.

This article has been retracted by Hindawi following an investigation undertaken by the publisher [1]. This investigation has uncovered evidence of one or more of the following indicators of systematic manipulation of the publication process:

- (1) Discrepancies in scope
- (2) Discrepancies in the description of the research reported
- (3) Discrepancies between the availability of data and the research described
- (4) Inappropriate citations
- (5) Incoherent, meaningless and/or irrelevant content included in the article
- (6) Peer-review manipulation

The presence of these indicators undermines our confidence in the integrity of the article's content and we cannot, therefore, vouch for its reliability. Please note that this notice is intended solely to alert readers that the content of this article is unreliable. We have not investigated whether authors were aware of or involved in the systematic manipulation of the publication process.

In addition, our investigation has also shown that one or more of the following human-subject reporting requirements has not been met in this article: ethical approval by an Institutional Review Board (IRB) committee or equivalent, patient/participant consent to participate, and/or agreement to publish patient/participant details (where relevant).

Wiley and Hindawi regrets that the usual quality checks did not identify these issues before publication and have since put additional measures in place to safeguard research integrity.

We wish to credit our own Research Integrity and Research Publishing teams and anonymous and named external researchers and research integrity experts for contributing to this investigation.

The corresponding author, as the representative of all authors, has been given the opportunity to register their agreement or disagreement to this retraction. We have kept a record of any response received.

### References

- [1] A. Lu and G. Lu, "Application of MRI and CT Images in Surgical Treatment of Early Cervical Cancer," *Scanning*, vol. 2022, Article ID 1592449, 9 pages, 2022.



## *Retraction*

# **Retracted: Postoperative Nursing and Functional Rehabilitation of Ultrasound Diagnosis of Lower Rotator Cuff Injury**

### **Scanning**

Received 20 June 2023; Accepted 20 June 2023; Published 21 June 2023

Copyright © 2023 Scanning. This is an open access article distributed under the Creative Commons Attribution License, which permits unrestricted use, distribution, and reproduction in any medium, provided the original work is properly cited.

This article has been retracted by Hindawi following an investigation undertaken by the publisher [1]. This investigation has uncovered evidence of one or more of the following indicators of systematic manipulation of the publication process:

- (1) Discrepancies in scope
- (2) Discrepancies in the description of the research reported
- (3) Discrepancies between the availability of data and the research described
- (4) Inappropriate citations
- (5) Incoherent, meaningless and/or irrelevant content included in the article
- (6) Peer-review manipulation

The presence of these indicators undermines our confidence in the integrity of the article's content and we cannot, therefore, vouch for its reliability. Please note that this notice is intended solely to alert readers that the content of this article is unreliable. We have not investigated whether authors were aware of or involved in the systematic manipulation of the publication process.

In addition, our investigation has also shown that one or more of the following human-subject reporting requirements has not been met in this article: ethical approval by an Institutional Review Board (IRB) committee or equivalent, patient/participant consent to participate, and/or agreement to publish patient/participant details (where relevant).

Wiley and Hindawi regrets that the usual quality checks did not identify these issues before publication and have since put additional measures in place to safeguard research integrity.

We wish to credit our own Research Integrity and Research Publishing teams and anonymous and named external researchers and research integrity experts for contributing to this investigation.

The corresponding author, as the representative of all authors, has been given the opportunity to register their agreement or disagreement to this retraction. We have kept a record of any response received.

### **References**

- [1] R. Hou, "Postoperative Nursing and Functional Rehabilitation of Ultrasound Diagnosis of Lower Rotator Cuff Injury," *Scanning*, vol. 2022, Article ID 8319082, 7 pages, 2022.

## Retraction

# Retracted: Effect of Microscope Combined with Wechat Smart Platform on Clinical Efficacy and Gastrointestinal Function of Patients with Cholecystolithiasis Combined with Common Bile Duct Stones

### Scanning

Received 20 June 2023; Accepted 20 June 2023; Published 21 June 2023

Copyright © 2023 Scanning. This is an open access article distributed under the Creative Commons Attribution License, which permits unrestricted use, distribution, and reproduction in any medium, provided the original work is properly cited.

This article has been retracted by Hindawi following an investigation undertaken by the publisher [1]. This investigation has uncovered evidence of one or more of the following indicators of systematic manipulation of the publication process:

- (1) Discrepancies in scope
- (2) Discrepancies in the description of the research reported
- (3) Discrepancies between the availability of data and the research described
- (4) Inappropriate citations
- (5) Incoherent, meaningless and/or irrelevant content included in the article
- (6) Peer-review manipulation

The presence of these indicators undermines our confidence in the integrity of the article's content and we cannot, therefore, vouch for its reliability. Please note that this notice is intended solely to alert readers that the content of this article is unreliable. We have not investigated whether authors were aware of or involved in the systematic manipulation of the publication process.

Wiley and Hindawi regrets that the usual quality checks did not identify these issues before publication and have since put additional measures in place to safeguard research integrity.

We wish to credit our own Research Integrity and Research Publishing teams and anonymous and named

external researchers and research integrity experts for contributing to this investigation.

The corresponding author, as the representative of all authors, has been given the opportunity to register their agreement or disagreement to this retraction. We have kept a record of any response received.

### References

- [1] X. Xu, D. Guo, Y. Zhang et al., "Effect of Microscope Combined with Wechat Smart Platform on Clinical Efficacy and Gastrointestinal Function of Patients with Cholecystolithiasis Combined with Common Bile Duct Stones," *Scanning*, vol. 2022, Article ID 9661506, 5 pages, 2022.

## Retraction

# Retracted: Application of MRI in the Prevention of Sports Injuries in Physical Education Teaching

### Scanning

Received 20 June 2023; Accepted 20 June 2023; Published 21 June 2023

Copyright © 2023 Scanning. This is an open access article distributed under the Creative Commons Attribution License, which permits unrestricted use, distribution, and reproduction in any medium, provided the original work is properly cited.

This article has been retracted by Hindawi following an investigation undertaken by the publisher [1]. This investigation has uncovered evidence of one or more of the following indicators of systematic manipulation of the publication process:

- (1) Discrepancies in scope
- (2) Discrepancies in the description of the research reported
- (3) Discrepancies between the availability of data and the research described
- (4) Inappropriate citations
- (5) Incoherent, meaningless and/or irrelevant content included in the article
- (6) Peer-review manipulation

The presence of these indicators undermines our confidence in the integrity of the article's content and we cannot, therefore, vouch for its reliability. Please note that this notice is intended solely to alert readers that the content of this article is unreliable. We have not investigated whether authors were aware of or involved in the systematic manipulation of the publication process.

In addition, our investigation has also shown that one or more of the following human-subject reporting requirements has not been met in this article: ethical approval by an Institutional Review Board (IRB) committee or equivalent, patient/participant consent to participate, and/or agreement to publish patient/participant details (where relevant).

Wiley and Hindawi regrets that the usual quality checks did not identify these issues before publication and have since put additional measures in place to safeguard research integrity.

We wish to credit our own Research Integrity and Research Publishing teams and anonymous and named external researchers and research integrity experts for contributing to this investigation.

The corresponding author, as the representative of all authors, has been given the opportunity to register their agreement or disagreement to this retraction. We have kept a record of any response received.

### References

- [1] J. Zhao, "Application of MRI in the Prevention of Sports Injuries in Physical Education Teaching," *Scanning*, vol. 2022, Article ID 7738233, 6 pages, 2022.

## *Retraction*

# **Retracted: Preparation and Performance Analysis of Bacterial Cellulose-Based Composite Hydrogel Based on Scanning Electron Microscope**

### **Scanning**

Received 20 June 2023; Accepted 20 June 2023; Published 21 June 2023

Copyright © 2023 Scanning. This is an open access article distributed under the Creative Commons Attribution License, which permits unrestricted use, distribution, and reproduction in any medium, provided the original work is properly cited.

This article has been retracted by Hindawi following an investigation undertaken by the publisher [1]. This investigation has uncovered evidence of one or more of the following indicators of systematic manipulation of the publication process:

- (1) Discrepancies in scope
- (2) Discrepancies in the description of the research reported
- (3) Discrepancies between the availability of data and the research described
- (4) Inappropriate citations
- (5) Incoherent, meaningless and/or irrelevant content included in the article
- (6) Peer-review manipulation

The presence of these indicators undermines our confidence in the integrity of the article's content and we cannot, therefore, vouch for its reliability. Please note that this notice is intended solely to alert readers that the content of this article is unreliable. We have not investigated whether authors were aware of or involved in the systematic manipulation of the publication process.

Wiley and Hindawi regrets that the usual quality checks did not identify these issues before publication and have since put additional measures in place to safeguard research integrity.

We wish to credit our own Research Integrity and Research Publishing teams and anonymous and named external researchers and research integrity experts for contributing to this investigation.

The corresponding author, as the representative of all authors, has been given the opportunity to register their agreement or disagreement to this retraction. We have kept a record of any response received.

### **References**

- [1] M. Shao, Z. Shi, B. Zhai, X. Zhang, and Z. Li, "Preparation and Performance Analysis of Bacterial Cellulose-Based Composite Hydrogel Based on Scanning Electron Microscope," *Scanning*, vol. 2022, Article ID 8750394, 7 pages, 2022.

## Retraction

# Retracted: Evaluation of the Effect of Refined Nursing Intervention on Coronary CT Imaging Microscopy

### Scanning

Received 20 June 2023; Accepted 20 June 2023; Published 21 June 2023

Copyright © 2023 Scanning. This is an open access article distributed under the Creative Commons Attribution License, which permits unrestricted use, distribution, and reproduction in any medium, provided the original work is properly cited.

This article has been retracted by Hindawi following an investigation undertaken by the publisher [1]. This investigation has uncovered evidence of one or more of the following indicators of systematic manipulation of the publication process:

- (1) Discrepancies in scope
- (2) Discrepancies in the description of the research reported
- (3) Discrepancies between the availability of data and the research described
- (4) Inappropriate citations
- (5) Incoherent, meaningless and/or irrelevant content included in the article
- (6) Peer-review manipulation

The presence of these indicators undermines our confidence in the integrity of the article's content and we cannot, therefore, vouch for its reliability. Please note that this notice is intended solely to alert readers that the content of this article is unreliable. We have not investigated whether authors were aware of or involved in the systematic manipulation of the publication process.

Wiley and Hindawi regrets that the usual quality checks did not identify these issues before publication and have since put additional measures in place to safeguard research integrity.

We wish to credit our own Research Integrity and Research Publishing teams and anonymous and named external researchers and research integrity experts for contributing to this investigation.

The corresponding author, as the representative of all authors, has been given the opportunity to register their

agreement or disagreement to this retraction. We have kept a record of any response received.

### References

- [1] T. Qian, "Evaluation of the Effect of Refined Nursing Intervention on Coronary CT Imaging Microscopy," *Scanning*, vol. 2022, Article ID 4870548, 6 pages, 2022.

## Retraction

# Retracted: Application of CT Ultrasonography Combined with Microscopic Intraperitoneal Hyperthermic Perfusion Chemotherapy in Postoperative Treatment of Oocyst Carcinoma

### Scanning

Received 20 June 2023; Accepted 20 June 2023; Published 21 June 2023

Copyright © 2023 Scanning. This is an open access article distributed under the Creative Commons Attribution License, which permits unrestricted use, distribution, and reproduction in any medium, provided the original work is properly cited.

This article has been retracted by Hindawi following an investigation undertaken by the publisher [1]. This investigation has uncovered evidence of one or more of the following indicators of systematic manipulation of the publication process:

- (1) Discrepancies in scope
- (2) Discrepancies in the description of the research reported
- (3) Discrepancies between the availability of data and the research described
- (4) Inappropriate citations
- (5) Incoherent, meaningless and/or irrelevant content included in the article
- (6) Peer-review manipulation

The presence of these indicators undermines our confidence in the integrity of the article's content and we cannot, therefore, vouch for its reliability. Please note that this notice is intended solely to alert readers that the content of this article is unreliable. We have not investigated whether authors were aware of or involved in the systematic manipulation of the publication process.

In addition, our investigation has also shown that one or more of the following human-subject reporting requirements has not been met in this article: ethical approval by an Institutional Review Board (IRB) committee or equivalent, patient/participant consent to participate, and/or agreement to publish patient/participant details (where relevant).

Wiley and Hindawi regrets that the usual quality checks did not identify these issues before publication and have since put additional measures in place to safeguard research integrity.

We wish to credit our own Research Integrity and Research Publishing teams and anonymous and named external researchers and research integrity experts for contributing to this investigation.

The corresponding author, as the representative of all authors, has been given the opportunity to register their agreement or disagreement to this retraction. We have kept a record of any response received.

### References

- [1] Z. Xia and H. Jin, "Application of CT Ultrasonography Combined with Microscopic Intraperitoneal Hyperthermic Perfusion Chemotherapy in Postoperative Treatment of Oocyst Carcinoma," *Scanning*, vol. 2022, Article ID 5444552, 6 pages, 2022.

## *Retraction*

# **Retracted: Efficacy Evaluation of the Combined Platelet-Rich Plasma and Hyaluronic Acid after Arthroscopic Joint Debridement in Treating Knee Osteoarthritis**

### **Scanning**

Received 20 June 2023; Accepted 20 June 2023; Published 21 June 2023

Copyright © 2023 Scanning. This is an open access article distributed under the Creative Commons Attribution License, which permits unrestricted use, distribution, and reproduction in any medium, provided the original work is properly cited.

This article has been retracted by Hindawi following an investigation undertaken by the publisher [1]. This investigation has uncovered evidence of one or more of the following indicators of systematic manipulation of the publication process:

- (1) Discrepancies in scope
- (2) Discrepancies in the description of the research reported
- (3) Discrepancies between the availability of data and the research described
- (4) Inappropriate citations
- (5) Incoherent, meaningless and/or irrelevant content included in the article
- (6) Peer-review manipulation

The presence of these indicators undermines our confidence in the integrity of the article's content and we cannot, therefore, vouch for its reliability. Please note that this notice is intended solely to alert readers that the content of this article is unreliable. We have not investigated whether authors were aware of or involved in the systematic manipulation of the publication process.

In addition, our investigation has also shown that one or more of the following human-subject reporting requirements has not been met in this article: ethical approval by an Institutional Review Board (IRB) committee or equivalent, patient/participant consent to participate, and/or agreement to publish patient/participant details (where relevant).

Wiley and Hindawi regrets that the usual quality checks did not identify these issues before publication and have since put additional measures in place to safeguard research integrity.

We wish to credit our own Research Integrity and Research Publishing teams and anonymous and named external researchers and research integrity experts for contributing to this investigation.

The corresponding author, as the representative of all authors, has been given the opportunity to register their agreement or disagreement to this retraction. We have kept a record of any response received.

### **References**

- [1] M. Lu and Y. Jin, "Efficacy Evaluation of the Combined Platelet-Rich Plasma and Hyaluronic Acid after Arthroscopic Joint Debridement in Treating Knee Osteoarthritis," *Scanning*, vol. 2022, Article ID 6994017, 5 pages, 2022.

## Retraction

# Retracted: Effect of Rehabilitation Physical Training on Basketball Injury under Ultrasound Examination

### Scanning

Received 20 June 2023; Accepted 20 June 2023; Published 21 June 2023

Copyright © 2023 Scanning. This is an open access article distributed under the Creative Commons Attribution License, which permits unrestricted use, distribution, and reproduction in any medium, provided the original work is properly cited.

This article has been retracted by Hindawi following an investigation undertaken by the publisher [1]. This investigation has uncovered evidence of one or more of the following indicators of systematic manipulation of the publication process:

- (1) Discrepancies in scope
- (2) Discrepancies in the description of the research reported
- (3) Discrepancies between the availability of data and the research described
- (4) Inappropriate citations
- (5) Incoherent, meaningless and/or irrelevant content included in the article
- (6) Peer-review manipulation

The presence of these indicators undermines our confidence in the integrity of the article's content and we cannot, therefore, vouch for its reliability. Please note that this notice is intended solely to alert readers that the content of this article is unreliable. We have not investigated whether authors were aware of or involved in the systematic manipulation of the publication process.

In addition, our investigation has also shown that one or more of the following human-subject reporting requirements has not been met in this article: ethical approval by an Institutional Review Board (IRB) committee or equivalent, patient/participant consent to participate, and/or agreement to publish patient/participant details (where relevant).

Wiley and Hindawi regrets that the usual quality checks did not identify these issues before publication and have since put additional measures in place to safeguard research integrity.

We wish to credit our own Research Integrity and Research Publishing teams and anonymous and named external researchers and research integrity experts for contributing to this investigation.

The corresponding author, as the representative of all authors, has been given the opportunity to register their agreement or disagreement to this retraction. We have kept a record of any response received.

### References

- [1] E. Wenjie and Q. Yu, "Effect of Rehabilitation Physical Training on Basketball Injury under Ultrasound Examination," *Scanning*, vol. 2022, Article ID 2554581, 8 pages, 2022.



## Retraction

# Retracted: Application of Multislice Spiral CT and Three-Dimensional Image Reconstruction Technology in the Observation of Ankle Sports Injury under the Microscope

### Scanning

Received 20 June 2023; Accepted 20 June 2023; Published 21 June 2023

Copyright © 2023 Scanning. This is an open access article distributed under the Creative Commons Attribution License, which permits unrestricted use, distribution, and reproduction in any medium, provided the original work is properly cited.

This article has been retracted by Hindawi following an investigation undertaken by the publisher [1]. This investigation has uncovered evidence of one or more of the following indicators of systematic manipulation of the publication process:

- (1) Discrepancies in scope
- (2) Discrepancies in the description of the research reported
- (3) Discrepancies between the availability of data and the research described
- (4) Inappropriate citations
- (5) Incoherent, meaningless and/or irrelevant content included in the article
- (6) Peer-review manipulation

The presence of these indicators undermines our confidence in the integrity of the article's content and we cannot, therefore, vouch for its reliability. Please note that this notice is intended solely to alert readers that the content of this article is unreliable. We have not investigated whether authors were aware of or involved in the systematic manipulation of the publication process.

In addition, our investigation has also shown that one or more of the following human-subject reporting requirements has not been met in this article: ethical approval by an Institutional Review Board (IRB) committee or equivalent, patient/participant consent to participate, and/or agreement to publish patient/participant details (where relevant).

Wiley and Hindawi regrets that the usual quality checks did not identify these issues before publication and have since put additional measures in place to safeguard research integrity.

We wish to credit our own Research Integrity and Research Publishing teams and anonymous and named external researchers and research integrity experts for contributing to this investigation.

The corresponding author, as the representative of all authors, has been given the opportunity to register their agreement or disagreement to this retraction. We have kept a record of any response received.

### References

- [1] D. Zhao, "Application of Multislice Spiral CT and Three-Dimensional Image Reconstruction Technology in the Observation of Ankle Sports Injury Under the Microscope," *Scanning*, vol. 2022, Article ID 8174310, 7 pages, 2022.

## *Retraction*

# **Retracted: Analysis of Infertility Factors Caused by Gynecological Chronic Pelvic Inflammation Disease Based on Multivariate Regression Analysis of Logistic**

### **Scanning**

Received 20 June 2023; Accepted 20 June 2023; Published 21 June 2023

Copyright © 2023 Scanning. This is an open access article distributed under the Creative Commons Attribution License, which permits unrestricted use, distribution, and reproduction in any medium, provided the original work is properly cited.

This article has been retracted by Hindawi following an investigation undertaken by the publisher [1]. This investigation has uncovered evidence of one or more of the following indicators of systematic manipulation of the publication process:

- (1) Discrepancies in scope
- (2) Discrepancies in the description of the research reported
- (3) Discrepancies between the availability of data and the research described
- (4) Inappropriate citations
- (5) Incoherent, meaningless and/or irrelevant content included in the article
- (6) Peer-review manipulation

The presence of these indicators undermines our confidence in the integrity of the article's content and we cannot, therefore, vouch for its reliability. Please note that this notice is intended solely to alert readers that the content of this article is unreliable. We have not investigated whether authors were aware of or involved in the systematic manipulation of the publication process.

In addition, our investigation has also shown that one or more of the following human-subject reporting requirements has not been met in this article: ethical approval by an Institutional Review Board (IRB) committee or equivalent, patient/participant consent to participate, and/or agreement to publish patient/participant details (where relevant).

Wiley and Hindawi regrets that the usual quality checks did not identify these issues before publication and have since put additional measures in place to safeguard research integrity.

We wish to credit our own Research Integrity and Research Publishing teams and anonymous and named external researchers and research integrity experts for contributing to this investigation.

The corresponding author, as the representative of all authors, has been given the opportunity to register their agreement or disagreement to this retraction. We have kept a record of any response received.

### **References**

- [1] L. Liu, G. Yang, J. Ren, L. Zhang, T. Wu, and Q. Zheng, "Analysis of Infertility Factors Caused by Gynecological Chronic Pelvic Inflammation Disease Based on Multivariate Regression Analysis of Logistic," *Scanning*, vol. 2022, Article ID 7531190, 7 pages, 2022.

## *Retraction*

# **Retracted: Application of CT Multimodal Images in Rehabilitation Monitoring of Long-Distance Running**

### **Scanning**

Received 5 December 2023; Accepted 5 December 2023; Published 6 December 2023

Copyright © 2023 Scanning. This is an open access article distributed under the Creative Commons Attribution License, which permits unrestricted use, distribution, and reproduction in any medium, provided the original work is properly cited.

This article has been retracted by Hindawi, as publisher, following an investigation undertaken by the publisher [1]. This investigation has uncovered evidence of systematic manipulation of the publication and peer-review process. We cannot, therefore, vouch for the reliability or integrity of this article.

Please note that this notice is intended solely to alert readers that the peer-review process of this article has been compromised.

Wiley and Hindawi regret that the usual quality checks did not identify these issues before publication and have since put additional measures in place to safeguard research integrity.

We wish to credit our Research Integrity and Research Publishing teams and anonymous and named external researchers and research integrity experts for contributing to this investigation.

The corresponding author, as the representative of all authors, has been given the opportunity to register their agreement or disagreement to this retraction. We have kept a record of any response received.

### **References**

- [1] X. Du and Y. He, "Application of CT Multimodal Images in Rehabilitation Monitoring of Long-Distance Running," *Scanning*, vol. 2022, Article ID 6425448, 7 pages, 2022.

## Research Article

# Application of CT Multimodal Images in Rehabilitation Monitoring of Long-Distance Running

Xufeng Du <sup>1</sup> and Yaye He <sup>2</sup>

<sup>1</sup>Physical Education Department of Shanxi Medical University, Taiyuan Shanxi 030001, China

<sup>2</sup>Science and Education Department Taiyuan Central Hospital, Taiyuan Shanxi 030001, China

Correspondence should be addressed to Xufeng Du; 201701360103@lzpcc.edu.cn

Received 1 August 2022; Revised 10 September 2022; Accepted 16 September 2022; Published 4 October 2022

Academic Editor: Balakrishnan Nagaraj

Copyright © 2022 Xufeng Du and Yaye He. This is an open access article distributed under the Creative Commons Attribution License, which permits unrestricted use, distribution, and reproduction in any medium, provided the original work is properly cited.

In order to monitor the rehabilitation of athletes injured in long-distance running, the author proposes a method for rehabilitation monitoring of long-distance running based on CT multimodal images. This method combines the latest multimodal image technology, integrates multimodal technology into CT images to improve the accuracy, performs image segmentation on CT multimodal images through medical segmentation methods, and analyzes the segmented images; finally, it can achieve the effect of rehabilitation treatment for athletes in long-distance running. Experimental results show that the total time taken by the authors' method is 10.9 hours, with an average time of 8 seconds, which is much shorter than the other two control methods. In conclusion, the authors' method allows for better rehabilitation monitoring of long-distance running sports injuries.

## 1. Introduction

Middle-distance running is short for middle-distance running and long-distance running [1]. In middle- and long-distance running, athletes may cause sports injuries due to the consumption of energy substances in the body and the accumulation of metabolites, the decline of exercise ability, technical deformation, and weak awareness of self-protection. Therefore, it is of great significance to study the causes and preventive measures of injuries in middle- and long-distance running; at the same time, the rehabilitation monitoring of the injured part is also very important [2, 3].

In recent years, with the continuous development of the mobile Internet and the continuous popularization of multimedia and smart portable devices, more and more information such as images, voices, and texts are stored on the network and smart devices in the form of data. Images and videos have become another main information carrier after text; now, billions of images are uploaded every day; in the future, there will be a lot of search work related to images and videos; therefore, machines automatically understand image semantics and establish a relationship between images

and texts; the relationship between them has become a research topic of practical significance. In recent years, various university laboratories, research institutions, and company laboratories have been carrying out this research in depth. Based on deep learning, researchers have conducted in-depth research on applications in computer vision and natural language processing and achieved excellent results. Multimodal image semantic understanding (image description), as a high-level image semantic understanding task, also involves multimodal problems related to computer vision and natural language processing and is an important exploration for the application of deep learning to multiple modal fields [4].

Medical image segmentation is the basis of medical image processing and analysis, the solution of this problem not only directly affects the successful application of computer graphics and image technology in medicine but also has important theoretical and practical significance [5–7]. Medical image segmentation is a process of extracting regions of interest, and the segmentation results can provide reference for subsequent disease diagnosis, treatment plan planning, and treatment effect evaluation. Because of its high resolution, CT can more clearly highlight the characteristics

of anatomical structure and diseased tissue, which makes it widely used in the diagnosis of diseases in many systems. Therefore, it is very important to study the application of image segmentation methods in CT images, as shown in Figure 1.

## 2. Literature Review

With the increase of competition intensity and the improvement of athletes' competitive level, the training intensity of middle-distance runners is also increasing. However, due to the relatively weak awareness of self-protection of athletes, sports injuries occur from time to time. There are five common injuries:

- (1) Overuse injury
- (2) Joint sprain
- (3) Strain
- (4) Abdominal pain during exercise
- (5) Muscle spasm

For these five kinds of injuries, relevant parties have made rehabilitation methods for these five methods and achieved ideal therapeutic effects. But it does not apply to all types of damage.

The multimodal image understanding task can be applied in many aspects and has strong practicality [8]. For example, it can be used for search functions, including image-text search and text-image search, so that the traditional tag-based search is converted into a tag and content-based search, and the search results are more accurate; at the same time, the search time is saved, and it has high practical significance. Multimodal image understanding can also be used for assistive functions, specifically assisting those systems without visual systems or visually impaired, such as intelligent robots assisting the blind; the robot can observe the external environment according to the visual system and convert it into text information is described, then use speech synthesis technology to achieve text-to-speech conversion, so as to better help visually impaired people, and can also be used in early childhood education; multimodal image understanding technology can teach children to see pictures and speak, and at the same time, in medical imaging, multimodal image understanding technology can automatically generate diagnostic results and assist doctors in seeing patients. Therefore, the multimodal image understanding task has a wide range of application scenarios in real life and has extremely high academic value and research significance that cannot be ignored in scientific research [9].

The current mainstream solutions for multimodal image understanding tasks are based on encoder-decoder frameworks. For example, Teng and Wu use an encoder to encode an input image and a decoder to generate captions for the image [10]. Among them, the common encoder is a deep convolutional neural network, and the decoder often uses an autoregressive decoder such as a recurrent neural network, such as LSTM; the autoregressive decoder sequentially

generates each word in a serialized manner, resulting in a complete descriptive sentence. Since the autoregressive decoder is based on the previously generated word sequence and image content to generate the words of the current time step, this is a serialization process, which cannot be parallelized, so there is a problem of slow generation speed. Moreover, in the process of generating words by reasoning, if the previous words are inappropriate or there is a deviation error, it is easy to affect the words generated later, resulting in cumulative errors. At the same time, the autoregressive decoder treats the sentence as a serialized structure instead of a hierarchical structure, this process cannot model the inherent hierarchical structure of natural language, and this makes the autoregressive decoder extremely favor N-gram phrases with high frequency in the training data and is more inclined to predict common phrases [11]. Therefore, autoregressive decoders run the risk of incorrect semantics and lack of sentence diversity. In the neural machine translation model (NMT), the nonautoregressive decoder is proposed to solve the problem that the generation speed of the autoregressive decoder is too slow, but this nonautoregressive decoder indirectly models the real target modal distribution, rather than modeling its distribution directly. Direct modeling follows the conditional generation method of language, that is, it predicts the word at the current moment based on the condition of the sentence above, and the autoregressive decoder adopts the direct modeling method. Indirect modeling follows the condition-independent generation method of language, that is, each word in the entire sentence is independently generated without being conditioned on the context. Therefore, indirect modeling does not follow the conditional distribution of the language, which inevitably introduces another problem, called the "multimodal problem."

CT has created a precedent for digital imaging, but it is different from ordinary X-ray imaging. CT displays sectional anatomical images, and its density resolution capability is much higher than that of X-ray images, so that X-ray imaging cannot develop anatomical structures and their lesions. Organization is visualized; thus, the inspection scope of the human body is significantly expanded, and the detection rate of lesions and the accuracy of diagnosis are improved. As the first digital imaging device developed, CT has greatly promoted the development of medical imaging. At present, CT has been widely used in the diagnosis of the following systems and organ diseases in clinic: central nervous system, head and neck, lungs, heart and great vessels, abdomen and pelvis, and musculoskeletal system.

Based on the above research, the author proposes a rehabilitation monitoring method for long-distance running sports injuries based on CT multimodal images. Combining CT medical segmentation technology and multimodal image technology, we form a CT multimodal image technology and use CT image cutting technology and multimodal image technology to medically cut and analyze CT multimodal images; this not only achieves the use of CT images for the rehabilitation of long-distance running injuries but also speeds up the monitoring speed and improves the rehabilitation effect.

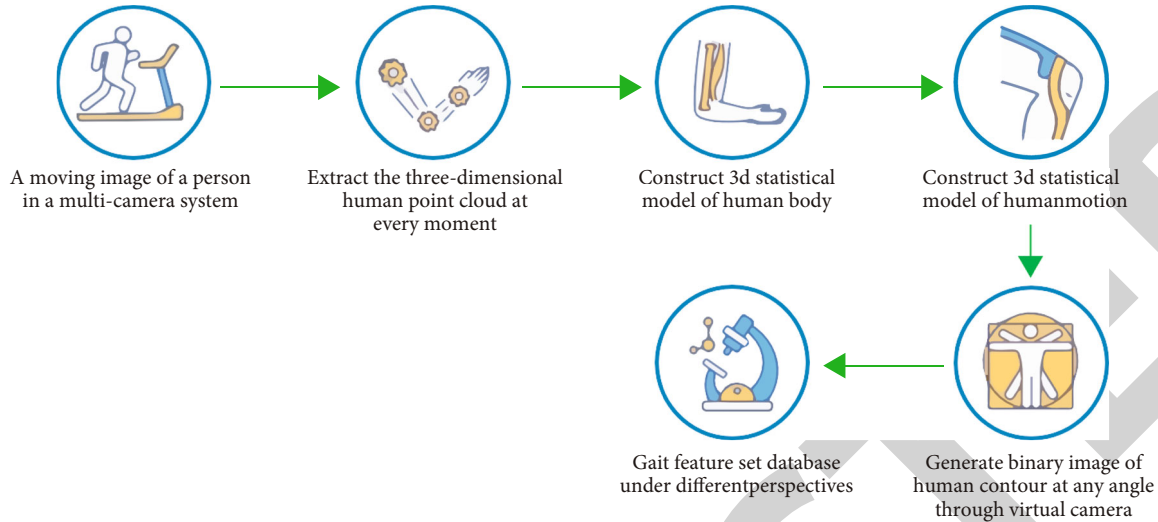


FIGURE 1: Application of CT multimodal images in long-distance running rehabilitation monitoring.

### 3. Research Methods

**3.1. Multimodal Image Understanding Model.** The algorithm of multimodal image understanding model mainly includes algorithm based on template matching, search, and multimodal image understanding based on neural network. The method based on template matching first recognizes visual elements such as objects existing in it, the relationship between objects, scene locations, etc. through scene recognition and target monitoring, then fill in the sentence template designed by hand; the disadvantage is that the sentence pattern is fixed, the generated sentence is too simple and lacks flexibility, and at the same time, this method requires identifying the relationship between objects, scene content, and objects in advance; the workload is large in the early stage, which will overrely on the performance of the experiment, and is prone to error accumulation; this is a way of inducing biases directly using the dataset. The search-based algorithm is used to search for similar images in the training dataset, and the description sentence of the most similar image is used as the description sentence of the image; compared with the template matching method, the sentences generated by this method are more fluent. The disadvantage is that similar pictures will have different content, so it is difficult to generate accurate sentences describing the images. The sentences generated by these methods are relatively simple and have a high error rate. For this reason, many researchers are constantly exploring new solutions, including multimodal image understanding models based on neural networks. The following will mainly introduce the multimodal image understanding model based on neural network.

The current popular algorithms for multimodal image understanding models are mainly based on deep neural network algorithms, inspired by the successful application of neural network training in machine translation; such algorithms usually use an encoder-decoder framework. The specific process is as follows: Use an encoder (such as a convolutional neural network CNN) to extract the features of the image, and then use a decoder (such as a recurrent

neural network LSTM) to decode the image features into smooth sentences. At prediction time, each step of the LSTM generates a word until a period is generated. Here, the word predicted at the previous moment and the internal state are input into LSTM, and then LSTM predicts the distribution of words and takes the word with the highest probability as the word at this moment. During training, a supervised method is generally used, so pairs of images and text are required. The input of each moment of LSTM is the word of the correct text at the previous moment, and then the probability of the word of the correct text at this moment is optimized. This is a calculation method of maximum likelihood estimation, which increases the probability of text in the dataset. This model breaks through the confinement of traditional multimodal image understanding and achieves high scores in various evaluation indicators, laying a theoretical guide for today's multimodal image understanding models.

#### 3.2. Theories Related to CT Images

**3.2.1. CT Images and CT Values.** A CT image consists of two parts: the intensity and size of the pixel, where the intensity of the pixel reflects the absorption of X-rays by the organ or tissue, and the size of the pixel reflects the fineness of the image, that is, the spatial resolution of the image [12]. In the process of CT imaging, the measurement accuracy of the X-ray absorption coefficient of organs or tissues can reach 0.5%. Therefore, compared with X-ray images, CT images have higher density resolution. In reality, for the convenience of expression, the CT value is usually used instead of the absorption coefficient to express the degree of X-ray absorption by an organ or tissue.

Figure 2 shows the CT values corresponding to various tissues of the human body. A careful study of the figure shows that the CT value corresponding to the bone is the highest, the CT value corresponding to the air is the lowest, and the CT value of the other tissues of the human body is in between.

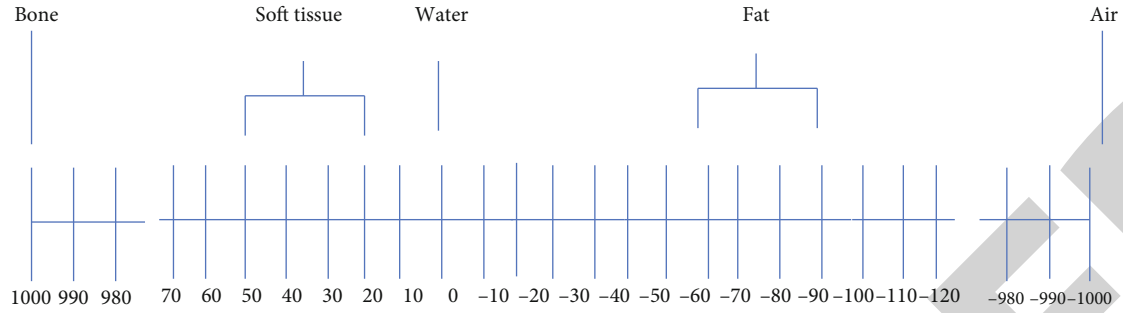


FIGURE 2: CT values corresponding to each tissue in the human body (unit: HU).

3.2.2. *CT Slice*. CT images are three-dimensional images of the human body, and CT images are often observed and analyzed from different directions in practical applications [13]. In human anatomy, the section that cuts the human body into two parts longitudinally along the left and right directions is called the coronal plane. The plane passing through the vertical axis and longitudinal axis of the human body and all parallel planes are called sagittal planes. The surface exposed after cutting the human body perpendicular to the axis of the human body is called the transverse plane.

3.2.3. *Research Characteristics of CT Image Segmentation Methods*. Compared with general images, CT images have the characteristics of anatomical tissue structure and shape complexity, inherent ambiguity of the image, inhomogeneity of grayscale within the tissue, and massive data. Therefore, the research on CT image segmentation methods correspondingly presents the following characteristics: (1) Due to the potential complexity and diversity of CT images and the difficulty of the segmentation problem itself, so far, there is no segmentation method that can be applied to various tasks, and it is usually the right segmentation for a specific task algorithm. Furthermore, due to the limitations of various segmentation methods, people are trying to explore new methods for CT image segmentation and pay more attention to the combination of multiple segmentation methods. (2) Although the obtained CT images exist in the form of two-dimensional slices, with the improvement of computer performance, the research on three-dimensional segmentation methods has received more and more attention; the reason is that the integrity of human organs ensures the continuity of CT images of adjacent slices, so the 3D segmentation method can use more information between slices to guide the segmentation process, making the segmentation results more accurate. (3) Medical images can be divided into anatomical images and functional images according to their functions, the former mainly describes human anatomical information, while the latter mainly describes human function and metabolic information. CT images belong to anatomical images. In the process of CT image segmentation, it has gradually become a new trend to fuse other functional images, such as positron emission tomography images, in order to guide CT image segmentation [14]. (4) Image segmentation algorithms can be divided into three categories according to their degree of automation: automatic, interactive, and manual segmentation [15–17]. Due

to the increasing precision of modern instruments, the volume of CT data is increasing, making manual segmentation almost impossible, and the results of manual segmentation have a lot to do with the experience of the operator; at the same time, the results are not repeatable, which greatly limits its application. Therefore, automatic segmentation is the goal of the segmentation algorithm design process. However, the complexity of the CT image itself makes the current automatic segmentation algorithms have achieved some successes, but they are far from meeting the requirements for the accuracy of the results in the process of clinical practical application. Therefore, user-initiated and user-guided interactive CT image segmentation methods have received more and more attention. The human-machine interactive segmentation method can not only give play to the subjective initiative of people; therefore, the accuracy of the segmentation algorithm is ensured, and the performance of the computer can be fully utilized, thereby ensuring the practicability of the segmentation algorithm

### 3.3. *Multimodal Image Segmentation of Hip CT Based on Adaptive Classification and Normal Direction Correction*

3.3.1. *Image Initial Segmentation*. After preprocessing the hip CT multimodal image, the initial segmentation of the image consists of two steps, the first step is to binarize the image using the global optimal threshold method [18]. Due to the higher density of bone relative to its surrounding soft tissue, bone has a higher intensity than the surrounding soft tissue in CT multimodal images. The threshold method is often used as the preferred method for rough bone segmentation due to its simple operation and high algorithm execution efficiency [19]. In the binarized image, the approximate area of the bone has been segmented, but due to the nonuniformity of bone density and the existence of lesions in the bone, the threshold method often causes holes in the bone in the binarized image, and bone boundaries produce discontinuities. In view of the above problems, in the second step, the 3D mathematical morphology method is used to fill the holes and connect the boundaries of the binarized images.

3.3.2. *Histogram-Based Thresholding*. The segmentation of the hip joint is achieved using a multistep method, and the basic steps are to first perform an initial segmentation of the CT multimodal images; then we use this segmentation

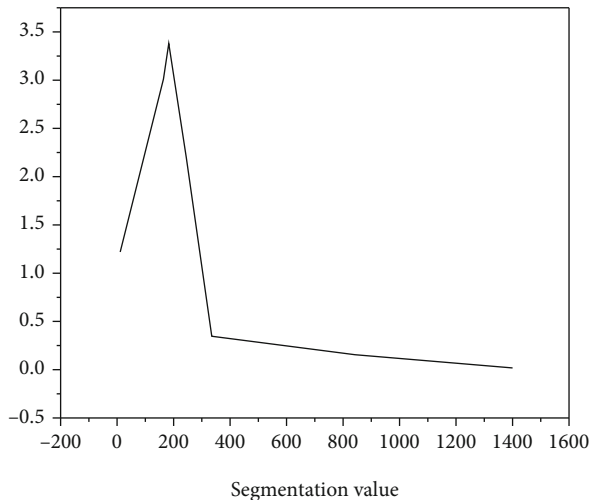


FIGURE 3: Threshold selection based on histogram.

result to initialize the iterative adaptive segmentation algorithm to achieve complete separation of bone and nonbone tissue and finally use the normal direction correction algorithm to achieve accurate positioning of the bone boundary.

There are many methods for initial segmentation of bone, such as threshold method, serpentine method, region growth method, watershed segmentation method, etc. Compared with other segmentation methods, threshold segmentation method is one of the most commonly used bone CT image segmentation methods, the reason is that in CT multimodal images, the bone tissue generally has a higher density than the surrounding soft tissue, and the threshold method can be used to achieve a simple and fast segmentation of the bone, then realizing the fast initialization of the iterative adaptive classification process; thereby, the execution efficiency of the whole algorithm is improved; due to the large amount of computation, the efficiency of other methods is much lower than that of threshold segmentation [20].

The advantage of threshold segmentation is that it is simple and fast. When the gray value of objects belonging to different types or their eigenvalues are very different, it can effectively segment the objects. The thresholding segmentation method mainly includes two steps:

- (1) Determine the required segmentation threshold
- (2) Compare the segmentation threshold with the voxel gray value to divide the voxels

In the above steps, determining the threshold is the key to segmentation. When using the threshold method to segment a grayscale image, there are generally certain assumptions about the image. In other words, it is based on a certain image model, for example, it is assumed that the gray distribution of different categories in the image conforms to the Gaussian distribution. Specifically applied to the CT multimodal image of the hip joint, considering that the bone has a significantly higher intensity than other soft tissues, and the internal intensity of the soft tissue does not change

much, the gray histogram of the hip joint can basically be regarded as composed of a mixture of two unimodal histograms corresponding to bone tissue and soft tissue.

For the grayscale histogram composed of the mixture of two unimodal histograms, the author determines the initial segmentation threshold according to the Otsu algorithm. The basic idea of Otsu algorithm is to find a threshold; this threshold maximizes the between-class variance and, at the same time, minimizes the within-class variance. According to the theory of discriminant analysis, such a threshold is the optimal segmentation threshold.

The specific steps for determining the optimal threshold are as follows: Firstly, calculate the grayscale histogram of the region of interest (ROI) of the hip joint. Since the CT value of soft tissue is smaller than that of bone tissue and the number of soft tissue voxels in the ROI accounts for a larger proportion, therefore, it can be judged from the histogram that high peaks correspond to soft tissue types, and low peaks correspond to bone tissue types. In this chapter, it is assumed that both soft tissue and bone tissue obey the Gaussian distribution. During the calculation of the optimal threshold, two Gaussian curves are used to fit the histogram curve; it can be known that the gray value corresponding to the intersection of the two Gaussian curves is the optimal segmentation threshold, as shown in Figure 3.

**3.3.3. Binary Image Morphological Operations.** In the binary image obtained by the above thresholding method, there are often holes in the bone tissue, discontinuity at the edge of the bone, and wrong connection between the bones. These phenomena are due to the nonuniformity of bone tissue density, the weak edge nature of bone, and the partial volume effect during CT multimodal imaging. In order to roughly obtain the bone tissue area for subsequent accurate edge segmentation, the author uses mathematical morphology to fill the “holes” in the obtained binary image. In general, the choice of structural elements (size and shape) affects the results of morphological operations. Commonly used structuring element shapes are sphere, cube, and rhombus. In order to minimize bone-to-bone misconnections due to morphological methods, the authors took  $3 \times 3 \times 3$  diamond-shaped structural elements.

#### 3.3.4. Iterative Reclassification Algorithm Computation

(1) *Calculate the Bone Boundaries from the Current Segmentation.* For a given voxel, if its directly connected neighbor voxels can be divided into two different classes, the voxel is located at the edge of the bone area  $B$  or the nonbone area  $\bar{B}$ . In order to calculate the voxels of the bone edge, a six-voxel neighborhood structure is first defined, and the voxel set of the spine edge in this chapter is  $E$ . Specifically, for each voxel  $x$  in  $B$ , if any one of its six neighboring voxels belongs to  $\bar{B}$ , then the voxel belongs to the set  $E_B$ . For the convenience of the following description, the authors here specifically label voxels  $x$  belonging to set  $E_B$  as  $x^*$ .

**3.3.5. Reclassification of Bone Boundary Regions Based on Bayesian Decision Criteria.** For each bounding voxel  $x$ , first define a window  $W(x^*)$  centered on the position of  $x$ . All



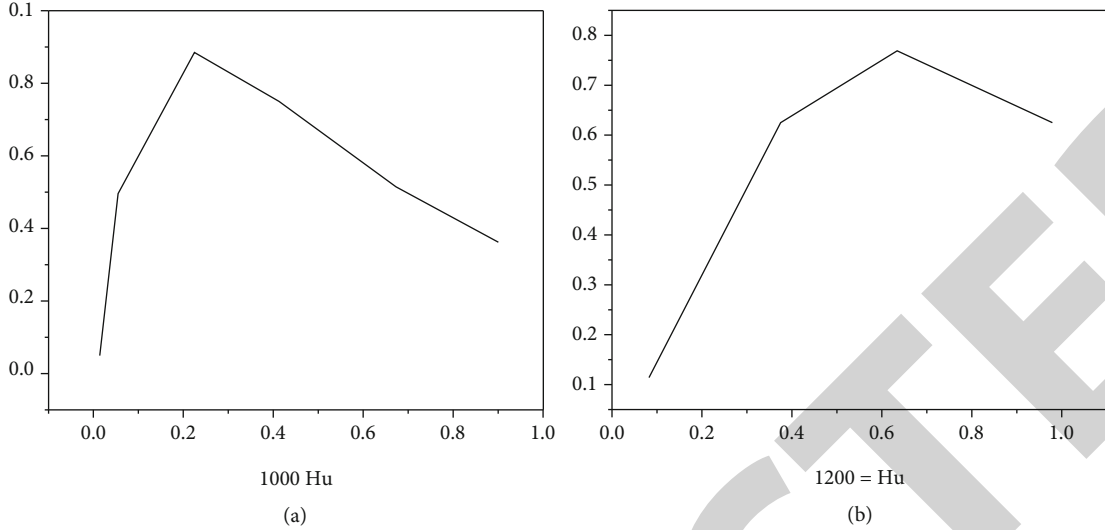


FIGURE 4: (a, b) show the values of  $p(a^x|y_x)$  under different intensities.  $p(a^x|y_x)$  values at different intensities.

voxels in  $W(x^*)$  are assumed to be derived from two Gaussian distributions (bone region  $B$  and nonbone Region  $\bar{B}$ ) with mean and standard deviation  $(\mu_1, \sigma_1)$  and  $(\mu_2, \sigma_2)$ , respectively. For convenience, note  $\varphi_1=(\mu_1, \sigma_1)$ ,  $\varphi_2=(\mu_2, \sigma_2)$ . The estimation method of parameters  $\varphi_1, \varphi_2$  will be discussed in detail later Figure 4.

According to Bayes' theorem, for a given voxel  $x$ , the proportion of bone components in the voxel can be calculated by the following formula:

$$p(a^x|y_x) = \frac{p(y_x|a^x)p(a^x)}{p(y_x)}. \quad (1)$$

**3.3.6. Update the Current Segmentation Result.** After each voxel in  $E_B$  has been traversed, the new bone area  $B$  and nonbone area  $\bar{B}$  are obtained again by using the three-dimensional mathematical morphology method. After the new bone and nonbone areas are obtained, the boundary voxel set  $E_B$  will be recalculated. If the voxels in  $E_B$  do not change during the two iterations before and after, the iteration process will be stopped. Otherwise, turn to the first step to recalculate the bone boundary voxels and perform the entire iterative process until convergence.

## 4. Results and Discussion

The authors conducted a retrospective analysis of the experimental results. In this experiment, 55 sets of CT multimodal data images were collected, including a total of 110 hip joints. The experimental data comes from a GE Pro Speed CT machine, the slice plane resolution is  $512 \times 512$ , the in-plane pixel pitch is 0.68 mm, the distance between slices is 1.5 mm, and the number of slices is 85 to 95. The experimental environment is MATLAB6.5, 2.33 GHz processor, 2 GB memory. Among the 110 hip joints, data ranging from normal to severe lesions were included. Manual segmentation results of all data were given by radiologists.

TABLE 1: Comparison results of three methods in 110 hip joint data segmentation time.

	Zoroofi's method	Yokota's method	Our method
Total (h)	12.9	18.5	10.9
Average time (s)	9.5	13.6	8

In order to verify the applicability of the proposed method, the authors based on anatomical and imaging features (e.g., the proximity of the femoral head to the acetabulum, the degree of deformity of the femoral head, and the degree of inhomogeneity of bone density); the obtained 110 hip joints were divided into four groups, and the numbers of the four groups were 16, 31, 51, and 12, respectively. Further research can be found that this method belongs to the model-based segmentation method; in the segmentation process, the shape information of the object to be segmented is added as a priori constraint knowledge; therefore, the segmentation method is more robust for hip joints with severe lesions. Table 1 shows the comparison results of this method and the other two methods in terms of segmentation time.

It can be seen that the author's method takes a total of 10.9 hours, and the average time is 8 seconds, which is much shorter than the other two methods, indicating that the author's method has great advantages in the field of image segmentation. Therefore, the injuries caused by long-distance running can be better treated.

## 5. Conclusion

The author proposes a method for rehabilitation monitoring of long-distance running injuries based on CT multimodal images. This method integrates multimodality technology into CT images. By medically cutting CT multimodal images and analyzing them; finally, the treatment of injuries caused by long-distance running can be achieved. Experimental results show that the method used by the author took a total

## *Retraction*

# **Retracted: Visual Dissemination of Intangible Cultural Heritage Information Based on 3D Scanning and Virtual Reality Technology**

### **Scanning**

Received 26 September 2023; Accepted 26 September 2023; Published 27 September 2023

Copyright © 2023 Scanning. This is an open access article distributed under the Creative Commons Attribution License, which permits unrestricted use, distribution, and reproduction in any medium, provided the original work is properly cited.

This article has been retracted by Hindawi following an investigation undertaken by the publisher [1]. This investigation has uncovered evidence of one or more of the following indicators of systematic manipulation of the publication process:

- (1) Discrepancies in scope
- (2) Discrepancies in the description of the research reported
- (3) Discrepancies between the availability of data and the research described
- (4) Inappropriate citations
- (5) Incoherent, meaningless and/or irrelevant content included in the article
- (6) Peer-review manipulation

The presence of these indicators undermines our confidence in the integrity of the article's content and we cannot, therefore, vouch for its reliability. Please note that this notice is intended solely to alert readers that the content of this article is unreliable. We have not investigated whether authors were aware of or involved in the systematic manipulation of the publication process.

Wiley and Hindawi regrets that the usual quality checks did not identify these issues before publication and have since put additional measures in place to safeguard research integrity.

We wish to credit our own Research Integrity and Research Publishing teams and anonymous and named external researchers and research integrity experts for contributing to this investigation.

The corresponding author, as the representative of all authors, has been given the opportunity to register their agreement or disagreement to this retraction. We have kept a record of any response received.

### **References**

- [1] W. Xu, X. Sun, and S. Pan, "Visual Dissemination of Intangible Cultural Heritage Information Based on 3D Scanning and Virtual Reality Technology," *Scanning*, vol. 2022, Article ID 8762504, 7 pages, 2022.

## Research Article

# Visual Dissemination of Intangible Cultural Heritage Information Based on 3D Scanning and Virtual Reality Technology

Wulong Xu , Xijie Sun , and Shihui Pan 

School of Journalism and Communication, Huanggang Normal University, Huanggang, Hubei 438000, China

Correspondence should be addressed to Shihui Pan; 0107045@yzpc.edu.cn

Received 1 August 2022; Revised 4 September 2022; Accepted 10 September 2022; Published 25 September 2022

Academic Editor: Balakrishnan Nagaraj

Copyright © 2022 Wulong Xu et al. This is an open access article distributed under the Creative Commons Attribution License, which permits unrestricted use, distribution, and reproduction in any medium, provided the original work is properly cited.

In order to meet the needs of modern people for the acquisition of intangible cultural heritage information, the authors propose a research method that combines 3D scanning and virtual reality technology. Taking the production process of Xiuyu as an example, using Unity3D virtual reality technology combined with a digital platform, 3D modeling of Xiuyu is carried out, so that people can view the intangible cultural heritage information intuitively. The experimental results show that after using this method, more than 60% of more than 1000 people surveyed in the questionnaire want to experience intangible cultural heritage. In a survey of visualization platforms conducted at the same time, 90% of users are willing to combine jade carving technology with 3D scanning virtual reality technology. *Conclusion.* 3D scanning and virtual reality technology can further promote the process of inheritance and dissemination of intangible cultural heritage, accelerate the cultivation of intangible cultural heritage talents through the visualization platform, and promote the sustainable development of intangible cultural heritage, in order to better pass down the life memory and cultural genes of our ancient nation.

## 1. Introduction

With the changes in production and lifestyle in modern society, the living soil of intangible cultural heritage has undergone major changes and is now facing a rapid decline. The data shows that there are currently 1082 representative inheritors of intangible cultural heritage in my country, with an average age of 63 years, and only 7 young adults under the age of 40 inheritors, as shown in Figure 1. It can be seen that the national intangible cultural heritage has been aging; if the inheritance of intangible cultural heritage is weak, then some handicrafts inherited by word of mouth and behavior will gradually be forgotten by people; the traditional skills mastered by the old artists will not be inherited and practiced, and the national intangible cultural heritage culture will eventually disintegrate or even die out.

Therefore, innovative exploration of the inheritance and dissemination of intangible cultural heritage can make intangible cultural heritage play a more important role in national development, international social exchanges, and

sustainable social development; this will further enhance the cultural self-confidence of the nation. Using the visualization platform as the communication medium, explore the feasibility and necessity of the application of digital technology in the inheritance and dissemination of intangible cultural heritage. Using virtual reality technology for “real” reproduction of intangible cultural heritage jade craftsmanship allows users to immensely experience traditional technological processes and processing methods and explore other new modes of inheritance and dissemination of intangible cultural heritage from point to point.

Changes in the media environment and the popularity of new communication methods have led to changes in information transmission methods. Information transmission has shifted from the era of writing to the era of reading pictures, and traditional media have shown obvious disadvantages in the protection and dissemination of intangible cultural heritage. Information visualization not only gives people a new experience but also makes people more pleasant and more engaged and allows viewers to gain insight

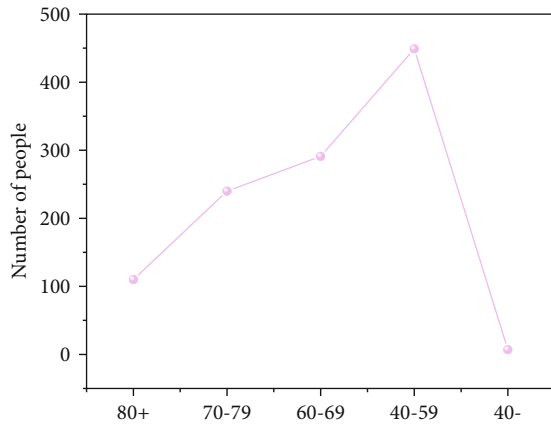


FIGURE 1: Age distribution of the fifth batch of national nongenetic inheritors.

into more information. At the same time, it can provide protection for the inheritance and dissemination of intangible cultural heritage and make the inheritance of intangible cultural heritage more artistic, communicative, and educational [1].

In this big environment, it is still very difficult to efficiently find, understand, and analyze information connections [2]. Visualization can transform obscure and complicated information content into simple and easy-to-read information graphics through visual methods, which greatly improves the efficiency of information acquisition. In the era of global diversification and informatization, it is a very effective and practical way to use digital technology to protect and inherit national intangible cultural heritage [3].

## 2. Literature Review

Conrad et al.'s book series "Virtual Reality Basic Course" proposes that dynamic environment modeling will become a bridge between the real environment and the virtual environment [4]. Integrate decentralized virtual reality systems to build a new virtual system that matches each other in time and space, which is convenient for participants to use and experience. Toktas and O'Neal in the journal *The Application of Virtual Reality Technology in the Protection and Inheritance of Intangible Cultural Heritage* proposed that intangible cultural heritage culture is inherited between families, teachers and apprentices, and ethnic groups, the communication method is very limited, and the use of virtual reality technology is in line with the development of the times and can attract more young people to experience and learn intangible cultural heritage [5]. Yang et al. in the "Research Review of the Application of Virtual Reality Technology in Tourism Abroad" proposed to use virtual reality technology to revive it and reproduce a certain place's heyday society through virtual images [6]. Zi-Jun et al. used 3D scanning and modeling technology to store and apply traditional Chinese medicine knowledge for the first time in "Research and Application of Acupuncture Tongren 3D Visualization" and developed acupuncture Tongren interac-

tive system, which realized TCM visual interactive query of acupoints, meridians, and common diseases [7]. The team led by Lei et al. solved the problems of functional module analysis, model establishment, scene import, and sky box addition of the scenic 3D roaming system and established a 3D interactive roaming system for scenic spots [8]. Yuan et al. used AutoCAD, 3dsmax, Photoshop, and other software to design the virtual hometown scene and finally realized the human-computer interaction functions such as season selection, scene roaming, and information interaction in Unity3D [9]. Aokage et al. pointed out in the analysis of the network influence factor (WIF) that the internal links of websites are often centered on navigation; if a website is large in scale, the number of internal links will increase accordingly, and the importance of the website cannot be judged [10]. Therefore, they adjusted the network impact factor (WIF): if the target "A" is at a specified time, after excluding the number of pages of "A" itself, the number of web pages linked to a website or a certain area on the Internet, if  $Z$  is used to represent, that is,  $Z$  is the number of external links, and the number of web pages of this website or area is expressed as  $y$ , then the network impact factor of "A" is  $WIF = z/y$ .

On the basis of current research, the author proposes a variety of research methods, such as literature reading, actual historical research, case study, and practical research, combined with Xiuyu craftsmanship. Using the method of interdisciplinary research, the author uses computer science, pedagogy, human-computer interaction technology, and simulation technology to conduct cross-disciplinary research and organically combines his research theories for the study of this topic. Using the historical research method, the origin of nonhereditary inheritance is explored in detail, and the longitudinal time comparison of inheritance is carried out. By using the case study method, by comparing the domestic and foreign intangible cultural heritage measures, the method and methods of virtual reality applied to the inheritance and dissemination of intangible cultural heritage are investigated. Using the experimental research method, the theoretical guidance of the paper is used as the support point of practice, and case design is carried out to disprove the validity of the theoretical research content. The author fully integrates theoretical research into specific practice and plays a directional guiding role; the practice process and results are summarized and refined to further improve the theory; this method of combining theory and practice makes virtual reality more systematic and scientific in the research of interaction design platforms.

## 3. Methods

### 3.1. Visual Content

**3.1.1. Visual Content and Direction Sorting.** Intangible cultural heritage has multiple attributes, including temporal attributes (such as birth year and approval year), spatial attributes (such as birthplace and place of circulation), relationship attributes (including inheritance), hierarchical attributes, people-related attributes, and multidimensional

synthesis attributes (such as spatiotemporal multidimensional attributes); it is suitable for visualization by combining time-based visualization methods (such as time series diagrams and calendar diagrams), geographic information-based visualization methods (such as GIS), hierarchical information visualization, and multidimensional visualization methods in the visualization discipline [11]. In order to dig out the feasible visualization direction and content, in-depth interviews were conducted with experts in the field of intangible cultural heritage and visualization, and the following research directions were summarized: (1) Time sequence diagram of the development of intangible cultural heritage: it reflects the evolution of the whole or part of the intangible cultural heritage list at different time stages in chronological order and can clearly see the production sequence and evolution law of intangible cultural heritage. (2) Intangible cultural heritage heat map: describe the intangible cultural heritage items, perform keyword search, get the search popularity according to the search results, and determine the heat value according to color, size, orientation, etc. (3) Intangible cultural heritage relationship diagram: describe the relationship between the intangible cultural heritage items and use the relationship between different nodes to represent the relationship between the intangible cultural heritage items, such as derivative relationship and joint relationship. (4) Intangible cultural heritage and region: the classic mode in the visualization map, which combines intangible cultural heritage attributes with space, describes the overall information of intangible cultural heritage in space and grasps the geographical location of intangible cultural heritage through the map. (5) Nongenetic inheritance relationship diagram: use the relationship between nodes and nodes in the relationship diagram to describe the relationship between the inheritors; the relationship line can be undirected or directional, such as the relationship between master and apprentice, father and son, and brother and sister. (6) Detailed introduction map of key intangible cultural heritage: decompose and reconstruct a single intangible cultural heritage item, interpret key and hot items in detail, and use interesting forms or storylines to express the data readability.

*3.1.2. Create a Metadata Database.* Refer to the formulation standards of international metadata databases, such as CDWA, a database of artworks and digital image resources, and VRA, a database of art and folk culture, in order to determine the attributes of the intangible cultural heritage metadata database. The intangible cultural heritage database attributes are determined as general attributes and core attributes [12]. The core attributes include the basic information of intangible cultural heritage such as name, type, batch, and application area. The general attributes include more than 30 items such as inheritance method, distribution, subject matter, derivation, and origin; for example, the Softmax classifier is based on the Softmax classifier connection, the deep convolutional neural network can classify and process specific target objects, and based on the classification to fully popularize the logistic regression model, the Softmax regression is obtained [13]. The labeled  $m$  samples constitute the

logistic regression training set. In formula  $\{(x^{(1)}, y^{(1)}), \dots, (x^{(m)}, y^{(m)})\}$ ,  $x^{(i)} \in R^{n+1}$  is the input feature.  $n+1$  is the  $x$  dimension of the feature vector, and  $x_0 = 1$  corresponds to the intercept term. Because binary classification is the goal of logistic regression, there is  $y^{(i)} \in \{0, 1\}$ . If the following functions exist,

$$h_{\theta} = \frac{1}{1 + \exp(-\theta^T x)} \quad (1)$$

Train the model parameters, which are essentially functions that allow it to minimize the loss:

$$J(\theta) = -\frac{1}{m} \left[ \sum_{i=1}^m y^{(i)} \log h_{\theta}(x^{(i)}) + (1 - y^{(i)}) \log (1 - h_{\theta}(x^{(i)})) \right] \quad (2)$$

The number of  $y$  (category labels) values is different  $k$ , mainly because it is a multiclassification problem that needs to be dealt with. So, for  $\{(x^{(1)}, y^{(1)}), \dots, (x^{(m)}, y^{(m)})\}$ , there are  $(i) \in \{1, 2, \dots, k\}$  class labels, and for a sample input (given)  $X$ , the probability  $p(y = i|x)$  of each classification result can be represented by a  $k$ -dimensional vector output.

*3.2. Implementation of Virtual Reality Technology in Xiuyu Craftsmanship.* The conventional methods of acquiring images are usually cameras, video cameras, scanners, etc. What these means only acquire is the two-dimensional image of the scanned object, that is, the two-dimensional plane information of the outline of a single side. At present, more and more 3D scanning technologies have replaced the previous scanning methods, made up for the shortcomings of 2D scanning in spatial data, and can accurately reflect the data information of entities in real space [14]. A 3D scanner is a scientific instrument used to detect and analyze the shape (geometric structure) and appearance data (such as color and surface albedo) of an object. It can accurately obtain the three-dimensional coordinates and three-dimensional digital model of the outer surface of the object in space. 3D scanning technology has now developed into the fourth generation of handheld scanning technology [15]. For the collection of the original model of the jade, the complete data of the jade can be obtained by using a handheld laser scanner. It has the characteristics of precision, efficiency, flexibility, and ease of use. The scanner and the computer update the recorded data in real time through the data interface, which provides a basic guarantee for the further processing of jade.

The virtual reality design includes five parts: designing, cutting, carving, polishing, and outputting the scanned jade model. First, analyze the scanned jade from multiple angles, design the model through two-dimensional graphics software, use convenient tools such as copying and mirroring to assist in the drawing of drawings, repeatedly adjust the matching degree between the graphics and the jade, then use the MAYA cutting tool to cut the jade, use various brushes in ZBrush to carve the jade model in detail, and

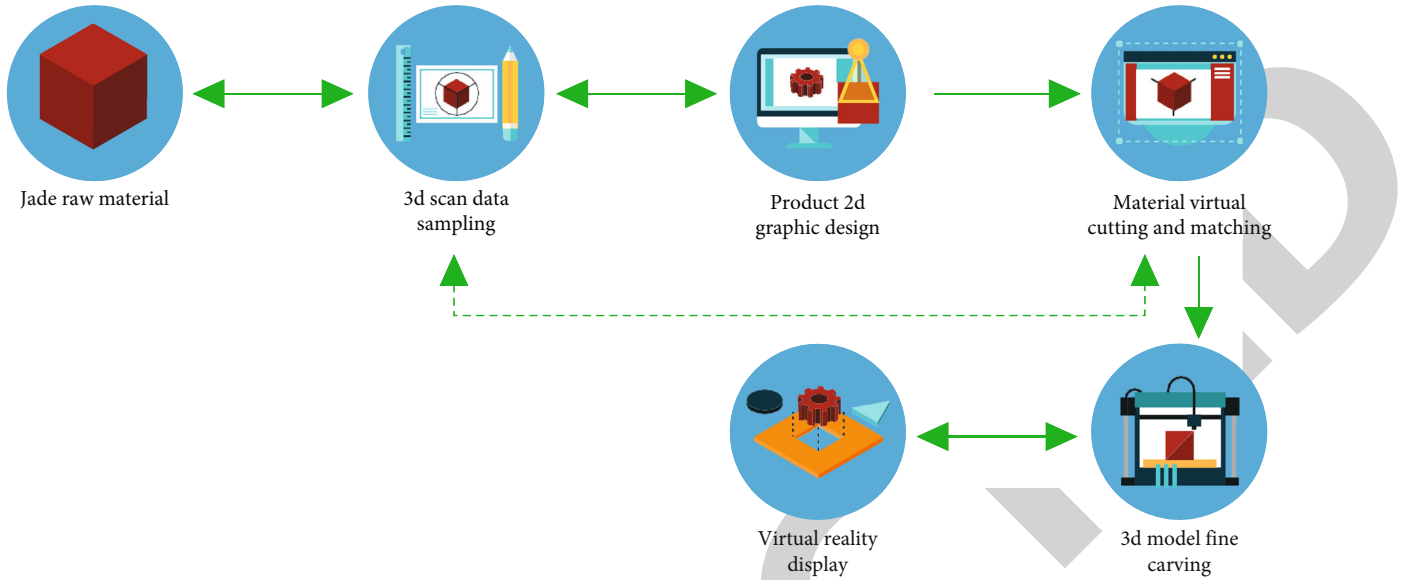


FIGURE 2: Implementation step diagram.

increase the subdivision level to achieve the effect of polishing. Finally, the prepared model is imported into Unity3D, and the human-computer interaction interface for editing operations such as displacement, rotation, and scaling is further set up [16].

In the jade processing process, virtual technology is used to carry out specific operations such as design, simulation, modeling, and interaction, and the product modeling, cost, process, and other aspects are simulated in advance; it not only brings predictability to jade processing but also adds more artistic creativity. The virtual reality design model has absolute advantages; especially for jade processing with excellent raw materials, virtual reality technology is particularly important. It has fundamentally changed the characteristics of the traditional production mode, such as being complex, repetitive, and closed. Taking the interactive 3D model in virtual design as the carrier, the design concept and processing process of the craft master are conveyed in a more intuitive way, so that the designer can repeatedly speculate and analyze the beautiful appearance, reasonable structure, and processing technology. Customers can deeply appreciate the value of Xiuyu craftsmanship through immersive viewing. Engraving students can practice the jade carving craftsmanship through virtual reality. As a result, Xiuyan jade carving can be maximized in the fields of creation, processing, production, sales, and training.

**3.3. Xiuyu Process Flow Based on Virtual Reality Technology.** The specific steps of introducing virtual reality technology in Xiuyu processing are shown in Figure 2.

**3.3.1. 3D Scan Data Sampling.** The image of jade material is converted into a format that can be read, stored, and edited by the computer through 3D scanning. The data sampling is to reproduce the jade material by means of cloud points, so that the outline features of the jade material are virtualized. The cloud point collection can directly generate the block

TABLE 1: Digital collection content.

Collection object	Collect content
Design patterns	Pattern, animal pattern, plant pattern, figure pattern, plain pattern
Machining tools	Jade carving flat knitting machine, jade carving electronic pen, saw blade, grinding head, grinding needle, drill bit
Jade scan	Hemo jade, lao jade, new mountain jade, hua jade, jia cui

surface structure, section line, etc., of the jade material, which makes the 3D model construction more accurate and convenient, and quickly switches the entity to the computerized digital management mode.

**3.3.2. Product Two-Dimensional Graphic Design.** Based on three-dimensional scanning, the computer converts the jade in the virtual space into digital graphics and obtains the drawing object of the two-dimensional graphics, so that the design can be targeted. The two-dimensional editing software adopts another digital expression of the outline image of the design graphics; in the two-dimensional design software, the design image is drawn on the two-dimensional coordinate position of the model through the pressure-sensitive pen of the hand-painted board, so as to maximize the use of the whole piece of jade; the material is used for creation; finally, the two-dimensional visual expression graphic information is presented on the computer [17].

**3.3.3. Virtual Cutting and Matching of Raw Materials.** To map the 2D design image to the main view in the 3D software, in order to avoid stretching after mapping, it is necessary to unfold the UV lines of the jade model in the 3D software in advance. Cut and extrude the model according to the line draft on the stone and further stretch, rotate, zoom, and other three-dimensional algorithms to control

TABLE 2: Judgment matrix and weight of first-level indicators in the evaluation system of intangible cultural heritage websites.

	C1	C2	C3	C4	C5	$W_i$ (权重)
C1	1.000	1.369	2.191	3.509	5.618	0.377
C2	0.731	1.000	1.601	2.563	4.105	0.276
C3	0.456	0.625	1.000	1.601	2.564	0.172
C4	0.285	0.390	0.625	1.000	1.601	0.108
C5	0.178	0.244	0.390	0.625	1.000	0.067
Consistency ratio: 0.000			Largest characteristic root: 5.000			

the point, line, and surface of the model in three views, symmetrical objects are mirrored and replicated, and finally, a three-dimensional digital display of the jade model in the design drawings is constructed. When operating, it is necessary to combine both the two-dimensional design drawings and the three-dimensional scanning data and constantly try and modify in the most reasonable interactive way to achieve the final effect [18].

**3.3.4. 3D Model Carving.** After completing the above steps, the computer has stored the basic model parameters of the jade product, but the model at this time is a rough model designed according to the drawings, and the relief and texture in the jade need to be further refined [19]. In the engraving software ZBrush, the rich engraving brushes are used to simulate the effect of various drill bits in the Xiuyu process for processing jade. After the model is made, the subdivision level is increased to achieve the effect of polishing.

**3.3.5. Virtual Reality Display.** Import the produced jade model into Unity3D for an all-round virtual immersive display.

#### 3.4. Digital Data Collection and Digital Model Establishment

**3.4.1. Digital Data Collection.** In order to obtain more detailed information on Xiuyu, the author went deep into the local area of Xiuyan, conducted a field investigation on the processing technology, and collected relevant information. The main contents include the following: the processing design patterns of Xiuyu are collected, the traditional Xiuyu processing tools are collected, and the digital model of jade is scanned and collected [20]. After the inspection, the materials such as pictures and patterns are further classified, screened and processed, and turned into digital material files required for virtual reality design. The contents of digital collection are shown in Table 1.

**3.4.2. Digital Pattern Processing.** The evolution of Xiuyu design has evolved from simple patterns in primitive society to rough patterns in slave society, then to exquisite patterns of flowers, birds, fish, insects, birds, and animals and auspicious patterns in feudal society, all of which embody the unique aesthetics of each period. In the interactive design, the platform will provide users with traditional Chinese jade carving patterns and the shapes of Xiuyu plain furnaces, bottles, tripods, and smokes [21]. The collected pictures are

processed into outline graphics by the vector software CorelDRAW, which makes the designer's material calling and reference more concise and intuitive.

In the Unity3D engine, the texture space coordinates of the collision point can be ray-detected by using RaycastHit.textureCoord. When users pick brushes or other tools through the VR handle, they can modify the texture space through the ray collision points in the virtual space. Similar to drawing operations, many intersections and UV coordinates of the model's normal map are generated every second. We can modify the bump on the jade surface by fusing the normal map. The original model after jade scanning itself has a flat normal map, and we constantly operate to superimpose the normal map of the engraving point to appear scratches and patterns [22].

## 4. Experimental Results and Analysis

The judgment matrix of the evaluation indicators of the intangible cultural heritage website and the weight and consistency test of each indicator are as follows; after three rounds of expert survey and scoring, the full frequency of the first-level indicators is information content (C1) 100%, website design (C2) 85.71%, website function (C3) 64.29%, website influence (C4) 42.86%, and website security (C5) 21.43%. Based on this, the judgment matrix is constructed and the relative weight is calculated, as shown in Table 2.

According to a big data survey of intangible cultural heritage culture, most users prefer to understand intangible cultural heritage culture through "experience" and feel that personal experience is more intuitive and interesting, as shown in Figure 3. This provides a broad market prospect for virtual intangible cultural heritage experience [23].

The dissemination of intangible cultural heritage information through virtual reality technology through questionnaires enables more people to experience intangible cultural heritage culture; the questionnaire survey shows that more than 60% of more than 1000 people experience intangible cultural heritage culture.

At the same time, a total of 30 users were selected to test the visualization platform; the target audience includes three types of groups: heritage artists, factory apprentices, and college students; the research includes four factors, namely, the interactive performance of the visualization platform, system speed, module experience accuracy, and professionalism technical acquaintance, as shown in Table 3. The test results show that 90% of users are willing to combine jade carving

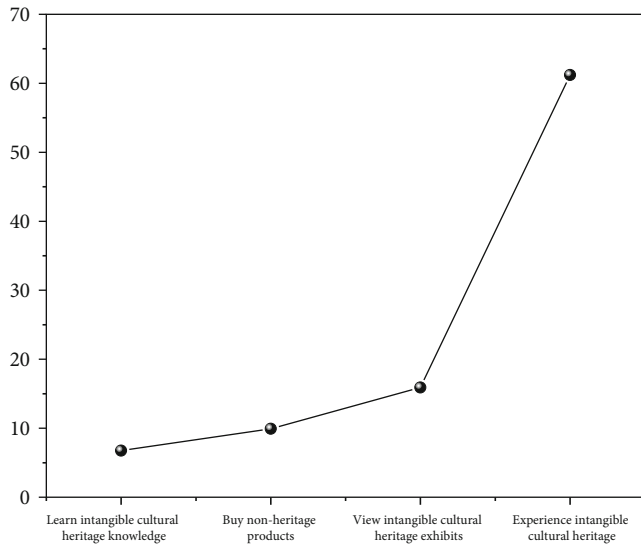


FIGURE 3: Proportion of participation in intangible cultural heritage.

TABLE 3: Experience evaluation of the engraving part of the platform.

Test number	Test items	The proportion
1	Most concerned about the platform engraving part	95%
2	Satisfaction with the engraving part	72%
3	Degree of expectation after modification	85%

technology with 3D scanning virtual reality technology, and only 15% of the test users have some understanding of virtual technology and 3D scanning technology; it shows that there are few practical cases of 3D scanning virtual technology combined with manual skills, which also increases the difficulty of promoting the visualization platform; in the later stage, it is necessary to further improve the operation performance of the system, reduce the technical difficulty of visualization, and increase the matching degree of technology [24, 25].

## 5. Conclusion

In general, 3D scanning and virtual reality technology have spawned a new concept of subversive visual communication, challenged the traditional static visual communication form, and attracted people's attention and recognition with a more flexible and dynamic form of expression. The research on the visualized Xiuyu platform realizes the function of combining technology and inheritance, breaks the single inheritance mode of traditional skills, and makes the dissemination of traditional skills more efficient. Display and disseminate intangible cultural heritage through digital media and digital platforms and further realize the cultural inheritance of intangible cultural heritage in the digital space. With the rapid

development of science and technology, virtual reality technology will definitely become an important way for the inheritance and dissemination of my country's intangible cultural heritage. Due to its digital and virtual nature, it has broken through many limitations in the way of protection and solved the singleness and limitations of traditional intangible cultural heritage protection methods. The intangible cultural heritage graphic database, intangible cultural heritage model database, intangible cultural heritage digital aided design, intangible cultural heritage virtual technology innovation process, etc., will definitely make more contributions to the inheritance and dissemination of intangible cultural heritage in my country.

## Data Availability

The data used to support the findings of this study are available from the corresponding author upon request.

## Conflicts of Interest

The authors declare that they have no conflicts of interest.

## Acknowledgments

This study is funded by the General project of Philosophy and Social Science research of Hubei Provincial Department of Education in 2021 "Research on the All-media Communication of Folk Embroidery art in Eastern Hubei under the Background of Rural Revitalization," Project No.: 21Y231.

## References

- [1] A. Behan, "The historiography of the twentieth-century classical performer: life, work, artistry," *Twentieth Century Music*, vol. 18, no. 2, pp. 161–184, 2021.
- [2] T. Hosoya, Y. Yamanashi, and N. Yoshikawa, "Compact superconducting lookup table composed of two-dimensional memory cell array reconfigured by external dc control currents," *IEEE Transactions on Applied Superconductivity*, vol. 31, no. 3, pp. 1–6, 2021.
- [3] J. Tang, "Dimensional modeling method discussion for the profits from mineral rights transfer management," *Modern Economics & Management Forum*, vol. 3, no. 2, pp. 81–88, 2022.
- [4] R. Conrad, T. Ruth, F. Lffler, S. Hadlak, and K. Narayan, "Efficient skeleton editing in a VR environment facilitates accurate modeling of highly branched mitochondria," *Microscopy and Microanalysis*, vol. 26, no. S2, pp. 1158–1161, 2020.
- [5] S. Toktas and M. L. O'Neil, "How do women receive inheritance? The processes of Turkish women's inclusion and exclusion from property," *The Journal of Asian Women*, vol. 29, no. 4, pp. 25–50, 2020.
- [6] Y. G. Yang, B. P. Wang, S. K. Pei, Y. H. Zhou, W. M. Shi, and X. Liao, "Using m-ary decomposition and virtual bits for visually meaningful image encryption," *Information Sciences*, vol. 580, no. 4, pp. 174–201, 2021.
- [7] S.-K. Yao, Y. Li, Z.-J. Jia et al., "A systematic review and meta-analysis of randomized controlled trials on treating ulcerative colitis by the integration method of heat-clearing, damp-excreting, spleen-strengthening, and stasis-removing of



## *Retraction*

# **Retracted: MRI View of Rehabilitation Methods to Relieve Anterior Cruciate Ligament Injury in Dancers**

### **Scanning**

Received 5 December 2023; Accepted 5 December 2023; Published 6 December 2023

Copyright © 2023 Scanning. This is an open access article distributed under the Creative Commons Attribution License, which permits unrestricted use, distribution, and reproduction in any medium, provided the original work is properly cited.

This article has been retracted by Hindawi, as publisher, following an investigation undertaken by the publisher [1]. This investigation has uncovered evidence of systematic manipulation of the publication and peer-review process. We cannot, therefore, vouch for the reliability or integrity of this article.

Please note that this notice is intended solely to alert readers that the peer-review process of this article has been compromised.

Wiley and Hindawi regret that the usual quality checks did not identify these issues before publication and have since put additional measures in place to safeguard research integrity.

We wish to credit our Research Integrity and Research Publishing teams and anonymous and named external researchers and research integrity experts for contributing to this investigation.

The corresponding author, as the representative of all authors, has been given the opportunity to register their agreement or disagreement to this retraction. We have kept a record of any response received.

### **References**

- [1] P. Yang, "MRI View of Rehabilitation Methods to Relieve Anterior Cruciate Ligament Injury in Dancers," *Scanning*, vol. 2022, Article ID 1544440, 7 pages, 2022.

## Research Article

# MRI View of Rehabilitation Methods to Relieve Anterior Cruciate Ligament Injury in Dancers

Pin Yang 

Hunan Institute of Engineering, Xiangtan, Hunan 411104, China

Correspondence should be addressed to Pin Yang; 20152800073@m.scnu.edu.cn

Received 25 July 2022; Revised 20 August 2022; Accepted 1 September 2022; Published 14 September 2022

Academic Editor: Balakrishnan Nagaraj

Copyright © 2022 Pin Yang. This is an open access article distributed under the Creative Commons Attribution License, which permits unrestricted use, distribution, and reproduction in any medium, provided the original work is properly cited.

In order to solve the problem of the difference in the diagnostic effect of different sequences of magnetic resonance imaging (MRI) examinations for anterior and posterior cruciate ligament injuries, the author proposes an MRI rehabilitation method to relieve anterior cruciate ligament injury in dancers. This method retrospectively analyzed the clinical data of 60 patients with knee anterior and posterior cruciate ligament injuries in our hospital, and all patients were diagnosed with knee anterior and posterior cruciate ligament injuries. All patients underwent MRI 3D sequence and 2D sequence examination successively to compare anatomical measurements. This study aimed at comparing the measurements of the posterior cruciate ligament (PCL) and anterior cruciate ligament (ACL) between the two examination sequences; comparing the diagnosis; comparing the grading and judgment of the anterior and posterior cruciate ligament injuries of the knee joint between the two inspection sequences; and comparing the diagnostic coincidence rates of the two examination sequences in the complete tear of the anterior and posterior cruciate ligaments of the knee. Experimental results show that, in terms of PCL and ACL, the angle, thickness, and length of two-dimensional MRI examination were significantly different from those of MRI examination and anatomical measurement ( $P < 0.05$ ); for PCL and ACL, the angle, thickness, and length of 3D MRI were not significantly different from anatomical measurements ( $P > 0.05$ ). The diagnostic accuracy of 2D MRI was 83.33%, which was lower than 95.00% of 3D MRI ( $P < 0.05$ ). There was no significant difference in the grading of anterior and posterior cruciate ligament injuries between the two examination sequences ( $P > 0.05$ ). The diagnostic coincidence rates of 3D MRI and 2D MRI for complete tear of the anterior and posterior cruciate ligaments were 95.55% and 80.00%, respectively ( $P < 0.05$ ). In conclusion, three-dimensional MRI examination can obtain higher diagnostic value for patients with knee joint anterior and posterior cruciate ligament injury.

## 1. Introduction

Sports dance is an emerging sport with strong technical and artistic qualities; it integrates art, sports, music, and dance, and it is called a model of the combination of “health” and “beauty” [1]. While the male and female players showed vigorous sports movements, it is also necessary to show the attractive artistic beauty of dance movements. The causes of sports injuries in sports dance are closely related to the lack of common knowledge of sports injuries among coaches and students [2]. Due to the lack of basic knowledge of sports injuries and the lack of knowledge of various preventive measures, the cause of the injury cannot be properly analyzed and lessons learned in the event of an injury, resulting in the frequent occurrence of the same injury.

In order to achieve outstanding competition results in sports dance, first of all, in order to ensure the health of the body, it is necessary to have sufficient muscle strength, such as explosive power, balance, coordination, and good quality and state [3]. At the same time, it can avoid the occurrence of sports injury or reduce the degree of injury. In addition, for different types of sports dance, we should pay attention to strengthening the exercise of weak parts and weak links, improve local functions, and meet special requirements. Dance sports is a contest of strength and beauty. In dancing, athletes make good use of loose knee force, strong leg strength and waist, and abdominal strength to make some difficult technical movements [4]. However, the artistry of the project requires the athletes to have the beauty of muscular lines, upright posture, and the perfect

combination of strength and beauty. Therefore, correct grasp of the priority order of muscle strength, coordination in the relationship between strengths, improvement in the processing ability of muscles, improvement in the internal coordination ability of muscles, and exercises that avoid muscle bulk and weight gain are especially important [5].

Sports injury (Figure 1) is a common situation for sports dancers in training or competition; it is due to the poor quality of the athletes or mistakes in technical movements; excessive exercise in teaching, sports training, and competition; insufficient preparation for warm-up activities; the venue, equipment, and clothing not meeting the requirements; and factors such as improper organization and management of competition events [6]. Injuries that occur during training have not been adequately rested and properly treated, and you have to continue training with the injury or without waiting for the injury to heal, over time, which will cause the injury to worsen, and this will directly affect the improvement of the level of sports dancers [7]. The injury problem of sports dancers should arouse the great attention of sports dance teachers and sports dancers, improve their awareness of injury prevention, and avoid the occurrence of sports injuries [8]. For this highly technical and artistic combination of sports and dance, sports injuries often trouble and restrict the normal performance of players [9]. Therefore, it is very important to study the sports injury of sports dance.

## 2. Literature Review

The cruciate ligament of the knee joint is also called the cruciate ligament clinically; it is mainly located in the latter part of the center of the knee joint, it has high strength and is covered by the synovial membrane, and it is mainly divided into anterior cruciate ligament and posterior cruciate ligament [10]. The two ligaments work together to limit excessive knee movement. However, knee cruciate ligament injuries are more common after a sports injury or injury from other factors. Due to the low self-healing ability of the cruciate ligament of the knee joint, after the injury, if it is not diagnosed in time and effective measures are taken to intervene, it is very easy to develop into a complete tear, which will adversely affect the stability of the joint, called secondary traumatic osteoarthropathy [11]. MRI is a commonly used imaging examination method in clinical practice; it has played a good role in the diagnosis of various diseases, it can achieve parametric and multidirectional imaging, and it has strong advantages in displaying articular cartilage and intra-articular structures. However, there are few studies on the difference in the effect of different examination sequences in the diagnosis of knee cruciate ligament injury, which limits the rational selection of clinical examination sequences to a certain extent. The three-dimensional fast spin echo sequence has the characteristics of high signal-to-noise ratio and high spatial resolution, which can realize thin-slice and no interval scanning and then clearly display the complex joint anatomy, which can play an important reference value in judging soft tissue damage.

Anterior cruciate ligament injury is one of the common diseases of the knee joint, which can lead to complications

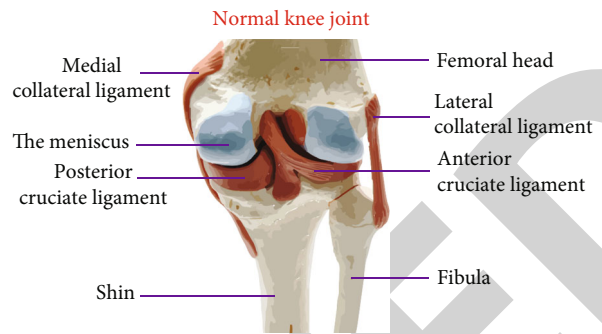


FIGURE 1: Ligament injury.

such as knee joint rotation imbalance, osteoarthritis, and cartilage degeneration; due to the early symptoms of joint swelling and pain in patients after injury, imaging diagnosis has caused certain difficulties. MRI is currently the main imaging method for diagnosing anterior cruciate ligament injury; however, there are still great limitations in diagnosing based on MRI signal intensity changes, resulting in low accuracy and specificity in the diagnosis of partial anterior cruciate ligament tear, which seriously affects the anterior cruciate ligament injury and the early diagnosis and treatment of cruciate ligament injury. Diffusion tensor imaging (DTI), as a quantitative diagnostic imaging technique, has so far been mainly used in the clinical diagnosis of central nervous system lesions; however, with the gradual popularization of DTI technology, there have been reports locally and abroad that it has been applied to other soft tissue lesions other than the central nervous system, along with the use of MRI and DTI to study normal anterior cruciate ligament and anterior cruciate ligament injury reconstruction. Moreover, there are few DTI studies on the grading of cruciate ligament injury; the application of DTI-based tractography (DTT) to evaluate the diagnostic effect of different grades of anterior cruciate ligament injury has not been seen [12]. In this study, DTI and DTT techniques were used to observe the fractional anisotropy (FA) value and apparent diffusion coefficient (ADC) value of the anisotropy fraction (FA) and apparent diffusion coefficient (ADC) of the injured anterior cruciate ligament and the corresponding parts of the normal group and with different degrees of injury, and its correlation with the degree of injury, in order to compare the diagnostic value of DTT in grading the degree of anterior cruciate ligament injury.

The author conducted a retrospective analysis of the clinical data of patients with cruciate ligament injury of the knee joint who underwent MRI examination in our hospital and were clinically diagnosed; the research content is described as follows [13].

## 3. Methods

### 3.1. Research Objects and Methods

**3.1.1. Research Objects.** The clinical data of 60 patients with knee anterior and posterior cruciate ligament injuries were retrospectively analyzed in a hospital, the inspection time

was between January 2020 and January 2021, and all patients were diagnosed with anterior and posterior knee injuries such as cruciate ligament injury. Among the 60 patients, 28 were female and 32 were male; the age ranged from 25 to 45 years, and the average age was  $32.71 \pm 4.15$  years. Injury factors were 24 cases of traffic accidents, 15 cases of falling from heights, 13 cases of heavy objects smashing, and 8 cases of other reasons; There were 45 complete tears and 15 partial tears [14].

The inclusion criteria were as follows: (i) clinical manifestations and surgical results were all diagnosed as anterior and posterior cruciate ligament injury; (ii) the clinical data were complete; (iii) the compliance was good, and the patients were able to cooperate with the examination; (iv) the affected knee joint had swelling, pain, and movement disorders; and for performance, (v) drawer test results were positive.

The exclusion criteria were as follows: (i) patients who have undergone knee surgery; (ii) women who are pregnant or breastfeeding; (iii) those who have a history of severe fractures; (iv) those who have a history of rheumatoid arthritis; (v) those who have tumor diseases; (vi) those who have congenital bone deformities; and (vii) patients with heart, liver, kidney, and lung organic function damage.

**3.1.2. Research Methods.** All patients were examined using the MAGNETOM Skyra 3.0 T magnetic resonance imaging system, using a special coil for the knee joint. The patients were assisted in a supine position and instructed to externally rotate the knee by  $15^\circ$  and maintain this angle during the examination. The 2D MRI scan parameters were as follows: (i) For the horizontal axis, the repetition time is 2000 ms, the recovery time is 38 ms, the matrix is  $300 \times 230$ , the field of view is  $150 \text{ mm} \times 150 \text{ mm}$ , the layer spacing is 0.5 mm, the layer thickness is 2.8 mm, the scanning time is 160 s, and the number of excitations is 2. (ii) For the sagittal plane, the repetition time is 2900 ms, the recovery time is 30 ms, the matrix is  $240 \times 240$ , the field of view is  $155 \text{ mm} \times 155 \text{ mm}$ , the slice interval is 0.41 mm, the slice thickness is 2.4 mm, the scanning time is 150 s, and the number of excitations is 2 times. (iii) For the coronal plane, the repetition time is 2600 ms, the recovery time is 30 ms, the matrix is  $300 \times 230$ , the field of view is  $155 \text{ mm} \times 155 \text{ mm}$ , the layer spacing is 0.41 mm, the layer thickness is 2.4 mm, the scanning time is 160 s, and the number of excitations is 2 times. The 3D MRI scanning parameters were as follows: for the sagittal plane, the repetition time is 1100 ms, the recovery time is 38 ms, the matrix is  $300 \times 230$ , the field of view is  $150 \text{ mm} \times 150 \text{ mm}$ , the slice spacing is 0 mm, the slice thickness is 0.5 mm, the scanning time is 320 ms, and the number of excitations is 1 time [15]. After three-dimensional MRI scans, all images were reconstructed in all planes, with a slice thickness of 1.5 mm and a slice interval of 0 mm. The operation was performed by 2 radiologists with rich clinical experience, and the images were read together to judge the knee joint injury situation and degree; when there was disagreement, a unified conclusion could be reached after discussion.

### 3.2. Research and Analysis

**3.2.1. Observation Items.** The posterior cruciate ligament (PCL) and anterior cruciate ligament (ACL) measurements were compared between the two examination sequences. The diagnosis of the two examination sequences were compared, as well as the grading and judgment of the anterior and posterior cruciate ligament injuries of the knee joint between the two inspection sequences. The contour and direction of the anterior and posterior cruciate ligaments of the knee joint were normal, and no abnormal signal was observed, which belonged to grade 0. Focal or diffuse swelling of the anterior and posterior cruciate ligaments of the knee joint as well as a high signal can be observed, the ligament continuity is acceptable, and the contour is clear and no notch is classified as grade 1. Incomplete rupture of the anterior and posterior cruciate ligaments of the knee joint as well as a thickening of the ligament can be observed, local notch may be present, the contour at the center of the injured area is incomplete, the ligament is interrupted, and the continuity is poor, but there are still some ligament connections belonging to grade 2. The anterior and posterior cruciate ligaments of the knee joint were completely ruptured, and the rupture site was incised or displaced, contraction at the ligament origin and insertion point was observed, and different degrees of dissolution and absorption at the rupture site belonged to grade 3. The diagnostic coincidence rates of the two examination sequences in the complete tear of the anterior and posterior cruciate ligaments of the knee were compared [16].

**3.2.2. Athletes' Assessment of Injury Risk from Sports Injuries.** It is shown in Table 1 that among the physical factors of sports dance professional athletes, injury history, physical fatigue, poor physical condition, and poor flexibility are the moderate risk factors for injury. The movement range of sports dance is large and flexible, and most of the sports dance movements are in contradiction with the anatomical structure of the human body; for example, most movements require a large range of motion and high flexibility of the hip joint, amplitude, and flexibility, directly affecting the quality of dance postures and technical movements. Moreover, the anatomical structure of the hip joint is characterized by good joint stability and poor flexibility; for example, the athlete's flexibility quality is poor, and when forcibly performing large-scale and high-speed hip joint movements that exceed the body's tolerance limit, it is easy to cause corresponding damage to the site [17]. The above four factors remind coaches and athletes that they should pay enough attention. Poor physical coordination, strength, and endurance are low-risk factors and are acceptable risks, but they cannot be ignored in normal training.

From Table 2, it can be seen that among the risk factors of injury caused by technical factors of sports dance professional athletes, incorrect technical essentials and improper self-prevention measures for injury are medium risk factors, and improper cooperation between dance partners and dance style are low. The risk factor is the incorrect technical essentials which refer to the damage to the body tissue

TABLE 1: Risk assessment results of physical factors for sports dance professional athletes.

Physiological factors	Amount of risk (Rv)	Risk level	Risk warning signs	Sort
Poor health (such as illness)	43.25 ± 15.42	Medium risk	Yellow	3
Injury history	62.25 ± 31.74	Medium risk	Yellow	1
Physical fatigue	49.63 ± 31.76	Medium risk	Yellow	2
Poor strength	29.25 ± 16.91		Green	6
Poor endurance	25.50 ± 17.72	Low risk	Green	7
Poor flexibility	40.75 ± 17.95	Medium risk	Yellow	4
Poor coordination	37.88 ± 19.67	Low risk	Green	5

TABLE 2: Risk assessment results of technical factors for sports dance professional athletes.

Physiological factors	Amount of risk (Rv)	Risk level	Risk warning signs	Sort
Incorrect technical essentials	45.25 ± 9.79	Medium risk	Yellow	1
Dance style	25.63 ± 12.05	Low risk	Green	4
Improper cooperation between dance partners	30.38 ± 4.84	Low risk	Green	3
Improper self-prevention measures	41.75 ± 11.88	Medium risk	Yellow	2

caused by the athlete's technical shortcomings and mistakes, violating the characteristics of the human body structure and the laws of activity of various organ systems, as well as the mechanical principles during exercise.

From Table 3, it can be seen that among the psychological factors of sports dance professional athletes, inattention and excessive mental stress are medium risk factors for injury, while depression and high excitement during training or competition are low risk factors. The research of domestic and foreign scholars shows that psychological factors are not only related to the performance of sports performance but also directly related to the pathogenesis of sports injuries.

From Table 4, it can be seen that among the risk of injury caused by other factors of professional dance athletes, accidents and emergencies are ranked first, followed by irregular life and rest, collisions during competitions, and referee factors; the above four factors are all low-risk factors, which are acceptable risks [18]. Accidents and emergencies are unforeseeable and mainly reflect the ability of athletes to respond to stress; for example, in research on the relationship between the stress level and sports injuries of sports students, high stress levels are one of the important causes of sports injuries. Athletes with high levels of stress are more easily affected by the external environment, such as obstacles to marriage and love, the death of relatives and friends, and emergencies on the training ground or on the field, all of which can affect the emotional state of athletes, thus affecting the physiological state and attention, so that sports injuries are prone to occur, and irregular life and rest can easily lead to the athletes' decline in function and easy fatigue, thereby increasing the risk of injury.

Based on the assessment results of the injury risk of professional sports dance athletes in the above four dimensions, we can see the main characteristics of the injury risk of sports dance athletes; the most important injury risks of ath-

letes during training or competition are as follows: injury training or competition, injury history, physical fatigue, partial overload, incorrect technical essentials, poor physical condition, inattention, etc. (Figure 2). This is basically consistent with the results of the open-ended questionnaire Pareto analysis. Athletes should take different preventive measures when dealing with different injury risks [19]. Coaches and athletes can generally take two types of measures when preventing injuries: risk avoidance and risk reduction. Among all the factors investigated, coaches and athletes generally believe that training or competition with injuries is the most likely to lead to the occurrence of injuries; therefore, for such risk factors, it is necessary to consider giving up training or competitions, or change the original training program to avoid risks. Excessive partial load or excessive exercise load on the body can easily lead to physical fatigue, resulting in decreased function and injury; therefore, coaches should scientifically arrange training plans to control exercise load, and especially to avoid single repetition of the same part of the training to reduce local burden to reduce the risk of injury [20]. Technical errors or mistakes are also the main cause of injury, so athletes should standardize their movements in their usual training and strengthen the learning of correct technical essentials, thereby reducing the risk of injury. Among the psychological factors, factors such as inattention and excessive mental tension may also lead to the occurrence of injuries such as technical deformation or errors in athletes during training and competition; for such factors, prevention and response should start from normal, strengthening the training of psychological adjustment ability to reduce the risk.

3.2.3. *Data Processing.* In this study, the data were calculated using SPSS22.0 software, and the measurement data were expressed in the form of  $(\bar{x} \pm s)$ , the  $t$  test was implemented,

TABLE 3: Risk assessment results of psychological factors for sports dance professional athletes.

Physiological factors	Amount of risk (Rv)	Risk level	Risk warning signs	Sort
Feeling down during training or competition	37.00 ± 19.09	Low risk	Green	3
Excessive excitement during training or competition	32.75 ± 9.19	Low risk	Green	4
Inattention	42.75 ± 11.56	Medium risk	Yellow	1
Nervousness	40.13 ± 13.25	Medium risk	Yellow	2

TABLE 4: Risk assessment results of other factors for sports dance professional athletes.

Physiological factors	Amount of risk (Rv)	Risk level	Risk warning signs	Sort
Referee factor	11.88 ± 5.19	Low risk	Green	4
Irregular life	35.13 ± 16.14	Low risk	Green	2
Collision during game	29.50 ± 10.93	Low risk	Green	3
Accident, accident	36.00 ± 17.63	Low risk	Green	1

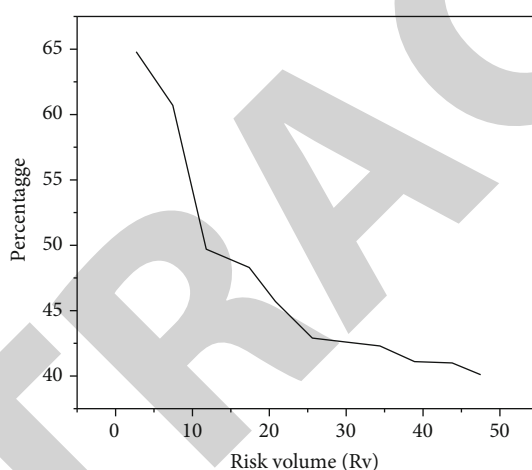


FIGURE 2: The main risks of injury caused by professional dance sports athletes.

TABLE 5: PCL measurement values of two groups of inspection sequences.

Check the sequence	Number of cases	Angle (°)	Thickness (cm)	Length (cm)
2D MRI	60	119.62 6.51	0.71 0.07	3.82 0.31
3D MRI	60	115.70 5.03	0.53 0.04	3.71 0.19
Anatomical measurements	60	115.53 5.12	0.52 0.03	3.70 0.24
<i>F</i>	—	10.260	278.110	4.200
<i>P</i>	—	<0.05	<0.05	<0.05
$X^2_1/P_1$	—	3.825/<0.05	19325/<0.05	2.371/<0.05
$X^2_2/P_2$	—	0.235/>0.05	1.560/>0.05	0.308/>0.05
$X^2_3/P_3$	—	3.691/<0.05	17.294/<0.05	2.343/<0.05

and the *F* value test was implemented for comparison between multiple groups. The enumeration data is expressed in the form of percentage, and the  $X^2$  test is implemented; when the test result shows  $P < 0.05$ , it indicates that the data has research value [21].

#### 4. Results and Discussion

In terms of PCL and ACL, the angle, thickness, and length of two-dimensional MRI examination were significantly different from those of MRI examination and anatomical

TABLE 6: ACL measurement values of the two groups of examination sequences.

Check the sequence	Number of cases	Angle (°)	Thickness (cm)	Length (cm)
2D MRI	60	37.40 4.18	0.73 0.05	3.22 0.11
3D MRI	60	39.35 4.98	0.63 0.02	3.57 0.16
Anatomical measurements	60	39.38 4.93	0.62 0.04	3.62 0.25
$F$	—	3.480	148.000	85.330
$P$	—	<0.05	<0.05	<0.05
$X^2_1/P_1$	—	2.373/<0.05	13307/<0.05	11.344/<0.05
$X^2_2/P_2$	—	0.049/>0.05	2.000/>0.05	2.1 19/>0.05
$X^2_3/P_3$	—	2.323/<0.05	14.384/<0.05	13.963/<0.05

measurement ( $P < 0.05$ ) [22, 23]. In terms of PCL and ACL, the angle, thickness, and length of 3D MRI were not significantly different from the anatomical measurements ( $P > 0.05$ ). See Tables 5 and 6.

## 5. Conclusion

The author proposes the MRI view of rehabilitation methods to relieve ACL injury in dancers. The main risks of injury caused by sports dancers are as follows: injury training or competition, injury history, physical fatigue, partial overload, incorrect technical essentials, poor physical condition, inability to concentrate, etc. Athletes can take different preventive measures when dealing with different risks of injury; generally, two types of measures can be taken: risk avoidance and risk reduction. Among them, risk reduction is the most widely used preventive coping strategy for athletes.

## Data Availability

The data used to support the findings of this study are available from the corresponding author upon request.

## Conflicts of Interest

The authors declare that they have no conflicts of interest.

## References

- [1] R. Ventura, P. Daley-Yates, I. Mazzoni, K. Collomp, and M. Stuart, "A novel approach to improve detection of glucocorticoid doping in sport with new guidance for physicians prescribing for athletes," *British Journal of Sports Medicine*, vol. 55, no. 11, pp. 631–642, 2021.
- [2] S. Mann and T. B. Grnlykke, "Does the spraino low-friction shoe patch prevent lateral ankle sprain injury in indoor sports? A pilot randomised controlled trial with 510 participants with previous ankle injuries," *British Journal of Sports Medicine*, vol. 55, no. 2, pp. 92–98, 2021.
- [3] C. Ekins, P. R. Wright, G. Schlee, and D. Owens, "Effects of a drums Alive® intervention versus hand-foot coordination training on motor, cognitive and motivational parameters in seniors," *Advances in Aging Research*, vol. 11, no. 3, pp. 51–77, 2022.
- [4] J. P. Ambegaonkar, L. Chong, and P. Joshi, "Supplemental training in dance: a systematic review," *Physical Medicine and Rehabilitation Clinics of North America*, vol. 32, no. 1, pp. 117–135, 2021.
- [5] M. Siejka, "The use of AHP to prioritize five waste processing plants locations in Krakow," *International Journal of Geo-Information*, vol. 9, no. 2, p. 110, 2020.
- [6] Y. Xu, "Repairing waist injury of sports dance based on multi-functional nano-material particles," *Ferroelectrics*, vol. 581, no. 1, pp. 172–185, 2021.
- [7] M. Lovalekar, K. A. Keenan, K. Beals et al., "Incidence and pattern of musculoskeletal injuries among women and men during marine corps training in sex-integrated units," *Journal of Science and Medicine in Sport*, vol. 23, no. 10, pp. 932–936, 2020.
- [8] J. Honrado, R. C. Bay, and K. C. Lam, "Epidemiology of patients with dance-related injuries presenting to emergency departments in the United States, 2014-2018," *Sports Health: A Multidisciplinary Approach*, vol. 13, no. 5, pp. 471–475, 2021.
- [9] Q. Liu, M. Huang, and W. S. Lee, "A look-ahead method for forecasting the concrete price," *Journal of Applied Mathematics and Physics*, vol. 10, no. 5, pp. 1859–1871, 2022.
- [10] D. Suh, M. J. Chang, H. J. Park, C. B. Chang, and S. B. Kang, "Assessment of anterolateral ligament of the knee after primary versus revision anterior cruciate ligament reconstruction," *Orthopaedic Journal of Sports Medicine*, vol. 9, no. 10, 2021.
- [11] J. Yin, K. Yang, D. Zheng, and N. Xu, "Anatomic reconstruction of the anterior cruciate ligament of the knee with or without reconstruction of the anterolateral ligament: a meta-analysis," *Journal of Orthopaedic Surgery*, vol. 29, no. 1, 2021.
- [12] J. Abbas, A. K. Ruhaima, A. I. Alanssari, and V. V. Pyliavskiy, "Perceptual method for MRI medical images improvement in presence of impulse noise," *Telecommunications and Radio Engineering*, vol. 79, no. 1, pp. 81–89, 2020.
- [13] G. Trudel, S. Duchesne-Bélanger, J. Thomas, G. Melkus, and O. Laneuville, "Quantitative analysis of repaired rabbit supraspinatus tendons ( $\pm$  channeling) using magnetic resonance imaging at 7 tesla," *Quantitative Imaging in Medicine and Surgery*, vol. 11, no. 8, pp. 3460–3471, 2021.
- [14] S. Zhang and Z. Lv, "Diagnosis and exercise rehabilitation of knee joint anterior cruciate ligament injury based on 3D-CT reconstruction," *Complexity*, vol. 2020, Article ID 3690124, 13 pages, 2020.

## Retraction

# Retracted: Effects of Sports Functional Food on Physical Function of Athletes under Ultrasound Observation

### Scanning

Received 11 July 2023; Accepted 11 July 2023; Published 12 July 2023

Copyright © 2023 Scanning. This is an open access article distributed under the Creative Commons Attribution License, which permits unrestricted use, distribution, and reproduction in any medium, provided the original work is properly cited.

This article has been retracted by Hindawi following an investigation undertaken by the publisher [1]. This investigation has uncovered evidence of one or more of the following indicators of systematic manipulation of the publication process:

- (1) Discrepancies in scope
- (2) Discrepancies in the description of the research reported
- (3) Discrepancies between the availability of data and the research described
- (4) Inappropriate citations
- (5) Incoherent, meaningless and/or irrelevant content included in the article
- (6) Peer-review manipulation

The presence of these indicators undermines our confidence in the integrity of the article's content and we cannot, therefore, vouch for its reliability. Please note that this notice is intended solely to alert readers that the content of this article is unreliable. We have not investigated whether authors were aware of or involved in the systematic manipulation of the publication process.

In addition, our investigation has also shown that one or more of the following human-subject reporting requirements has not been met in this article: ethical approval by an Institutional Review Board (IRB) committee or equivalent, patient/participant consent to participate, and/or agreement to publish patient/participant details (where relevant).

Wiley and Hindawi regrets that the usual quality checks did not identify these issues before publication and have since put additional measures in place to safeguard research integrity.

We wish to credit our own Research Integrity and Research Publishing teams and anonymous and named external researchers and research integrity experts for contributing to this investigation.

The corresponding author, as the representative of all authors, has been given the opportunity to register their agreement or disagreement to this retraction. We have kept a record of any response received.

### References

- [1] Z. Cheng, H. Lin, and Z. Zhou, "Effects of Sports Functional Food on Physical Function of Athletes under Ultrasound Observation," *Scanning*, vol. 2022, Article ID 7769653, 7 pages, 2022.



## Research Article

# Effects of Sports Functional Food on Physical Function of Athletes under Ultrasound Observation

Zhao Cheng <sup>1</sup>, Hong Lin <sup>1</sup>, and Zhenmao Zhou <sup>2</sup>

<sup>1</sup>School of Sport and Health, Anhui University of Chinese Medicine, Hefei, Anhui 230012, China

<sup>2</sup>Department of Physical Education, Anhui Medical University, Hefei, Anhui 230031, China

Correspondence should be addressed to Hong Lin; 20160617@ayit.edu.cn

Received 24 July 2022; Revised 20 August 2022; Accepted 3 September 2022; Published 14 September 2022

Academic Editor: Balakrishnan Nagaraj

Copyright © 2022 Zhao Cheng et al. This is an open access article distributed under the Creative Commons Attribution License, which permits unrestricted use, distribution, and reproduction in any medium, provided the original work is properly cited.

In order to improve the physical function of athletes under hypoxic training, the authors propose to observe the effect of functional food with active ingredients of polypeptide polyamines in deer antler on the physical function of athletes under ultrasound observation. According to the characteristics of physiological changes during hypoxic training, functional foods containing the active ingredients of polypeptide polyamines in deer antler were selected and given to athletes under simulated hypoxic training, observe the changes of red blood cells (RBC), hemoglobin (Hb), hematocrit (Hct), blood lactic acid, free radical metabolism and immune function of athletes, and musculoskeletal under ultrasound observation, discuss how to improve the physical function and athletic ability of athletes under hypoxic training. Experimental results show that athletes after 6 weeks of hypoxic training, red blood cells and hemoglobin were significantly increased, there was a significant difference compared to the control group ( $P < 0.05$  or  $P < 0.01$ ). After 6 weeks of hypoxic training, hemoglobin increased by 10.1%, a 5.6 percentage point increase compared to the control group. *Conclusion.* The antler peptides used by the authors can enhance the effect of hypoxic training.

## 1. Introduction

China has attached great importance to functional foods for a long time. In ancient medicine, China attaches great importance to dietary therapy and dietary supplements, and has formed a unique theory of the homology of medicine and food, which is recorded in many ancient Chinese documents. In “Shan Hai Jing”, “Huangdi Neijing”, “Shen Nong’s Classic of Materia Medica”, “Treatise on Febrile Diseases”, “Qian Jin Fang”, “Medical Therapy Materia Medica”, “Compendium of Materia Medica”, and other monographs, all have the theory of diet therapy, food supplement, food nourishment, and medicine and food homology. It can be said that functional food originated from the theory of dietary therapy, food nourishment, food supplement, and medicine and food homology in my country, medicine tonic is not as good as food tonic, which has been recognized by scholars all over the world [1]. Since the implementation of the functional food management measures in 1996, the state has strengthened the management and approval of func-

tional food, stipulating functional food refers to food with specific health care functions, that is, food suitable for specific groups of people, with the ability to regulate body functions, and not for the purpose of treating diseases [2].

The deer is the most representative special economic animal with a high reputation both at home and abroad, and its body is full of treasures. Modern research has proved that deer antler has the functions of regulating body metabolism, enhancing physical strength, improving hematopoietic function, promoting growth and development, improving body immunity, and promoting various physiological functions, in addition to deer antler, other deer products, such as antlers, deer whips, deer tails, deer tires, and deer blood, are important nutritional and health care products, therefore, the use of deer antler and by-products to develop functional food is the need for the development of the deer industry, it is the fundamental way to broaden the utilization of deer products, extend the industrial chain, increase the added value of products, and then improve the economic benefits of the deer industry [3].

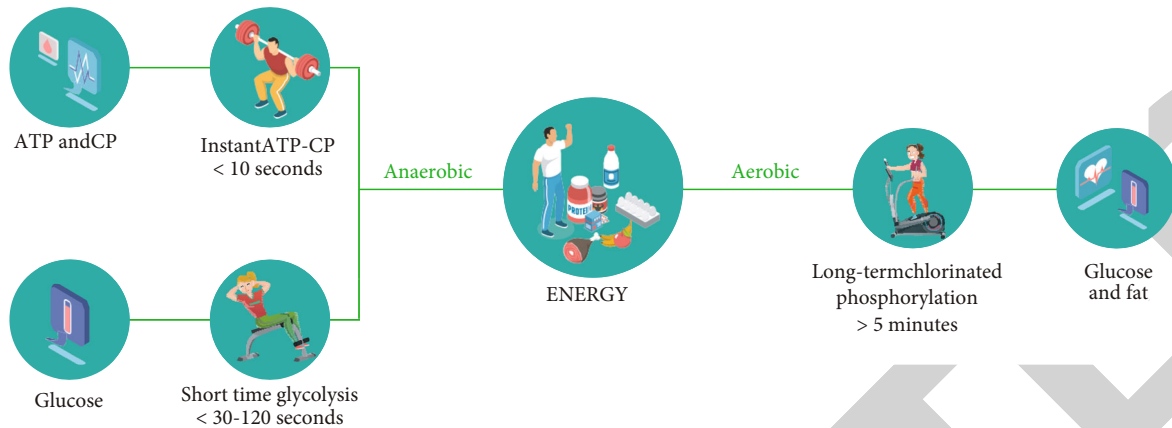


FIGURE 1: Endurance training.

At present, there are 22 functions of functional food accepted by the Ministry of Health. The specific functions are: Antifatigue, antimutation, anti-radiation, promoting growth and development, promoting lead excretion, promoting lactation, regulating blood quality, regulating blood pressure, regulating blood sugar, regulating immunity, improve memory, improve vision, improve sleep, improve nutritional anemia, improve osteoporosis, improve gastrointestinal tract, delay aging, it is resistant to hypoxia, lose weight, beautify, clear the throat and moisten the throat, and has a protective effect on chemical liver damage.

## 2. Literature Review

Mhb et al. found that deer antler polypeptide can accelerate the repair of back skin defects in rats and promote fracture healing, and can also significantly stimulate the proliferation of chondrocytes and osteoblast-like cells, and show a dose-effect relationship, and there is no species specificity [4]. Lane et al. treated spinal cord injured rats with deer antler peptides; it was found that it has a significant promoting effect on the recovery of motor function in rats [5]. Fang et al. tested cytokine production and lymphocyte proliferation, etc., it was found that velvet antler polypeptide can activate macrophages to secrete IL-12, promote the proliferation of mouse T and B lymphocytes, and enhance the immune function of the body. The peptides in velvet antler have obvious inhibitory effects on various acute and chronic inflammations, and are one of the material bases for the anti-inflammatory and analgesic effects of velvet antler. Polypeptides isolated from deer antler can significantly increase serum cortisol levels, and reduce ascorbic acid and cholesterol levels in rat adrenal glands, the results confirmed that the anti-inflammatory effect of velvet antler polypeptide is related to the stimulation of the adrenal cortex, and the anti-inflammatory effect is obvious [6]. Zhan et al. isolated and cultured osteoarthritic chondrocytes in vitro and added low, medium, and high doses (6.25, 12.5, and 25.0  $\mu\text{g}/\text{ml}$ ) of velvet antler polypeptide, respectively, the results showed

that velvet antler polypeptide has a reversal effect on the oxidative damage of osteoarthritic chondrocytes [8]. Lepelley and Crow have shown that antler polypeptide can promote the increase of testosterone and luteinizing hormone in male rat plasma which indicates that velvet antler polypeptide is one of the effective components of velvet antler affecting sexual function. In addition, studies have shown that cyclophosphamide-induced damage to mouse genetic material, deer antler polypeptide also has a certain protective effect [9]. Hu et al. observed the rod climbing time and weight-bearing swimming time of mice in the deer antler polypeptide (PAP) group and the control group, the changes of serum lactic acid content in mice before and after swimming were measured, and the experimental results showed that, deer antler polypeptide can significantly prolong the survival time of mice under normal pressure and hypoxia, gasping time after decapitation and hypoxia, pole climbing time and weight-bearing swimming time. It can also significantly reduce the increase in serum lactate in mice after swimming. Experiments show that velvet antler polypeptide has obvious antifatigue ability [10].

Hypoxic endurance training (Figure 1) is a compensatory change in function induced by a hypoxic environment. High altitude hypoxia training is generally divided into three stages—namely, the adaptation period, the training period, and the end period. During the whole training, hypoxia and low pressure stimulate the body very strongly, and the body's physiology changes accordingly under the stimulation, but the body is prone to fatigue and excessive free radicals when exercising in a hypoxic environment, damage to the body's homeostasis, resulting in damage to the body's health, decline in the body's immune system function, etc., affecting the training progress and training effect.

Therefore, according to the characteristics of physiological changes during hypoxic training, we have targeted the selection of functional foods containing the active ingredients of polypeptide polyamines in deer antler and given them to athletes under simulated hypoxia training, in order to observe the changes of red blood cells (RBC), hemoglobin (Hb), hematocrit (Hct), blood lactic acid, free radical metabolism and immune function of athletes, and musculoskeletal under ultrasound observation, according to the corresponding

data, the active ingredients of the drug are improved, so as to be able to explore the special food for hypoxic training that can help improve the physical function and athletic ability of athletes, and make up for the lack of nutritional supplementation in hypoxic training.

### 3. Research Methods

*3.1. Musculoskeletal Ultrasound.* Musculoskeletal ultrasound (US) is a fast, convenient, nonradiation imaging method with low cost, there is high acceptance and real-time dynamic examination of the musculoskeletal system. Ultrasound is widely used and is being used by more and more doctors, and its application in different medical disciplines is also increasing, covering almost every speciality of medicine: Anesthesia, Cardiology, Intensive Care, Emergency Medicine, Gynecology, Neurology, Obstetrics and Gynecology, Orthopedics, Pediatrics, Pulmonology and Rehabilitation, etc. Ultrasound has also become more portable, and every year businesses are developing smaller and more convenient devices [11]. In recent years, with the continuous improvement of ultrasound resolution, contrast-enhanced ultrasound, elastography, and other methods, also gaining increasing approval and practice, the medical community has witnessed significant progress in potential applications of musculoskeletal ultrasound, among them, the use of ultrasonography in the treatment of musculoskeletal diseases has attracted special attention, musculoskeletal ultrasound has gradually become a new type of ultrasound imaging technology practiced in clinic, it is also used in multidisciplinary clinical applications, such as joint, muscle and tendon injuries, peripheral nerves, musculoskeletal tumors, bone and cartilage diseases, skeletal muscle function evaluation, rheumatoid arthritis, pediatric hip dysplasia, rehabilitation therapy, pelvic floor muscles, intervention, elastography, contrast-enhanced ultrasound, and ultrasound biomicroscopy.

Mindray Resona ultrasound equipment was used, and the ultrasound probe frequency was 7-15 MHz, the relevant data of the subjects were measured before and after the experiment, including the thickness and elastic modulus of the transversus abdominis in the resting and contracting positions, thickness and elastic modulus of multifidus muscles in resting and contracted positions. The color ultrasound room was kept at 23-27°C and properly ventilated, before and after the experiment, the data of all subjects were measured by the same professional ultrasound doctor, avoid errors caused by different personnel experience [12].

(1) Resting position: The subject is in a supine position, the body is relaxed, the upper limbs are placed on the side of the body, and the probe is placed vertically with the skin, the thickness and elastic modulus of the transversus abdominis were measured along the upper border of the iliac crest, and the echo of the oblique stripe muscle was observed, the measurement was performed at the end of inspiration, three images were intercepted and the average value was taken.

(2) Contracted position: The subject completed the supine position of the suspension group training, and the measurement was performed while maintaining this action

and the transversus abdominis was activated, the thickness and elastic modulus of the transversus abdominis were measured by the probe along the upper border of the iliac crest, and three pictures were intercepted and the average value was taken.

The reasons for choosing the suspended supine position for real-time dynamic data measurement of the transversus abdominis are: the prone position is inconvenient to measure the transversus abdominis, and the distance between the transversus abdominis and the bed surface is not enough for the probe to be placed. At the same time, the left lateral position is more difficult to control than the right lateral position, and the subject is prone to shaking, which affects the measurement efficiency. Therefore, the supine position is the best choice of all positions.

*3.2. Materials and Methods.* The author selected 100 athletes as the research observation objects of the experiment, and carried out adaptive training according to the relevant behavioral indicators. After acclimatization training, athletes with significant differences in weight and athletic ability and average developmental levels were eliminated. The selected athletes were randomly divided into two groups with 50 animals in each group, and the two groups of athletes were defined as the hypoxic endurance training control group and the deer antler polypeptide hypoxic endurance training group. The hypoxia control group and the deer antler polypeptide hypoxia training group were given the same dose of normal saline, and each group continued to take it for 30 days. Afterwards, two groups of athletes were tested in a hypoxic chamber provided by a university sports college at the same time, the oxygen concentration in the chamber was defined at 15.4%, which was equivalent to simulated hypoxia training at an altitude of about 2,500 meters [13]. Blood samples were collected in the first 4 weeks of the experiment, and the physiological and biochemical indicators of the athletes in the hypoxic training group were recorded and observed by the influence of velvet antler polypeptide, that is, the generation speed and quantity of RBC, Hb, Hct, and Epo, the samples were tested by respective kits and detection methods.

*3.3. Test Indicators.* Red blood cell parameters: Red blood cell count (RBC), hemoglobin concentration (Hb), hematocrit (HCT), transverse abdominal muscle thickness, and elastic modulus.

*3.4. Test Equipment.* The method of measuring the changes of RBC, Hb, and Hct is sampling blood from athletes according to the specified time, and using the Coulter three-category whole blood analyzer to analyze the four indicators of Epo, RBC, Hb, and Hct, Mindray Resona ultrasound equipment.

*3.5. Statistical Processing.* The existing data were analyzed by the statistical software spss11.0, and the results of all data were shown in the following formula (1):

$$Y = X \pm S \quad (1)$$

In the formula,  $X$  represents the mean;  $S$  represents the standard deviation.

The independent samples  $t$  test was used for the data analysis between groups, and the paired samples  $t$  test was used for the analysis within the group, and the significance level was  $P < 0.05$  [14].

## 4. Analysis of Results

### 4.1. Changes in Red Blood Cell Parameters

**4.1.1. Changes in Erythropoietin.** After comparative analysis of the data, it was found that there was no significant difference in the basal values measured before training between the hypoxic control group and the hypoxic peptide group, after entering the training period, the basal values of the hypoxic control group increased significantly, on the 4th, 10th, 16th, and 21st day after the start of hypoxic training and the 5th day after the end of hypoxic training, compared with the baseline values measured before training, there were significant improvements ( $P < 0.05$ ), As in Table 1:

**4.1.2. Changes in Red Blood Cells.** Analysis from this set of data. On the base value before training, there was no significant difference between the hypoxic control group and the hypoxic peptide group, which indicated that the basic conditions and natural conditions of the two groups of athletes were consistent, in the 28 days after entering the hypoxic training period, there were significant changes in both groups, the degree of red blood cell changes in the hypoxic polypeptide group was significantly higher than that in the hypoxic control group on the 4th, 11th, 17th, and 22nd day of the training period, and the difference was significant ( $P < 0.05$ ). This shows that during hypoxic training, velvet antler polypeptide has the effect of stimulating the hematopoietic system and thus promoting erythropoiesis. Figure 2:

**4.1.3. Changes in Hemoglobin.** The data results show there was no significant difference in the basal value of hemoglobin before training between the hypoxic training group and the hypoxic peptide group. After entering the hypoxic training period, there was no significant change in the hypoxic training group in the hypoxic training period, but the hemoglobin content of the polypeptide group increased after entering the hypoxic training period, with a significant effect ( $P < 0.05$ ). As shown in Table 2:

**4.1.4. Changes in Hematocrit.** The experimental data show that there was no significant difference in the baseline values of the two groups of samples before the test, after entering the hypoxic environment training, the body's hematocrit increased on the 9th and 15th day and on the 5th and 8th day after the end of hypoxia, respectively, and the elevated value of the hypoxic polypeptide group was higher than that of the control group, which was significantly different ( $P < 0.05$ ). As shown in Table 3:

### 4.2. Changes in Oxidative Stress Indicators

**4.2.1. Changes of Erythrocyte Malondialdehyde.** The statistical results of Table 4 show that 4 weeks ago and 4 weeks

TABLE 1: Erythropoietin (unit: IU/ml).

EPO	Hypoxia control group	Hypoxic peptide group
Base value	13.3 ± 1.6	13.5 ± 2.3
Hypoxia begins day 1	13.3 ± 1.4	13.8 ± 2.1
Hypoxia begins day 4	13.2 ± 2.4	14.5 ± 3.7
Day 10 of hypoxia	12.4 ± 2.5	15.8 ± 2.3
Day 16 of hypoxia	14.7 ± 1.9	14.7 ± 3.1
Hypoxic training day 21	15.3 ± 2.3	15.2 ± 3.2
End of hypoxia day 5	14.6 ± 3.1	16.9 ± 2.1
End of hypoxia day 8	14.7 ± 3.5	14.6 ± 3.1

later, after performing incremental load exhaustive exercise, the MDA production and the respective resting values of the hypoxic control group and the hypoxic polypeptide group were compared, showing a significant increase ( $P < 0.05$ ). After 4 weeks, compared to the control group and itself 4 weeks ago, there was no significant change in MDA production in the hypoxic group after intermittent hypoxic training.

**4.2.2. Changes in Superoxidase.** The statistical results in Table 5 show that before and after 4 weeks, after performing exhaustive exercise with increasing load, the SOD activity of the hypoxic control group and hypoxic polypeptide group did not change significantly, and it showed a downward trend. After 4 weeks, through intermittent hypoxia training, both the activity of SOD in the hypoxia group at rest and after exhaustive exercise showed a significant increase, it was higher than the values at rest 4 weeks ago and after exhaustive exercise, respectively ( $P < 0.05$ ).

**4.2.3. Changes of Glutathione Peroxidase.** The statistical results in Table 6 show that 4 weeks ago and 4 weeks later, after performing exhaustive exercise with increasing load, the GSH-PX activity and the respective resting values of the hypoxic polypeptide group and the hypoxic control group were compared, showed a significant increase ( $P < 0.05$ ). After 4 weeks of intermittent hypoxia training in the hypoxic group, the activity of GSH-PX both at rest and after exhaustive exercise showed a significant increase, higher than 4 weeks before at rest and after exhaustive exercise, respectively ( $P < 0.05$ ) [15].

**4.3. Comparison of Transverse Abdominis.** The transversus abdominis in the core muscle group of the control group and the hypoxic group was measured and evaluated, and a comparative analysis was performed. Compared with the control group, the thickness of the transversus abdominis in the hypoxia group was not statistically significant ( $P < 0.05$ ) [16].

**4.4. The Effect of Velvet Antler Polypeptide on the Antioxidant System under Hypoxia.** The method used by the authors is to increase the load to exhaustion, during this process, the lipid peroxidation reaction, its metabolite MDA increases significantly, while the SOD activity does not

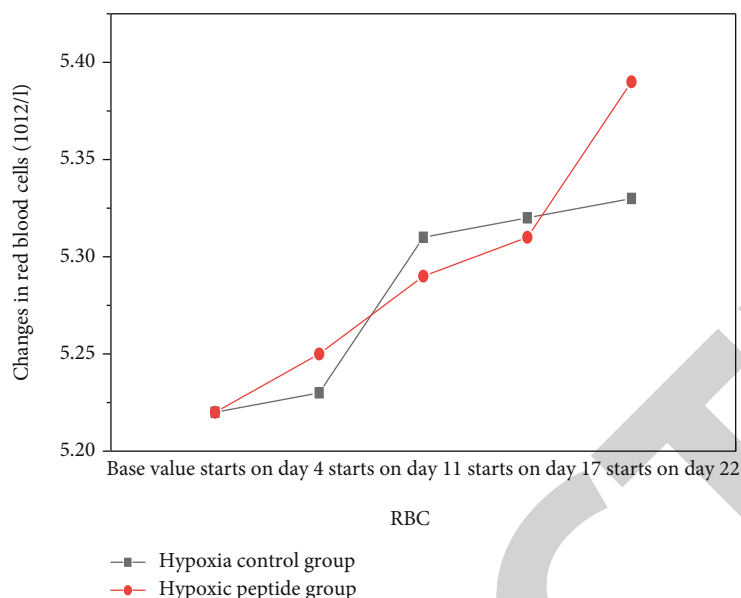


FIGURE 2: Changes in red blood cells (unit: 1012/l).

TABLE 2: Changes in hemoglobin (unit: g/l).

Hb	Hypoxic training group	Hypoxic peptide group
Base value	148 ± 5	150 ± 4
Hypoxia begins day 3	149 ± 6	152 ± 5
Day 10 of hypoxia	150 ± 4	160 ± 7
Day 16 of hypoxia	150 ± 5	163 ± 6
Day 21 of hypoxia	152 ± 5	165 ± 7
Day 28 of hypoxia	153 ± 6	166 ± 8

TABLE 3: Changes in hematocrit (unit: %).

Hct	Hypoxic training group	Hypoxic peptide group
Base value	43.8 ± 2.5	43.9 ± 1.4
Hypoxia begins day 1	43.7 ± 1.9	44.2 ± 1.5
Hypoxia begins day 9	44.2 ± 2.2	45.0 ± 1.8
Day 15 of hypoxia	44.5 ± 1.5	45.4 ± 1.7
Day 17 of hypoxia	43.2 ± 1.9	44.9 ± 2.4
Day 22 of hypoxia	44.4 ± 2.3	44.5 ± 2.0
Day 24 of hypoxia	44.2 ± 2.3	45.0 ± 2.6
End of hypoxia day 5	44.0 ± 2.4	45.5 ± 1.7
End of hypoxia day 8	43.5 ± 1.7	44.9 ± 1.9
End of hypoxia day 15	44.0 ± 2.5	45.1 ± 2.1

change significantly, but decreases. The activity of GSH-PX increased. The activity of SOD did not differ significantly immediately after exercise, but increased significantly after exercise, and returned to the original normal level within a few hours afterward. At the same time, by measuring OFR and MDA in plasma, they both achieved a significant

increase after exercise [17]. However, the fluidity of the RBC membrane was significantly reduced due to lipid peroxidation. Different degrees of exercise intensity and exercise time will cause different degrees of free radical and antioxidant system reactions. After the exhaustive exercise with increasing load, the free radicals increased immediately, the SOD enzyme did not change significantly, and the GSH-PX showed a significant increase, which may be related to the different exercise methods used. In the experimental results, the SOD enzyme activity did not change, which is related to the increase in the autooxidation of hemoglobin after exercise, a large number of accumulated in red blood cells, and promote SOD to catalyze O<sub>2</sub>-disproportionation reaction, the generated H<sub>2</sub>O<sub>2</sub> feedback inhibition, inhibiting SOD activity. A large amount of H<sub>2</sub>O<sub>2</sub> activates glutathione peroxidase GSH-PX, which significantly increases glutathione peroxidase (GSH-PX). The significant increase in MDA proves that the number of free radicals generated increases, which intensifies the peroxidation of lipids, and may cause oxidative damage to red blood cells, leading to changes in red blood cell structure and function, and ultimately resulting in reduced exercise capacity due to tissue hypoxia [18]. Therefore, by using specific training methods to improve the antioxidant capacity of red blood cells, so as to effectively improve the sports ability of athletes, which is very important for the development of sports training ability.

*4.5. Effects of Antler Polypeptides on Exercise Capacity under Hypoxic Training.* In a hypoxic environment, velvet antler polypeptide can promote the release of EPO from the kidneys, and promote the increase of blood indicators Hct, Rbc, and Hb, thereby improving the blood's ability to absorb and transport oxygen, this is an important factor in rapidly improving aerobic capacity during hypoxic training, the main task of Hb is to transport oxygen from the lungs to

TABLE 4: Malondialdehyde (unit: nmol/ml).

MDA	Before training		After four weeks of training	
	Quiet value	Immediately after exercise	Quiet value	Immediately after exercise
Control group	16.9 ± 1.5	18.7 ± 1.6 *	17.6 ± 2.1	20.2 ± 2.4 *
Hypoxia group	17.9 ± 1.8	20.8 ± 2.1 *	15.9 ± 1.9	19.8 ± 1.9 *

\*Paired test before and after exercise was significantly different,  $P < 0.05$ .

TABLE 5: Superoxidase (unit: Nu/gHb).

SOD	Before training		After four weeks of training	
	Quiet value	Immediately after exercise	Quiet value	Immediately after exercise
Control group	17383.8 ± 1895.7	15726.6 ± 2879.2	17475.8 ± 1342.7	16034.3 ± 2801.9
Hypoxia group	16183.5 ± 1465.0	14319.6 ± 2013.5	18830.3 ± 1952.2	17786.3 ± 2285.2

\*Paired test before and after exercise was significantly different,  $P < 0.05$ . There is a significant difference from the paired test of the quiet value four weeks ago,  $P < 0.05$ . Compared with the value immediately after exercise four weeks ago, there is a significant difference,  $P < 0.05$ .

TABLE 6: Glutathione peroxidase (unit: Nu/gHb).

SOD	Before training		After four weeks of training	
	Quiet value	Immediately after exercise	Quiet value	Immediately after exercise
Control group	72.8 ± 14.5	102.2 ± 20.2 *	73.3 ± 13.6	104.2 ± 19.9 *
Hypoxia group	68.7 ± 6.9	94.95 ± 7.5 *	74.3 ± 8.0	105.1 ± 8.8 ***

other tissues in the body, and then transport the carbon dioxide produced by the various tissues of the body back to the lungs during exercise. The increase of Hb will directly affect the aerobic exercise capacity index  $VO_{2max}$  of the human body, at the same time, the reduction of Hb is a very powerful buffer and the increase of Hb content can provide a certain compensatory function for the decline of human alkali reserve. When the human body performs strenuous exercise, the concentration of  $H^+$  will increase, and the increase of the concentration of  $H^+$  will accelerate the generation of exercise fatigue and affect the exercise ability of the human body [19]. At this time, the conversion between oxy-hemoglobin and reduced hemoglobin reduces the acid concentration of the human body and improves the antacid buffering capacity of the human body.

The lack of oxygen is an important factor in the decline of exercise capacity. The experimental group and the control group in this experiment were experimented under the conditions and intensity of simulated altitude training. The result shows, athletes after 6 weeks of hypoxic training, erythrocytes, and hemoglobin were significantly increased compared with the control group ( $P < 0.05$  or  $P < 0.01$ ). After 6 weeks of hypoxic training, hemoglobin increased by 10.1%, a 5.6 percentage point increase compared to the control group. This shows that, in theory, the oxygen transport capacity of the blood has been significantly improved.

In the exhaustion experiment, we found that the average exhaustion time of the peptide was 43 minutes longer than that of the control group, which was significantly higher than that of the control group, the velvet antler peptides taken promote the rise of RBC and HB in the body, which enhances the oxygen-carrying capacity of the blood, the cir-

culatory system is the main factor affecting the maximum oxygen uptake, in the absence of other factors, changes in hemoglobin concentration during exercise are a direct factor affecting  $VO_{2max}$  and athletic performance [20]. After one month of peptide-assisted training and normal hypoxia training, we found that HB in the peptide group was significantly higher than that in the control group, which provided a reasonable explanation for the longer exhaustion time in the peptide group than in the control group in the exhaustion experiment [21].

The above conclusions show that in 4 weeks of hypoxic training, the performance of the athletes in the antler polypeptide group was higher than that in the control group, deer antler polypeptide has a good effect on promoting the production of red blood cells in the body, and can significantly improve the oxygen-carrying capacity of the body.

## 5. Conclusion

The antler peptides used by the authors can enhance the effect of hypoxic training. Given that there was no change in hemoglobin concentration in this experiment, it is recommended to strengthen nutritional control and intervention in future studies, and measure blood volume or total hemoglobin, in order to understand the effect of intermittent hypoxic training on hemoglobin synthesis.

After four weeks of hypoxic training, red blood cell antioxidant enzymes SOD, glutathione antioxidant enzyme (GSH-PX) activity, and red blood cell antioxidant protein levels were significantly increased both at rest and after exhaustive exercise. It shows that deer antler peptides can be used in hypoxic training, induces an increase in the

## *Retraction*

# **Retracted: Efficacy Evaluation of the Combined Platelet-Rich Plasma and Hyaluronic Acid after Arthroscopic Joint Debridement in Treating Knee Osteoarthritis**

### **Scanning**

Received 20 June 2023; Accepted 20 June 2023; Published 21 June 2023

Copyright © 2023 Scanning. This is an open access article distributed under the Creative Commons Attribution License, which permits unrestricted use, distribution, and reproduction in any medium, provided the original work is properly cited.

This article has been retracted by Hindawi following an investigation undertaken by the publisher [1]. This investigation has uncovered evidence of one or more of the following indicators of systematic manipulation of the publication process:

- (1) Discrepancies in scope
- (2) Discrepancies in the description of the research reported
- (3) Discrepancies between the availability of data and the research described
- (4) Inappropriate citations
- (5) Incoherent, meaningless and/or irrelevant content included in the article
- (6) Peer-review manipulation

The presence of these indicators undermines our confidence in the integrity of the article's content and we cannot, therefore, vouch for its reliability. Please note that this notice is intended solely to alert readers that the content of this article is unreliable. We have not investigated whether authors were aware of or involved in the systematic manipulation of the publication process.

In addition, our investigation has also shown that one or more of the following human-subject reporting requirements has not been met in this article: ethical approval by an Institutional Review Board (IRB) committee or equivalent, patient/participant consent to participate, and/or agreement to publish patient/participant details (where relevant).

Wiley and Hindawi regrets that the usual quality checks did not identify these issues before publication and have since put additional measures in place to safeguard research integrity.

We wish to credit our own Research Integrity and Research Publishing teams and anonymous and named external researchers and research integrity experts for contributing to this investigation.

The corresponding author, as the representative of all authors, has been given the opportunity to register their agreement or disagreement to this retraction. We have kept a record of any response received.

### **References**

- [1] M. Lu and Y. Jin, "Efficacy Evaluation of the Combined Platelet-Rich Plasma and Hyaluronic Acid after Arthroscopic Joint Debridement in Treating Knee Osteoarthritis," *Scanning*, vol. 2022, Article ID 6994017, 5 pages, 2022.

## Research Article

# Efficacy Evaluation of the Combined Platelet-Rich Plasma and Hyaluronic Acid after Arthroscopic Joint Debridement in Treating Knee Osteoarthritis

Min Lu <sup>1</sup> and Yanquan Jin <sup>2</sup>

<sup>1</sup>Department of Orthopedics, People's Hospital of Ningbo University, Ningbo Zhejiang 315000, China

<sup>2</sup>Taizhou Orthopedics Hospital Orthopedics, Taizhou, Zhejiang 318000, China

Correspondence should be addressed to Min Lu; 201903525@stu.ncwu.edu.cn

Received 12 July 2022; Revised 25 July 2022; Accepted 3 August 2022; Published 6 September 2022

Academic Editor: Balakrishnan Nagaraj

Copyright © 2022 Min Lu and Yanquan Jin. This is an open access article distributed under the Creative Commons Attribution License, which permits unrestricted use, distribution, and reproduction in any medium, provided the original work is properly cited.

**Objective.** The study is aimed at observing the efficacy of the combined platelet-rich plasma and hyaluronic acid after arthroscopic joint debridement in treating knee osteoarthritis (KOA). **Methods.** 126 patients with KOA admitted to the Affiliated People's Hospital of Ningbo University and Taizhou Orthopaedic Hospital from 2018-11 to 2021-11 were selected. All nominees were grouped by random drawing; group B (63 cases) received arthroscopic joint debridement while group A (63 cases) received platelet-rich plasma and hyaluronic acid based on group B. The following metrics are counted, including total efficiency, knee joint pain and function, inflammatory cytokines levels, and oxidative stress indicator levels; the complication rate is counted. **Results.** The total effective rate of group A (93.65%) was higher than that of group B (77.78%) ( $P < 0.05$ ), and there was no significant difference in the incidence of complications between the groups ( $P > 0.05$ ). Three months after treatment, knee joint pain and function, inflammatory cytokine levels, and oxidative stress indicators levels in group A were better than in group B ( $P < 0.05$ ). **Conclusion.** The combined platelet-rich plasma and hyaluronic acid after arthroscopic joint debridement in treating KOA can achieve significant effects, reduce knee pain, accelerate the recovery of knee joint function, relieve inflammation, and inhibit oxidative stress and has high safety.

## 1. Introduction

Knee osteoarthritis (KOA) is common in orthopedics, with an incidence of approximately 20% in people over 45 years of age [1]. At present, the use of step-by-step, individualized treatment and surgery is an indispensable means for the treatment of middle and advanced KOA. Arthroscopic joint debridement is one of the commonly used surgical methods; cleaning up the diseased tissue in the joint cavity can achieve the purpose of relieving clinical symptoms [2]. Besides, drug injection is also a definitive therapy. For example, commonly used drugs are hyaluronic acid and platelet-rich plasma. The former plays a role in lubricating joints through its unique physicochemical properties and molecular structure. At the same time, the latter contains many growth factors, which

can stimulate cell proliferation, induce vascular formation, and promote tissue healing [3, 4]. However, there is a lack of research on the effect of arthroscopic joint debridement combined with platelet-rich plasma and hyaluronic acid in treating KOA in China. Herein, this current study focuses on this topic to provide a clinical reference. The report is as follows.

## 2. Material and Methods

**2.1. General Information.** 126 patients with KOA admitted to the Affiliated People's Hospital of Ningbo University and Taizhou Orthopaedic Hospital from 2018-11 to 2021-11 were selected; all nominees were grouped by random drawing. Group B consisted of 63 cases, with a male-to-



female ratio of 21 : 42; aged 43-70 years (average age,  $55.46 \pm 6.03$  years); disease duration 0.5-11.0 years (average disease duration,  $5.45 \pm 2.37$  years); and side: 30 left and 33 right. Group A consisted of 63 cases, with a male-to-female ratio of 24 : 39; aged 45-68 years (average age,  $57.39 \pm 5.21$  years); disease duration of 0.5-12.5 years (average disease duration,  $6.09 \pm 2.68$  years); and side: 26 left and 37 right. The general data of the two groups were comparable ( $P > 0.05$ ).

## 2.2. Selection Criteria

- (1) The following are the inclusion criteria: the study conforming to KOA diagnostic guidelines [5]; Kellgren-Lawrence grades which are III to IV; conservative treatment which is ineffective for 3 to 6 months, with indications for arthroscopic joint debridement; and unilateral disease
- (2) The following are the exclusion criteria: combined with other joint diseases, such as rheumatoid arthritis and rheumatoid arthritis; skin damage in the injection area; combined with knee joint trauma; accompanied by the abnormal liver and kidney function, infectious diseases, coagulation dysfunction, severe cardiovascular and cerebrovascular diseases, malignant tumors, diseases of the immune system, and diseases of the nervous system; previous knee surgery; received medication within the past one month; poor compliance; and lack of clinical data

## 2.3. Methods

- (1) Group B received arthroscopic joint debridement, spinal anesthesia, supine position, routine disinfection, and drape, and an incision was made on the anterolateral and anteromedial aspects of the knee joint, and the arthroscope was placed through the anterolateral approach; observe the suprapatellar capsule, intermuscular groove, and patellar articular surface in sequence; assist the patient in bending the knee to  $90^\circ$ ; observe the cruciate ligament, articular cartilage, and meniscus; place the planer from the anteromedial approach; then, inflammatory synovium, proliferative tissue, osteophyte and necrotic cartilage were cleaned with a planer under the microscope. The edge of the meniscus and the cartilage defect area were trimmed, the debris in the joint cavity was sucked, the incision was closed, and finally, pressure bandaging was performed
- (2) Group A received platelet-rich plasma and hyaluronic acid based on group B. Platelet-rich plasma needs to be prepared first. The instrument uses a sterile centrifuge and a platelet-rich plasma preparation kit produced by Shandong Weigao Medical Equipment Co. Ltd. 30 min before arthroscopic joint debridement; collect and centrifuge 40 mL of the patient's cubital venous blood (1500 r/min, 19 cm, 10 min); remove the lower 1/5 red blood cell layer

and continue centrifugation (centrifugation conditions are the same as above); add calcium chloride (2 mL) to the remaining 1/4 liquid, and mix well to obtain 4 mL of platelet-rich plasma. Before closing the incision under arthroscopic joint debridement, platelet-rich plasma was injected into the joint cavity from the anterolateral entrance, and 2 mL of hyaluronic acid was injected at 10 min intervals (Chinese Medicine Zhunzi: H10960136); close the incision, and apply a pressure dressing. Clean once during the operation, 2 weeks, 4 weeks and 6 weeks after the operation, a total of 4 times

## 2.4. Observation Indicators

- (1) Efficacy: it is assessed by the improvement rate of the Western Ontario and McMaster university osteoarthritis index (WOMAC) score (improvement rate =  $(\text{pretreatment score} - \text{treatment posttreatment score}) / \text{pretreatment score} \times 100\%$ ). Improvement rates of  $\geq 75\%$ , 30% to 74%, and  $\leq 29\%$  represent markedly effective, practical, and ineffective [6]. The sum of practical efficiency and apparent efficiency is the total effective efficiency
- (2) Knee joint pain and function: visual analog scales (VAS) and WOMAC score were used to evaluate the knee joint pain and function in group A and group B. The total score on the VAS scale is 0-10, with 0 representing no pain and 10 representing severe pain. WOMAC includes 24 items and percentage system; the lower the score, the better the function of the knee joint [7, 8]. The evaluation was performed once before treatment and three months after treatment
- (3) Levels of inflammatory cytokines and oxidative stress indicators: before treatment and three months after treatment, 5 mL of joint cavity fluid was collected from the affected side of the patient. The supernatant was centrifuged to determine inflammatory cytokines by ELISA (interleukin-6 (IL-6), tumor necrosis factor- $\alpha$  (TNF- $\alpha$ ), and interleukin- $1\beta$  (IL- $1\beta$ ) levels and malondialdehyde (MDA), superoxide dismutase (SOD), and other oxidative stress index levels)
- (4) Complication rate: pay attention to thromboembolism, wound infection and lower limb swelling

2.5. *Statistical Methods.* The data were analyzed by SPSS 22.0, and the test level was  $\alpha = 0.05$ .

## 3. Results

3.1. *Curative Effect.* The curative effect of group A was better than that of group B ( $P < 0.05$ ), as shown in Table 1.

3.2. *Knee Joint Pain and Function.* Three months after treatment, the VAS and WOMAC score of group A were lower than that of group B ( $P < 0.05$ ), as shown in Table 2.

TABLE 1: Curative effects ( $n$  (%)).

Group	Number of cases	Effective	Efficient	Invalid	Total efficiency
Group A	63	24 (38.10)	35 (55.56)	4 (6.35)	59 (93.65)
Group B	63	17 (26.98)	32 (50.79)	14 (22.22)	49 (77.78)
$\chi^2$					6.481
$P$					0.011

TABLE 2: Knee joint pain and function ( $\bar{x} \pm s$ , points).

Group	Number of cases	VAS score		WOMAC score	
		Before treatment	Three months after treatment	Before treatment	Three months after treatment
Group A	63	6.69 $\pm$ 0.90	2.35 $\pm$ 0.22	57.28 $\pm$ 8.33	35.14 $\pm$ 5.62
Group B	63	6.45 $\pm$ 0.83	3.21 $\pm$ 0.38	55.57 $\pm$ 7.64	41.68 $\pm$ 6.47
$t$		1.556	15.546	1.201	3.205
$P$		0.122	<0.001	0.232	0.002

TABLE 3: Levels of inflammatory cytokines ( $\bar{x} \pm s$ ).

Group	Number of cases	IL-6 (ng/L)		TNF- $\alpha$ ( $\mu$ g/L)		IL-1 $\beta$ (ng/L)	
		Before treatment	Three months after treatment	Before treatment	Three months after treatment	Before treatment	Three months after treatment
Group A	63	105.34 $\pm$ 10.27	75.90 $\pm$ 7.46	9.71 $\pm$ 2.56	4.22 $\pm$ 1.29	2.78 $\pm$ 0.33	1.32 $\pm$ 0.16
Group B	63	102.82 $\pm$ 9.44	88.59 $\pm$ 8.23	9.13 $\pm$ 2.08	6.34 $\pm$ 1.67	2.69 $\pm$ 0.30	1.88 $\pm$ 0.24
$t$		1.434	9.068	1.396	7.974	1.602	15.410
$P$		0.154	<0.001	0.165	<0.001	0.112	<0.001

TABLE 4: Levels of oxidative stress indicators ( $\bar{x} \pm s$ ).

Group	Number of cases	MDA ( $\mu$ mol/L)		SOD (U/mL)	
		Before treatment	Three months after treatment	Before treatment	Three months after treatment
Group A	63	14.15 $\pm$ 1.79	5.88 $\pm$ 1.02	88.65 $\pm$ 6.69	120.32 $\pm$ 8.73
Group B	63	13.72 $\pm$ 1.53	9.34 $\pm$ 1.27	86.58 $\pm$ 6.17	104.41 $\pm$ 7.24
$t$		1.449	16.860	1.805	11.923
$P$		0.150	<0.001	0.073	<0.001

TABLE 5: Complication rate ( $n$  (%)).

Group	Number of cases	Thromboembolism	Wound infection	Lower extremity swelling	Total incidence
Group A	63	0 (0.00)	2 (3.17)	2 (3.17)	4 (6.35)
Group B	63	1 (1.59)	2 (3.17)	3 (4.76)	6 (9.52)
$\chi^2$					0.434
$P$					0.510

3.3. *Levels of Inflammatory Cytokines.* Three months after treatment, the levels of IL-6, TNF- $\alpha$ , and IL-1 $\beta$  in group A were lower than those of group B ( $P < 0.05$ ), as shown in Table 3.

3.4. *Levels of Oxidative Stress Indicators.* Three months after treatment, the levels of MDA and SOD in group A were better than those in group B ( $P < 0.05$ ), as shown in Table 4.

3.5. *Complication Rate.* There was no significant difference in the incidence of complications between the two groups ( $P > 0.05$ ), as shown in Table 5.

#### 4. Conclusion

With the acceleration of the aging process in China, KOA has gradually become a common disease. However, its pathogenesis has not been fully elucidated. It is believed by the most scholars that KOA are involved in mechanical stress, oxidative stress, and chronic inflammation [9, 10]. Arthroscopic joint debridement is an effective procedure for the treatment of KOA. For instance, arthroscopic joint debridement can remove loose bodies and osteophytes, reduce cartilage wear, and joint pain and optimize joint function. Besides, it can clean up inflammatory and proliferative tissue and inhibit its erosion of other parts. Cleaning the joint cavity can prevent inflammatory cytokines from entering the blood affecting other joints. However, the effect of single arthroscopic joint debridement is limited. Hence, it is usually used in combination with other drugs.

Hyaluronic acid is a high molecular weight polysaccharide that exists widely in various tissues in the body. Hyaluronic acid can combine with glycoproteins to form aggregates, improve the stability of collagen fiber scaffolds and synovial cells, and improve the viscoelasticity of tissue matrix and synovial fluid when injected into the knee joint cavity. At the same time, hyaluronic acid can reduce mechanical friction and wear, provide nutrition for articular cartilage, repair damaged cartilage, and relieve joint pain. After the platelet-rich plasma is injected into the joint cavity, a large number of growth factors are released, which can accelerate the proliferation of chondrocytes and the synthesis of cartilage matrix and stimulate the activation of vascular endothelial cells, facilitate the formation of new capillaries and increase the blood supply of damaged tissues, thereby repairing damaged cartilage. It is obtained by centrifugation of autologous blood, which can avoid immune rejection with high safety. The literature has reported that platelet-rich plasma is rich in platelets; activated platelets can release a variety of antimicrobial peptides, which play a role of bacteriostatic and bactericidal [11, 12]. It can be seen from this study that the combined treatment method has a significant effect and can improve the symptoms and function of knee joint pain in KOA patients. The reason may be that the combination of the above two drugs can stimulate the proliferation of chondrocytes and rebuild the defective cartilage based on surgical treatment of internal lesions of the knee joint. The drug is injected once every two weeks, which has a sustained effect; it can relieve pain and dysfunction significantly.

TNF- $\alpha$ , IL-6, and IL-1 $\beta$ , as inflammatory cytokines, are involved in the inflammatory response during the KOA occurrence [13]. TNF- $\alpha$  and IL-1 $\beta$  can stimulate the production of chondrocytes and synovial cells as well as secrete prostaglandins and collagenase. Furthermore, it causes the degradation and destruction of articular cartilage. IL-6 is an amplifying factor for the biological effects of TNF- $\alpha$  and IL-1 $\beta$  and can also reflect the severity of the body's inflam-

matory response [14, 15]. Relevant studies have confirmed that the concentration of IL-1 $\beta$  in the joint cavity positively correlates with the severity of KOA [16]. Some scholars have pointed out that high levels of TNF- $\alpha$  in the joint cavity can promote the activation of polymorphonuclear cells, increase the secretion of prostaglandin E<sub>2</sub>, cause the aggregation of inflammatory cells, increase vascular permeability, and increase local edema [17]. In this study, combining surgery and drugs can reduce the inflammatory response. The reason is that, on the one hand, hyaluronic acid can inhibit matrix metalloproteinases and interleukins and resist the invasion of inflammatory cytokines. On the other hand, platelet-rich plasma enters the lesion, and anti-inflammatory factors are released, which can inhibit the excessive activation of nuclear factor  $\kappa$ B; it can stimulate the production of many inflammatory cytokines and trigger an inflammatory response.

Oxidative stress plays a massive role in the pathogenesis of KOA. In healthy people, oxygen-free radicals are generated and eliminated in a balanced state. In contrast, in KOA patients, excessive oxygen free radicals hinder the proliferation of chondrocytes and promote the degradation of the cartilage matrix, resulting in cartilage damage [18]. Under the action of disproportionation, SOD can scavenge oxygen free radicals and prevent cell lysis and apoptosis, and its level is proportional to the body's antioxidant capacity. MDA is one of the membrane lipid peroxidation products, which will aggravate membrane damage and reflect the degree of tissue peroxidative damage [19, 20]. This study confirms that combining surgery and drugs can reduce oxidative stress in KOA patients. The reason may be related to the activation of the Keap1/Nrf2/HO1 signaling pathway by platelet-rich plasma to increase the expression of SOD. The elevated SOD level can effectively scavenge excess oxygen free radicals and reduce oxidative stress. In addition, the safety of the treatment regimen in this study was confirmed.

To sum up, arthroscopic joint debridement combined with platelet-rich plasma and hyaluronic acid in treating KOA achieves significant effects; can reduce knee pain, accelerate the recovery of knee joint function, relieve inflammation, and inhibit oxidative stress; and has high safety. Hence, it is worthy of promotion and application.

#### Data Availability

The data used to support the findings of this study are available from the corresponding author upon request.

#### Conflicts of Interest

The authors declare that they have no conflicts of interest.

#### Authors' Contributions

Min Lu and Yanquan Jin contributed equally to this work and should be considered the co-first authors.

## *Retraction*

# **Retracted: Digital Image Restoration Based on Multicontour Batch Scanning**

### **Scanning**

Received 5 December 2023; Accepted 5 December 2023; Published 6 December 2023

Copyright © 2023 Scanning. This is an open access article distributed under the Creative Commons Attribution License, which permits unrestricted use, distribution, and reproduction in any medium, provided the original work is properly cited.

This article has been retracted by Hindawi, as publisher, following an investigation undertaken by the publisher [1]. This investigation has uncovered evidence of systematic manipulation of the publication and peer-review process. We cannot, therefore, vouch for the reliability or integrity of this article.

Please note that this notice is intended solely to alert readers that the peer-review process of this article has been compromised.

Wiley and Hindawi regret that the usual quality checks did not identify these issues before publication and have since put additional measures in place to safeguard research integrity.

We wish to credit our Research Integrity and Research Publishing teams and anonymous and named external researchers and research integrity experts for contributing to this investigation.

The corresponding author, as the representative of all authors, has been given the opportunity to register their agreement or disagreement to this retraction. We have kept a record of any response received.

### **References**

- [1] Y. Ding, Y. Wei, S. Zhang, and S. Yu, "Digital Image Restoration Based on Multicontour Batch Scanning," *Scanning*, vol. 2022, Article ID 8106516, 8 pages, 2022.

## Research Article

# Digital Image Restoration Based on Multicontour Batch Scanning

Yongsheng Ding , Yunbo Wei , Shuisheng Zhang , and Shihang Yu 

School of Science Qiqihar University, Qiqihar, Heilongjiang 161006, China

Correspondence should be addressed to Yongsheng Ding; 3100501039@caa.edu.cn

Received 30 July 2022; Revised 12 August 2022; Accepted 17 August 2022; Published 5 September 2022

Academic Editor: Balakrishnan Nagaraj

Copyright © 2022 Yongsheng Ding et al. This is an open access article distributed under the Creative Commons Attribution License, which permits unrestricted use, distribution, and reproduction in any medium, provided the original work is properly cited.

In order to explore the problem of digital image restoration, the authors propose a research on digital image restoration based on multicontour batch scanning. This method recommends key technical problems and solutions based on information represented by multicontour batch scans, exploring research in digital image restoration. Research has shown that the research on digital image restoration based on multicontour batch scanning is about 40% more efficient than traditional methods. Aiming at the new application of digital image inpainting, the application of image inpainting in image compression is studied in depth, and the technical principles of image inpainting and image compression are complemented.

## 1. Introduction

Digital image restoration technology is widely used because of its wide application background; it has become a popular research topic in the field of image processing in recent years [1]. In-depth research on digital image inpainting technology is carried out, and targeted improvements are proposed to improve the image inpainting quality, thereby enhancing the practicability of image inpainting [2]. The application of images is ubiquitous, and a large proportion of the information obtained by human beings in daily life comes from the visual system; with the vigorous development of the computer industry and the advent of the information age, the application value of images as a carrier of information is getting higher and higher. For example, the Bureau of Meteorology can study climate change and environmental pollution through satellite aerial images, and astronomers can study the laws of galaxies by observing astronomical images and observing cosmic celestial bodies such as black holes. Doctors in the hospital inspect relevant parts of the body by taking CT and MRI scans, and the public security department uses fingerprints, faces, and other images to identify and extract the basis for solving cases, etc.; the development of more and more technologies requires the use of images; it can be said that the development of modern technology is inseparable from images.

The concept of “image restoration” originally originated from the restoration of ancient paintings and other works of art [3]. Some cultural relics such as calligraphy and painting are damaged to a certain extent due to environmental factors, human factors, and other factors during the preservation process, such as scratches and missing [4]. The initial image restoration is to repair and fill in the damaged parts of the work by specialized experienced art maintainers; the purpose is to restore the damaged image into a complete and clear work as much as possible by means of image restoration, which is the predecessor of image restoration technology. There is undoubtedly a great risk in directly repairing the original precious artwork; some simple negligence and carelessness may lead to unpredictable consequences or even irreversible losses. With the realization and popularization of image digitization, a new restoration idea has emerged, which can scan the original work into digital form and store it in the computer and only need to use the image restoration technology to perform related processing on the scanned digital files. In this way, manipulation of the original work can be avoided, which greatly reduces the risk of repairing the image. In the above-mentioned “correlation processing,” image restoration technology plays a pivotal role; after years of research and development, digital image restoration technology has now developed into an increasingly mature subject.

Due to the advent of the mobile Internet era and the medical information revolution, images and videos have become more and more popular, and image processing has received more and more attention and has developed into a promising discipline [5]. Images will inevitably be damaged in the process of acquisition and transmission, which undoubtedly brings great difficulties to researchers. For different processing purposes, image processing is mainly divided into image enhancement, image restoration, image reconstruction, and image segmentation.

In recent years, the popular wavelet transform has developed very rapidly and has gradually become the frontier and hotspot in the field of image compression [6]. Wavelet transform takes into account the visual characteristics of the human eye while eliminating image redundancy and has a wide range of applications in the field of compression of static images and dynamic images [7]. The image compression of wavelet transform has greater advantages than discrete cosine transform, it has high compression ratio and no block effect, it has strong processing ability for detail noise and can display image data at multiple resolutions, and therefore, the image compression method based on wavelet transform replaces DCT and becomes a main research direction in the field of image compression. The current popular JPEG2000 is a new standard for image compression based on wavelet transform, as shown in Figure 1.

## 2. Literature Review

Jiao and Wu said that since images are a direct way for people to obtain information, the processing of images is particularly important [8]. With the development of modern science and technology, image processing technology has been widely used. Choi et al. said that in the field of medical research, radiography and micrographs have been used to diagnose diseases for a long time [9]. Jiu and Pustelnik said that at present, computer image processing has become an important processing method for disease diagnosis [10]. Agnes et al. said that the internal conditions of the body that were previously undetectable by general inspection methods can now be obtained by special medical imaging modalities [11]. One of the most representative diagnostic methods is X-ray CT (computed tomography). The development of digital image processing and reconstruction to today's level is mainly due to (1) the development of the computer itself. Early computers were difficult to meet the requirements of real-time processing of massive data in terms of processing speed and storage capacity. With the development of computer hardware and digital technology, the prices of computers, storage devices, and peripheral devices have dropped sharply, and their performance has been significantly improved. Processing that was previously only possible with mainframe computers is now possible with personal computers. (2) The development of mathematics. In particular, the emergence and development of discrete mathematics has laid a theoretical foundation for digital image processing.

Zheng believed that people usually process images in order to obtain high-quality images in order to achieve satisfactory results [12]. For example, removing noise in the image, enhancing or suppressing some parts of the image, or changing the brightness of the image thereby improves the quality of the image. Neilson et al. believe that extracting information or certain features contained in images to facilitate computer analysis is also a factor that people consider image processing, including preprocessing for computer vision [13]. Espriella et al. believe that the last reason is to facilitate the storage of images, so as to complete the encoding and shrinking of images [14]. Digital image processing mainly includes geometric processing, image coding, image enhancement, image restoration, image reconstruction, and image segmentation. Any image processing process can be simply modeled using an input-output system. Unfortunately, most image processing problems are ill-posed inverse problems that do not satisfy uniqueness, existence, or stability. Therefore, how to solve ideal solutions from these under-determined problems brings great challenges to people. Since the image is disturbed in the process of acquisition, transmission, or storage, the image will be degraded; for example, the image contains noise and is blurred. Therefore, prior knowledge of the degenerate system is used to construct suitable mathematical models to reduce or eliminate the distortion of the observed images, resulting in high-quality images that are easy to observe and study.

The idea of image restoration has a long history, but it is a relatively new topic in the field of image processing to be studied as a technology. Until 2000, the concept of image restoration (image inpainting) was introduced at the International Graphics Annual Conference, a more formal and internationally influential conference, formally proposed by Bertalmio et al. Since then, digital image restoration technology has become a general term for a type of work that uses computer programs to run autonomously, or to restore missing images with a small amount of human-computer interaction. Image restoration is not only a simple image processing problem but also involves many fields such as computer vision, computer graphics, and human visual psychology; there are many influencing factors and various processing methods, and because of its high practical value, it has attracted the research of many scholars; the related technology of digital image restoration has become a relatively popular research topic.

Because digital image restoration technology involves technologies in many fields, various research methods emerge one after another, and the classification of image restoration methods is also different based on different classification standards. According to different inpainting ideas and focus, digital image inpainting can be simply divided into two categories: structure-based inpainting methods and texture-based inpainting methods. Most of the structure-based image inpaintings are processing methods in the form of solving partial differential equations; the main idea is to imitate the skills of manual inpainting and gradually diffuse from the boundary of the missing area to the interior through an iterative method to achieve image filling. In the original repair scheme proposed, iterative repair is

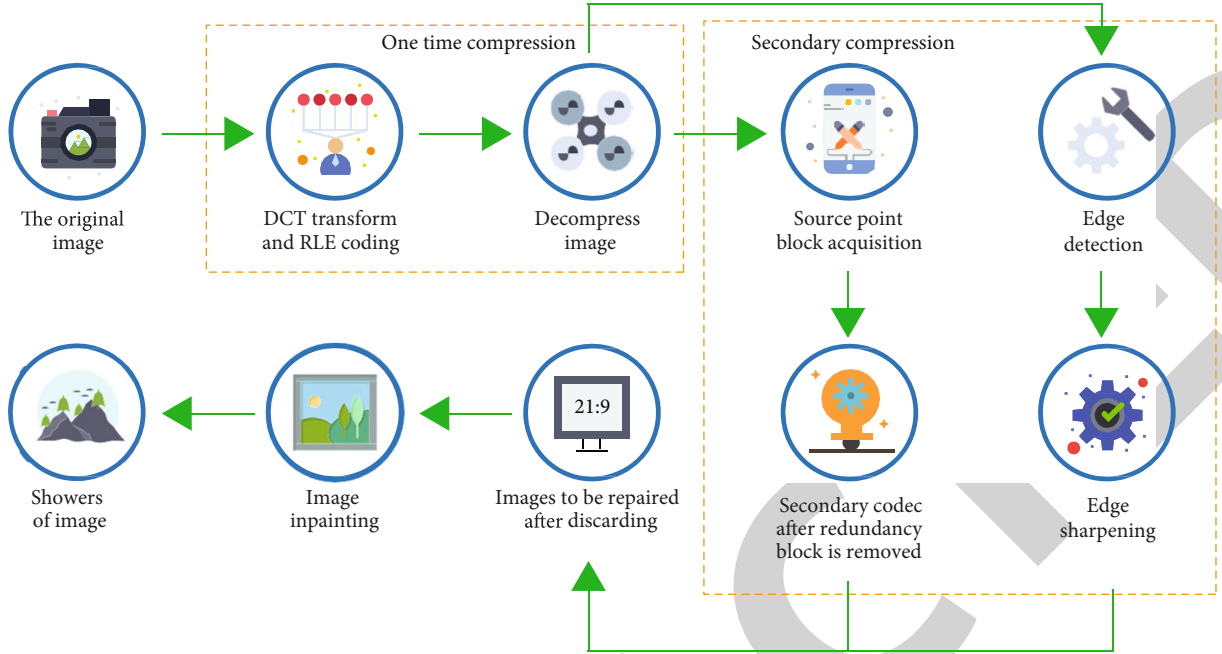


FIGURE 1: Compression scheme combining image inpainting and image compression.

performed in sequence from the outside to the inside along the isoilluminance line with a single pixel as the basic unit; the repair process is realized by solving a third-order PDE, which is based on an early classical approach to the structure of the BSCB model. The repair idea and mathematical modeling of the BSCB model are easy to understand and implement, but the repair feature of this repair method is based on pixels, which determines that the repair speed must be very slow, and the repair effect lacks overall beauty and coordination; therefore, the BSCB model is often only used as a reference model for image inpainting.

### 3. Methods

**3.1. The Process of Adding Blur and Poisson Noise.** Typically, blur and Poisson noise are added to the process, where  $u$  is the real image,  $H$  is the blurred point spread function (PSF), and Poisson represents the effect of Poisson noise [15, 16]. The formula for this problem is shown in

$$z = \text{Poisson}(Hu). \quad (1)$$

Degradation of acquired signals caused by Poisson noise is a common phenomenon in applications such as biomedical imaging, night vision, and astronomy [17, 18]. Therefore, Poisson noise removal is especially important for further processing such as image classification and recognition. Poisson noise is a type of signal-dependent noise. It is very different from Gaussian noise and does not satisfy the simple additivity principle, so the commonly used Gaussian noise removal algorithms cannot be directly applied to Poisson noise suppression. Specifically, assuming that the observed noise-contaminated image obeys a Poisson distribution, the

discrete probability is shown in

$$P(f|u_i) = \frac{e^{-u_i} u_i^f}{f!}. \quad (2)$$

In the subnetwork SubNet1, Taylor's formula and convolution operator are successively employed to simulate the generalization of the regular forward transform. More specifically, by introducing a transformation and applying Taylor's formula, it can be obtained as shown in

$$g_i = 2\sqrt{\frac{f_i + 3}{8}}. \quad (3)$$

The convolutional operator created by "Conv" is usually an integral part of the convolutional neural network architecture. Each convolutional layer is a neuron with learned weights  $\{w\}$  and biases  $\{b\}$ , as shown in

$$y_{i_2, j_2, d_2} = \text{Conv}(x)_{i_2, j_2, d_2}. \quad (4)$$

First, for stability purposes, the equation is generalized using the multiple "Conv" layers and summation operators in SubNet1, i.e., as shown in

$$g \approx \sqrt{\frac{6}{2}} + 2\sqrt{\frac{6\phi f}{3}}, \quad (5)$$

$$g \approx \text{Conv}(1) + \text{Conv}(f). \quad (6)$$

Suppose there is a damaged image  $I$ , the middle irregular area  $Q$  is the area to be repaired,  $t$  is the boundary, and the known area is in it. The repair process is an iterative process

TABLE 1: Correlation values between the first Conv convolutional layers of the training network.

	Conv-kernel-Gaussian	Conv-kernel-average	Conv-kernel-motion
Conv-kernel-Gaussian	1.01	0.89	0.88
Conv-kernel-average	0.81	1.04	0.83
Conv-kernel-motion	0.89	0.83	1.08

that gradually diffuses along the image boundary in a coarse-to-fine and external-to-interior manner, and its iterative equation can be expressed as

$$I^{n+1}(i, j) = I^n(i, j). \quad (7)$$

In the formula,  $n$  is the number of iterations,  $n + 1$  is the current number of iterations,  $(i, j)$  is the pixel coordinates in the two-dimensional image, and  $\Delta t$  is the step size of each iteration, which can usually be set to one constant value. The improvement amount is a key amount in the formula, which is directly related to the diffusion mode of the repair process; its calculation expression is shown in

$$I_t^n(i, j) = \overline{\delta L}(i, j) \overline{N}(i, j). \quad (8)$$

The CDD model is the curvature-driven diffusion model; on the basis of the TV model, the curvature-driven term  $s$  is introduced into the expression of the diffusion intensity factor; its mathematical expression is shown in

$$s = \nabla \left( \frac{\nabla I}{|\nabla I|} \right). \quad (9)$$

For the convenience of calculation, we can simply take  $g(|s|) = |s|$ , so as to obtain the repair expression of the CDD model as shown in

$$-\nabla \left[ \frac{g(|s|)}{|\nabla I|} \nabla I \right] + \chi(I - I_0) = 0. \quad (10)$$

The values in Table 1 show that the three convolutional filters are indeed similar in terms of quantitative metrics [19, 20]. In particular, the network trained with the Gaussian blur kernel is more correlated than the other two blur kernels. Second, the transform layer in the residual subnet contains not only smooth features but also some detailed features similar to noise. That is, the residual block does play a role in non-Gaussian noise removal, as shown in Table 1.

#### 4. Results and Analysis

For the convenience of comparison, the repair time and various repair indicators of the above three groups of experiments are listed in a table [21]. The number of repaired pixels of the image to be repaired is directly related to the repair time; the more pixels to be repaired, the longer the repair time is required. The total number of repaired pixels reflects the search range of the sample block, which indirectly affects the repair time; the ratio of repaired pixels to

total pixels can also reflect the difficulty of image repairing. The number of sample replications reflects the specific number of block replications in the repairing process; this parameter is determined by the average size of the replicated blocks, which can indirectly reflect texture complexity and structure information of the block to be repaired. The influence of the number of Poisson treatments to the number of sample replications on the repair time is also an important parameter worth referring to [22, 23]. It can be seen from Table 2 that the repair time of the three images to be repaired is in the unit of 100 seconds, which is within the acceptable range, and the proportion of repaired pixels to the total pixels is 3.5%, 6.8%, and 20.0%, different loss ratios represent different inpainting difficulties, and all three groups of images to be inpainted with different ratios have been inpainted, indicating that the proposed inpainting algorithm has good versatility [24, 25]. In the three groups of experiments, the number of Poisson processing accounts for about 20% of the total number of sample replications; it can be verified that Poisson processing indeed repairs only the outermost circle of sample blocks as expected. The algorithm repair indicators are shown in Table 2.

In the field of image restoration, there is currently no reliable and consistent objective evaluation standard for restoration effects; the most widely used in traditional restoration technology researchers is peak signal-to-noise ratio; since the object removal experiment does not have a known image as a comparison benchmark, this index cannot be calculated, so this objective evaluation criterion cannot be applied in the repair experiment in such a situation. This experiment uses a subjective evaluation criterion; that is, the observer evaluates the inpainted image without knowing the inpainted area [26, 27], as shown in Table 3.

As shown in Table 3, the repair method used in the experiment has achieved good results in terms of repair time and repair quality; the traditional Criminisi AIEI model has the shortest repair time; however, it is difficult to guarantee the repair quality for a specific image; the proposed improvement method improves the repair quality to a certain extent, but it increases the time cost significantly; the proposed improvement method can significantly improve the image repair quality without increasing too much repair time, which is an effective improvement scheme.

The discrete cosine transform can play a role in concentrating the data energy of the correlation in the image; after the DCT transform, the image information is concentrated in the upper left corner of the matrix; it represents the low-frequency component of the image, and most of the image information is reflected here. While most of the values in the lower right part are zero or near-zero fractional values, this information represents the high-frequency components



TABLE 2: Algorithm repair indicators.

Indicator records/experimental images	Table	Horse	Jumper
Repair time (s)	130.38	197.63	97.28
Repair pixel(s)	3426	6730	12690
Total pixels (pieces)	98304	98304	63448
Sample replication times (times)	134	212	225
Number of Poisson treatments (times)	35	49	40

of the image. Before performing inverse discrete cosine transform, discarding these coefficient values close to zero has little effect on the picture quality of the reconstructed image but achieves the purpose of expressing the image with less data, thus enabling the compression of image data [28].

After the original image is subjected to discrete cosine transform and some coefficients are discarded, the coefficient matrix is coded, and the compression method adopts relatively simple RLE coding. RLE coding is also known as run-length coding; during image coding, adjacent elements with the same pixel value in a specified direction are defined as a round, and the length of the retention is a continuous run, referred to as a run for short. The main principle of run-length coding is to represent the same value string in the image matrix with a representative value plus the run length, so that the representation length of the matrix data is smaller than the length of the original data, thereby realizing data compression.

The selection of reserved block and discarded block is a key step in image inpainting applied to image compression; if there are too few discarded blocks, it is not conducive to improving the compression ratio; and if there are too many reserved blocks, it is difficult to guarantee the repair effect. Especially if important feature blocks are discarded by mistake, it will cause no repair or obvious repair traces after repair. Therefore, the goal to be achieved in this step is to find the most suitable balance between discarding redundant blocks and retaining important feature blocks. The method adopted is to extract the edge of the compressed image first and then sharpen it; at the same time, the extreme points in the image block are counted; Finally, the pixel on the sharp edge and all the extreme points of the statistics are processed, that is, the expansion processing. Then all the selected blocks can be obtained and then the unselected blocks will be deleted.

The edge of an image generally refers to the position where the gray value of the image changes significantly, the principle of edge detection is usually realized by using the differences in gray, color, and texture characteristics between the object and the background; common detection operators include Prewitt operator, Robert operator, Sobel operator, and Canny operator.

The Canny edge detection operator can process image edges from multiple stages such as filtering, enhancement, and detection, and its gradient is calculated using the derivative of the Gaussian filter. First, smooth the image with a Gaussian filter, then calculate the magnitude and direction of the filtered image gradient, and then apply nonmaximum suppression processing to the gradient value; finally, the double threshold method is used to connect the edges.

Considering that the image matrix is composed of discrete pixels, the above operators all use the difference method to approximate the partial derivatives. The adopted edge detection and sharpening methods are as follows: first, the Sobel horizontal edge sharpening filter is used to extract and sharpen the image edge, and then, the Prewitt horizontal edge filter is used to extract and sharpen the image twice. Sharpening twice with different filters can obtain contours that are beneficial to inpainting. The source point of the image is a key point with strong structure, usually such a key point is a mathematical extreme point, and the extreme point includes a maximum point and a minimum point, and such key points are calculated and marked. The image to be repaired can be obtained by expanding the extracted and sharpened contours and the obtained source points by several pixel widths.

Table 4 is a comprehensive comparison of the three groups of experiments; after using the compression scheme of this experiment for compression and redundancy elimination, each can obtain different compression ratios. By vertical comparison, it can be found that the overall compression ratio is related to the encoding and decoding method used in the first compression and the redundancy elimination amount of the second “compression”, and the encoding and decoding processing of the first compression scheme of the three images and the redundancy elimination method in the second “compression” are the same, but since the redundancy of the three images themselves are different, this leads to the difference in the amount of culling, which directly leads to the difference in the compression rate. Horizontal comparison, the choice of the image restoration method after secondary “compression,” has a very important influence on obtaining a complete image; the CDD restoration model can be judged from the objective evaluation index of PSNR (peak signal-to-noise ratio); the AIEI repair model and the repair effect of the repair method used in the experiment show an increasing trend, as shown in Table 4.

Three sets of experiments demonstrate the feasibility of applying image inpainting to image compression; however, since the inpainting mechanism of image inpainting technology uses the correlation of the image itself, therefore, the prerequisite for applying image restoration technology to image compression is that the image content has a certain correlation. If the correlation of the image is large, a relatively large compression ratio can be obtained, but if the image itself is an image with low correlation and complex texture, the compression ratio obtained by this scheme will be correspondingly reduced. For example, the image in experiment 3 is relatively complex due to its relatively complex texture; the obtained compression ratio is lower than that of experiments 1 and 2.

The compression ratio obtained by this scheme is limited, and the highest compression ratio obtained in the three groups of experiments is less than 5:1, while the compression ratio that can be achieved by the existing mainstream compression standard JPEG is usually above 10:1; the emerging development of JPEG2000 can even achieve more, indicating that the compression ratio obtained by this

TABLE 3: Comparison of repair evaluation and repair time.

Experimental image/repair method		Criminisi repair	Regular Poisson processing fix	Repair method used in experiments
Table	Subjective evaluation (score/total score)	7.1/10.0	8.1/10	8.8/10
	Repair time (s)	11903	140.43	130.36
Horse	Subjective evaluation (number of approvals/sample)	6.2/10	6.5/10	8.1/10
	Repair time (s)	188.71	226.03	197.63
Jumper	Subjective evaluation (number of approvals/sample)	5.2/10	7.2/10	8.3/10
	Repair time (s)	90.23	112.81	97.28

TABLE 4: Comparison of compression and repair schemes.

Number of experimental groups	Original image size (KB)	Compressed size (KB)	Compression ratio (%)
Experiment 1	65.12	15.04	23.47
Experiment 2	65.27	14.78	22.92
Experiment 3	88.17	28.37	32.73

scheme cannot be compared with special compression standards. As far as the compression ratio is concerned, the application of digital image restoration technology to image compression cannot establish its own advantages, but the significance of this scheme is an attempt to a new compression idea other than traditional compression methods; from this perspective, the scheme of applying image inpainting to image compression enhances the flexibility of image compression techniques. Compared with traditional compression methods such as JPEG, the scheme applying image restoration to image compression has the capability of restoration processing in addition to compression. If the image itself is damaged after compression by JPEG compression, the desired image cannot be recovered due to no follow-up processing mechanism; on the contrary, this scheme can repair the damage caused by the compression itself due to subsequent repair processing; thus, the fault tolerance of compression can be enhanced.

At the same time, the compression ratio that can be obtained by this scheme is also directly related to the restoration capability of the image restoration technology; when the image is fixed, the reason why a higher compression ratio cannot be obtained is because the existing digital image restoration technology has considerable limitations on the restoration ability of compressed images. For the restoration after compression, the restoration algorithm obtains a better restoration effect than the CDD model and the AIEI model. The compression ratios obtained in the three sets of experiments are all the maximum values obtained under the premise that the repair algorithm studied can be repaired; that is, in the case of more discarded blocks, the existing repair algorithms have been difficult to complete the repair task. In theory, with the further development of image restoration technology, under the condition that the new repair technology has more powerful repair ability, a higher compression ratio can be obtained.

Since VST-Net-joint performs better than VST-Net-part, this section only discusses VST-Net-joint. Some variants of the network VST-Net-joint are studied from different

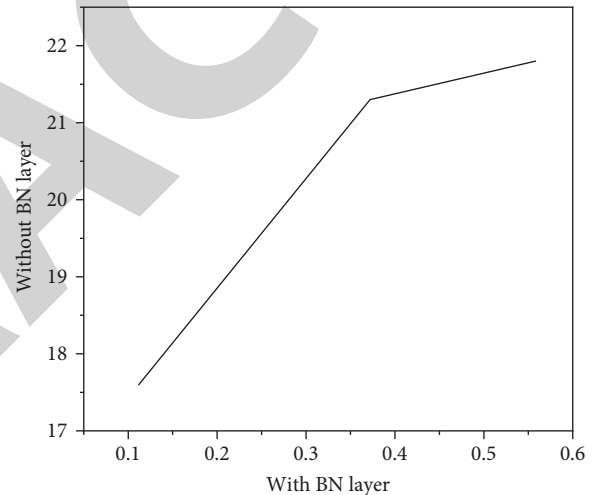


FIGURE 2: Average PSNR (dB) and SSIM values with/without BN in SubNet2.

aspects, i.e., with/without BN layers in SubNet2, the number of Conv layers in SubNet1 and SubNet3, and the number of channels and filter sizes in the entire network. First, the proposed networks with and without BN layers are compared in SubNet2. Figure 2 lists the average PSNR and SSIM values on Set11. It can be seen that in the network with BN layers, it can achieve better performance with regard to medium and large peaks. Conversely, in terms of peaks, better performance can be obtained in networks without BN layers. This phenomenon shows that the first stage used for variation stabilization is indeed imprecise, and the noise produced subsequently in the second stage is not exact Gaussian noise. BN layers are great for removing Gaussian noise, not for non-Gaussian noise, as shown in Figure 2.

## 5. Conclusion

Image restoration and reconstruction have always received extensive attention from researchers. Traditional algorithms

can achieve satisfactory results to a certain extent, but with the increasing maturity of convolutional neural networks, network learning algorithms have brought more research directions to people. The work mainly focuses on image restoration and reconstruction based on convolutional neural networks; first, the network is simply constructed; after the image deblurring has a certain effect, the network is improved to make it better applicable to Poisson image denoising task. Subsequently, medical CT images were explored.

The application of image restoration is studied, including conventional applications such as restoration of art works, cultural relics, photo text removal, and new applications such as relatively complex video transmission error concealment and virtual scene generation, the application feasibility of image inpainting in the above application fields is expounded, and relevant application examples are made by using the existing image inpainting technology. A “secondary compression” scheme is proposed by extracting and removing information from conventionally compressed images and then repairing the compressed images with restoration technology to obtain complete images for normal use.

## Data Availability

The data used to support the findings of this study are available from the corresponding author upon request.

## Conflicts of Interest

The authors declare that they have no competing interests.

## Acknowledgments

This study is funded by the Scientific Research Projects of Heilongjiang Provincial Education Department (135509313).

## References

- [1] X. M. Gao, Y. L. Li, B. L. Lu, Q. X. Xiong, and J. F. Li, “Estimation of spad value in waterlogged winter wheat based on characteristic indices of hyperspectral and digital image,” *Ying yong sheng tai xue bao = The journal of applied ecology/Zhongguo sheng tai xue xue hui, Zhongguo ke xue yuan Shenyang ying yong sheng tai yan jiu suo zhu ban*, vol. 32, no. 3, pp. 959–966, 2021.
- [2] B. S. Sindu, A. Thirumalaiselvi, and S. Sasmal, “Investigations on fracture related properties of strain hardened concrete using digital image correlation and acoustic emission techniques,” *European Journal of Environmental and Civil Engineering*, vol. 10, pp. 1–23, 2021.
- [3] S. Khalilzadehtabrizi, A. Seifiasl, and M. H. Asl, “Measurement of deformation patterns in steel plate shear walls subjected to cyclic loading based on multi-target digital image correlation (MT-DIC),” *Structure*, vol. 33, no. 8, pp. 2611–2627, 2021.
- [4] T. U. Haq, T. Shah, G. F. Siddiqui, M. Z. Iqbal, and H. Jamil, “Improved twofish algorithm: a digital image enciphering application,” *Access*, vol. 9, pp. 76518–76530, 2021.
- [5] G. Jing, Y. Du, R. You, and M. Siahkouhi, “Comparison study of crack propagation in rubberized and conventional prestressed concrete sleepers using digital image correlation,” *Proceedings of the Institution of Mechanical Engineers, Part F: Journal of Rail and Rapid Transit*, vol. 236, no. 4, pp. 350–361, 2022.
- [6] Y. Kai, T. Ogawa, Z. Wang, and Y. Adachi, “Strain distribution analysis of two perpendicular planes in sus310s austenitic stainless steel using digital image correlation,” *ISIJ International*, vol. 61, no. 1, pp. 481–486, 2021.
- [7] W. M. Ahmed, T. V. Verhaeghe, and A. P. McCullagh, “Maxillary complete-arch implant-supported restoration: a digital scanning and maxillomandibular relationship workflow,” *The Journal of Prosthetic Dentistry*, vol. 125, no. 2, pp. 216–220, 2021.
- [8] J. Jiao and L. Wu, “Image restoration for the mra-based pan-sharpening method,” *Access*, vol. 8, pp. 13694–13709, 2020.
- [9] K. Choi, J. S. Lim, and S. K. Kim, “Statnet: statistical image restoration for low-dose CT using deep learning,” *IEEE Journal of Selected Topics in Signal Processing*, vol. 14, no. 6, pp. 1137–1150, 2020.
- [10] M. Jiu and N. Pustelnik, “A deep primal-dual proximal network for image restoration,” *IEEE Journal of Selected Topics in Signal Processing*, vol. 15, no. 2, pp. 190–203, 2021.
- [11] S. S. Agnes, D. Akshaya, M. Kaviya, and K. Kiruthiga, “A comprehensive survey on crack detection of bone using various techniques,” *Bulletin of Scientific Research*, vol. 2, no. 2, pp. 1–7, 2020.
- [12] X. Zheng, “Rationality modeling of 3D scanning image of digital print laser based on block matching texture information repair,” *IEEE Sensors Journal*, vol. 20, no. 20, article 11975, p. 11982, 2020.
- [13] B. N. Neilson, C. M. Craig, R. Y. Curiel, and M. I. Klein, “Restoring attentional resources with nature: a replication study of Berto’s (2005) paradigm including commentary from Dr. Rita Berto,” *Human Factors: The Journal of Human Factors and Ergonomics Society*, vol. 63, no. 6, pp. 1046–1060, 2021.
- [14] M. C. Espriella, V. Lecours, P. C. Frederick, E. V. Camp, and B. Wilkinson, “Quantifying intertidal habitat relative coverage in a Florida estuary using UAS imagery and GEOBIA,” *Remote Sensing*, vol. 12, no. 4, pp. 677–717, 2020.
- [15] G. Song and H. Wang, “Artificial intelligence-assisted fresco restoration with multiscale line drawing generation,” *Complexity*, vol. 2021, no. 4, Article ID 5567966, p. 12, 2021.
- [16] N. H. Salman and S. Rafea, “The arithmetic coding and hybrid discrete wavelet and cosine transform approaches in image compression,” *Xinan Jiaotong Daxue Xuebao/Journal of Southwest Jiaotong University*, vol. 55, no. 1, pp. 1–9, 2020.
- [17] X. Wang, H. Wang, and S. Niu, “An intelligent forensics approach for detecting patch-based image inpainting,” *Mathematical Problems in Engineering*, vol. 2020, no. 8, Article ID 8892989, p. 10, 2020.
- [18] A. V. Sidorenko and I. V. Shakinko, “The digital watermarking algorithm using discrete chaotic maps,” *system analysis and applied information science*, vol. 2, no. 2, pp. 72–76, 2020.
- [19] V. Yatnalli, B. G. Shivaleelavathi, and K. L. Sudha, “Review of inpainting algorithms for wireless communication application,” *Engineering, Technology and Applied Science Research*, vol. 10, no. 3, pp. 5790–5795, 2020.

## Retraction

# Retracted: Injury Prevention Effect of MRI Imaging Technology in Physical Education and Sports Training

### Scanning

Received 11 July 2023; Accepted 11 July 2023; Published 12 July 2023

Copyright © 2023 Scanning. This is an open access article distributed under the Creative Commons Attribution License, which permits unrestricted use, distribution, and reproduction in any medium, provided the original work is properly cited.

This article has been retracted by Hindawi following an investigation undertaken by the publisher [1]. This investigation has uncovered evidence of one or more of the following indicators of systematic manipulation of the publication process:

- (1) Discrepancies in scope
- (2) Discrepancies in the description of the research reported
- (3) Discrepancies between the availability of data and the research described
- (4) Inappropriate citations
- (5) Incoherent, meaningless and/or irrelevant content included in the article
- (6) Peer-review manipulation

The presence of these indicators undermines our confidence in the integrity of the article's content and we cannot, therefore, vouch for its reliability. Please note that this notice is intended solely to alert readers that the content of this article is unreliable. We have not investigated whether authors were aware of or involved in the systematic manipulation of the publication process.

In addition, our investigation has also shown that one or more of the following human-subject reporting requirements has not been met in this article: ethical approval by an Institutional Review Board (IRB) committee or equivalent, patient/participant consent to participate, and/or agreement to publish patient/participant details (where relevant).

Wiley and Hindawi regrets that the usual quality checks did not identify these issues before publication and have since put additional measures in place to safeguard research integrity.

We wish to credit our own Research Integrity and Research Publishing teams and anonymous and named external researchers and research integrity experts for contributing to this investigation.

The corresponding author, as the representative of all authors, has been given the opportunity to register their agreement or disagreement to this retraction. We have kept a record of any response received.

### References

- [1] J. Liu, "Injury Prevention Effect of MRI Imaging Technology in Physical Education and Sports Training," *Scanning*, vol. 2022, Article ID 9991523, 6 pages, 2022.

## Research Article

# Injury Prevention Effect of MRI Imaging Technology in Physical Education and Sports Training

Jianxin Liu 

Pingdingshan University, Pingdingshan, Henan 467000, China

Correspondence should be addressed to Jianxin Liu; 20150235127@mail.sdufe.edu.cn

Received 29 July 2022; Revised 12 August 2022; Accepted 17 August 2022; Published 31 August 2022

Academic Editor: Balakrishnan Nagaraj

Copyright © 2022 Jianxin Liu. This is an open access article distributed under the Creative Commons Attribution License, which permits unrestricted use, distribution, and reproduction in any medium, provided the original work is properly cited.

In order to solve the problem of observing and analyzing the clinical value of MRI diagnosis in patients with knee sports injury and guiding clinical targeted treatment, the author proposed a sports injury prevention method in sports training teaching based on MRI image observation. This method retrospectively analyzed the imaging data of 101 patients with knee joint MRI examination due to osteoarthritis, sports injury and synovitis in joint surgery, and arthroscopic exclusion of true meniscus tear, MR multisequence and multiplane scans were performed to observe the anatomical features of TGL and MFL images and the occurrence rate of the lateral meniscus “false tear sign,” and the  $\chi^2$  test was used to compare the occurrence rate of “pseudo-tear sign” between genders and sides. Experimental results show that the incidence of TGL on MRI was about 67.3% (68/101), and the incidence of “pseudo-tear sign” in the anterior horn of the lateral meniscus caused by TGL was 2.9% (2/68). The overall appearance rate of MFL on MRI was 91.1% (92/101), the appearance rate of plate anterior ligament (HL) was 13.9% (14/101), and the occurrence rate of “pseudo-tear sign” in the posterior horn of the lateral meniscus caused by HL was 7.1% (1/14). The occurrence rate of the posterior ligament (WL) was 77.2% (78/101), and the incidence of “pseudo-tear sign” in the posterior horn was 20.5% (16/78). According to the shape and course of TGL and MFL on MRI, and the direction and position of the lateral meniscus pseudotear, combined with MRI sagittal plane and coronal plane observation, it can effectively identify the true and false attributes of lateral meniscus anterior and posterior horn tears, thereby reducing unnecessary surgical treatment.

## 1. Introduction

In daily physical education training, it can not only improve the physical quality of students but also master training techniques to provide help for the healthy development of students' bodies; in special sports, many students enjoy the fun of sports and will also be injured during exercise. With the continuous innovation and reform of physical education, higher requirements are put forward for students' physical quality. Therefore, through the analysis of the situation and causes of sports injuries, students are reminded to pay attention to the possibility of preventing injuries, in order to ensure their own safety [1]. In daily sports training, the main reason for students' injury in sports training lies in their physical fitness. Students lack of systematic exercise, resulting in excessive muscle tension and excitement during training, resulting in poor physical coordination; therefore,

the muscle strength of the students is insufficient, resulting in some impairment of sports training activities. In addition, the students are unable to respond quickly to the movement due to technical factors, resulting in poor flexibility of the limbs and substandard movements, which can easily cause the body to lose balance and eventually cause injury. Students will also suffer from unresolved fatigue of the body, which will affect their subsequent training, or train and compete with injuries, resulting in more injuries. In sports training, students lack coordination and cooperation with each other, resulting in the phenomenon of limb collision leading to injury [2]. Figure 1 shows the sports injury prevention method. The knee joint is a vital weight-bearing joint in the human body with a complex structure. Once it is over-exercised, it may cause knee joint injury, which will not only cause local pain and discomfort in the patient's knee joint but also damage the surrounding tissues. Although CT and



FIGURE 1: Sports injury prevention.

TABLE 1: Occurrence rate of transverse knee ligament and anterior and posterior ligaments of femoral plate in 101 patients.

Side exception	Transverse knee ligament	Anterior plate femoral ligament	Plate posterior ligament
Left knee 43	29 (67.4%)	5 (11.6%)	32 (74.4%)
Right knee 58	39 (67.2%)	9 (15.5%)	46 (79.3%)
Total 101	68 (67.3%)	14 (13.9%)	78 (77.2%)
$\chi^2$ value	0.000	0.313	0.336
$P$ value	0.983	0.576	0.562

X-ray have certain value for the diagnosis of knee joint injury, their spatial resolution is poor, and it is difficult to accurately judge the degree of knee joint injury. Arthroscopy, the “gold standard” for diagnosis, although it can help clinically identify the actual damage of the knee joint, in-depth analysis of the anatomical structure can guide effective clinical diagnosis and treatment, but it is more invasive, and is likely to cause greater trauma to the physical and mental health of patients, limiting its clinical application [3]. MRI is noninvasive. This not only enables multiplanar imaging but also has high soft tissue resolution, which can clearly observe the cruciate ligament meniscus, synovial membrane, articular cartilage and joint capsule, and other tissues. So, the process of clinical diagnosis of patients with knee sports injury has been widely used.

## 2. Literature Review

There is a risk of injury in sports training, most of which are due to the insufficient preparation of the trainee, the incompatibility of the trainee’s physical reserve and the training intensity, the irregular training venue, and the imperfect training facilities or disrepair. Among them, the personal physical quality and skill level of trainees vary from person to person; so, the probability of sports injury risk for different training objects is also different. In the process of training, some common training mistakes can easily lead to sports injuries [4]. For example, the preparatory activities before training are insufficient and unreasonable, and the coaches ignore the necessity of proper relaxation during the training process and arranged a lot of load sports that do not match the physical fitness level of the trainees, some athletes insisted on training with injuries in order to

improve their competition performance and competitive skills, and the coaches did not organize training programs, especially confrontational training programs. Athletes’ physical factors limit their athletic ability to a certain extent; if athletes and coaches do not realize this, and arrange training programs that are not in line with their own physiological level, it is very easy to cause sports injuries [5]. Physiological factors mainly include muscle strength, flexibility, sensitivity, coordination, injury history, and degree of fatigue [6]. Among them, the main reasons for sports injuries are insufficient muscle strength, insufficient flexibility, and excessive fatigue of the body. The knee joint is the largest and most complex joint in the human body, due to sports injuries, high-energy injuries, and degenerative changes, and the meniscus is prone to damage. MRI can perform multidirectional, arbitrary cross-section, and multiparameter imaging and has high resolution of soft tissue density. It is currently the best method for noninvasive diagnosis of meniscus injury [7]. In the clinical practice of joint surgery, preoperative knee MRI is sometimes misjudged as “pseudo-tear sign.” “Pseudo-tear sign” is often manifested in the lateral meniscus. The formation of the “pseudo-tear sign” in the anterior horn of the lateral meniscus is often related to the course of the transverse knee ligament (TGL), and the cause of the “pseudo-tear sign” in the posterior horn of the lateral meniscus is often related to the course of the menisco-femoral ligament (MFL). MFL can be divided into anterior ligament (Humphrey’s ligament, HL) and posterior ligament (Wrisberg’s ligament, WL) according to the location of the insertion point [8]. Although TGL, HL, and WL have gradually attracted attention, there is still a lack of quantitative research on these three ligament systems. The author retrospectively analyzed the MRI data of 101 knee joint subjects, counted the occurrence rate of TGL, HL and WL, and observed the cross-sectional morphology of TGL, HL and WL, the midpoint sagittal diameter and coronal diameter were measured, and the fascicles of the three ligaments and the occurrence rate of the lateral meniscus “pseudo-tear sign” were calculated to improve the understanding of TGL, HL, and WL, establish an effective identification method for true and false tears in the anterior and posterior horns of the lateral meniscus caused by TGL, HL, and WL, and avoid unnecessary surgery such as arthroscopy [9].

## 3. Methods

3.1. *Information.* The data of 101 adult patients who underwent MRI examination due to knee joint degeneration,

TABLE 2: The transverse ligament of the knee and the midpoint diameter of the anterior and posterior ligaments of the plate and femur.

Midpoint diameter (mm)	Ligament name					
	Transverse knee ligament		Anterior plate femoral ligament		Plate posterior ligament	
	Sagittal diameter	Coronal diameter	Sagittal diameter	Coronal diameter	Sagittal diameter	Coronal diameter
	1.88 ± 0.35	1.79 ± 0.60	1.53 ± 0.39	2.82 ± 0.92	2.04 ± 1.03	3.1 ± 1.08

TABLE 3: The course of the transverse knee ligament and the anterior and posterior ligaments of the plate and femur.

Way of walking	Transverse knee ligament	Ligament name	
		Anterior plate femoral ligament	Plate posterior ligament
Loose	57 (83.82%)	2 (14.29%)	28 (35.90%)
Compact	11 (16.18%)	12 (85.71%)	50 (64.10%)

traffic accident injury, sports injury, etc. were selected for retrospective analysis; among them, there were 60 males and 41 females, with an average age of 42 (18-75) years old, 43 left knees, and 58 right knees. Inclusion criteria were as follows: age  $\geq 18$  years old; MRI data were complete; arthroscopic examinations were completed, and meniscus tears were excluded [10]. Exclusion criteria were as follows: severe knee trauma, severe degeneration, and significant motion artefacts indicated by arthroscopy and/or MRI.

### 3.2. Inspection Method

**3.2.1. MR Scanning Method and Sequence Parameters.** The German-made Siemens Verio 3.0T superconducting MR machine and the wrapped surface coil are used for scanning. The patient was placed in the supine position with the knee extended, the center of the coil was positioned at the level of the lower border of the patella, and the knee was fixed with a plastic fixator. Sagittal, coronal, and axial scans of the knee joint were routinely performed. Scanning sequence and parameters were as follows: conventional scanning sagittal, coronal, and axial [11]. Sagittal PDW-TSE-SPiR were as follows: TR1500 ms, TE15 ms, slice thickness 4 mm, slice spacing 0.4 mm, matrix  $216 \times 512$ , and FOV150 mm. Sagittal TSE-T1WI were as follows: TR400 ms, TE9 ms, slice thickness 3 mm, slice spacing 0.4 mm, matrix  $384 \times 256$ , and FOV 150 mm. Coronal FS-PDWI were as follows: TR3600 ms, TE29 ms, layer thickness 3 mm, layer spacing 1 mm, matrix  $448 \times 320$ , and FOV150 mm. Coronal TSE-T2WI were as follows: TR4000 ms, TE61.6 ms, layer thickness 3 mm, layer spacing 1 mm, matrix  $352 \times 288$ , and FOV150 mm. Cross-sectional FS-T2WI were as follows: TR4000 ms, TE80 ms, layer thickness 1 mm, layer spacing 1 mm, matrix  $352 \times 288$ , and FOV150 mm [12].

**3.2.2. Observation Method.** One each of the chief physicians of the Department of Radiology and the Department of Joint Surgery and the occurrence rate of TGL, HL and WL were observed on MRI multisequence and multiplanar images by single-blind method, the running mode, cross-sectional shape, midpoint diameter, and beam splitting, whether there

is a “pseudo-tear sign” in the anterior and posterior angles of the lateral meniscus, etc. [13]. If the result is a quantitative index, it will be measured twice and averaged for statistical analysis. If the qualitative index of observation is inconsistent, it will be determined after discussion.

**3.2.3. Definition of Midpoint Diameter and Determination of Anatomical Landmarks.** The midpoint diameter defined by the author is divided into midpoint sagittal diameter and midpoint coronal diameter. The midpoint sagittal diameter refers to the anteroposterior diameter (width) of the ligament observed in the sagittal plane; in order to unify the observation plane, a standardized plane that is clearly displayed on the anterior and posterior cruciate ligaments is selected for measurement. The midpoint coronal diameter refers to the upper and lower diameter (thickness) of the ligament observed in the coronal plane; in order to unify the observation plane, a standardized plane above the intercondylar spine that clearly shows the observed ligament is selected for measurement [14].

**3.3. Data Statistical Processing.** SPSS 16.0 statistical software was used for data processing. Measurement data obeyed or approximately obeyed normal distribution, expressed as  $(\bar{x} \pm s)$ , count data were analyzed by  $\chi^2$  test, and  $P < 0.05$  was considered statistically significant.

The  $\chi^2$  test is a widely used hypothesis test method, but it is often used in the hypothesis test of categorical count data in medical papers; that is, for the comparison of the rate of two specimens, the rate of multiple specimens, the internal structure of the specimen, and the rate of specimens, compared with the overall rate, the actual distribution of a phenomenon is compared with its theoretical distribution [15]. However, when the samples meet the normal approximation conditions, such as the number of samples  $n$  and the sample rate  $p$  meet the conditions  $np$  and  $n(1-p)$  that are greater than 5, the hypothesis test statistic  $u$  value can be calculated to make judgments. Commonly used  $\chi^2$  test is divided into the following categories: ①  $2 \times 2$  table  $\chi^2$  test: applicable to the comparison of 2 specimen rates or composition ratios and ② paired data  $\chi^2$  test: it is suitable for the comparison of the ratios or composition ratios of two samples in a paired design, that is, whether there is a significant difference between the two treatment results through the data of a single sample; ③  $R \times C$  table  $\chi^2$  test is suitable for the comparison of the ratios or composition ratios of multiple samples [16].

**3.4. Identification Method.** (1) Observe the lateral meniscus image in successive slices on the sagittal plane image. Pseudotears of the meniscus are discontinuous and mostly

TABLE 4: Cross-sectional morphology of transverse knee ligament and anterior and posterior plate femoral ligaments.

Example	Round	Oval	Flat	Short stick	Irregular shape
Knee transverse ligament (68)	23 (33.8%)	31 (45.6%)	2 (2.9%)	2 (2.9%)	10 (14.7%)
Anterior plate femoral ligament (14)	1 (7.1%)	6 (42.8%)	5 (35.7%)	1 (7.1%)	1 (7.1%)
Posterior plate femoral ligament (78)	2 (2.6%)	12 (15.4%)	28 (35.9%)	9 (11.5%)	27 (34.6%)

TABLE 5: The transverse ligament of the knee and the anterior and posterior ligaments of the plate and femoral ligament.

Example	1 bunch	2 bunches	$\geq 3$ beams
Knee transverse ligament (68)	62 (91.2%)	4 (5.9%)	2 (2.9%)
Anterior plate femoral ligament (14)	9 (64.3%)	3 (21.4%)	2 (14.3%)
Posterior plate femoral ligament (78)	66 (84.6%)	11 (14.1%)	1 (1.3%)

confined to the vicinity of the anterior and posterior horns of the meniscus, while TGL and MLF can be displayed continuously on other sagittal planes. (2) Observe the running direction and appearance position of the linear high signal [17]. The running direction of true meniscus tear is complex, and its location is not constant, while the running direction of pseudotear caused by TGL band is from the back to the front, and it is fixed at the anterior horn of the meniscus. The linear running direction of the pseudotear caused by MLF is one of the following two directions: one is from the posterior superior border of the lateral meniscus to the posterior and inferior, and the other is fixed in the vertical direction of the medial part of the posterior corner of the lateral meniscus. (3) Observation of meniscus morphology is as follows: in a true tear, the meniscus is irregularly shaped and appears to be completely hyperintense. However, in the pseudotear of the anterior and posterior horns of the lateral meniscus caused by TGL and MLF, there is no abnormality in the lateral meniscus itself, and the edges of the lateral meniscus are smooth and maintain a regular “bow tie” shape. (4) The role of coronal position in the identification of true and false tears: coronal images often show the full picture of TGL and MLF; in the true meniscus tear, high signal can be observed in both the sagittal and coronal views, while the pseudotear coronal view has wireless-like high signal between the TGL and MLF and the lateral meniscus [18]. The purpose of this study was to systematically observe the lateral meniscus “pseudo-tear sign” and related TGL and MLF by MRI and deepen the understanding of TGL and MLF imaging anatomy, the mechanism of the false tear sign of the lateral meniscus of the knee joint in MRI was discussed, and an effective method for identifying the true and false tear of the lateral meniscus was established.

#### 4. Results and Analysis

Among the 101 knees in this group, TGL was observed on MRI in 68 cases, the incidence rate of TGL was 67.3%, the incidence of TGL in the left knee was 67.4%, and that in the right knee was 67.2%. HL was observed on MRI in 14 cases, and the incidence of HL was 13.9%; among them,

the incidence of HL in the left knee was 11.6%, and the incidence of HL in the right knee was 15.5%. WL was observed in 78 cases on MRI, and the incidence of WL was 77.2%; among them, the incidence of WL in the left knee was 74.4%, and the incidence of WL in the right knee was 79.3% [19]. Three target ligaments appeared at the same time in 2 cases, accounting for 2.0%, and in 5 cases, none of the three ligaments appeared, accounting for 5.0%. There was no significant difference in the occurrence rates of TGL, HL, and WL between the left and right sides (all  $P$  values  $>0.05$ ), see Table 1.

In sagittal MRI, the TGL is located anterior to the tibiofemoral joint and posterior to the infrapatellar fat pad, and the mean midpoint diameter of the TGL is as follows: sagittal diameter ( $1.88 \pm 0.35$ ) mm and coronal diameter ( $1.79 \pm 0.60$ ) mm. The walking patterns can be divided into two types: the first one is the common one, which is loosely related to the tibial plateau; that is, it passes through the middle of the infrapatellar fat pad, and there are 57 cases of this type, accounting for 83.8% (57/68); the other one is less common, which is closely related to the tibial plateau, that is, crawls on the articular surface of the tibial plateau, and there are 11 cases of this type, accounting for 16.2% (11/68). In the sagittal view, the cross-sectional morphology of TGL was oval in 45.6% (31/68), round in 33.8% (23/68), irregular in 14.7% (10/68), and flat in 2.9% (2/68), the short bar accounts for 2.9% (2/68) and 91.2% (62/68) of TGLs were single beam, 5.9% (4/68) were two beams, and 2.9% (2/68) were three beams or more, and the midpoint diameter of the three ligaments measured by MRI is shown in Table 2 [20].

The HL originates from the medial border of the posterior horn of the lateral meniscus, runs obliquely inward and upward through the posterior cruciate ligament, and ends in front of the posterior cruciate ligament on the lateral side of the medial condyle of the femur. The mean midpoint diameter of HL was as follows: sagittal diameter ( $1.53 \pm 0.39$ ) mm and coronal diameter ( $2.8 \pm 0.92$ ) mm. There are two ways of HL running: the first type was closely related to the posterior cruciate ligament, accounting for 85.7% (12/14) in 12 cases. The other type was loosely related to the posterior



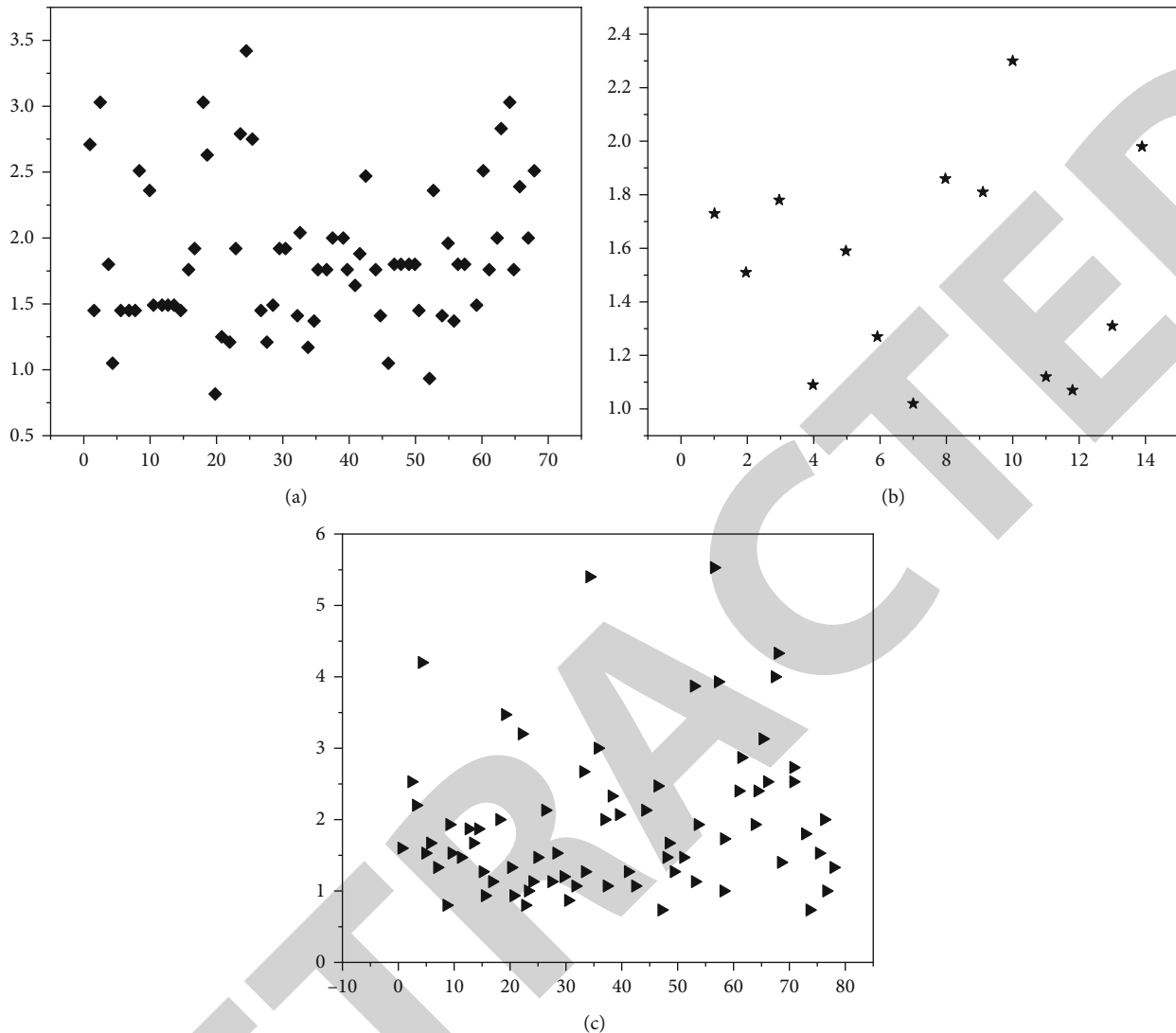


FIGURE 2: Scatter distribution of the midpoint diameter of the transverse knee ligament and the anterior and posterior ligaments of the plate and femur. (a) Sagittal diameter at the midpoint of the transverse ligament of the knee. (b) Sagittal diameter at the midpoint of the anterior femoral ligament. (c) Sagittal diameter at the midpoint of the posterior femoral ligament.

cruciate ligament, accounting for 14.3% (2/14) in 2 cases. The cross-sectional morphology of HL was observed in the sagittal view: 42.9% (6/14) were oval, 35.7% (5/14) were flat, and 7.1% were round, short rod, and irregular (1/14/14). HL splitting was as follows: 9 cases of single bundle, accounting for 64.3%, 3 cases of two bundles, accounting for 21.4%, and 2 cases of three bundles or more, accounting for 2.9%, and the running mode is shown in Table 3.

The WL originates from the medial edge of the posterior horn of the lateral meniscus, is located posterior to the HL, and continues upward obliquely through the posterior cruciate ligament, ending at the rear of the posterior cruciate ligament on the lateral side of the medial femoral condyle. The mean midpoint diameter of WL was as follows: sagittal diameter ( $2.04 \pm 1.03$ ) mm and coronal diameter ( $3.10 \pm 1.08$ ) mm. WL can also be divided into two types: one is closely related to the posterior cruciate ligament, 50 cases of this type, accounting for 64.1% (50/78); among

them, 11 cases were directly merged into the posterior cruciate ligament, accounting for 14.1% (11/78). A loose type is related to the posterior cruciate ligament, 28 cases of this type, accounting for 35.9% (28/78). The WL cross-sectional morphology observed in the sagittal view was as follows: the flat shape accounted for 35.9% (25/78), the irregular shape accounted for 34.6% (27/78), the oval shape accounted for 15.4% (12/78), and the short rod shape had 11.5% (9/78) and 2.6% (2/78) round. WL beam splitting was as follows: 66 cases of single beam, accounting for 84.6%, 11 cases of two beams, accounting for 14.1%, 1 case of three beams or more, accounting for 1.3%, the cross-sectional shape is shown in Table 4, the beam splitting is shown in Table 5, and the scatter distribution of the midpoint diameter is shown in Figures 2(a)–2(c).

In Figure 2, (a) is the scatter diagram of the midpoint sagittal diameter of the transverse ligament of the knee, (b) is the distribution of the midpoint sagittal diameter of the

## Retraction

# Retracted: Application of MRI in the Prevention of Sports Injuries in Physical Education Teaching

### Scanning

Received 20 June 2023; Accepted 20 June 2023; Published 21 June 2023

Copyright © 2023 Scanning. This is an open access article distributed under the Creative Commons Attribution License, which permits unrestricted use, distribution, and reproduction in any medium, provided the original work is properly cited.

This article has been retracted by Hindawi following an investigation undertaken by the publisher [1]. This investigation has uncovered evidence of one or more of the following indicators of systematic manipulation of the publication process:

- (1) Discrepancies in scope
- (2) Discrepancies in the description of the research reported
- (3) Discrepancies between the availability of data and the research described
- (4) Inappropriate citations
- (5) Incoherent, meaningless and/or irrelevant content included in the article
- (6) Peer-review manipulation

The presence of these indicators undermines our confidence in the integrity of the article's content and we cannot, therefore, vouch for its reliability. Please note that this notice is intended solely to alert readers that the content of this article is unreliable. We have not investigated whether authors were aware of or involved in the systematic manipulation of the publication process.

In addition, our investigation has also shown that one or more of the following human-subject reporting requirements has not been met in this article: ethical approval by an Institutional Review Board (IRB) committee or equivalent, patient/participant consent to participate, and/or agreement to publish patient/participant details (where relevant).

Wiley and Hindawi regrets that the usual quality checks did not identify these issues before publication and have since put additional measures in place to safeguard research integrity.

We wish to credit our own Research Integrity and Research Publishing teams and anonymous and named external researchers and research integrity experts for contributing to this investigation.

The corresponding author, as the representative of all authors, has been given the opportunity to register their agreement or disagreement to this retraction. We have kept a record of any response received.

### References

- [1] J. Zhao, "Application of MRI in the Prevention of Sports Injuries in Physical Education Teaching," *Scanning*, vol. 2022, Article ID 7738233, 6 pages, 2022.

## Research Article

# Application of MRI in the Prevention of Sports Injuries in Physical Education Teaching

Jing Zhao 

Department of Public Physical Education, Taiyuan University, Shanxi, China 030032

Correspondence should be addressed to Jing Zhao; 2020212360@mail.chzu.edu.cn

Received 21 July 2022; Revised 12 August 2022; Accepted 17 August 2022; Published 29 August 2022

Academic Editor: Balakrishnan Nagaraj

Copyright © 2022 Jing Zhao. This is an open access article distributed under the Creative Commons Attribution License, which permits unrestricted use, distribution, and reproduction in any medium, provided the original work is properly cited.

In order to explore the situation of ankle sports injury in physical education, the author proposed the application method of MRI in sports injury prevention in physical education. In a retrospective analysis of 28 patients with clinically diagnosed ankle injuries, taking ankle arthroscopy/incision as the standard, the sensitivity and diagnostic value of MRI examination for ankle sports injury were analyzed statistically. The result shows that 6 cases of ankle fracture were correctly diagnosed by MRI, and the diagnostic sensitivity for bone marrow contusion and edema was 100%. Among the 19 cases of clinically diagnosed ankle ligament injury, 16 cases were diagnosed by MRI, and the overall sensitivity was 84%. Of the 8 cases of calcaneofibular ligament injury, 6 cases were correctly diagnosed by MRI, with a sensitivity of 75%. *Conclusion.* 3.0 T MRI examination has high sensitivity for ligament, tendon, and cartilage injury, which can well show ankle joint injury and provide an objective basis for early clinical treatment and rehabilitation.

## 1. Introduction

It is the obligatory responsibility and obligation of schools and society to create a safe campus physical education environment, strengthen the safety management of the campus body and teaching environment, and carry out campus sports safety education activities for teachers and students [1]. At present, the country is paying more and more attention to sports, and the variety of campus sports activities has also increased; students also like sports more and love sports; physical education is playing an increasingly important role in quality education; lack of certain sports hygiene knowledge, sports safety knowledge, and emergency measures after sports injuries often cause unnecessary pain after injury. In physical education, sports injury accidents occur from time to time, which not only directly damages the physical and mental health of students but also contradicts the purpose of “health first” in physical education. And one of the biggest obstacles for students to carry out sports practice is the occurrence of sports injuries in campus sports teaching activities.

Sports injury is a difficult problem that needs to be faced in physical education; this phenomenon has seriously

affected the normal progress of physical education; the occurrence of sports injuries in physical education activities has caused students to be physically and mentally injured to varying degrees, adding a heavy burden. It directly affects students' learning and life [2]. As the organizer of physical education, physical education teachers should consider all aspects; it is very important to take the initiative to prevent the occurrence of sports injuries and to deal with them promptly and correctly. The occurrence of sports injuries is not scary; its serious impact is that it is difficult to recover from the impact on the students themselves, and later, sports injuries may leave a shadow on the students' minds, so that students are afraid of physical education classes and are tired of physical education classes.

## 2. Literature Review

Asselin et al. found that the clinical diagnostic accuracy of the drawer test was the lowest among the three tests in 85 patients with anterior cruciate ligament injury; nevertheless, the drawer test is still widely used in clinical practice because of its simple implementation application [3]. Prasanna et al. combined mechanical testing with a noncontact full-field

strain measurement system and quantified the surface strain distribution of the anterolateral collateral ligament and the functional movement of the knee joint; it is of great significance to study the rupture mechanism of the anterolateral collateral ligament [4]. Vidhya et al. reconstructed the three-dimensional anatomical structure of the hip joint by CT and found that the center of the femoral ball head of DDH patients was more anterior, superior, and lateral than normal people, which provided an anatomical reference for the treatment and classification of DDH patients [5]. By comparing the preoperative and postoperative CT images of DDH patients, Weiss et al. found that the preoperative hip anatomical parameters could predict the postoperative hip anteversion angle, which provided a reference for the formulation of the surgical plan [6]. CT also has its limitations. It has poor imaging effects on soft tissues such as cartilage, ligaments, and muscles; therefore, when using CT for joint function evaluation, it is generally only from the perspective of bone.

MRI is also a tomography technology (Figure 1); its principle is through the application of high-intensity magnetic field and radio frequency field, using atomic nuclear magnetic resonance (NMR) to scan specific parts of the human body; compared with CT technology, MRI has no ionizing radiation and is harmless to human tissues and organs, and MRI technology can image different human tissues in a targeted manner by setting different imaging parameters and can clearly image soft tissues, providing more abundant joint anatomy than CT for orthopedic information. Clement et al. collected MRI image data of knee joint of 180 patients with anterior cruciate ligament injury; by measuring the position of the anterior cruciate ligament on the femur and tibia in three-dimensional MRI images, it was found that the insertion point of the anterior cruciate ligament on the femur location is a susceptibility factor for its noncontact injury [7]. This study well demonstrates the advantages of MRI in imaging joint anatomy; excellent spatial resolution and clear ligament imaging are the prerequisites for this study; compared with CT, MRI has great advantages in both areas. Nielsen et al. quantified the T2 relaxation time of knee articular cartilage using T2-mapping sequence, a quantitative MRI technique, which found that OA patients had higher T2 relaxation time of articular cartilage compared to healthy individuals and found that T2 mapping can distinguish OA of different severity, indicating that this technology can reflect the level of knee cartilage degeneration [8]. Toomey et al. used glycosaminoglycan chemical exchange saturation transfer (gagCEST) imaging technique to measure a total of 96 lumbar intervertebral discs in 24 volunteers; the gagCEST signal was found to be higher in degenerated discs, indicating that this technique can quantify disc degeneration [9]. Different quantitative MRI techniques have different sensitivities to the biochemical components of joint tissue, so different quantitative MRI detection methods are often used for different diseases.

MRI has the advantage of the best soft tissue resolution for complex soft tissue anatomy and can display image resolution in multidirectional imaging and can simultaneously

display abnormal signal changes after bone marrow injury. The author aims to provide an objective basis for the early clinical treatment of ankle sports injury and its rehabilitation and focuses on evaluating the diagnostic ability of MRI for ankle injury in 28 cases.

### 3. Research Methods

*3.1. General Information.* A retrospective analysis of 28 hospitalized cases of ankle injury from January 2018 to December 2021 in the department of orthopedics in a hospital was done, all of which received ankle arthroscopy or/and arthrotomy. Twenty-eight injured ankles had complete medical records and preoperative MRI examination data; 19 were males and 9 were females (Figure 2), ranging in age from 16 to 70 years old, with an average age of 42 years. Clinical manifestations: all affected ankle joints have a clear history of injury, manifested as ankle joint swelling, pain, and limited mobility. Among them, 6 cases were sprained while walking, and 22 cases were sports injuries (Figure 3); 17 cases were left ankle, and 11 cases were right ankle (Figure 4), postinjury ankle pain, swelling, subcutaneous ecchymosis, lameness, local tenderness, and positive ankle inversion test [10]. The 28 injured ankle joints were routinely taken anterior and lateral ankle X-rays before operation; among them were 5 cases of medial malleolus or/lateral malleolus fractures, 1 case of posterior triangular bone avulsion, and 2 cases of inferior tibia and fibula separation, and no abnormal bone structure was found in the remaining patients. All patients underwent the first examination within 1 to 5 days after trauma. The interval between MRI examination and ankle arthroscopy/incision was 1 to 9 days (mean, 4 days).

*3.2. MRI Instruments, Examination Methods, and Scanning Sequences.* A Siemens 3.0 T Verio superconducting magnetic resonance imager was used. Use flexible FLEX surface coils. Scan the ankle on the injured side of the patient. Take the supine position and adopt the foot advanced method. The lower limbs on both sides are straight, the affected foot is in a natural relaxed position (usually, the ankle joint is planted flexed 20° and slightly supinated), and the inspection site should be fixed to avoid internal and external rotation of the affected foot as much as possible [11]. The conventional scanning sequences are PD + Tse + Fs, TR/TE is 2650/31; T1-Tse, TR/TE is 750/16. Scanning orientations include (1) transverse axis scan: parallel to the top of the talus, from the lower tibiofibular syndesmosis to the lower edge of the calcaneus; (2) coronal scan: take the transverse axis as the orientation and perform coronal scan from the front of the anterior navicular bone to the posterior edge of the heel in a plane parallel to the line connecting the inner and outer malleolus; (3) sagittal scan: take the transverse axis as the orientation and scan from the edge of the medial malleolus (or lateral malleolus) to the edge of the lateral malleolus (or medial malleolus) perpendicular to the plane connecting the inner and outer malleolus; the scanning field of view (FOV) of the above sequence is 210 mm, the layer thickness is 3-4 mm, and the matrix is 256 × 240.

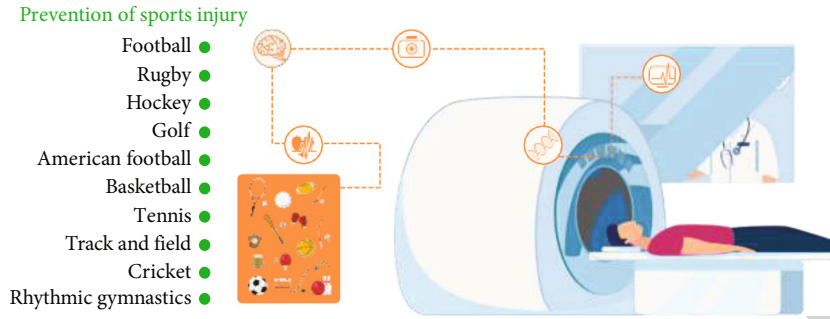


FIGURE 1: MRI technology.

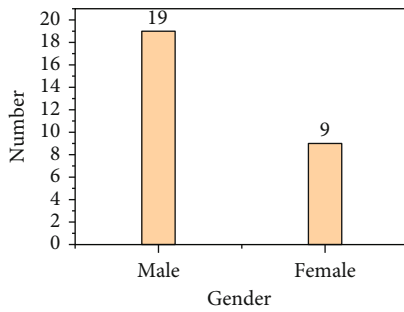


FIGURE 2: Gender ratio.

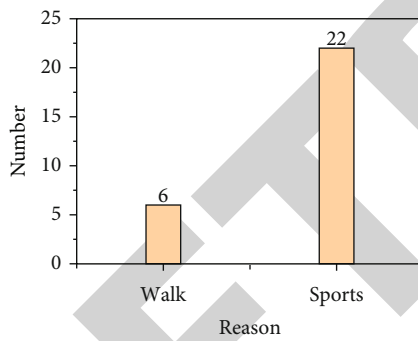


FIGURE 3: Causes of damage.

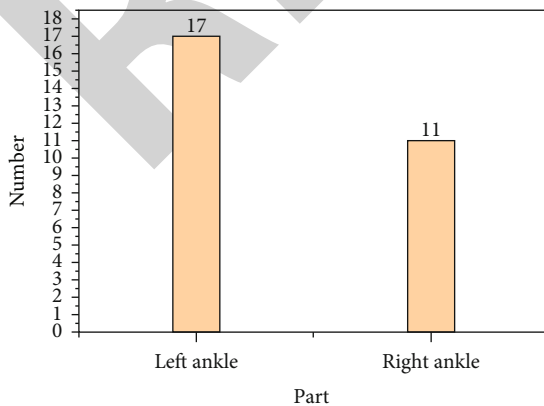


FIGURE 4: Injury site.

3.3. *Ankle Arthroscopy/Arthrotomy.* Orthopedic surgeons employed standard ankle arthroscopy techniques/arthrotomy and detailed documentation.

3.4. *Statistical Analysis.* MRI findings were compared with ankle arthroscopy technique/incision surgery, and the four-table data  $\chi^2$  test was used; the consistency between the findings of MRI and the findings of ankle arthroscopy/incision was analyzed, and  $P < 0.05$  was considered statistically significant.

The mathematical definition formula for the correlation analysis of factors using the chi-square test is shown in

$$\chi^2 = \sum_{i=1}^r \sum_{j=1}^c \frac{(f_{ij}^0 - f_{ij}^e)^2}{f_{ij}^e}. \quad (1)$$

In the formula,  $r$  is the number of rows in the contingency table;  $c$  is the number of columns in the contingency table;  $f_{ij}^0$  is the observed frequency;  $f_{ij}^e$  is the expected frequency.

The formula for calculating the expected frequency of  $f^e$  is as follows:

$$f^e = \frac{RT}{n} * \frac{CT}{n} * n = \frac{RT * CT}{n}. \quad (2)$$

In the formula,  $RT$  is the sum of the observation frequency of the row;  $CT$  is the sum of the observation frequency of the column.

By deriving the chi-square statistic from the above formula, it can be seen that if the expected frequency and the observed frequency are the same, the chi-square statistic is the smallest, which is 0; it can be inferred that these two variables are completely independent and have no correlation. The greater the difference between the expected frequency and the observed frequency, the greater the chi-square statistic that can be obtained, and the higher the degree of correlation [12].

## 4. Analysis of Results

4.1. *MRI Diagnosis of Ankle Fracture and Bone Contusion.* Of all 28 ankle arthroscopy/otomies, a positive diagnosis was made for 6 fractures. A total of 6 fractures were found

by MRI, with a sensitivity of 100% and a 95% CI of 54.07% to 100.00%, as shown in Table 1, fracture line or bone fragment displacement, and showed bone marrow contusion and edema associated with the fracture; MR showed patchy long T1 and long T2 signals in the bone marrow, and fat-suppressed sequences showed high signal.

**4.2. MRI Diagnosis of Ankle Ligament Injury.** In this group of 28 cases of ankle arthroscopy or/and arthrotomy, there were 19 cases of ankle ligament injury. Among them, there were 16 cases of lateral collateral ligament injury, including 8 cases of simple rupture of the anterior talofibular ligament, 5 cases of simultaneous rupture of the anterior talofibular ligament and calcaneofibular ligament, and 3 cases of simple rupture of the calcaneofibular ligament, with 1 case of medial deltoid ligament injury, 1 case of simple rupture of anterior tibiofibular ligament, and 1 case of rupture of anterior tibiofibular ligament combined with deltoid ligament injury (see Table 2). MRI correctly diagnosed 16 cases with a sensitivity of 84% and a 95% CI of 60.42% to 96.62% (Table 3). The MR manifestations of ligament injury are mainly partial or complete discontinuity of the ligament, thickening, shrinking, abnormal signal, and widening of the joint space; 1 case was missed, which was avulsion of the anterior talofibular ligament without obvious displacement. Among the 8 cases of calcaneofibular ligament rupture, 6 cases were correctly diagnosed by MRI with a sensitivity of 75%, and 2 cases were misdiagnosed as normal. In 1 case, the calcaneofibular ligament was normal and MRI suggested a suspicious tear. No posterior talofibular ligament injury was found in this group of patients. Statistical analysis showed that the difference between the two was not statistically significant, and the MRI findings were in good agreement with ankle arthroscopy techniques/incision surgery [13].

**4.3. MRI Diagnosis of Tendon Injury.** Tendon injury was rare in this group of cases; in 2 cases of Achilles tendon rupture, MRI correctly showed the continuity of the tendon; in 4 cases of tendon tenosynovitis, MRI showed effusion in the tendon sheath.

**4.4. Cartilage Damage.** Arthroscopic and MRI diagnoses were consistent in 3 cases, joint effusion in 10 cases; MRI showed muscle and soft tissue contusion in 17 cases.

**4.5. Discussion.** The ankle joint is one of the major joints of the lower extremity, and sports injuries are very common, mostly caused by excessive force during running and jumping, improper landing posture, or uneven ground; most fracture-dislocation lesions can be initially diagnosed, and occult fractures can be further diagnosed by CT spiral scan multiplanar reconstruction. However, for soft tissue trauma and cartilage trauma, ordinary X-ray and CT scans cannot provide sufficient diagnostic information. If the diagnosis of these injuries is ignored in clinical practice and treatment is not given in time, it is easy to cause persistent joint pain or joint instability [14]. Therefore, in order to carry out an early, accurate, and comprehensive evaluation of ankle sports injuries, in addition to plain X-ray films, it is neces-

TABLE 1: 28 cases of ankle MRI diagnosis of ankle fractures ( $n$ ).

MR	Operation		Total
	+	-	
+	6	0	6
-	0	22	22
Total	6	22	28

sary to use MRI technology with comprehensive evaluation advantages [15]. Due to its inherent advantages of multiparameter, multidirectional, and the best soft tissue resolution, MRI can clearly display fractures, bone contusions, and joint attachment structure damage at the same time, which can play a good supplementary role to ordinary X-rays in damage evaluation.

The results of this study show that MRI has 100% sensitivity for the diagnosis of fracture injury and bone contusion and bone marrow edema, as well as the assessment of fracture and dislocation. The T2-weighted fat-suppressing sequence of MRI cannot detect the large-scale patchy long T2 signal of bone contusion and edema, which cannot be found in X-ray plain film and arthroscopy/incision. Its high sensitivity is because MRI technology can accurately reflect a series of pathological changes such as bone marrow edema after bone injury and intraosseous hemorrhage after microfracture and show corresponding abnormal signals and can obtain timely and comprehensive diagnosis of lesions. Bone contusion is a concept put forward after MRI is applied to clinical bone and joint examination, edema, hemorrhage of phalanx trabecular, and even tiny fracture of trabecular bone. It is the common main cause of pain after bone and joint injury, and sometimes, it may be the only cause. The diagnosis through MRI can avoid unnecessary or invasive examinations, guide the injured person to rest and recover in time, and promote the recovery of bone contusion, so as to avoid excessive weight-bearing which further collapses the already weak trabecular bone, the formation of compression fractures or cartilage degeneration, and other sequelae changes. For patients with severe clinical symptoms and no abnormality in plain X-rays or only suspicious fractures, further MRI examinations play an important role [16].

MRI also has high sensitivity for the diagnosis of ligament injury. The sensitivity of this study was 84% based on the number of ligament injuries. MRI diagnosis of ankle ligament injury criteria: (1) ligament continuity is interrupted; (2) ligament shape is wavy or curved; or ligament contour disappears [17]. Satisfying two diagnostic criteria at the same time can make the diagnosis more accurate. Since ankle sprains are mostly varus and internal rotation injuries, usually the lateral collateral ligament is more involved in ankle sports injuries, including three lateral collateral ligaments, the anterior talofibular ligament, the calcaneofibular ligament, and the posterior talofibular ligament. It is easier to diagnose the injury of the anterior talofibular ligament by observing the multidirectional and multiparameter imaging of MRI, but it is relatively difficult to diagnose the injury of the calcaneofibular ligament; analysis of the reasons considers that under the conventional scanning method, the

TABLE 2: 19 cases of ankle ligament injury ( $n$ ).

Damage	Number
Lateral collateral ligament injury	16
Simple anterior talofibular ligament rupture	8
Anterior talofibular ligament and calcaneofibular ligament rupture at the same time	5
Simple calcaneal ligament rupture	3
Medial deltoid ligament injury	1
Simple anterior tibiofibular ligament rupture	1
Rupture of anterior tibiofibular ligament combined with deltoid ligament injury	1

TABLE 3: Comparison of 28 cases of ankle joint MRI diagnosis and ankle arthroscopy/incision ( $n$ ).

MR	Operation		Total
	+	-	
+	16	1	17
-	3	8	11
Total	19	9	28

anterior talofibular ligament can be displayed completely on the single-layer transverse axial image and can also be displayed on the coronal image, and it is easy to observe part or all of its continuity interruption, thickness changes, and signal abnormalities. The calcaneofibular ligament, whether on the transverse axial image or the coronal image, is completely displayed on the single-layer image and intermittently displayed on several consecutive layers. In this way, MRI is often difficult to accurately determine whether the continuity of the calcaneofibular ligament is intact, and the main signs of judging the injury are decreased calcaneofibular ligament tension and increased ligament signal swelling on T2WI, resulting in a decline in diagnostic ability [18]. Usually, ankle varus injury results in rupture of the anterior talofibular ligament or/and calcaneofibular ligament, of which the anterior talofibular ligament alone is the most ruptured. The second is the simultaneous rupture of the anterior talofibular ligament and the calcaneofibular ligament, while the posterior talofibular ligament is rarely damaged. In 3.0T MRI thin-layer 3D scanning, especially isotropic high-resolution 3D scanning, high-quality images along the calcaneofibular ligament can be obtained. At the same time, the MRI technique is used to display these ligaments at the best angle. The scanning method is taken in the supine natural position, and the 20° oblique section to the head side can better observe the anterior talofibular ligament. Observe the calcaneofibular ligament in a 15° oblique section on the side of the foot, or adjust the inclination angle to the direction of 25° on the side of the foot; most of them can show that the basic requirements for diagnosis are met; the injury of the posterior talofibular ligament can be observed in conventional coronal scanning [19].

In this group of 28 cases of ankle injury, 6 cases of tendon injury, MRI showed abnormal morphology and signal

to make a definite diagnosis. MRI technology has the best soft tissue resolution and multiparameter and multidirectional imaging capabilities, which provide it with irreplaceable advantages. At present, MRI is considered to be the best diagnostic method for ankle tendon injury. Although there are many tendons around the ankle joint and their course is more complicated, through a comprehensive analysis, pay attention to the following two normal conditions: (1) there may be a small amount of effusion in the normal tendon sheath, especially in the flexor tendon sheath; (2) when the calf tendon is transferred to the sole of the foot through the medial and lateral malleolus, the “magic angle phenomenon” is often seen, that is, the signal of the tendon is increased on the short TE image ( $TE \leq 20$  ms), but the signal of the tendon on the long TE image is normal. Tendon injuries can be easily diagnosed. MRI for the diagnosis and grading of ankle talar osteochondral injury is an effective and noninvasive evaluation method. The diagnostic sensitivity of talar osteochondral injury in this group was high (75%) [20].

## 5. Conclusion

MRI technology has the advantages of multiparameter, multidirectional, and high soft tissue resolution and can sensitively reflect the abnormal signal changes of bone cortex, bone marrow, ligament, tendon, articular surface osteochondral, etc. during ankle injury. It has extremely high sensitivity to the common fractures of the ankle joint, bone marrow damage, ligament, tendon, and cartilage damage; it provides a more “direct” and clear diagnostic basis for clinical diagnosis, which cannot be compared and replaced by other imaging methods. But at the same time, there are also some shortcomings; the optimization of ankle MRI examination imaging scanning technology plays a key role in the diagnosis of ligament injury, which cannot be recognized by most scanning staff; at the same time, due to the relatively short application time of imaging technology compared with other imaging technologies and the complexity of imaging image display, clinicians generally have limited reading and understanding. Relying on the combination and communication of imaging and clinical, more promotion and interpretation of image information, so clinicians can better grasp and apply it to guide the choice of clinical treatment. It is believed that MRI technology, as a noninvasive, painless, and nonradiative damage examination method, will have more and more broad application prospects in ankle injury.

## Data Availability

The data used to support the findings of this study are available from the corresponding author upon request.

## Conflicts of Interest

The author declares that there are no conflicts of interest.

## *Retraction*

# **Retracted: Postoperative Nursing and Functional Rehabilitation of Ultrasound Diagnosis of Lower Rotator Cuff Injury**

### **Scanning**

Received 20 June 2023; Accepted 20 June 2023; Published 21 June 2023

Copyright © 2023 Scanning. This is an open access article distributed under the Creative Commons Attribution License, which permits unrestricted use, distribution, and reproduction in any medium, provided the original work is properly cited.

This article has been retracted by Hindawi following an investigation undertaken by the publisher [1]. This investigation has uncovered evidence of one or more of the following indicators of systematic manipulation of the publication process:

- (1) Discrepancies in scope
- (2) Discrepancies in the description of the research reported
- (3) Discrepancies between the availability of data and the research described
- (4) Inappropriate citations
- (5) Incoherent, meaningless and/or irrelevant content included in the article
- (6) Peer-review manipulation

The presence of these indicators undermines our confidence in the integrity of the article's content and we cannot, therefore, vouch for its reliability. Please note that this notice is intended solely to alert readers that the content of this article is unreliable. We have not investigated whether authors were aware of or involved in the systematic manipulation of the publication process.

In addition, our investigation has also shown that one or more of the following human-subject reporting requirements has not been met in this article: ethical approval by an Institutional Review Board (IRB) committee or equivalent, patient/participant consent to participate, and/or agreement to publish patient/participant details (where relevant).

Wiley and Hindawi regrets that the usual quality checks did not identify these issues before publication and have since put additional measures in place to safeguard research integrity.

We wish to credit our own Research Integrity and Research Publishing teams and anonymous and named external researchers and research integrity experts for contributing to this investigation.

The corresponding author, as the representative of all authors, has been given the opportunity to register their agreement or disagreement to this retraction. We have kept a record of any response received.

### **References**

- [1] R. Hou, "Postoperative Nursing and Functional Rehabilitation of Ultrasound Diagnosis of Lower Rotator Cuff Injury," *Scanning*, vol. 2022, Article ID 8319082, 7 pages, 2022.



## Research Article

# Postoperative Nursing and Functional Rehabilitation of Ultrasound Diagnosis of Lower Rotator Cuff Injury

Riying Hou 

College of Gerontic Education, Jilin Open University, Changchun, Jilin 130022, China

Correspondence should be addressed to Riying Hou; 202003526@stu.ncwu.edu.cn

Received 19 July 2022; Revised 12 August 2022; Accepted 17 August 2022; Published 28 August 2022

Academic Editor: Balakrishnan Nagaraj

Copyright © 2022 Riying Hou. This is an open access article distributed under the Creative Commons Attribution License, which permits unrestricted use, distribution, and reproduction in any medium, provided the original work is properly cited.

In order to explore the postoperative nursing effect and functional rehabilitation of rotator cuff repair under ultrasound diagnosis, a method of nursing and rehabilitation functional training for athletes' wrist injury under the assistance of microscopic B-ultrasound was proposed. This study retrospectively analyzed the therapeutic effect of tendon anastomosis in 237 patients with wrist tendon injury, adopted nursing measures such as health education and functional exercise, and observed its clinical effect. The results showed that after 3-6 months of follow-up, all patients had satisfactory recovery of tendon function. Of these, 132 patients recovered well. 84 patients recovered well. The excellent and good rate of patients was 91%. Ultrasound diagnosis of rotator cuff repair combined with functional exercise promotes good recovery of shoulder joint function in patients.

## 1. Introduction

B-ultrasound is a commonly used medical equipment in hospitals. It utilizes the characteristics of ultrasonic wave, such as excellent directivity, strong penetration ability, and obvious reflection characteristics. According to the basic situation of the recovery of ultrasonic signal, it completes ultrasonic imaging by using the recovery part of acoustic signal. Hospital B-ultrasound can complete the diagnosis and observation of diseases, providing a basis for pathological diagnosis and treatment. And it has the characteristics of simple, painless diagnosis, low diagnosis cost, and high acceptance by patients [1].

Wrist joint is one of the joints with the most complex structure and the most frequent movement in the human body, which is also an organ necessary for people to complete daily work. The wrist joint is mainly composed of the distal ulnar and radial bones, eight carpal bones, and the proximal end of the 1st to 5th metacarpal bones. The complex motion is usually accomplished by the cooperation of the ulnar deflection force, the dorsiflexion force, and the rotation force. The three forces affect each other and easily cause the injury of bone, cartilage, and soft tissue. Therefore, wrist injuries are mostly mixed injuries, often multiple wrist

fractures, joint dislocation, and soft tissue edema. Wrist joint injury is a common and frequently occurring clinical disease. If it cannot be treated timely and accurately, it is easy to lead to wrist joint function and activity disorders. Therefore, accurate diagnosis of wrist joint injury is particularly important. Imaging examination plays an important role in wrist joint injury and is the most important auxiliary diagnosis method, which can provide clinicians with clear and intuitive image information and provide reliable basis for subsequent clinical treatment plan. X-ray is the preferred clinical method in the imaging examination of wrist joint injury, but its two-dimensional image has some limitations in the imaging diagnosis, which is prone to misdiagnosis and missed diagnosis. In recent years, multislice spiral CT (MSCT) and nuclear magnetic resonance (MRI) techniques have been widely used to improve the accuracy of wrist injury imaging diagnosis. With the improvement of ultrasound technology and the improvement of sensitivity, the application of ultrasound in wrist joint injury has been further expanded [2].

X-ray has the advantages of simple operation and low price, which is widely used in the diagnosis of tumors and bone and joint injuries. It can clearly display fracture and joint dislocation, which has always been the preferred

imaging examination method for wrist joint injuries. Patients with wrist trauma are routinely diagnosed by X-ray anteroposterior and lateral radiography. Changes in the morphology of some wrist joints on radiographs suggest abnormalities in the wrist joint. For example, there are “three arcs” in the wrist joint, namely, the two arcs on the far and far sides of the scaphoid bone, lunate bone, and deltoid bone and the arc on the proximal articular surface of the head and scaphoid bone on the orthographic film. Changes in any one of the arcs indicate joint abnormalities. The width of the wrist joint space is basically the same, 1~2 mm. If the joint space narrowed or even disappeared, indicating the possibility of dislocation. The lunate bone is located in the middle of the articular surface of the distal radius on the lateral radiographs and is basically quadrilateral on the anteroposterior radiographs. If the shape and position of the lunate bone change significantly, it suggests the occurrence of lunate bone dislocation. On lateral wrist radiographs, lunate bone, skull, and radial longitudinal axis should be basically in a straight line, and severe deviation would be considered as dislocation [3]. The change of “triangle shadow” has important diagnostic value for most carpal dislocation. The determination of “tear drop angle” on X-ray lateral film is instructive to the determination of step and fissure of articular surface. It is important to remember that the measurement of length and width is helpful to analyze the changes and damage degree of radial sigmoid notch. Parameters such as the width of the distal radius are helpful for diagnosing the degree of articular surface injury and wrist instability. Dorsal deltoid fractures can be diagnosed by clinical manifestations combined with lateral wrist radiographs. “Terry-Thomas sign” and “overflow cup sign” are helpful for the early and late diagnosis of perilunate dislocation, respectively. The anatomical structure of wrist joint is complex, the shape of carpal bone is diverse, and the injury situation is also complex and diverse. In addition to fracture or fracture accompanied by dislocation, there can be structural disorder and deformity. If accompanied by soft tissue swelling, bleeding gauze wrapping, etc., it will form interference to the examination. There are still many deficiencies in the diagnosis of wrist joint injury by X-ray plain film. For complex fractures or multiple fractures, many hidden fractures and microfractures are often missed and misdiagnosed due to overlapping. Although X-ray is the first choice in clinical examination of ulna impingent syndrome, it cannot accurately diagnose the patients with early ulna impingent syndrome. X-ray has low sensitivity in the diagnosis of lunate dislocation and perilunate dislocation, which is easy to be missed and misdiagnosed. The probability of missed diagnosis and misdiagnosis is also high for dorsal fracture of the wrist triangle bone. Patients with wrist trauma are usually in passive position. And it is often difficult to take the standard projection position due to pain, which leads to carpal bone overlap and deformation, affecting the accuracy of diagnosis. In the case of wrist plaster external fixation, accurate diagnosis is more difficult [4].

Ultrasonic examination, which is widely used in tumor, cardiovascular, oral, and other diseases, has the advantages of safety, speediness, no radiation, and so on. With the

improvement of ultrasonic technology, its sensitivity has been continuously improved, further expanding the application of ultrasonic examination in wrist joint injury and reducing the dependence of wrist joint lesions on CT and MRI. As shown in Figure 1, the Ultrasound Institute and the Radiological Society recommend the use of a broadband, high-resolution ultrasound probe for wrist examination due to the relatively shallow position of the wrist. This probe can obtain better images, which is helpful for doctors to observe wrist joint injury. Ultrasonic examination of wrist joint injury can not only be used to evaluate the traumatic injured muscles, tendons, ligaments, and peripheral nerves but also clearly display joint effusion [5]. The use of 3D ultrasound provides more images of normal and abnormal tissues than conventional two-dimensional ultrasound, allowing for more evaluation of damage. Ultrasound can clearly show the adjacent situation of the tissues such as blood vessels and nerves around the wrist and some soft tissue lesions such as tendinitis, tenosynovitis, bursitis, tenosynovitis, ganglion cyst, joint effusion, nerve compression, and injury. The diagnosis of injury tenosynovitis is convenient and fast. High-frequency ultrasound can accurately display and diagnose TFCC injury and bone erosion in patients with early and active rheumatoid arthritis (RA), which can be applied to the diagnosis and follow-up of RA. Combined with angiography, it can also conduct qualitative and semiquantitative analysis of RA synovial blood perfusion [6].

However, the penetration of ultrasound is weak, and the anatomical structure of the carpal bone cannot be completely and clearly displayed by ultrasound examination. In addition, the compression of the ultrasonic probe will cause discomfort in patients with wrist trauma, etc., and there are still some limitations in the examination of wrist injury.

To sum up, different imaging examination methods have their own advantages and disadvantages in wrist joint injury. If a single examination is used for analysis and diagnosis, missed diagnosis and misdiagnosis may often occur.

## 2. Literature Review

Sagar et al. proposed the theory of wave-particle duality, believing that the motion of electrons is similar to the propagation of visible light [7]. Taa et al. proposed the motion theory of electron in magnetic field and pointed out that the magnetic field with axial symmetry has the effect of deflection and focusing on electron beam [8]. The discovery of wave-particle duality theory and magnetic focusing theory provides important theoretical guidance for the invention of electron microscope. Using electron beam instead of visible light as illumination source can greatly improve the geometric resolution and effective magnification of electron microscope, which is an important basis for the existence of electron microscope. Ashkenazi et al. confirmed the possibility of electronic imaging for the first time and obtained an electronic image of copper net magnified 12 times [9]. Subsequently, with the joint efforts of El-Rosasy and Ayoub, transmission electron microscopy of commodities was developed and gradually popularized [10]. The resolution

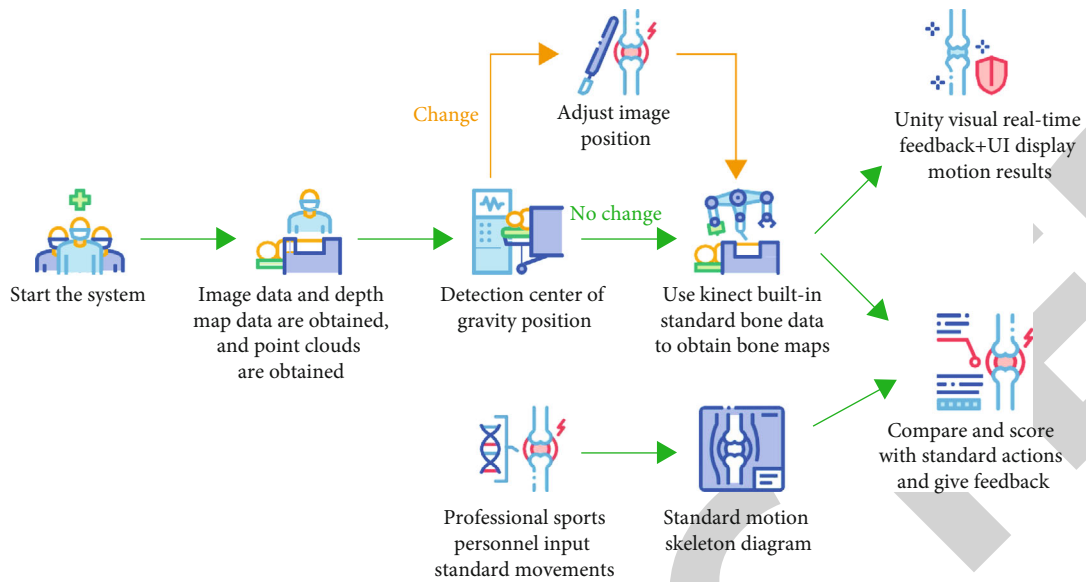


FIGURE 1: Athlete's wrist injury assisted by B-ultrasound.

of Elmiskop I transmission electron microscope developed by Mc et al. was better than 1 nm [11]. Chi et al. first proposed the principle and design idea of scanning electron microscopy [12]. On the basis of the secondary electron detector designed and improved by Mlha et al., the first practical scanning electron microscope was specially developed for the Canadian Pulp and Paper Research Institute, which made a great contribution to the development of modern scanning electron microscopy and was in the National Science Museum of Canada [13]. Ncha et al. made the first commercial scanning electron microscope of model Mark I [14]. The secondary electron detector (ET-D) improved and perfected by Chen et al. had also become a necessary secondary electron detector for all current scanning electron microscopy [15]. At the end of 1980s, Lotzien et al. successfully developed the environmental scanning electron microscope and began to sell them [16].

Improving the image quality and resolution of electron microscope was the direction of continuous efforts of scientists and electron microscope engineers all over the world. In terms of electron emission sources, tungsten filament cathode had gradually developed to lanthanum hexaboride cathode and then to high resolution field emission cathode. Field emission cathodes could be divided into cold field and hot field, respectively. The electron energy divergence of the cold field emission cathode was smaller, and the current density was larger. Although the electron energy divergence of the hot field emission cathode was slightly larger than that of the cold field and the current density was slightly smaller than that of the cold field, the total emission current of the hot field emission cathode was larger, the stability was better, and the anti-interference ability was stronger. In the electronic imaging technology, Americans invented the eight pole astigmatism device and then gradually invented the spherical aberration correction device, monochromator, and other parts which helped to improve the resolution of the image. In terms of image recording media, the tradi-

tional photosensitive film mode had been replaced by the CDD camera mode, and more advanced CMOS cameras had been gradually popularized and used [17]. With the continuous development and deepening of these new technologies, the current highest resolution of transmission electron microscopy and scanning electron microscopy had reached the high level of 0.07 nm and 0.4 nm, respectively [18].

In addition, energy dispersive spectrometer, spectrograph, EBSD, FIB, freezing technology, and 3D reconstruction technology have also developed rapidly in recent decades [19]. The combination and integration of these techniques with the electron microscope greatly enhance the detection function and analytical ability of the electron microscope.

### 3. Methods

**3.1. Surgical Methods.** In previous literature, brachial plexus block anesthesia was performed with the patient in supine position. The shoulder joint was placed on the side table with the extension 90°. The index finger, middle finger, and ring finger were put into the traction finger sleeve. Traction tower was used to tract the radial fracture end longitudinally. After the C-arm perspective was satisfying, the fracture end was fixed by a 1.5 mm Kirschner wire at the styloid process of the radius, and the finger sleeve was removed from the traction tower. The forearm was horizontally positioned. The skin and fascia were longitudinally cut between the flexor carpi radialis tendon and radial artery. The anterior rotator muscle was cut from the radial insertion to expose the extra-articular fracture. If the traction reduction was not satisfactory, the Kirschner wire could be withdrawn to the distal side of the fracture, and the finger press could be used to continue the Kirschner wire after the reduction was satisfactory [20]. The plate was placed close to the volar side of the radius. After the adjustment of the lower C-arm was

satisfied, the plate was fixed with ordinary compression screws through the sliding hole to make it close to the radius, and then the locking screws on the lower part of the ordinary nail were inserted. Again, the traction finger sleeve was hung on the traction tower for traction, and the traction force was 5-7 kg. It approached on 3/4 and 4/5 of the dorsal side of the wrist joint, each about 0.3 cm long. And the arthroscope and plane were inserted to attract the blood stasis in the joint and make the field of vision clear [21]. The radial articular surface and surrounding ligaments were observed. Kirschner wire and probe hook were used to pry the joint fracture block to make it smooth. The joint space was less than 1.0 mm, and the joint step was less than 1.0 mm. Kirschner wire was used to fix temporarily. After C-arm fluoroscopic reduction was satisfactory, the plate distal screw was placed. Arthroscopy was used to assist to observe whether the screw entered the articular cavity and whether the length of the screw penetrated out of the dorsal bone cortex. The traction device was removed, the wound was rinsed, the radial edge of the anterior muscle was sutured, and the subcutaneous and skin were sutured. Posterior external fixation was assisted for C3 distal radial fractures. And antirotation flexion and extension bracing was assisted for C1 and C2 distal radial fractures complicated with TFCC injury.

### 3.2. Nursing Methods

**3.2.1. Postoperative Day Care.** Postures care were taken immediately after patients entered the ward after surgery. The affected limb was placed on a 30° elevation pad to ensure that the wrist was about 10.0 cm higher than the heart level. At the same time, psychological counseling was carried out to eliminate patients' tension. According to the surgical records, the patients and their families were instructed about the precautions for the affected limb, and the pamphlet *Early Rehabilitation Guide for Arthroscopic Treatment of Distal Radius Fracture* was issued. The injured wrist was wrapped with a medical ice pack to help stop bleeding and detumescence and prevent compartment syndrome. Anti-infective and detumescent drugs were administered intravenously [22].

**3.2.2. 2~7 Days Postoperative Nursing.** On the 2nd day after surgery, patients could get out of bed and carried out rehabilitation training of shoulder, elbow, and finger, especially the inflexible flexor tendon caused by the stimulation of surgery and steel plate. Early finger flexion and extension training were beneficial to prevent tendon adhesion and joint stiffness. The six-step method was used for training. Because the flexor thumb tendon was located in the deepest layer and the plate was the largest, the thumb could be used for opposite finger and opposite palm training to the other four fingers in the early stage. At the same time, thumb dorsiflexion, adduction, and abduction training could be conducted, with 30 min each time and 6 times a day.

**3.2.3. 7~14 Days Postoperative Nursing.** On the 7th day after surgery, early health equipment (grip ball, grip machine, finger extension and flexion trainer, etc.) could be assisted. Pas-

sive wrist flexion and extension training could be used for non-C3 distal radius fractures, with passive flexion and extension ranging from -10° to 10° at week 1 and passive flexion and extension ranging from -20° to 20° at week 2. Patients were encouraged to perform active wrist flexion and extension training after passive flexion and extension. Patients without TFCC injury could passively train pronation and supination movements [23].

**3.2.4. 3~6 Weeks Postoperative Nursing.** Postoperative 3 weeks of wrist range of motion were -30°~30°, and postoperative 4 weeks of wrist range of motion were -40°~40°. At the same time, the strength training was strengthened. At this time, auxiliary grip and pinch force training could be conducted. Patients without TFCC injury could be passively trained in pronation and supination. Five to six weeks after the operation, patients could take active training, with the forearm placed on the flat table and wrist joint located at the table. And when the healthy hand assisted pulling the affected wrist, flexion and extension training were conducted at the same time [24].

**3.2.5. 7~8 Weeks Postoperative Nursing.** At the 7th week after surgery, wrist weight-bearing drafting was started, starting with 0.5 kg weight-bearing and progressing step by step. At this time, the brace was removed for patients with TFCC injury, and passive pronation and supination training were conducted. Passive wrist flexion and extension and lateral deflection training were performed. The activity limit remained 10-20 s. The patient was instructed to carry out fine motor coordination exercises, such as writing, typing on the keyboard, and twisting bottle caps. At the 8th week after surgery, muscle strength training and resistance training of wrist joint and forearm were mainly started. At this time, flexion, extension, pronation, supination, and ulnar deviation were trained with rubber strips with different elastic forces [25].

## 4. Experiment Results and Discussions

In previous literature and general data, 237 patients with hand tendon injury were selected, including 150 males and 87 females. The age ranged from 18 to 83 years, with an average age of (41.6 ± 11.4) years. There were 180 cases of cutting injury, 20 cases of smashing, 17 cases of rolling, 5 cases of fracture complication, and 15 cases of strangulation. Of the 237 patients, 12 had edema, 5 had tendon adhesion, 2 had tendon rupture, and 2 had joint stiffness after surgery, see Figures 2-5, Table 1.

The patients were followed up for 3-6 months. All the 237 patients had satisfactory recovery of tendon function. 132 patients had excellent recovery. 84 patients had good recovery. 11 patients had moderate recovery. And 10 patients had poor recovery. The rate of excellent and good treatment was 91%.

Hand is an important tool in daily life and work, which plays an important role in life and work. With the development of economy, people's living standards have improved significantly, and their expectation for treatment is

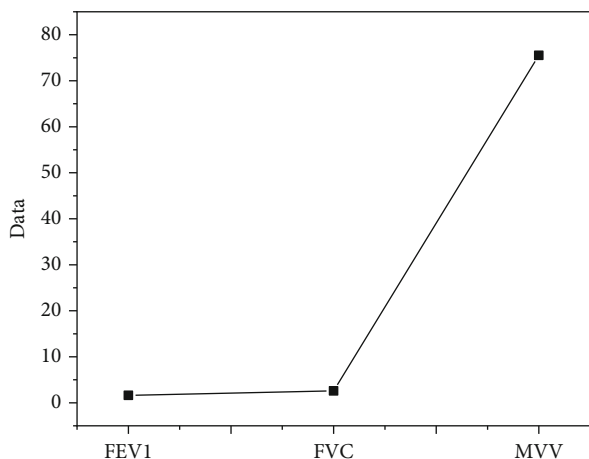


FIGURE 2: Comparison of minimum indexes of lung function in the control group.

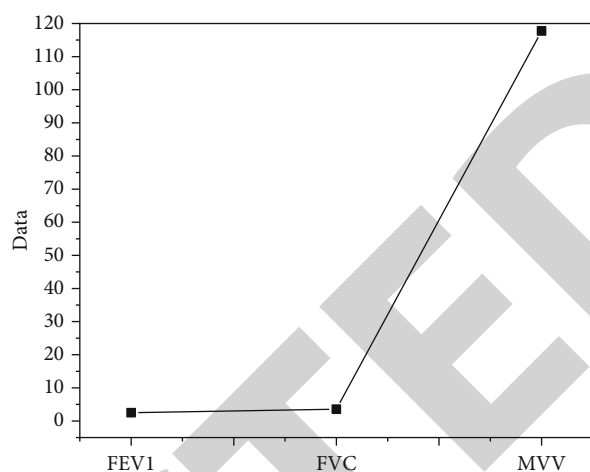


FIGURE 5: Comparison of maximum indexes of lung function in the treatment group.

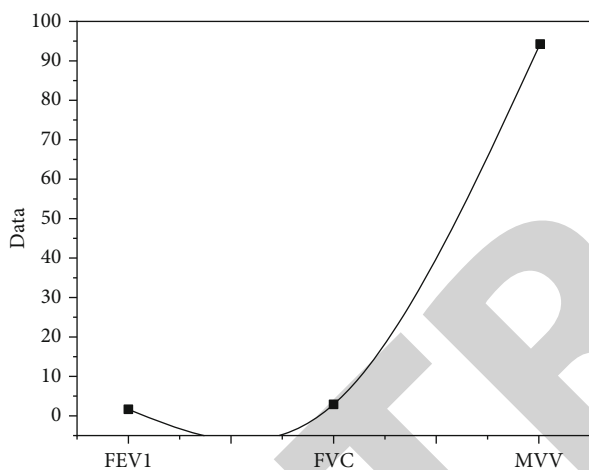


FIGURE 3: Comparison of maximum indexes of lung function in the control group.

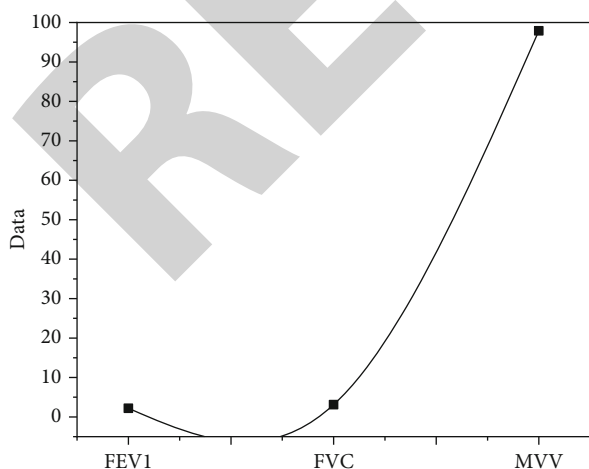


FIGURE 4: Comparison of minimum indexes of lung function in the treatment group.

TABLE 1: Comparison of average hospitalization expenses and days in the hospital between the two groups ( $x \pm s$ ).

Group	Cases	Hospitalization expenses	Days in hospital
The treatment group	119	4068.91 ± 746.32	11.12 ± 2.14
The control group	118	5176.39±	14.93 ± 3.21
<i>t</i>		4.92	3.09
<i>P</i>		0.001	0.003

increasing. For hand trauma patients, functional recovery of the affected finger after operation is not only simple morphological repair but more attention is paid to the effect of functional modification. And the medical concept is also changed from simple surgical treatment to rehabilitation treatment. Postoperative nursing and functional exercise guidance are particularly important after hand tendon injury. Proper treatment can reduce complications such as tendon adhesion and joint stiffness and maximize the maintenance of hand function.

To sum up, hand tendon injury nursing is a comprehensive, systematic, and effective nursing method, which is mainly through improving patients' awareness of disease knowledge to effectively improve the symptoms of patients and promote the rehabilitation of patients ultimately.

### 5. Conclusion

In the research, a method of nursing and rehabilitation function training of athletes' wrist joint injury assisted by microscope B-ultrasound was proposed. The method was as follows. Brachial plexus block anesthesia was performed with the patient in supine position. The shoulder joint was placed on the side table with the extension 90°. The index finger, middle finger, and ring finger were put into the traction finger sleeve. Traction tower was used to tract the radial fracture end longitudinally. After the C-arm perspective was satisfying, the fracture end was fixed by a 1.5 mm Kirschner

wire at the styloid process of the radius, and the finger sleeve was removed from the traction tower. The nursing method of nursing and rehabilitation measures was taken from the beginning to the seventh or eighth week after surgery. The patients were followed up for 3-6 months by retrospective analysis and observation. All the 237 patients had satisfactory recovery of tendon function. 132 patients had excellent recovery. 84 patients had good recovery. 11 patients had moderate recovery. And 10 patients had poor recovery. The rate of excellent and good treatment was 91%. It proved the effectiveness of the experience of nursing and rehabilitation function of athletes' wrist joint injury assisted by microscope B-ultrasound. In the future, it is believed that more and more cases of nursing and rehabilitation function exercise of athletes' wrist injury will be completed with the help of microscope and B-ultrasound.

### Data Availability

The data used to support the findings of this study are available from the corresponding author upon request.

### Conflicts of Interest

The author declares no conflicts of interest.

### References

- [1] Y. A. Novikov, "Calibration of a scanning electron microscope: 2. Methods of signal processing," *Journal of Surface Investigation: X-Ray, Synchrotron and Neutron Techniques*, vol. 15, no. 5, pp. 987–998, 2021.
- [2] X. Zhou, L. Tang, D. Lin, and W. Han, "Virtual & augmented reality for biological microscope in experiment education," *Virtual Reality & Intelligent Hardware*, vol. 2, no. 4, pp. 316–329, 2020.
- [3] V. Muthukumar, D. Karki, and B. Jatin, "Concept of lethal triad in critical care of severe burn injury," *Indian Journal of Critical Care Medicine*, vol. 23, no. 5, pp. 206–209, 2019.
- [4] J. L. Bowden, R. Lamberts, D. J. Hunter, L. R. Melo, and K. Mills, "Community-based online survey on seeking care and information for lower limb pain and injury in Australia: an observational study," *BMJ Open*, vol. 10, no. 7, article e035030, 2020.
- [5] S. R. Piedade, M. R. Hutchinson, and N. Maffulli, "Presently PROMs are not tailored for athletes and high-performance sports practitioners: a systematic review," *Sports Medicine*, vol. 4, no. 5, pp. 248–253, 2019.
- [6] D. J. Keene and K. Willett, "Implications of the ankle injury management (aim) trial," *Bone and Joint Journal*, vol. 101-B, no. 12, pp. 1472–1475, 2019.
- [7] S. Sagar, S. Malhotra, A. Swarup, and R. Kaushik, "Evaluation of mri findings in chronic painful knee joint," *Journal of Evidence Based Medicine and Healthcare*, vol. 6, no. 43, pp. 2818–2823, 2019.
- [8] T. Apivatthakakul, J. L. Koerner, S. Luangsod et al., "Size and location of posterior wall fragment on ct can predict hip instability in a cadaveric model," *Injury*, vol. 52, no. 8, pp. 2104–2110, 2021.
- [9] I. Ashkenazi, H. Schermann, A. Gold et al., "Tranexamic acid in hip hemiarthroplasty," *Injury*, vol. 51, no. 11, pp. 2658–2662, 2020.
- [10] M. A. El-Rosasy and M. A. Ayoub, "Traumatic composite bone and soft tissue loss of the leg: region-specific classification and treatment algorithm," *Injury*, vol. 51, no. 6, pp. 1352–1361, 2020.
- [11] M. Chen, X. Jin, G. W. Fryhofer et al., "The application of the nice knots as an auxiliary reduction technique in displaced comminuted patellar fractures," *Injury*, vol. 51, no. 2, pp. 466–472, 2020.
- [12] Y. L. Chi, X. Gao, Y. J. Xu, X. M. Bu, and B. Wu, "Open total dislocation of ankle joint without fractures: a case report," *Medicine*, vol. 100, no. 22, article e26247, 2021.
- [13] M. Le Hanneur, M. Colas, J. Serane-Fresnel et al., "Endoscopic brachial plexus neurolysis in the management of infraclavicular nerve injuries due to glenohumeral dislocation," *Injury*, vol. 51, no. 11, pp. 2592–2600, 2020.
- [14] N. C. Hagemeyer, J. Saengsin, S. H. Chang et al., "Diagnosing syndesmotism instability with dynamic ultrasound - establishing the natural variations in normal motion," *Injury*, vol. 51, no. 11, pp. 2703–2709, 2020.
- [15] J. Y. Chen, G. R. She, S. M. Luo et al., "Hemiarthroplasty compared with internal fixation for treatment of nondisplaced femoral neck fractures in elderly patients: a retrospective study," *Injury*, vol. 51, no. 4, pp. 1021–1024, 2020.
- [16] S. Lotzien, T. Rosteijs, V. Rausch, T. A. Schildhauer, and J. Gemann, "Trochanteric femoral nonunion in patients aged over 60 years treated with dynamic condylar screw," *Injury*, vol. 51, no. 2, pp. 389–394, 2020.
- [17] P. A. Li, X. Ning, L. Jia et al., "A minimally invasive incision and loop drainage technique for the treatment of lower limb Morel-Lavallee lesions: nose ring drainage technique," *Injury*, vol. 51, no. 2, pp. 570–573, 2020.
- [18] Y. Miyashima, Y. Kaneshiro, K. Yano, H. Teraura, H. Sakanaka, and T. Uemura, "Size and stabilization of the dorsoulnar fragment in ao c3-type distal radius fractures," *Injury*, vol. 50, no. 11, pp. 2004–2008, 2019.
- [19] N. Yamamoto, S. Tsukada, J. Kawai, D. Ueda, and T. Ozaki, "Calcaneal insufficiency fractures following total knee arthroplasty: classification and clinical findings," *Injury*, vol. 50, no. 12, pp. 2339–2345, 2019.
- [20] D. I. Chun, J. Kim, Y. S. Kim, J. H. Cho, and Y. Yi, "Relationship between fracture morphology of lateral malleolus and syndesmotism stability after supination-external rotation type ankle fractures," *Injury*, vol. 50, no. 7, pp. 1382–1387, 2019.
- [21] G. Dhiman, V. Kumar, A. Kaur, and A. Sharma, "Don: deep learning and optimization-based framework for detection of novel coronavirus disease using x-ray images," *Interdisciplinary Sciences Computational Life Sciences*, vol. 13, no. 2, pp. 260–272, 2021.
- [22] N. Balakrishnan, A. Rajendran, and P. Ajay, "Deep embedded median clustering for routing misbehaviour and attacks detection in ad-hoc networks," *Ad Hoc Networks*, vol. 126, pp. 102757, 2021.
- [23] X. Liu, J. Liu, J. Chen, F. Zhong, and C. Ma, "Study on treatment of printing and dyeing waste gas in the atmosphere with Ce-Mn/GF catalyst," *Arabian Journal of Sciences*, vol. 14, no. 8, pp. 1–6, 2021.

## *Retraction*

# **Retracted: DSA Image Analysis of Clinical Features and Nursing Care of Cerebral Aneurysm Patients Based on the Deep Learning Algorithm**

### **Scanning**

Received 5 December 2023; Accepted 5 December 2023; Published 6 December 2023

Copyright © 2023 Scanning. This is an open access article distributed under the Creative Commons Attribution License, which permits unrestricted use, distribution, and reproduction in any medium, provided the original work is properly cited.

This article has been retracted by Hindawi, as publisher, following an investigation undertaken by the publisher [1]. This investigation has uncovered evidence of systematic manipulation of the publication and peer-review process. We cannot, therefore, vouch for the reliability or integrity of this article.

Please note that this notice is intended solely to alert readers that the peer-review process of this article has been compromised.

Wiley and Hindawi regret that the usual quality checks did not identify these issues before publication and have since put additional measures in place to safeguard research integrity.

We wish to credit our Research Integrity and Research Publishing teams and anonymous and named external researchers and research integrity experts for contributing to this investigation.

The corresponding author, as the representative of all authors, has been given the opportunity to register their agreement or disagreement to this retraction. We have kept a record of any response received.

### **References**

- [1] J. Wang, L. Ti, X. Sun, R. Yang, N. Zhang, and K. Sun, "DSA Image Analysis of Clinical Features and Nursing Care of Cerebral Aneurysm Patients Based on the Deep Learning Algorithm," *Scanning*, vol. 2022, Article ID 8485651, 6 pages, 2022.

## Research Article

# DSA Image Analysis of Clinical Features and Nursing Care of Cerebral Aneurysm Patients Based on the Deep Learning Algorithm

Jian Wang , Lin Ti , Xiaorui Sun , Ruping Yang , Nafei Zhang , and Kejuan Sun 

The First Hospital of Hebei Medical University, Shijiazhuang, Hebei 050031, China

Correspondence should be addressed to Kejuan Sun; 20160550@ayit.edu.cn

Received 10 June 2022; Revised 27 July 2022; Accepted 3 August 2022; Published 13 August 2022

Academic Editor: Balakrishnan Nagaraj

Copyright © 2022 Jian Wang et al. This is an open access article distributed under the Creative Commons Attribution License, which permits unrestricted use, distribution, and reproduction in any medium, provided the original work is properly cited.

**Objective.** A deep learning algorithm was developed for automatic detection and localization of intracranial aneurysms in DSA, and its clinical characteristics were analyzed, and targeted nursing measures were formulated. **Methods.** Using a retrospective multicenter study method based on radiology reports, DSA images of aneurysms were randomly divided into 75 cases in the training set, 20 cases in the internal test set, and 35 cases in the external test set. Using a computer-aided detection method based on the three-dimensional U-Net (3D U-Net), after preprocessing DSA images, automatic segmentation of intracranial blood vessels is performed to obtain regions of interest, and based on the segmentation results, physicians' annotations are introduced. The 3D U-Net network model is trained and adjusted, and the obtained model is used to automatically detect the cerebral aneurysm area. **Results.** Fivefold cross-validation was used for the training set and the internal test set, and a sensitivity of  $(94.4 \pm 1.1)\%$  was obtained. Automatic detection of aneurysms was performed on the external test set, and the average false positive rate was 0.86 FPs/case (false positives/case). The resulting sensitivity was 82.9%. The classification comparison of external test sets showed that the sensitivity of the method for detecting aneurysms with sizes of 5.00~<10.00 mm and  $\geq 10.00$  mm (88.2% and 100.0%) was higher than that for aneurysms with sizes of <3.00 mm and 3.00~<5.00 mm (50.0% and 72.7%). The sensitivity of patients aged 50-60 years and >60 years (90.0% and 87.5%) was higher than that of patients aged <50 years (66.7%), and there was little difference between different genders (84.6% in males and 81.8% in females). **Conclusion.** The deep learning algorithm has high diagnostic performance in detecting intracranial aneurysms, which is verified by external datasets.

## 1. Introduction

An intracranial aneurysm (IA) is a tumor-like dilation caused by abnormal local cerebrovascular changes and is a relatively common cerebrovascular disease, with an incidence of about 3%~5% in the general population [1]. Most (about 90%) patients with unruptured intracranial aneurysms (UIAs) usually have no obvious clinical manifestations, and only about 10% of patients will have special manifestations such as headaches and unilateral facial numbness (an aneurysm that affects an adjacent nerve or brain structure) [2]. Rupture of IAs is the main cause of non-traumatic subarachnoid hemorrhage (SAH), with an annual incidence of about 1% [3, 4] but high mortality and disability

rates [5-7]. About 12% of patients are diagnosed before treatment. They have died, and there is still a 40% mortality rate within one month after treatment. About 30% of patients will be left with neurological dysfunction, and only a small number of patients have a slightly better prognosis [8, 9]. Early accurate detection is of great significance to the clinical management and prognosis of patients with intracranial aneurysms.

Medical imaging plays an increasingly important role in the diagnosis and treatment of diseases and is an important tool for doctors to carry out disease screening, clinical diagnosis, treatment guidance, and efficacy evaluation. In recent years, with the development of medical imaging technology, the detection rate of IAs is also increasing. Magnetic



resonance angiography (MRA), computed tomography angiography (CTA), and digital subtraction angiography (DSA) are the common examination methods for IAs. At this stage, the “gold standard” for the diagnosis of IAs is still DSA, with a sensitivity of more than 95%, but the operation is more complicated, the equipment and technical requirements are high, and it has disadvantages such as difficult repetition, high price, invasiveness, and many complications. Clinical application is limited. However, due to the different shapes and sizes of IAs and the complex morphology of parent arteries, the workload of routine physical examination for rapid screening is large, and it is easy to miss diagnose and misdiagnose simply by relying on manual reading.

Computer-aided diagnosis (CAD) is a branch of artificial intelligence (AI) technology, which uses the machine learning algorithm to analyze and judge medical images. Deep learning (DL) is currently the most promising machine learning algorithm and a key technology to revolutionize AI+ medical imaging (i.e., CAD). The DL method generally refers to a deep segmentation network model based on convolutional neural networks (CNN), which can automatically learn features layer by layer from a large number of input data and complete classification and recognition tasks, forming an end-to-end structure. It has strong robustness and generalization ability. The CAD system based on DL has great potential and clinical application value in improving the accuracy of pathological diagnosis, reducing missed or misdiagnosis, and reducing the workload of doctors. In this study, a set of automatic detection methods for cerebral aneurysms based on DSA technology was established. With this method, doctors could obtain three-dimensional (3D) sectional models of suspected aneurysm areas and intracranial arteries for hemodynamic analysis after the input of cranial DSA images. The core of the whole method is the use of 3D FCN, and the detection results can be obtained after the input of images conforming to the standard of Digital Imaging and Communications in Medicine (DICOM).

## 2. Materials and Methods

**2.1. Research Object.** The image data of 130 patients with unruptured intracranial cystic aneurysms who underwent routine physical examination or saw a doctor in our hospital from January 2020 to December 2021 were selected. According to the ratio of the training set and internal test set of about 4:1, the patients were randomly divided into three groups: training set (75 cases), internal test set (20 cases), and external test set (35 cases). The age of the patients in the training set and internal test set was 28–86 years old, and 37.5% were aged >60 years. Among them, the average age of the training set patients was  $(56 \pm 11)$  years old, the average age of male patients (24 cases) was  $(56 \pm 10)$  years old, and the average age of female patients (51 cases) was  $(58 \pm 13)$  years old. The average age of patients in the internal test set was  $(56 \pm 10)$  years old, and the average age of male patients (7 cases) was  $(56 \pm 10)$  years old. The average age of female patients (13 cases) was  $(56 \pm 10)$  years. Age > 60 years old accounted for 42%. Aneurysm sizes in the training set and the internal test set ranged from 1.39 mm to

21.00 mm, and 38.5% of patients had aneurysm sizes < 5.00 mm. The training set had a total of 79 aneurysms (4 double cases, 71 single cases), and the internal test set had a total of 26 aneurysms (4 double cases, 1 triple case, and 15 single cases). Aneurysm sizes in the external test set ranged from 2.00 to 23.10 mm, with 40% of patients having aneurysm sizes < 5.00 mm, with a total of 35 aneurysms (all single cases). See Table 1. The training set and the internal test set were marked by two radiologists with more than 5 years of experience, and the external test set was marked by two radiologists with more than 3 years of experience, and the DSA results were used as the gold standard.

**2.2. Training Environment and Imaging Methods.** The training environment used in this study is as follows: the central processor is Intel Core i9-9900k, the memory is Nvidia DDR4 2400 MHz 32 GB, the graphics card is Nvidia GeForce RTX 2080 Ti, and the operating system is Microsoft Windows 10 professional edition. In this environment, the training process of 200 iterations takes 16 hours, and when detecting aneurysms, the average detection speed is 58 s/case, including the output of blood vessel segmentation results and the output of detection results. Whole cerebral angiography images of all patients with the same parameters were collected: GE Innova 4100 digital flat panel angiography system and three-dimensional workstation. According to the Seldinger method, the femoral artery was punctured, and the internal carotid artery and vertebral artery underwent angiography with a 5F angiography catheter, and the frontal and lateral DSA examinations were performed to obtain DSA images. Due to retrospective data analysis, all cases with unclear images were excluded at enrollment.

**2.3. Research Methods.** First, the dataset is expanded, and the training set is expanded to 600 cases, and the internal test set is expanded to 160 cases by using flipping, discrete Gaussian filtering, and histogram equalization filtering in turn. At the same time, all the data were treated as isotropic and the blank parts around the data were cut out.

The automatic aneurysm detection method designed in this study is divided into 2 main steps: (1) automatic segmentation of intracranial arteries and (2) aneurysm detection performed using an FCN-based method.

**2.3.1. Cerebral Artery Segmentation.** After the DICOM image is preprocessed, nonlinear filtering is used to enhance the grayscale range of blood vessels. The bounding box method is used to automatically select seed points on the surrounding surface of the skull, and through the area growth of the adaptive threshold, the voxels of the skull region can be obtained, and the skull can be automatically removed. Since the voxels in the high-signal value area are mainly blood vessels in the DSA image, binarization is performed on the volume data after removing the skull, and the connected domain statistics are performed on the binarized data [10]. According to the size of the connected domain, pick a seed point. The gray value distribution of blood vessels in the DSA image data is similar to the Gaussian distribution. Using the statistical results of the connected

TABLE 1: Aneurysm condition of the training set and inner and outer test sets.

Groups	N	Number of aneurysms ( $n$ )	Average aneurysm size ( $\bar{x} \pm s$ , mm)	Number of aneurysms ( $n$ )			
				<3.00 mm	3.00~<5.00 mm	5.00~<10.00 mm	>10.00 mm
Training set	75	79	6.86 $\pm$ 4.23	9	23	30	17
Internal test set	20	26	6.30 $\pm$ 3.56	3	6	15	2
External test set	35	35	6.48 $\pm$ 4.00	2	11	17	5

domain, according to the characteristics of the Gaussian distribution, the gray distribution range of the blood vessel region can be automatically determined, and the obtained seed points and the range are used to determine the region. Upon growth, the intracranial arterial vascular tree can be obtained. A 3D reconstruction of the surface of the vessel tree is performed, and the resulting vessel tree model can be used for hemodynamic analysis.

**2.3.2. Aneurysm Detection.** An optimized 3D U-Net network is used as the detection core [11]. The network is able to handle  $128 \times 128 \times 128$  voxel data. When training the model, all the data in the training set is first resampled to  $128 \times 128 \times 128$ , and the labeled area is inflated with uniform parameters. There are two kinds of labels in the labeled area, namely, blood vessels and aneurysms. The network training adopts the form of online learning, the learning rate is  $5e-2$ , and the optimization method is adaptive moment estimation (Adam)+stochastic gradient descent (SGD). The training is completed after about 200 iterations and takes about 16 hours.

After the training of the network model is completed, the model is used to detect aneurysms. The data of the test set is firstly segmented, and then the segmented vessel tree is detected. The model can give the probability value of aneurysms for each voxel on the vessel tree and adopts the automatic threshold selection method based on the hyperbolic function to classify the detection results into two categories: blood vessels and aneurysms. When displaying the detection result, the center of all voxels of the aneurysm label is taken, and the aneurysm existing in the spherical space with a certain radius (the radius is consistent with the radius of the expansion process) is marked as a prompt to the user. See Figure 1.

**2.4. Observation Indicator.** The Dice coefficient was used to determine whether the marked area overlapped with the aneurysm, and the overlapping and nonoverlapping areas were counted. According to whether there is an aneurysm in the marked area as the basis for evaluating the performance of this method, the following two indicators are used: (1) sensitivity: the ratio of the number of labeled areas covered to the total number of aneurysms actually existing and (2) false positive rate: the ratio of the number of labeled areas without aneurysms to the sample size.

**2.5. Statistical Treatment.** Microsoft Excel 2013 software was applied. The normally distributed measurement data are represented by  $\bar{x} \pm s$ , and the count data are represented by frequency ( $n$ ) and percentage (%).

### 3. Results

In this study, the dataset is randomly divided into three subsets: training set, internal test set, and external test set. Among them, the external test set does not participate in the training and parameter adjustment process at all.

This study used fivefold cross-validation on the training set and internal test set with an average sensitivity of (94.4  $\pm$  1.1)%. For the external test set, the detection sensitivity of this method is 82.9%, and the false positive rate is 0.86 FPs/case (false positives/case). A classification comparison of the external test set data showed that the sensitivity (88.2% and 100.0%) of the method for detecting aneurysms with a size of 5.00~<10.00 mm and  $\geq 10.00$  mm was higher than that for aneurysms with a size of <3.00 mm and 3.00~<5.00 mm (50.0% and 72.7%). The detection sensitivity of patients aged 50-60 years and >60 years (90.0% and 87.5%) was higher than that of patients aged <50 years (66.7%). The difference in detection sensitivity between different genders (84.6% and 81.8% for males and females, respectively) was small. See Table 2.

Among the 6 undetected aneurysms (false negatives) in the external test set, there were 4 females and 2 males, aged 35-69 years, with aneurysm sizes ranging from 2.60 to 5.67 mm. There were 30 false positive results: 17 cases were found, 5 cases were 2 cases, and 1 case was 3 cases; the remaining 12 cases had no false positive results.

### 4. Discussion

Intracranial aneurysms are cerebral hemangioma-like protrusions caused by abnormal changes in local blood vessel morphology. The etiology of aneurysms is still unclear. Congenital factors include the following: the wall thickness of the cerebral artery is about 1/3 thinner than that of other parts of the same diameter, and it lacks the support of surrounding tissues, so it bears a large blood flow, especially at the bifurcation. Acquired factors include infection, trauma, tumor, and atherosclerosis; most of them are congenital factors. The formation mechanism of intracranial aneurysms is the stress damage of blood flow to the arterial wall. Due to the change in blood flow, a part of the arterial wall protrudes outward, forming a permanent local expansion. The magnitude of the stress is usually related to the velocity and angle of the blood vessel. Intracranial aneurysm is classified as a serious cerebrovascular disease due to its insidious onset, complex pathogenesis, and critical onset [12].

DSA combines rotational angiography, DSA technology, and computer three-dimensional image processing technology. After secondary rotation DSA collects image data, it

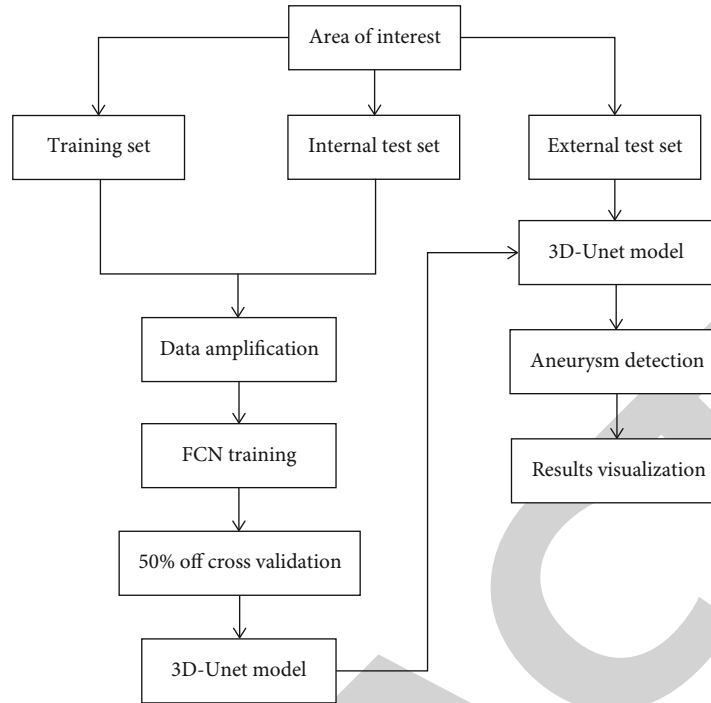


FIGURE 1: Aneurysm detection procedure.

TABLE 2: External test set comparison of aneurysm detection methods ( $N = 35$ ).

Clinical features		N	Aneurysm detection methods		Detection sensitivity (%)
			Manual marking+DSA (n)	Automatic detection (n)	
Gender	Male	13	13	11	84.6
	Female	22	22	18	81.8
Age	<50 years old	9	9	6	66.7
	50~60 years old	10	10	9	90.0
	>60 years old	16	16	14	87.5
Aneurysm size	<3.00 mm	2	2	1	50.0
	3.00~<5.00 mm	11	11	8	72.7
	5.00 mm~<10.00 mm	17	17	15	88.2
	$\geq 10.00$ mm	5	5	5	100.0

can observe and accurately measure lesions at any angle, thereby reducing the number of angiography images. From the aspect of morphology, clear observation is needed. The relationship between the tumor body and the parent artery and the diameter of the tumor diameter can be analyzed, and the adjacent relationship with the surrounding blood vessels and the blood circulation can be analyzed, the quality of image acquisition and the safety of interventional diagnosis and treatment can be improved, and the corresponding treatment can be performed after angiography [13].

All data in this study were DSA images collected with uniform parameters from outpatients and routine physical examinations. The age, gender, aneurysm location, and aneurysm size of the subjects were randomly distributed. By analyzing the results on the external test set, it can be seen that in the detection method of this study, different genders and different ages have little effect on the processing

performance, but the aneurysm size has a greater impact on the processing performance. In this study, the sensitivity of the method for detecting aneurysm samples with size  $\geq 10.00$  mm was 100.0% (including the internal test set and external test set), and the sensitivity for detecting aneurysms with size  $5.00 \sim < 10.00$  mm was better than that for aneurysms with size  $3.00 \sim < 5.00$  mm. Therefore, considering the detection performance of aneurysms of different sizes, the detection ability of aneurysms with a size of  $\geq 5$  mm is better than that of aneurysms with a size of  $< 5.0$  mm. The results could not demonstrate the detection performance of this method for aneurysms of this size. In terms of false positives, the average false positive rate in this study was 0.86 FPs/case, and the number of false positives in each case was 0-3.

The results of this study show that the detection method is not sensitive to the age of the samples. The ability of these methods to detect aneurysms in patients  $\geq 50$  years old is

better than that in patients < 50 years old. Since the data used in this study all use a unified acquisition matrix, the sharpness of the images does not change in different samples, so the detection performance of the detection method in this study on other sharpness samples cannot be proved. However, in terms of the distribution of the false negative results of this method in the samples, the FCN used in the study is suitable for the task of aneurysm detection, and increasing the data volume of the training samples is expected to improve the performance of the method. In terms of false positive performance, the false positive results obtained in this study are mainly aneurysms with a size of < 3.00 mm. Due to the process, the false positive results are all located on the cerebral arteries, which need to be confirmed by the user twice, but the average false positive rate is higher. In addition, the number of false positives in a single sample is at most 3, and the workload of secondary confirmation is relatively small. Under the current false positive rate conditions, it is considered to give priority to improving the sensitivity of the method to avoid missed diagnosis.

This study is based on the detection method of deep learning, with a sample size of 130 cases, and the obtained result has a sensitivity of 82.9% and a false positive rate of 0.86 FPs/case. Ueda et al. [14] used a two-dimensional ResNet-18 network, Nakao et al. [15] used a 4-layer CNN and sliced the data in multiple directions, and Hanaoka et al. [16] used a method based on artificial features and support vector machines to detect aneurysms. The comparison shows that the sensitivity and false positive rate of this study are better than the results of Hanaoka et al. (sensitivity 80.0%, false positive rate 3.00 FPs/case). Its effect is better than the traditional artificial feature method. However, the sample size in the study by Nakao et al. is smaller than that in the study by Ueda et al., and the network with fewer layers achieves better results, which may indicate that in the case of sufficient sample size, the network structure has a significant impact on the detection results. Shallow networks have the potential to outperform deep networks in the task of aneurysm detection. The sample size of this study is significantly smaller than that of Nakao et al. (450 cases) and Ueda et al. (1271 cases), but the number of samples required by the 3D FCN used is larger than that of the two-dimensional network (the two-dimensional network can convert each slice that is regarded as 1 sample), while the 3D network treats each aneurysm as 1 sample), so the sensitivity is lower than that of Nakao et al. and Ueda et al. The study by Ueda et al. (2.90 and 6.60 FPs/case) also illustrates the potential of 3D FCN in aneurysm detection.

To sum up, the detection method in this study has similar detection performance for different types of data (age, gender, and aneurysm size), and it also proves that 3D FCN has a good effect on structures such as bends, bifurcations, and aneurysms on blood vessels (recognition ability). However, 3D networks have higher requirements on the amount of training data, and the noise in the data has a greater impact on the training results. At present, the sensitivity of the detection method in this study is 82.9%, which is still a certain distance from clinical application. In future research, we will focus on improving methods, such as data

expansion and network model layer reduction, in order to improve the detection method in this study and overall performance.

## Data Availability

The data used to support the findings of this study are available from the corresponding author upon request.

## Conflicts of Interest

The authors declare that they have no conflicts of interest.

## References

- [1] M. H. M. Vlak, A. Algra, R. Brandenburg, and G. J. E. Rinkel, "Prevalence of unruptured intracranial aneurysms, with emphasis on sex, age, comorbidity, country, and time period: a systematic review and meta-analysis," *The Lancet Neurology*, vol. 10, no. 7, pp. 626–636, 2011.
- [2] E. H. Witvoet, N. Pelzer, G. M. Terwindt et al., "Migraine prevalence in patients with unruptured intracranial aneurysms: a case-control study," *Brain and Behavior*, vol. 7, no. 5, article e00662, 2017.
- [3] S. Juvela and M. Korja, "Intracranial aneurysm parameters for predicting a future subarachnoid hemorrhage: a long-term follow-up study," *Neurosurgery*, vol. 81, no. 3, pp. 432–440, 2017.
- [4] T. Steiner, S. Juvela, A. Unterberg, C. Jung, M. Forsting, and G. Rinkel, "European Stroke Organization guidelines for the management of intracranial aneurysms and subarachnoid haemorrhage," *Cerebrovascular Diseases*, vol. 35, no. 2, pp. 93–112, 2013.
- [5] T. Ingall, K. Asplund, M. Mähönen, and R. Bonita, "A multinational comparison of subarachnoid hemorrhage epidemiology in the WHO MONICA stroke study," *Stroke*, vol. 31, no. 5, pp. 1054–1061, 2000.
- [6] M. Edjlali, C. Rodriguez-Régent, J. Hodel et al., "Subarachnoid hemorrhage in ten questions," *Diagnostic and Interventional Imaging*, vol. 96, no. 7-8, pp. 657–666, 2015.
- [7] J. B. Bederson, E. S. Connolly, H. H. Batjer et al., "Guidelines for the management of aneurysmal subarachnoid hemorrhage: a statement for healthcare professionals from a special writing group of the stroke council, American heart association," *Stroke*, vol. 40, no. 3, pp. 994–1025, 2009.
- [8] Z. Taufique, T. May, E. Meyers et al., "Predictors of poor quality of life 1 year after subarachnoid hemorrhage," *Neurosurgery*, vol. 78, no. 2, pp. 256–264, 2016.
- [9] J. Vilkki, S. Juvela, K. Malmivaara, J. Siironen, and J. Hernesniemi, "Predictors of work status and quality of life 9–13 years after aneurysmal subarachnoid hemorrhage," *Acta Neurochirurgica*, vol. 154, no. 8, pp. 1437–1446, 2012.
- [10] L. Wen, X. Wang, Z. Wu, M. Zhou, and J. S. Jin, "A novel statistical cerebrovascular segmentation algorithm with particle swarm optimization," *Neurocomputing*, vol. 148, pp. 569–577, 2015.
- [11] F. Isensee, P. Kickingereder, W. Wick, M. Bendszus, and K. H. Maier-Hein, "Brain tumor segmentation and radiomics survival prediction: contribution to the BRATS 2017 challenge," in *Brainlesion: Glioma, Multiple Sclerosis, Stroke and Traumatic Brain Injuries*, pp. 287–297, Quebec, Canada, 2017.

## Retraction

# Retracted: Effect of Rehabilitation Physical Training on Basketball Injury under Ultrasound Examination

### Scanning

Received 20 June 2023; Accepted 20 June 2023; Published 21 June 2023

Copyright © 2023 Scanning. This is an open access article distributed under the Creative Commons Attribution License, which permits unrestricted use, distribution, and reproduction in any medium, provided the original work is properly cited.

This article has been retracted by Hindawi following an investigation undertaken by the publisher [1]. This investigation has uncovered evidence of one or more of the following indicators of systematic manipulation of the publication process:

- (1) Discrepancies in scope
- (2) Discrepancies in the description of the research reported
- (3) Discrepancies between the availability of data and the research described
- (4) Inappropriate citations
- (5) Incoherent, meaningless and/or irrelevant content included in the article
- (6) Peer-review manipulation

The presence of these indicators undermines our confidence in the integrity of the article's content and we cannot, therefore, vouch for its reliability. Please note that this notice is intended solely to alert readers that the content of this article is unreliable. We have not investigated whether authors were aware of or involved in the systematic manipulation of the publication process.

In addition, our investigation has also shown that one or more of the following human-subject reporting requirements has not been met in this article: ethical approval by an Institutional Review Board (IRB) committee or equivalent, patient/participant consent to participate, and/or agreement to publish patient/participant details (where relevant).

Wiley and Hindawi regrets that the usual quality checks did not identify these issues before publication and have since put additional measures in place to safeguard research integrity.

We wish to credit our own Research Integrity and Research Publishing teams and anonymous and named external researchers and research integrity experts for contributing to this investigation.

The corresponding author, as the representative of all authors, has been given the opportunity to register their agreement or disagreement to this retraction. We have kept a record of any response received.

### References

- [1] E. Wenjie and Q. Yu, "Effect of Rehabilitation Physical Training on Basketball Injury under Ultrasound Examination," *Scanning*, vol. 2022, Article ID 2554581, 8 pages, 2022.

## Research Article

# Effect of Rehabilitation Physical Training on Basketball Injury under Ultrasound Examination

Wenjie E.  and Qiufen Yu 

Physical Education College, Qiqihar University, Qiqihar, Heilongjiang 161006, China

Correspondence should be addressed to Wenjie E.; 1710700627@hbut.edu.cn

Received 21 June 2022; Revised 15 July 2022; Accepted 22 July 2022; Published 8 August 2022

Academic Editor: Balakrishnan Nagaraj

Copyright © 2022 Wenjie E. and Qiufen Yu. This is an open access article distributed under the Creative Commons Attribution License, which permits unrestricted use, distribution, and reproduction in any medium, provided the original work is properly cited.

In order to solve the problem of observing the effect of rehabilitation physical training on basketball player injury, a kind of observation study on the effect of rehabilitation physical training on basketball player injury based on memory ultrasound examination was proposed. This study makes a comprehensive analysis of physical fitness training factors such as physical fitness test plan, training arrangement, training method, training monitoring, and effect evaluation. Through the experiment, it is found that there are still gaps in physical training, diagnostic standards, training plans and requirements, load monitoring, standardization of operation, nutrition, and recovery in the training organization. There are only 23.81% of full-time physical coaches and 25.40% of professional team doctors at all levels of sports teams. There were only 23.81% of full-time physical fitness coaches and 25.40% of professional team doctors in all levels of sports teams. Basketball players in the basketball injury survey had 67 sports injuries throughout the year, with a rate of 3.35 injuries per person and 2.48 injuries per 1000 hours. The location of chronic injuries is usually the lower back, knee joint, and ankle. The main injuries are due to the physical component, with injuries occurring most frequently throughout the training season in July, August, and September. Experiments show that good and professional physical training can reduce the risk of injury to a greater extent than strengthening the specific skills of athletes.

## 1. Introduction

Basketball is one of the most popular sports among contemporary college students. With the development of Internet media and the increase of international exchanges and the excellent performance of basketball stars in NBA, basketball and basketball culture have been widely spread on campus. In particular, basketball has become a part of college students' after-school life with the successful promotion of basketball competitions such as NBA and CBA and College Basketball Super League. Basketball is a strong competition, combined with running jump shooting and other comprehensive sports. With the continuous high level of basketball, the athletes are in all aspects of the ability of higher and higher requirements for athletes to adapt to the needs of the development of basketball now. Frequent physical contact in the process of intense on-field confrontation is easy to cause various injuries. Knee joint injury is one of the most

common and fatal injuries, which seriously affects the sports career of athletes. Therefore, how to reduce knee joint injury and prevent injury in basketball has become the research goal of experts from all over the world for many years. With the rapid development of modern competitive sports, traditional physical training theories and methods can no longer meet the needs of competition and training, and what is conceived is a major breakthrough in the theory and method of physical training under the background of professional sports. The United States has formed a whole set of physical training system dominated by the principles and methods of functional training, which has attracted worldwide attention. The physical function training system includes movement mode training, strength training, sensitivity and balance training, energy metabolism system training, and recovery and regeneration training, as shown in Figure 1. Many elements in the body function training, combined with the characteristics of basketball special physical strength quality

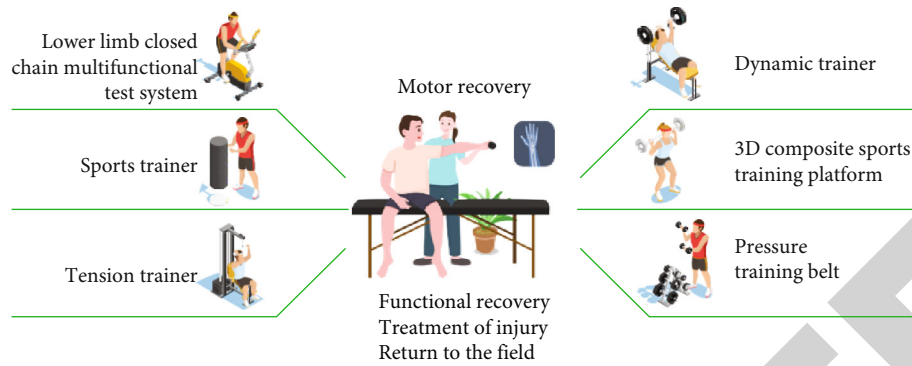


FIGURE 1: Flow chart of rehabilitation physical training.

training is always an important training contents of body function training. At the same time, China's long-term training time has been confirmed, and the body muscle strength is the key to the sports technical mastery, improvement is the guarantee of prevention, and treatment of sports injuries is the key to the sports level. Therefore, through the study of the mechanism and symptoms of knee joint injury, the results of the study can be applied to teaching in the process of basketball training and put forward the cause and the prevention and treatment of knee injuries and reduce the athlete knee joint injury in training or competition; the knee joint to minimize the damage rate prolongs the life of sports and basketball athlete's knee injury prevention, to reduce the damage and prevent to provide some reference and provide certain theoretical basis for further practical research.

## 2. Literature Review

Basketball is one of the most popular sports in the world, and it has a solid mass base. Chun et al. said that 15 cities in China have been named national basketball cities [1]. Park and Lee say that basketball is the top game loved by audiences all over the world, so there must be more personalized and perfect requirements for athletes' basic physical ability and technical and tactical level in training [2]. Sene-Mir et al. said that according to the definition of Chinese experts, physical training ability refers to the improvement of athletes' technical level and tactical level, which is reflected in three aspects, including basic physical ability, good physical quality, and technical and tactical level, which is based on the ability to create excellent competition results [3]. Lee et al. say that the development of physical ability will be one of the key factors in the ultimate success and provide a strong athletic life [4]. The training process is usually divided into basic training and special training. Kim et al. said that the former tried to improve and enhance the basic physical quality and ability of athletes, while the latter mainly made adjustments based on the characteristics of special needs and the development of different training content methods and intensity of athletes, to effectively improve the physical strength and technical and tactical level of athletes in this sport [5]. Xue et al. said that Chinese athletes still lack targeted and individualized physical training system, which is unable to transform basic physical training

into special physical training. Sports injury is a subject that every athlete will face, which is most likely to happen in training and competition [6]. Ji et al. said that the factors were related to athletes' sports types, skills, tactics, physical basic athletic ability training, competition facilities, environment, and psychological factors [7]. Jafarpour and others say that basketball is also one of the sports with a high injury rate due to overuse of joints, muscles, and ligaments due to the high-intensity confrontation and high-speed collision [8]. Yang et al. say that modern basketball is so physical and confrontational that players are at increased risk of injury during practice and play [9]. In the whole basketball sport of different intensity levels, the problem of injury has been an urgent problem to be solved. According to studies and reports, the common acute injuries of basketball players include bruise, contusion, fracture, joint sprain, and muscle strain. The incidence of sports injury is as high as 71.1%. Baniaghil and others said that sports injury not only has a negative impact on the physical and mental health of individual athletes but also affects their competitive level and restricts the development of the whole team, forming a vicious circle [10]. Damage preventive physical training is combined with rehabilitation physical training basic physical training special physical fitness training and special requirements of special technique and method, applied to athletes in different special physical training under the supervision of sports injury and functional status, in order to reduce the damage to the athletes in competitive conditions risk of injury. It combines physical fitness training and rehabilitation training as a means of intervention, supported by the knowledge of rehabilitation medicine, to ensure the physical health of daily training, mainly for athletes to provide a basis for postinjury recovery training and combined with the training concept based on injury prevention, so as to improve and develop training quality. On the basis of injury prevention, this study mainly studies the status quo between basic physical fitness and special physical fitness training of basketball players outside China, explores the current operation mechanism of sports training in China, and constructs the feasibility of injury training content and prevention sports training theory. In this study, the physical training system for basketball sports is mainly to reduce and prevent the incidence of sports injury, provide effective scientific basis and methods, ensure the physical and mental health of athletes, and prolong the life of sports career.

### 3. Method

The premise of data complementarity and fusion is that the data of both sides have unified standard requirements. The data coordinates of human skeleton joints obtained by two Kinect are recorded and output according to their respective machine coordinate systems in order to unify the fusion processing. Firstly, the two data are registered and calibrated, and the coordinate systems of the two are transformed with unified constraints, that is, the space coordinate position is transformed. The starting position of the reference coordinate system of each Kinect is in the infrared camera. The  $x$ -axis,  $y$ -axis, and  $z$ -axis with fixed coordinates are all fixed to the left of the infrared camera, and the top is in the direction of the center of the detection angle. Based on this, it is considered that the coordinate position transformation of two Kinect devices with an angle of  $a$  and a distance of  $d$  is unified, and the transformation between coordinate systems is unified, as shown in Figure 2.

The data of rotation matrix  $R_{x,y,z}$  and translation vector  $T$  of the position difference between two coordinate systems should be obtained according to the calculation of actual parameters in the process of three-dimensional space coordinate transformation. The data of the first Kinect whose three-dimensional coordinate point was originally  $(x, y, z)$  were unified to the reference coordinate standard of the second Kinect. Therefore, the transformed data  $(x', y', z')$  and the second Kinect marked the three-dimensional coordinate position of the same bone joint in the same coordinate system 130. The theoretical derivation results should be consistent, and the actual noise error can also be solved by calculation and derivation, which is convenient for comparison and analysis of the differences between the data collected by two Kinect machines and is conducive to processing and obtaining more reliable three-dimensional coordinate rotation and translation corresponding to the coordinates of human skeleton joints. The formula is shown in

$$\begin{pmatrix} x' \\ y' \\ z' \end{pmatrix} = R_{x,y,z} \begin{pmatrix} x \\ y \\ z \end{pmatrix} + T. \quad (1)$$

After coordinate calibration, the two machines unified the processing reference standard of the data of the two Kinect, but the different noise errors of each Kinect were not processed and solved. The existing data fusion technology merges two sets of data by simple summation of weighted average when data is successfully captured by either machine and compensates the prediction by simple summation average of bone data of the same node before and after frames of data image when data is lost by both machines. Although the advantages of dual Kinect are complementary and fused to a certain extent, there is still a poor fusion effect, which does not distinguish the different data changes caused by different noises caused by dual Kinect and the reliability of human data. For nonlinear

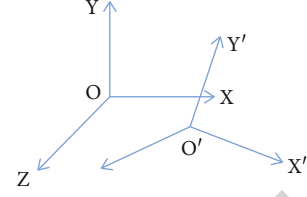


FIGURE 2: Transformation diagram between coordinate systems.

motion features, in-depth analysis considering errors, in order to solve such problem, will improve the fusion algorithm; in combination with characteristics of human physiological conditions after a trusted part of the first selected two groups of data, according to the double platform to access different angle of view to capture the human body skeleton key points, the credibility of the contribution to effect changes the contribution weight when there are two groups of data fusion. And in view of the two machines at the same time, data loss situation, the comprehensive nonlinear characteristics of human body, can ensure real time and accuracy for Kalman filter to compensate key points of state data; data fusion for data processing in the process of making not only can ensure the high accuracy of the data and can reduce the requirement of the amount of calculation and ensure real-time need. In order to reduce the amount of computation for data fusion of the two groups and optimize and improve the stability and reliability of human skeleton junction position after data fusion, reliable data screening operation is given priority during data fusion [11, 12]. There is an interdependent and restricted relationship between the joint positions of human bones. According to the physiological characteristics of human body, the bone length is fixed, so the bone length is calculated and derived according to the coordinates of the obtained data, and the bone position data is constrained and optimized [13]. The corresponding bone length  $L$  obtained by two groups of different Kinect: in calculation and comparison, the length should be consistent. According to the data of  $L_{ij11}$ ,  $L_{ij21}$ ,  $L_{ij12}$ ,  $L_{ij22}$ ,  $L_{ij1N}$ , and  $L_{ij2N}$  solved by the  $N$  frames before and after the two sets of data, the bone length with large deviation should be excluded by comprehensive consideration. The remaining  $K$  valid data were averaged to obtain the fixed value of effective bone length for data constraint optimization. The corresponding calculation formula of bone length  $L_{ij}$  is shown in

$$L_{ij} = \frac{1}{k} \sum_{k=0}^{k-1} L_{ijk}. \quad (2)$$

According to the characteristics of human motion joint rotation, it can be found that the bone rotation angle also has certain limitations, and the data can be optimized according to the rotation angle threshold constraint. Because of the human body fixed-point action, the joint twist rotation, such as rotation of the wrist, the fixed wrist joint relative to the unified reference coordinate system,



and the fixed point action space coordinates did not change, but the position orientation changed the angle. Since the range of position orientation change was not taken into account in the original data obtained, the data of human bone joints with high reliability can be screened in more detail by constraining rotation characteristics under the condition of a certain bone length, to calculate the rotation angle value of each joint point, including its flexion and extension. The calculation of the change of angle value is the Euler angle problem of rigid body in space coordinate system [14]. Rotating angle values for said joint activities, according to the actual physical joints angle threshold for data selection, convert the rotation matrix  $R$  here to form Euler angle of 60, according to the  $z$ - $y$ - $x$  axis order change, respectively, corresponding to transform angle value alpha, beta, and gamma, which converts the rotation matrix  $R$  specific formula in the form of Euler angle as shown in

$$R = R(\alpha)R(\beta)R(\gamma) = \begin{pmatrix} \cos \alpha & -\sin \alpha & 0 \\ \sin \alpha & \cos \alpha & 0 \\ 0 & 0 & 1 \end{pmatrix} \begin{pmatrix} \cos \beta & 0 & \sin \beta \\ 0 & 1 & 0 \\ -\sin \beta & 0 & \cos \beta \end{pmatrix} \begin{pmatrix} 1 & 0 & 0 \\ 0 & \cos \gamma & -\sin \gamma \\ 0 & \sin \gamma & \cos \gamma \end{pmatrix}. \quad (3)$$

At this point, the solution is shown in

$$\alpha = \arctan \frac{p_{32}}{p_{33}}, \beta = \arctan \frac{-p_{31}}{\sqrt{p_{32}^2 + p_{33}^2}}, \arctan \frac{p_{21}}{p_{11}}. \quad (4)$$

The rotation Euler angle of different joints can be selected by referring to the angle threshold of normal physiological activity of joints in medical data [15]. In order to ensure the accuracy and real time of the calculation of nonlinear human complex motion by the improved prediction method, the nonlinear motion features are linearized and transformed; to meet the nonlinear motion conditions, the idea of Kalman filter can be used to quickly predict and solve the problem and achieve high efficiency state position prediction. Here, the nonlinear motion of human body is expressed in the form of Taylor series expansion, and the position change of human skeleton junction is expressed as  $p(x)$ . When Taylor series expansion is performed at  $x_0$ , the speed change is represented by the  $-$ derivative  $p'(x)$  of  $p(x)$  at  $x_0$ .

Similarly, Taylor series expansion formula of the first two terms can be used to convert the complex real-time nonlinear change information of speed of human movement

into a linear expression, as shown in

$$p(x) = \frac{p(x_0)}{0} + \frac{p'(x_0)}{1}(x - x_0) + \dots + \frac{p^{(n)}(x_0)}{n}(x - x_0)^n + R_n(x). \quad (5)$$

Taylor series expansion of multidimensional variables is carried out in the specific form of the following 3-5 formulas, where  $J_p$  represents Jacobian matrix;  $H(\vec{x}_k)$  is represented as Hessian matrix, as shown in

$$p(\vec{x}) = p(\vec{x}_k) + J_p(\vec{x} - \vec{x}_k) + \frac{1}{2}(\vec{x} - \vec{x}_k)^T H(\vec{x}_k)(\vec{x} - \vec{x}_k) + 0^n. \quad (6)$$

The state change transfer variance formula of the improved Kalman filter is shown in

$$s_k = p(s_{k-1}) + q_k. \quad (7)$$

The corresponding formula of observed changes can be expressed as

$$o_k = h(s_k) + r_k. \quad (8)$$

By using Taylor series expansion formula, the two variances correspond to

$$s_k = p(s_{k-1}) + q_k = p(\tilde{s}_{k-1}) + p_{k-1}(s_{k-1} - \tilde{s}_{k-1}) + q_k, \quad (9)$$

$$o_k = h(s_k)r_k = h(\tilde{s}_k) + H_k(s_k - \tilde{s}_k) + r_k. \quad (10)$$

The improved Kalman filter can quickly and accurately obtain the lost data of human bone joints in the nonlinear complex human motion state. After the prediction, the data accuracy can be verified again by the constraints of bone length and joint position rotation angle, in order to ensure that the predicted data can meet the high accuracy requirements of human bone joint data and establish a solid foundation for accurate identification of human knee joint movement rehabilitation action.

## 4. Experiments and Analysis

According to the statistics of 20 college basketball players above grade II who reported injuries, the cumulative incidence rate was 99.3%, and the athlete training rate was 2.33 times per thousand hours, as shown in Table 1.

The affected days are shown in Figure 3.

It can be seen from the research data that the acute injury of basketball sports is mainly acute injury, among which the knee injury is the most serious and frequent, affecting the training days as much as 18.25 days, followed by the foot and ankle injury 8.48 days, and the spinal injury still cannot be ignored. Because acute and chronic injuries accounted for 10.94 days of spinal injury, this is a significant percentage. The proportion of acute injury is more than 70%, and it occurs during training and competition. It

TABLE 1: Injuries to college basketball players.

	Ankle	Knee	Spinal	Wrist	Lower limbs
Acute	8.48	18.25	5.67	2	
Chronic		2.67	5.27		5

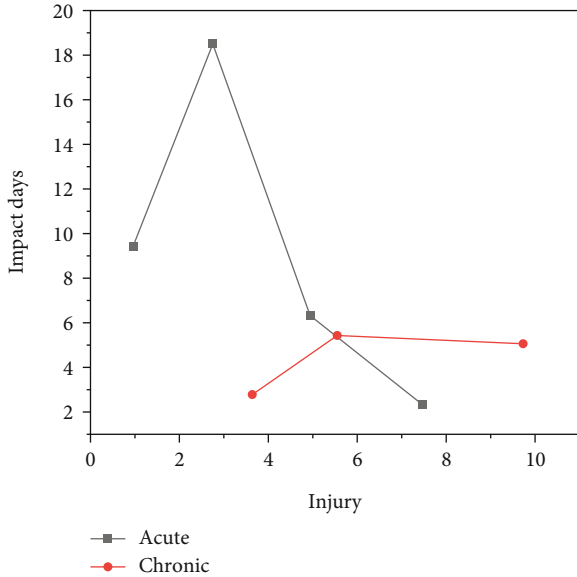


FIGURE 3: Injuries to college basketball players.

represents that the physical quality of athletes cannot bear such intense training and competition. The number of training days affected by injury is high, and the impact is huge and inestimable for a series of intensive basketball events [16, 17]. From the investigation, it is shown that the sports injuries of 20 male basketball players above grade 2 occurred in body position attributes, including acute injuries in 35 cases, accounting for 73%, and ankle injuries in 24 cases, accounting for most of them; knee injury (5 cases, 14%) was the second. There were 3 cases of spinal injury (9%). Shoulder injury in 2 cases (6%); wrist injury in 1 case accounted for 3%; There were 9 cases (75%) of chronic injuries in the spinal column. There were 3 cases of chronic injury in the knee joint, which accounted for 25% of the cases. It was found that in the nonstandard training mode received from childhood, not to mention the training of injury prevention, the pursuit of technical sports performance is the main cause of the biggest injury to the current athletes. In order to effectively reduce and prevent basketball injury, injury prevention measures and good physical training are necessary. Gradually increase the intensity of training and teaching competitions and let the athletes gain reasonable progress. Extensive evaluation and revision of the operation process are required to ensure the best preparation for injury prevention and competition excellence [18]. As coaches and team doctors, we must understand how to minimize sports injuries, which is the embodiment of the need to learn more relevant knowledge and practice, so as to help athletes grow up healthily. Common injury prevention strategies include the following aspects: pay attention to the field

condition of the sports ground at any time and the influence of equipment and facilities on the safety of the situation for a comprehensive inspection, no matter in the training or competition environment, or on the athletes, to reduce the incidence of injury, the software and hardware need to be complete, and reasonable and careful personalized training course planning. In order to improve the athletes' basic sports ability and strengthen the level of physical training, strengthening training load control, developing emergency plans, travel safety, and competitive strategy enhance athletes' competitive level and physical and mental health [19, 20]. From the feedback questionnaire of coaches and athletes, the most common methods adopted by coaches are the training method to avoid aggravating the injury and the strength exercise to strengthen the injured part, and the proportion is nearly 90%, which indicates that the training of trainers in the rehabilitation stage after the injury of athletes is mainly to avoid aggravating the injury and then strengthen other training of the injured part, hoping that the injured part of the athlete will not be degraded or other adverse effects due to the rest of the rehabilitation period. And in part of the athletes, it is give priority to in order to strengthen the power of the injured area to practice and strengthen the core strength training proportion similar to avoid aggravating the proportion of pain, showing athletes in convalescence after injury; choose the injured parts of the relevant training, to maintain the quality of their own body condition and to avoid physical injury [21]. It can be found from the feedback of these two degrees that sports injury has a great impact on athletes, even the whole sports team, and has a certain impact on the athletes' competitive state. How to prevent it through training in advance is a good solution to reduce or even avoid the occurrence of such situation. In the prevention of sports injury mechanism, the coach will focus on the amount of strength training, strengthen the ability to fight, and implement warm-up and relaxation exercises before and after the training; athletes also focus more on strength training [22, 23]. It can be seen that both trainers and athletes believe that strengthening strength training and improving body resistance can avoid sports injuries. However, compared with the ankle, which is the most common part of injuries, it can be found that the balance and stability of the body and joint flexibility are relatively neglected by trainers and athletes. It can be seen that in the measures to prevent sports injuries, trainers and athletes do not do specific injury prevention training for the project and part, resulting in the gap between prevention and reality, and unable to produce effective and meaningful effects [24]. Coaches have more perfect ideas and practices for injury prevention, but lack more complete ideas and practices for the core training of joint flexibility and body balance and stability. There are serious deficiencies in the concept and measures of athletes' prevention of sports injury. In the above research data, the overall data found was only maintained at about 50%. The best was 63.11% for strong core strength training to improve body collision ability, and the concept of improving joint flexibility was only 40.16 for the most lack of injury prevention. This phenomenon shows that the thinking of injury prevention and

TABLE 2: Measures adopted by coaches to prevent sports injuries ( $n = 15$ ).

Option	Percentage
Strengthen subjective understanding, always alert to the occurrence of injury accidents	93.33%
Standardize the technical movements of strength exercises, and apply soil to the existing injured parts to prevent injury support belt	93.33%
Strengthen strength training, improve the ability to fight	100.00%
Strengthen core strength training to improve body balance and stability	66.67%
Improve the athlete's joint flexibility	60.00%
Warm up and stretch before training or a race	100.00%
Finish with stretching and relaxation exercises	100.00%

TABLE 3: Measures adopted by athletes to prevent sports injury ( $n=128$ ).

Options	Percentage
Strengthen subjective understanding, always alert to the occurrence of injury accidents	54.10%
Standardize the technical movements of strength exercises, and apply soil to the existing injured parts to prevent injury support belt	56.56%
Strengthen strength training, improve the ability to fight	63.11%
Strengthen core strength training to improve body balance and stability	57.38%
Improve the athlete's joint flexibility	40.16%
Warm up and stretch before training or a race	54.10%
Finish with stretching and relaxation exercises	54.10%

the actual training effect are not fully played, and the injury rate of athletes is in a crisis, which not only affects sports performance, but also affects life and physical and mental health if the injury is serious, which is worth my strict prevention, as shown in Table 2 and Table 3.

It can affect our life and our health, and it is worth keeping a lid on. In the annual report, it is found that the rate of upper limb injury accounts for nearly 15% of the total, especially the waist injury is the most common chronic sports injury of basketball players. Studying abroad is similar to the results for the training process; only pay attention to the training methods, one-way as centripetal and centrifugal training proportion or pull and push action structure, especially for mechanical principle and features have failed to notice, so great pressure on the spine and large joints and incongruity caused serious imbalance between muscles and bones, so not only the former back, even left and right sides due to the inertia of the movement caused by uneven training phenomenon, so waist injury and knee and shoulder injuries are common [25, 26]. Therefore, in the course planning and design, focusing on the relationship between the corresponding and the two sides can effectively prevent injury. Because of careful training, athletes can have more achievements in sports performance. It can be found from the previous explanation that the prevention ideas and objects cannot be completely prevented, and it is more worrying when sudden injury really occurs in the process of training and competition. The coach's research shows that the treatment of the occurrence of injury is relatively clear and effective, and the treatment is more appropriate because of accumulated experience in the interview, whereas in ath-

lete's research found that not only prevent insufficient knowledge, together with the injury how emergency treatment is relatively lack of knowledge, the most striking is 39.34% of athletes to think in the arena to show oneself and to insist on playing for the injury in a patient and uncertainty and thus the best opportunity to impact damage emergency treatment. Moreover, only 50 percent of athletes knew whether they should seek medical attention or not. Immediate ice treatment is already the best emergency response measure, and there are only 68.85% of it. From the above, we can know that athletes' sports life and health-related knowledge need to be greatly improved and paid attention to. This is not only the injury problem, but also the key to improve the performance of athletes and sports literacy [27]. Regardless of athletes or coaches, encounter acute accidental damage, in ice compress and bandaging treatment as a priority, and subsequent processing is not to a hospital for medical checks, the impact of these sudden damages for the players is huge; not game is unable to training; the team's training policy and curriculum, will produce unexpected delays and the influence [28]. The most obvious effect of its physical signs is in the short distance, high intensity, and high explosive power events; effective anaerobic training can improve speed and explosive power and maintain strong muscle strength. Sprint acceleration, deceleration, and change of direction in training competitions all require anaerobic operation, and effective anaerobic training can strengthen the use and ability of muscles in these steering body parts. In the statistical table of sports trauma, the steering parts, such as ankle and knee, account for more than 53% of the acute injury sites. It can be

seen from the above points that injury prevention physical training method can effectively improve the anaerobic ability of athletes in the part of anaerobic ability and can effectively prevent the injury caused by anaerobic ability deficiency of athletes.

## 5. Conclusion

The investigation shows that the injury of basketball players is usually concentrated in the acute and excessive use of muscles, ligaments, and bones, resulting in long-term injury and inflammation. Chronic injury is the main injury of basketball players, which is mainly concentrated in the injured parts of waist, knee, and ankle. In the past, sports medicine focused on physiology-based recovery and rehabilitation treatment, but neglected to rehabilitation physical training and injury prevention physical training. Lead to basketball players is repeatedly injured, and injury recovery time is too long and other problems, at the same time, due to the impact of injury and lack of in-depth understanding of physical training unknowingly lead to increased risk of sports injury. Physical training in training organizations, diagnostic criteria, training program and requirements, load monitoring, operation standardization, nutrition, and recovery, there is gap between Chinese basketball training in the fitness test planning training arrangement training method training monitoring and evaluation, etc. There is a big board; this is the main cause of the high incidence of sports injuries. Based on the situation of sports injury of Chinese basketball players and the deficiency of physical training, the frame system of injury prevention physical training is constructed, which mainly includes the training principle evaluation system, content framework, stage division, and effect monitoring.

## Data Availability

The data used to support the findings of this study are available from the corresponding author upon request.

## Conflicts of Interest

The authors declare that they have no conflicts of interest.

## Acknowledgments

This study was supported by the Research Project of Basic Scientific Research Business Fee of Heilongjiang Provincial Higher Education Institutions "Innovation Research on Diversified Supply Path and Strategy of Public Service of Ice and Snow Sports Tourism in Heilongjiang province" with project no.: 135409337 and by the Qiqihar Philosophy Social Science Research Planning General Project "Qiqihar City Ice Sports Tourism Public Service Supply Model Innovation Research" with project number: QSX2021-20YB.

## References

- [1] H. Chun, Y. A. Jeong, and B. Lee, "The effect of action observation training on brain activity in children with cerebral palsy," *The Journal of Korean Academy of Physical Therapy Science*, vol. 27, no. 1, pp. 18–25, 2020.
- [2] G. H. Park and H. M. Lee, "Effect of action observation physical training for chronic stroke patients on the stairs walking ability and self-efficacy," *The Journal of Korean Physical Therapy*, vol. 33, no. 2, pp. 53–61, 2021.
- [3] A. M. Sene-Mir, M. Portell, M. T. Anguera, and S. Chacón-Moscoso, "Manual material handling training: the effect of self-observation, hetero-observational and intrinsic feedback on workers' knowledge and behaviour," *International Journal of Environmental Research and Public Health*, vol. 17, no. 21, article 8095, 2020.
- [4] H. J. Lee, J. S. Lee, and Y. M. Kim, "Effects of action observation training and mirror therapy on the electroencephalograms of stroke patients," *The Journal of Korean Physical Therapy*, vol. 33, no. 2, pp. 106–113, 2021.
- [5] T. Kim, C. Frank, and T. Schack, "The effect of alternate training of action observation and motor imagery on cognitive and skill performance," *International Journal of Sport Psychology*, vol. 51, no. 2, pp. 101–121, 2020.
- [6] X. Xiao, L. Xin, L. Yu et al., "Clinical observation on the time-effect relationship of moxibustion for primary dysmenorrhea due to stagnation and congelation of cold-damp," *Journal of Acupuncture and Tuina Science*, vol. 19, no. 1, pp. 62–66, 2021.
- [7] Y. K. Ji, Y. U. Ryu, and J. Park, "The effects of action observation with functional electrical stimulation on corticomuscular coherence," *The Journal of Korean Physical Therapy*, vol. 32, no. 6, pp. 365–371, 2020.
- [8] H. Jafarpoor, M. Hosseini, M. Sohrabi, and M. Mehmannaevazan, "The effect of direct observation of procedural skills/mini-clinical evaluation exercise on the satisfaction and clinical skills of nursing students in dialysis," *Journal of Education and Health Promotion*, vol. 10, pp. 1–6, 2021.
- [9] X. Yang, M. Zhang, L. Kong, Q. Wang, and J. C. Hong, "The effects of scientific self-efficacy and cognitive anxiety on science engagement with the "question-observation-doing-explanation" model during school disruption in covid-19 pandemic," *Journal of Science Education and Technology*, vol. 30, no. 3, pp. 380–393, 2021.
- [10] A. Baniaghil, S. Ghasemi, M. Rezaei Aval, and N. Behnampour, "Effect of communication skill training based on Calgary-Cambridge observation model on midwifery students' communication skills," *Journal of Research Development in Nursing and Midwifery*, vol. 17, no. 2, pp. 24–27, 2020.
- [11] S. M. Son and K. W. Kang, "Effect of action observation training using y-balance on balance capability in young adults," *The Journal of Korean Physical Therapy*, vol. 32, no. 2, pp. 65–69, 2020.
- [12] R. L. A. Touche, F. C.-M. Herranz-Gómez, A. Paris-Alemanay, and L. Suso-Martí, "Effect of brain training through visual mirror feedback, action observation and motor imagery on orofacial sensorimotor variables: a single-blind randomized controlled trial," *Journal of Oral Rehabilitation*, vol. 47, no. 5, pp. 620–635, 2020.
- [13] A. Karadeniz, C. K. Altundag, and A. S. Yucel, "Investigating the effects of worksheets supported with prediction-observation-explanation method on high school students opinions," *New Trends and Issues Proceedings on Humanities and Social Sciences*, vol. 7, no. 3, pp. 198–203, 2020.
- [14] D. Fazeli, H. R. Taheri, and A. S. Kakhki, "Utilizing the variability of practice in physical execution, action observation,

## *Retraction*

# **Retracted: Preparation and Performance Analysis of Bacterial Cellulose-Based Composite Hydrogel Based on Scanning Electron Microscope**

### **Scanning**

Received 20 June 2023; Accepted 20 June 2023; Published 21 June 2023

Copyright © 2023 Scanning. This is an open access article distributed under the Creative Commons Attribution License, which permits unrestricted use, distribution, and reproduction in any medium, provided the original work is properly cited.

This article has been retracted by Hindawi following an investigation undertaken by the publisher [1]. This investigation has uncovered evidence of one or more of the following indicators of systematic manipulation of the publication process:

- (1) Discrepancies in scope
- (2) Discrepancies in the description of the research reported
- (3) Discrepancies between the availability of data and the research described
- (4) Inappropriate citations
- (5) Incoherent, meaningless and/or irrelevant content included in the article
- (6) Peer-review manipulation

The presence of these indicators undermines our confidence in the integrity of the article's content and we cannot, therefore, vouch for its reliability. Please note that this notice is intended solely to alert readers that the content of this article is unreliable. We have not investigated whether authors were aware of or involved in the systematic manipulation of the publication process.

Wiley and Hindawi regrets that the usual quality checks did not identify these issues before publication and have since put additional measures in place to safeguard research integrity.

We wish to credit our own Research Integrity and Research Publishing teams and anonymous and named external researchers and research integrity experts for contributing to this investigation.

The corresponding author, as the representative of all authors, has been given the opportunity to register their agreement or disagreement to this retraction. We have kept a record of any response received.

### **References**

- [1] M. Shao, Z. Shi, B. Zhai, X. Zhang, and Z. Li, "Preparation and Performance Analysis of Bacterial Cellulose-Based Composite Hydrogel Based on Scanning Electron Microscope," *Scanning*, vol. 2022, Article ID 8750394, 7 pages, 2022.

## Research Article

# Preparation and Performance Analysis of Bacterial Cellulose-Based Composite Hydrogel Based on Scanning Electron Microscope

Meiling Shao , Zhan Shi , Bin Zhai , Xiangfei Zhang , and Zhongyi Li 

College of Chemistry and Chemical Engineering, Shangqiu Normal University, Shangqiu, Henan 476000, China

Correspondence should be addressed to Meiling Shao; 11231125@stu.wxica.edu.cn

Received 16 June 2022; Revised 16 July 2022; Accepted 22 July 2022; Published 6 August 2022

Academic Editor: Balakrishnan Nagaraj

Copyright © 2022 Meiling Shao et al. This is an open access article distributed under the Creative Commons Attribution License, which permits unrestricted use, distribution, and reproduction in any medium, provided the original work is properly cited.

In order to better prepare and analyze bacterial cellulose-based composite hydrogels, an experimental method based on scanning electron microscopy was proposed. The specific content of the method is to observe the hydrogel through scanning electron microscope, to observe the space between molecules through experiments, and to improve the effect of bacterial cellulose preparation of hydrogel. The experimental results show that the gel preparation effect is best when PEG concentration is not more than observed by scanning electron microscope. It is better to prepare bacterial cellulose complex hydrogel by scanning electron microscopy.

## 1. Introduction

Scanning electron microscope (SEM) is a kind of observation means between transmission electron microscope and optical microscope [1]. It uses a very narrow focused high-energy electron beam to scan the sample. Through the interaction between the beam and the material, various physical information is stimulated, and the information is collected, amplified, and reimaged to achieve the purpose of characterization of the microscopic morphology of the material. New scanning electron microscopes have a resolution of 1 nm. Magnification can reach 300,000 times and above continuous adjustable. In addition, scanning electron microscope and other analysis instruments can be combined to observe the microscopic morphology and analyze the composition of the material in small areas. Scanning electron microscope is widely used in the study of rock and soil graphite ceramics and nanomaterials. Therefore, scanning electron microscope plays an important role in scientific research.

The signals used for scanning electron microscopy imaging come from the interaction of the incident light beam with atoms at different depths in the sample. Under electron beam bombardment, the samples will produce many kinds

of signals including back scattering, electron secondary electron, characteristic X-ray, absorption electron, transmission electron, auger electron, cathode fluorescence electron, and beam induced effect [2–4]. While it is difficult for a single machine to have all the detectors, the backscattered electron (BSE) and secondary electron (SEI) characteristic X-ray detector is the standard detector of general scanning electron microscopes.

Cellulose is the most abundant natural biodegradable polymer in the world, which exists widely in the plant kingdom and is one of the main research objects in the birth and development stage of polymer chemistry [5]. Figure 1 shows the preparation of the collagen-based hydrogels. At present, there are two kinds of different ways to obtain cellulose. One is natural synthetic cellulose, which is synthesized by plants through photosynthesis or by microorganisms. The other is synthetic cellulose, which is synthesized by enzyme-catalyzed synthesis of cellulose and glucose from ring-opening polymerization of neopentyl derivatives in vitro. Synthetic cellulose has lower crystallinity and less regular morphology than natural cellulose. In today's world facing four major problems of population, resources, environment, and food, renewable natural resources have important strategic significance for sustainable development [6, 7].

In addition to plant cellulose, microorganisms can also ferment to produce cellulose, which is collectively known as bacterial cellulose [8]. When using *Acetobacter xyloxydum* for static culture, Pfdab et al. found that a membrane formed on the surface of the medium, which was named BC after physical and chemical analysis, confirmed that it had a structure similar to cellulose [9]. According to the research, bacterial cellulose is a chain polymer composed of glucopyranose residue to residue to glycosidic bond  $\beta-1$ . It has nanometer ultrafine network structure and has more excellent characteristics than natural plant cellulose, such as high purity, high crystallinity, large specific surface area, good hydrophilicity and biocompatibility, and easy to degrade in the environment. At present, in developed countries, bacterial cellulose industry has initially formed an annual value of more than 100 million dollars of market, involving food, chemical, pharmaceutical, textile, and papermaking industries. As a kind of environmentally friendly and renewable biological material, bacterial cellulose has great commercial value and good development prospect under the situation of increasing population and resource shortage in the world.

## 2. Literature Review

Bacterial cellulose exists in the form of pure cellulose and has a similar structure to cellulose produced by plants or algae, with unique physical and chemical properties. BC has a dense three-dimensional network structure, and the fiber diameter is between 30 and 100 nm, which is 1/10-1/100 of the plant cellulose fiber. The bacteria that can produce cellulose are mainly acetic acid bacteria, rhizobia, soil bacteria, octadiococcus, etc. The most effective species used in microbial research is the Gram-negative *Acetobacter xyloxydum*, which was renamed as *Gluconacetobacter xylinus* internationally.

Studies on bacterial cellulose synthesis contribute to a better understanding of the biological origin of plant cellulose. At the beginning, the research on BC biosynthesis has been limited to physiological and biochemical properties, but in recent decades, with the development of molecular biology, the research on the mechanism of BC biosynthesis has been accelerated. The synthesis of bacterial cellulose is a specifically controlled multistep reaction process involving a complex system of unique enzymes that catalyze and regulate protein reactions. These processes include the synthesis of the cellulose precursor glucose uridine diphosphate, followed by glucose polymerization  $\beta-1$ , and the synthesis of 4-glucan chains, whereby the terminal complex continuously transfers pyranoid glucose residues from UDPGlu to the newly formed polysaccharide chain. Supramolecular network structure was thus formed. The synthesis pathway of UDPGlu has been reported, but the molecular mechanism of the assembly and combination of multiple dextran chains into fibrils needs to be further elucidated.

The pentose phosphate cycle and tricarboxylic acid cycle are two main metabolic pathways in cellulose synthesis by *Acetobacter xyloxydum*. The pentose phosphate cycle is a metabolic process through glucose alienation and effective sugar alienation synthesis of cellulose. Because of the possi-

bility of mutual conversion between pyruvate and glucose, the glycolysis pathway should be inhibited so that pyruvate is continuously converted to glucose. In the tricarboxylic acid cycle, glycogen dissimilation occurs from oxaloacetate through pyruvate, oxaloacetate decarboxylase, and pyruvate kinase, and hexose phosphate synthesizes cellulose through isomerization and phosphorylation. When the energy charge is high, that is, when the activity of 6-phosphate glucose dehydrogenase is inhibited by ATP, glucose metabolism is conducive to the synthesis of cellulose, whereas glucose metabolism enters HMP (Table 1).

In view of this research problem, Ji et al. believed that bacterial cellulose in wet state had high tensile strength, high elastic modulus, high water holding capacity, and smooth internal and external surface, which could be used as artificial blood vessels in surgery [10]. Vasava and Panchal believed that bacterial cellulose had a special three-dimensional network structure, high wet strength, high water absorption, and water retention due to nanoeffect and could be formed by in situ processing in wet state. Because of its high purity and excellent performance, bacterial cellulose fiber can be widely used in medical dressings, tissue engineering scaffolds, artificial blood vessels, artificial skin, and other aspects. It is one of the hot fields of international biomedical material research [11]. Babu believes that the combination of scanning electron microscope and other analytical instruments can be used to observe the microscopic morphology and analyze the composition of the material in small areas [12].

An experimental method based on scanning electron microscope is proposed in this paper. The specific content of this method is to observe the hydrogel through scanning electron microscope and observe the intermolecular space through experiment to prove the effect of this method to solve the problem of preparing hydrogel from bacterial cellulose.

## 3. Method

*3.1. Secondary Electron Morphology Contrast Principle.* Secondary electron is a kind of free electron produced by bombarding the sample with an electron beam so that the outer electrons of the atom in the sample are separated from the atom. Secondary electron has a lower energy, generally less than 50 eV. Since the secondary electrons are generated very close to the surface of the sample (generally 5-10 nm away from the surface), the secondary electron imaging (SEI) can characterize the sample surface with a high resolution up to 1 nm.

*3.2. Principle of Atomic Number Contrast of Backscattered Electrons.* Backscattered electrons (BSE) are part of the electrons reflected by the sample in the process of electron beam bombardment, including elastic backscattered electrons reflected by the nucleus and inelastic backscattered electrons reflected by the outer nucleus. The scattering angle of elastic backscattering electrons is greater than 90, and there is no energy loss. Therefore, the energy of elastic backscattering electrons is very high, generally reaching thousands to tens

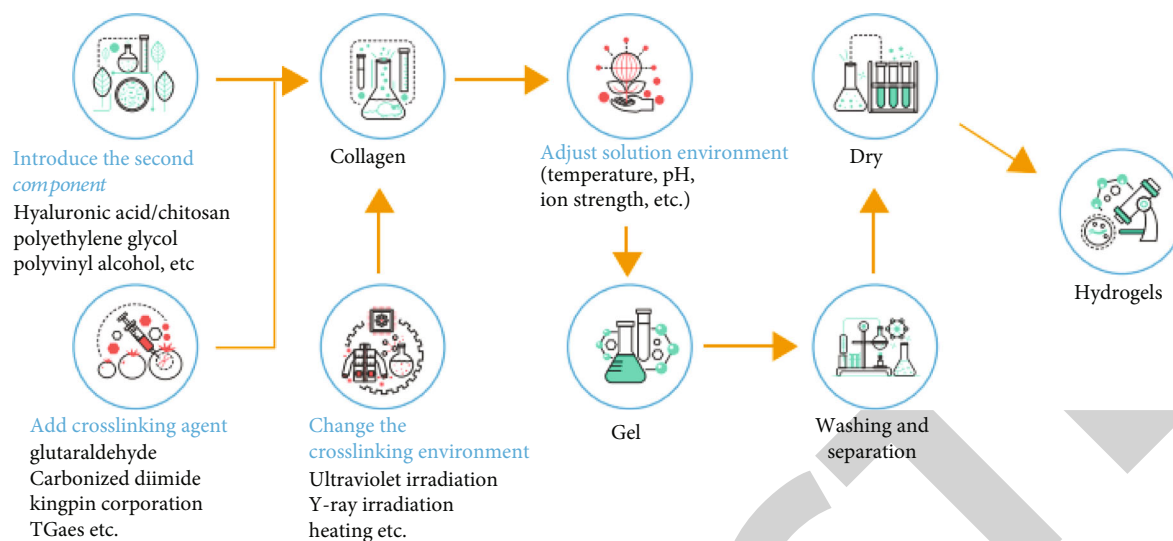


FIGURE 1: Preparation of collagen-based hydrogel.

TABLE 1: Characteristics of bacterial cellulose species.

Bacterial genus	Cellulose characteristics	Crystal form	Function
Acetobacter	Extracellular membrane cellulose	Type I of type II	Aerobic environment
Rhizobium	Extracellular microfibrils	Type I	Adsorb to parasitic plants
Agrobacterium	Extracellular microfibrils	Type I	Adsorb to plant tissue
Sarcina	Amorphous cellulose	Type I	Unclear

of thousands of volts. Inelastic backscattering electrons not only change direction but also have different degrees of energy loss due to collision with exonuclear electrons. Therefore, the energy distribution range of inelastic backscattering electrons is wide, generally tens of electron volts to thousands of electron volts. Since inelastic backscattered electrons need to be scattered many times before escaping from the sample surface, the number of inelastic backscattered electrons is much higher than that of inelastic backscattered electrons. Therefore, the backscattered electrons referred to in scanning electron microscopy mostly refer to elastic backscattered electrons. The resolution of the backscattered electron image is lower than that of the secondary electron image because the backscattered electron image is generated at a depth of several hundred nanometers from the sample surface. However, the yield of backscattered electrons is highly dependent on the atomic number of the sample, so it can be used to provide information on the atomic number contrast of the sample. In the backscattering mode, the region with large average atomic number on the sample surface has strong backscattering signal, which shows high brightness in the electron microscope image. On the contrary, the region with small atomic number is dark. Therefore, in the analysis of scanning electron microscope, backscattered electrons are usually combined with the energy spectrum produced by characteristic X-ray to do composition analysis. In addition, because the intensity of backscattered signal is related to the angle between the sample crystal plane and the incident electron beam, when the

angle between the incident electron beam and the crystal plane is larger, the backscattered signal is stronger, and the image is brighter and vice versa; the backscattered electron can be used for crystal orientation analysis [13, 14].

**3.3. Principle of Characteristic X-Ray and Application of Energy Spectrum.** When the high-energy electron beam bombards the sample and ionizes the electrons in the inner layer of the atom in the sample, the atom at this time is in a high excited state, and the high-energy electrons in the outer layer will transition to the inner layer to fill the vacancy in the inner layer and release energy, which is called characteristic X-ray. These characteristic X-rays can be used to identify components and determine the abundance of elements in samples.

**3.4. Experiment Reagent.** Experimental reagents and instruments are shown in Tables 2 and 3.

### 3.5. Minimal Medium

- (1) Inclined surface medium for *Acetobacter xylanoides*: glucose 25 g/L, peptone 3 g/L, yeast extract 5 g/L, agar sterilization 18 g/L, and pH 5; the sterilization was conducted under 121°C for 20 min (3 strains all use the same inclined plane medium)
- (2) Seed solution of *Acetobacter xylanoides* slant medium



TABLE 2: Test reagent list.

Name	Molecular formula	Actual size
Glucose	C <sub>6</sub> H <sub>12</sub> O <sub>6</sub>	Analytically pure
Xylose	C <sub>5</sub> H <sub>10</sub> O <sub>5</sub>	Analytically pure
Galactose	C <sub>6</sub> H <sub>12</sub> O <sub>6</sub>	Analytically pure
Arabinose	C <sub>5</sub> H <sub>10</sub> O <sub>5</sub>	Analytically pure
Mannose	C <sub>12</sub> H <sub>22</sub> O <sub>11</sub>	Analytically pure
Tryptone		Biochemical reagent
Yeast		Biochemical reagent
Citric acid	C <sub>6</sub> H <sub>8</sub> O <sub>7</sub> ·H <sub>2</sub> O	Analytically pure
Agar powder		Biochemical reagent
3,5-Trinitro	C <sub>7</sub> H <sub>4</sub> N <sub>2</sub> O <sub>7</sub>	Analytically pure
Trinitro-seignette salt	C <sub>4</sub> H <sub>4</sub> KNaO <sub>6</sub> ·4H <sub>2</sub> O	Analytically pure
Phenol	C <sub>6</sub> H <sub>5</sub> OH	Analytically pure
Anhydrous sodium sulfate	Na <sub>2</sub> SO <sub>4</sub>	Analytically pure
Sodium hydroxide	NaOH	Analytically pure

TABLE 3: Experimental apparatus.

Name of instrument	Model
Sartorius electronic scales	BS224
Magnetic stirring apparatus	85-1B
Lightning magnetic laboratory digital pH meter	PHSJ-4A
Automatic autoclave cooker	YXQ-LS-SH
Peying full temperature control shaker	HYG-B
Water-jacket incubator	9080
Double single clean table	SW-CJ-2FD
Digital display electric thermostatic water bath	XMTB
Electrothermostatic blast oven	DHG-914OA
Lyophilizer	Alpha 1-2 LD
Scanning electron microscope	BSESEI
Fully automatic specific surface and porosity analyzer	TriStar II 3020
Fourier transform infrared Raman spectroscopy	NEXUS-670

- (3) Glucose 25 g/L, peptone 3 g/L, yeast extract 5 g/L, and pH 5.0; the sterilization was conducted under 121°C for 20 min
- (4) Fermentation medium for *Acetobacter xyloxydans* seed liquor
- (5) Fermentation medium: carbon source 25 g/L, peptone 3 g/L, and yeast extract 5 g/L; the sterilization was conducted under 121°C for 20 min
- (6) Note: the carbon source is xylose glucose, arabinose galactose, or mannose

3.5.1. *Acetobacter xyloxydans* Seed Rejuvenation. The medium used for rejuvenation is liquid seed medium, and the configuration method is shown in 3.4 [15]. The seed medium and activated strain inclined surface were taken, and two ring

TABLE 4: Orthogonal experimental factors and level tables.

	Bacterial strain	Inoculum age	Inoculum size
1	ATCC23770	18 h	6%
2	ZGD201301	24 h	8%
3	ATCCZ200801	30 h	10%

strains were selected by inoculation ring and inserted into 100 mL liquid medium. The whole process was sterile operation. After the medium was shaken well, it was placed in a temperature-controlled shaker and incubated at a speed of 160 RPM for 24 hours.

3.5.2. *Preparation of Bacterial Cellulose Membrane*. The finished seed liquid was inoculated into 100 mL different fermentation medium by 6% (wt%) and incubated for 30 days at constant temperature. Gel-like bacterial cellulose film with certain thickness was generated at the interface between medium and air [16].

3.5.3. *Posttreatment of Bacterial Cellulose Membrane*. The bacterial cellulose membrane, which had been incubated for 10 days, was removed and rinsed with deionized water. After 2 hours immersion in NaOH aqueous solution of 0.1% (wt%) at 80 °C, they were then immersed in deionized water at 80 degrees Celsius for two hours. Cyclic treatment was performed at least 3 times to remove the remaining thal- lus and culture medium, resulting in a transparent gel-like bacterial cellulose membrane. Rinse repeatedly with deionized water until the pH is about 7, and the film appears milky and translucent [17]. Put it into deionized water and store it at room temperature after sterilization for 20 min. The wet film is bacterial cellulose. The wet film is quick-frozen with liquid nitrogen and then freeze-dried with a freeze dryer to obtain bacterial cellulose dry [18].

3.5.4. *Effects of Inoculum Amount on Bacterial Cellulose Yield and Fermentation Initiation on Bacterial Cellulose Yield*. Three strains of *Acetobacter xyloxydans* used fermentation medium of E -carbon source D-grapes. The shaking time of the seed solution was 30 hours. Then the inoculum was inoculated into 50ml of fermentation medium at 2%, 4%, 6%, 8% and 10%. The initial pH was 5.5 and incubated at 30°C for 10 days. The initial pH was 5.5 and incubated at 30°C for 10 days. Bacterial cellulose membranes were harvested and then dried, weighed and averaged.

The fermentation medium of three strains of *A. xyloxydans* strains is D-glucose. The shaking time of seed liquid was then inoculated into fermentation medium according to the inoculation amount, starting at 4, 4.5, 5, 5.5, and 6. The bacterial cellulose film was harvested and then dried and weighed for average value [19].

Orthogonal experiment design is to use mathematical statistics and orthogonality principle, through the reasonable arrangement of experiments, through a few test times, quickly obtain experimental results [20]. Orthogonal experiment is within the scope of the investigation; the purpose of the selected typical minority test conditions and find the

TABLE 5: DNS sample list.

Glucose (mL)	0.1	0.2	0.3	0.4	0.5	0.6	0.7	0.8	0.9	1.0
Water (mL)	0.9	0.8	0.7	0.6	0.5	0.4	0.3	0.2	0.1	0
Sugar concentration (mg/mL)	0.2	0.4	0.6	0.8	1.0	1.2	1.4	1.6	1.8	2.0

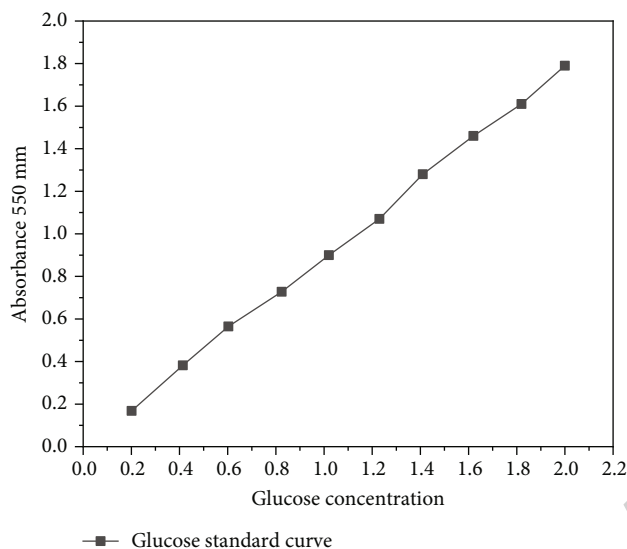


FIGURE 2: Glucose standard curve.

best condition of production and scientific research. Selecting strains of ages and the quantity of the experiment, to design the orthogonal scheme with three factors three levels, each child three parallel experiment, initial 5, fermentation time for 10 days, harvest bacterial cellulose membrane. Then dry weight average. Table 4 shows the orthogonal experimental factors and level tables.

**3.6. Effect of Fermentation Days on Bacterial Cellulose Fermentation.** The shaking time of carbon source glucose seed solution in fermentation medium used by three strains of *Acetobacter xylobacter* was selected for 30 hours, and then, 50 mL of carbon source glucose seed solution was inoculated into fermentation medium at an inoculation rate of 8% and incubated for 10 days at a constant temperature starting at 5 and 30, respectively. Samples were taken every two days to measure the change in yield and the concentration of residual carbon source in fermentation liquid. The carbon source utilization rate and cellulose conversion rate of the three strains were calculated [21].

$$\begin{aligned} &\text{Carbon source utilization ratio (\%)} \\ &= \frac{(\text{initial carbon source concentration} \\ &\quad - \text{final carbon source concentration})}{\text{initial carbon source concentration}}, \end{aligned}$$

$$\begin{aligned} &\text{BC percent conversion (g/g)} \\ &= \frac{\text{BC output}}{\text{Total initial carbon source} - \text{Total final carbon source}}. \end{aligned} \quad (1)$$

**3.7. Determination of Residual Sugar in Fermentation Broth.** The DNS method was used to prepare standard glucose solution; then, 10 test tubes (25 mL) were taken, and corresponding reagents were added according to Table 5. Then, DNS reagents were added, respectively, and the boiling water bath was conducted for 5 minutes. Figure 2 shows the blood glucose standard curve. After cooling, deionized water was added. After mixing, the absorption value was measured at the wavelength with the standard glucose concentration as the abscissa and the absorbance value as the ordinate. The standard curve was drawn, and the regression equation was calculated [22].

**3.8. Observing Colloidal Structure.** BC/PVA/PEG composite hydrogel: add corresponding PEG to the dissolved PVA solution, place it in a water bath, and form a homogeneous solution after mixing. After mechanical dewatering, the thickness of the purified membrane was about, and the membrane was immersed in the corresponding mixed solution of PVA and PEG. The impregnation and freeze-thaw process were the same as above, and the freeze-thaw process was repeated for 2-6 times to obtain the composite BC/PVA/PEG hydrogel [23].

The prepared bacterial cellulose film was freeze-dried and sprayed with gold; then, the microspatial structure and colloid mesh aperture of bacterial cellulose were observed by BSE SEI scanning electron microscope, and the micro-morphology of BC and its composite hydrogels were observed by scanning electron microscope [24].

## 4. Results and Discussion

Experiments show that the three-dimensional network observed by scanning electron microscope has a dense structure with criss-crossing fibers and an average size of 40-60 nm. The corresponding results are as follows: the gel preparation effect is the most ideal when PEG concentration is below 6%. In addition, adding the following PEG will not produce a significant increase in hydrophobicity of phase separation when PEG concentration is above [25].

## 5. Conclusion

This paper presents an experimental method based on scanning electron microscope. The specific content of this method is to observe the hydrogel through scanning electron microscope and observe the intermolecular space through experiment to prove the effect of this method to solve the problem of preparing hydrogel from bacterial cellulose. Bacterial cellulose is a kind of biocellulose with high application value. It has many excellent physical and chemical properties. However, in practical application, some properties of

bacterial cellulose cannot meet the requirements perfectly, so its structural characteristics need to be improved.

## Data Availability

The data used to support the findings of this study are available from the corresponding author upon request.

## Conflicts of Interest

The authors declare that they have no conflicts of interest.

## Acknowledgments

This work was supported by the National Natural Science Foundation of China (NSFC) (Project No. 21905168). This work was supported by the Science and Technology Fund of Henan Province (Project No. 20A430021).

## References

- [1] X. Xu, L. Li, and A. Sharma, "Controlling messy errors in virtual reconstruction of random sports image capture points for complex systems," *International Journal of Systems Assurance Engineering and Management*, vol. 1, 2021.
- [2] M. Bradha, N. Balakrishnan, A. Suvitha et al., "Experimental, computational analysis of butein and lanceoletin for natural dye-sensitized solar cells and stabilizing efficiency by IoT," *Environment, Development and Sustainability*, vol. 24, no. 6, pp. 8807–8822, 2022.
- [3] J. Chen, J. Liu, X. Liu, W. Gao, J. Zhang, and F. Zhong, "Degradation of toluene in surface dielectric barrier discharge (SDBD) reactor with mesh electrode: synergistic effect of UV and TiO<sub>2</sub> deposited on electrode," *Chemosphere*, vol. 288, Part 3, p. 132664, 2022.
- [4] R. Huang, S. Zhang, W. Zhang, and X. Yang, "Progress of zinc oxide-based nanocomposites in the textile industry," *IET Collaborative Intelligent Manufacturing*, vol. 3, no. 3, pp. 281–289, 2021.
- [5] H. Xie, Y. Wang, Z. Gao, B. Ganthia, and C. Truong, "Research on frequency parameter detection of frequency shifted track circuit based on nonlinear algorithm," *Nonlinear Engineering*, vol. 10, no. 1, pp. 592–599, 2021.
- [6] B. Yaneva and E. Karaslavova, "Erbium-doped yttrium aluminium garnet (er:yag) laser instrumentation in periodontal treatment – scanning electron microscope study," *Oxidation Communications*, vol. 44, no. 1, pp. 162–170, 2021.
- [7] A. A. Borzunov, D. V. Lukyanenko, E. I. Rau, and A. G. Yagola, "Reconstruction algorithm of 3D surface in scanning electron microscopy with backscattered electron detector," *Journal of Inverse and Ill-Posed Problems*, vol. 29, no. 5, pp. 753–758, 2021.
- [8] R. A. Rosenberg, E. A. Rozhkova, and V. Novosad, "Investigations into spin- and unpolarized secondary electron-induced reactions in self-assembled monolayers of cysteine," *Langmuir*, vol. 37, no. 9, pp. 2985–2992, 2021.
- [9] P. F. Dong, R. Z. Xie, K. R. Wang et al., "Kernel crack characteristics for X-ray computed microtomography ( $\mu$ CT) and their relationship with the breakage rate of maize varieties," *Journal of Integrative Agriculture*, vol. 19, no. 11, pp. 2680–2689, 2020.
- [10] H. H. Ji, K. H. Shin, and J. L. Yun, "Scalable binder-free free-standing electrodes based on a cellulose acetate-assisted carbon nanotube fibrous network for practical flexible li-ion batteries," *ACS Applied Materials and Interfaces*, vol. 13, no. 5, pp. 6375–6384, 2021.
- [11] D. V. Vasava and S. S. Panchal, "Biodegradable polymeric materials - synthetic approach," *ACS Omega*, vol. 5, no. 9, pp. 4370–4379, 2020.
- [12] L. G. Babu, "Influence on the tribological performance of the pure synthetic hydrated calcium silicate with cellulose fiber," *Journal of the Balkan Tribological Association*, vol. 23, no. 3, pp. 104–111, 2020.
- [13] O. T. Tiomnova, F. Coelho, T. Pellizaro, J. Chanfrau, and A. C. Guastaldi, "Preparation of scaffolds of amorphous calcium phosphate and bacterial cellulose for use in tissue regeneration by freeze-drying process," *Biointerface Research in Applied Chemistry*, vol. 11, no. 1, pp. 7357–7367, 2021.
- [14] W. Sahyouni and A. Nassif, "Effect of atomic number on plasma pinch properties and radiative emissions," *Advances in High Energy Physics*, vol. 2021, Article ID 6611925, 5 pages, 2021.
- [15] B. Achary, "Electron micrograph studies on the effects of fluoxetine in depression-induced adult female rat ovaries," *Indian Journal of Science and Technology*, vol. 14, no. 5, pp. 406–414, 2021.
- [16] Q. Wang and P. Geng, "Fatigue life prediction method of face-centered cubic single-crystal metals under multiaxial nonproportional loading based on structural mechanical model," *Fatigue and Fracture of Engineering Materials and Structures*, vol. 45, no. 1, pp. 133–158, 2022.
- [17] X. Li, R. Wang, H. Zhang, Z. Xin, and Y. Dong, "Study on micro - melt polishing and strengthening mechanism of scanning electron beam surface," *Nuclear Instruments and Methods in Physics Research Section B Beam Interactions with Materials and Atoms*, vol. 504, no. 5, pp. 58–63, 2021.
- [18] J. A. Ruiz, M. Artica, and L. Landeo, "66 effect of the co-culture system and the culture medium on invitro embryo development in alpacas (Vicugna pacos)," *Reproduction, Fertility, and Development*, vol. 33, no. 2, p. 140, 2021.
- [19] D. Zhu, Q. Chen, T. Qiu, G. Zhao, and X. Fang, "Optimization of rare earth carbonate reactive-crystallization process based on response surface method," *Journal of Rare Earths*, vol. 39, no. 1, pp. 98–104, 2021.
- [20] E. M. Thurman, Y. Yu, I. Ferrer, K. A. Thorn, and F. L. Rosario-Ortiz, "Molecular identification of water-extractable organic carbon from thermally heated soils: C13 NMR and accurate mass analyses find benzene and pyridine carboxylic acids," *Environmental Science and Technology*, vol. 54, no. 5, pp. 2994–3001, 2020.
- [21] R. Yang, C. Hong, Z. Huang, H. Wen, and J. Chen, "Liquid nitrogen fracturing in boreholes under true triaxial stresses: laboratory investigation on fractures initiation and morphology," *SPE Journal*, vol. 26, no. 1, pp. 135–154, 2021.
- [22] L. M. Prayogo and A. Basith, "The effect of sunglint correction for estimating water depth using rationing, thresholding, and mean value algorithms," *Rekayasa*, vol. 14, no. 1, pp. 39–48, 2021.
- [23] H. Liu, T. Cui, and M. He, "Product optimization design based on online review and orthogonal experiment under the background of big data," *Proceedings of the Institution of Mechanical Engineers, Part E: Journal of Process Mechanical Engineering*, vol. 235, no. 1, pp. 52–65, 2021.

## Retraction

# Retracted: Nursing Education of Lateral Oblique Complications of Neurosurgery under Microscope

### Scanning

Received 20 June 2023; Accepted 20 June 2023; Published 21 June 2023

Copyright © 2023 Scanning. This is an open access article distributed under the Creative Commons Attribution License, which permits unrestricted use, distribution, and reproduction in any medium, provided the original work is properly cited.

This article has been retracted by Hindawi following an investigation undertaken by the publisher [1]. This investigation has uncovered evidence of one or more of the following indicators of systematic manipulation of the publication process:

- (1) Discrepancies in scope
- (2) Discrepancies in the description of the research reported
- (3) Discrepancies between the availability of data and the research described
- (4) Inappropriate citations
- (5) Incoherent, meaningless and/or irrelevant content included in the article
- (6) Peer-review manipulation

The presence of these indicators undermines our confidence in the integrity of the article's content and we cannot, therefore, vouch for its reliability. Please note that this notice is intended solely to alert readers that the content of this article is unreliable. We have not investigated whether authors were aware of or involved in the systematic manipulation of the publication process.

In addition, our investigation has also shown that one or more of the following human-subject reporting requirements has not been met in this article: ethical approval by an Institutional Review Board (IRB) committee or equivalent, patient/participant consent to participate, and/or agreement to publish patient/participant details (where relevant).

Wiley and Hindawi regrets that the usual quality checks did not identify these issues before publication and have since put additional measures in place to safeguard research integrity.

We wish to credit our own Research Integrity and Research Publishing teams and anonymous and named exter-

nal researchers and research integrity experts for contributing to this investigation.

The corresponding author, as the representative of all authors, has been given the opportunity to register their agreement or disagreement to this retraction. We have kept a record of any response received.

### References

- [1] K. Hu, "Nursing Education of Lateral Oblique Complications of Neurosurgery under Microscope," *Scanning*, vol. 2022, Article ID 2158181, 8 pages, 2022.

## Research Article

# Nursing Education of Lateral Oblique Complications of Neurosurgery under Microscope

Kecui Hu 

School of Nursing, Anhui University of Chinese Medicine, Hefei, Anhui 230012, China

Correspondence should be addressed to Kecui Hu; 31115327@njau.edu.cn

Received 2 June 2022; Revised 4 July 2022; Accepted 22 July 2022; Published 5 August 2022

Academic Editor: Balakrishnan Nagaraj

Copyright © 2022 Kecui Hu. This is an open access article distributed under the Creative Commons Attribution License, which permits unrestricted use, distribution, and reproduction in any medium, provided the original work is properly cited.

In order to solve the problem of nursing education of lateral oblique complications, a nursing education solution of lateral oblique complications of neurosurgery under the microscope was proposed. The method used subjective evaluation and objective evaluation to systematically evaluate the basic training module. In subjective evaluation, the authenticity score of surgical simulator was  $3.65 \pm 0.01$ , the realism score of surgical instruments was  $3.81 \pm 0.01$ , the realism score of tactile sense was  $3.75 \pm 0.01$ , the operating environment score was  $3.60 \pm 0.01$ , and the overall effect score was  $3.63 \pm 0.01$ . The difficulty score of the whole training was  $3.15 \pm 0.01$ . In the aspect of objective evaluation, the entropy method was used to process the data of training track, training angle, training time, trigger times, success times, failure times, and other indicators of 24 trainers collected, and the experiment verified the nursing education of lateral oblique complications of neurosurgery under the microscope.

## 1. Introduction

As one of the most technically demanding medical specialties, neurosurgery requires neurosurgeons not only to have a high level of theoretical knowledge but also to have high operational skills, in order to ensure the reduction of any unnecessary mistakes, because any mistakes will lead to serious consequences, so simulation surgery has become a daily training for every neurosurgeon to maintain their surgical skills, as shown in Figure 1. In modern times, simulation plays an extremely important role in both medical and nonmedical fields, especially in fields with high risk and high cost, including the training of military personnel, pilots, car drivers, and nuclear power plant operators. Through simulation, trainers can study and experiment with process interactions with different processes, consider various processes, monitor the impact of ideas on models and methods, perform, and select the best ideas. In medicine, simulated surgery is generally divided into physical simulation and virtual simulation. Physical simulations typically include cadaver models, live animal models, and artificial limb simulation models. Cadaver model and live animal model are the best training

methods for surgeons to practice their surgical skills, but they have some problems such as lack of cadaver source and ethics. Prosthesis simulation is an alternative scheme, which can achieve 1:1 reduction through 3D printing. However, due to the limitation of materials, this scheme has low repeatability and cannot improve the real feeling of surgeons. Virtual simulation includes virtual reality, augmented reality, and mixed reality. Combined with the real operation environment, real-time tactile feedback can improve the immersion of training physicians, achieve the purpose of training physicians spatial sense, and improve surgical skills, which is a very promising training method at present.

## 2. Literature Review

Yan et al. said that the 2019 China Cancer Report released by the China Cancer Center indicated that about 10,000 people are diagnosed with cancer every day, an average of seven people every minute. The report pointed out that the most important treatment for cancer is surgery, so the training of surgical skills for surgeons has become particularly important [1]. Swiatek et al. said that with the rapid

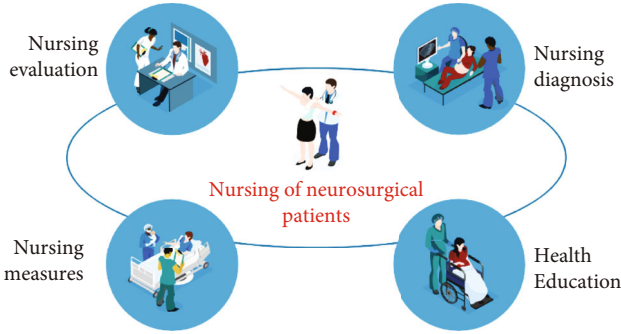


FIGURE 1: Flow chart of neurological examination under microscope.

expansion of the enrollment of medical colleges in China, the difficulty in obtaining cadavers, the unguaranteed surgical training, the low efficiency, and high cost of the training of surgeons would greatly prolong the training cycle of a surgeon [2]. Krych et al. said that neurosurgery includes craniocerebral surgery, spinal neurosurgery, spinal neurosurgery, and peripheral neurosurgery. Craniocerebral surgery and spinal neurosurgery are the most important components of neurosurgery and also the two most studied directions outside China [3]. Martins et al. say that with the development of science and technology, the concept of minimally invasive surgery has permeated the whole process of neurosurgery and treatment. Not only can patients undergo painless neurosurgery, but with the development of visualization techniques such as magnetic resonance imaging (MRI), computed tomography (CT), and neuroendoscopy. Diagnosis and treatment of neurological diseases have become more reliable [4]. Tamborska et al. stated that the Neurosurgical Navigation System (NNS) concept originated in the 1990s [5]. Ivanov et al. stated that NSS uses a high-performance computer to closely correlate patient preoperative image data (MRI and CT) with the actual location of intraoperative lesions. Surgeons can display three-dimensional (3D) images of surgical sites and instruments in real time through a monitoring screen [6]. Aibar-Duran et al. said that preoperative imaging often fails to provide accurate guidance to the surgeon due to changes in the patient's position or surgical environment [7]. Therefore, intraoperative imaging technology has attracted more and more attention, such as intraoperative MRI, intraoperative three-dimensional ultrasound, intraoperative CT, and other imaging technology 1. Agrawal et al. said that surgeons can fuse intraoperative images with preoperative planning images or omit preoperative images to simplify the intraoperative imaging process of image-guided neurosurgery work and provide more auxiliary information [8]. Andreev et al. said that the development of neurosurgery depends on advances in existing surgical techniques [9]. According to Febns et al., the results of computed tomography and magnetic resonance imaging have ushered in a new era in neurosurgery, with medical applications including surgical microscopy, ventricular endoscopy, intraoperative navigation, and multidirectional clinical trials. The idea of minimally invasive surgery has flooded [10]. However, current methods only use two test models, which

is also a limitation for most new surgeons. VR was first used in medicine in the early 1990s to view difficult medical records during surgery and plan preoperative procedures. For 3D reconstruction, VR is considered one of the most promising surgical plans.

### 3. Methods

It indicates that the algorithm is a classical swarm algorithm. It is one of the partitioning process. The  $k$ -word algorithm uses  $k$  as a measure and divides  $n$  models into  $k$  groups. The goal is to make the samples within the cluster have high similarity, while the similarity between samples belonging to different clusters is low. The algorithm tries to find  $k$  partitions that reduce the squared error value, usually ending up in a local optimum. The  $k$ -language algorithm uses distance as a measure of similarity, that is, the closer the distance between two models, the greater the probability [11]. The algorithm considers that clusters are composed of samples that are close to each other, but samples belonging to different clusters are far apart, so compact and independent clusters can be obtained.  $k$  is assuming that there are  $n$  models in the configuration file, and each model has the characteristics of  $P$ ; then, each model can be used as the following vector, as shown in the following formula:

$$X_i = (X_{1i}, X_{2i}, \dots, X_{pi}), i = 1, 2, 3, \dots, n. \quad (1)$$

$k$  samples were selected as the initial clustering centers, and the following vectors of each clustering center are shown in the following formula:

$$Z_i = (z_{1j}, z_{2j}, \dots, z_{pj}), j = 1, 2, 3, \dots, k. \quad (2)$$

The calculation method usually uses the error sum of squares criterion function as a function of the group. The error sum of squares criterion function is defined by the following equation:

$$J_c = \sum_{j=1}^k \sum_{i=1}^{n_j} \|x_i - m_j\|^2, \quad (3)$$

where  $k$  is the number of clustering to be formed,  $n_j$  is the number of samples in the  $j$ -th class,  $m_j$  is the mean value of class  $J$  samples and represents the center of gravity of this type of data set, as shown in the following formula:

$$m_j = \frac{1}{n} \sum_{i=1}^{n_j} x_i, j = 1, 2, \dots, k. \quad (4)$$

The method of iterative updating is adopted: in each iteration,  $k$  clusters are formed according to the sample points around  $k$  cluster centers, and the centroid of each cluster obtained by recalculation (namely, the average value of all points in the cluster, namely, the set center) will be used as the reference point of the next iteration [12, 13]. The reference points selected iteratively are closer

and closer to the real center of mass of the cluster, so the objective function is smaller and smaller, and the clustering effect is better and better [14]. First, select  $k$  points as the starting point according to the understanding of  $k$ , and then, calculate the distance from each model to the center point. Center the model where it is closest to it and adjust the position of the new group. If there is no change in the clustering center of two adjacent iterations, it indicates that the sample adjustment is over, the li number  $J_c$  of the clustering criterion has converged, and the algorithm is over.

Set the sample set size  $n$ , the number of clusters  $k$ , and the convergence criterion  $\varepsilon$ , let the number of iterations  $mark = I$ , and select  $k$  initial focal points  $z(j)(l)$  from the sample set,  $j = 1, 2 \dots k$ . The location  $D(X, Z, (l)), i = 1, 2, \dots$  of each sample object from the cluster center was calculated,  $j = 1, 2 \dots k$  as shown in the following formula:

$$D(X_i, Z(l)) = \min \{D(X_i, Z(l)), j = 1, 2, 3, \dots, n\}. \quad (5)$$

The standard function  $J_c$  of calculation error is shown in the following formula:

$$J_c(l) = \sum_{j=1}^k \sum_{m=1}^{n_i} \|X_m^{(j)} - Z(l)\|^2. \quad (6)$$

AP algorithm is a new unsupervised clustering algorithm developed by Sc IENCC in 2007. The algorithm is a clustering algorithm based on data transfer between nodes. The goal of the job is to find the slope at the best position in the group such that the result for each data point is similar to the content of the group. The algorithm is fast and effective and has good application results in face image clustering, gene recognition, handwriting character recognition, and optimal air route planning. In the AP algorithm, two data types, responsible and available, are usually exchanged, where  $r(i, k)$  represents the number sent from point  $i$  to candidate group  $k$ , considering whether point  $k$  corresponds to the midpoint of point  $i$ .  $A(i, k)$  represents the number sent to me by candidate group  $k$ , considering how I choose  $k$  as its midpoint [15]. In fact, the process of AP algorithm iteration is to constantly update the attractiveness and belonging values of each data point and finally generate  $M$  cluster center points and then allocate the remaining data points to the corresponding cluster according to the similarity. The relationship between attractiveness and belonging is shown in Figure 2.

The core steps of AP clustering algorithm are the iterative updating of  $r(i, k)$  and  $a(i, k)$ , and the updating formulas are shown as follows:

$$r(i, k) = s \left( i, k - \max_{j \neq k} \{a(i, j) + s(i, j)\} \right), \quad (7)$$

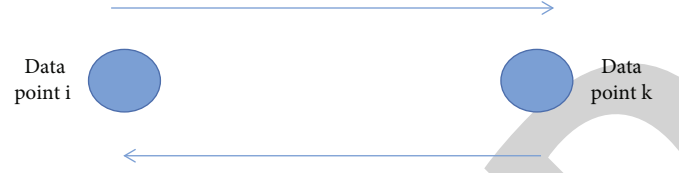


FIGURE 2: The relationship between attractiveness and belonging.

$$a(i, k) = \min \left\{ 0, r(i, k) + \sum_{j \neq i, j \neq k} \max\{0, r(j, k)\} \right\}, i \neq k. \quad (8)$$

As shown in the following formula,

$$a(i, k) = \sum_{j \neq k} \max\{0, r(j, k)\}. \quad (9)$$

During the entire iterative process of the algorithm, the  $r(i, k)$  and  $a(i, k)$  information values of each sample point are constantly updated by the algorithm until the convergence of the algorithm is completed. Thus,  $k$  high-quality exemplar can be generated, and then, the nonclustering centered exemplar. Data points are allocated to the corresponding cluster. Damping factor  $\text{lam} \in [0.5, 1]$  is introduced to avoid oscillation. Increasing dayani factor can effectively eliminate the oscillation and make the algorithm converge.  $\text{lam} = 0.9$  can be obtained, as shown in the following formula:

$$r^{(t)}(i, k) = (1 - \text{lam}) * \left[ s(i, k) - \max_{j \neq k} \{a^{t-1}(i, j) + s(i, j)\} + \text{lam} * r^{(t-1)}(i, k) \right]. \quad (10)$$

Means algorithm is widely used because of its simple theory and fast calculation speed. However, it also has many defects: the number of clustering in  $k$ -means algorithm needs to be given in advance. The clustering result depends on the reasonable choice of user parameters, but the selection of the number of clustering is very difficult to estimate, especially when we do not know the given data distribution form, so it is impossible to determine how many classes the data set should be divided into. The algorithm has great dependence on the selection of initial value. Different initial values often lead to different results, which leads to poor stability of the algorithm [16]. The  $k$ -means algorithm needs to update the distribution model regularly and continuously count new sites after modification. Therefore, when the data cost is very large, the time cost of the algorithm is very large. And the algorithm is sensitive to noise and outliers. In the face of the original data with complex human quantity and errors (action: operation of fire failure data), we first consider how to convert the original data into data in accordance with the requirements of mathematical analysis methods. The nursing bed movement history in the system of "multi-functional nursing and physiological parameters remote monitoring device" is the source data object of this paper. This data sheet includes six attributes: control mode

TABLE 1: Comparison of nursing satisfaction score between intervention group and control group ( $n(\%)$ ).

	Quite satisfied	Satisfied	So-so	Dissatisfied	Z value	P value
Intervention group ( $n = 50$ )	7 (14)	31 (62)	10 (20)	2 (4)	-3.208	0.001
The control group ( $n = 50$ )	4 (8)	15 (30)	26 (52)	5 (10)		

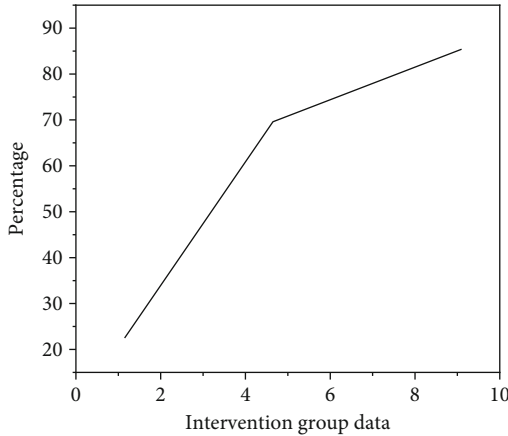


FIGURE 3: Pie chart of satisfaction score of intervention group.

(manual, voice, and timing control), action type, action time, action value, operation result, fault analysis, and remarks. Due to inevitable objective reasons, there are errors and omissions in the data, and the quality of the data will directly affect the clustering algorithm results, so it is necessary to preprocess the source data [17]. Nonparametric rank-sum test analysis showed that patients' satisfaction with nursing work in the intervention group was significantly better than that in the control group, and the difference between the two groups was statistically significant ( $Z = 3.479$ ,  $P < 0.05$ ), as shown in Table 1 and Figure 3.

#### 4. Experiment and Analysis

The overall framework of the nursing bed experimental platform is shown in Figure 4.

The main control computer as a human-computer interaction interface and user input control signal platform, care bed motor control drive system to complete the analysis of control signal, and drive the corresponding control bed parts of the motor [18, 19]. The nursing bed should meet the various necessary positions and postures which are conducive to the nursing person's rehabilitation and self-care. For example, in order to prevent bedsores and a series of complications caused by poor blood flow due to a long time in bed, nursing bed can realize the bed surface left and right side turn over action. To speed up the healing of a patient's injured leg, the nursing bed offers leg lifts and more. The nursing bed has 12 single movements in total, and all single movements of the nursing bed are shown in Table 2 below.

They are left turn up, left turn down, right turn up, right turn down, back up, back down, leg up, leg down, head of the bed up, head of the bed down, bed end up, and bed end down. There are also two combined movements: bed

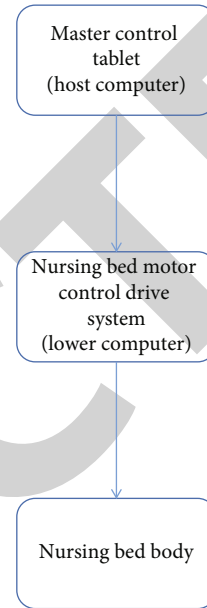


FIGURE 4: Overall framework of nursing bed experimental platform.

rise and bed fall, which are made by the head and tail of the bed in coordination [20]. If bed body rises, namely, the head of a bed and bed end rise at the same time, bed body drops, namely, the head of a bed and bed end drop at the same time, because this nurses a bed to share 14 action types. The nursing bed consists of a number of independent institutions in mechanical structure, each corresponding to more than one degree of freedom. Under the unified and coordinated control of the control system, these institutions form a multichain system, through the cooperative movement of each bed panel, so that the nursing bed completes a specific posture [21]. Therefore, the design and implementation of the control system is one of the most important parts of the whole nursing bed. In order to make the control system realize intelligent control of nursing bed and timely understand the current working state of nursing bed, the necessary number of position sensors is installed on the nursing bed body. By detecting the data transmitted back through the sensor, the control system can understand the motion state of each bed panel in real time, to avoid the mutual interference of different institutions or the overimpact of the linear motor and other unnecessary damage to the bed and the user. Nursing bed movement control system adopts the control mode of cascade and feedback between upper and lower computers [22]. The upper computer is a full-touch tablet PC under Windows XP system with a resolution of  $800 * 600$ . The familiar window operating system makes it easy



TABLE 2: Basic monomer movements of nursing bed.

Left side	Left turn up Left turn down	Right side	Right turn up Right turn down
North	Back up Back down	Legs	The leg up The leg down
The head of a bed	Bed body rise Bed body down	The end of the bed	Bed rise Bed down

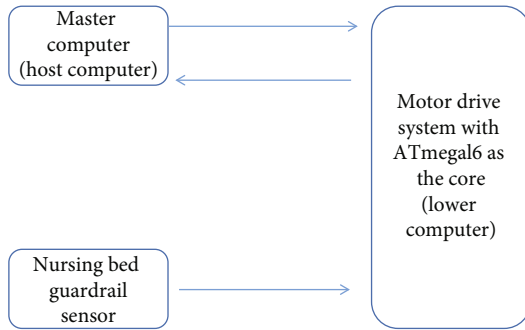


FIGURE 5: Control system block diagram of nursing bed.

for users to master the operation, while the large high-resolution screen also enhances the user experience. The lower computer is a motor drive system based on ATmega16 chip [23, 24]. The user input the control (button or voice) signal of nursing bed action through the upper computer, and the lower computer is responsible for driving the corresponding motor to perform the corresponding nursing bed action. At the same time, the lower computer detects the limit signal of the relevant position sensor, motor pulse, and voice recognition trigger signal in real time and feeds these signals back to the upper computer for relevant processing. The control system block diagram of nursing bed is shown in Figure 5.

Retrospective analysis was conducted in this study, and 100 subjects were selected, including 50 in the control group and 50 in the intervention group. By comparing the age composition, gender, education level, marital status, per capita monthly income (yuan), payment method of medical expenses, nature of work, and residence of patients in the two groups, the results show that there were no significant differences in age composition, gender, education level, marital status, per capita monthly income (yuan), payment method of medical expenses, nature of work, and residence between the two groups ( $P > 0.05$ ), indicating that the two groups were comparable. In this study, the patients' lumbar function was scored based on the postoperative JOA lumbar function score. Cronbach's A coefficient of this scale was 0.89, which had high reliability and validity. The results showed that there was no significant difference in the JOA lumbar function score between the control group and the day control group ( $P > 0.05$ ). The JOA lumbar spine function scores of the affected group at 1 month and 3 months after operation were  $21.2 \pm 1.010$  and  $28.34 \pm 0.939$ , respectively, which were higher than those of the control group

( $20.74 \pm 1.046$  and  $27.56 \pm 0.951$ , respectively). There was significant difference between the two groups ( $P < 0.05$ ). Repeated measure anOVA showed that lumbar function was restored at 1 and 3 months after surgery in both groups over time. However, the recovery of lumbar function in the intervention group was better than that in the control group ( $P < 0.05$ ) [25]. It indicates that the implementation of preoperative lumbar function training guidance, early postoperative exercise, and timely psychological intervention in clinical nursing pathway under ERAS concept can promote the recovery of patients' lumbar function more quickly. It has also been confirmed that ERAS has positive significance for postoperative functional recovery and postoperative pain recovery of patients after knee surgery. ERAS as a concept has been recognized and widely used by medical professionals. The control group was given routine care, while the intervention group was given ERAS care. ERAS care covers multiple aspects of preoperative, intraoperative, and postoperative care, which can reduce the occurrence and duration of postoperative lumbar pain and achieve rapid recovery. Fifteen patients were enrolled in the ERAS observation group. Preoperative drug diagnosis and minimally invasive surgery should be taken to reduce tissue stimulation and dissection in the wound. Postoperative combined analgesic drugs, early functional exercise, reasonable diet, and other methods were used to evaluate the therapeutic effect using VAS. The results showed that VAS score of the observation group was significantly different from that of the control group 1 day after surgery, 3 days after surgery, and at discharge follow-up,  $P < 0.05$ ; ERAS is considered to be an advanced rehabilitation guidance strategy based on evidence-based medicine research, which optimizes management measures for the entire treatment process and every link to embody humanistic care, better communication, and cooperation between patients and medical staff. Early postoperative rehabilitation exercise enhances patient confidence, reduces back pain, prevents nerve root adhesion, and has a good effect [26]. ERAS-assisted modeling has also been shown to improve postoperative pain in perioperative patients. The results of this study showed that there was no significant difference in the VAS scores of the two groups in the days of enrollment ( $P > 0.05$ ). The VAS scores of the patient group on the 1st, 2nd, and 3rd days after operation were  $3.38 \pm 1.008$ ,  $2.30 \pm 0.931$ , and  $1.48 \pm 0.677$ , respectively. The lower the control group ( $4.12 \pm 1.466$ ,  $2.74 \pm 1.225$ , and  $1.88 \pm 0.872$ ), the difference was significant,  $P < 0.05$ . For time ( $P < 0.05$ ), compared with the control group, the pain relief in the affected group was significantly better than the control group ( $P < 0.05$ ). This indicates that during

the implementation of clinical nursing pathway under ERAS philosophy for patients, the medical staff has optimized management measures for every link. Timely psychological support for patients, teaching patients to relieve pain methods, enhancing patient confidence, and advancing analgesia and the implementation of multimode analgesia effectively reduce the pain of patients, to achieve the purpose of rapid recovery. Cerebrospinal fluid leakage caused by dura injury is a common complication of lumbar spine surgery. It has been reported that the incidence of cerebrospinal fluid leakage in primary lumbar surgery is 5.5%-9%. Cerebrospinal fluid leakage can cause direct consequences including wound sensation and wound healing, and long time without improvement can cause headache symptoms. The main cause of cerebrospinal fluid leakage is adhesion of ossification and dura, careless operation during the operation, and damage of dura and arachnoid membrane. Prevention is the key to avoid cerebrospinal fluid leakage. Therefore, surgeons must first be familiar with local anatomy, and fully evaluate the adhesion degree between the compressor and the dura, whether there is dura ossification, and fully expose the surgical field during the operation, so as to avoid cerebrospinal fluid leakage as much as possible by improving surgical techniques. For the occurrence of cerebrospinal fluid leakage, actively take the correct treatment method, and strive to achieve good results. The results of this study showed that the incidence of postoperative cerebrospinal fluid leakage was 2% (1 case) in the intervention group and 2% (1 case) in the control group, and there was no statistical significance between the two groups ( $P > 0.05$ ). This may be related to the small sample size of this study, and a large number of clinical trials are still needed in the future to verify the significance of the implementation of clinical nursing pathway under ERAS concept in reducing the incidence of cerebrospinal fluid leakage after lumbar interbody fusion fixation. Urinary retention is a common complication after lumbar surgery. Some studies have found that the incidence of urinary retention after lumbar surgery is 15%. At the same time, patients with lumbar spinal stenosis are prone to urinary tract infection due to routine indwelling catheter after general anesthesia. Foreign studies have reported that the incidence of urinary tract infection after scoliosis and kyphosis surgery is 3.9% and 4.8%, respectively. The study found that 10.5% of patients developed urinary tract infections after spinal surgery. The incidence of postoperative urinary tract infection varies depending on the population, study, and surgical approach, and patients may experience severe recurrence of postoperative urinary tract infection. Therefore, great attention should be paid to actively intervene to minimize the occurrence of urination and urination [27, 28]. The results of this study showed that the incidence of urinary incontinence and voiding was 4% (2 cases) in the study group and 18% (9 cases) in the study group. The incidence of urinary incontinence and urinary incontinence in the control group was lower than that in the control group, and the difference between the two groups was significant ( $P < 0.05$ ). Li et al. showed that by using therapy in an ERAS strategy, caregivers could reduce urination and urination by educating patients about timely preoperative and appropri-

ate interventions and timely handling of catheters during and after surgery. It is of great significance to prevent urinary retention and urinary tract infection after lumbar interbody fusion and fixation. Abdominal distention often occurs 1~3 days after lumbar spine surgery, which seriously affects the patient's health and mood, diet, and sleep, and increases the patient's pain. Long-term abdominal distention may lead to intestinal adhesion and intestinal obstruction. Abdominal distention may squeeze both lungs and cause dyspnea and dyspnea, which requires extensive attention. Relevant studies on the effects of ERAS on abdominal distention after lumbar spine surgery showed that the incidence of abdominal distention in the observation group (using ERAS nursing) and the control group (using routine nursing) was 7% and 21%, respectively, and the abdominal distention was completely relieved in the observation group 7 days after surgery, while the rate of abdominal distention in the control group was 5%. The difference between the two groups was statistically significant. It is believed that nursing measures under the guidance of BRAS concept can reduce the occurrence of postoperative abdominal distention and relieve abdominal distention as soon as possible, which has great promotion significance. Studies have found that the incidence of postoperative abdominal distention can be significantly reduced through early postoperative activities and functional exercises for patients with lumbar degenerative diseases. In this study, the incidence of postoperative abdominal distention was compared between the two groups. The results showed that the incidence of postoperative abdominal distention was 14% (7 cases) in the intervention group and 32% (16 cases) in the control group, and the difference between the two groups was statistically significant ( $P < 0.05$ ). The results of this study are consistent with the studies of experts outside China, suggesting that the incidence of abdominal distention can be reduced by implementing relevant measures of clinical nursing pathway under ERAS concept, such as fasting for 6 h and 2 h before surgery, small amount of water intake early after surgery, and early ambulation. Deep vein thrombosis of lower limbs is a common complication after orthopedic surgery, which is usually caused by longer operation time, longer postoperative bed time, advanced age, fear of wound pain, and poor postoperative functional exercise. The patient has no obvious symptoms in the early stage, but if not handled in time, the severe case may lead to embolus shedding and pulmonary embolism, endangering the patient's life. Foreign literature has reported that the incidence of venous thrombosis in lower limbs after spinal surgery is 0.3%-31%, and the incidence of deep venous thrombosis in lower limbs in patients with spinal trauma and spinal surgery is 1.2%-3.6%, among which 50%-70% can be secondary to pulmonary embolism. The results vary depending on the population and methods studied. The results of this study showed that the incidence of postoperative deep vein thrombosis in the lower extremity was 0% (0 cases) in the patient group and 2% (1 case) in the control group. There was no significant difference in any one group ( $P > 0.05$ ). There was 1 case of lower extremity deep vein thrombosis in the control group and no case of lower extremity deep vein thrombosis in the intervention group,

which was less in both groups. Firstly, it may be closely related to the high attention paid by medical staff, and secondly, it may be related to the small sample size of the study, which still needs to be confirmed by studies with large samples in the future. Wound infection can be seen in a variety of factors. Studies have found that the causes of wound infection after lumbar interbody fusion fixation are often diabetes, infection history, long operation time, smoking, and interbody fusion device implantation. Previous back surgery and diabetes were reported to be significant risk factors for wound infection. It has been reported that the incidence of incisions after lumbar spinal stenosis is 4% to 6%, and the incidence of incisions after lumbar spinal stenosis and interbody fusion is 2.5%. The results of this study showed that the incidence of postoperative pain in the intervention group was 2% (1 case), and that in the control group was 10% (5 cases), with no value in either group ( $P > 0.05$ ). This may be related to the small sample size of this study and the improvement of medical asepsis technology. Future studies with large samples are still needed to confirm the significance of clinical nursing pathway implementation under ERAS concept in preventing wound infection after lumbar interbody fusion fixation.

## 5. Conclusion

Here, a BTS (brain tumor) operation training simulator was developed from the training of neurosurgery, aiming to solve the practical problems of difficult training and high cost in neurosurgery. And the existing problems in virtual neurosurgery are introduced, and the key problems in virtual neurosurgery are studied. The basic training module of BTS surgery was designed, and the simulator was analyzed subjectively and objectively to verify its effectiveness. The main work of this essay includes the following aspects: surface rendering and volume rendering in 3D reconstruction of medical images are compared, and volume rendering of medical images based on Ray Casting algorithm is realized in Unity3D, which plays a crucial role in preoperative planning of virtual surgical simulator. The soft tissue modeling and cutting in neurosurgery were realized based on XPBD algorithm, and surgical training modules such as skin cutting were realized in Unity3D, which further improved the simulator of brain tumor surgery. A grid voxel method was proposed to reconstruct the skull, and a training module for craniotomy was designed to solve the problem of unreal tactile simulation in orthopedic surgery.

## Data Availability

The data used to support the findings of this study are available from the corresponding author upon request.

## Conflicts of Interest

The authors declare that they have no conflicts of interest.

## References

- [1] X. Yan, D. Kang, Y. Lin, S. Qi, and C. Jiang, "CBX4-dependent regulation of HDAC3 nuclear translocation reduces Bmp2-induced osteoblastic differentiation and calcification in adamantinomatous craniopharyngioma," *Cell Communication and Signaling*, vol. 20, no. 1, pp. 1–12, 2022.
- [2] P. R. Swiatek, M. H. Mccarthy, J. Weiner, S. Bhargava, and S. Iyer, "Intraoperative image guidance for lateral position surgery," *Annals of Translational Medicine*, vol. 9, no. 1, pp. 90–90, 2021.
- [3] A. J. Krych, M. D. LaPrade, C. S. Cook et al., "Lateral meniscal oblique radial tears are common with ACL injury: a classification system based on arthroscopic tear patterns in 600 consecutive patients," *Orthopaedic Journal of Sports Medicine*, vol. 8, no. 5, p. 2325967120921737, 2020.
- [4] R. S. Martins, S. U. Saqib, M. Gillani, S. R. T. Sania, and H. Zafar, "Patterns of traumatic injuries and outcomes to motorcyclists in a developing country: a cross-sectional study," *Traffic Injury Prevention*, vol. 22, no. 2, pp. 162–166, 2021.
- [5] M. Butler, A. Tamborska, G. K. Wood et al., "Considerations for causality assessment of neurological and neuropsychiatric complications of SARS-CoV-2 vaccines: from cerebral venous sinus thrombosis to functional neurological disorder," *Journal of Neurology, Neurosurgery and Psychiatry*, vol. 92, no. 11, pp. 1144–1151, 2021.
- [6] P. I. Ivanov, I. S. Zubatkina, D. A. Butovskaya, and T. I. Kozhokar, "Radiosurgical treatment of medically refractory Parkinson's tremor," *Russian Journal of Neurosurgery*, vol. 23, no. 1, pp. 16–25, 2021.
- [7] J. Á. Aibar-Durán, M. J. Á. Holzapfel, R. R. Rodríguez, R. B. Nieto, C. R. Arnall, and J. M. Teixeira, "Occipital nerve stimulation and deep brain stimulation for refractory cluster headache: a prospective analysis of efficacy over time," *Journal of Neurosurgery*, vol. 134, no. 2, pp. 1–8, 2020.
- [8] M. Agrawal, R. Samala, R. S. Doddamani, and P. S. Chandra, "Letter: predictors of postoperative complications after selective dorsal rhizotomy," *Acta Neurochirurgica*, vol. 163, no. 2, pp. 475–475, 2021.
- [9] D. N. Andreev, M. A. Kutin, P. L. Kalinin, A. N. Shkarubo, and I. V. Chernov, "Complications caused by excessive hemostatic tamponade in the removed tumor area in transnasal endoscopic surgery of pituitary adenoma," *Russian Journal of Neurosurgery*, vol. 22, no. 1, pp. 21–30, 2020.
- [10] A. Febns, T. R. M. D. Febns, F. A. Ringel, and K. Schaller, "Postural ergonomics and micro-neurosurgery: microscope has an edge over loupes," *Journal of the American College of Surgeons*, vol. 231, no. 2, pp. 300–301, 2020.
- [11] I. V. Valkov and M. N. Mladenovski, "Meningeal melanocytoma of the middle cranial fossa: a case report," *Journal of Biomedical and Clinical Research*, vol. 13, no. 1, pp. 71–75, 2020.
- [12] H. Suzuki and R. J. Wood, "Origami-inspired miniature manipulator for teleoperated microsurgery," *Nature Machine Intelligence*, vol. 2, no. 8, pp. 437–446, 2020.
- [13] E. Engelhardt, "Marcello Malpighi: the nervous system under a microscope," *Arquivos de Neuro-Psiquiatria*, vol. 79, no. 4, pp. 346–349, 2021.
- [14] C. Klinkert, R. Szabó, C. Stieger, D. Campi, N. Marzari, and M. Luisier, "2-D materials for ultrascaled field-effect transistors: one hundred candidates under the ab initio microscope," *ACS Nano*, vol. 14, no. 7, pp. 8605–8615, 2020.

## Retraction

# Retracted: Application of MRI and CT Images in Surgical Treatment of Early Cervical Cancer

### Scanning

Received 20 June 2023; Accepted 20 June 2023; Published 21 June 2023

Copyright © 2023 Scanning. This is an open access article distributed under the Creative Commons Attribution License, which permits unrestricted use, distribution, and reproduction in any medium, provided the original work is properly cited.

This article has been retracted by Hindawi following an investigation undertaken by the publisher [1]. This investigation has uncovered evidence of one or more of the following indicators of systematic manipulation of the publication process:

- (1) Discrepancies in scope
- (2) Discrepancies in the description of the research reported
- (3) Discrepancies between the availability of data and the research described
- (4) Inappropriate citations
- (5) Incoherent, meaningless and/or irrelevant content included in the article
- (6) Peer-review manipulation

The presence of these indicators undermines our confidence in the integrity of the article's content and we cannot, therefore, vouch for its reliability. Please note that this notice is intended solely to alert readers that the content of this article is unreliable. We have not investigated whether authors were aware of or involved in the systematic manipulation of the publication process.

In addition, our investigation has also shown that one or more of the following human-subject reporting requirements has not been met in this article: ethical approval by an Institutional Review Board (IRB) committee or equivalent, patient/participant consent to participate, and/or agreement to publish patient/participant details (where relevant).

Wiley and Hindawi regrets that the usual quality checks did not identify these issues before publication and have since put additional measures in place to safeguard research integrity.

We wish to credit our own Research Integrity and Research Publishing teams and anonymous and named external researchers and research integrity experts for contributing to this investigation.

The corresponding author, as the representative of all authors, has been given the opportunity to register their agreement or disagreement to this retraction. We have kept a record of any response received.

### References

- [1] A. Lu and G. Lu, "Application of MRI and CT Images in Surgical Treatment of Early Cervical Cancer," *Scanning*, vol. 2022, Article ID 1592449, 9 pages, 2022.

## Research Article

# Application of MRI and CT Images in Surgical Treatment of Early Cervical Cancer

An Lu  and Guohua Lu 

Obstetrics and Gynecology Department, Yixing City People's Hospital, Yixing, Jiangsu 214200, China

Correspondence should be addressed to Guohua Lu; 201804306@stu.ncwu.edu.cn

Received 4 June 2022; Revised 1 July 2022; Accepted 12 July 2022; Published 2 August 2022

Academic Editor: Balakrishnan Nagaraj

Copyright © 2022 An Lu and Guohua Lu. This is an open access article distributed under the Creative Commons Attribution License, which permits unrestricted use, distribution, and reproduction in any medium, provided the original work is properly cited.

In order to understand the problems of the application of MRI and CT images in the early cervical cancer surgery, a method that the application of MRI imaging and CT images in early cervical cancer surgery was proposed. For the cervical cancer in clinical practice, the applications of the modern imaging examination and the clinical staging classification were investigated and analyzed. Compared with the surgical pathology results, the application value of common modern imaging in clinical staging of cervical cancer was evaluated. It was found that the sensitivity of MRI and CT in diagnosing lymph node metastasis was 56% and 58%, and the specificity was 93% and 92%, respectively. The experiment proved the application value of MRI and CT in clinical staging of cervical cancer.

## 1. Introduction

Since the 1940s, with the popularization of cervical cytology, HPV testing and other cervical cancer screening methods, patients with cervical cancer have been diagnosed and treated at the early stage or even precancerous stage, thus blocking the occurrence and development of cervical cancer. After the successful application of cervical cancer vaccine in clinic, the World Health Organization has put forward the ambitious goal of global elimination of cervical cancer. However, despite a significant decline in the incidence and mortality of cervical cancer in developed countries, cervical cancer is still one of the major malignant tumors threatening women's health worldwide, ranking fourth in the incidence and mortality of female malignant tumors, most of which occur in developing countries. In China, according to the tumor monitoring data of the National Cancer Center, cervical cancer ranks first among female reproductive tract malignancies. The prevention and treatment of cervical cancer is not only a simple medical issue but also affected by social, economic, cultural, and other complex factors in addition to medical factors. Research on the prevention and treatment of cervical cancer in China and other developing countries is not only necessary to reduce the imbalance in the

prevention and treatment of cervical cancer, but also the only way to achieve the elimination of cervical cancer in the world.

## 2. Literature Review

Tuchina et al. believed that since tumor progression was a continuous process, patients with cervical cancer were presented as heterogeneous groups with different clinicopathological features and survival prognosis when they sought treatment [1]. Dong et al. believed that clinicians first judged patients' cancer stage and then conducted doctor-patient communication, prognosis judgment, and treatment plan selection according to their stages [2]. Therefore, Xiaodan et al. believed that accurate clinical staging was an important influencing factor in evaluating patient prognosis, selecting appropriate treatment mode, and implementing individualized surgery [3]. Low or high preoperative staging may lead to inadequate or excessive treatment of cervical cancer. Voronin et al. believed that the high staging caused some patients to lose the chance of surgery and accept direct radiotherapy instead, thus losing the advantages of surgical treatment in preserving ovarian and vaginal functions and reducing long-term complications. Some patients lost the

opportunity to receive a smaller range of conservative surgery and received unnecessary extensive hysterectomy, resulting in increased perioperative complications and decreased quality of life [4]. Eley et al. believed that low staging could lead to inadequate treatment, and postoperative radiotherapy and chemotherapy were often needed, resulting in a significant increase in total complications and seriously affecting the quality of life. Or the scope of the lesion was found to be beyond the expectation during the operation, resulting in increased difficulty of the operation or even having to give up the operation [5]. In addition, Masselli et al. believed the clinical staging classification should be judged according to unified standards in patients with tumor staging, which could make the data of the world different medical institutions being comparable, so as to carry out data summary and analysis of therapeutic effect evaluation and the implementation of clinical trials. It could make cancer research results applied to the worldwide eventually [6]. Capozza et al. believed that cervical cancer was one of the earliest malignant tumors with clinical staging. Its history could be traced back to 1928 [7]. Reinhold et al. believed that the clinical staging classification was born in the context of radiotherapy as the main treatment for cervical cancer [8]. At that time, Marchenko et al. believed that in order to compare the therapeutic efficacy of cervical cancer among different institutions, different doctors, and different radiotherapy methods, a standard radiotherapy regimen for cervical cancer was established, which changed the chaotic situation of radiotherapy at that time. The following radiotherapy committee of the International Health Union commissioned three professors to develop clinical staging of cervical cancer [9]. After the staging was proposed, Silvestro et al. believed that it was gaining worldwide recognition because of its simplicity, practicality, and its ability to reflect prognosis to a certain extent. It was adopted by the Federation International of Gynecology and Obstetrics (FIGO) in 1954 and was used to today [10]. Although it was modified for many times, its periodization principle and framework remained unchanged. Compared with other malignant tumors using clinical staging, such as lung cancer, for a long time, the clinical staging of FIGO cervical cancer mainly relied on pelvic examination and some simple imaging methods, such as IVP and chest X-ray, while modern imaging examinations such as CT and MRI were excluded, as shown in Figure 1.

### 3. Methods

Full convolutional neural networks are widely used in image segmentation. At present, full convolutional neural network is used for organ segmentation in medical image. On the basis of full convolutional neural network, many improved network structures are derived. In the research, the basic structure and training method of convolutional neural network were introduced, and the three-dimensional convolutional neural network Vnet network was introduced, and then, the defects of Vnet network in the field of organ segmentation were pointed out. Full convolutional neural network is used to solve the problem of image semantic segmentation [11]. Since there is no full connection layer,

the full convolutional neural network does not need to fix the feature graph into the feature vector of the same length, so it can receive the input image of any size. Full convolutional neural network is an end-to-end network structure, and the same size segmentation results can be obtained directly from the input image data. In essence, full convolutional neural network classifies every pixel of the image [12, 13]. The full convolutional neural network is mainly composed of convolution layer, pooling layer, and upsampling layer. The function of convolution layer is to extract local features of image data. The function of pooling layer is to enhance receptive field and narrow data dimension. The function of the upsampling layer is to restore the feature map to the same size as the input image [14]. The overall process is as follows. The image is input first. Then, feature is extracted through convolution layer and pooling layer to compress feature dimension. Then, the dimension of the feature map is restored through the upper sampling layer. Finally, Softmax is calculated for the feature graph to obtain the category probability of each pixel. According to the probability, each pixel is classified and the final segmentation result is obtained. According to the dimension of input image, full convolutional neural network can be divided into two-dimensional full convolutional neural network and three-dimensional full convolutional neural network. Common two-dimensional full convolutional neural network includes FCN, Unet, and DeepLab. Three-dimensional full convolutional neural network includes 3D Unet, Vnet, and DenseVnet. Full convolutional neural network is generally composed of the following parts including convolution, pooling, activation function, upsampling, and Softmax. Schematic diagram of the simple structure of full convolutional neural network is shown in Figure 2.

Pooling, namely, downsampling, is used to reduce data dimensions. Pooling typically reduces the dimension of the image data by a factor of 2. Due to the statistical properties of features, the feature graph can still describe the image after the pooling operation. And the pooling operation reduces the data dimensions, which can effectively avoid overfitting. There are three main types of pooling: maximum pooling, mean pooling, and convolution pooling. In maximum pooling, the maximum value of the region is selected as the output. In mean pooling, the mean value of the region is calculated as the output. In convolution pooling, the convolution is calculated, and the stride is set to 2 to achieve the effect of pooling [15]. After the input convolution calculation, another function will be applied, and this function is the activation function. The function of activation function is to introduce nonlinear relation so that the neural network can approximate to any nonlinear function.

Common activation functions are as follows.

Sigmoid function is shown in the following formula:

$$f(x) = \frac{1}{1 + e^{-x}}. \quad (1)$$

Hyperbolic tangent (tanh) function is shown in the

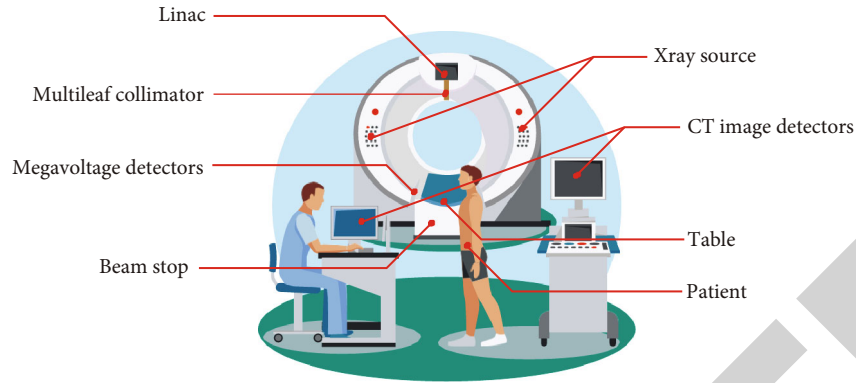


FIGURE 1: Application of MRI and CT images in the surgical treatment of early cervical cancer.

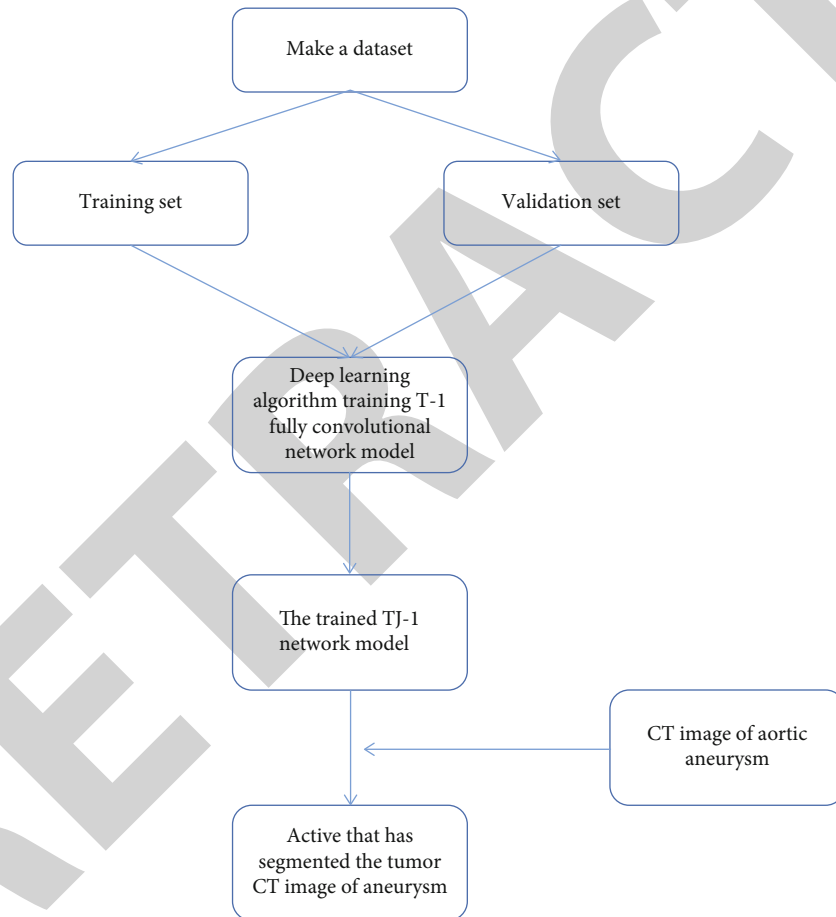


FIGURE 2: Schematic diagram of simple structure.

following formula:

$$f(x) = \frac{e^x - e^{-x}}{e^x + e^{-x}}. \quad (2)$$

ReLU function is shown in the following formula:

$$f(x) = \max(0, x). \quad (3)$$

PreLU function is shown in the following formula:

$$f(y_i) = \begin{cases} y_i, & \text{if } y_i > 0, \\ a_i y_i, & \text{if } y_i \leq 0. \end{cases} \quad (4)$$

Sigmoid function is prone to cause the problem of gradient disappearance. Compared with sigmoid, tanh is improved but still has the problem of gradient disappearance. At the same time, these two functions are more

complicated and require a large amount of calculation. ReLU function is greatly improved in these two aspects. ReLU not only does not appear gradient disappearance but also is easy to calculate. Meanwhile, ReLU function can also introduce sparsity into neural network. The PReLU function is unsaturated and converges faster than ReLU. After the convolution and pooling of the input image, the size of the feature map is smaller than the original image. The image segmentation network needs to restore the feature map to the same size as the input image for further calculation. Therefore, the size of the feature map needs to be expanded to improve the resolution of the feature map, which is called upsampling [16]. There are three common methods of upsampling: bilinear interpolation, transposed convolution, and antipooling. At present, transposed convolution is mainly used. Transposed convolution is performed by first enlarging the size of the input by adding zeros, then rotating the convolution kernel, and finally convolving the input. The operation is shown in Figure 3.

Softmax is used to deal with multiclassification problems. The final output of neural network needs to be processed by Softmax function. The definition of Softmax function is shown in the following formula:

$$s_i = \frac{e^{V_i}}{\sum_j e^{V_j}}. \quad (5)$$

Full convolutional neural network is a supervised learning algorithm, and the parameters of the convolution kernel in the network need to be obtained through the supervised training. In the supervised training of convolutional neural network, three parts are mainly considered including labeled data, loss function, and gradient descent algorithm.

Loss function is used to measure the difference between the predicted value and the real value of the model. It is a nonnegative real value function. The smaller the loss function, the better the robustness of the model. For image segmentation, there are two commonly used loss functions.

Cross entropy loss function: it describes the difference between two probability distributions. The smaller the difference is, the closer the probability distribution is. For the two probability distributions  $p$  and  $q$ ,  $q$  is used to represent the cross entropy of  $p$ , as shown in the following formula:

$$H(p, q) = -\sum_x P(x) \log q(x). \quad (6)$$

Dice loss function: it describes the degree of overlap between the predicted region and the real region in the image segmentation result, as shown in the following formula:

$$D = \frac{2\sum_i^N p_i g_i}{\sum_i^N p_i^2 + \sum_i^N g_i^2}. \quad (7)$$

Gradient descent algorithm is a kind of iterative method. Gradient descent is one of the most commonly used methods for solving model parameters of machine learning

algorithms, namely, unconstrained optimization problems. The minimum value of the target loss function was iteratively solved step by step by gradient descent method, and the minimum loss function and model parameter values were obtained. Commonly used gradient descent algorithms are as follows.

The full name of SGD is Stochastic Gradient Descent. A batch of samples are randomly selected. Each input in the sample is output by using the existing parameters, and then, all the errors are compared with the actual output. After averaging, the average error is obtained. Based on this, parameters are updated as shown in the following formulas:

$$\begin{aligned} \hat{g} &\leftarrow +\frac{1}{m} \nabla_{\theta} \sum_i L(f(x_i; \theta), y_i), \\ \theta &\leftarrow \theta - \varepsilon \hat{g}. \end{aligned} \quad (8)$$

One problem with SGD is that the gradient calculated in each iteration is noisy. Using the idea of momentum for reference, the previous several gradients are added into the calculation of this gradient, which can effectively alleviate the noise problem and speed up learning. The cumulative gradient decays each turn, as shown in the following formulas:

$$\begin{aligned} s &\leftarrow \rho_1 s + (1 - \rho_1) g, \\ r &\leftarrow \rho_2 r + (1 - \rho_2) g \odot g. \end{aligned} \quad (9)$$

In the case of preparing the training data, the loss function and gradient descent algorithm are determined. Then, the full convolutional neural network can be trained to fit the parameter values of the neural network. However, the models trained based on training data sets often have poor generalization ability, which can be mainly divided into two reasons, namely, underfitting and overfitting. Underfitting is caused by the poor fitting degree of the model to the data, which can be solved by increasing the depth of the neural network or improving the network structure. Overfitting is because during the training of the model, if there is less training data, that is, the training data cannot estimate the distribution of the whole data or the number of training iterations is too many, the noise in the training data and the unrepresentative features in the training samples are fitted, which leads to the poor generalization ability of the model. The overall network structure is the encoder decoder structure. The left part is the encoding process, which is composed of convolution and pooling layer, with a total of 4 convolution layers and 4 pooling layers. The right part is decoding process, with a total of 4 convolution layers and 4 upsampling layers. In the middle of the network bottom is convolution layer, which is located between encoding and decoding process. In the encoding part and decoding part, the convolution layer with the same size of feature graph is connected by the cascade layer. Each convolution layer contains 1 to 2 convolution units, among which the first left convolution layer and the first right convolution layer contain 1 convolution unit, and the remaining convolution layers contain 2 convolution units. In the convolution



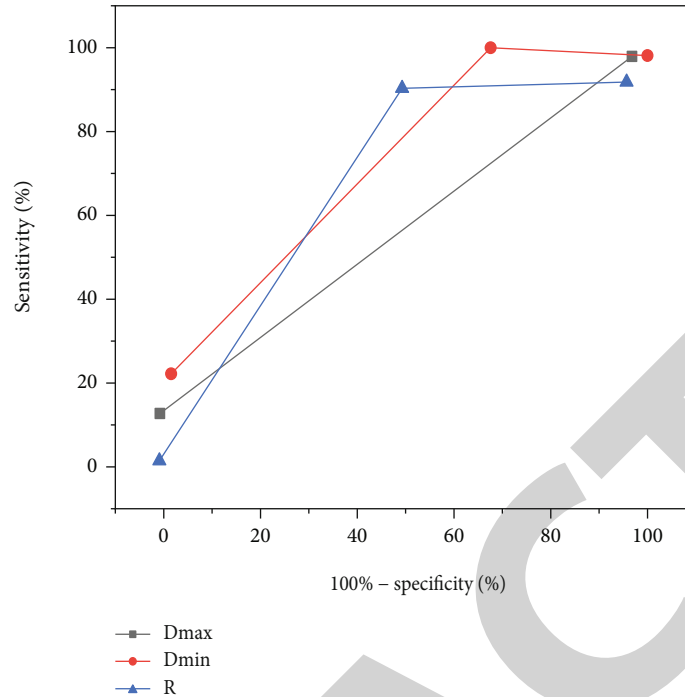


FIGURE 3: ROC comparison of different variables.

layer, residual learning structure is adopted to add the input of the convolution layer and the final output of the convolution layer. And then, subsequent calculation is carried out, so as to alleviate the problem of gradient disappearance. The pooling layer of Vnet-S network is the convolution pooling. There are two  $1 \times 1 \times 1$  convolution kernels behind the right 1 convolution layer, which is responsible for the number of compression channels. At the end of the network is Softmax, which generates the category probability of each pixel of the image. Specific network parameters are shown in Table 1.

The overall process of network coding calculation is as follows. First, in the coding process, features are extracted continuously by the convolutional layer, feature dimensions are reduced by the pooling layer, and receptive fields are increased. When reaching the middle layer, feature dimensions reach the minimum and the number of feature channels reaches 256. Then, in the decoding process, the convolution layer extracts and combines the features, the upsampling layer restores the size of the feature image, and the cascade layer compensates the fine granularity image features and target location information. On the right 1, the size of the feature map of the convolution layer is restored to the same size as the input image. Then, two  $1 \times 1 \times 1$  convolution kernels are combined and the number of channels is compressed to obtain two feature images with the same size as the original image. Then, Softmax function is used to obtain the probability of each voxel in the original image belonging to foreground and background. If the foreground probability is greater than the background probability, the prediction is the foreground target and marked as 1. If the foreground probability is less than the background probability, the prediction is the background and marked 0. The loss

function selected by training Vnet-S network is Dice loss function.

#### 4. Experiment and Analysis

Twenty patients with LACC admitted to Nanfang Hospital of Southern Medical University from September 2020 to May 2021 were selected for a retrospective analysis. The original data sets of preoperative CTA and DSA images during arterial chemotherapy were collected. The patients were 29-52 years old, with an average age of  $43.28 \pm 7.98$  years. All patients were evaluated by two chief gynecologic oncologists based on the 2009 Federation International of Gynecology and Obstetrics (FIGO) staging, and the size of the tumor was more than 4 cm. All patients were excluded from basic cardiovascular diseases, hyperthyroidism, pregnancy, etc., and had no history of drug or seafood allergy. After being informed of the efficacy and risks of arterial chemotherapy and other alternative treatment plans, they voluntarily accepted preoperative neoadjuvant arterial chemotherapy, underwent preoperative CTA examination, and signed relevant informed consent, as shown in Table 2.

Dual source CT (SOMATOM Definition) produced by Siemens, Uvixian (370 mgI/ml, Schering Guangzhou Pharmaceutical Co., LTD.) and double syringe were used. Scanning conditions were tube voltage 120 kV, tube current 320 mA, scanning layer thickness 5 mm, layer spacing 5 mm, fasting for 4 h to 6 h before examination, and without other special treatment. During the scanning, the patient was in supine position in the middle of the bed with his head in his hands and his legs straight and together. The midsagittal plane of his body was perpendicular to the bed. The scanning range was from the lower margin of the third lumbar

TABLE 1: Vnet-S network parameters.

Convolution layer	Composition	Convolution layer	Composition
Left 1	Convolution unit X1 Channel number 16	Right 1	Convolution unit X2 Channel number 128
Left 2	Convolution unit X2 Channel number 32	Right 2	Convolution unit X2 Channel number 64
Left 3	Convolution unit X2 Channel number 64	Right 3	Convolution unit X2 Channel number 32
Left 4	Convolution unit X2 Channel number 128	Right 4	Convolution unit X1 Channel number 16
Middle layer	Convolution unit X2 Channel number 256	Output	$1 \times 1 \times 1$ convolution Channel number 2

TABLE 2: FIGO staging of cervical cancer patients.

Staging	Cases
IB2 stage	9 cases
IIA2 stage	3 cases
IIB stage	7 cases
IIIA stage	1 case
In total	20 cases

spine to the lower margin of the symphysis pubis [17]. After the routine plain scanning was performed (plain scanning period), contrast agent 80ml was injected through the patient's right median cubital vein at the flow rate of 4.0ml/s (A tube) with a double simple high-pressure syringe, followed by 20ml normal saline injection at 4.0 ml/s (B tube) and bolus tracking. The region of interest (ROI) at 2.0 cm above the abdominal aortic bifurcation was selected for dynamic CT value monitoring, and the scanning was automatically triggered when the CT value in ROI reached 100 Hu (arterial phase). Finally, the images of each period were thinned to a thickness of 1.0mm and saved by disc carving. First, the original data set in plain scanning period was imported into the Mimics software. After automatic positioning images, tissue images, and interpolation processing, the minimum reconstruction threshold was set at 100Hu. After region growing, a complete digital 3D model of pelvis was directly reconstructed. Finally, the constructed pelvic digital 3D model was exported and saved in STL format by binary STL command in export tool, in preparation for subsequent registration and reconstruction of vascular network model [18]. The original data set of arterial phase was imported into the Mimics software, and the minimum reconstruction threshold was set to 90Hu~100Hu according to the display of arterial blood network after automatic positioning image, tissue image, and interpolation processing. Then, the bone tissue of each layer was automatically generated, and the outline of arterial blood network was enhanced (initial mask) by region growth. The STL format file of pelvis was imported into the reconstruction file of arterial phase, and the 3D model data was inverted into 2D mask data by calculate mask from subject. After separating the pelvis from the connected part of the pelvic arterial network layer by layer, the pelvic mask was created by using

erase tools in edit masks. Boolean operations were used to subtract the pelvic mask from the initial mask. A new digital 3D model of cervical cancer arterial blood network was further generated by using the region growth tool, which was exported and saved in JPEG format. On the basis of the digital 3D model of uterine arterial blood network for cervical cancer in vivo, 3Dview, Rotation, and Rescale were used to scale and rotate the model at any size and angle, so as to observe the branches and direction of each artery. The source and number of uterine blood supply arteries were identified. Using the function of Cut with polyplane and Cut with curve in the Mimics software, the uterine arterial blood network model was segmented into uterine or cervical arterial blood network, left or right uterine arterial blood network, and left or right cervical arterial blood network. For each part, the blood volume could be calculated by using 3D properties—volume and the blood supply ratio could be further calculated. For cervical cancer patients with original clinical IB1~IIA2 stage included in the research, lymph node metastasis was first determined according to MRI or CT examination reports. For patients with positive pelvic lymph nodes, IICr stage was defined according to the new FIGO cervical cancer staging standard. Since para-aortic lymph node dissection was performed in only a few cases, IIC stage in the research referred to the cases with positive pelvic lymph nodes. Then, according to the surgical pathological report, lymph node metastasis was determined, which was defined as IHICp stage in the same way. And then, IICr and IIICp were compared. The measurement data were expressed as mean  $\pm$  standard deviation ( $X \pm S$ ), and the counting data were expressed as  $N$  (%). According to data type, intergroup comparison was performed by independent sample  $t$  test, and intergroup rate comparison was performed by  $\chi^2$  test or Fisher's exact probability method. When lymph node metastasis was confirmed, it was defined as true positive if both MRI and pathological reports indicated the presence of at least one lymph node metastasis [19, 20]. If only MRI showed lymph node metastasis, it was defined as false positive. If neither MRI nor pathology showed lymph node metastasis, it was defined as true negative. If only pathology showed lymph node metastasis, it was defined as false negative. The sensitivity, specificity, positive predictive value, and negative predictive value of imaging

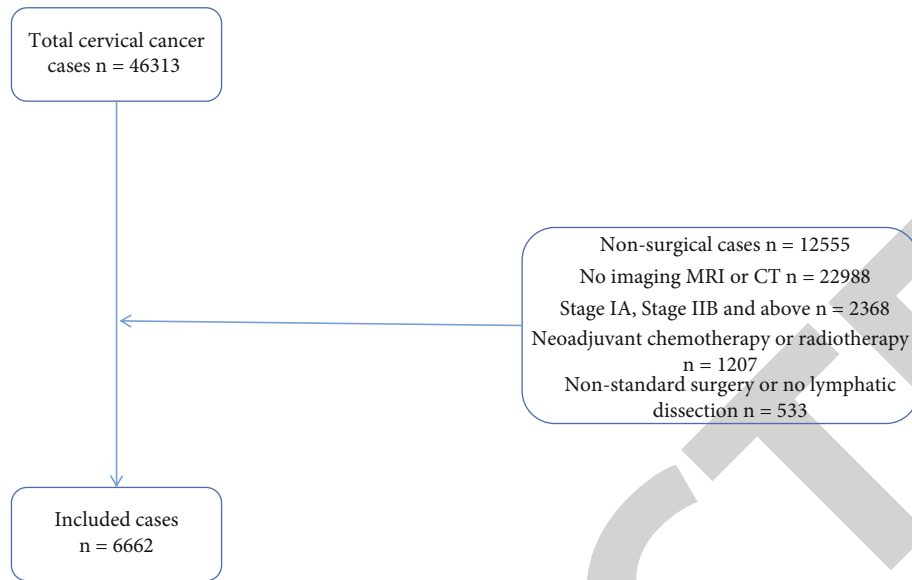


FIGURE 4: Case inclusion process.

examination in diagnosing lymph node metastasis were calculated using surgical pathological results as the gold standard. The SPSS 21.0 software was used for statistical analysis. A total of 46313 cases of cervical cancer were screened from the big database of clinical diagnosis and treatment of cervical cancer in China, and 6662 cases were selected for final analysis. The case screening process is shown in Figure 4.

With the gradual popularization of cervical cytology screening, HPV testing, and cervical cancer vaccine, there are great changes in the epidemiology of cervical cancer. Firstly, there are obvious national and regional differences [21]. In developed countries, cervical cancer on a whole has appeared a downward trend. But in the developing world, because of the disequilibrium of medical and health conditions, cervical cancer has not been effectively controlled. Even due to factors such as lifestyle changes, new cases continue to rise. Cervical cancer is still a serious threat to women's health gynecologic malignant tumor. Secondly, the wide application of cervical cancer screening makes more women get diagnosed at the early stage, and the diagnosis proportion of early cervical cancer increases. Thirdly, the incidence of cervical cancer shows an obvious trend of younger age. And patients often have the desire to preserve ovarian function or fertility. Finally, researches on the staging methods of cervical cancer show that in many countries worldwide, especially developed countries, the clinical staging of modern imaging examinations such as MRI is not strictly excluded but affected by these examinations [22]. The exclusion of modern imaging tests such as MRI from clinical staging is in fact not universally followed, leading to a decline in the comparability of clinical staging between different countries and regions worldwide. From the perspective of the change of treatment mode, with the increase of cases of early cervical cancer, the proportion of patients with cervical cancer undergoing surgical treatment is on the rise due to the advantages of surgical treatment in pre-

serving ovarian function, tissue elasticity, and reproductive function [23]. Nowadays, the treatment mode of cervical cancer has changed into a comprehensive prevention and treatment mode. It is mainly diversified surgical treatments for early cancer and the radiotherapy combined with immunotherapy and gene therapy for middle and late cancer. Tumor staging is not static, but it should be regularly updated as clinical practice changes, so as to adapt to current clinical practice. Therefore, with the changes in the epidemiology and treatment mode of cervical cancer, the clinical staging of cervical cancer should be changed accordingly. For a long time, a large number of researches have believed that lymph node metastasis is an adverse factor affecting the prognosis of patients with early cervical cancer. The 5-year survival rate of patients with negative lymph node metastasis can reach 91%, while the 5-year survival rate of patients with positive lymph node metastasis decreases to 67%. Lymph node metastasis is also a determinant of post-operative supplementary radiotherapy. Therefore, in the new stage classification of cervical cancer, lymph node metastasis is included in the stage and defined as IIC stage. At the same time, modern imaging examinations such as MRI and CT are allowed to be included in the clinical stage, making it possible to assess the presence of lymph node metastasis through imaging examination before treatment. Since positive lymph nodes are one of the clear indications of postoperative supplementary radiotherapy, it is of great clinical significance to determine whether there is lymph node metastasis and whether it is IIC before treatment. On the one hand, if there is no actual lymph node metastasis and the imaging is determined to be stage IIC, the patient may be advised to direct radiation therapy, thus losing the opportunity for surgical treatment. For the women of child-bearing age, radiotherapy may result in loss of ovarian function. And for the women who need to have children, radiotherapy may also result in loss of fertility. On the other hand, if positive lymph nodes are not found before surgical

treatment, patients will need to receive supplementary radiotherapy after surgery, resulting in higher total complications of cervical cancer patients than direct radiotherapy and decreased quality of life [24, 25].

Therefore, if imaging methods can be used to accurately diagnose the presence of lymph node metastasis and improve the accuracy of IICr, it will certainly help improve the treatment prognosis of patients. At present, the accuracy of MRI and CT in diagnosing lymph node metastasis is not ideal. A meta-analysis showed that MRI and CT had a sensitivity of 56% and 58% and specificity of 93% and 92%, respectively, in diagnosing lymph node metastasis. Bourgioti et al. reported that MRI had a sensitivity of 50.00% and specificity of 98.99% in the diagnosis of positive pelvic lymph nodes. In the research, the sensitivity of MRI and CT in diagnosing lymph node metastasis was only 26.56% and 12.21%, respectively. Most patients with lymph node metastasis confirmed after surgery could not be accurately diagnosed by CT or MRI before surgery. The diagnostic efficacy of CT and MRI in diagnosing lymph nodes was not ideal. The reasons were analyzed, which may be related to the multicenter retrospective research, long time span, and the lack of advanced early imaging equipment. Therefore, in the clinical practice of cervical cancer in China, MRI and CT examination is used to diagnose lymph node metastasis, and the diagnostic efficacy of IIC stage is low [26]. Pelvic lymphatic dissection should still be considered for patients with cervical cancer whose MRI or CT examination does not indicate positive lymph nodes [27, 28]. Currently, the commonly used imaging techniques for detecting lymph node status in clinical practice include B-ultrasound, CT, MRI, and PET-CT. Among them, CT and MRI are the most commonly used imaging examinations for detecting lymph node status of cervical cancer due to their high popularity. MRI and CT are mainly used to judge benign and malignant lymph nodes by observing the size of lymph nodes, and the positive standard is usually shorter axis diameter  $\geq 1$  cm. However, normal-sized metastatic lymph nodes are not uncommon. And enlarged lymph nodes can also be benign lesions, such as inflammatory enlargement and reactive hyperplasia. Morphological criteria alone cannot distinguish whether the enlarged lymph nodes are metastatic lymph nodes and cannot distinguish inflammatory lesions from tumor metastasis. And normal size metastatic lymph nodes also cannot be found.

## 5. Conclusions

The application of FIGO clinical staging of cervical cancer in China was described in detail, including standardization and accuracy. The proportion of clinical staging not conforming to FIGO staging standard was 22.6%, and the nonstandard staging was more common in age  $> 70$  years old. Nonexogenous lesions and other staging parameters were difficult to determine. The proportion of inaccurate clinical staging was 34.2%, and the incidence of higher stage was significantly higher than that of lower stage. The inconsistent judgment of tumor maximum diameter and vaginal involvement was the main factor leading to inaccurate staging classifica-

tion. Imaging examination, such as MRI and CT, has application value in the clinical staging of cervical cancer. The inclusion of imaging examination in cervical cancer staging is helpful to improve the accuracy of clinical staging. In the past clinical practice of cervical cancer in China, the low diagnostic efficiency of imaging examination may be related to the relatively backward imaging examination equipment and technology and the insufficient attention of gynecological oncologists to imaging examination. MRI has the advantage of high soft tissue resolution, which can accurately display the size of cervical tumor lesions, especially suitable for early cervical cancer. CT scanning has the advantages of fast speed and clear images, which is more suitable for the late stage of cervical cancer.

## Data Availability

The data used to support the findings of this study are available from the corresponding author upon request.

## Conflicts of Interest

The authors declare that they have no conflicts of interest.

## References

- [1] D. Y. Tuchina, I. G. Meerovich, O. G. Sindeeva et al., "Prospects for multimodal visualisation of biological tissues using fluorescence imaging," *Quantum Electronics*, vol. 51, no. 2, pp. 104–117, 2021.
- [2] Y. Dong, S. Dong, Z. Wang, L. Feng, and P. Yang, "Multimode imaging-guided photothermal/chemodynamic synergistic therapy nanoagent with a tumor microenvironment responded effect," *ACS Applied Materials & Interfaces*, vol. 12, no. 47, pp. 52479–52491, 2020.
- [3] X. Yang, T. Han, Y. Zhang et al., "The application of 3D printing in the development of recist standard for evaluating tumor efficacy," *Oncology and Translational Medicine*, vol. 6, no. 1, pp. 43–46, 2020.
- [4] V. Voronin, A. Zelensky, and S. Agaian, "3-D block-rooting scheme with application to medical image enhancement," *IEEE Access*, vol. 9, pp. 3880–3893, 2020.
- [5] K. A. Eley and G. Delso, "Imaging of bone in the head and neck region, is there more than CT?," *Current Radiology Reports*, vol. 10, no. 6, pp. 69–82, 2022.
- [6] G. Masselli, E. Casciani, C. D. Angelis, S. Sollaku, and G. Gualdi, "Clinical application of 18F-DOPA PET/TC in pediatric patients," *American Journal of Nuclear Medicine and Molecular Imaging*, vol. 11, no. 2, pp. 64–76, 2021.
- [7] M. Capozza, A. A. Anemone, C. Dhakan, M. D. Peruta, and S. Aime, "GlucocEST MRI for the evaluation response to chemotherapeutic and metabolic treatments in a murine Triple-Negative breast cancer: a comparison with [18F]F-FDG-PET," *Molecular Imaging and Biology*, vol. 24, no. 1, pp. 126–134, 2022.
- [8] C. Reinhold, Y. Ueno, E. A. Akin, P. R. Bhosale, and E. Imaging, "ACR appropriateness criteria pretreatment evaluation and follow-up of endometrial cancer," *Journal of the American College of Radiology*, vol. 17, no. 11, pp. S472–S486, 2020.

## Retraction

# Retracted: Nursing Methods and Experience of Local Anesthesia Patients under Arthroscope

### Scanning

Received 26 September 2023; Accepted 26 September 2023; Published 27 September 2023

Copyright © 2023 Scanning. This is an open access article distributed under the Creative Commons Attribution License, which permits unrestricted use, distribution, and reproduction in any medium, provided the original work is properly cited.

This article has been retracted by Hindawi following an investigation undertaken by the publisher [1]. This investigation has uncovered evidence of one or more of the following indicators of systematic manipulation of the publication process:

- (1) Discrepancies in scope
- (2) Discrepancies in the description of the research reported
- (3) Discrepancies between the availability of data and the research described
- (4) Inappropriate citations
- (5) Incoherent, meaningless and/or irrelevant content included in the article
- (6) Peer-review manipulation

The presence of these indicators undermines our confidence in the integrity of the article's content and we cannot, therefore, vouch for its reliability. Please note that this notice is intended solely to alert readers that the content of this article is unreliable. We have not investigated whether authors were aware of or involved in the systematic manipulation of the publication process.

In addition, our investigation has also shown that one or more of the following human-subject reporting requirements has not been met in this article: ethical approval by an Institutional Review Board (IRB) committee or equivalent, patient/participant consent to participate, and/or agreement to publish patient/participant details (where relevant).

Wiley and Hindawi regrets that the usual quality checks did not identify these issues before publication and have since put additional measures in place to safeguard research integrity.

We wish to credit our own Research Integrity and Research Publishing teams and anonymous and named external researchers and research integrity experts for contributing to this investigation.

The corresponding author, as the representative of all authors, has been given the opportunity to register their agreement or disagreement to this retraction. We have kept a record of any response received.

### References

- [1] X. Zhang, J. Wang, W. Gao et al., "Nursing Methods and Experience of Local Anesthesia Patients under Arthroscope," *Scanning*, vol. 2022, Article ID 3689344, 9 pages, 2022.

## Research Article

# Nursing Methods and Experience of Local Anesthesia Patients under Arthroscope

Xiaowei Zhang <sup>1</sup>, JingWang <sup>2</sup>, Weixu Gao <sup>2</sup>, Lijuan Li <sup>1</sup>, LiangYu <sup>3</sup>, Kun Liu <sup>4</sup>, and Nan Li <sup>5</sup>

<sup>1</sup>Department of Nursing, Huaxin College of Hebei Geo University, Shijiazhuang, Hebei 050700, China

<sup>2</sup>Shijiazhuang Vocational College of Technology and Information, Shijiazhuang, Hebei 050000, China

<sup>3</sup>Hebei Yiling Hospital, Shijiazhuang, Hebei 050091, China

<sup>4</sup>The First Hospital of Hebei Medical University, Shijiazhuang, Hebei 050031, China

<sup>5</sup>Shijiazhuang Jilian Medical Secondary School, Shijiazhuang, Hebei 050071, China

Correspondence should be addressed to JingWang; 202005000015@hceb.edu.cn

Received 18 June 2022; Revised 9 July 2022; Accepted 18 July 2022; Published 27 July 2022

Academic Editor: Balakrishnan Nagaraj

Copyright © 2022 Xiaowei Zhang et al. This is an open access article distributed under the Creative Commons Attribution License, which permits unrestricted use, distribution, and reproduction in any medium, provided the original work is properly cited.

In order to solve the nursing problems of local anesthesia patients under arthroscopy, a nursing method and experience based on local anesthesia patients under arthroscopy was proposed. From June 2019 to May 2021, 478 patients who underwent knee arthroscopy under spinal anesthesia or local anesthesia were retrospectively investigated, including 186 cases (38.9%) under local anesthesia and 292 cases (61.1%) under spinal anesthesia. 2% lidocaine plus epinephrine was injected locally and intra-articular in patients with local anesthesia, and 0.75% bupivacaine in patients with spinal anesthesia. It was found that in the local anesthesia group and spinal anesthesia group, 94.1% (175/186) and 98.3% (287/292) patients did not feel pain during operation. 93.0% (173/186 cases) and 96.2% (281/292 cases) of patients in the two groups were satisfied or very satisfied with the effect of anesthesia, respectively. The experimental results showed that local anesthesia was a simple and effective anesthesia method for knee arthroscopy, which was more reliable and safer than spinal anesthesia. Local anesthesia could be used for knee arthroscopy or cleaning and rinsing, free body removal, or even common meniscinoplasty.

## 1. Introduction

Arthroscopic knee surgery is a minimally invasive knee surgery that has been widely carried out at present. As an invasive surgery, it is inevitable to involve anesthesia, complications, postoperative pain, and other problems. At present, spinal anesthesia is the most commonly used anesthesia method in China, while local anesthesia as a simpler anesthesia method has not been widely developed. In the research, a retrospective research of 478 patients who underwent arthroscopic knee surgery under spinal anesthesia or local anesthesia was conducted to compare and analyze the

clinical results. Arthroscopic knee surgery is one of the best methods for the treatment of knee osteoarthritis. Postoperative pain and swelling of the affected limb are common complications. Pain affects the recovery of patients and even delays into chronic pain, which affects the daily life of patients in the future, thus affecting the efficacy of surgery. Arthroscopic knee surgery avoids the large surgical incision, reduces many surgical operations, and reduces superficial trauma, but does not reduce the degree of pain. Because the surgically repaired structures inside the joint (such as synovial tissue, anterior fat pad, and joint capsule) are rich in nerve endings, patients can feel painful stimulation, which

causes severe pain. The local peripheral nerve compressed by edema or stimulated by inflammatory reaction substances is also one of the causes of pain.

## 2. Literature Review

Niwas, R. et al. believed that the United Nations World Health Organization (WHO) designated 2000-2010 as the “Bone and Joint Decade” [1]. In osteoarthropathy, Jrgensen, L. et al. believed that as the largest joint in the human body, the knee joint was the most frequently involved joint [2]. Huang, W. et al. believed that knee osteoarthritis was a disease associated with osteoarthrosis, degenerative arthritis, hyperplastic arthritis, hypertrophic arthritis, and senile arthritis caused by degenerative changes of articular cartilage, resulting in cartilage loss and destruction, and also known as osteoarthrosis, degenerative arthritis, hyperplastic arthritis, and senile arthritis, which were often affected by middle-aged and old people [3]. Bayahya, R. A. et al. believed that the knee joint included two articular surfaces, tibia joint and patella joint. In daily activities, the two articular surfaces were not only heavily stressed but also had more complex movement patterns than other joints in the human body, so the knee joint was one of the joints that were most vulnerable to damage or aging [4]. With the high prevalence of knee osteoarthritis, the number of patients coming to the hospital for knee surgery was also increasing. Khoshkesht, S. et al. believed that the postoperative pain was inevitable for most surgical patients. And improper and timely postoperative analgesia measures would bring serious influence to patients, which would make patients doubt the operation and affect doctor-patient and nurse-patient relationship [5]. Thorarinsdottir, K. et al. believed that the International Association for the Study of Pain (IASP) defined pain as an unpleasant feeling and emotional experience with actual or potential tissue damage, belonging to a subjective feeling [6]. Suza, D. E. et al. believed that the inability to communicate could not negate the possibility that an individual had the pain experience and needed the appropriate pain relief [7]. Mutsonziwa, G. A. et al. believed that in recent years, perioperative analgesia was paid more and more attention to the researches in various countries. And it was advocated that postoperative pain should be treated as “the fifth vital sign,” which was equal to vital signs such as blood pressure, heart rate, respiration, and temperature, and timely treatment should be given [8]. Yu, A. et al. believed that the Joint Commission on Accreditation of Healthcare Organizations (JCAHO) (2001) also added the pain assessment and the pain treatment to the hospital assessment items [9]. Zhu, L. et al. believed that learning surgical knowledge and understanding the pain mechanism of the disease could better grasp the characteristics of pain and alleviate the unpleasant pain of patients by taking effective analgesic measures in time [10]. Using active and effective analgesia not only could reduce the degree of pain and eliminate mental tension, so that patients felt more comfortable through the postoperative recovery period. It could also reduce the incidence of perioperative cardiovascular complications, which was beneficial to get out of bed early and pro-

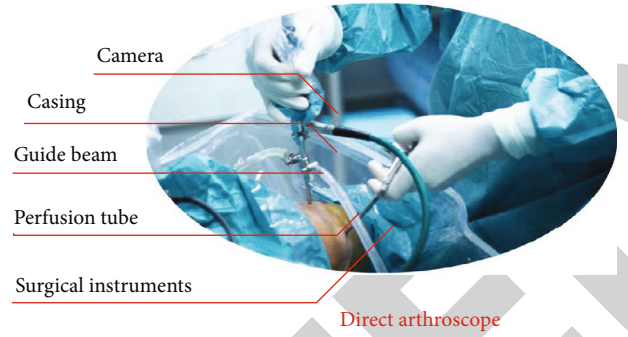


FIGURE 1: Nursing methods of patients under arthroscopic local anesthesia.

mote the recovery of gastrointestinal function for patients. In addition, effective analgesia could also improve sleep quality, enhance immunity, and promote the body's early recovery. Therefore, active perioperative analgesia is very necessary. The nursing methods of local anesthesia patients under arthroscopy are shown in Figure 1.

## 3. Methods

Cluster statistics mainly includes distance, similarity coefficient, and correlation coefficient. The distance and similarity coefficient statistics are used to count the similarity between objects. According to the different types of objects involved in cluster analysis, their definitions are also different. In general, the value range of the distance is a positive real number, and the value of the similarity coefficient is generally between  $[-1, 1]$ . In order to divide data objects reasonably, cluster analysis is based on the degree of affinity between data points, so the definition of similarity measure for data objects is the basis of cluster analysis. One is similarity coefficient. The more similar the two sample points are, the greater the similarity coefficient value is (the closer to the maximum value 1). On the contrary, the more dissimilar the sample points are, the smaller the similarity coefficient value between them is (the closer to the minimum value 0). The other one is distance function. According to the number of characteristic attributes of sample points, the sample is regarded as a point in multidimensional space, so as to define a distance to measure the similarity relationship between sample points. Sample points with a closer distance have a higher similarity, while sample points with a longer distance have a greater difference [11, 12]. There are many ways to measure the distance between sample points. Let  $d(x, x_i)$  be the distance between sample points  $x$  and  $x_i$ , which is generally required to meet the following conditions as shown in Formula (1).

$$\begin{aligned} d(x_i, x_j) &\geq 0, \text{ 且 } d(x_i, x_j) \Leftrightarrow x_i = x_j \\ d(x_i, x_j) &= d(x_j, x_i) \end{aligned} \quad (1)$$

The Euclidean distance is shown in Formula (2).

$$d(x_i, x_j) = \sqrt{\sum_{k=1}^n (x_{ik} - x_{jk})^2}. \quad (2)$$

The absolute distance is shown in Formula (3).

$$d(x_i, x_j) = \sum_{k=1}^n |x_{ik} - x_{jk}|. \quad (3)$$

The variance-weighted distance is shown in Formula (4).

$$d(x_i, x_j) = \sqrt{\sum_{k=1}^n \frac{(x_{ik} - x_{jk})^2}{S_k^2}}. \quad (4)$$

As shown in Formula (5),

$$\bar{x} = \frac{1}{n} \sum_{l=1}^n x_{lk}, S_k^2 = \frac{1}{n-1} \sum_{l=1}^n (x_{lk} - \bar{x}_k)^2. \quad (5)$$

The Mahalanobis distance is shown in Formula (6).

$$d(x_i, x_j) = \sqrt{(x_i - x_j)^T S^{-1} (x_i - x_j)}. \quad (6)$$

In Formula (6),  $S$  is the mountain sample point  $x_1, x_2, \dots$ , and the calculated covariance matrix is shown in Formula (7).

$$\bar{x} = \frac{1}{n} \sum_{l=1}^n x_l, S = \frac{1}{n-1} \sum_{l=1}^n (x_l - \bar{x})(x_l - \bar{x})^T. \quad (7)$$

The correlation coefficients of polymorphic qualitative variables are mainly as follows.

The correlation coefficient related to  $\gamma^2$  is shown in Formula (8).

$$\gamma^2 = nss * \left[ \sum_{i=1}^p \sum_{j=1}^q \frac{n_{ij}^2}{nS_{ai}nS_{bj}} - 1 \right]. \quad (8)$$

$\gamma^2$  itself is also a correlation coefficient, which can be expressed as Formula (9).

$$G_{ij}(1) = nss * \left[ \sum_{i=1}^p \sum_{j=1}^q \frac{n_{ij}^2}{nS_{ai}nS_{bj}} - 1 \right]. \quad (9)$$

That is, one variable is used to predict another variable, and its prediction ability is used as the correlation between the two variables. When the state of variable A is unknown, variable B needs to be predicted. Then, the middle edge and maximum are used as the prediction of state of variable B, which is expressed as Formula (10).

$$nS_b = \max \{nS_{b1}, nS_{b2}, \dots, nS_{bj}, \dots, nS_{bq}\}. \quad (10)$$

The principle of pain after knee arthroscopy is as follows. Most articular structures, including synovial tissue, joint capsule, and fat pad, have autonomic nerve endings that can feel pain stimulation and produce pain sensation. Innervation of joints and synovium is reviewed and it is pointed out that the nerves connecting any joint originate in the spinal cord. The joint is usually the primary nerve, the accessory nerve that passes the peripheral nerve near the joint, and the intramuscular nerve branch that passes through the joint capsule. The knee joint also receives cutaneous nerves in the skin. About half of axons are composed of fine fibers, either thin or unmyelinated. Part of them are unmyelinated C fibers, which are responsible for pain transduction that is not active under normal conditions but released when tissue is damaged [13]. Moreover, in the inflammatory response after surgical trauma, many mediators such as prostaglandins are released, which sensitize the fibers so that they can stimulate and release pain sensation in ordinary activities. Pain signals produced by pain receptors in peripheral nerves are transmitted along the dorsal root ganglia to the dorsal cord, then processed, and then transmitted to higher centers. Risk factors for pain after knee surgery are a complex, subjective, and emotional experience that is influenced by multiple factors, including surgical factors, anesthesia factors, and patient factors. Surgical factors include the type of surgery, duration of surgery, and duration of intraarticular analgesic tourniquet removal. Anesthesia factors include the way of using anesthesia, whether to apply advanced analgesia and the size of analgesic drug dose inside the joint. Patient factors include gender of the patient, preoperative pain rating and duration, previous pain experience, and psychological expectations of the patient after surgery. Recent researches show that female patients are the most important risk factor for pain after arthroscopic surgery. The type of surgery, duration of surgery, and tourniquet use are less important factors. This may explain the conflicting results in previous researches of pain management after arthroscopy.

#### 4. Experiment and Analysis

In recent years, arthroscopic surgery has increased greatly, which brings new challenges to the postoperative analgesia. Although arthroscopic knee surgery allows patients to avoid the large surgical incisions associated with traditional open surgery, some patients still have persistent pain that can last up to two weeks and result in a slow recovery. A recent research of more than 5,700 surgical patients found that orthopedic surgery was the third most common procedure postoperative pain, accounting for 47.7%. In addition, the same survey found that moderate to severe postoperative pain occurred in 44.5% of arthroscopic knee surgeries. Therefore, postoperative analgesia in arthroscopic surgery is still a problem. And effective postoperative analgesia is very important for arthroscopic surgery, which is also very helpful for hand rehabilitation [14]. Effective analgesia is very important for knee arthroscopy and postoperative rehabilitation, which should be started on the day of operation. The ideal postoperative analgesia technique should have



specific effects, long duration, easy operation, and high safety. At present, there are many analgesics and techniques with different principles of action that can be used to relieve pain after knee arthroscopy and have been proved to be effective. These techniques can be divided into the following three categories: pharmaceutical analgesia (including systemic and intraarticular analgesia), local anesthesia techniques, and nonpharmaceutical techniques. But all kinds of analgesic drugs and techniques have the potential side effects and toxicity. Many drugs can act on the pain sensation pathway, so as to effectively relieve the pain after knee arthroscopy, but the potential toxic side effects are inevitable [15]. In general analgesia, opioids (such as morphine, pethidine, fentanyl, and tramadol) may cause respiratory obstruction, static and dizziness, nausea and vomiting, intestinal obstruction, urinary retention, itching, and other side effects. N-benzyloxypropionamide may cause bleeding, gastritis, renal tubular dysfunction, allergic reactions, bronchospasm, fluid retention, thromboembolism, and other side effects. COX-2 inhibitors may cause renal tubular dysfunction, allergic reactions, severe skin adverse reactions, thromboembolism, and other symptoms. Acetaminophen may cause liver poisoning and granulocytosis. Clonidine may cause silence, hypotension, and bradycardia. Gabapentin may cause drowsiness, dizziness, blurred vision, etc. In intra-articular analgesia, arrhythmias due to systemic absorption of local anesthetics, poisoning of the central nervous system, sympathetic-like effects, and catheter insertion techniques can lead to infection. Opioids can cause side effects through systemic absorption. The principle of cold therapy and pressure method is applied to the experimental group. The patient's limb is stimulated by cold compression. The human body system will make control response to this input information, respectively, starting physiological regulator and cognitive regulator to adjust and adapt. The system responds in an adaptive way that is healthy for the body. It is fed back into the system as a feedback signal, slowing down nerve conduction. The excitement of nerve endplate decreases and the pain threshold increases, which improves the pain after knee arthroscopy. Vascular permeability and local exudation are reduced, so as to reduce swelling. Motor function and the ability of daily living activities should be enhanced to restore and maintain health (see Figure 2).

The basic framework of nursing is the concept of holistic nursing. Holistic nursing lays the foundation for nursing practice and research. The basic orientation of the present situation and future is that the human body and mind are regarded as one, and it is needed to completely take a person as the center. It is not only seeing the disease but also not seeing the patient (centering on the disease), nor is it just the patient but not the health (centering on the patient). The most important thing for people is health, so we must take the health of the people as a whole (centering on health) for the concepts, including their psychological, physical, and social aspects, serving the whole process of life, the whole process of health and disease, and the fitness of people with family, society, taking all as a consideration of factors. Patients are provided with preventive care (environment, immunization, nutrition knowledge), nurturing care (daily

care), promoting care (self-care, health education), so that nurses can not only treat patients' diseases but also take care of all aspects of health. It can not only provide standardized medical care services for patients but also develop targeted care plans. It not only provides high-quality care to patients during hospitalization but also takes into account the continuous care of patients after they return home to ensure that patients can receive whole-process, continuous, and high-quality care [16]. After the knee arthroscopy, patients often experience limb pain and swelling several hours after surgery. At this time, the orthopedic clinical nurses cannot be "inactive." After the pain and swelling have occurred on the patient, they passively ask the doctor for corresponding symptomatic treatment (such as oral administration, intramuscular injection, and intravenous infusion of analgesics), which increases the pain of the patient imperceptibly [17, 18]. At this point, the clinical nurse should be proactive in assessing pain and swelling. They should communicate with the doctor in advance to do advance analgesia measures, which can greatly relieve the pain and swelling of the patient. And it can lay a foundation for establishing a good nurse-patient relationship and improving the quality of nursing and patient satisfaction. Experts were selected according to the following criteria. Willingness: Be willing to participate in the research. Working experience and professional title: Intermediate or above professional title and more than 10 years of working experience. Education: Bachelor degree or above. Specialty: Clinical medicine, nursing management, clinical nursing, rehabilitation medicine. Finally, 12 experts were selected for Delphi expert consultation. All 12 experts had rich clinical experience and scientific research ability to provide reliable opinions or suggestions. The details of general information of experts are shown in Table 1.

Thirty patients from a 3-level hospital were selected to carry on the preliminary experiments. And with the approval of the department head and patients, the cold therapy watch list was designed. Qualitative interviews were conducted with 5 clinical nurses with the title of head nurse and 5 postoperative patients using this treatment. In order to ensure the orderly and smooth conduct of the interview, the interview outline was prepared according to the research purpose and characteristics of the interviewees. During the interview, appropriate questioning should be conducted according to the specific situation to gain an in-depth understanding of relevant issues. In order to know whether they were easy to use, the automatic circulation system of compression cold therapy, clinical effects (effect of relieving pain and swelling), and complaints of discomfort in the process of use were recorded. Then, the opinions were recorded, summarized, and fed back to 3 orthopedic experts (two well-known chief orthopedic physicians and a head orthopedic nurse with decades of clinical experience) and 1 college nursing expert for consultation. The survey items were modified and supplemented to optimize the research program. The information of experts and interviewees is shown in Table 2.

The patients' data are shown in Table 3.

Clinical nurses believed that they preferred to apply the automatic circulation system of compression cold therapy

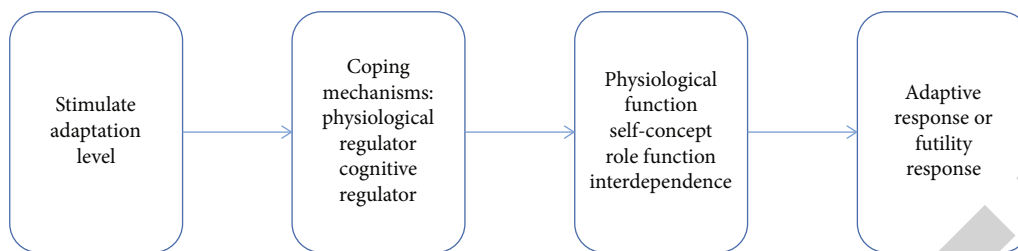


FIGURE 2: Schematic diagram of the adaptive system.

TABLE 1: General information of experts.

Items	Age	The number of specialists	Composition ratio (%)
Age (years old)	30-39	5	41.67
	40-49	6	50.00
	≥50	1	8.33
Years of work (years)	10-19	3	25.00
	20-29	7	58.33
	≥30	2	16.67
	Intermediate	4	33.33
	Sub-high and above	8	66.67

TABLE 2: General information of interviewees (nurses).

Interview subjects	Clinical professional	Age (years old)	Years of work (years)	Title	Education
Nurse A	Orthopedic care	44	26	Supervisor nurse	Bachelor
Nurse B	Orthopedic care	44	26	Supervisor nurse	Bachelor in reading
Nurse C	Orthopedic care	43	25	Supervisor nurse	Bachelor in reading
Nurse D	Orthopedic care	36	17	Supervisor nurse	Bachelor
Nurse E	Orthopedic care	35	16	Supervisor nurse	Bachelor

TABLE 3: General information of interviewees (patients).

Interview subjects	Gender	Age (years old)	Hospitalization (days)	Diagnosis
Patient A	Female	58	5	Osteoarthropathy of the right knee
Patient B	Female	51	6	Osteoarthropathy of the left knee joint
Patient C	Female	41	9	Degenerative lesion of the right knee
Patient D	Male	56	7	Degenerative disease of the left knee joint
Patient E	Male	37	7	Osteoarthropathy of the right knee

for cold therapy operation. Because traditional ice cold therapy used ice to apply towels externally, which was not easy to fix the patient and easy to move when they moved. Frequent visits are required. When ice melted, it would wet towels and contaminate the wound. The traditional ice treatment required the nurse to grab ice with bare hands each time she was frostbitten in her youth and the amount of ice was only enough for one patient at a time. The ice compression bag of the automatic circulation system of compression cold therapy is designed in the form of the wrapped cuff style, which was easier to fix and basically did not shift. And the new device could hold enough ice water for more than eight hours with each replacement. It reduced the workload and did not have to worry about the problem of contaminat-

ing the wound after dissolving the traditional cold treatment ice, because the ice bucket kept the temperature constant. There were no cases of chilblains. Inpatients believed that the automatic circulation system of compression cold therapy was more comfortable and effective. Patients still liked to use pressure cold treatment automatic circulation system for cold treatment, which was more comfortable. Traditional cold therapy was not fixed well, and it would drop when moving, affecting the patient's activities. It was very cool at the beginning and then was wet. The automatic circulation system of compression cold therapy was a new equipment, which was better than the traditional method. The wound was less painful and the leg was less swollen. The cold treatment was affecting the patient's activity too long. No

chilblains had occurred so far, regardless of the cold treatment method.

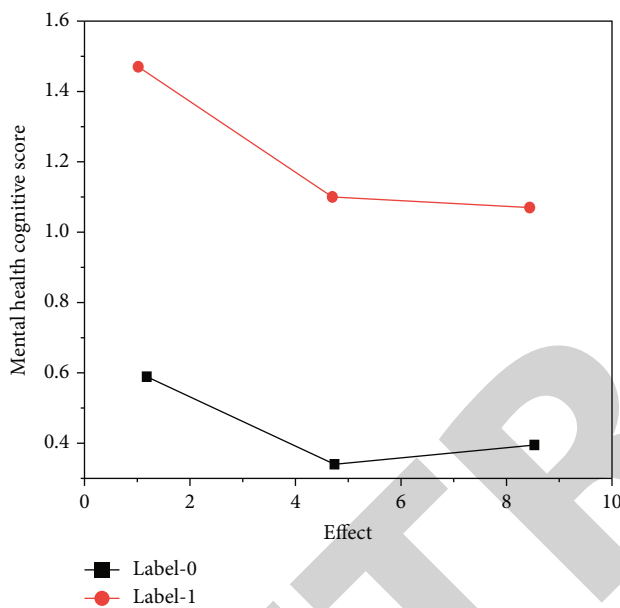
Experts believed that the automatic circulation system of compression cold therapy was a new cold therapy method, which theoretically had the advantages of both cold therapy and pressure therapy. It reduced the nursing work burden and facilitated the operation. But the specific clinical efficacy must be verified through the clinical practice and patients' feelings should be taken into account [19]. The self-made cold therapy satisfaction questionnaire could effectively evaluate the efficacy of postoperative detumescence and analgesia, which reflected the subjective feelings of patients.

A total of 64 patients admitted to the research after the informed consent were randomly divided into the experimental group (the compression cold therapy automatic circulation system treatment group) and the control group (the ice treatment group), with 32 patients in each group. The anesthesia methods used were subarachnoid anesthesia (lumbar anesthesia), continuous epidural anesthesia, or combined lumbar and epidural anesthesia [20, 21]. The inclusion criteria were as follows. Patients were with clear consciousness, no communication barriers, and willing to cooperate with the research. Patients underwent arthroscopic surgery on one knee. The primary disease was one of the following three, including knee osteoarthritis, knee meniscus injury, and knee free body. The exclusion criteria were as follows: the diseases complicated with serious cardiovascular and cerebrovascular, severe anemia, diabetes, hypoproteinemia, and other factors affecting healing; Raynaud's syndrome or other vascular spasmodic diseases such as thrombotic arteritis, hypersensitivity to low temperature, poor local circulation; hypoesthesia or impairment of lower extremities; other infectious lesions throughout the body; patients with indwelling drainage tube after surgery. Two groups of patients began to perform postoperative functional exercises under the guidance of nurses 8 h after surgery. Quadriceps femoris isometric exercises, namely, thigh muscles, tightened and relaxed. More should be done without increasing pain. Equal length exercise of popliteal muscle, namely, the affected leg, pressed the pillow to tighten and relax the muscles on the back of the thigh. Ankle movement was the slow and full range of ankle movement. Cold therapy was performed every 8 h after surgery for both groups. The pain was assessed by Visual Analogue Scale/Score (VAS), and the swelling was assessed by the difference of leg circumference between the affected side and the healthy side. Pain and swelling were evaluated at 24 h and 48 h postoperatively, and knee HSS score and comfort were evaluated at 48 h postoperatively. Two groups of patients were treated with different methods of cold therapy; 32 cases in experimental group were treated with automatic circulation system of compression cold therapy and 32 cases in control group were treated with traditional water ice pack ice treatment. The experimental group was treated with Aircast Cryo/Cuff Systems (automatic circulation system of compression cold therapy). The ice water in the ice bucket was changed every 8 h, and 30 min treatment was performed every 8 h after sur-

gery. The control group was treated with ice pack wrapped with double cotton cloth for 30 minutes every 8 hours after the operation. The ice pack could be replaced when the ice pack completely melted. Postoperatively, the affected limb was routinely raised and the thigh was actively moved to promote blood circulation and edema regression [22, 23]. It should be paid attention to the patient's complaints during the cold therapy, and the changes in skin color, tension, and temperature. The pain was assessed by Visual Analogue Score (VAS). The specific approach was as follows. There was a 10 cm horizontal line on the scoring ruler, and one end of the horizontal line was 0, indicating no pain. The other end was 10, indicating severe pain. The middle part represented different levels of pain. The patient was asked to mark the level of pain on the line according to how he felt. This method was sensitive and comparable [24, 25]. The knee function was scored by Hospital for Special Surgery (HSS) under the guidance of medical staff. VAS and swelling were recorded 24 h and 48 h after surgery, and knee HSS score 48 h after surgery. Patients' satisfaction with the automatic circulation system of compression cold therapy before discharge was measured by self-designed satisfaction questionnaire, which was a self-made questionnaire designed to investigate patients' subjective feelings and efficacy satisfaction after application of compression cold therapy [26]. Questionnaire formulation process was as follows. After reviewing the literature, two directors of orthopedic joint experts and one nursing expert were invited to judge whether each item of self-made questionnaire could effectively reflect the effect of compression cold therapy and the treatment satisfaction of patients. Expert opinions were collected and summarized, and the questionnaire was modified according to expert opinions. Again, the specialists were invited to evaluate the content validity of the revised questionnaire. Finally, the content and items of the questionnaire were compiled under the guidance, review, modification, and approval of three orthopedic experts before they were applied to the clinical research. The questionnaire consisted of five parts. The first part was basic information of patients. The second part was the method of analgesia. The third part was the evaluation of analgesic effect. The fourth part was the evaluation of patients' adverse reactions. The fifth part was the subjective feelings of the patients for the analgesia method. The patients were invited to write down their own experience of the analgesia method for improving pain and reducing limb swelling, as well as their opinions and suggestions. The third and fourth parts were multiple-choice questions, with four answers including very satisfied, satisfied, average, and dissatisfied, with scores of 3, 2, 1, and 0, respectively. There were 13 multiple choice questions in the satisfaction questionnaire, and the total score was 39 points. The unit was points. A total of 64 patients were included, including 19 males and 45 females, with an average age of  $55.31 \pm 15.03$  years, 34 on the left side and 30 on the right side. There were no significant differences in age, gender, disease type, anesthesia method, preoperative pain, and swelling between the two groups in terms of

TABLE 4: Comparison of postoperative pain, swelling, and knee HSS score between the two groups.

Comparison items	Automatic circulation system of compression cold therapy group	Ice treatment group	Statistic	P value
Postoperative 24 h VAS	2.75 ± 1.48	3.59 ± 1.27	$t = -2.449$	0.017
Postoperative 48 h VAS	1.06 ± 1.67	1.88 ± 1.13	$t = -2.174$	0.027
Swelling 24 h after surgery (cm)	2.28 ± 0.88	3.21 ± 1.23	$t = -3.453$	0.001
Swelling 48 h after surgery (cm)	1.60 ± 0.83	2.36 ± 1.14	$t = -3.035$	0.004
Postoperative HSS score	78.65 ± 9.10	73.84 ± 13.13	$t = 1.704$	0.093

FIGURE 3: Clustering effect of  $K=2$  (not considering nursing).

24 h and 48 h postoperative pain and swelling ( $P > 0.05$ ). There was no significant difference in HSS score of knee joint 48 h after operation ( $P > 0.05$ ), as shown in Table 4.

The application of compression cold therapy after knee arthroscopy is an important method to prevent and cure postoperative pain and swelling of patients, which can promote the early activity and early recovery of patients, so as to reduce the length of hospital stay and the dosage of analgesics. Local cold therapy can make local blood vessel contraction, slow blood flow, so that the permeability of capillaries is reduced, tissue fluid extravasation is reduced, local metabolism is slowed down, oxygen consumption is reduced, and muscle tension is weakened, so as to alleviate the pain. Compression reduces the joint leakage and reduces the swelling, which reduces the pain. Compression cold therapy makes full use of the advantages of the cold therapy and compression to reduce the joint blood accumulation and relieve the pain, thus playing an important role in the prevention and treatment of the pain and swelling after the knee arthroscopy. After the introduction of automatic circulation system products of compression cold therapy and the train-

ing of knowledge of compression cold therapy, the director, the head nurse, and nurses of the orthopedic joint group jointly worked out the observation table of the cold therapy. Through the preliminary test of compression cold therapy for patients after knee arthroscopy as a case control, the effect of swelling, pain, and other indicators was observed, and good preliminary results were achieved. The results of clinical trials showed that the pain and swelling of the cold therapy group were lower than those of the control group. Patients in the compression cold therapy group had a good compliance, and many patients experienced swelling and pain relief due to the ice treatment [27, 28]. Based on the psychological nursing of patients' cognition of their own mental health, only the cognitive score of patients' mental health was considered to construct a psychological grading model based on  $K$ -Means of pigeons. In this chapter, the experiment verified the differences between grades formed by different  $K$  values, and the appropriate grades for the classification model were selected according to the experimental results (see Figure 3).

## 5. Conclusions

On the one hand, postoperative compression therapy of the affected limb not only can stop bleeding and prevent exudation through the physical compression but also can promote exudation and congestion to squeeze into the surrounding normal tissues, thus expanding the absorption area, facilitating absorption, and reducing tissue and joint adhesion, degeneration, and a series of pathological changes. As the situation and trend of postoperative bleeding and exudation are gradually under control, continuous compression cold therapy should be stopped. And prolonging the time of compression cold therapy will cause muscle stiffness, which is not conducive to patients' functional exercise. In addition, the continued compression cold therapy can reduce the venous blood flow and even increase the risk of deep vein thrombosis. This retrospective research showed that local anesthesia in arthroscopic knee surgery was simple and effective and had obvious advantages of light postoperative pain, fewer complications, early recovery of physiological functions, and higher reliability and safety under the conditions of intraoperative analgesia and patient satisfaction similar to spinal anesthesia. Local anesthesia could be used for

knee arthroscopy, cleaning and rinsing, free body removal, and even common meniscoplasty, which was the first choice for outpatient knee arthroscopy. Anesthesia effect and patient satisfaction were expected to be higher when combined with intravenous administration. It was not recommended for patients with infectious arthritis or diffuse proliferative synovitis. Patients with bilateral knee arthroscopy were not involved in this research, which required the further research.

## Data Availability

The data used to support the findings of this study are available from the corresponding author upon request.

## Conflicts of Interest

The authors declare that they have no conflicts of interest.

## References

- [1] R. Niwas and S. A. Devi, "Experience of hypertensive patients attending services of district hospital" sapam asha devi original research paper nursing," *Indian Journal of Applied Research*, vol. 7, no. 8, pp. 123–125, 2021.
- [2] L. Jrgensen, S. K. Jensen, and B. Brogaard, "Situational awareness in the outpatient encounter between patients with breast cancer or malignant melanoma and healthcare professionals: patients' perceptions," *Journal of Clinical Nursing*, vol. 29, no. 11-12, pp. 1981–1990, 2020.
- [3] W. Huang and X. Peng, "Study on the effect of lean management in optimizing nucleic acid testing process in outpatient department," *Advanced Journal of Nursing*, vol. 2, no. 3, pp. 64–67, 2021.
- [4] R. A. Bayahya and O. Z. Alsharqi, "A cross sectional study to identify the factors influence implementation of changes in healthcare organization," *American Journal of Nursing Research*, vol. 9, no. 6, pp. 200–205, 2021.
- [5] S. Khoshkesht, L. Mardanian, and A. N. Nasrabadi, "Experience of nursing students in the first exposure to the patient under chemotherapy," *Iranian Journal of Nursing Research*, vol. 15, no. 1, pp. 19–28, 2020.
- [6] K. Thorarinsdottir and K. Kristjansson, "Meaningful text: total hip replacement patients' lived experience of a nursing care plan written in lay language," *The Open Nursing Journal*, vol. 14, no. 1, pp. 325–333, 2020.
- [7] D. E. Suza, T. Eltrikanawati, R. S. Tarigan, and J. Gunawan, "The lived experience of patients from an ethnic group in Indonesia undergoing diabetic foot ulcer treatment," *British Journal of Nursing*, vol. 29, no. 5, pp. S20–S26, 2020.
- [8] G. A. Mutsonziwa, J. Green, and J. Blundell, "A phenomenological exploration of source isolation in patients infected with multi-drug resistant organisms," *Journal of Advanced Nursing*, vol. 78, no. 1, pp. 211–223, 2022.
- [9] A. Yu, L. C. Maclagan, C. Diong, P. C. Austin, and S. E. Bronskill, "Sex differences in care need and survival in patients admitted to nursing home poststroke," *Canadian Journal of Neurological Sciences*, vol. 47, no. 2, pp. 153–159, 2020.
- [10] L. Zhu, L. Chen, H. Kan, and P. Cai, "Staged versus conventional nursing for patients receiving chemotherapy for advanced non-small cell lung cancer: a before and after study," *Annals of Palliative Medicine*, vol. 10, no. 1, pp. 250–257, 2021.
- [11] S. H. Lim, L. L. Mei, F. Aloweni, and S. Y. Ang, "Audit of the appropriateness and accuracy of fluid intake and output monitoring: experience in a tertiary hospital," *British Journal of Nursing*, vol. 30, no. 11, pp. 660–664, 2021.
- [12] A. Amberg, "Making alliances with patients dependent on benzodiazepines: a provider's experience," *Journal of Psychosocial Nursing and Mental Health Services*, vol. 58, no. 1, pp. 29–32, 2020.
- [13] L. A. Bove and C. Kleman, "Using video technology to educate students, patients, and legislators," *Journal of Nursing Education*, vol. 59, no. 8, pp. 457–460, 2020.
- [14] C. Lindauer, K. G. Speroni, K. Godinez, T. Lurz, and A. Zakes, "Effect of a nurse-led, patient-centered, gratitude intervention on patient hospitalization experience," *The Journal of Nursing Administration*, vol. 51, no. 4, pp. 192–199, 2021.
- [15] M. Fan and A. Sharma, "Design and implementation of construction cost prediction model based on svm and lssvm in industries 4.0," *International Journal of Intelligent Computing and Cybernetics*, vol. 14, no. 2, pp. 145–157, 2021.
- [16] A. Mazo, M. Waddell, J. Raddatz, K. Blankenship, and A. B. Christmas, "Screening of acute traumatic stress disorder and posttraumatic stress disorder in pediatric trauma patients: a pilot study," *Journal of Trauma Nursing*, vol. 28, no. 4, pp. 235–242, 2021.
- [17] M. Raj, P. Manimegalai, P. Ajay, and J. Amose, "Lipid data acquisition for devices treatment of coronary diseases health stuff on the internet of medical things," *Journal of Physics: Conference Series*, vol. 1937, article 012038, 2021.
- [18] V. Lebel and S. Charette, "Nursing interventions to reduce stress in families of critical care patients: an integrative review," *Critical Care Nurse*, vol. 41, no. 1, pp. 32–44, 2021.
- [19] Q. Li, T. Liu, S. Zhang, and X. Miao, "Illness perception and treatment experience in patients with gout: a descriptive qualitative study," *Clinical Rheumatology*, vol. 41, no. 4, pp. 1185–1195, 2022.
- [20] X. Liu and Z. Ahmadi, "H<sub>2</sub>O and H<sub>2</sub>S adsorption by assistance of a heterogeneous carbon boron nitrogen nanocage: Computational study," *Main Group Chemistry*, vol. 21, no. 1, pp. 185–193, 2022.
- [21] R. Haren, A. M. Correa, B. Sepesi, D. C. Rice, and M. B. Antonoff, "Hospital readmissions after pulmonary resection: post-discharge nursing telephone assessment identifies high risk patients," *Journal of Thoracic Disease*, vol. 12, no. 3, pp. 184–190, 2020.
- [22] E. Kang, G. A. Tobiano, W. Chaboyer, and B. M. Gillespie, "Nurses' role in delivering discharge education to general surgical patients: a qualitative study," *Journal of Advanced Nursing*, vol. 76, no. 7, pp. 1698–1707, 2020.
- [23] R. Huang, "Framework for a Smart Adult Education Environment2015," *World Transactions on Engineering and Technology Education*, vol. 13, no. 4, pp. 637–641, 2015.
- [24] K. Y. Chiang, S. Y. Fan, L. H. Chang, W. Y. Chang, and J. J. Wang, "Development and psychometric validation of a tool for assessing the care needs of families of patients with dementia," *Hu Li Za Zhi The Journal of Nursing*, vol. 67, no. 4, pp. 39–49, 2020.
- [25] S. Filiz and S. A. Ate, "What are the factors affecting nursing care satisfaction of patients hospitalized in palliative care

## Retraction

# Retracted: Construction of Biologic Microscopic Image Segmentation Model Based on Smoothing of Fourth-Order Partial Differential Equation

### Scanning

Received 11 July 2023; Accepted 11 July 2023; Published 12 July 2023

Copyright © 2023 Scanning. This is an open access article distributed under the Creative Commons Attribution License, which permits unrestricted use, distribution, and reproduction in any medium, provided the original work is properly cited.

This article has been retracted by Hindawi following an investigation undertaken by the publisher [1]. This investigation has uncovered evidence of one or more of the following indicators of systematic manipulation of the publication process:

- (1) Discrepancies in scope
- (2) Discrepancies in the description of the research reported
- (3) Discrepancies between the availability of data and the research described
- (4) Inappropriate citations
- (5) Incoherent, meaningless and/or irrelevant content included in the article
- (6) Peer-review manipulation

The presence of these indicators undermines our confidence in the integrity of the article's content and we cannot, therefore, vouch for its reliability. Please note that this notice is intended solely to alert readers that the content of this article is unreliable. We have not investigated whether authors were aware of or involved in the systematic manipulation of the publication process.

Wiley and Hindawi regrets that the usual quality checks did not identify these issues before publication and have since put additional measures in place to safeguard research integrity.

We wish to credit our own Research Integrity and Research Publishing teams and anonymous and named external researchers and research integrity experts for contributing to this investigation.

The corresponding author, as the representative of all authors, has been given the opportunity to register their agreement or disagreement to this retraction. We have kept a record of any response received.

### References

- [1] Y. Ma, "Construction of Biologic Microscopic Image Segmentation Model Based on Smoothing of Fourth-Order Partial Differential Equation," *Scanning*, vol. 2022, Article ID 1908644, 8 pages, 2022.

## Research Article

# Construction of Biologic Microscopic Image Segmentation Model Based on Smoothing of Fourth-Order Partial Differential Equation

Ye Ma 

Department of Biomedical Engineering, Jilin Medical University, Jilin, China 132013

Correspondence should be addressed to Ye Ma; 20160443@ayit.edu.cn

Received 2 June 2022; Revised 3 July 2022; Accepted 13 July 2022; Published 25 July 2022

Academic Editor: Balakrishnan Nagaraj

Copyright © 2022 Ye Ma. This is an open access article distributed under the Creative Commons Attribution License, which permits unrestricted use, distribution, and reproduction in any medium, provided the original work is properly cited.

In order to solve the problem of microscopic image noise, a biological microscopic image segmentation model based on the smoothing of the fourth-order partial differential equation was proposed. Based on the functional description of image smoothness by directional curvature mode value, a fourth-order PDE image denoising model is derived, which can effectively reduce noise while preserving edges. The result of this method is piecewise linear image, and the gradient at the edge of the target has a step. Using the feature of noise reduction, a new geodesic active contour model is proposed. The experiment result shows that when the variance of Gaussian white noise is 15, the enhancement and denoising effects of the proposed method are 80.35% and 69.84 higher than those of the original vibration filtering method and L. Alvarez method. In terms of time, the proposed method is 1.3075 seconds slower than the original vibration filtering method and 17.5754 seconds faster than the L. Alvarez method. When the variance of Gaussian white noise is 25, the enhancement and denoising effects of the proposed method are 97.79% and 81.16 higher than those of the original vibration filtering method and L. Alvarez method. In terms of time, the proposed method is 1.3246 seconds slower than the original vibration filtering method and 17.5796 seconds faster than the L. Alvarez method. *Conclusion.* The new model is not only stable but also has strong ability of contour extraction and fast convergence.

## 1. Introduction

Medical imaging is an important part of the noninvasive diagnostic process implemented by today's healthcare systems. It involves the creation of visual and functional representations of the body's interior and organs for clinical analysis. Medical imaging technology is mainly divided into imaging based on X-ray (examples include traditional x-rays, computed tomography (CT), and mammography), microimaging, magnetic resonance imaging (MRI), ultrasound (US), and optical coherence tomography (OCT). Based on these medical imaging technologies, various types of biomedical images are increasingly being used to diagnose various diseases [1]. Medical imaging consists of two parts: (1) image formation and reconstruction and (2) image processing and analysis. Image formation involves the process of forming a two-dimensional (2D) image of a three-

dimensional (3D) object, while image reconstruction relies on a set of iterative algorithms, usually forming two-dimensional and three-dimensional images from projected data of the object. Image processing, on the other hand, involves the use of algorithms to enhance the properties of the image, such as noise removal, while image analysis extracts quantitative information or a set of features from the image for target identification or classification, such as medical image segmentation techniques [2].

In the field of computer vision, image segmentation refers to the process of dividing an image into multiple regions. The goal of segmentation is to simplify and/or change the representation of the image, making it more meaningful and easier to analyze [3]. Some of the practical applications of image segmentation include medical imaging to study anatomical diagnosis, treatment planning or locating tumors, and other

pathological diagnoses. In addition, image segmentation technology is also widely used in face recognition, machine vision, satellite target positioning, and other fields, as shown in Figure 1.

## 2. Literature Review

Özdür et al. combined the excellent time-frequency localization characteristics of wavelet in the field of filtering and denoising with the threshold method to overcome the influence of noise in cell images. This method has a good segmentation effect on simple adhesions of quasicircular cells (adhesions of less than 3 cells), but poor segmentation effect on complex adhesions of irregular shape cells [4]. Chen et al. proposed a multithreshold segmentation method for cell images; that is, cell images are segmented into multiple regions by using gray distribution. This method is effective when there is a significant difference between two adjacent regions of the target in the image, but when the cell edge is blurred and the gray distribution of the image is seriously uneven, the segmentation result is not satisfactory [5]. Inspired by the features, Li et al. proposed a multithreshold segmentation algorithm of color histogram with block overlapping for cell graphs stained under the microscope, although this method is better than the traditional color histogram segmentation method. However, it is necessary to update a histogram with a large color change in real time and calculate the Euclidean distance between the reference model and the reference model, which requires a large amount of calculation and is difficult to ensure the segmentation efficiency and robustness to the light [6]. Liu et al. used Delaunay triangulation to divide the cell image into irregular triangles [7]. Chen et al. noted that in addition to dividing the cell image horizontally and vertically, the image was also split in two at 45 and 275 directions [8]. In order to solve the problem of fixed segmentation location, Wang and Chen chose the optimal location to achieve horizontal or vertical segmentation. The above algorithms do not take into account the actual boundary shape of cells but artificially divide the image into some fixed shapes and approach the boundary of cells by constantly subdividing the shapes, which is easy to produce block effect or oversegmentation at the edge of cells [9]. Nlü and Kiri proposed a cell segmentation method based on Sobel operator for the feature of strong speckle noise in the image of gastric adenocarcinoma cells. This method suppressed the speckle noise by making cursive changes to the image, but the edge continuity detected by Sobel operator was not good, and the edge was easy to miss detection when the gray difference between cells and background was small [10]. Liu et al. proposed a method of calculating the segmentation of oval cells. On the basis of ROI extraction and Canny operator's preliminary detection of cell edges, Gauss conic curve fitting was used to accurately locate cell edges. This method has a good segmentation effect on elliptical cells, but not on irregular shape cells [11].

Image noise has a great influence on the segmentation effect of active contour model, especially for the edge based model. Therefore, the regional global partition method is introduced into the region-based model to partially solve this problem. But in some cases, image smoothing pretreatment is still needed. In this paper, the directional curvature mode is used to measure the image smoothness, and a method of biological

microscopic image smoothness based on the fourth-order partial differential equation is derived from the functional. The result of this method is a piecewise linear image, and there is a step in the gradient of the target edge. Experimental results show that the proposed denoising method can greatly improve the segmentation effect of both edge- and region-based active contour models.

## 3. Research Method

### 3.1. Design and Image Acquisition of Fluorescence Microscopic Imaging System Based on Structured Light Illumination

*3.1.1. Principle of Fluorescence Microscopic Imaging.* High-performance fluorescence microscopic imaging system (including automatic focusing platform) provides high-quality cell images for subsequent postprocessing of medical microscopic cell images, which is the premise and key of medical microscopic cell image segmentation in this paper. This section is the key and core content of the whole article [12].

As a kind of optical microscope, fluorescence microscope plays an important role in biomedical research. Fluorescence microscopy uses fluorescence molecules as probes to label biological tissues and obtain spatial information of samples by detecting the distribution of fluorescence signals emitted by excited fluorescence molecules. When a substance is irradiated by a light wave with a shorter wavelength, it emits a light with a longer wavelength, as shown in Figure 2. The energy of phosphorescence is lower than that of fluorescence, so its wavelength is longer than that of fluorescence, and its life span can reach several hours. Excitation materials emit fluorescent light called excitation light; its spectrum includes ultraviolet blue light and has been extended to yellow-green light band [13].

The process of fluorescence is the interaction between light and matter. Fluorescent groups (fluorescent substances probe dye proteins, etc.) that stain cell samples absorb excitation light at a specific central wavelength and undergo an energy-level transition from the ground state to the excited state. Then, the Stokes shift occurs, the frequency shifts to the intermediate state, and finally, the transition back to the lower energy order (ground state) and the emission of fluorescent photons (emission of light). Due to the Stokes frequency shift, the energy of the emitted fluorescent photon is lower than that of the excited photon; that is, the wavelength of the emitted light is longer than that of the excited light.

*3.1.2. How Fluorescence Microscopy Works.* Fluorescence microscope based on fluorescence characteristics has the basic structure of optical microscope and optical magnification; it also has the following unique properties: high fluorescence contrast, selective excitation, high sensitivity, and the red shift of the signal light relative to the excitation light (which is conducive to the separation of the signal light and the excitation light). These unique features improve the image quality of the optical microscope [14]. Given the Stokes shift, how do you build a fluorescence microscope that irradiates a sample at a single wavelength, filters out the light reflected back, and only sees the fluorescence with a longer wavelength shift?



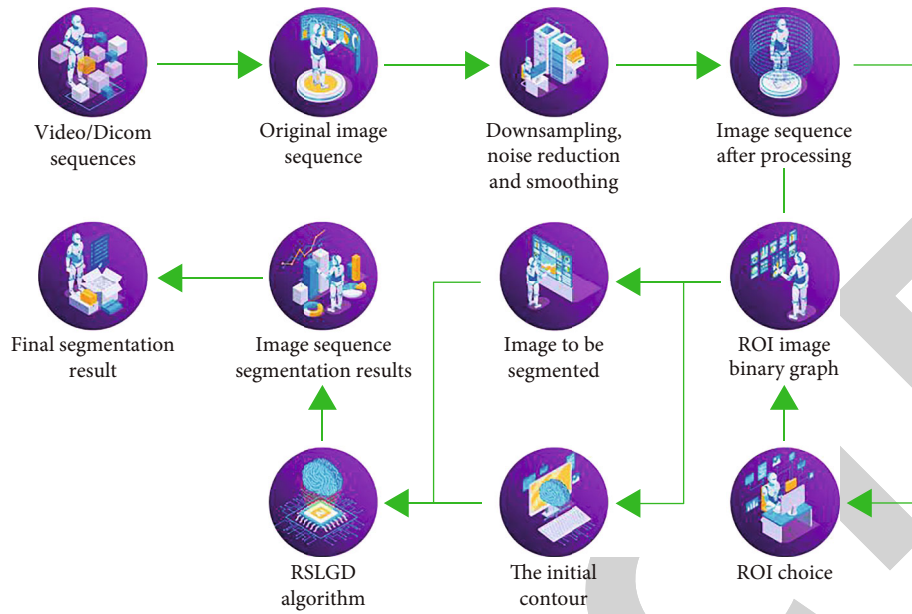


FIGURE 1: A fourth-order partial differential equation-smoothed biomicroscopic image segmentation model.

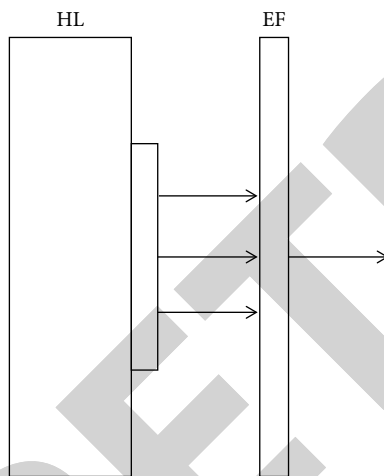


FIGURE 2: Phosphorescence and fluorescence generation diagram.

In fact, it is very similar to how George Gabriel Stokes first noticed fluorescence: a purple glass window allegedly filtered sunlight onto a bottle of tonic water, which he then observed was filled with white wine, blocking out the purple light. The preferred method of modern fluorescence microscopy is surface illumination, that is, falling fluorescence microscopy, which uses an objective lens to illuminate and image the sample. An upright microscope with a slide at the bottom, in this case the light source, is an arc lamp that sends full-spectrum light to the sample through a fluorescent cube that selectively illuminates the sample with the wavelength that excites the particular fluorophore [15]. The excited red fluorescence sends photons in all directions, some of which are collected by the objective and sent to the camera port above through the cube which has two

filters, a dichromatic mirror and a barrier filter, to prevent the excited wavelength from reaching the detector.

In this structure, the microscope objective not only has the usual role of imaging and magnifying the sample but also acts as a condenser to illuminate the sample. The advantage of this approach over transmission fluorescence microscopy (in which the excited light passes through the condenser and the emission is collected by the objective) is that, although the excitation of the fluorophore is the same as that of the transmission microscope, only a small portion of the excited light reflected from the sample needs to be blocked in the return path in the fall-illumination mode.

The main technical obstacle of falling fluorescence microscopy is the overlapping of excitation light and fluorescence emission in the light path, which requires a special beam splitter, namely, dichromatic mirror, to separate excitation and emission. The design of dichromatic beam splitter uses a 45-degree light path. In an ordinary fluorescence microscope, dichromatic mirror reflects the light from the source at shorter wavelengths and transmits the longer wavelengths of the fluorescence emitted. Each dichromatic mirror is designed to have a transition from reflection to transmission between the excitation and emission peaks of the fluorophore for which it is designed. Dichromatic mirrors are rarely used without two additional filters: an excitation filter with a preselected excitation wavelength and a barrier filter that only allows light of longer wavelengths to return to the detector. All three of these filters are typical interference filters with very specific wavelength selectivity, and these are engineering marvels made up of many thin stacks of materials with alternating refractive indices. With the exciter beam splitting bicolor circuit and the barrier circuit, these three components can be very good separation of excitation light and emitted light.

**3.2. Image Smoothing Based on Fourth-Order Partial Differential Equation.** The image function  $I$  is regarded as the surface defined in the three-dimensional space  $(x, y, I(x, y))$ , as shown in Figure 3. Specify a point  $p$  and a direction  $\vec{d}$  on  $I$ , and then, the change of the normal vector of the surface of the point  $p$  in the direction  $\vec{d}$  is expressed by the directional curvature  $\vec{n}$ . Directional curvature is a second-order description of the change speed of the surface along the tangent direction of a certain point on the surface, which can quantitatively express the change of the surface around a certain point:

$$m^2 = 0.5 \cdot (I_{xx}^2 + I_{yy}^2) + I_{xy}^2. \quad (1)$$

Thus, we consider the following defined functional over the region as shown in

$$E(I) = \int_{\Omega} F(m^2) dx dy. \quad (2)$$

$m^2$  is shown in equation (1) and  $I \in C^4(\Omega)$ . Function  $F(\cdot) \geq 0$  is an increasing function, namely,  $F'(\cdot) > 0$ . The operator  $m^2$  can describe the roughness of the local surface. Therefore, the larger the roughness (noise) of the image surface  $I$  is, the larger the functional value of equation (2) is, and the minimization of  $E(I)$  is equivalent to image smoothness [16]. Euler equation about equation (2) is obtained by using variational method:

$$\frac{\partial^2}{\partial x^2} (F'(m^2)I_{xx}) + 2 \frac{\partial}{\partial x \partial y} (F'(m^2)I_{xy}) + \frac{\partial^2}{\partial y^2} F'(m^2)I_y = 0. \quad (3)$$

Euler equation shown in formula (3) can be solved by gradient descent method as shown in

$$\frac{\partial I}{\partial t} = \& - \left[ \frac{\partial^2}{\partial x^2} (F'(m^2)I_{xx}) + 2 \frac{\partial^2}{\partial x \partial y} (F'(m^2)I_{xy}) + \frac{\partial^2}{\partial y^2} (F'(m^2)I_{yy}) \right]. \quad (4)$$

The conduction function is shown in

$$F'(m^2) = \frac{1}{1 + m^2/K^2}. \quad (5)$$

$K$  is threshold of conductivity coefficient; selecting different  $K$  values can control the retention and smoothing of different image features. The original image is taken as the input, and the final solution  $t \rightarrow \infty$  is obtained at that time so that the image is not overly smooth; the iteration must be terminated within a limited time.

The image whose gray function satisfies the plane equation is a linear image. Obviously, when the image  $I$  is a linear image, the gradient  $\nabla I = (\partial I / \partial x) \vec{i} + (\partial I / \partial y) \vec{j}$  is constant. Laplace  $\nabla^2 I$  evaluates to zero and the operator  $m^2 = 0.5 \cdot (I_{xx}^2 + I_{yy}^2) + I_{xy}^2$  is

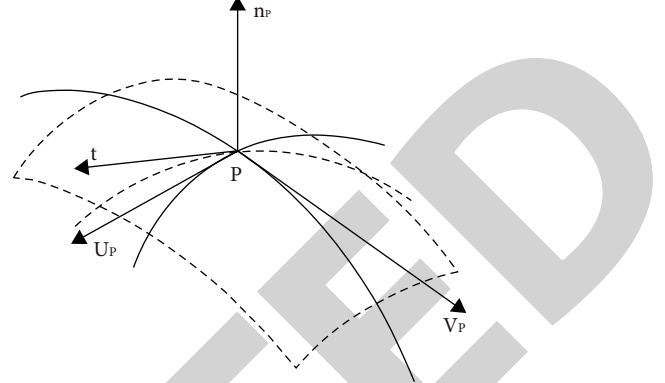


FIGURE 3: Schematic diagram of directional curvature.

zero, so that the left end of equation (3) is equal to

$$\begin{aligned} F'(0)(I_{xxxx} + 2I_{xxyy} + I_{yyyy}) &= F'(0) \left( \frac{\partial^2}{\partial x^2} (I_{xx} + I_{yy}) + \frac{\partial^2}{\partial y^2} (I_{xx} + I_{yy}) \right) \\ &= F'(0) \left( \frac{\partial^2}{\partial x^2} (\nabla^2 I) + \frac{\partial^2}{\partial y^2} (\nabla^2 I) \right) = 0. \end{aligned} \quad (6)$$

It can be seen that the linear image satisfies Euler equation (3), and since the function  $F(\cdot)$  is nonnegative, the functional  $E(I)$  satisfies

$$E(I) \geq 0. \quad (7)$$

At the same time, the function  $F(m^2)$  is an increasing function, and the global minimum is obtained when the linear image  $m^2 = 0$  is drawn, that is, the global minimum of the functional.

Other minima may exist in the functional  $E(I)$ , and we show that piecewise linear images satisfy Euler's equations.

Set  $\Omega_i, i = 1, 2, \dots, n$  as the division of image region, and the piecewise linear image is shown in

$$I(x, y) = \sum_{i=1}^n I_i(x, y), \quad (8)$$

where,

$$I_i(x, y) = \begin{cases} \text{planar image, } (x, y) \in \Omega_i, \\ 0. \end{cases} \quad (9)$$

$I_i \in C^4(\Omega_i)$ ; the composite image  $I(x, y)$  should be continuous. Any two adjacent images  $I_i, I_j$  shown in formula (9) must satisfy different plane equations; otherwise, they can be combined.  $\partial \Omega_i$  is the boundary of area  $\Omega_i$ ;  $\Omega_i - \partial \Omega_i$  is the internal part of  $\Omega_i$ , satisfying the following equations:

$$\nabla I_i(x, y) = \text{constant } (x, y) \in (\Omega_i - \partial \Omega_i), \quad (10)$$

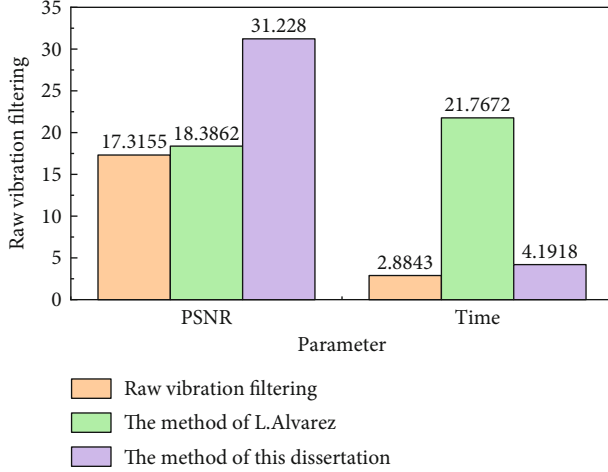


FIGURE 4: Comparison of synthetic image enhancement and denoising effect measures (Gaussian white noise variance = 15).

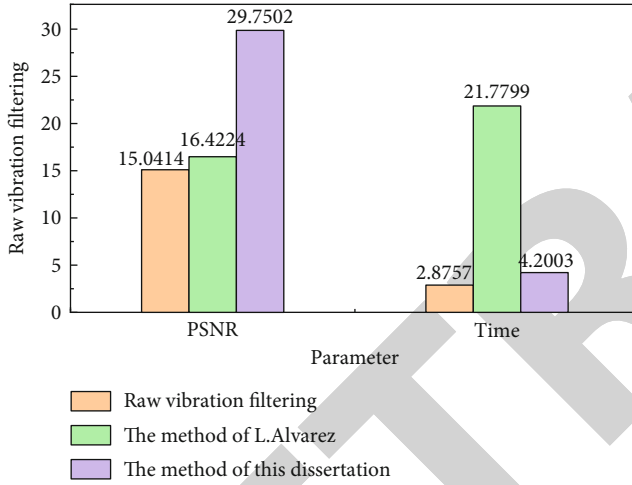


FIGURE 5: Comparison of composite image enhancement and denoising effect measures (Gaussian white noise variance = 25).

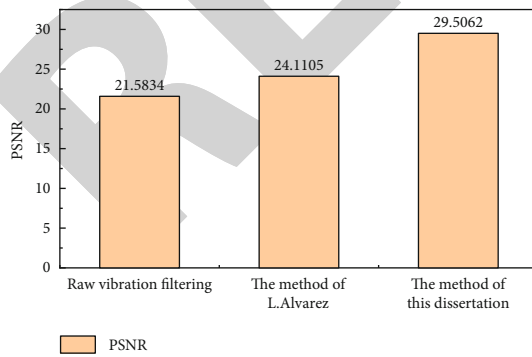


FIGURE 6: Comparison of image enhancement and denoising effect measures (variance of Gaussian white noise = 15).

$$\begin{aligned} \nabla^2 I_i(x, y) &= 0, \\ (x, y) &\in (\Omega_i - \partial\Omega_i), i = 1, 2, \dots, n. \end{aligned} \quad (11)$$

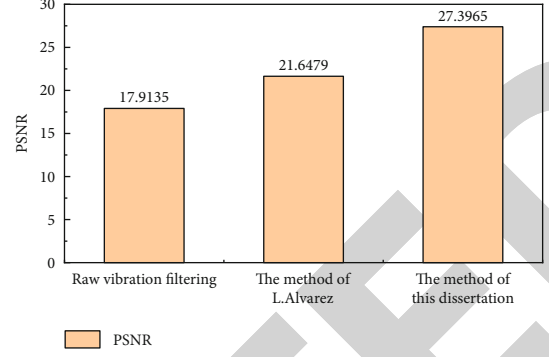


FIGURE 7: Comparison of image enhancement and denoising effect measures (Gaussian white noise variance = 25).

Therefore, the algorithm is shown in

$$\begin{aligned} \nabla^2 I(x, y) &= 0, \\ m^2(x, y) &= 0.5^\circ (I_{xx}^2 + I_{yy}^2) + I_{xy}^2 = 0. \end{aligned} \quad (12)$$

$(x, y) \in (\Omega - \partial\Omega)$ ,  $\partial\Omega = \bigcup_{i=1}^n \partial\Omega_i$ . Since any two adjacent  $I_i$  and  $I_j$  sums are on different planes, the gradient at the boundary  $\partial\Omega$  is discontinuous, as shown in

$$\nabla I_i \neq \nabla I_j. \quad (13)$$

As shown in formula (14),

$$\nabla^2 I(x, y) = \infty, (x, y) \in \partial\Omega. \quad (14)$$

For the operator  $m^2(x, y)$ , the calculation formula is shown in

$$\begin{aligned} m^2 &= \frac{1}{2} (I_{xx}^2 + I_{yy}^2) + I_{xy}^2 = \frac{I_{xx}^2 + I_{xy}^2 + I_{yy}^2 + I_{xy}^2}{2} \\ &\geq \frac{2I_{xx}I_{xy} + 2I_{yy}I_{xy}}{2} = I_{xy}(I_{xx} + I_{yy}) = I_{xy}\nabla^2 I. \end{aligned} \quad (15)$$

$(x, y) \in \partial\Omega$ . If  $I_{xy}$  equals to zero, then the calculation method is shown in

$$\begin{aligned} m^2 &= \frac{1}{2} (I_{xx}^2 + I_{yy}^2) + I_{xy}^2 = \frac{I_{xx}^2 + I_{yy}^2}{2}, \\ (\nabla^2 I(x, y))^2 &= \infty = I_{xx}^2 + I_{yy}^2 + 2I_{xx}I_{yy} \leq 2(I_{xx}^2 + I_{yy}^2). \end{aligned} \quad (16)$$

So we get

$$m^2 = \frac{1}{2} (I_{xx}^2 + I_{yy}^2) + I_{xy}^2 = \infty. \quad (17)$$

The result is shown in

$$F'(\infty) = 0. \quad (18)$$

If  $I_{xx}$  equal to infinity ( $\infty$ ), then the calculation method is shown in

$$F'(m^2)I_{xx} = \frac{1}{(1/I_{xx}) + \left( (0.5 * (I_{xx} + I_{yy}^2/I_{xx})) + I_{xy}^2/I_{xx} \right) / K^2} = 0. \quad (19)$$

It is a similar case for  $I_{xx}$  and  $I_{yy}$ .

Therefore, when it is a piecewise linear image, the result is shown in

$$\frac{\partial^2}{\partial x^2} \left( F'(m^2)I_{xx} \right) + 2 \frac{\partial^2}{\partial x \partial y} \left( F'(m^2)I_{xy} \right) + \frac{\partial^2}{\partial y^2} F'(m^2)I_{yy} = 0, \quad (x, y) \in \Omega. \quad (20)$$

It can be seen that the segmented linear image satisfying Euler equation (formula (4)) is the noise reduction model of the fourth-order partial differential equation derived in this paper [17].

**3.3. New Geodesic Active Contour Model Based on Smoothing of Fourth-Order Partial Differential Equation.** Geodesic active contour (GAC) proposed by Caselles et al. is a model based on curve evolution theory and level set method. It can deal with topological structure changes of curve movement freely without any external control conditions, and it is the most widely used edge model [18].

Geodesic active contour identifies image features (such as edges) with functions  $g(I)$  and was aimed at minimizing energy functions. The motion equation of the corresponding contour curve  $C$  is shown in

$$\frac{\partial C}{\partial t} = g(I)(k + V_0)\vec{N} - \left( \nabla g(I) \cdot \vec{N} \right) \vec{N}, \quad (21)$$

where  $k$  is the curvature of the curve,  $\vec{N}$  is the normal unit vector of the curve,  $V_0$  is the constant, and  $g(I)$  takes a minimum value at the edge, as shown in

$$g(I) = \frac{1}{1 + |\nabla[G_\sigma * I]|^2}, \quad (22)$$

where  $G_\sigma$  represents the two-dimensional Gaussian filter operator with the standard deviation of  $\sigma$  and  $*$  is the convolution operator.

The last term  $g(I)$  is edge attraction, which is an image force pointing towards the edge of the image. When the curve moves near the target edge, this term applies an external force pointing towards the edge of the curve, thus pulling the curve towards the target. In the actual image processing, the target edge is not the ideal edge, and it is not zero at the edge  $g(I)$ . At this point, the curve motion stops near the target by the balance of the edge attraction and the force of the first term, so the target positioning performance is limited [19].

On the basis of image smoothing by the denoising model derived in this paper, we propose a new edge identification

function as shown in

$$G(I) = \frac{1}{1 + |\nabla^2 I|^2}. \quad (23)$$

The corresponding new geodesic active contour (NEW-GAC) model is shown in

$$\frac{\partial C}{\partial t} = g(I)(k + V_0)\vec{N} - \left( \nabla G(I) \cdot \vec{N} \right) \vec{N}. \quad (24)$$

As we know from the above, different images  $K$  can be selected to control the smoothness of image features, and the smoothed image is a piecewise linear image with a step in the gradient at the target edge, as shown in

$$\nabla^2 I(x, y) = \infty, (x, y) \in \partial\Omega. \quad (25)$$

Therefore, the new edge identification function can better achieve the effect of the ideal geodesic active contour model. In the experimental results, we will see that compared with the traditional geodesic active contour model, the new geodesic active contour model proposed in this paper is more ideal in edge positioning.

## 4. Interpretation of Result

In order to verify the effect of the proposed method in image enhancement and denoising, the synthetic images and brain images with different variances of Gaussian white noise and salt and pepper noise were selected for enhancement and denoising. The original vibration model, L. Alvarez method model, and the method in this paper are used to process the noise image, and the results are compared [20, 21].

The results of image enhancement and denoising of Gaussian white noise and appropriate amount of salt and pepper noise are given when the number of iterations is 100. It is obvious that the vibration filtering equation can enhance the image and amplify the noise signal at the same time. The L. Alvarez method has some effect on image enhancement and denoising. However, when the noise is large, the original image structure cannot be well maintained, and the sharp corner information is seriously lost. Compared with the previous two methods, the method in this paper has a better effect, and the original image structure is relatively intact, and the sharp corner information is also well maintained [22, 23].

The enhancement and denoising results of several methods in medical images are given, in which the variance of the image noise is 15 Gaussian white noise, and the number of iterations is 15. It can be seen from the figure that the processing effect of the method in this paper is significantly better than that of the first two methods, which not only enhances the image and removes the noise but also maintains more image details.

In this paper, peak signal-to-noise ratio (PSNR) is also used as the enhancement and denoising effect measurement index. PSNR reflects the statistical average of image signal-to-noise ratio changes. It is a widely used method to measure the subjective quality of images. The greater the PSNR, the

better the image quality and the worse the image quality. As shown in Figures 4–7, it can be seen that the effect obtained by using this algorithm is superior to other methods when the variance of Gaussian white noise is 15. The enhancement and denoising effects of the proposed method are 80.35% and 69.84% higher than those of the original vibration filtering method and L. Alvarez method. In terms of time, the proposed method is 1.3075 seconds slower than the original vibration filtering method and 17.5754 seconds faster than the L. Alvarez method. When the variance of Gaussian white noise is 25, the enhancement and denoising effect of the proposed method is 97.79% and 81.16% higher than that of the original vibration filtering method and L. Alvarez method. In terms of time, the proposed method is 1.3246 seconds slower than that of the original vibration filtering method and 17.5796 seconds faster than that of L. Alvarez method. At the same time, we give the calculation time of various algorithms in the composite image and find that the time of the method in this paper is much smaller than that of the method, mainly because the linear smooth Gaussian kernel  $G_\sigma$  is no longer used to denoise the vibration item in each iteration [24, 25].

## 5. Conclusion

This paper proposes a functional to describe the image smoothness based on the directional curvature mode value and then deduces a fourth-order PDE image denoising model. The processing result is piecewise linear image (including linear image), and the gradient at the edge has a step. In this paper, a new geodesic active contour (NEW-GAC) model is proposed, which improves the contour extraction performance of the original vibration filtering method and the L. Alvarez method with good speed. It is worth noting that NEW-GAC makes full use of the characteristics of the denoising model derived in this paper, and the two methods together constitute a new image segmentation method. The region-based active contour model has some robustness to noise, but the processing of strong noise graph is still limited. The noise reduction model in this paper also greatly improves the segmentation effect of region-based active contour model.

## Data Availability

The data used to support the findings of this study are available from the corresponding author upon request.

## Conflicts of Interest

The author declares that there are no conflicts of interest.

## References

- [1] M. Ebihara and K. Katayama, "Anomalous charge carrier decay spotted by clustering of a time-resolved microscopic phase image sequence," *The Journal of Physical Chemistry C*, vol. 124, no. 43, pp. 23551–23557, 2020.
- [2] Y. Du, G. Xiao, L. Liu, Y. Gui, D. Wei, and X. Yang, "Study of solidification and microstructure characteristics for aircraft icing," *International Journal of Thermophysics*, vol. 41, no. 2, pp. 1–11, 2020.
- [3] Y. J. Kim and Y. Chai, "Splitting of concrete with steel, glass fiber-reinforced polymer, and basalt fiber-reinforced polymer bars exposed to mgso\_4," *ACI Structural Journal*, vol. 117, no. 3, pp. 3–16, 2020.
- [4] N. A. Özdür, I. B. Üçel, J. Yang, and C. C. Aydinler, "Residual intensity as a morphological identifier of twinning fields in microscopic image correlation," *Experimental Mechanics*, vol. 61, no. 3, pp. 499–514, 2020.
- [5] Y. M. Chen, F. I. Chou, W. H. Ho, and J. T. Tsai, "Classifying microscopic images as acute lymphoblastic leukemia by resnet ensemble model and taguchi method," *BMC Bioinformatics*, vol. 22, no. S5, pp. 1–21, 2021.
- [6] M. Li, S. Gao, H. Han, and C. Zhang, "L 0 optimization using laplacian operator for image smoothing," *Jisuanji Fuzhu Sheji Yu Tuxingxue Xuebao/Journal of Computer-Aided Design and Computer Graphics*, vol. 33, no. 7, pp. 1000–1014, 2021.
- [7] Y. Liu, X. Ma, X. Li, and C. Zhang, "Two-stage image smoothing based on edge-patch histogram equalisation and patch decomposition," *IET Image Processing*, vol. 14, no. 6, pp. 1132–1140, 2020.
- [8] W. Chen, J. Bai, X. Gu, Y. Li, and Z. Gui, "Separation-based model for low-dose CT image denoising," *The Journal of Engineering*, vol. 2020, no. 12, pp. 1198–1208, 2020.
- [9] W. Wang and Y. Chen, "An accelerated smoothing gradient method for nonconvex nonsmooth minimization in image processing," *Journal of Scientific Computing*, vol. 90, no. 1, pp. 1–28, 2022.
- [10] R. Nlü and R. Kiri, "Detection of damaged buildings after an earthquake with convolutional neural networks in conjunction with image segmentation," *The Visual Computer*, vol. 38, no. 2, pp. 685–694, 2022.
- [11] L. Liu, L. Wang, D. Xu et al., "CT image segmentation method of liver tumor based on artificial intelligence enabled medical imaging," *Mathematical Problems in Engineering*, vol. 2021, 8 pages, 2021.
- [12] Y. Zhang and Y. Tian, "A new image segmentation method based on fractional-varying-order differential," *Journal of Beijing Institute of Technology*, vol. 30, no. 3, pp. 254–264, 2021.
- [13] A. Renugambal and K. S. Bhuvanewari, "Kapur's entropy based hybridised WCMFO algorithm for brain MR image segmentation," *IETE Journal of Research*, vol. 2, pp. 1–20, 2021.
- [14] J. Xue, Y. Wang, A. Qu, J. Zhang, and H. Sun, "Image segmentation method for Lingwu long jujubes based on improved fcn-8s," *Nongye Gongcheng Xuebao/Transactions of the Chinese Society of Agricultural Engineering*, vol. 37, no. 5, pp. 191–197, 2021.
- [15] Y. Tian, X. Cao, X. Li, H. Zhang, and R. Boulatov, "A polymer with mechanochemically active hidden length," *Journal of the American Chemical Society*, vol. 142, no. 43, pp. 18687–18697, 2020.
- [16] L. Fang, X. Wang, and L. Wang, "Multi-modal medical image segmentation based on vector-valued active contour models," *Information Sciences*, vol. 513, pp. 504–518, 2020.
- [17] H. Lv, F. Zhang, and R. Wang, "Fuzzy active contour model using fractional-order diffusion based edge indicator and fuzzy local fitted image," *IEEE Access*, vol. 8, pp. 172707–172722, 2020.
- [18] X. Yan and G. Weng, "Hybrid active contour model driven by optimized local pre-fitting image energy for fast image

## *Retraction*

# **Retracted: Corner Detection of the Computer VR Microscope Image Based on the 3D Reconstruction Algorithm**

### **Scanning**

Received 11 July 2023; Accepted 11 July 2023; Published 12 July 2023

Copyright © 2023 Scanning. This is an open access article distributed under the Creative Commons Attribution License, which permits unrestricted use, distribution, and reproduction in any medium, provided the original work is properly cited.

This article has been retracted by Hindawi following an investigation undertaken by the publisher [1]. This investigation has uncovered evidence of one or more of the following indicators of systematic manipulation of the publication process:

- (1) Discrepancies in scope
- (2) Discrepancies in the description of the research reported
- (3) Discrepancies between the availability of data and the research described
- (4) Inappropriate citations
- (5) Incoherent, meaningless and/or irrelevant content included in the article
- (6) Peer-review manipulation

The presence of these indicators undermines our confidence in the integrity of the article's content and we cannot, therefore, vouch for its reliability. Please note that this notice is intended solely to alert readers that the content of this article is unreliable. We have not investigated whether authors were aware of or involved in the systematic manipulation of the publication process.

Wiley and Hindawi regrets that the usual quality checks did not identify these issues before publication and have since put additional measures in place to safeguard research integrity.

We wish to credit our own Research Integrity and Research Publishing teams and anonymous and named external researchers and research integrity experts for contributing to this investigation.

The corresponding author, as the representative of all authors, has been given the opportunity to register their agreement or disagreement to this retraction. We have kept a record of any response received.

### **References**

- [1] J. Huang, "Corner Detection of the Computer VR Microscope Image Based on the 3D Reconstruction Algorithm," *Scanning*, vol. 2022, Article ID 8621103, 8 pages, 2022.

## Research Article

# Corner Detection of the Computer VR Microscope Image Based on the 3D Reconstruction Algorithm

Junjun Huang 

Fujian Vocational College of Agriculture, Fuzhou, Fujian 350119, China

Correspondence should be addressed to Junjun Huang; 2013071430@stu.zjhu.edu.cn

Received 26 May 2022; Revised 5 July 2022; Accepted 9 July 2022; Published 20 July 2022

Academic Editor: Balakrishnan Nagaraj

Copyright © 2022 Junjun Huang. This is an open access article distributed under the Creative Commons Attribution License, which permits unrestricted use, distribution, and reproduction in any medium, provided the original work is properly cited.

In order to solve the problem of multisolution and ill-formedness of the 3D reconstruction method of a single image (purpose), the author proposes a microscope image segmentation algorithm based on the Harris multiscale corner detection. Separating complex engineering images into several simple basic geometric shapes, rebuild them separately to avoid the ill-conditioned solution problem of directly recovering depth information. In order to improve the registration accuracy of the corner-based image registration algorithm, the idea of multiresolution analysis was introduced into the classic Harris corner detection, and a gray intensity variation formula based on the wavelet transform was constructed, and a scale transformation characteristic was obtained so that the improved Harris corner detection algorithm is invariant to rotation, translation, and scale. Experimental results show that after reconstruction, the error between the length of the object measured based on the point cloud data and the actual length of the object is small, and both remain within the error range of 3 mm. The experiment verifies the fast, accurate, and stable characteristics of the improved algorithm.

## 1. Introduction

80% of the information that humans understand and explore the world is the visual information obtained by the eyes. With the rapid development of modern computer technology, people have begun to try to make computers have visual functions similar to those of humans, replacing human eyes with cameras, capturing images through cameras, and then using computers to analyze and understand the captured images; the output of advanced visual information helps us to recognize and understand the world faster and better, resulting in the new discipline of computer vision [1].

3D reconstruction technology is one of the important branches of computer vision technology (Figure 1), and it is a popular research field combining computer vision and industrial measurement. Among them, in the fields of rapid design of industrial products, automatic detection and measurement, quality inspection and control, 3D printing, and other fields, the demand for fast, accurate, and convenient acquisition of 3D information on the surface of objects is increasing [2].

At present, structured light technology is the most reliable and effective technology to achieve the three-dimensional reconstruction of the object surface [3]. This technology first projects the structured light coding pattern onto the surface of the target object to be measured through a projector and then uses a camera to shoot the surface of the target object; the camera will capture the structured light image whose coding pattern is deformed due to the shape of the surface of the target object, decode the deformed structured light image, and then calculate the 3D point cloud data of the object surface based on the principle of triangulation so as to realize the three-dimensional reconstruction of the surface of the measured object. With the rapid development of science and technology, various fields hope to achieve the high-precision 3D reconstruction of the surface of high-speed moving objects; in order to achieve the 3D reconstruction of moving objects, only a single image can be used for 3D reconstruction; therefore, 3D reconstruction based on a single image has become an important research direction in the field of structured light technology.



FIGURE 1: 3D reconstruction algorithm.

## 2. Literature Review

Research on the application of the active structured light method in the detection of the three-dimensional topography of objects started in the 1970s. Huang et al. proposed a method for projecting slit structured light to identify polyhedra. With the development of structured light technology, projection modes have also been developed; in particular, the emergence of encoded structured light solves the limitation of additional geometric constraints. Coding structured light can be divided into temporal coding and spatial coding according to different coding methods. The time coding method uses the preprojected image to the surface of the object and then creates the code, so the complete final code pattern cannot be formed until all the patterns are completely projected, and the encoding is closely related to the projection position [4]. Li et al. projected a grayscale-encoded pattern with marked sinusoidal intensities onto the object surface, solving the problem of ambiguity of the projected signal at each different time [5]. Based on the use of  $N$ -ary, Tang et al. proposed a color-based projection scheme and established a reflection model, which contains  $n^m$  fringes in the RGB color space, and the number of fringe projections directly affects the measurement efficiency of the system [6]. In order to reduce the number of streaks, Pan and Zhu developed a hybrid system that can simultaneously fuse temporal and spatial encoding; the system has a fast processing speed and high measurement accuracy and can be applied to dynamic measurement; the projected structured light can be encoded according to the time axis; at the same time, it can also be encoded according to the spatial neighborhood points [7]. Gao et al. proposed a pseudorandom sequence; due to the uniqueness of the window, each different subsequence can find the absolute position in the whole sequence; it is widely used in spatial coding schemes. Spatial encoding can be regarded as a sequence set based on pseudorandom numbers; the encoding pattern is generated by a Hamming window or an  $N$ -dimensional Euler path; the feature positions are determined by observing the line colors stored in the same window [8]. In 1998, Peng et al.

proposed an orthogonal vertical grid color coding, which uses the peak concentration to detect the intersection, and at the same time, it converts the color from the RGB space to the HSI space for encoding, but in the decoding process, due to the different reflection of illuminance, the H channel is sensitive, which leads to new problems [9]. Feng et al. proposed an encoding scheme combining traditional stripes and multislit structured light, which again improved the measurement accuracy [10].

For the 3D reconstruction of a single 2D engineering geometry, the author proposes a new research method, which avoids the ill-conditioned solution problem of traditional methods. Firstly, using the microscope image segmentation algorithm based on the Harris multiscale corner detection, a complex combined graph is separated into several simple primitives, and then each primitive is reconstructed in 3D, which not only reduces the complexity of the reconstruction algorithm but also improves the real-time performance. The improved corner detection algorithm can obtain corners at different scales, thus overcoming the possible corner information loss, the position offset and susceptibility to noise in the Harris corner detection of a single scale, and the extraction of false corners and other problems. Secondly, the relationship between image matching and image corner matching is studied; the algorithm takes the corner as the feature point of the image and uses four indicators, such as the corner value, the number of neighborhood corners, the distance between the corners, and the consistency of parameters; filter the set of corner points step by step; the unmatched corners are effectively eliminated; the matching accuracy is ensured, and at the same time, the heavy calculation of template matching in the traditional algorithm is avoided, and the matching speed is greatly improved.

## 3. Research Methods

### 3.1. Harris Multiscale Corner Detection Principle and Corner Extraction

3.1.1. *The Principle and Limitation of the Classic Harris Corner Detection.* The corner point is an important image



feature point, which contains rich two-dimensional structural information; in the fields of feature-based image registration, shape recognition, and three-dimensional reconstruction, corner point extraction is of great significance. The most representative corner detection algorithm is the Harris corner detection algorithm [11]. The Harris operator is a signal-based corner feature extraction operator proposed by Harris and Stephens; it has the characteristics of simple calculation, uniform and reasonable extraction of corner features, quantitative extraction of feature points, and a stable operator. The processing process of the classic Harris corner detection algorithm is expressed as the following formulas:

$$M = G(\tilde{s}) \otimes \begin{bmatrix} g_x^2 & g_x g_y \\ g_x g_y & g_y^2 \end{bmatrix}, \quad (1)$$

$$R = \det(M) - k \cdot \text{tr}^2(M), \quad k = 0.04,$$

where  $g_x$  and  $g_y$  are the gradients in the  $x$  and  $y$  directions, respectively,  $G(\tilde{s})$  is the Gaussian template,  $\det$  is the determinant of the matrix,  $\text{tr}$  is the straight trace of the matrix,  $k$  is a constant, and  $R$  represents the interest value of the corresponding pixel in the graph. If the interest value of a certain pixel is in the largest neighborhood and is greater than the threshold ( $R_0$ ), the pixel is called a corner, and the corresponding interest value is called a corner value. Although the Harris corner detection is a classic algorithm, it has the following shortcomings. (1) Since corners can only be detected at a single scale, nonmaximum suppression is performed on the corner metric to determine local maxima, and the extraction effect depends on the setting of the threshold. The threshold will lose corner information, and if the threshold is small, false corners will be extracted. Therefore, the lack of scale function makes the positioning accuracy of the algorithm poor, and it may also miss some actual corner points, which are also sensitive to noise. (2) The Harris corner detection uses a Gaussian smoothing function with an adjustable window, but the size of the Gaussian window is not easy to control. If the window is small, many false corners will appear due to the influence of noise. If the window is larger, the position of the corner points will be greatly offset due to the rounded corner effect of the convolution, and the calculation amount will be increased [12]. (3) Smoothing the image with an infinitely smooth Gaussian function will result in the loss of corner information due to oversmoothing.

**3.1.2. Improved Harris Multiscale Corner Detection.** In view of the problems existing in the Harris corner detection algorithm, the idea of multiresolution analysis is introduced into the algorithm so that the Harris algorithm has the characteristics of multiscale detection of corners. This is based on the following principles. In the Harris algorithm,  $g_x$  and  $g_y$  reflect the gray level change direction of each pixel of the image, and if the brightness of pixel  $(x, y)$  changes sufficiently in all directions, it is extracted as a corner [13]. The wavelet  $\Psi_{u,s}(t)$  is a function with a mean of 0, and the wavelet transform of the signal  $g$  is

$$W_g(u, s) = g * \Psi_{u,s}(t) = \int_{-\infty}^{+\infty} g(t) \Psi_{u,s}(t) dt. \quad (2)$$

It measures the variation of the signal within a neighborhood centered on  $u$  and whose length is proportional to  $s$ . And if the wavelet has a first-order or  $n$ -order vanishing moment, the wavelet transform is a multiscale differential operator [14]. Therefore, use the wavelet transform of the image to redefine the gray intensity change formula of the image, that is, the following formula:

$$\begin{aligned} E_{u,y}(x, y) &= S_{2^j}(uW_{2^{j+1}}^1 f + vW_{2^{j+1}}^2 f)^2 \\ &= (S_{2^j} u^2 (W_{2^{j+1}}^1 f)^2 + 2uvW_{2^{j+1}}^1 f W_{2^{j+1}}^2 f + v^2 (W_{2^{j+1}}^2 f)^2) \\ &= Au^2 + 2Cuv + Bv^2 = (u, v) \begin{pmatrix} A & C \\ C & B \end{pmatrix} (u, v)^T. \end{aligned} \quad (3)$$

Among them,  $W_{2^{j+1}}^1 f$  and  $W_{2^{j+1}}^2 f$ , respectively, represent the wavelet transform of the image  $f$  in the  $x$  and  $y$  directions, that is, the following formulas:

$$\begin{aligned} W_{2^{j+1}}^1 f &= S_{2^j}^d f \otimes (G_j, D), \\ W_{2^{j+1}}^2 f &= S_{2^j}^d f \otimes (D, G_j). \end{aligned} \quad (4)$$

And  $S_{2^j}$  represents the smoothing operator, so we have

$$\begin{aligned} A &= S_{2^j}[(W_{2^{j+1}}^1)^2] = (W_{2^{j+1}}^1)^2 \otimes (H_j, H_j), \\ B &= S_{2^j}[(W_{2^{j+1}}^2)^2] = (W_{2^{j+1}}^2)^2 \otimes (H_j, H_j), \\ C &= S_{2^j}[(W_{2^{j+1}}^1 W_{2^{j+1}}^2)] = (W_{2^{j+1}}^1 W_{2^{j+1}}^2) \otimes (H_j, H_j). \end{aligned} \quad (5)$$

$\otimes$  is the convolution operation,  $H$  and  $G$  are the low-pass and high-pass filters, respectively,  $D$  is the Dirac filter, and  $H_j$  and  $G_j$  represent the insertion of  $2^j - 1$  zeros between the filter coefficients of  $H$  and  $G$ , respectively. In this way, the autocorrelation matrix of pixel point  $(x, y)$  at scale  $j + 1$  is obtained as follows:

$$M_2^{j+1} = \begin{pmatrix} A & C \\ C & B \end{pmatrix}. \quad (6)$$

It is worth noting that Equation (3) not only reflects the gray intensity change of each pixel but also reflects the information of the scale space change, which enables corner detection at different scales [15]. At the same time, the central B-spline function with low-pass characteristics is selected as the smoothing function; it can make up for the insufficiency of the Gaussian function window that is difficult to control and oversmooth in the Harris algorithm and enhance the corner detection performance.

Like the Harris algorithm, if the two eigenvalues  $\lambda_1$  and  $\lambda_2$  of the autocorrelation matrix are large enough, the pixel is

detected as a corner point. In order to avoid the eigenvalue decomposition of the matrix  $M_2^{j-1}$ , the corner response function (CRF) under the scale  $s = 2^{j+1}$  is defined as the following formula:

$$C_2^{j+1}(x, y) = \det \left( M_2^{j+1} \right) - k \left( \text{trace} \left( M_2^{j+1} \right) \right)^2. \quad (7)$$

Among them,  $\det \left( M_2^{j+1} \right) = \lambda_1 \lambda_2 = AB - C^2$ ,  $\text{trace} \left( M_2^{j+1} \right) = \lambda_1 + \lambda_2 = A + B$ , and  $k$  is a given constant ranging from 0.04 to 0.06. At this time, the noise is eliminated by setting a threshold value, and nonmaximum value suppression is performed to determine the corner points; that is, the pixel point  $(x, y)$  that satisfies  $C_2^{j+1}(x, y) > T$  is determined as the corner point. The new Harris multiscale corner detection method obtains corner information at multiple scales, reducing the restriction of threshold setting on corner extraction. Usually, the detection operator of small-scale parameters can detect subtle changes in the gray level and reflect more singular point information, but it is more sensitive to noise. The detection operator of large-scale parameters can detect rough changes in the gray level and reflect sharply changing singular points, and it has strong suppression of noise. Therefore, the multiscale Harris corner detection achieves precise localization at small scales and removal of falsehoods and preservation of truth at large scales [16]. After the Harris multiscale corner detection, the author proposes the following “fine-to-coarse” method to accurately screen corners at different scales.

Firstly, for the modulus maximum point  $P_j$  that appears in the  $2^j$  and  $j = 1$  scales, the corner response function  $C_2^j(x_j, y_j)$  is calculated; when its value exceeds the threshold  $T_j$ , this point is extracted as a candidate corner point. Selecting the scales of  $2^j$  and  $j = 1$  is to use the wavelet transform to accurately locate the corners at small scales to determine the position of the corners; therefore, all corners can be included in this step.

Secondly, at the scale of  $2^{j+1}$ , observe whether there is a maximum point in  $C_2^{j+1}(x_j, y_j)$  near the candidate corner point  $P_j$  obtained in the previous step; if it exists, it is determined that the point is a corner point; if not, the point can be eliminated from the candidate corner points.

### 3.1.3. Analysis of the Experimental Results of the Algorithm.

In the experiment, the central B-spline function with low-pass characteristics is selected as the smooth function of the corner detection operator because the function has good approximation ability and compact support and other excellent properties. When the order of the B-spline function tends to infinity, it converges to the Gaussian function, and its derivative converges to the derivative of the Gaussian function. The statistics in Table 1 fully demonstrate the superiority of the improved algorithm in terms of localization, effectiveness, and noise immunity in extracting corners [17].

TABLE 1: Statistics of the number of corner points.

Detector	Exact corner	Missing corner	Pseudocorner
Classic Harris algorithm	40	7	11
Improved algorithm	45	2	3

**3.2. Body Segmentation Algorithm Based on Corner Detection.** The basic idea of the adopted body segmentation algorithm is as follows. The basic geometric primitives in the field of engineering drawing are as follows: cylinder, cuboid, sphere, wedge, cone, etc. If all kinds of basic primitives contained in complex two-dimensional engineering drawings can be detected, it is easy to segment them. The process of detecting the basic primitives from the combined image is actually an image registration process; that is, the images to be separated are sequentially registered with the standard images of the basic shapes. Based on this, the categories and positions of the basic primitives contained in the image to be separated are determined. But there are two deficiencies in the common matching algorithms based on image features. First, the matching accuracy of the algorithm is not high and the stability is not good. Since the matching algorithm only uses a small part of the information of the image, the matching result is easily affected by factors such as noise and image information distribution, and it is highly dependent on the accuracy and stability of the feature points. Second, the matching search speed of feature points still needs to be improved [18]. Most of the matching algorithms use the template correlation method to perform the ergodic matching search; therefore, the algorithm is computationally expensive and slow.

Aiming at the above two shortcomings, the author proposes a new matching algorithm based on corner detection. Firstly, the feature points of the image are extracted by the multiscale Harris operator with less computational complexity and better stability, and the corner sets of the reference image and the image to be matched are obtained, respectively. Then, according to the relationship between the matching of corner sets, the image corners are gradually screened from three aspects: alignment, the number of neighborhood corners, and the distance between corners; due to the instability of the corner detection algorithm and other factors, the image matching is affected, and finally, an accurate and stable matching corner set is obtained [19].

Figure 2 is a graph in which the cylinder is rotated 45 degrees clockwise, and it can also be regarded as a projection graph obtained from different viewing angles for the same three-dimensional entity, which requires the registration algorithm to map them as an entity, and the improved Harris multiscale corner detection algorithm has rotation invariance, translation invariance, and scale invariance, which solves the problem of “many” versus “one” very well [18].

When matching the feature points of two images, choosing an appropriate similarity algorithm can improve the matching efficiency and accuracy. The alignment degree of the corner point pair (CPAM) is defined to determine the

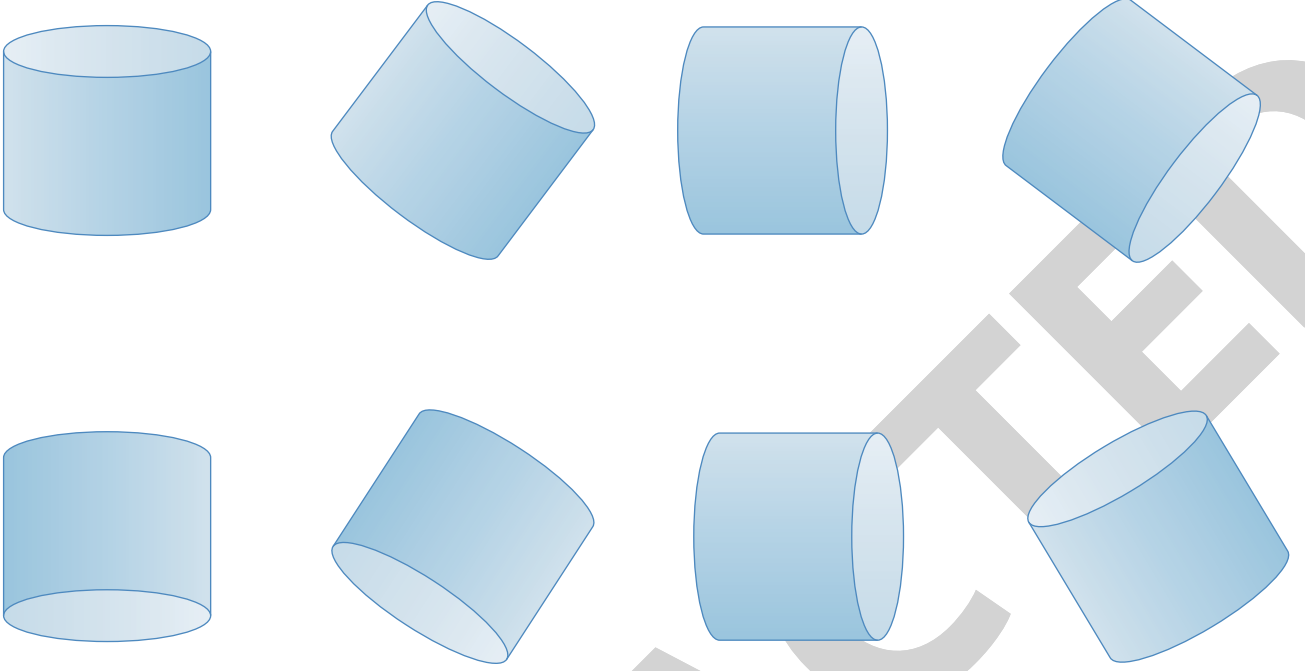


FIGURE 2: The various rotation effects of the cylinder.

matching point pair; that is, on the basis of the corner point and its gradient information extracted by the Harris multi-scale corner point detection algorithm, the approximate rotation angle is obtained according to the angle histogram statistics, the feature submaps centered on the corners are extracted from the two images to be registered, and the alignment of all these feature submaps is calculated.

**3.2.1. Angle Histogram for Corner Point Pairs.** Assuming that there are two images  $f_1(x, y)$  and  $f_2(x, y)$  to be registered, the extracted corner sets are  $P_{f_1} = \{p_i = (p_x^i, p_y^i)\}_{i=1,2,\dots,N}$  and  $P_{f_2} = \{q_j = (q_x^j, q_y^j)\}_{j=1,2,\dots,N}$ , respectively, where  $\theta_{p_1}$  and  $\theta_{q_1}$  are the gradient vector directions of  $p_i$  and  $q_j$ , respectively. Define the angle histogram  $H(\theta)$  of the corner point pair, indicating the number of the corresponding corner point pairs in  $P_{f_1}$  and  $P_{f_2}$  when the angle difference is  $\theta$ . The  $\theta$  value when  $H(\theta)$  takes the maximum value also represents the rotation angle between the images  $f_1(x, y)$  and  $f_2(x, y)$ . In order to improve the accuracy of the algorithm, modify  $H(\theta)$ .

The rotation angle  $\theta$  between images can be estimated by searching for the angle corresponding to the maximum value of  $H(\theta)$ . This method of using statistics to obtain the rotation angle has the advantages of the small amount of calculation and accurate calculation.

**3.2.2. Alignment of Corner Point Pairs.** The alignment of the corner point pair is defined as the following formula:

$$\overline{\text{CPAM}}(p, q, \theta) = \frac{1}{100 \cdot \text{CI}(I_1, I_2) + 1}. \quad (8)$$

In the formula,  $I_1$  and  $I_2$  are the corresponding two feature submaps, and CI is the interaction variance of the two

feature submaps, which reflects the stability of the corresponding gray levels of the two feature submaps. For the corner point  $q_j$  in the image  $f_2(x, y)$  to be registered, its matching corner point  $p$  is determined in the corner point set  $P_{f_1}$  of another image  $f_1(x, y)$  to be registered. If and only if  $p$  and  $q_j$  satisfy the following conditions,  $\{p \leftrightarrow q_j\}$  becomes a candidate matching point pair.

$$\begin{aligned} |\theta_{i,j} - \theta| < 5^\circ, \quad \theta_{i,j} = \theta_p - \theta_{q_j}, \\ \overline{\text{CPAM}}(p, q_j) = \max_{p_i \in P_{f_1}} \overline{\text{CPAM}}(p_i, q_j), \quad (9) \\ \overline{\text{CPAM}}(p, q_j) > T_a, \quad T_a \text{ is the threshold.} \end{aligned}$$

In the formula,  $\theta_p$  represents the gradient direction of the corner point  $P$ , and the threshold ( $T_a$ ) is the mean of the variance of the two feature submaps. Finally, the candidate matching point pairs are linearly weighted to eliminate the wrong matching point pairs, and a subset of matching corner point pairs is initially obtained. It should be noted that the corner points in subsets  $C_1$  and  $C'_1$  whose corner point values are matched do not necessarily correspond one-to-one; that is, the number of corner points contained in  $C_1$  and  $C'_1$  may be different.

**3.2.3. Neighborhood Corner Matching.** If images A and B match, the two matching corners on them should have the same number of corners in the same neighborhood. Therefore, the corner points in  $C_1$  and  $C'_1$  that do not meet this condition are eliminated through the number of neighborhood corner points matching, and new corner point sets  $C_1 = \{c_1, c_2, \dots, c_g\}$  and  $C'_1 = \{c'_1, c'_2, \dots, c'_h\}$  are obtained.

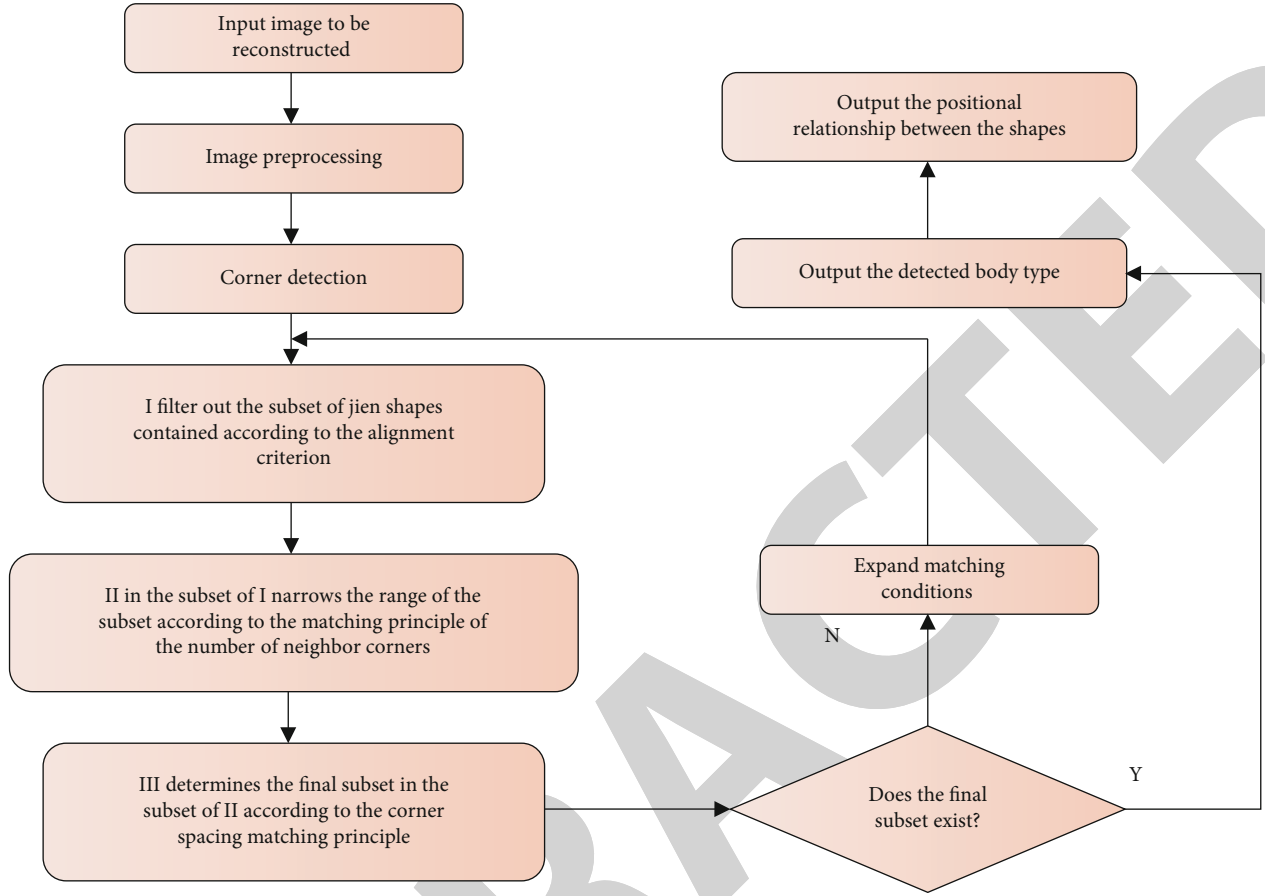


FIGURE 3: Flowchart of the body segmentation algorithm.

Similarly, the number of corner points in  $C_2$  and  $C'_2$  may also be different [20].

**3.2.4. Corner Spacing Match.** If images A and B match, the distances between the corresponding two corner points and the other corresponding corner points in their respective neighborhoods should be the same; therefore, the corner point spacing matching is to further eliminate the corner points in  $C_2$  and  $C'_2$  that do not meet this condition and get new subsets  $C_3$  and  $C'_3$ . The specific operations are as follows. Let  $c_i$  and  $c'_i$  be a pair of corner points that have satisfied the matching of the value of corner points and the matching of the number of neighborhood corner points. Let the number of neighborhood corner points be  $p$ , and the distances from  $c_i$  and  $c'_i$  to the corner points of their neighborhoods are arranged in descending order as  $\{d_1, d_2, \dots, d_p\}$  and  $\{d'_1, d'_2, \dots, d'_p\}$ ; if  $\{d_1, d_2, \dots, d_p\}$  and  $\{d'_1, d'_2, \dots, d'_p\}$  are equal in one-to-one correspondence within the allowable deviation range,  $c_i$  and  $c'_i$  are considered to be matching corners; otherwise, they are not. After the above steps, the number of corner points contained in the two corner point sets ( $C_3$  and  $C'_3$ ) may still be inconsistent. For the convenience of calculation, the “one-to-one correspondence” or “one-to-many correspondence” corners can be

directly eliminated so that  $C_3$  and  $C'_3$  contain the same number of corners, that is,  $C_3 = \{c_1, c_2, \dots, c_f\}$  and  $C'_3 = \{c'_1, c'_2, \dots, c'_f\}$ .

**3.2.5. Body Segmentation Algorithm Flow.** After the above three steps of detection, it is possible to basically determine which basic geometric primitives are included in the two-dimensional graphics to be reconstructed and then determine the positional relationship between the basic geometric shapes included; these relationships are the basis for the BOOL operation on the reconstructed basic shape. The flow of the whole body segmentation algorithm is shown in Figure 3. When the final matching subset does not exist, it is necessary to expand the matching condition to continue the matching search, but the matching condition has a threshold; when the maximum search condition is reached and still no valid subset is obtained, it is considered that the image to be reconstructed does not have any valid subset and contains any of the basic shape classes.

## 4. Analysis of Results

For the combined graph shown in Figure 4(a), it is extremely difficult to reconstruct it directly in 3D, but if it is separated into several basic geometric shapes and then 3D

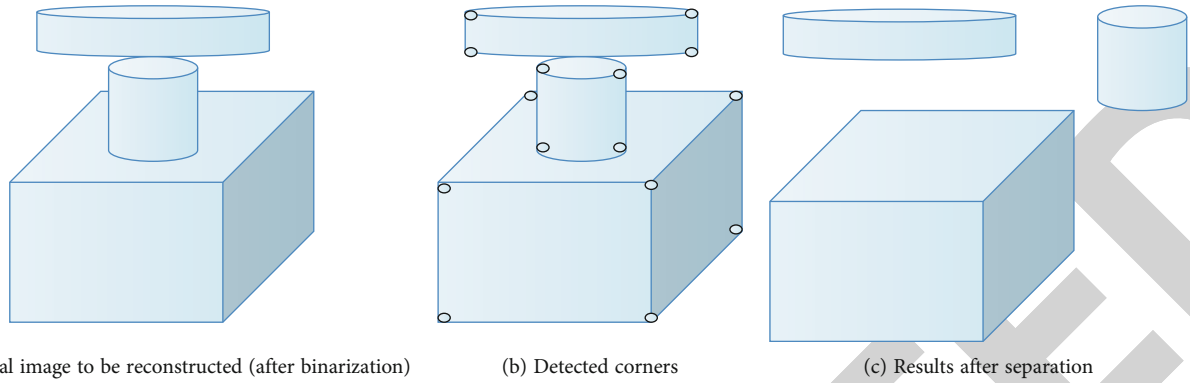


FIGURE 4: 3D reconstruction example.

reconstruction is carried out separately, a complex problem is solved. Figure 4 is an example of a 3D reconstruction. Among them, Figure 4(b) shows the corner points extracted by the Harris multiscale corner point detection algorithm [21]; the extracted corner point sets are sequentially registered with the standard corner point subsets of various basic shapes in order to confirm the basic shape type contained in the 2D image to be reconstructed. Part of the shape may be occluded; as shown in Figure 4(b), a corner of the lower cuboid is covered by the middle cylinder, and sometimes, there will be more interference corners, such as the intersection of the middle cylinder and the two edges of the cuboid; the generated corners, for these cases, require the shape separation algorithm to appropriately relax the conditions when making matching criteria. Figure 4(c) is the result of the shape separation algorithm, which is composed of two cylinders and a cuboid.

Taking the reconstruction of a cuboid as an example to illustrate the 3D reconstruction process of a single basic geometric body, because it is known that the type of the shape is a cuboid, in order to reconstruct its contour information in the three-dimensional space, it is necessary to know the dimensions of the length, width, and height of the cuboid and the coordinates of its centroid [22]. The centroid coordinates are easy to determine. Then, using the calculation result of the corner point histogram in Section 3.2, we can know the rotation angle of the cuboid in the reconstructed image relative to the standard shape, use the rotation angle to correct the cuboid in the image to be reconstructed, and then easily calculate the length, width, and height information according to the distance between the corresponding corner pairs. The rest of the geometry reconstruction process is similar.

The number of reconstructed point clouds proposed by the author is more than 15,000; in addition, as shown in Figure 5, the average error and standard deviation of the three-dimensional point cloud data statistics and the measurement results are compared; the average error and standard error can show that the author's reconstruction algorithm has high accuracy; after reconstruction, the length of the object measured based on the point cloud data and the actual length of the object have a small error, which are kept

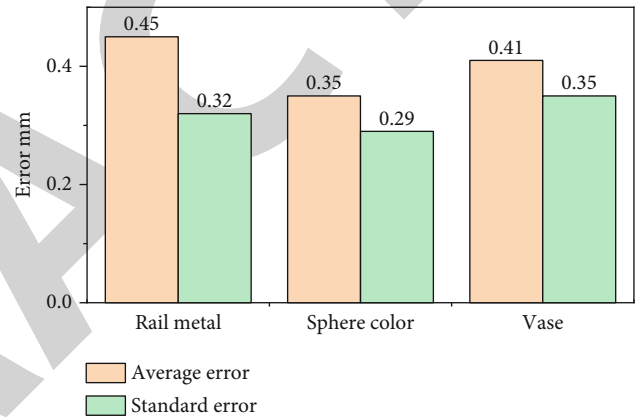


FIGURE 5: Average error and standard deviation of 3D point cloud data statistics and measurement results.

within the error range of 3 mm; through these experimental data, it is fully verified that the algorithm proposed by the author can effectively improve the accuracy of 3D reconstruction [23].

Finally, each reconstructed single shape is drawn in the three-dimensional space through the BOOL operation. The system is based on the VC++ 6.0 development platform through the embedded Open Inventor 3D graphics library for 3D data processing [24].

## 5. Conclusion

3D reconstruction based on a single image is one of the major challenges faced by human beings in basic and applied research, and there are still many difficulties that have not been satisfactorily resolved. The improved algorithm provides a new idea for the 3D reconstruction of engineering drawings, which is to separate the complex composite body into simple basic geometric shapes, then reconstruct them, respectively, and divide the reconstructed basic shapes according to their relative positions; the relationship performs BOOL operations to obtain the geometric entity model in the 3D space. The image registration algorithm

## Retraction

# Retracted: Comparison of Improved Surgical Eight-Step Handwashing Combined with ATP Fluorescence in Detecting the Infection Rate at the Site of Seven-Step Surgical Handwashing and 30-Day Orthopaedic Surgery: A Randomized Study

### Scanning

Received 11 July 2023; Accepted 11 July 2023; Published 12 July 2023

Copyright © 2023 Scanning. This is an open access article distributed under the Creative Commons Attribution License, which permits unrestricted use, distribution, and reproduction in any medium, provided the original work is properly cited.

This article has been retracted by Hindawi following an investigation undertaken by the publisher [1]. This investigation has uncovered evidence of one or more of the following indicators of systematic manipulation of the publication process:

- (1) Discrepancies in scope
- (2) Discrepancies in the description of the research reported
- (3) Discrepancies between the availability of data and the research described
- (4) Inappropriate citations
- (5) Incoherent, meaningless and/or irrelevant content included in the article
- (6) Peer-review manipulation

The presence of these indicators undermines our confidence in the integrity of the article's content and we cannot, therefore, vouch for its reliability. Please note that this notice is intended solely to alert readers that the content of this article is unreliable. We have not investigated whether authors were aware of or involved in the systematic manipulation of the publication process.

Wiley and Hindawi regrets that the usual quality checks did not identify these issues before publication and have since put additional measures in place to safeguard research integrity.

We wish to credit our own Research Integrity and Research Publishing teams and anonymous and named

external researchers and research integrity experts for contributing to this investigation.

The corresponding author, as the representative of all authors, has been given the opportunity to register their agreement or disagreement to this retraction. We have kept a record of any response received.

### References

- [1] X. Chen, T. Wang, Q. Li et al., "Comparison of Improved Surgical Eight-Step Handwashing Combined with ATP Fluorescence in Detecting the Infection Rate at the Site of Seven-Step Surgical Handwashing and 30-Day Orthopaedic Surgery: A Randomized Study," *Scanning*, vol. 2022, Article ID 3123565, 7 pages, 2022.

## Research Article

# Comparison of Improved Surgical Eight-Step Handwashing Combined with ATP Fluorescence in Detecting the Infection Rate at the Site of Seven-Step Surgical Handwashing and 30-Day Orthopaedic Surgery: A Randomized Study

Xiong Chen <sup>1</sup>, Tao Wang <sup>2</sup>, Qinglian Li <sup>1</sup>, Lixia Cheng <sup>3</sup>, Zhimin Xie <sup>3</sup>, Jianping Xu <sup>3</sup>, and Dejian Yang <sup>1</sup>

<sup>1</sup>Department of Operating Room, Xianyou County General Hospital, Putian 351200, China

<sup>2</sup>Department of Orthopedics, Beijing Jishuitan Hospital, Beijing 100035, China

<sup>3</sup>Department of Orthopedics, Putian Medical District, The 900th Hospital of Joint Logistic Support Force, PLA, Putian 351100, China

Correspondence should be addressed to Dejian Yang; 11233318@stu.wxlc.edu.cn

Received 26 May 2022; Revised 1 July 2022; Accepted 8 July 2022; Published 19 July 2022

Academic Editor: Balakrishnan Nagaraj

Copyright © 2022 Xiong Chen et al. This is an open access article distributed under the Creative Commons Attribution License, which permits unrestricted use, distribution, and reproduction in any medium, provided the original work is properly cited.

**Context.** Surgical site infection prolongs hospital stay and is one of the main causes of incidence rate and a source of high medical expenses. There are few clinical studies comparing the risk of infection in orthopaedic surgery after different washing methods. **Objectives.** To compare the effects of two hand cleaning schemes on the prevention of surgical site infection in routine orthopaedic surgery. Compared with the standard surgical seven-step washing technique and detected by ATP fluorescence method, the handwashing effects of the improved surgical eight-step washing technique and the standard surgical seven-step washing technique were compared, so as to provide a basis for eliminating the handwashing blind area of the surgical seven step washing technique and improving the surgical handwashing method. **Methods.** A total of 800 consecutive patients who underwent clean and clean-contaminated orthopaedic surgery between January 1, 2020 and December 31, 2020. Twenty orthopaedic doctors in the operating room of our research team were randomly divided into the improved eight-step washing technique group (improved group) and the traditional seven-step washing technique group (traditional group), with 10 people in each group. Each person was randomly sampled 40 times, 400 people in each group, a total of 800 people, and completed by stages in 12 months. **Main Outcome Measures.** The infection rate of surgical site 30 days after operation was the primary end point. The qualified rate of fingertip culture was combined with ATP fluorescence in the two groups and three new culture areas in the two groups: the lateral edge of the palm, the medial edge of the palm, and the nail groove of the middle finger and the nail root were secondary end points. **Results.** The 2 protocols were comparable in regard to surgical site infection risk factors. The infection rate of surgical site in the traditional group was 10 cases (2.50%) in 400 cases and 0 cases (0%) in the improved group. Three culture areas were added: the qualified rate of lateral edge of palm, medial edge of palm, and nail groove and nail root of middle finger, and the nosocomial infection rate of surgical incision between the two groups was statistically significant ( $P < 0.05$ ). There was no significant difference in the qualified rate of fingertip culture ( $P > 0.05$ ). The handwashing scheme in this study meets the recommended duration of hand disinfection and has good tolerance, and the skin dryness and skin irritation after using aqueous solution are similar. **Conclusions.** The improved surgical eight-step washing technique combined with ATP fluorescence detection is helpful to eliminate the “blind area” of handwashing. It is also necessary to add three training areas. Handwashing and training are more scientific, rigorous, and effective. They are effective in reducing orthopaedic surgical infection and have application value. They can safely replace the traditional surgical seven-step washing technique, which is worthy of clinical promotion.

## 1. Background

Due to China's large population, limited medical resources, large-scale medical institutions, dense patients, and heavy workload of medical staff, medical staff often ignore hand hygiene, resulting in pollution and hospital infection; Hand is an important way to spread the sense of hospital. Surgical site infection prolongs hospital stay, is one of the main causes of incidence rate, and is also the source of high medical expenses [1]. Hand hygiene is the simplest, most direct, and effective measure to prevent nosocomial infection, and it is also one of the most important tasks in nosocomial infection management [2, 3]. Few clinical studies have compared the risk of infection in orthopaedic surgery after different cleaning methods. Orthopaedic surgery has more open fractures, and the incision is polluted incision, which is more prone to infection, because most of them have built-in objects, and orthopaedic doctors' fingers are more prone to occupational exposure, especially the fingertips of index fingers and nail grooves are easily pierced by Kirschner wire tips, broken ends of bones, and other accidents, resulting in occupational exposure. The nosocomial infection rate of surgical incision is high. Therefore, orthopaedic doctors have higher requirements for handwashing. Handwashing is the most economical and effective means of prevention and control. The standard surgical seven-step washing technique is improved compared with the previous six-step washing technique, and the technology has become mature, but there are still "blind areas" where the cleaning is not in place. It is more necessary to sample and cultivate the "blind areas" after handwashing, and there is a lack of relatively objective evaluation criteria for washing to 10 cm above the elbow and applying disinfectant to 6 cm above the elbow. The current standard surgical seven-step washing technique has three handwashing blind areas and training blind areas. The seven-step washing technique lacks relatively objective evaluation criteria to wash hands to 10 cm above the elbow and apply disinfectant to 6 cm above the elbow, which needs to be further improved.

## 2. Introduction

In this study, three handwashing blind areas and training blind areas existed in the standard surgical seven-step washing technique were improved. While using the standard fingertip sampling culture, the sampling culture of handwashing blind areas was increased. The qualified rate of handwashing and the nosocomial infection rate of orthopaedic surgical incision were compared between the two groups.

## 3. Data and Methods

**3.1. Clinical Data.** From January to December 2020, the handwashing environment and other conditions were the same. 20 orthopaedic doctors in the operating room environment were selected and randomly divided into the improved group and the traditional group, with 10 people in each group. Each person was randomly sampled 40 times, with 400 people in each group, a total of 800 people. They

were completed in stages in 12 months. Combined with ATP fluorescence method, the qualified rates of three new culture areas in the two groups: the lateral edge of the palm, the medial edge of the palm, and the nail groove and nail root of the middle finger, were detected and compared, and the qualified rates of fingertip culture and the nosocomial infection rate of the incision after operation were compared between the two groups. The sampling work was completed by the members of this study in stages.

### 3.2. Research Method

**3.2.1. Handwashing Method.** ① The traditional group used standard surgical seven-step washing to wash hands. ② The improved group used the improved surgical eight-step washing technique and washed the arm for the first time: washing hands to 5 horizontal fingers on the elbow was the objective standard. Wash your arms for the second time: wash your hands to 4 horizontal fingers on the elbow as the objective standard, and apply disinfectant to 3 horizontal fingers on the index finger, middle finger, and ring finger as the objective standard. The first seven steps are the same as above. Step 8: similar to step 6, close your fingers together and put them on the other hand. There are three blind areas: the outer edge of the palm, the inner edge of the palm, and the nail groove and the nail root, which are carried out alternately.

**3.2.2. Sampling Method.** Before and after handwashing, each subject took 4 samples from four culture areas, including conventional fingertips, and three new culture areas: the outer edge of the palm, the inner edge of the palm, and the nail groove of the middle finger and the root of the nail. Spin and smear the cotton swab of the bacterial culture tube at the above four sampling places twice and submit it for inspection; biological detection method: take the samples stored in PBS and shake them sufficiently to make the microorganisms on the cotton swab dissolve in PBS as much as possible. After the Petri dish is numbered, add 0.5 ml of the sample into the Petri dish, spread it evenly with a sterile l rod, and make 3 copies of each sample. After all smearing and culture, put it into 37°C incubator for 72 hours. Record the number of growing colonies and calculate the average value as the test result. The control adopts PBS solution control and empty Petri dish control. The positive control of *Escherichia coli* is added to the Petri dish. It is cultured at 37°C for 72 hours with the sample for observation and detected by ATP fluorescence method. Observe and record the results of finger improved surgical eight-step handwashing combined with ATP fluorescence detection and bacterial culture+drug sensitivity test after surgical washing manipulation.

**3.2.3. Interventions.** Calculation formula of biological monitoring quantity is as follows: total bacteria (CFU/cm<sup>2</sup>) = plate colony × dilution multiple/sampling area (cm<sup>2</sup>). The ATP fluorescence test of the operator is negative, and the bacterial culture ≤ 5 CFU/cm<sup>2</sup> is qualified. The infection rate of the operation site was calculated when the patient had no infection at the operation site within 30 days after the



operation, which was negative and positive. 30 days after operation, the infection rate of operation site in the two groups was the primary end point. The qualified rate of fingertip culture in the two groups and three new culture areas in the two groups: the lateral edge of the palm, the medial edge of the palm, and the nail groove of the middle finger and the nail root were detected by ATP fluorescence method. The qualified rate of culture after operation was the secondary end point. The SPSS23.0 statistical software was used for data analysis. The normal measurement data is expressed by "mean  $\pm$  SD," and the counting data is expressed by the number of cases or percentage.

## 4. Result

**4.1. Bioassay Results before and after Handwashing.** Before handwashing, the number of bacteria in the hands of orthopaedic doctors in the traditional group was 29.32~593.32 CFU/cm<sup>2</sup> respectively, and the detection result of ATP fluorescence method was positive. Before handwashing, the number of bacteria in the hands of orthopaedic doctors in the improved group was 28.32~596.32 CFU/cm<sup>2</sup>, respectively, and the detection result of ATP fluorescence method was positive. The hand hygiene of the two groups before handwashing was similar. After handwashing, the total number of bacteria in the hands of orthopaedic doctors in the traditional group is 1.32~62.67 CFU/cm<sup>2</sup>, respectively, which indicates that careful handwashing with flowing water and hand sanitizer can significantly reduce the amount of bacteria in the hands, and as long as they are cleaned according to the normal operation, they can basically meet the hygienic standard. In the improved group, the total number of bacteria in the hands of orthopaedic doctors was 1.32~32.67 CFU/cm<sup>2</sup>, respectively, indicating that the amount of bacteria in the hands can be greatly reduced by carefully washing hands with improved step washing method with flowing water and hand sanitizer, and the hygienic standard can be reached as long as they are cleaned according to the normal operation. The infection rate between the two groups was statistically significant.

**4.2. Pass Rate after Handwashing.** From January 2020 to December 2020, according to the biological monitoring results after handwashing by orthopaedic doctors, the qualified rate of conventional fingertips, lateral edge of palm, medial edge of palm and nail groove and nail root of middle finger were 97%, 91%, 90% and 92%, respectively. In the improved group, the qualified rates of conventional fingertip, lateral edge of palm, medial edge of palm, and nail groove and root of middle finger were 98%, 97%, 98%, and 99%, respectively. There was no significant difference in the qualified rate of fingertip samples between the two groups ( $P > 0.05$ ). There were significant differences in the samples of the lateral edge of the palm, the medial edge of the palm, and the nail groove of the middle finger and the nail root ( $P < 0.05$ ) (Table 1).

**4.3. Biological Monitoring Results after Handwashing.** After 800 orthopaedic doctors washed their hands, the number

of samples in the traditional group was 400, and the incision infection rate was 2.5%. The number of samples in the improved group was 400, and the incision infection rate was 0%. The difference was statistically significant ( $P < 0.05$ ) (Table 2).

See Table 1 for the comparison of the qualified rate of handwashing between the two groups.

See Table 2 for the comparison of infection rate of handwashing surgical incision between the two groups.

## 5. Discussion

In the 19th century, Semmelweis first noted the link between hospital-acquired diseases and hand hygiene [4]. Nosocomial infection places a heavy burden on patients and health care providers and economically affects health care institutions [5]. Hand is the main carrier of transmitting bacteria, viruses, and microorganisms. Bacteria carried by surgeons' hands or arms are the culprit of surgical incision infection and one of the most important factors. Surgical cleaning and surgical handwashing disinfection are effective methods to prevent handwashing. Hospital surgical wound infection is an important measure to prevent infection. Hand hygiene has always been an important part of perioperative practice. Effective handwashing is one of the most simple and easy means, an important measure to prevent exogenous hospital feeling, and an effective means of two-way protection between patients and medical staff. The sense of hospital has brought great economic impact to medical institutions. However, studies [6] have proved that the audit cycle can improve the efficiency of surgical handwashing. Among all tested compounds, the local skin microflora was significantly lower than that before scrubbing at two time points after scrubbing and operation [7]. Research [8] shows that handwashing feedback video monitoring is an effective tool to measure hand hygiene and improve compliance. Surgical site infection (SSI) remains a major problem for patients and medical systems. Paying attention to nursing and standardized quality measures continue to promote the improvement of surgical sterility, but there are still some disputes in the field of surgical hand disinfection [9]. It has been reported [10, 11] that the preoperative surgical hand disinfection scheme of hand is related to surgical wound infection (SSI). Preoperative handwashing is essential to prevent surgical site infection (SSI) [12]. Careful surgical scrubbing can reduce the number of bacteria on the skin, but it cannot completely eliminate bacteria. There are temporary microorganisms left on the hands after surgery. Studies [13] have proved that two-layer wound closure during surgical handwashing is not only an effective barrier to prevent microbial transmission, but also an effective barrier to protect surgeons. Handwashing is a necessary measure to prevent nosocomial infection [14]. Studies [15–17] have shown that effective hand hygiene, such as effective handwashing and hand disinfection, is the basis for slowing down the spread of COVID-19. The novel coronavirus pneumonia is being studied and popularized by studying the [18] medical staff's handwashing and hand disinfection. After hand disinfection, nails coated with conditioner or mixed varnish

TABLE 1: Comparison of qualified rate of 4 samples of handwashing between two groups.

Group	Fingertip sample		Sample of lateral margin of palm		Sample of medial margin of palm		Nail groove and nail root samples of middle finger	
	Number of samples	Qualified rate (%)	Number of samples	Qualified rate (%)	Number of samples	Qualified rate (%)	Number of samples	Qualified rate (%)
Improvement group	400	98	400	97	400	98	400	99
Traditional group	400	97	400	91	400	90	400	92
$\chi^2$		0.410		6.383		11.348		11.402
P		>0.05		<0.05		<0.05		<0.05

TABLE 2: Comparison of incision infection rate between two groups.

Group	Number of samples	Incision infection rate (%)
Improvement group	400	0
Traditional group	400	2.5
$\chi^2$	5.063	
$P$	<0.05	

have a similar risk of pathogenic microorganisms as natural nails. Lasting regular nail polish will increase the risk of hand disinfection ineffective [19]. Clinical application of handwashing brush although the skin is common all over the world, the feeling, appearance, and integrity of the skin are obvious. It even causes serious damage. Pittet et al. [20] confirmed that after the pathogen is discharged from the infection source, it needs five consecutive steps to colonize or infect the new host. The seven-step washing technique includes the outer edge of the palm, the inner edge of the palm, and the nail groove of the middle finger and the root of the nail. There are “blind areas” in the seven-step washing technique. There are many wrinkled skin, and it is relatively difficult to clean and disinfect. Young medical personnel, especially interns, are mostly limited to textbooks, and their handwashing is easy to miss or insufficient, resulting in infection at the surgical site. ATP bioluminescence is a sensitive and rapid method for evaluating the quality of end cleaning. We emphasize the value of using quantitative methods to monitor the cleanliness of hospital environment [21]. Studies have shown that ATP biological fluorescence method has a certain correlation with the traditional bacterial culture method, can better reflect the cleaning status of hands, can help measure the sanitary quality of hospital surface, and can be used as a useful agent of microbial pollution [22]. By providing rapid feedback, ATP analysis helps to raise the awareness of operators and allows immediate action in case of emergency [23]. The research shows that ATP biological fluorescence detection method can provide an objective and real-time analysis method and effectively reduce the nosocomial infection rate [24–27]. After the application of ATP biological fluorescence on-site monitoring method, the hand hygiene compliance of all kinds of personnel in the operating room is higher than that before the application, and the qualified rate of hand hygiene is higher than that before the application, indicating that the hand hygiene compliance and qualified times of all kinds of personnel can be improved. Through regular on-site random sampling inspection, strengthen supervision and ensure the safety of patients and personnel. At the same time, formulate scientific, simple, and fast on-site hand hygiene monitoring standards, reduce the monitoring cost, eliminate the occurrence of nosocomial infection caused by poor hand disinfection effect, and improve the quality and image of medical services, which is expected to provide reference basis for on-site standardized management of hand hygiene. However, there is still a certain infection rate of surgical incision

after rubbing and washing hands, especially in patients with orthopaedic surgery, surgical treatment, large incision surgery, long operation time, large intraoperative bleeding, and so on. It is easy to be infected and affect the treatment effect of infection in patients undergoing orthopaedic surgery. In serious cases, it will endanger the life of patients. Orthopaedic surgery has more open fractures, and the incision is polluted incision, which is more prone to infection, because most of them have built-in objects, and orthopaedic doctors’ fingers are more prone to occupational exposure, especially the fingertips of index fingers and nail grooves are easily pierced by Kirschner wire tips, broken ends of bones, and other accidents, resulting in occupational exposure. The nosocomial infection rate of surgical incision is high. Therefore, orthopaedic doctors have higher requirements for handwashing.

This study focuses on orthopaedics with higher risk of implant infection, which requires higher and more rigorous surgical procedures. If it can reduce the infection of orthopaedic surgery, the improved eight-step washing technique is suitable for preoperative handwashing in orthopaedics and other surgeries with built-in objects, and it is also more suitable for preoperative handwashing in other surgeries. ATP fluorescence method and traditional bacterial culture method are effective and scientific. ATP fluorescence method is simpler than traditional bacterial culture method.

Therefore, this study selected a group of orthopaedic doctors as the research object. It was found that the two handwashing methods were handwashing and sampling according to the requirements of disinfection technical specifications. There was no significant difference in the qualified rate of fingertip samples ( $P > 0.05$ ). It shows that the disinfection of fingertips by standard seven-step washing technique is qualified. However, there were three new culture areas: the lateral edge of the palm, the medial edge of the palm, and the nail groove and nail root of the middle finger. The difference of the infection rate of the surgical incision was statistically significant. The difference was statistically significant ( $P < 0.05$ ). It shows that the seven-step washing technique has a “blind area.” The improved surgical eight-step washing technique combined with ATP fluorescence detection is helpful to eliminate the “blind area” of handwashing. It is also necessary to add three training areas. Handwashing and training are more scientific, rigorous, and effective. They are effective in reducing orthopaedic surgical infection and have application value. They are worthy of preoperative handwashing with built-in devices in clinical orthopaedics and are also more suitable for preoperative handwashing in other surgeries. In addition, orthopaedic doctors wear double gloves to prevent occupational exposure caused by accidental puncture of Kirschner wire tip and broken bone end, which is also worthy of promotion. Novel coronavirus pneumonia, which is now safe, more scientific, more rigorous, and effective, is also worth promoting in the new crown pneumonia epidemic. It can reduce cross infection, protect the patients who are fighting the epidemic, and protect the people in the isolated area. The eight-step washing technique is also worth promoting in the COVID-19.

## Data Availability

The data used to support the findings of this study are available from the corresponding author upon request.

## Conflicts of Interest

The authors declare that they have no conflicts of interest.

## Authors' Contributions

Xiong Chen and Tao Wang contributed equally to this work and should be considered co-first authors.

## Acknowledgments

This study was supported by the Fujian Putian Science and Technology Plan Project (2021SXY001).

## References

- [1] J. J. Parienti, P. Thibon, R. Heller et al., "Hand-rubbing with an aqueous alcoholic solution vs traditional surgical hand-scrubbing and 30-day surgical site infection rates: a randomized equivalence study," *Journal of the American Medical Association*, vol. 288, no. 6, pp. 722–727, 2002.
- [2] B. Simmons, J. Bryant, K. Neiman, L. Spencer, and K. Arheart, "The role of handwashing in prevention of endemic intensive care unit infections," *Infection Control and Hospital Epidemiology*, vol. 11, no. 11, pp. 589–594, 1990.
- [3] Geneva, WHO, "WHO guidelines on hand hygiene in health care: first global patient safety challenge clean care is safer care. Geneva: World Health," *Organization*, 2009, <https://pubmed.ncbi.nlm.nih.gov/23805438/>.
- [4] N. Kadar, "Rediscovering Ignaz Philipp Semmelweis (1818–1865)," *American Journal of Obstetrics and Gynecology*, vol. 220, no. 1, pp. 26–39, 2019.
- [5] E. Tchouaket Nguemeleu, S. Boivin, S. Robins et al., "Development and validation of a time and motion guide to assess the costs of prevention and control interventions for nosocomial infections: a Delphi method among experts," *PLoS One*, vol. 15, no. 11, p. e0242212, 2020.
- [6] R. Mukherjee, P. Roy, and M. Parik, "Achieving perfect hand washing: an audit cycle with surgical internees," *Indian Journal of Surgery*, vol. 83, no. 5, pp. 1166–1172, 2021.
- [7] H. E. Eitzen, M. A. Ritter, M. L. French, and T. J. Gioe, "A microbiological in-use comparison of surgical hand-washing agents," *The Journal of Bone and Joint Surgery. American Volume*, vol. 61, no. 3, pp. 403–406, 1979.
- [8] A. Khan and S. Nausheen, "Compliance of surgical hand washing before surgery: role of remote video surveillance," *The Journal of the Pakistan Medical Association*, vol. 67, no. 1, pp. 92–96, 2017.
- [9] B. S. Oriel and K. M. Itani, "Surgical hand antisepsis and surgical site infections," *Surgical Infections*, vol. 17, no. 6, pp. 632–644, 2016.
- [10] J. Tanner, J. C. Dumville, G. Norman, and M. Fortnam, "Surgical hand antisepsis to reduce surgical site infection," *Cochrane Database of Systematic Reviews*, vol. 1, no. 1, 2016.
- [11] S. Pirie, "Hand washing and surgical hand antisepsis," *Journal of Perioperative Practice*, vol. 20, no. 5, pp. 169–172, 2010.
- [12] Y. H. Ho, Y. C. Wang, E. W. Loh, and K. W. Tam, "Antiseptic efficacies of waterless hand rub, chlorhexidine scrub, and povidone-iodine scrub in surgical settings: a meta-analysis of randomized controlled trials," *The Journal of Hospital Infection*, vol. 101, no. 4, pp. 370–379, 2019.
- [13] C. Yoon, H. S. Gong, J. S. Park, H. S. Seok, J. W. Park, and G. H. Baek, "Wound sealing before surgical hand washing for surgeons with a minor cut injury on the hand," *Surgical Infections*, vol. 20, no. 5, pp. 390–394, 2019.
- [14] M. V. Launay-Savary and K. Slim, "Le lavage chirurgical des mains. Surgical hand washing," *Journal De Chirurgie (Paris. 1908)*, vol. 139, no. 2, pp. 85–87, 2002.
- [15] M. A. Johansson, T. M. Quandelacy, S. Kada et al., "SARS-CoV-2 transmission from people without COVID-19 symptoms," *JAMA Network Open*, vol. 4, no. 1, p. e2035057, 2021.
- [16] Z. Wang, Y. Fu, Z. Guo et al., "Transmission and prevention of SARS-CoV-2," *Biochemical Society Transactions*, vol. 48, no. 5, pp. 2307–2316, 2020.
- [17] G. Kampf, Y. Brüggemann, H. E. J. Kaba et al., "Potential sources, modes of transmission and effectiveness of prevention measures against SARS-CoV-2," *Journal of Hospital Infection*, vol. 106, no. 4, pp. 678–697, 2020.
- [18] X. N. Yuan, Q. Y. Meng, N. Shen et al., "Detection and evaluation of SARS-CoV-2 nucleic acid contamination in corona virus disease 19 ward surroundings and the surface of medical staff's protective equipment," *Beijing Da Xue Xue Bao. Yi xue Ban= Journal of Peking University. Health Sciences*, vol. 52, no. 5, pp. 803–808, 2020.
- [19] M. Walaszek, W. Kwapniewska, B. Jagiencarz-Starzec et al., "Effectiveness of hand disinfection depending on the type of nail plate coating - a study among nurses working in a specialist hospital," *Medycyna Pracy*, vol. 72, no. 1, pp. 29–37, 2021.
- [20] D. Pittet, B. Allegranzi, H. Sax et al., "Evidence-based model for hand transmission in patient care and the role of improved practices," *The Lancet Infectious Diseases*, vol. 7, no. 5, pp. 304–305, 2007.
- [21] Y. S. Huang, Y. C. Chen, M. L. Chen et al., "Comparing visual inspection, aerobic colony counts, and adenosine triphosphate bioluminescence assay for evaluating surface cleanliness at a medical center," *American journal of Infection Control*, vol. 43, no. 8, pp. 882–886, 2015.
- [22] E. Amodio, L. Cannova, M. R. Villafrate, A. M. Merendino, L. Aprea, and G. Calamusa, "Analytical performance issues: comparison of ATP bioluminescence and aerobic bacterial count for evaluating surface cleanliness in an Italian hospital," *Journal of occupational and Environmental Hygiene*, vol. 11, no. 2, pp. D23–D27, 2014.
- [23] T. Sanna, L. Dallolio, A. Raggi et al., "ATP bioluminescence assay for evaluating cleaning practices in operating theatres: applicability and limitations," *BMC Infectious Diseases*, vol. 18, no. 1, p. 583, 2018.
- [24] L. Paciello, F. C. Falco, C. Landi, and P. Parascandola, "Strengths and weaknesses in the determination of *Saccharomyces cerevisiae* cell viability by ATP-based bioluminescence assay," *Enzyme and Microbial Technology*, vol. 52, no. 3, pp. 157–162, 2013.
- [25] M. C. Chan, T. Y. Lin, Y. H. Chiu et al., "Applying ATP bioluminescence to design and evaluate a successful new intensive care unit cleaning programme," *Journal of Hospital Infection*, vol. 90, no. 4, pp. 344–346, 2015.

## Retraction

# Retracted: Identification of Sports Athletes' High-Strength Sports Injuries Based on NMR

### Scanning

Received 11 July 2023; Accepted 11 July 2023; Published 12 July 2023

Copyright © 2023 Scanning. This is an open access article distributed under the Creative Commons Attribution License, which permits unrestricted use, distribution, and reproduction in any medium, provided the original work is properly cited.

This article has been retracted by Hindawi following an investigation undertaken by the publisher [1]. This investigation has uncovered evidence of one or more of the following indicators of systematic manipulation of the publication process:

- (1) Discrepancies in scope
- (2) Discrepancies in the description of the research reported
- (3) Discrepancies between the availability of data and the research described
- (4) Inappropriate citations
- (5) Incoherent, meaningless and/or irrelevant content included in the article
- (6) Peer-review manipulation

The presence of these indicators undermines our confidence in the integrity of the article's content and we cannot, therefore, vouch for its reliability. Please note that this notice is intended solely to alert readers that the content of this article is unreliable. We have not investigated whether authors were aware of or involved in the systematic manipulation of the publication process.

In addition, our investigation has also shown that one or more of the following human-subject reporting requirements has not been met in this article: ethical approval by an Institutional Review Board (IRB) committee or equivalent, patient/participant consent to participate, and/or agreement to publish patient/participant details (where relevant).

Wiley and Hindawi regrets that the usual quality checks did not identify these issues before publication and have since put additional measures in place to safeguard research integrity.

We wish to credit our own Research Integrity and Research Publishing teams and anonymous and named external researchers and research integrity experts for contributing to this investigation.

The corresponding author, as the representative of all authors, has been given the opportunity to register their agreement or disagreement to this retraction. We have kept a record of any response received.

### References

- [1] W. Zhou and H. Chu, "Identification of Sports Athletes' High-Strength Sports Injuries Based on NMR," *Scanning*, vol. 2022, Article ID 1016628, 7 pages, 2022.

## Research Article

# Identification of Sports Athletes' High-Strength Sports Injuries Based on NMR

Wenyong Zhou  and Huan Chu 

Jiangxi Institute of Fashion Technology, Nanchang, Jiangxi 330201, China

Correspondence should be addressed to Wenyong Zhou; 31115317@njau.edu.cn

Received 1 June 2022; Revised 24 June 2022; Accepted 1 July 2022; Published 15 July 2022

Academic Editor: Balakrishnan Nagaraj

Copyright © 2022 Wenyong Zhou and Huan Chu. This is an open access article distributed under the Creative Commons Attribution License, which permits unrestricted use, distribution, and reproduction in any medium, provided the original work is properly cited.

In order to study the high-strength sports injury in sports, this paper proposes a method based on NMR to identify the high-strength sports injury of sports athletes. This method carries out a questionnaire survey and research on the athletes who are excellent in sports dance major from 2019 to 2021 in the Institute of Physical Education. The athletes' age range is 18-25 years, and the training period of sports dance is 3-5 years. The results show that compared with other recognition methods, the recognition method based on NMR has higher accuracy and efficiency. The method of this study is helpful to improve the recognition efficiency and accuracy. Athletes are very easy to get injured during sports. In order to reduce the degree of injury of athletes, we should strictly follow the action standards in the training process to avoid serious injury.

## 1. Introduction

Any injury occurring in the course of sports training is closely related to the sports and the technical characteristics of the sports. For example, sports dance events require athletes to do a lot of somersaults, jumps, supports, and other actions, which is easy to cause sports injuries to the waist, shoulders, and wrists of sports dance athletes [1]. Tennis players and javelin throwers are prone to "tennis elbow." The main causes of injury are improper training methods, poor physical fitness, wrong technical movements, athletes' lack of self-protection awareness, lack of attention to warm-up activities, accumulation of body fatigue, inappropriate environment, and unfavorable training and competition organization [2]. Sports injury can be divided into acute sports injury and chronic injury (Figure 1). Acute sports injury can be caused by external factors, such as fierce physical confrontation with other athletes, or by their own factors. Muscle strain and ligament strain are common in training. Acute sports injury can be distinguished as follows according to the specific location of the injury: (1) skin damage, (2) muscle injury, (3) joint injury, (4) nerve injury, etc.,

or classified according to the type of injury, such as strain, dislocation, and fracture. Chronic sports injury may be caused by local overburden, accumulation of repeated minor injuries, and failure to deal with acute injuries in time or improper treatment methods. The characteristics of chronic injury are slow onset, gradual deepening of symptoms, and long recovery time, such as fatigue periostitis and patella strain [3].

Khodov et al. pointed out that sports dance competition and training cause more injuries, mainly soft tissue injuries. The knee, ankle, waist, back, and shoulder are easy to be pulled, and the toe is easy to be abraded and bruised. Secondly, the injuries of ligaments, muscle bonds, muscles, and joint capsules were mostly soft injuries. Chronic strain, repeated accumulation of minor injuries, and failure to heal major injuries may cause chronic injuries to sports dancers [4]. Novakovic et al. pointed out that the psychological causes of sports injury mainly include anxiety, stress response, personality characteristics, motivation, life events, psychological preparation, and psychological fatigue. Intervention measures mainly include guiding athletes' correct attribution, setting feasible rehabilitation goals, mastering psychological coping skills, and problem oriented analysis

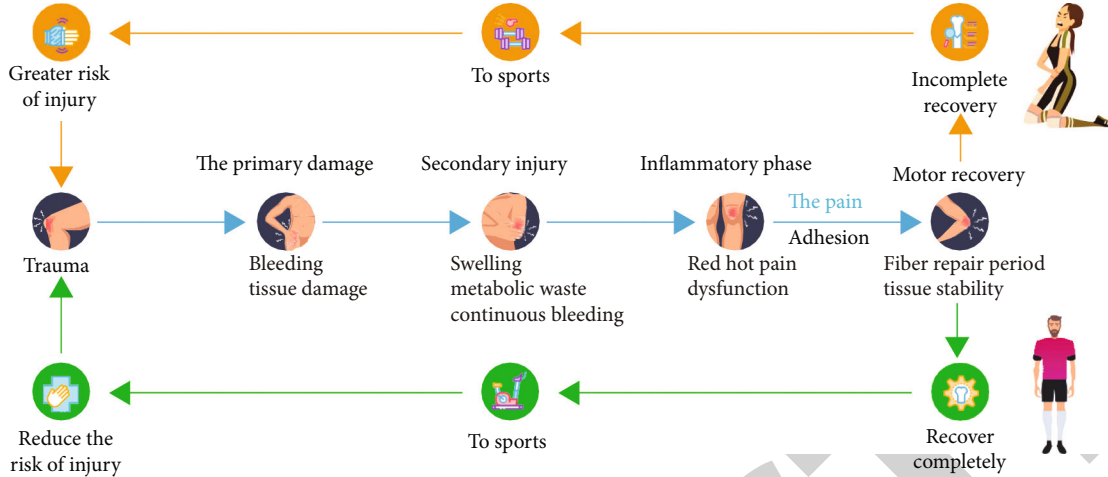


FIGURE 1: Sports injury.

[5]. Gkoura et al. started with the mechanism analysis of sports injury; focused on the circular relationship between muscle balance, abnormal posture, and movement mode and injury; and analyzed and pointed out the key factors of posture and movement mode, as well as the role of rehabilitation functional exercise on human motion system and the basic principle of injury rehabilitation. Then, it puts forward the process of injury rehabilitation functional exercise from the aspects of posture, movement, and muscle balance assessment, mainly including assessment process and detail requirements, targeted muscle tension and muscle weakness treatment methods and processes, proprioceptive training, and integration training points [6]. Siudem et al. pointed out that the hot spots of sports injury research mainly focus on four categories: sports related concussion, anterior cruciate ligament injury, joint instability, and overuse injury; and each research is closely focused on the mechanism of sports injury, injury prevention, treatment, rehabilitation, and rehabilitation standards that can return to the field [7]. Derman et al. proposed a recognition method based on linear discrimination and ultrasonic image features. This method has good recognition efficiency, but its recognition accuracy is relatively low [8]. Wang and Li proposed a recognition method based on improved spectral clustering, which has certain recognition effect, but its accuracy is not high [9]. Sollerhed et al. proposed a recognition method based on wavelet coefficient  $H_u$ , which can obtain more accurate recognition effect, but it takes a long time [10]. Therefore, this paper will study a recognition method based on NMR to investigate and analyze the sports dancers in the Institute of Physical Education, in order to improve the accuracy and efficiency of recognition.

## 2. Athletes' High-Strength Sports Injury Identification

Firstly, it is necessary to perform gray-scale conversion on the sports injury image. For the color image, the pixels can be represented by 3 bytes, and their bytes correspond to the brightness generated by 3 components [11], of which 3

components are represented by R, G, and B, respectively. When the 3 components are the same, it is a gray-scale image; otherwise, it is a color image. The gray-scale value conversion formula is as follows:

$$\text{Gray}(i, j) = 0.299 \cdot R(i, j) + 0.587 \cdot G(i, j) + 0.114 \cdot B(i, j). \quad (1)$$

After conversion, the 24 bit image representation of the image still does not change. The main function of the gray conversion is to improve the efficiency of damage recognition [12].

In order to improve the accuracy of damage identification, it is necessary to extract its contour. In this study, mathematical morphology and adaptive thresholding are used to extract the contour, and curve fitting method is also used to obtain a curve, that is, the damaged contour [12]. The damage active contour model is a snake model, which can obtain the contour of the damaged part. When the snake point is at an equilibrium position, the energy will be at a very small value, and the obtained contour will converge to the edge of the identified damaged part. Therefore, in order to identify the damaged part, it is necessary to make the contour energy reach a very small value. The expression formula of contour energy is as follows:

$$E(C) = [\alpha E_{in}(C) + \beta E_{ex}(C)] \text{Gray}(i, j), \quad (2)$$

where  $\alpha$  and  $\beta$  are the weighted values and  $E_{ex}(C)$  and  $E_{in}(C)$  are the complementary energy and internal energy, respectively. After the damage contour is obtained, the damaged part can be preliminarily identified by using the  $K-L$  transformation analysis method. After obtaining the contour, the number of damaged pixels and other relevant information can be obtained, so the digital matrix is established by using these information [13]. In order to improve the accuracy of identifying the damaged position, it is necessary to arrange the images into 64 feature vectors, which are arranged in series according to the column. Then, there are

$m$  images, and the formula for  $X = \{x_1, x_2, \dots, x_n\}$  to calculate the overall mean vector of images is

$$\mu = \frac{1}{m} \sum_{i=1}^m x_i E(C). \quad (3)$$

Arrange the eigenvalues  $A$  in a decreasing manner. After the arrangement, select the first  $J$  eigenvalues  $\lambda$  that are not zero, and then, extract their corresponding vector  $O$ . Then, the covariance matrix eigenvector  $\mu$  can be calculated according to the following formula. Select the first 60% of the eigenvalues, so that most of the damage images can be retained.

**2.1. Pixel Calculation of Damage Location Based on NMR.** Through the above analysis, the damage location can be preliminarily identified, but the exact location cannot be obtained. Therefore, the article will further identify the damaged part by using NMR, so as to obtain a more accurate damaged part and calculate the area of the damaged area. Using NMR in image damage recognition is to treat each solution as a fish and then form a solution set of all solutions. There are two ways to find the final solution in the solution set: taking the cluster center as the solution and the cluster result as the solution [9]. In order to improve the recognition accuracy, this paper uses the cluster center as the solution. That is, the objective function (4) of fish can be expressed by the following formula:

$$j_g = \sum_{i=1}^E \|V_i - x_k\|^2 \cdot d(x, y), \quad (4)$$

where  $g$  represents the number of cluster centers,  $x_k$  represents the cluster object, and  $V_i$  represents the pixel cluster centers. When  $j_g$  is the minimum value in the formula, it is set as the best clustering point, which is helpful to achieve the purpose of damage image segmentation [14]. After clustering, the gray pixel value of the image will reach the corresponding effect with the original pixel. After clustering results, the color rendering of pixels is realized, so different colors in the image will represent different representations. Thus, the RGB representation value of pixels can be calculated by accumulating the GRB flux of each type of pixel value and dividing it by the total number of pixels.

### 3. Research and Analysis

**3.1. Research Object.** A questionnaire survey was conducted on the professional athletes of sports dance major from 2019 to 2021 in the Institute of Physical Education [15]. The athletes were 18-25 years old, and the training period of sports dance was 3-5 years.

**3.2. Research Methods.** We conducted face-to-face interviews with experts in aerobics, sports dance, sports injury, sports statistics, and sports art in the Institute of Physical Education; solicited their opinions on the research content, questionnaire, and other aspects; and obtained valuable

information. At the same time, during the period of issuing the questionnaire, the coaches and principals of sports dance examinee training institutions in various colleges and universities had an in-depth understanding of the relevant contents of this article and obtained valuable information [16].

In order to fully understand the sports injury of college sports dance candidates, a questionnaire for college sports dance candidates in 2021 is designed according to a large number of data, the opinions and suggestions of relevant experts, and the characteristics of the survey object.

Ten experts (associate professors or professors) were employed to evaluate the contents of the questionnaire design, content design, and structure design according to the five grades of indicators (a) very appropriate, (b) relatively appropriate, (c) average, (d) inappropriate, and (e) very inappropriate. After the first round of evaluation, the experts put forward many valuable opinions. After the modification of the questionnaire, the same experts were asked to evaluate again. Experts do not disagree with the questionnaire design, questionnaire content, and structure design. 27.7% think it is very appropriate, and 58.7% think it is more appropriate [17].

The reliability test adopts the retest method. After two weeks of issuing the questionnaire, 50 candidates are randomly selected from the sports dance candidates and sent the questionnaire again by e-mail. After recovery, the scores are given to each option, and the two-time correlation coefficient is calculated ( $r = 0.882$ ,  $p < 0.01$ ), indicating that the survey results have high reliability [18].

**3.3. Data Statistics.** After the questionnaire was collected, the questionnaire data were analyzed, the invalid questionnaires were eliminated, all the survey results were carefully counted, and the data were analyzed by SPSS, mainly using chi-square test, factor analysis, and other statistical methods, which provided strong data support for this paper. The questionnaire information is sorted and summarized by Excel software, and the database is established on the software, and the software is used for statistical analysis.

**3.4. Result Analysis.** Figure 2 shows the time-consuming results of different recognition methods. From the figure, it can be seen that when the number of images to be recognized is different, the recognition method based on NMR is the shortest among the three methods. Therefore, it can be concluded that the method studied in this paper has faster recognition efficiency than other methods. Because this method has gone through image gray conversion before recognition, this step is conducive to improve the recognition efficiency.

**3.4.1. Comparison of Injury Rates of Athletes of Different Genders.** Table 1 shows that the injury rate of women is 52.6% and that of men is 51%. It shows that no matter in Latin dance, the injury rate of women in modern dance is higher than that of men. Women's dance steps are complex and fancy, so the requirements for women's flexibility and body coordination are higher than that of men. The injury rate of women is bound to be higher than that of men.



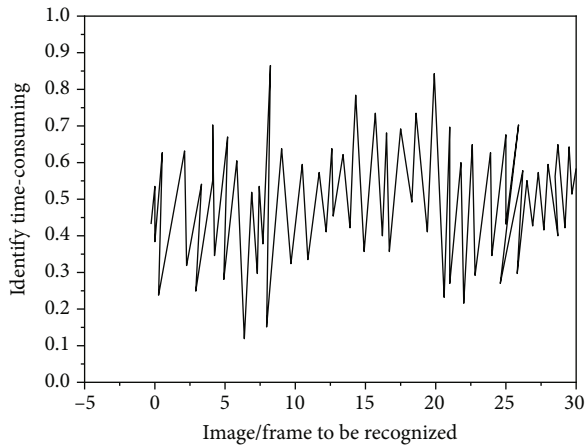


FIGURE 2: Time-consuming of damage identification method based on NMR.

As can be seen from Figure 3, Latin dancers suffer more injuries than modern dancers in general. The injury rate of female Latin dancers is higher than that of modern dancers, and that of male Latin dancers is also higher than that of modern dancers.

So the conclusion is as follows: (1) the probability of injury in Latin dance competition training is higher than that in modern dance. (2) The injury rate of women is higher than that of men, whether they are Latin dancers or modern dancers. This result is closely related to the technical style characteristics of the two dances. Compared with modern dance, Latin dance is more complex and changeable in technical movements, and the music rhythm is more cheerful and passionate, all of which have higher requirements for athletes [19]. Whether it is Latin dance or modern dance, women's technical movements are more abundant, mainly to show women. Women's coordination and flexibility are highly required, and it is inevitable that their injury rate is higher than that of men.

According to the classification of injury nature, 112 Latin dancers were counted, including 47 men and 65 women.

From Table 2, we find that the skin abrasion rate caused by Latin dance competition training is as high as 65.6% for women and 58.6% for men. Latin dancers have varied shapes. In addition to the basic dance steps, there are many different styles of modeling actions, such as the man kneeling at the end of the dance in the Paso. Repeated training is very easy to cause skin abrasion or even subcutaneous bleeding.

In Latin dance, the probability of muscle strain and muscle contusion is also very high. Among them, the probability of female muscle strain is 51.7%, and the probability of muscle contusion is 45.6%; In men, the probability of muscle strain is as high as 54.2%, and the probability of muscle contusion is as high as 43.6%. The results show that the probability of muscle strain and muscle contusion of women is higher than that of men [20]. This is because the Latin dance mainly shows women's dance posture. Except for the bullfight dance, women's dance moves are more difficult and complex than men's. Frequent muscle control during com-

petition and training, muscle stretching is very easy to cause muscle strain, and the probability of joint dislocation and fracture during competition and training is very low.

**3.4.2. Cause Analysis of Sports Injury.** Many factors can cause sports injuries to sports dancers, such as (1) no warm-up activities or perfunctory warm-up activities before exercise; (2) poor technical level of athletes; (3) poor physical quality; (4) unscientific training methods, excessive exercise volume, and intensity; (5) the training time is unreasonable and too long; (6) choose difficult dance movements that do not meet their own level; (7) uncoordinated cooperation between male and female athletes; (8) unreasonable music rhythm; (9) decreased physical fitness during the competition; (10) unable to reasonably adjust their own state before the competition; and (11) collision with other players during the competition.

From Table 3, in the investigation of sports dance athletes, it is found that the main factors leading to athletes' injury are insufficient warm-up preparation; poor physical fitness; unscientific training methods; it is too difficult to select technical action; and poor condition before the game [21].

- (1) Sports dancers do not pay attention to warm-up activities, or insufficient warm-up activities are an important factor causing sports injuries. Both Latin dance and modern dance need a high degree of coordination of athletes' bodies. In particular, Latin dance has very high requirements for movement speed and strength. Without preparatory activities or without systematic preparatory activities, the excitability of nervous system cannot be reached, and the stiffness and uncoordinated muscles and joints are very easy to cause sports injuries to athletes. In the survey, it is found that most sports dancers are dismissive of preparatory activities. Some athletes mistakenly think that doing preparatory activities will appear to be their own low level and directly start training their unskilled movement routines or difficulties. Another situation is that sports dance athletes lack targeted special preparation warm-up, only basic preparation activities. Sports dance includes two categories, ten dance types with different styles and simple and single preparation activities, which simply cannot meet the requirements of this sports art project
- (2) The physical quality of sports dancers is poor. During the investigation of the athletes in the Institute of Physical Education, it is found that although the institute has set up a ballet body course, the athletes generally lack basic physical quality training and special physical quality training. It is difficult to effectively improve strength, explosiveness, speed, and endurance, which is unfavorable to the development of sports dance. With the continuous development of sports dance competition towards difficulty and beauty, the competition is becoming increasingly fierce. Athletes' poor physical quality makes it

TABLE 1: Comparison of injury rates of athletes of different genders.

Female			Male			Total		
Number of people investigated	Number of injured	Damage rate	Number of people investigated	Number of injured	Damage rate	Number of people investigated	Number of injured	Damage rate
123	66	52.6%	60	30	51%	183	96	52.5

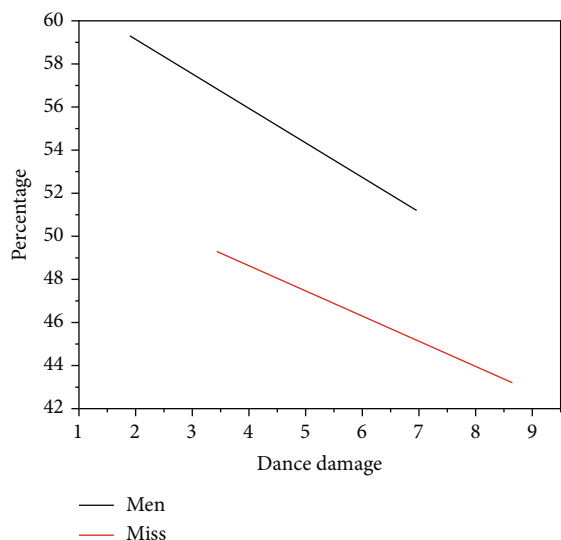


FIGURE 3: Comparison of injury rates of athletes of different dances.

TABLE 2: Investigation and research on injury nature of Latin dancers.

Injuries	Lady		Man	
	Number of injured	Injury probability	Number of injured	Injury probability
Skin abrasion	20	65.6%	15	58.6%
Muscle strain	10	51.7%	14	54.2%
Muscle contusion	11	45.6%	11	43.6%
Ligament injury	21	46.6%	6	40.4%
Dislocation of joint	2	1.8%	1	4.3%
Fracture	1	1.6%	0	0

difficult to support technical requirements and competition intensity. Except for a few athletes in sports dance training institutions who will invite professional physical fitness coaches to carry out physical fitness training, most of them also have the same problem, or even more serious

#### 4. Discussion

In the process of competition performance, athletes must first do a good job in warm-up activities to make the nervous

system and joint muscles active and excited. Athletes should scientifically and systematically formulate training programs and training plans. In combination with the characteristics of special projects, special physical quality training is carried out to better support the development of special projects, such as strength, explosiveness, flexibility, and endurance. Athletes should reasonably choose the technical difficulty, avoid aiming too high, aim too high and do too little, and resolutely follow the principle of step-by-step training. Athletes should learn to adjust their physical state before the competition or before the performance. They should reduce heavy load training about a week before the competition and avoid long-term training. They can do some low-intensity adaptive exercises, get familiar with the music rhythm, review the competition routine with their dance partners, and adjust their diet and sleep to prepare for the competition.

The athletes' preparatory activities should consist of free hand exercises, stretching exercises, and basic pace exercises. This can not only improve the flexibility of athletes' joints and muscles but also significantly improve the excitability of the nervous system, effectively prevent sports injuries caused by uncoordinated joint muscle stiffness and athletes' inattention, and greatly improve the training efficiency of athletes. The intensity of warm-up preparation activities should be controlled at low to medium intensity [22]. Athletes should feel their bodies warm and sweat slightly and do not make their bodies feel tired. According to the characteristics of sports, it is appropriate to control the time of daily training warm-up preparation activities to about 10 minutes. In the competition, the athletes should prepare for warm-up according to the actual situation, dance types, and weather factors.

In the training process, athletes of different levels should be different from person to person when formulating training plans. They must follow the principle of step-by-step and persistent sports training. They should formulate annual training plans, monthly training plans, and weekly training plans to deal with competitions and performances, so as to avoid temporary cramming before competitions. In the training process, it is not that the greater the amount of training, the faster the improvement of technical level. The improvement of technical level is a cumulative process. Excessive training will only cause physical and mental fatigue of athletes, reduce training enthusiasm, and increase the risk of sports injury.

By massaging the joints, the elasticity of the ligaments can be enhanced and the range of motion of the joints can be increased, especially for the damaged joints, ligaments, and muscle bonds, which can greatly accelerate the recovery effect. When massaging and relaxing, you can choose to focus on the parts that are easy to be damaged, such as the soleus, gastrocnemius, and quadriceps femoris of the lower limbs in Latin dance. You can also massage and relax the

TABLE 3: Factors of sports injury of municipal sports dancers.

Cause of damage	Number of persons	Proportion
Insufficient warm-up preparation	45	23%
Poor physical fitness	36	19.1%
Unscientific training methods	31	16.5%
Difficult to choose technical action	27	14.3%
Poor preparation before the game	19	11.4%
Other	25	12.7%

tired parts according to your body feeling. When athletes feel very tired, they need to massage and relax their muscles and joints [23]. The timing of massage and relaxation can be carried out together with stretching activities after the end of competition and training, or after bathing or before going to bed after the end of competition and training. During the massage, the strength shall be from light to heavy, and the feedback of the massaged athletes shall be listened to, and the strength and massage parts shall be adjusted appropriately according to the feedback.

## 5. Conclusion

Athletes will inevitably be injured during sports. The identification of injury pictures is helpful to improve the therapeutic effect of athletes. In this paper, the damaged parts are identified based on NMR; the method in this paper helps to improve the identification efficiency and accuracy. Athletes are very easy to get injured during sports. In order to reduce the degree of injury of athletes, we should strictly follow the action standards in the training process to avoid serious injury. The strategies to deal with the risk of acute sports injury are risk control and risk transfer. There are two methods for risk control: take risk prevention measures before the occurrence of risk events and take risk mitigation measures during and after the occurrence of risk events. The main measure to transfer the risk of acute sports injury is insurance. As an advanced noninvasive and nonradioactive diagnostic method, NMR provides an effective auxiliary diagnostic method for doctors with high accuracy, and its examination results are an important basis for arthroscopic examination. However, its cost is high, and there are still a certain degree of false positives and false negatives, but with the reduction of inspection costs, the development of MRI technology, and the accumulation of clinical data, NMR will become the first choice for early diagnosis of sports injuries.

In the future, we will formulate the archives of sports dance athletes' acute sports injury risk events, study the quantitative probability of sports dance athletes' acute sports injury risk, and establish the sports athletes' acute sports injury risk model, in order to obtain the correlation between sports injury and sports performance.

## Data Availability

The data used to support the findings of this study are available from the corresponding author upon request.

## Conflicts of Interest

The authors declare that they have no conflicts of interest.

## Acknowledgments

This study is supported by the Sports Research Project of Jiangxi Sports Bureau, Research on the Development of Rural Public Sports Service Governance in Jiangxi Province under the Background of Rural Revitalization Strategy in the New Era, Project No. 202141.

## References

- [1] C. Covelli, S. Yuan, D. Grewell, and K. Schmidt-Rohr, "Structural changes from vibration welding of maple and pine woods analyzed by solid-state NMR," *Welding in the World*, vol. 66, no. 5, pp. 961–971, 2022.
- [2] M. Zhu and N. Liu, "Research on NMR noise reduction method based on improved CEEMD," *IEEE Access*, vol. 8, pp. 122864–122873, 2020.
- [3] A. S. Tarasov, I. Z. Rakhmatullin, G. S. Shurshalova, A. V. Klochkov, K. A. Il'Yasov, and V. V. Klochkov, "The affect of gadolinium ion on micelles and reverse micelles by NMR spectroscopy," *BioNanoScience*, vol. 11, no. 1, pp. 136–141, 2021.
- [4] I. A. Khodov, K. V. Belov, M. A. Krestyaninov, and M. G. Kiselev, "Conformational equilibria of a thiadiazole derivative in solvents of different polarities: an NMR study," *Russian Journal of Physical Chemistry A*, vol. 96, no. 4, pp. 765–772, 2022.
- [5] M. Novakovic, M. D. Battistel, H. F. Azurmendi, M. G. Concilio, D. I. Freedberg, and L. Frydman, "The incorporation of labile protons into multidimensional NMR analyses: glycan structures revisited," *Journal of the American Chemical Society*, vol. 143, no. 23, pp. 8935–8948, 2021.
- [6] L. Gkoura, G. Diamantopoulos, M. Fardis, D. Homouz, and G. Papavassiliou, "The peculiar size and temperature dependence of water diffusion in carbon nanotubes studied with 2d NMR diffusion-relaxation d-t2eff spectroscopy," *Biomicrofluidics*, vol. 14, no. 3, pp. 034114–034116, 2020.
- [7] P. Siudem, J. Bukowicki, R. Wa We, and K. Paradowska, "Structural studies of two capsaicinoids: dihydrocapsaicin and nonivamide.13C and15N MAS NMR supported by genetic algorithm and GIAO DFT calculations," *RSC Advances*, vol. 10, no. 31, pp. 18082–18092, 2020.
- [8] W. Derman, P. Runciman, J. C. Brown, and M. Badenhorst, "093 promotion of para athlete well-being in South Africa (the propel studies), part ii: identification of sleep-associated risk factors," *British Journal of Sports Medicine*, vol. 54, no. 1, 2020.
- [9] H. Wang and Z. Li, "Gray image segmentation algorithm based on one-dimensional image complexity," *Journal of Intelligent and Fuzzy Systems*, vol. 40, no. 1, pp. 1–10, 2020.
- [10] A. C. Sollerhed, A. Horn, I. Culpan, and J. Lynch, "Adolescent physical activity-related injuries in school physical education and leisure-time sports," *Journal of International Medical Research*, vol. 48, no. 9, 2020.

## *Retraction*

# **Retracted: Application of Color Doppler Ultrasound Combined with Magnetic Resonance Imaging in Placenta Accreta**

### **Scanning**

Received 5 December 2023; Accepted 5 December 2023; Published 6 December 2023

Copyright © 2023 Scanning. This is an open access article distributed under the Creative Commons Attribution License, which permits unrestricted use, distribution, and reproduction in any medium, provided the original work is properly cited.

This article has been retracted by Hindawi, as publisher, following an investigation undertaken by the publisher [1]. This investigation has uncovered evidence of systematic manipulation of the publication and peer-review process. We cannot, therefore, vouch for the reliability or integrity of this article.

Please note that this notice is intended solely to alert readers that the peer-review process of this article has been compromised.

Wiley and Hindawi regret that the usual quality checks did not identify these issues before publication and have since put additional measures in place to safeguard research integrity.

We wish to credit our Research Integrity and Research Publishing teams and anonymous and named external researchers and research integrity experts for contributing to this investigation.

The corresponding author, as the representative of all authors, has been given the opportunity to register their agreement or disagreement to this retraction. We have kept a record of any response received.

### **References**

- [1] X. Sun, R. Ren, X. Yu, F. Peng, and X. Gao, "Application of Color Doppler Ultrasound Combined with Magnetic Resonance Imaging in Placenta Accreta," *Scanning*, vol. 2022, Article ID 1050029, 7 pages, 2022.

## Research Article

# Application of Color Doppler Ultrasound Combined with Magnetic Resonance Imaging in Placenta Accreta

Xue Sun <sup>1</sup>, Runrun Ren <sup>2</sup>, Xiaoqian Yu <sup>1</sup>, Fang Peng <sup>2</sup>, and Xia Gao <sup>1</sup>

<sup>1</sup>Department of Obstetrics, The Affiliated People's Hospital of Hubei University of Medicine, Shiyuan, Hubei 442000, China

<sup>2</sup>Department of Ultrasound Imaging Center, The Affiliated People's Hospital of Hubei University of Medicine, Shiyuan, Hubei 442000, China

Correspondence should be addressed to Fang Peng; 201904012233@stu.zjrsru.edu.cn

Received 9 May 2022; Revised 16 June 2022; Accepted 1 July 2022; Published 13 July 2022

Academic Editor: Balakrishnan Nagaraj

Copyright © 2022 Xue Sun et al. This is an open access article distributed under the Creative Commons Attribution License, which permits unrestricted use, distribution, and reproduction in any medium, provided the original work is properly cited.

In order to improve the diagnostic value of color Doppler ultrasonography in placenta accreta and make the diagnosis more accurate, a method to detect placenta accreta by combining color Doppler ultrasonography and magnetic resonance is proposed. The patients with placenta accreta were selected for color Doppler ultrasonography and MRI examination. Kappa test was used to analyze the consistency between the results of ultrasound and MRI examination alone and combined diagnosis and pathological examination results, and the receiver operating characteristic (ROC) was drawn. Price compliance, sensitivity, specificity, good estimate rate, negative bid success rate, and Youden index were chosen as the basis for measuring the value of our tests. The results showed that the Kappa combined test rate was 0.609, the equivalent efficiency was 80.90%, and the correlation was good; ROC curve analysis showed that the sensitivity and specificity of articular placenta accreta were 91.75% and 89.26%. The sensitivity, uniqueness, good estimate, negative predictive value, and Youden index of color Doppler ultrasound combined with magnetic resonance imaging > magnetic resonance imaging > color Doppler ultrasound in our laboratory were compared, and the difference was significant ( $P < 0.05$ ). The experimental results show that color Doppler ultrasound and MRI are effective in the diagnosis of placenta accreta, and each has advantages and disadvantages. Therefore, it has been improved in the diagnosis of placenta accreta, is helpful for the diagnosis of placenta accreta, and is suitable for popularization and use.

## 1. Introduction

Placenta accreta is a rare obstetric critical illness due to hypoplasia or absence of the decidua of the uterus, and the placental villi invade the uterine serosal layer and even penetrate the serosal layer and involve surrounding organs. In patients with placenta accreta, the placenta is partially stripped, and the subplacental blood sinus is open for a long time. It is easy to cause severe bleeding and urinary system damage that are difficult to control during the operation, which seriously endangers the life of the mother. Therefore, the correct diagnosis of placenta accreta in the early prenatal period and the determination of the type of placenta accreta are very important for the selection of treatment methods and the prevention and control of intraoperative bleeding [1]. Color Doppler ultrasound is easy to operate, and it not

only has the advantages of traditional two-dimensional ultrasound structural images but also provides rich hemodynamic information for the diagnostic staff, as shown in Figure 1. However, the diagnosis results are greatly influenced by the operating factors and diagnosis experience of the diagnosing personnel. In addition, in patients with placenta accreta, if the abdominal fat is thicker, the fat is produced in the intestinal lumen, which may adversely affect the diagnosis and distort the diagnosis. Magnetic resonance imaging is a medical technique that was only used in medicine in the 1980s. It uses static and radio frequency magnetic fields to acquire image data of human tissue. HD images without using different materials can be seen in [2]. Although magnetic resonance imaging has high spatial resolution, it is easily affected by the specific structure of the uterus in the diagnosis of placenta accreta, and misdiagnosis

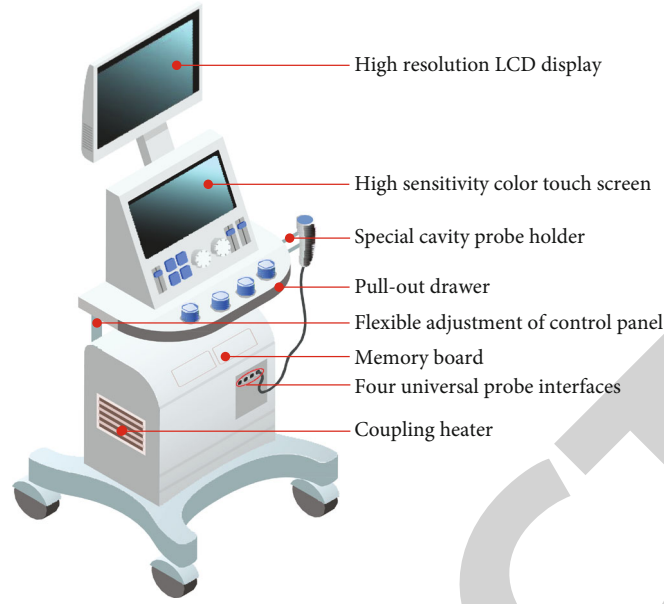


FIGURE 1: Color Doppler ultrasound.

and missed diagnosis are inevitable. Since color Doppler ultrasound and magnetic resonance have their own advantages and disadvantages, the combined application of the two diagnostic methods can become an important method to improve the diagnostic accuracy and avoid unnecessary hysterectomy. This article analyzes the effect of combined diagnosis [3].

## 2. Literature Review

Shanker et al. showed that placenta accreta is an obstetric complication in which placental tissue invades the myometrium due to a variety of reasons, and while placenta accreta penetrates the serosa and involves parametrial tissues, it can lead to hemorrhage, miscarriage, damage to pelvic organs, and even death in severe cases, endangering the safety of patients [4]. Xu et al. showed that for the diagnosis of placenta accreta, magnetic resonance imaging has a high evaluation value, especially for preoperative risk assessment. There are relatively specific indicators of preestimated bleeding, which can well help clinicians make decisions [5]. Apgm et al.'s study showed that magnetic resonance imaging (MRI) examination can show signs such as myometrial thinning or discontinuity, placental type, and abnormal blood vessels in the placenta. Clinically, it can be determined according to the type of placental bulge and the accumulation of blood vessels in the serosal layer of the uterus. Signs to differentiate between penetrating and nonpenetrating placenta accreta have high clinical application value [6]. Hong et al. showed that MRI has high resolution, has simple operation, is not easily affected by other factors, and can display placental structure well. Ultrasound diagnosis of placenta accreta, although simple and low cost, is easily affected by the patient's body size and bladder filling degree, and its accuracy and sensitivity are not high [7]. Horng et al. combined the advantages and disadvantages of color Doppler

ultrasound and MRI, and the combined results were identified and demonstrated that the application of color Doppler ultrasound combined with magnetic resonance imaging in clinical trials of placenta accreta can improve sensitivity and specificity of prenatal testing. Fewer diagnoses and invalid diagnoses can be seen in [8]. Bao et al. showed that placenta accreta is caused by the invasion of placental villi into the myometrium caused by traumatic defects of the endometrium and primary decidual dysplasia and has a high incidence. The incidence of placenta accreta is acute and very dangerous. During childbirth, the placenta is difficult to be stripped, resulting in intrapartum and postpartum hemorrhage, secondary infection, and uterine rupture, which seriously threatens the safety of mothers and fetuses [9]. Experiments have shown that color Doppler ultrasound (US) and magnetic resonance imaging (MRI) and alpha-fetoprotein (AFP) imaging are currently used for prenatal screening for placenta accreta. Among them, AFP is not specific because of its many influencing factors and can only be used as a screening method, while the clinical reports of US and MRI diagnosis of placenta accreta are mostly used alone [10]. Zhi et al. stated that the current prenatal diagnosis of placenta accreta mainly relies on two-dimensional color ultrasound, three-dimensional ultrasound Doppler ultrasound, three-dimensional color power Doppler ultrasound and magnetic resonance imaging (MRI), and other methods. Among them, two-dimensional color ultrasound is a widely used method in clinical practice, but it cannot display the blood flow of the posterior wall of the placenta and requires high medical skills for the operator, so the misdiagnosis is common [11]. Wei et al. believed that three-dimensional color Doppler ultrasound can clearly display the blood flow of the posterior placenta, with simple operation and high resolution, which greatly improves the diagnostic coincidence rate [12]. Hussein et al. stated that MRI also has the advantages of noninvasiveness, repeatability, and no ionizing

radiation, but the price is relatively expensive and the imaging speed is slow and sensitive [13].

### 3. Research Methods

**3.1. General Information.** A total of 89 patients with suspected placenta accreta were selected from January 2019 to January 2020 in A Central Hospital and B People's Hospital. BMI was  $21.12 \pm 1.45 \text{ kg/m}^2$ , including 20 primiparas, 69 multiparous women, gestation times  $3.40 \pm 2.40$ , parity times  $2.30 \pm 2.00$ , 26 cases of previous abortion, uterine cavity surgery history of 21 cases, and 28 cases of cesarean section history [14]. Among them, there were 25 patients with placenta accreta. This study has been approved by the hospital ethics committee.

**3.2. Inclusion and Exclusion Criteria.** (1) Inclusion criteria are as follows: ① The patient has a history of abortion, placenta previa, a history of uterine cavity operation, and a history of cesarean section and other high-risk factors; ② the routine ultrasound examination after 28 weeks before delivery indicates placenta previa, that is, the lower edge of the placenta is less than 20 mm from the internal cervical os; ③ the patients were informed and signed the informed consent. (2) Exclusion criteria are as follows: ① pregnancy complicated with pelvic mass; ② the existence of other underlying diseases such as heart, liver, and kidney dysfunction; ③ the existence of malignant tumor; and ④ placental stagnation caused by congenital malformation of the uterus

**3.3. Instruments and Equipment.** The VolusionE8 three-dimensional color Doppler ultrasound diagnostic apparatus (GE, USA) and the Siemens Symphony 1.5T superconducting MRI scanner (Siemens, Germany) were used, and the apparatus was equipped with a workstation for image post-processing [15].

#### 3.4. Inspection Method

**3.4.1. Color Doppler Ultrasonography.** The VolusionE8 3D color Doppler ultrasound diagnostic instrument was used with built-in virtual computer-aided analysis software, and the 4Dview software was used for 3D reconstruction [16]. The patient has a proper bladder, and the patient is in a supine or lateral position. The probe is placed on the patient's abdominal wall, perpendicular to the abdomen, for horizontal, vertical, and dynamic detection. The direction of the probe is constantly changed during observation, and the body position is changed if necessary. Pay attention to observe the routine fetal and amniotic fluid indicators, the space area of the posterior wall of the placenta, the relationship between the edge of the placenta and the cervical foramen, and the blood flow in the placenta. Three-dimensional image observation of blood vessels at the placenta implantation site was performed to analyze the location of suspicious placental lesions and the three-dimensional structure of blood supply around them. All patient examination images were jointly completed by 2 deputy chief physicians of obstetrics [17].

TABLE 1: Value analysis of color Doppler ultrasonography in the diagnosis of placenta accreta.

3D ultrasound	Gold standard		Coincidence rate (%)	Kappa value
	Positive	Negative		
Positive	42	10	71.91	0.410
Negative	15	22		

TABLE 2: Analysis of the value of MRI in the diagnosis of placenta accreta.

MRI diagnosis	Gold standard		Coincidence rate (%)	Kappa value
	Positive	Negative		
Positive	36	7	68.91	0.376
Negative	21	25		

TABLE 3: Value analysis of the combined diagnosis of placenta accreta by the two methods.

Joint diagnosis	Gold standard		Coincidence rate (%)	Kappa value
	Positive	Negative		
Positive	44	4	80.90	0.609
Negative	13	28		

**3.4.2. MRI Examination.** Image postprocessing was performed using a Siemens Symphony 1.5T superconducting MRI scanner and a LEONARDO workstation equipped with the instrument. The patient had a full bladder, and the patient was placed in the supine position. Temporary scan mode is Fast Low Angle Shot (FLASH)/T1WI, while T2WI is Half-Fourier Fast Acquire One Shot. Echo Sequence (HASTE) Transient Time (TR) is 1000 ms, Echo Sequence (TE) is 74 ms, transverse slice thickness is 5 mm, slice spacing is 2.4 mm, excitation times (NEX) are 1 second, the field of view (FOV) is 25 cm, the matrix is  $164 \times 256$ , the fast spin echo (TSE) series is used in the sagittal position, the slice thickness is 6 mm, the slice spacing is 1.8 mm, the NEX times are 2, and the matrix is  $240 \times 320$ . At the same time, fat suppression and flow compensation techniques are used, and the contrast agent used in some stillborn or postpartum patients is the nonspecific extracellular space contrast agent gadolinium-diethylenepentaacetic acid (Gd-DTPA) cubital vein injection [18]. The scanning range is from the lower border of the pubic symphysis to about 2 cm above the uterine fundus. All patient examination images were jointly completed by 2 senior radiologists.

**3.5. Observation Indicators.** Select value coincidence, sensitivity, particularity, positive estimate, negative estimate, and Youden index according to the measured values of our test rating, sensitivity (%) =  $\frac{\text{really good}}{\text{true good} + \text{false false}} \times 100\%$ ; specificity (%) =  $\frac{\text{true negatives}}{\text{true negatives} + \text{false positives}} \times 100\%$ ; positive predictive value (%) =  $\frac{\text{true positives}}{\text{true positives} + \text{false positives}} \times 100\%$ ; negative

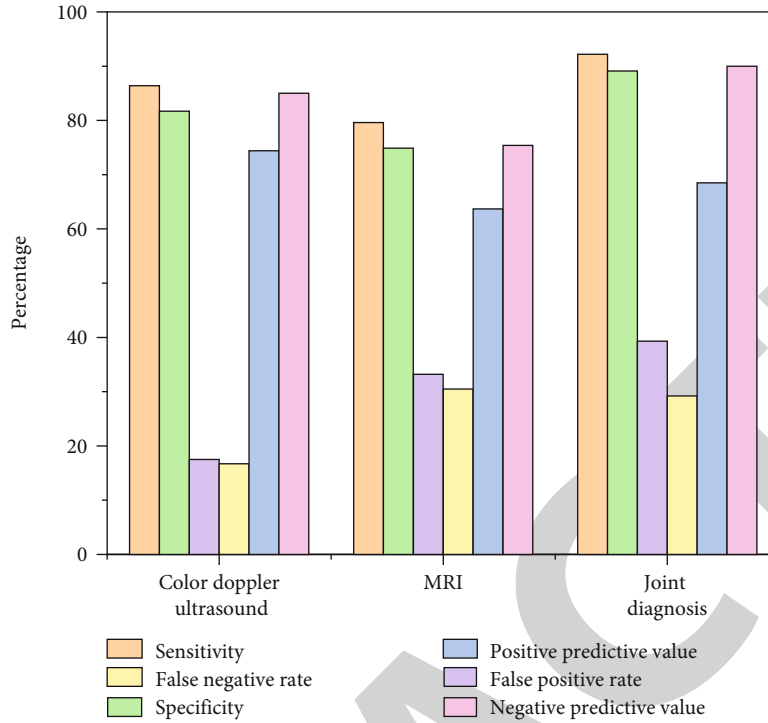


FIGURE 2: ROC curve analysis of the value of the two methods alone and combined in the diagnosis of placenta accreta (%).

TABLE 4: Comparison of the coincidence rates of the three diagnostic scheme.

Diagnostic program	Placenta piercing
Color Doppler ultrasound	15 (78.95)
Magnetic resonance imaging	17 (89.47)
Color Doppler ultrasound combined with magnetic resonance imaging	19 (100.00)

predictive value (%) =  $\frac{\text{true false}}{(\text{false true} + \text{false false})} \times 100\%$ ; Youden index = sensitive + special - 1.

**3.6. Statistical Methods.** The data of this study were analyzed using the SPSS 20.0 software. Data expressed as a percentage (%) was calculated using the  $\chi^2$  test. The Kappa coefficient is used to measure the similarity of two measurement models. The diagnostic value of the two methods for placenta accreta was determined by recipient characteristics and ROC curves. The statistical results show that the difference is significant when  $P < 0.05$  [19].

## 4. Result Analysis

**4.1. Analysis of Color Doppler Ultrasonography in Patients with Placenta Accreta.** Color Doppler ultrasonography showed that patients with penetrating placenta accreta had the following: abundant blood vessels between the uterine serosa layer and the bladder wall, interruption of the continuity between the uterine serosa layer and the bladder, and local mass of the placenta protruding into the bladder and other manifestations.

**4.2. Analysis of MRI Manifestations in Patients with Placenta Accreta.** MRI shows that patients with placenta accreta have the following: the placenta gathers and shows a hump-like change; the placenta signal is significantly uneven; the placenta is irregular in the internal cervical os; it has posterior wall, with unclear demarcation and other manifestations [20].

**4.3. Analysis of the Value of the Two Inspection Methods Alone and in Combination in the Diagnosis of Placenta Accreta.** The 89 patients with suspected placenta accreta were diagnosed as 57 by the “gold standard” such as clinical and pathological diagnosis, among which 42 were diagnosed as positive by ultrasound.  $\kappa = 0.410$ , the coincidence rate was 71.91%, and the consistency of the two diagnostic methods was acceptable [21]. Among the 57 confirmed patients, 36 patients were positive by MRI. The Kappa coefficient test was  $\kappa = 0.376$  for the two diagnostic methods of MRI and the “gold standard,” and the coincidence rate was 68.91%. The consistency of the two diagnostic methods was general. Among the 57 confirmed patients, 44 patients were positive in the joint examination. The Kappa coefficient method for the joint diagnosis and the “gold standard” diagnosis method had a  $\kappa = 0.609$ , and the coincidence rate was 80.90%. The two diagnostic methods had good consistency. ROC curve analysis showed that the sensitivity of ultrasonography in detecting placenta accreta was 86.49%, the specificity was 82.16%, the positive estimate was 75.19%, and the negative estimate was 85.31%; the sensitivity of MRI in the diagnosis of placental implantation was 79.43%. The placenta accreta rate was 79.43%, the primary sex was 79.43%, the specificity was 75.21%, the positive estimate rate was



TABLE 5: Comparison of diagnostic efficacy of three diagnostic schemes.

Diagnostic program	N	Sensitivity (%)	Specificity (%)	Positive predictive value (%)	Negative predictive value (%)	Youden index
Color Doppler ultrasound	64	78.13	81.25	80.65	78.79	0.59
Magnetic resonance imaging	64	93.75	87.50	88.24	93.33	0.81
Color Doppler ultrasound combined with magnetic resonance imaging	64	100.00	100.00	100.00	100.00	1.00
$\chi^2$		7.905	8.847	9.011	7.905	9.250
P		0.005	0.001	0.000	0.005	0.000

64.12%, and the negative estimate rate was 75.21%; the sensitivity of the two placenta accreta samples was 91.75%, the odds are 89.26%, the positive odds are 68.59%, and the odds are 89.67% (see Tables 1–3 and Figure 2).

**4.4. Sequence of Diagnostic Coincidence Rate and Analysis of Diagnostic Energy Efficiency.** The detection rate of color Doppler ultrasound, magnetic resonance, and color Doppler ultrasound combined with magnetic resonance on placental puncture was determined as follows: color Doppler ultrasound combined with magnetic resonance > magnetic resonance > color Doppler, and the difference was statistically significant ( $P < 0.05$ ) (see Table 4). In terms of performance evaluation, the sensitivity, specificity, positive estimate, negative estimate, and Youden index of each test were compared: color Doppler ultrasound combined with magnetic resonance imaging > magnetic resonance imaging > color Doppler ultrasound, and the contrast value is  $P < 0.05$  (see Table 5).

**4.5. Discussion.** In this study, the hypoechoic zone between the posterior wall of the lower placenta and the myometrium disappeared in patients with placenta accreta under two-dimensional ultrasonography, and there was no obvious protrusion of the uterus and bladder. The placenta showed abundant blood flow and obvious blood sinuses. There is a high-speed pulsed arterial blood flow with venous blood flow in the placental space. Three-dimensional color Doppler ultrasound in vascular transparency mode showed that the distribution of blood vessels between the uterine serosa and the bladder wall in patients with placenta accreta was significantly increased, and the local mass of the placenta protruded toward the bladder. In the images under 3D color power Doppler ultrasound, the distribution of blood vessels in the placenta of patients with placenta accreta was significantly increased, and it was difficult to distinguish the blood vessels between the villi and the intervilli. MRI images showed irregular mass shadows in the uterine cavity and strip-shaped signal shadows in the anterior abdomen, showing postoperative changes. The placenta is located in the uterine fundus, showing an arc-shaped soft tissue signal shadow, protruding into the myometrium of the uterine wall on the right side of the uterine fundus. In patients with placenta accreta, the space in the posterior wall of the placenta has largely disappeared with partial disappearance of the muscular layer, and there are multiple anechoic areas of dif-

ferent sizes and irregular shapes in the placental parenchyma and basal layer. The patient can see the appearance of irregular placenta in the internal cervical os. In order to further analyze the application value of color Doppler ultrasonography and MRI alone and in combination in the diagnosis of prenatal placenta accreta, in this study, 89 patients with suspected placenta accreta were diagnosed as 57 by the “gold standard” of clinical and pathological diagnosis. Among them, 42 patients were diagnosed as positive by ultrasound, and the consistency between the two diagnostic methods of ultrasound and the “gold standard” was acceptable. Among the 57 confirmed patients, 36 were positive by MRI, and the consistency between MRI and the “gold standard” diagnostic methods was general. Among the 57 confirmed patients, 44 patients were positive by the combined examination, and the two diagnostic methods of the combined diagnosis and the “gold standard” were in good agreement [22]. The ROC curve analysis in this study showed that the sensitivity and specificity of Doppler ultrasound in the diagnosis of placenta accreta were 86.49% and 82.16%, respectively; the sensitivity and specificity of MRI in the diagnosis of placenta accreta were 79.43% and 75.43%. The sensitivity of placenta accreta was 91.75%, and the specificity was 89.26%. It can follow color Doppler ultrasound, MRI diagnosis, color Doppler ultrasound combined with magnetic resonance imaging examination, the cost consistency, sensitivity, specificity, and good estimates of this examination can be compared with submitted surgical results. Price, negative bid, and Youden index were chosen as the basis for measuring the value of our tests. The surgical results confirmed that the diagnosis of patients with different placental pathways was as follows: color Doppler ultrasound combined with magnetic resonance imaging > magnetic resonance imaging > color Doppler ultrasound, and the difference was statistically significant ( $P < 0.05$ ), our diagnosis. There were significant differences in sensitivity, specificity, positive estimation rate, negative estimation rate, and Youden index between color Doppler ultrasound combined with magnetic resonance imaging > magnetic resonance imaging > color Doppler ultrasound ( $P < 0.05$ ). Based on this, it can be seen that in the diagnosis of placenta accreta, color Doppler ultrasound combined with magnetic resonance imaging is more effective, suggesting that color Doppler ultrasound and MRI have better value in the diagnosis of placenta accreta, which is helpful for physician. Early diagnosis and taking corresponding measures are extremely important for the treatment of placenta accreta.

## 5. Conclusion

This article discusses the application of color Doppler ultrasound combined with magnetic resonance imaging in placenta accreta. A feature of this method is the combination of color Doppler ultrasound and magnetic resonance imaging, which can improve the sensitivity and specificity of prenatal diagnosis and reduce the cost of misdiagnosis and non-diagnosis. Through the experimental analysis, the following conclusions were drawn: (1) ROC curve analysis showed that the sensitivity and specificity of the combined diagnosis of penetrating placenta implantation were higher than those of the single method. (2) Combined diagnosis and gold standard have good consistency and high coincidence rate. The "gold standard" diagnostic method has a high coincidence rate. (3) Compared with sensitive, specific, good estimate, negative estimate, and Youden index, color Doppler ultrasound combined with magnetic resonance imaging has the best effect. In the diagnosis of placenta accreta, since the placenta is attached to the posterior wall of the uterus, MRI scans are multifaceted and minimally invasive and can reveal information such as fresh and old bleeding. And it can reveal the information of fresh bleeding and old bleeding for the diagnosis personnel. The detection results are more in line with the actual characteristics. Color Doppler ultrasound has the advantages of simple operation, short diagnosis time, low cost, and patient cooperation, so it still has a high clinical status. Since the uterus is an important organ for women to conceive the next generation and also plays an important endocrine function in the body, it is the top priority to preserve the uterus as much as possible. In this case, the use of color Doppler ultrasound combined with magnetic resonance is promoted in the diagnosis work. Imaging can improve the sensitivity of the diagnosis of placenta accreta and make the diagnosis more accurate.

## Data Availability

The data used to support the findings of this study are available from the corresponding author upon request.

## Conflicts of Interest

The authors declare that they have no conflicts of interest.

## References

- [1] I. A. Hassan and L. K. Hamza, "Unique case of a tenth cesarean section in an Emirati woman," *Dubai Medical Journal*, vol. 3, no. 1, pp. 5–7, 2020.
- [2] S. Poddar and S. Sharma, "Diagnostic limitation and outcome of definitive surgical approach in placenta accreta spectrum disorders - a prospective case series study," *Journal of Evidence Based Medicine and Healthcare*, vol. 8, no. 7, pp. 359–363, 2021.
- [3] A. A. Khalifa, M. A. Elsemary, M. M. Ahmed, and M. M. Elshamandy, "Huge post-partum intra-myometrial hematoma (couvelaire uterus) in a preserved uterus in a case of placenta accreta: case report," *The Egyptian Journal of Hospital Medicine*, vol. 84, no. 1, pp. 2173–2175, 2021.
- [4] S. A. Shainker, R. M. Silver, A. M. Modest, M. R. Hacker, and S. A. Karumanchi, "Placenta accreta spectrum: biomarker discovery using plasma proteomics," *Obstetric Anesthesia Digest*, vol. 41, no. 2, pp. 77–78, 2021.
- [5] R. Xu, L. Cai, S. Xu, and J. Yan, "The effect of different diagnostic timings and types of placenta accreta on the pregnancy outcome," *Indian Journal of Pathology and Microbiology*, vol. 64, no. 2, pp. 288–293, 2021.
- [6] A. P. Gomes, A. Germano, M. Sousa et al., "Preoperative color Doppler ultrasound parameters for surgical decision-making in upper arm arteriovenous fistula maturation," *Journal of Vascular Surgery*, vol. 73, no. 3, pp. 1022–1030, 2021.
- [7] S. Hong, Y. Le, K. U. Lio, T. Zhang, Y. Zhang, and N. Zhang, "Performance comparison of ultrasonography and magnetic resonance imaging in their diagnostic accuracy of placenta accreta spectrum disorders: a systematic review and meta-analysis," *Insights Into Imaging*, vol. 13, no. 1, pp. 1–13, 2022.
- [8] H. C. Horng, M. J. Lai, W. H. Chang, and P. H. Wang, "Placenta accreta spectrum (pas) and peripartum hysterectomy," *Taiwanese Journal of Obstetrics and Gynecology*, vol. 60, no. 3, pp. 395–396, 2021.
- [9] Y. Bao, Y. Pang, Z. Sun, Q. Li, D. Tang, and L. Xia, "Functional diagnosis of placenta accreta by intravoxel incoherent motion model diffusion-weighted imaging," *European Radiology*, vol. 31, no. 2, pp. 740–748, 2021.
- [10] Y. Takaya, H. Chen, H. Ten et al., "Evaluation of the malignant potential of gliomas using diffusion-weighted and gadolinium-enhanced magnetic resonance imaging," *Brain Science Advances*, vol. 7, no. 4, pp. 248–256, 2021.
- [11] M. Zhi, M. Wang, W. Li, L. Ma, and Q. Lv, "Reliability of the application of transvaginal color Doppler ultrasound in the identification of pelvic tumors in women of childbearing age," *Annals of Translational Medicine*, vol. 8, no. 24, pp. 1662–1662, 2020.
- [12] Z. Wei, M. Mu, M. Li, J. Li, and Y. Cui, "Color Doppler ultrasound detection of hemodynamic changes in pregnant women with gdm and analysis of their influence on pregnancy outcomes," *American Journal of Translational Research*, vol. 13, no. 4, pp. 3330–3336, 2021.
- [13] A. M. Hussein and A. Kamel, "Reply to letter to the editor article "placenta accreta spectrum: "placenta accreta" is still used"," *Archives of Gynecology and Obstetrics*, vol. 303, no. 6, pp. 1631–1632, 2021.
- [14] L. K. Chen, Y. W. Lai, P. C. Li, and S. S. Chen, "Significant relationship between parameters measured by transrectal color Doppler ultrasound and sexual dysfunction in patients with BPH 12 months after TURP," *BMC Urology*, vol. 21, no. 1, pp. 1–7, 2021.
- [15] D. Li, X. Qian, R. Li et al., "High resolution adc for ultrasound color Doppler imaging based on mash sigma-delta modulator," *IEEE Transactions on Biomedical Engineering*, vol. 67, no. 5, pp. 1438–1449, 2020.
- [16] A. Jd, B. Mt, C. Sc, D. Gmr, and D. Ss, "Comparison of handheld acoustic Doppler with point-of-care portable color Doppler ultrasound in the assessment of venous reflux disease - sciencedirect," *Journal of Vascular Surgery: Venous and Lymphatic Disorders*, vol. 8, no. 5, pp. 831–839, 2020.
- [17] Y. Xu, Y. Wu, R. Zhang, and C. Liu, "Application of color Doppler ultrasound combined with fibroscan scoring system in the diagnosis of chronic hepatitis b fibrosis," *Yingxiang Kexue yu Guanghuaxue/Imaging Science and Photochemistry*, vol. 39, no. 1, pp. 67–74, 2021.

## *Retraction*

# **Retracted: Construction of Computer Microscope Image Segmentation Model Based on Fourth-Order Partial Differential Equation Smoothing**

### **Scanning**

Received 5 December 2023; Accepted 5 December 2023; Published 6 December 2023

Copyright © 2023 Scanning. This is an open access article distributed under the Creative Commons Attribution License, which permits unrestricted use, distribution, and reproduction in any medium, provided the original work is properly cited.

This article has been retracted by Hindawi, as publisher, following an investigation undertaken by the publisher [1]. This investigation has uncovered evidence of systematic manipulation of the publication and peer-review process. We cannot, therefore, vouch for the reliability or integrity of this article.

Please note that this notice is intended solely to alert readers that the peer-review process of this article has been compromised.

Wiley and Hindawi regret that the usual quality checks did not identify these issues before publication and have since put additional measures in place to safeguard research integrity.

We wish to credit our Research Integrity and Research Publishing teams and anonymous and named external researchers and research integrity experts for contributing to this investigation.

The corresponding author, as the representative of all authors, has been given the opportunity to register their agreement or disagreement to this retraction. We have kept a record of any response received.

### **References**

- [1] F. Li, "Construction of Computer Microscope Image Segmentation Model Based on Fourth-Order Partial Differential Equation Smoothing," *Scanning*, vol. 2022, Article ID 4355184, 8 pages, 2022.

## Research Article

# Construction of Computer Microscope Image Segmentation Model Based on Fourth-Order Partial Differential Equation Smoothing

Feng Li 

Yellow River Conservancy Technical Institute, Kaifeng Henan 475004, China

Correspondence should be addressed to Feng Li; 31115329@njau.edu.cn

Received 5 June 2022; Revised 26 June 2022; Accepted 1 July 2022; Published 12 July 2022

Academic Editor: Balakrishnan Nagaraj

Copyright © 2022 Feng Li. This is an open access article distributed under the Creative Commons Attribution License, which permits unrestricted use, distribution, and reproduction in any medium, provided the original work is properly cited.

In order to solve the problem of image noise, the author proposes a computer microscope image segmentation model based on the smoothing of fourth-order partial differential equations. On the basis of the functional describing the smoothness of the image by the directional curvature modulus, the author deduces a fourth-order partial differential equation (PDE) image noise reduction model, while effectively reducing noise, the edges are well preserved. The processing result of this method is a piecewise linear image, and there is a step in the gradient at the edge of the target. Taking advantage of this feature of the noise reduction results, the author proposes a new geodesic active contour model. The experimental results show that the reference method directly segments the results, iterates 10 times, and takes 160.721 seconds. Using the noise reduction model in the paper to preprocess and then using the reference method to segment the result, iterating 8 times, it takes 32.347 seconds. *Conclusion.* The new model is not only stable but also has strong contour extraction ability and fast convergence speed.

## 1. Introduction

Image processing serves two audiences, human and computer. The research content involves three levels: low-level, intermediate, and high-level, namely, image processing (image acquisition, denoising, enhancement, and segmentation), image analysis and understanding (edge, contour, and recognition), and computer vision (object and scene understanding) [1]. On the one hand, image processing is helpful for human analysis, such as image acquisition for space projects, medical images, earth remote sensing monitoring, and astronomy. Image contrast enhancement or colorization is used in the interpretation of X-rays, industry, medicine, biological sciences, geography, etc. Image enhancement and restoration are used in archaeology, physics, and other fields. On the other hand, image processing helps to solve the problem of machine perception, that is, extracting information from images that is more suitable for computer processing; the application fields include automatic character recognition, industrial machine vision for production inspection, military identification, automatic fingerprint processing,

X-ray processing, radiation and blood sample classification processing, and aerial and satellite image processing [2]. Therefore, in order to complete high-level computer vision tasks, the accurate acquisition of images and the proper representation of image visual information are the basic problems of image processing, which have very important theoretical significance and practical value. As a carrier of visual signals, images contain rich color, texture, and edge information. Ideally, images should objectively reflect the scene, and computers should be able to read image information that is meaningful to humans. However, these two requirements cannot be directly satisfied in practical applications. On the one hand, noise is inevitably introduced in the process of image acquisition and transmission. During image acquisition, the sensor may generate noise due to factors such as ambient light and temperature. During image transmission, noise may be generated due to transmission channel interference, such as when wireless channels are interfered with by light or atmospheric pollution. Therefore, image denoising is an important basic problem in image processing [3]. On the other hand, scientific studies have shown that, in

the process of observing and analyzing scenes and images, humans tend to focus on the outline of objects rather than trivial details, and it is easy to distinguish the main edges and understand information in complex natural images. Therefore, if the structural image can be extracted, it will help the computer to simulate the human visual system to understand the image and the scene and also help to improve the effect of a series of applications such as edge extraction, image abstraction, and tone mapping, as shown in Figure 1.

## 2. Literature Review

Wang and Chen express the deformation curve in a parametric form, imagine it as an elastic rubber line, and use the internal energy to describe the tension and smoothness of the curve. The external energy is defined based on the image and forms a minimal value. At the same time, internal and external energies are minimized to generate internal and external forces: the internal force contracts the curve and keeps the curve from being over-bent; the external force attracts the curve to the target edge [4]. Xh et al. proposed an attractive field based on the vector diffusion equation, by diffusing the gradient of the image boundary to a position far from the boundary, the attractive range of the boundary to the deformation curve was improved. The resulting force field is called the Gradient Vector Flow. This method is not only insensitive to the initial position of the curve but also can segment image boundaries with concave shapes [5]. Silva et al. proposed guided filter, which introduced a new image to guide the filtering of the current image in the linear translation transformation filtering process. The principle of the guided filter to preserve the edge is similar to the bilateral filter, but the bilateral filter is easy to cause gradient reversal, and the visual effect of the guided filter near the edge is better than that of the bilateral filter [6]. Ni and Kiri proposed the local Laplacian filter, which uses the classic Laplacian pyramid on the image after local enhancement processing. Its advantage is that it can handle multiscale details and obtain halo-free results [7]. Liu et al. proposed local extrema. The method first constructs the maximum and minimum envelopes on the extreme values selected in the local sliding window and then calculates a smooth mean envelope, so that the oscillations with high contrast can be removed [8]. Zhang and Tian proposed relative total variation (RTV). They observed that the intrinsic variation (cumulative sum of signed gradients) is much larger in the texture sliding window than in the structure window, and the purpose of smoothing the image can be achieved by controlling the relative total variation of the output image. RTV can remove the texture of mosaic images well, but due to the complex illumination and perspective distortion of natural images, some details of natural images may be oversmoothed [9]. Yang propose a nonlocal averaging algorithm over the spatial domain to solve the problem of image denoising. This method uses the similar pixel information in the image to estimate the true gray value of the target pixel, where the pixel similarity is measured by the similarity of the image block. The introduction of nonlocal self-similarity greatly

improves the image denoising effect, and it has created a new research idea for the field of denoising [10].

The image noise has a greater impact on the segmentation effect of the active contour model, especially for edge-based models. To this end, the region-based model introduces the method of region global division, which partially solves this problem. But in some cases, image smoothing preprocessing is still required. The author uses the directional curvature modulus to measure the smoothness of the image and deduces an image smoothing method based on the fourth-order partial differential equation from the functional, the processing result is a piecewise linear image, and there is a step in the gradient of the target edge. On this basis, we propose a new geodesic active contour model. Experimental results show that, using the noise reduction method as preprocessing, the segmentation effect of edge-based and region-based active contour models has been greatly improved.

## 3. Research Methods

*3.1. Anisotropic Diffusion Method.* The feature blurring caused by Gaussian filtering is mainly because the degree of diffusion is consistent across all image locations and does not distinguish features from noise [11]. If it is used as a feature detection operator to reduce the diffusion in the area with larger  $\nabla I$ , the features can be protected more, and the diffusion coefficient of the following formula is proposed

$$c(|\nabla I_0|) = \frac{1}{\sqrt{1 + (|\nabla I_0|^2/k^2)}}. \quad (1)$$

Among them,  $k > 0$  is used to judge features.

The diffusion equation corresponding to equation (1) is the following equation

$$\frac{\partial I}{\partial t} = \text{div} (c(|\nabla I_0|)\nabla I). \quad (2)$$

Compared with Gaussian filtering, equation (2) is more ideal for feature preservation. But on the other hand, when the time  $t$  is large, some pseudoedges that reflect the differential structure of the original image appear in the smooth image [12].

The easiest way to remove these false edges is to provide feedback to the diffusion coefficient  $c(\cdot)$  in the iterative process, so that it is adjusted according to the current image  $I(x, y, t)$  at time  $t$ , rather than calculated according to  $I_0$ . Accordingly, Perona and Malik proposed their famous P-M method as shown in the following formulas:

$$\frac{\partial I}{\partial t} = \text{div} (c_{P-M}(|\nabla I|)\nabla I). \quad (3)$$

Among

$$c_{P-M}(|\nabla I|) = \frac{1}{1 + (|\nabla I|/k)^2}. \quad (4)$$

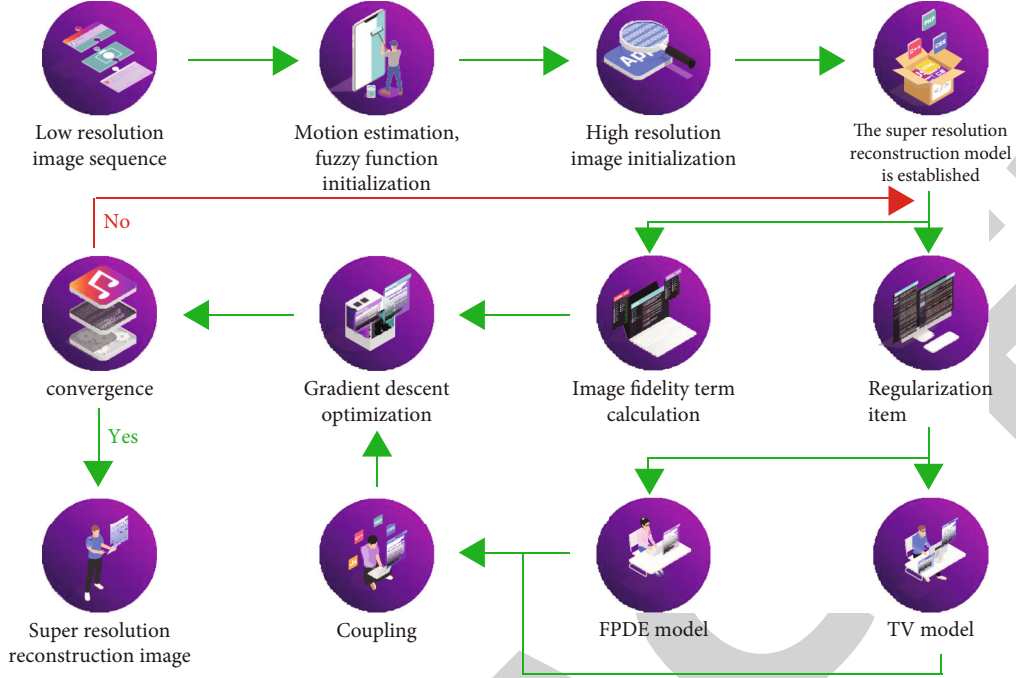


FIGURE 1: Computer microscope image of fourth order partial differential equation smoothing.

Or

$$c_{P-M}(|\nabla I|) = \exp\left(-\left(\frac{|\nabla I|}{k}\right)^2\right). \quad (5)$$

The P-M method does not have the blurring and “boundary drift” of Gaussian filtering, nor does it exist the pseudoedge of formula (2), it also has a strengthening effect on some features (such as brain outline), and the effect is ideal.

The P-M method has attracted extensive attention due to its good characteristics and has been rapidly applied to various fields of image processing; however, with the deepening of research, many problems of the P-M method have gradually emerged [13].

Starting from the one-dimensional signal, we analyze the reasons for the “ill-conditioned” and feature strengthening effects of the P-M method, then focus on the “staircase” effect of the P-M method, and give solutions to partial differential equations in the following chapters.

Set the flow function as follows

$$\Phi(s) = s * c(s). \quad (6)$$

If  $\Phi(s)$  is monotonically increasing; then, the P-M method is regular, and equation (3) is guaranteed to have a unique solution. But in the case of the actual diffusion coefficient such as (4),  $\Phi(s)$  can only guarantee a partial increase, as shown in Figure 2. At this time, the flow  $\Phi(s)$  satisfies  $\Phi(s) \geq 0, s \leq k; \Phi(s) < 0, s > k$ .

The reason why the P-M method produces the “staircase” effect is that its partial differential equation is the decisive factor. From the above, it can be seen that both image

smoothing and feature enhancement of the P-M method are performed autonomously. In a homogeneous region with a smaller gradient  $|\nabla I|$ , the diffusion coefficient  $c(|\nabla I|)$  is larger, and the diffusion proceeds rapidly, further reducing the gradient in this region and reducing noise. In the characteristic region with a larger gradient  $|\nabla I|$ , the diffusion coefficient  $c(|\nabla I|)$  is smaller, the diffusion is weakened, and a weak “barrier” is formed. As diffusion progresses, these barriers are strengthened by backward diffusion and rapidly evolve into discontinuities with infinite gradients and zero diffusion coefficients, called “shocks.” Accordingly, features are consolidated and maintained.

The bidirectional diffusion coefficient is the following equations:

$$c_1(s) = \frac{1}{1 + (s/k_f)^p} - \frac{\alpha}{1 + ((s - k_b)/\omega)^{2q}}. \quad (7)$$

$$c_2(s) = \begin{cases} 1 - \left(\frac{s}{k_f}\right)^p, & 0 \leq s \leq k_f, \\ \alpha \left[ \left(\frac{(s - k_b)}{\omega}\right)^{2q} - 1 \right], & k_b - \omega \leq s \leq k_b + \omega, \\ 0, & \text{otherwise.} \end{cases} \quad (8)$$

3 and 4 are schematic diagrams of diffusion coefficients  $c_1$  and  $c_2$  and flow rates, respectively. As can be seen, the diffusion coefficient of the P-M method is always greater than zero, although the gradient decreases rapidly after the gradient is greater than the threshold value  $k$ , the diffusion to the corresponding feature area is reduced, but the smoothing of

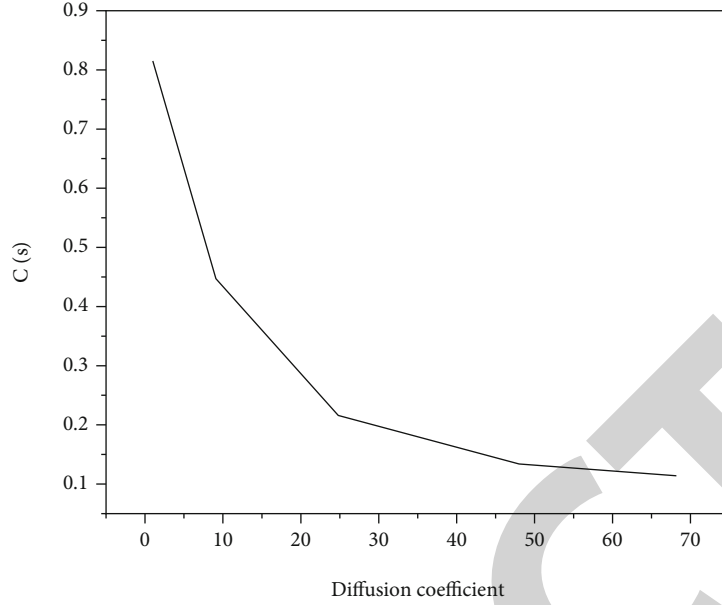


FIGURE 2: Diffusion coefficient and flow rate of P-M.

the important content of the image still exists. Whereas the bidirectional diffusion shown in Figures 3 and 4 consists of parameters  $k_f$ ,  $k_b$ , and  $\omega$ . The joint control includes both the smoothing of low-gradient noise and homogeneous regions, the enhancement of mid-gradient feature regions, and the prohibition of diffusion on high-gradient regions. Experiments show that bidirectional diffusion is an effective image smoothing and sharpening method, the processing results are not affected by “stairs,” and the details in the image can be well preserved.

Compared with the diffusion coefficient of P-M type, the diffusion coefficient of bidirectional diffusion is essentially the same, and both use the threshold to divide the image into two parts: feature and noise, but the processing of features is different. In order to obtain a better feature enhancement effect, the two-way diffusion must strictly control the range of backward diffusion [14].

**3.2. Image Smoothing Based on Fourth-Order Partial Differential Equations.** Consider the image function  $I$  as a surface defined in the three-dimensional space  $(x, y, I(x, y))$ , as shown in Figure 5, determine a point  $p$  and a certain direction  $\vec{d}$ , on  $I$ ; then, the change of the surface normal vector  $\vec{n}$  of point  $p$  in the direction  $\vec{d}$  is expressed by the directional curvature. The directional curvature is a second-order description of the speed of surface change along the tangent direction of a point on the surface, and it can quantitatively express the change of the surface around a point [15]. An operator describing the (direction) curvature modulus is the following formula:

$$m^2 = 0.5 \cdot (I_{xx}^2 + I_{yy}^2) + I_{xy}^2. \quad (9)$$

Therefore, we consider the following functional defined on the region  $\Omega$  as the following formula:

$$E(I) = \int_{\Omega} F(m^2) dx dy \quad (10)$$

Among them,  $m^2$  is as in formula (9),  $\in C^4(\Omega)$ . Function  $F(\cdot) \geq 0$  is an increasing function, i.e.,  $F'(\cdot) > 0$ . The operator  $m^2$  can describe the roughness of the local surface. Therefore, the greater the roughness (noise) of the image surface  $I$ , the greater the functional value of (10), and minimizing  $E(I)$  is equivalent to image smoothing. The Euler equation about (11) is obtained by using the variational method:

$$\frac{\partial^2}{\partial x^2} (F'(m^2) I_{xx}) + 2 \frac{\partial}{\partial x \partial y} (F'(m^2) I_{xy}) + \frac{\partial}{\partial y^2} F'(m^2) I_y = 0. \quad (11)$$

The Euler equation shown in equation (11) can be solved by the gradient descent method as the following equations:

$$\frac{\partial I}{\partial t} = - \left[ \frac{\partial^2}{\partial x^2} \left( \begin{matrix} F'(m^2) \\ I_{xx} \end{matrix} \right) + 2 \frac{\partial^2}{\partial x \partial y} (F'(m^2) I_{xy}) + \frac{\partial^2}{\partial y^2} (F'(m^2) I_{yy}) \right]. \quad (12)$$

Among

$$F'(m^2) = \frac{1}{1 + (m^2/K^2)}. \quad (13)$$

For the conduction function,  $K$  is the conduction coefficient threshold, and choosing different  $K$  values can control the preservation and smoothing of different image features.

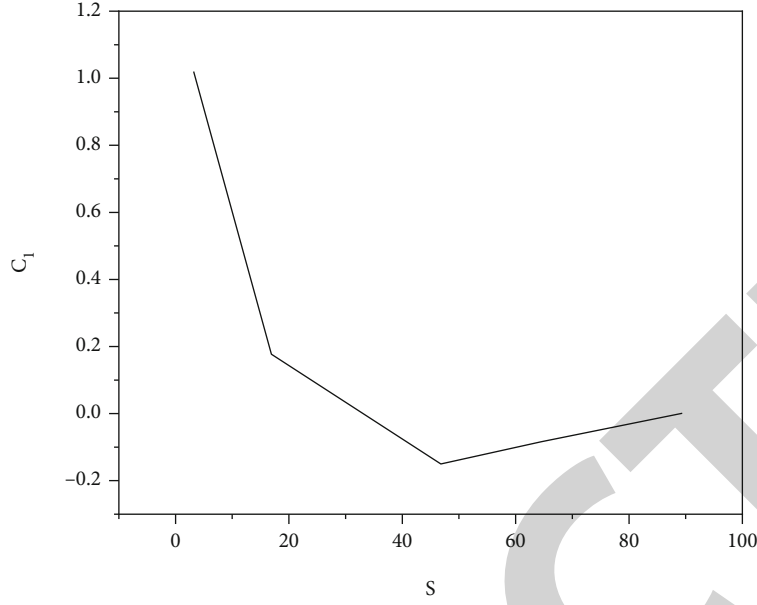


FIGURE 3: Diffusion coefficient and flow.

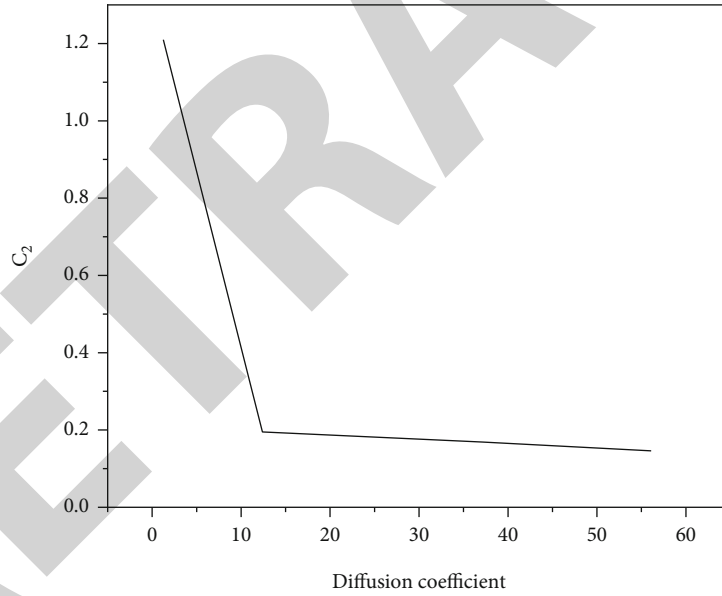


FIGURE 4: Diffusion coefficient and flow.

Taking the original image as input, the final solution is obtained when  $t \rightarrow \infty$ . In order for the image not to be oversmoothed, the iteration must be terminated with a time limit [16].

The image whose grayscale function satisfies the plane equation is a linear image (planar image). Obviously, when the image  $I$  is a linear image, the gradient  $\nabla I = \partial I / \partial x \vec{i} + \partial I / \partial y \vec{j}$  is constant, the Laplace calculation  $\nabla^2 I$  is zero, the value of operator  $m^2 = 0.5 \cdot (I_{xx}^2 + I_{yy}^2) + I_{xy}^2$  is also zero,

and at this time, the left-hand side of equation (13) is equal to the following equation:

$$\begin{aligned}
 &F'(0)(I_{xxxx} + 2I_{xxyy} + I_{yyyy}) =, \\
 &F'(0)\left(\frac{\partial^2}{\partial x^2}(I_{xx} + I_{yy}) + \frac{\partial^2}{\partial y^2}(I_{xx} + I_{yy})\right) =, \quad (14) \\
 &F'(0)\left(\frac{\partial^2}{\partial x^2}(\nabla^2 I) + \frac{\partial^2}{\partial y^2}(\nabla^2 I)\right) = 0.
 \end{aligned}$$



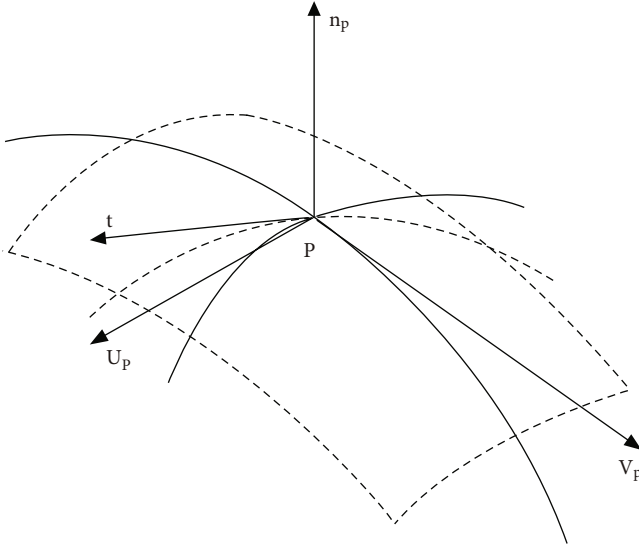


FIGURE 5: Schematic diagram of directional curvature.

It can be seen that the linear image satisfies Euler's equation (14). Since the function  $F(\cdot)$  is nonnegative, the functional  $E(I)$  satisfies the following equation:

$$E(I) \geq 0. \quad (15)$$

At the same time, the function  $F(m^2)$  is an increasing function, and the global minimum is obtained when  $m^2 = 0$  is a linear image, that is, the global minimum of the functional  $E(I)$  [17].

There may also be other minima of the functional  $E(I)$ ; below, we prove that the piecewise linear image satisfies the Euler equation.

Let  $\Omega_i, i = 1, 2, \dots, n$  be the division of the image area  $\Omega$ , and the piecewise linear image is the following formula:

$$I(x, y) = \sum_{i=1}^n I_i(x, y). \quad (16)$$

Among

$$I_i(x, y) = \begin{cases} \text{planar image, } (x, y) \in \Omega_i, \\ 0. \end{cases} \quad (17)$$

$I_i \in C^4(\Omega_i)$ , the composite image  $I(x, y)$  should be continuous. Any two adjacent images  $I_i$  and  $I_j$  shown in equation (17) must satisfy different plane equations; otherwise, the two can be merged.  $\partial\Omega_i$  is the boundary of the area  $\Omega_i$ ,  $\Omega_i - \partial\Omega_i$  is the interior of  $\Omega_i$ , which satisfies the following equations:

$$\nabla I_i(x, y) = \text{constant } (x, y) \in (\Omega_i - \partial\Omega_i), \quad (18)$$

$$\nabla^2 I_i(x, y) = 0, \quad (19)$$

Among them,  $(x, y) \in (\Omega_i - \partial\Omega_i), i = 1, 2, \dots, n$ .

So as the following formula:

$$\begin{aligned} \nabla^2 I(x, y) &= 0, \\ m^2(x, y) &= 0.5^\circ (I_{xx}^2 + I_{yy}^2) + I_{xy}^2 = 0. \end{aligned} \quad (20)$$

Among them,  $(x, y) \in (\Omega - \partial\Omega), \partial\Omega = \bigcup_{i=1}^n \partial\Omega_i$ . Since any two adjacent  $I_i$  and  $I_j$  are on different planes, the gradient on the boundary  $\partial\Omega$  is discontinuous, that is, as in the following equations:

$$\nabla I_i \neq \nabla I_j. \quad (21)$$

Then

$$\nabla^2 I(x, y) = \infty, (x, y) \in \partial\Omega. \quad (22)$$

For operator  $m^2(x, y)$ , as in the following equation

$$\begin{aligned} m^2 &= \frac{1}{2} (I_{xx}^2 + I_{yy}^2) + I_{xy}^2 = \frac{I_{xx}^2 + I_{yy}^2 + I_{yy}^2 + I_{xy}^2}{2} \geq, \\ \frac{2I_{xx}I_{xy} + 2I_{yy}I_{xy}}{2} &= I_{xy}(I_{xx} + I_{yy}) = I_{xy}\nabla^2 I. \end{aligned} \quad (23)$$

Among them  $(x, y) \in \partial\Omega$ . If  $I_{xy}$  is equal to zero, then

$$\begin{aligned} m^2 &= \frac{1}{2} (I_{xx}^2 + I_{yy}^2) + I_{xy}^2 = \frac{I_{xx}^2 + I_{yy}^2}{2}, \\ (\nabla^2 I(x, y))^2 &= \infty = I_{xx}^2 + I_{yy}^2 + 2I_{xx}I_{yy} \leq 2(I_{xx}^2 + I_{yy}^2). \end{aligned} \quad (24)$$

So the following formulas are obtained:

$$m^2 = \frac{1}{2} (I_{xx}^2 + I_{yy}^2) + I_{xy}^2 = \infty. \quad (25)$$

Then

$$F'(\infty) = 0. \quad (26)$$

If  $I_{xx}$  is equal to infinity ( $\infty$ ), then

$$F'(m^2)I_{xx} = \frac{1}{(1/I_{xx}) + (0.5 * (I_{xx} + (I_{yy}^2/I_{xx}))) + (I_{xy}^2/I_{xx})/K^2} = 0. \quad (27)$$

The situation is similar for  $I_{xx}$  and  $I_{yy}$ .

Therefore, when  $I$  is a piecewise linear image as in the following equation:

$$\begin{aligned} \frac{\partial^2}{\partial x^2} (F'(m^2)I_{xx}) + 2 \frac{\partial^2}{\partial x \partial y} (F'(m^2)I_{xy}) + \frac{\partial^2}{\partial y^2} F'(m^2)I_{yy} &= 0, \\ (x, y) &\in \Omega. \end{aligned} \quad (28)$$

It can be seen that the piecewise linear image satisfies the Euler equation.

**3.3. A New Geodesic Active Contour Model Based on the Smoothing of Fourth-Order Partial Differential Equations.** The geodesic active contour (GAC) proposed by Shokri and Pishbin is a model based on the curve evolution theory and the level set method; without any external control conditions, it is one of the most widely used edge models to deal with topological changes in curved motion freely [18].

The geodesic active contour uses the function  $g(I)$  to identify the image features (such as edges) and aims to minimize the energy function, and the motion equation corresponding to the contour curve  $C$  is the following formula:

$$\frac{\partial C}{\partial t} = g(I)(k + V_0)\vec{N} - (\nabla g(I) \cdot \vec{N})\vec{N}, \quad (29)$$

where  $k$  is the curvature of the curve,  $\vec{N}$  is the normal unit vector of the curve, and  $V_0$  is a constant.  $g(I)$  takes a minimum value at the edge, often using the following formula:

$$g(I) = \frac{1}{1 + |\nabla[G_\sigma * I]|^2}, \quad (30)$$

where  $G_\sigma$  represents a two-dimensional Gaussian filter operator with standard deviation  $\sigma$ , and  $*$  is a convolution operator.

The last term  $g(I)$  in equation (29) is the edge attractive force, which is an image force that points to the edge in the image. When the curve moves near the target edge, this term exerts an external force on the curve directed towards the edge, thereby pulling the curve towards the target [19]. In actual image processing, the target edge is not an ideal edge, and  $g(I)$  is not zero at the edge. At this time, the curve movement is terminated near the target by relying on the balance between the edge attraction force and the force of the first term in equation (29), so the target localization performance is limited [20, 21].

Based on the denoising model derived by the author for image smoothing, we propose a new edge identification function as follows:

$$G(I) = \frac{1}{1 + |\nabla^2 I|^2}. \quad (31)$$

And the corresponding new geodesic active contour (New-GAC) model is as follows:

$$\frac{\partial C}{\partial t} = g(I)(k + V_0)\vec{N} - (\nabla G(I) \cdot \vec{N})\vec{N}. \quad (32)$$

From the above, we know that selecting different  $K$  can control the smoothing of image features, the smoothed image is a piecewise linear image, and there is a step in the gradient at the target edge, that is, the following formula:

$$\nabla^2 I(x, y) = \infty, (x, y) \in \partial\Omega. \quad (33)$$

Therefore, the new edge identification function (31) can better achieve the effect of the ideal geodesic active contour model [22].

In the experimental results section, we will see that compared with the traditional geodesic active contour model, and the new geodesic active contour model proposed by the author is more ideal in edge localization [23–25].

## 4. Analysis of Results

The segmentation effect of the traditional geodesic model and the new model proposed by the author is compared, both of them segment the results processed by the noise reduction method. Among them, select the conduction coefficient threshold  $K = 2.0$ , and iterate 100 times. The segmentation result of the traditional geodesic model, with 514 iterations, takes 67.938 seconds. New-GAC segmentation results, iterating 310 times, takes 38.165 seconds. Traditional GAC uses gradient as edge detection operator, which is easily affected by nontarget features; however, New-GAC uses the Laplacian operator to detect and makes full use of the characteristics of noise reduction results. Not only the number of iterations is less, the time-consuming is shorter, but the segmentation results are also better than those of traditional GAC.

Examining the effect of noise reduction models on region-based active contour models. The author chooses the direct segmentation method because the model in the direct segmentation method is very robust and robust. Using the processing results of the noise reduction method, the threshold  $K = 3.5$  is selected, and the iteration is performed 300 times. The method iterates 10 times and takes 160.721 seconds. Using the noise reduction model to preprocess, and then using the direct segmentation method to segment the result, iterating 8 times, it takes 32.347 seconds. Although the global optimal division method has a certain robustness to noise, it is still greatly affected by it, after preprocessing using the author's method, the target edge is consolidated and strengthened, the number of iterations is reduced, the time consumption is greatly reduced, and the segmentation effect is reduced, also greatly improved.

## 5. Conclusion

The author proposes a functional describing the smoothness of the image based on the directional curvature modulus value and derives a fourth-order partial differential equation (PDE) image noise reduction model, the processing result is a piecewise linear image (including linear images), and there is a step in the gradient at the edge. Taking advantage of this feature, the authors propose a new geodesic active contour (New-GAC) model, which improves the contour extraction performance of traditional GAC and is much faster. It is worth noting that New-GAC makes full use of the characteristics of the denoising model derived by the author to process the results, and the two together constitute a new image segmentation method. The region-based active contour model has a certain robustness to noise, but the processing of strong noise maps is still limited, and the noise

## Retraction

# Retracted: Effect of Microscope Combined with Wechat Smart Platform on Clinical Efficacy and Gastrointestinal Function of Patients with Cholecystolithiasis Combined with Common Bile Duct Stones

### Scanning

Received 20 June 2023; Accepted 20 June 2023; Published 21 June 2023

Copyright © 2023 Scanning. This is an open access article distributed under the Creative Commons Attribution License, which permits unrestricted use, distribution, and reproduction in any medium, provided the original work is properly cited.

This article has been retracted by Hindawi following an investigation undertaken by the publisher [1]. This investigation has uncovered evidence of one or more of the following indicators of systematic manipulation of the publication process:

- (1) Discrepancies in scope
- (2) Discrepancies in the description of the research reported
- (3) Discrepancies between the availability of data and the research described
- (4) Inappropriate citations
- (5) Incoherent, meaningless and/or irrelevant content included in the article
- (6) Peer-review manipulation

The presence of these indicators undermines our confidence in the integrity of the article's content and we cannot, therefore, vouch for its reliability. Please note that this notice is intended solely to alert readers that the content of this article is unreliable. We have not investigated whether authors were aware of or involved in the systematic manipulation of the publication process.

Wiley and Hindawi regrets that the usual quality checks did not identify these issues before publication and have since put additional measures in place to safeguard research integrity.

We wish to credit our own Research Integrity and Research Publishing teams and anonymous and named

external researchers and research integrity experts for contributing to this investigation.

The corresponding author, as the representative of all authors, has been given the opportunity to register their agreement or disagreement to this retraction. We have kept a record of any response received.

### References

- [1] X. Xu, D. Guo, Y. Zhang et al., "Effect of Microscope Combined with Wechat Smart Platform on Clinical Efficacy and Gastrointestinal Function of Patients with Cholecystolithiasis Combined with Common Bile Duct Stones," *Scanning*, vol. 2022, Article ID 9661506, 5 pages, 2022.

## Research Article

# Effect of Microscope Combined with Wechat Smart Platform on Clinical Efficacy and Gastrointestinal Function of Patients with Cholecystolithiasis Combined with Common Bile Duct Stones

Xu Xu , Dongmei Guo , Yan Zhang , Dandan Yang , Guangbin Hou , Quanfu Li , Changqing Ge , Zengwang Qie , and Yonggang Zhong 

Department of Hepatobiliary Surgery, Second Hospital of Baoding, Baoding, Hebei 071051, China

Correspondence should be addressed to Quanfu Li; 20163064@ayit.edu.cn

Received 5 May 2022; Revised 20 May 2022; Accepted 16 June 2022; Published 30 June 2022

Academic Editor: Balakrishnan Nagaraj

Copyright © 2022 Xu Xu et al. This is an open access article distributed under the Creative Commons Attribution License, which permits unrestricted use, distribution, and reproduction in any medium, provided the original work is properly cited.

To explore the clinical efficacy of microscope combined with Wechat smart platform in patients with cholecystolithiasis and choledocholithiasis, this paper proposes the effect of microscope combined with Wechat smart platform intervention after laparoscopic lithotomy and choledocholithotomy on the clinical efficacy and gastrointestinal function of patients with cholecystolithiasis combined with choledocholithiasis. From February 2018 to March 2019, 78 patients with gastric cancer were selected by our clinic and included in the research team. Evaluate the efficacy of endoscopic biliary lithotomy (LBL) + bile duct lithotomy (TBL) + T-tube drainage therapy to provide reliable evidence for improved efficacy and efficacy in order to provide a strong reference for improving the effectiveness and safety of surgical treatment of choledocholithiasis. Safety of surgical treatment of diseases. Gallstone disease. The experiments did not show any significant differences between the two groups during surgery. Diabetes was lower in the control group, and hospital incidence was lower in the control group. There were no significant differences between the two groups for preoperative WHOQOL-100 scores. Two weeks and four weeks after surgery, the man-key-100 score was higher than that of the control group. Endoscopic cholecystectomy + choledocholithotomy + choledochoscopic lithotomy + T-tube fluid have been shown to be effective in promoting rapid intestinal function and improving patient quality of life and are appropriate for therapeutic use.

## 1. Introduction

Nowadays, young adults rely more on the online world for interpersonal communication. Wechat platform is a highly influential interactive information dissemination platform, which not only has text function, but also can add pictures, voice, and video. Through the health publicity of Wechat platform, patients and their families can obtain effective nursing knowledge related to diseases more directly and quickly [1]. It not only saves human resources, but also enables patients to continue to obtain relevant knowledge after discharge, and can communicate with medical staff anytime and anywhere. It is an efficient way of work. The degree of nursing knowledge of minimally invasive operation for gallstones was investigated in the continuous care

of patients. By investigating the patients' awareness of gallbladder disease and their satisfaction with health education, the clinical efficacy of wechat platform health education in the continuous care of patients undergoing minimally invasive gallstone surgery was explored [2, 3]. The incidence rate is about 12% ~ 18%. The incidence rate of gallstone is rising because of the change of living standard. However, 8%~25% of patients have choledocholithiasis, which may lead to serious complications if effective treatment is not taken in time [4, 5]. However, the treatment of cholecystolithiasis combined with common bile duct stones is more difficult. Therefore, it is necessary to innovate the treatment scheme to improve the treatment effect of cholecystolithiasis combined with common bile duct stones, as shown in Figure 1.

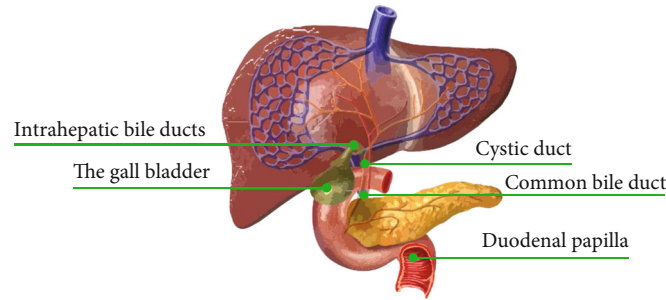


FIGURE 1: Cholecystolithiasis combined with choledocholithiasis.

TABLE 1: Comparison of surgical indexes between the two groups.

Group	Intraoperative time	Intraoperative bleeding	Postoperative hospital stay
Research group	94.37 ± 13.38	50.54 ± 10.17	6.73 ± 0.18
Control group	94.26 ± 13.32	106.61 ± 18.22	10.55 ± 0.37

TABLE 2: Comparison of postoperative intestinal function recovery between the two groups.

Group	Postoperative bowel sounds recovery time	First postoperative anal exhaust time
Research group	32.36 ± 5.12	15.34 ± 3.18
Control group	60.54 ± 9.85	41.27 ± 6.52

## 2. Literature Review

To solve this research problem, Rasheed, N. et al. studied the use of traditional open surgery for choledocholithiasis, and the postoperative complication rate was 20%, indicating that there were many postoperative complications. Laparoscopic cholecystectomy can explore and observe the abdominal cavity through high brightness and multiangle, and the operation field is enlarged under the display of endoscope, which is conducive to overall grasp and local fine operation [6]. Sebastian, M. and others used laparoscopic cholecystectomy to treat common bile duct stones. It shows that laparoscopic cholecystectomy combined with choledochotomy and choledochofiberscope lithotomy T-tube drainage can reduce blood loss and shorten abdominal drainage time, intestinal function normalization time, and hospital stay [7]. Akool, M. A. and others studied that laparoscopic cholecystectomy was used to treat common bile duct stones, and the postoperative complications were only 6% [8]. VV Boiko and others found that after cholecystectomy, it is easy to have insufficient bile, resulting in abdominal distension and diarrhea after eating. How to preserve the gallbladder and its functional integrity while ensuring the surgical effect is a hotspot in clinical research [9]. Boiko, V. V. and others performed duodenoscopy, choledochoscopy, and laparoscopy combined with cholelithotomy for the patients in the observation group. Different endoscopes can give full play to their own advantages and improve the stone clearance rate, and the clinical effect is definite [10]. Osuch, C. and others believe that after cholecystectomy, although the recurrence

of gallstones can be avoided, there is compensatory expansion of common bile duct, resulting in narrow opening of duodenal papilla, resulting in the change of bile flow characteristics of common bile duct, and increasing the recurrence rate of common bile duct stones [11]. Klarica, L. and others found that LC combined with bile duct exploration can significantly shorten the length of incision, improve the speed of postoperative recovery, and reduce the economic burden of patients because of its use of minimally invasive technology [12]. Hao, Jiang and others used LC combined with bile duct exploration to treat common bile duct stones combined with gallbladder stones, which helps to preserve the integrity of duodenal papilla, and can treat gallbladder stones and common bile duct stones at one time, which is more in line with normal physiological conditions [13].

Based on the current research, this paper proposes the effect of laparoscopic lithotomy and choledocholithotomy with microscope combined with Wechat smart platform on the clinical efficacy and gastrointestinal function of patients with cholecystolithiasis combined with choledocholithiasis. Laparotomy was performed in the study group and in the control group. There were no significant differences in the operating time of the two groups.

## 3. Method

3.1. *Data.* The medical records of 78 gallstones patients treated in our hospital from February 2018 to March 2019 were divided into two groups, with 39 patients in each group. The control group included 21 males and 18 females. Age range is 26 to 73 years and average (48.31 ± 2.11) years. The course of disease is 1 ~ 11 years, the average (5.57 ± 0.24) years. 21 men and 18 women on the board. Ages are between 25 and 74 years and average (48.33 ± 2.12) years. The course of disease is 1-11 years, the average (5.55 ± 0.25) years. There was no significant difference in clinical data such as gender and age between the two groups, indicating comparability. This study was approved by the Medical and Ethical Research Institute of our hospital. Inclusion criteria: surgical treatment was required for choledocholithiasis. Patients should be conscious and can actively cooperate with this study. In this study, laparoscopic cholecystectomy, choledochotomy, choledochoscopic lithotomy and T tube drainage were well tolerated, and there were no relevant contraindications. The number of calculi was less than 5 and the maximum diameter of calculi was less than 2 cm; patients and their families were fully

TABLE 3: Comparison of postoperative complications between the two groups.

Group	Subcutaneous effusion	Subcutaneous emphysema	Incision infection	Abdominal infection	Acute cholangitis	Acute pancreatitis	Total
Research group	0	2.57	0	0	0	2.57	5.14
Control group	7.68	0	2.57	2.57	2.57	0	17.96

TABLE 4: Comparison of wh0qol-100 scores between the two groups.

Group	Preoperative	2 weeks after operation	4 weeks after operation	8 weeks after operation
Research group	64.36 ± 6.12	72.55 ± 3.69	79.83 ± 3.92	85.27 ± 3.65
Control group	64.37 ± 6.11	64.32 ± 6.09	73.37 ± 4.56	85.26 ± 3.67

informed of the study contents and signed relevant agreements. Exclusion criteria are as follows: patients with recurrent choledocholithiasis [14, 15]; patients with other gallbladder diseases; patients with a history of abdominal surgery; patients with malignant tumors; female patients with choledocholithiasis in special physiological periods such as pregnancy, puerperium, and lactation; persons with mental illness; and those who refuse to sign informed consent [16].

### 3.2. Method

#### (1) Surgical Methods of Study Group

The study group was treated with laparoscopic cholecystectomy + common bile duct incision, choledochoscopic lithotomy + T-tube drainage. The details were as follows: drinking and fasting for 8 hours before operation, continuous ECG monitoring and oxygen inhalation after entering the room, and routine general anesthesia; the four hole method was used to enter the abdominal cavity, effectively separate the gallbladder triangle, and remove the gallbladder; fine needle puncture to confirm the position of the common bile duct, make a longitudinal incision (length 0.5 ~ 1.0 cm) on the front wall of the common bile duct, select the appropriate specification of choledochoscope according to the diameter of the common bile duct, and place it through the operation hole; routinely explore the location, quantity, and size of common bile duct stones, and reasonably expand the incision according to the exploration results [17]; the stones in the common bile duct were taken out with the stone taking basket, and the choledochoscope was used to explore again to determine whether there were stones left in the common bile duct and intrahepatic bile duct and to confirm that the duodenal papilla was unblocked; after washing the common bile duct effectively with 0.9% sodium chloride solution, place a "t" tube for drainage, close the incision of the common bile duct, place the drainage tube in the small omental hole, and close each incision of the abdominal wall. One month after operation, pull out the drainage tube after the T-tube cholangiography is clear that there is no stone residue and the common bile duct is unobstructed [18, 19].

(2) The details were as follows: the preoperative preparation was the same as that of the study group. After

general anesthesia, take the middle of the upper abdomen (slightly to the right) to make a straight incision, routinely explore the gallbladder, dissect the gallbladder triangle, and remove the gallbladder (combination of forward and reverse). After the common bile duct was cut, the stones were taken out, and the "t" drainage tube was routinely placed; the postoperative treatment was the same as that in the study group

3.3. *Observation Indicators.* Intestinal function: The recovery time of intestinal sounds and the first exhaust time of anus were recorded in the two groups. Complications: The occurrences of postoperative abdominal infection, acute cholangitis, acute pancreatitis, and other complications in the two groups were recorded [20]. Quality of life: The world Health Organization (WHO) quality of life measurement scale was used. The scores of each item of the WHOQOL-100 scale were 0 ~ 4 (involving social relations, psychology, environment, physiology, independence, spiritual pillar and other evaluation contents). The total score was 0 ~ 100 [21, 22].

## 4. Results

4.1. *Comparison of Surgical Indexes between the Two Groups.* Diabetes mellitus is lower in the control group, and after hospitalization, it is lower in the control group, with a significant difference ( $P < 0.05$ ), as shown in Table 1.

4.2. *Comparison of Intestinal Function between the Two Groups.* In the study group, postoperative bowel noise and the first time postoperative rectal excretion time are shorter in the control group as shown in Table 2 ( $P < 0.05$ ).

4.3. *Comparison of Complications between the Two Groups.* No patients had two or more problems occurring at the same time in this study. The incidence of problems in the control group was lower than in the control group, and the difference was significant ( $P < 0.05$ ) (see Table 3).

4.4. *Comparison of Quality of Life between the Two Groups.* There was no significant difference between the two groups in preoperative WHOQOL-100 scale score, at 2 and 4 weeks after operation (see Table 4 and Figure 2).

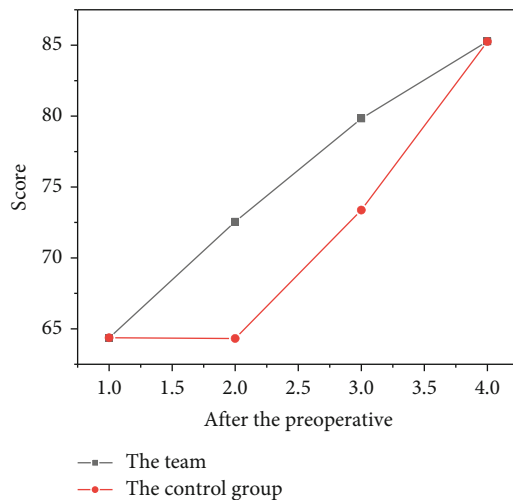


FIGURE 2: Comparison of wh0qol-100 scale scores between the two groups.

**4.5. Discussion.** The open surgery operation has been used in clinic to provide good surgical field for the operator and obtain ideal stone clearance rate. However, the patients with large trauma and high blood loss are not conducive to postoperative health recovery, and the incidence rate of postoperative complications is high, which may increase the hospitalization time and treatment cost of [23, 24]. Endoscopic retrograde cholangiopancreatography choledocholithotomy has been gradually applied to the treatment of choledocholithiasis. However, after this operation, the patient needs to choose another time for laparoscopic cholecystectomy, and the patient will suffer secondary trauma. Therefore, it is not conducive for them to actively accept this scheme and cooperate with the treatment room. Laparoscopic cholecystectomy + choledocholithotomy + choledochoscopy + T-tube drainage is one of the minimally invasive treatment schemes for choledocholithiasis popularized in the clinic at this stage. During the operation, choledochoscopy is used to explore the local bile duct lesions and take stones with the help of laparoscope, which can effectively reduce the surgical trauma and bleeding [25]. In addition, laparoscopic cholecystectomy + choledochotomy, choledochoscopic lithotomy + T-tube drainage can completely preserve the structure of duodenal papillary sphincter, reduce the risk of abnormal conditions such as biliary infection and intestinal reflux, and solve the operations such as lithotomy and cholecystectomy at one time, which can effectively avoid the injury of patients after secondary surgery, which is of great significance to promote the recovery of patients' health as soon as possible and ensure their quality of life. Postoperative intestinal function recovery, postoperative complications, postoperative quality of life, and other indicators of the study group are treated with laparoscopic cholecystectomy + choledochotomy + choledochoscopy + T-tube drainage.

Cholecystolithiasis combined with choledocholithiasis is a common surgical disease. With the continuous maturity of endoscopic technology such as choledochoscopy, laparoscopy, and duodenoscopy and the deepening of minimally

invasive concept, in recent years, there are many reports on the combination of endoscopic cholangiopancreatography, duodenal papillotomy, bile duct stone removal, and laparoscopic cholecystectomy. However, some scholars believe that the above operation requires cholecystectomy, which may damage the bile duct and cause a variety of complications. Another study found that after cholecystectomy, it is easy to have insufficient bile, resulting in abdominal distension and diarrhea after eating. How to preserve the gallbladder and its functional integrity while ensuring the surgical effect is a hotspot in clinical research.

## 5. Conclusion

In this paper, the combination of choledoscopy, choledochoscopy, and choledochoscopy for choledochoscopy shows that postoperative bowel movements in patients with gallstones affect the quality of life and the treatment rate of fluid in patients with gallstones. The 78 patients with biliary tract disease treated between February 2018 and March 2019 were divided into two groups, with 39 patients in each group. Bleeding was less in the control group during the study and less in the hospital after surgery than in the control group ( $P < 0.05$ ). Previously, there was no difference between the two groups of WHOQOL-100 scores. The WHOQOL-100 score in the study group was higher in the control group between 2 and 4 weeks after work ( $P < 0.05$ ). Endoscopic cholecystectomy + choledoscopy + T bronchial fluid plays an important role in the treatment of gallstones, which improves the function of the digestive tract and improves the patient's quality of life.

## Data Availability

The data used to support the findings of this study are available from the corresponding author upon request.

## Conflicts of Interest

The authors declare that they have no conflicts of interest.

## References

- [1] M. M. Halei, I. Y. Dziubanovskyi, and I. P. Marchuk, "Comparison of quality of life in postoperative patients with cholecystolithiasis and choledocholithiasis. The difference between open and laparoscopic treatment," *Biomedical and Biosocial Anthropology*, vol. 36, no. 36, pp. 47–51, 2020.
- [2] L. Feng, Z. You, J. Gou, E. Liao, and L. Chen, "Xanthogranulomatous cholecystitis: experience in 100 cases," *Annals of Translational Medicine*, vol. 8, no. 17, pp. 1089–1089, 2020.
- [3] M. Yang and Y. Shi, "Diagnostic value of ultrasound combined with mri in cholecystolithiasis: a protocol for systematic review and meta analysis," *Medicine*, vol. 100, no. 19, article e25896, 2021.
- [4] I. Vagelj, M. Vuko, M. Hrskanovi, and D. Vagelj, "Angiodysplasia of the gallbladder: an unknown risk factor for cholecystolithiasis," *Case Reports in Pathology*, vol. 2020, 3 pages, 2020.
- [5] B. Migda, M. A. Gabryelczak, A. Migda, and K. Prostacka, "A rare complication of cholecystolithiasis: perforation of the

## Retraction

# Retracted: Observation on the Effect of Rehabilitative Physical Training on Sports Injuries under Ultrasound Image Examination

### Scanning

Received 11 July 2023; Accepted 11 July 2023; Published 12 July 2023

Copyright © 2023 Scanning. This is an open access article distributed under the Creative Commons Attribution License, which permits unrestricted use, distribution, and reproduction in any medium, provided the original work is properly cited.

This article has been retracted by Hindawi following an investigation undertaken by the publisher [1]. This investigation has uncovered evidence of one or more of the following indicators of systematic manipulation of the publication process:

- (1) Discrepancies in scope
- (2) Discrepancies in the description of the research reported
- (3) Discrepancies between the availability of data and the research described
- (4) Inappropriate citations
- (5) Incoherent, meaningless and/or irrelevant content included in the article
- (6) Peer-review manipulation

The presence of these indicators undermines our confidence in the integrity of the article's content and we cannot, therefore, vouch for its reliability. Please note that this notice is intended solely to alert readers that the content of this article is unreliable. We have not investigated whether authors were aware of or involved in the systematic manipulation of the publication process.

In addition, our investigation has also shown that one or more of the following human-subject reporting requirements has not been met in this article: ethical approval by an Institutional Review Board (IRB) committee or equivalent, patient/participant consent to participate, and/or agreement to publish patient/participant details (where relevant).

Wiley and Hindawi regrets that the usual quality checks did not identify these issues before publication and have since put additional measures in place to safeguard research integrity.

We wish to credit our own Research Integrity and Research Publishing teams and anonymous and named external researchers and research integrity experts for contributing to this investigation.

The corresponding author, as the representative of all authors, has been given the opportunity to register their agreement or disagreement to this retraction. We have kept a record of any response received.

### References

- [1] L. Wang and H. Wang, "Observation on the Effect of Rehabilitative Physical Training on Sports Injuries under Ultrasound Image Examination," *Scanning*, vol. 2022, Article ID 9998265, 7 pages, 2022.



## Research Article

# Observation on the Effect of Rehabilitative Physical Training on Sports Injuries under Ultrasound Image Examination

Lanfeng Wang  and Haoyu Wang 

Gdansk University of Physical Education and Sport, Gdansk, Poland

Correspondence should be addressed to Haoyu Wang; [2021720147@yangtzeu.edu.cn](mailto:2021720147@yangtzeu.edu.cn)

Received 8 May 2022; Revised 9 June 2022; Accepted 16 June 2022; Published 29 June 2022

Academic Editor: Balakrishnan Nagaraj

Copyright © 2022 Lanfeng Wang and Haoyu Wang. This is an open access article distributed under the Creative Commons Attribution License, which permits unrestricted use, distribution, and reproduction in any medium, provided the original work is properly cited.

In order to observe the effect of rehabilitative physical training on sports injuries under ultrasound examination, this study firstly carried out experiments, induction and analysis of ultrasound examination, and evaluation-related content, especially the diagnosis of ultrasound examination in muscle and tendon injuries caused by various reasons. And the clinical application of treatment (clinical research) is reviewed, in order to provide reference data for clinical stage summary. Then, by determining the fasciculation and location of the tendon rupture injury by ultrasound, the clinic can decide whether or not to proceed with surgery. Small Achilles tendon tears only require conservative treatment to avoid the development of complete Achilles tendon rupture. Finally, 26 patients and 10 healthy adults were examined by ultrasonography, and each subject was segmented to examine 11 muscles, including the tongue muscle. The bilateral trapezius, bilateral biceps brachii, bilateral abductor pollicis brevis, bilateral quadriceps femoris, and bilateral tibialis anterior muscles were evaluated by ultrasound and statistical methods. The experimental results show that if the fasciculation of the Achilles tendon injury does not reach more than 3/11, it indicates that no surgical treatment is required; for those with a complete tear of the Achilles tendon, the distance between the broken ends should be further measured in the toe flexion state to evaluate whether surgical treatment is required. It effectively solves the problem of visual diagnosis of sports injuries.

## 1. Introduction

Common clinical imaging diagnostic techniques mainly include X-ray, computed tomography (CT), magnetic resonance imaging (MRI), and ultrasound [1]. In the diagnosis of soft tissue lesions such as muscles and tendons, X-ray examination is difficult to clearly display soft tissue lesions, and the detection sensitivity of early lesions is poor; so, it is not applicable for the diagnosis of such diseases (Figure 1). X-ray examination is more suitable for the detection of abnormal structural changes in bones and joints. CT and MRI have clear advantages in diagnosing the anatomical details of musculoskeletal system, muscles, tendons, and other soft tissue lesions; however, its clinical application is limited by the purchase of equipment in medical institutions, whether the operating physicians have professional skills and experience, etc., there are strict requirements for

the indication population. Ultrasonography is widely used in clinical practice because of its advantages of noninvasiveness, simple operation, and quick results. Existing studies have shown that ultrasonography can detect skeletal, muscular system muscles, tendons, joints and superficial soft tissue injuries, and even deep muscle lesions. Ultrasonography can dynamically observe the movement of muscles and tendons in real time [2]. However, both CT and MRI cannot perform real-time dynamic examination, which is the main deficiency in their clinical diagnostic applications.

Computed tomography (CT), magnetic resonance imaging (MRI), and ultrasound can be used to diagnose and treat musculoskeletal disorders, both positive and negative. Compared to CT and MRI, ultrasound is easier for patients to receive and can be transmitted in a hospital for the first time. This is a normal observation. In recent years, new ultrasound technology has increased the benefits of conventional

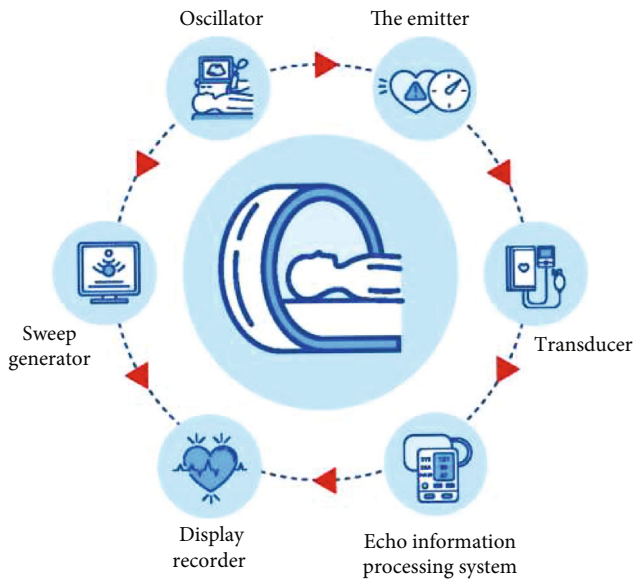


FIGURE 1: Ultrasonic examination.

ultrasound treatment and compensated for the inadequacy of imaging, especially in diagnostic and diagnostic procedures: treatment of musculoskeletal disorders. To this end, the author discusses the use of ultrasound in the diagnosis and treatment of bone and bone marrow to provide a summary of medical data [3].

## 2. Literature Review

In my country's competitive sports, "physical rehabilitation training" was formally proposed by Dr. Deshmukh et al., and it belongs to a relatively new discipline, but it does not deny that there is no relevant training in our country before [4]. Bertollo and others believe that in foreign countries, the application of rehabilitation physical training to physical training is relatively tight, the training is more refined, the training institutions are more commercial, there are sports rehabilitators, sports protectionists, and physical trainers in terms of personnel distribution, and these three professional talents play a very important role in the medical treatment and physical training of athletes [5]. Gr Bovi et al. believe that a new definition has been added on the basis of the definition of the concept of physical rehabilitation, which is roughly classified as adding attribution: a highly targeted functional training; adding functional value: enabling athletes who are injured or in poor competitive condition to reduce the risk of injury and improve their competitive status; add specificity: combined with special training, it is beneficial to improve the physical function and physical quality of athletes and help athletes prevent sports injuries; and add key differences: in physical rehabilitation training, rehabilitation is the core, and training is the soul [6]. Kudo-Saito and others believe that individualization and differentiated treatment should be emphasized, the impact of injuries on athletes' physical functions should be understood from training, and training plans should be adjusted in time

according to athletes' feedback. Among them, Kudo-Saito et al. believe that rehabilitation physical training belongs to a new comprehensive discipline [7]; Choi et al. believe that it is a training method and belongs to functional training; Liu Dongsen believes that it is a physical training program. The ultimate goal of rehabilitative physical training for athletes is not only to restore basic functions but also to improve physical function and sports performance and return to training ground and competition field. For the stage of acute injury of athletes and local inflammation after surgery, medical rehabilitation must be the main focus, and the rest of the body should be rehabilitative physical training by means of balance training [8]. Haller et al. found that there are various classifications of rehabilitation, classifying rehabilitation from the perspective of physiology, and there are sports system rehabilitation, nervous system rehabilitation, cardiopulmonary function rehabilitation, urinary system function rehabilitation, circulatory function rehabilitation, respiratory system function rehabilitation, digestive system function rehabilitation, reproductive system function rehabilitation, and endocrine system function rehabilitation [9]. Xun et al. found that, according to the stage of sports injury recovery, it can be divided into the following: it includes 4 stages: acute stage of injury, medical rehabilitation period, rehabilitation fitness period, and physical training period. It can be divided into upper extremity, lower extremity, and core area according to the part of injury recovery, which is further divided into muscle injury, ligament injury, fascia injury, muscle key sheath, and joint capsule injury. According to the specific purpose of rehabilitation, it can be divided into functional rehabilitation type, disease prevention type, functional rehabilitation type, core strengthening type, nerve rehabilitation type, muscle group rehabilitation type, balance and joint rehabilitation type, and stretching rehabilitation type of physical training [10]. Guo et al. found that physical fitness is divided into broad and narrow concepts, and generalized physical fitness refers to the physical ability elements stored by the human body in order to adapt to the needs of exercise, which is the performance of the basic ability of human activities. The narrow concept is the synthesis of the special strength system and related qualities that athletes need to complete high-level competition [11]. Traylor et al. divided the concept of physical fitness into physiological aspects and psychological aspects, physiological aspects represent sports performance and adaptability, and mental abilities represent the second manifestation of volitional qualities. Traylor et al. more comprehensively summarized the influence of nature and nurture, the elements of physical fitness, and the core quality in the elements [12].

The author takes the content system of rehabilitative physical training as the research object, from the theoretical basis of rehabilitative physical training, to the concept and principle of the programmatic construction of the content system, and the programmatic construction of the content system of rehabilitative physical training, etc.; to sort out the article, the program is used to construct the system, and the program of the rehabilitation physical training content is reflected through case presentation.

### 3. Research Methods

#### 3.1. Ultrasound Examination and Evaluation

**3.1.1. Ultrasound Inspection Equipment.** The authors used the Mindray M7 Ultrasonic System with 11 MHz linear high-frequency probe, and in all tests, all settings were stored in the factory preset tissue imaging facility, with a magnification of 50 and one seeks depth and breadth for each. Muscles and self are different [13].

Ultrasound was performed on 26 patients and 10 adults for good health, and each study examined 11 muscles, including the tongue, two-sided trapezius, two-sided biceps, two-sided abductor pollicis brevis, two lateral quadriceps, and both anterior tibial. The specific inspection methods are as follows: (1) medullary segment: check the tongue muscle and bilateral trapezius muscle and check the trapezius muscle from the back at the level of the cervical spinous process and the midclavicular line; (2) cervical segment: check bilateral biceps and bilateral abductor pollicis brevis; and (3) lumbosacral segment: check bilateral quadriceps and bilateral tibialis anterior muscles. All subjects were trained by 1 or 2 muscle ultrasound and the inspection by professionals who are proficient in muscle ultrasound technology, and the examiner knows the clinical findings of each subject but is unaware of the final diagnosis of each patient. The tongue and bilateral trapezius muscles were examined in a sitting position, and other muscles were examined in a supine position [14]. During the examination, the subject's muscles remain completely relaxed. With the exception of the trapezius, the rest of the muscles were imaged laterally at the largest diameter with B-mode.

**3.1.2. Counting Method of Ultrasonic Beam Flutter.** Referring to the method of Tsuji et al. to detect fasciculation by ultrasound, the probe was hit in the middle of the muscle belly of each muscle and observed for 30 seconds, ultrasound-identified fasciculations are unspontaneous twitching of a small part of the muscle, for 0.2 to 0.5 s, observe at least three fasciculations in the same muscle (three identical or independent fasciculations), and detected by ultrasound, and it is recorded as a fasciculation detected. In order to assess whether ultrasound can correctly identify fasciculations, when examining each muscle group, the probe detection area needs to be changed, in order to rule out the problem that the muscle structure itself and the surrounding tissue cannot be evaluated, the fasciculation detection is affected. Record the number and types of observed muscle fasciculations; according to the distribution of fasciculations, the fasciculations are divided into two types: focal and multifocal, and the number of fasciculations in each muscle is calculated separately. For muscles with continuous multifocal fasciculations that are difficult to count, count as a maximum of 30. Patients with suspected ALS and healthy adult controls were tested in the same way, and the number and distribution of muscle fasciculations were recorded.

**3.1.3. Ultrasound Beam Score.** To differentiate ALS patients from non-ALS patients, an "Ultrasonic fibrillation score" developed, which was determined by the number of muscles

seen by fasciculation in the muscle selection by ultrasound. Use the ROC curve to find the most important and measure the sensitivity and specificity of the number of fascicular muscles in a patient to differentiate ALS in non-ALS patients: diagnosis of ALS [15].

**3.1.4. Statistical Methods.** All data in this study were analyzed using SPSS statistics 22.0. Age, gender, number of muscle fasciculation, and amount of fasciculation detected were compared by ALS group, non-ALS control group, and health control group, and the measurement data are presented as the normal distribution. The measurement data conforming to normal distribution were expressed in the form of mean standard deviation (SD) and comparison of the two groups were designed using the independent model *t*-test; census data were presented at different frequencies, and differences between two or more digits were determined using the Kruskal-Wallis test or the Man-Whitney *U* test. Pearson's chi-square test was used to calculate muscle differences and differences between groups of ALS and non-ALS. ROC regression was used to verify the accuracy of the diagnosis, mark the ROC curve, calculate the area under the curve (AUC), find the optimal cut-off value, and identify the sensitivity and specificity. Spearman correlation analysis was used to filter the relationships between difference and nondifference. Each key test is a two-way test.  $P < 0.05$  was considered significant (Table 1).

**3.2. Distribution of Fasciculations Detected by Ultrasound in Each Group.** The classification of muscle fasciculation in the ALS group, the control group, and the health control group was 2.5, 0.6, and 0.3, respectively. The distribution of fasciculation differs between three groups ( $P < 0.001$ ) values [16]. Compared with the disease control group and the health control group, the distribution of muscle fasciculation in the group of ALS patients is constant, and the anatomical distribution is broad, generally living into 2 or more segments, and in the distal and near end and follows the results of electromyography, which showed the patient symptoms and upper and lower motor brain damage. Most patients in the control group had no more than 1 stage of fasciculation, but our results showed 2 stages of fasciculation per patient, and in healthy individuals, distribution of fasciculation is most often affected and involved in 2 segments (Figure 2).

**3.3. Comparison of Fasciculation Muscle Number and Fasciculation Detection Rate among Groups.** The number of fasciculations diagnosed in each of the 11 subgroups in the ALS group, the control group, and the health control group was 6.44, 1.20, and 0.50, respectively, and the numbers of people are very different. Of the three groups, the number of fascial muscles found in the ALS group was higher than that in the disease group and the health control group ( $P < 0.001$ ), and the difference was significant (see Table 2).

As shown in Tables 2 and 3, the overall detection rate of fibrillation in the ALS group, the non-ALS control group, and the health management group was 58.5%, 10.9%, and

TABLE 1: Demographic characteristics of the three groups undergoing muscle ultrasonography.

	ALS ( $n = 16$ )	Disease control group ( $n = 10$ )	Healthy control group ( $n = 10$ )	$P$ value
Gender: male, female	11 : 5	8 : 2	6 : 4	0.531
Age	61.69 $\pm$ 7.26	45.20 $\pm$ 16.03	54.50 $\pm$ 11.81	0.024
Disease duration (months)	15.13 $\pm$ 9.70	13.80 $\pm$ 18.55	N/A	0.234
ALSFRS-R score	38.40 $\pm$ 5.75	N/A	N/A	N/A

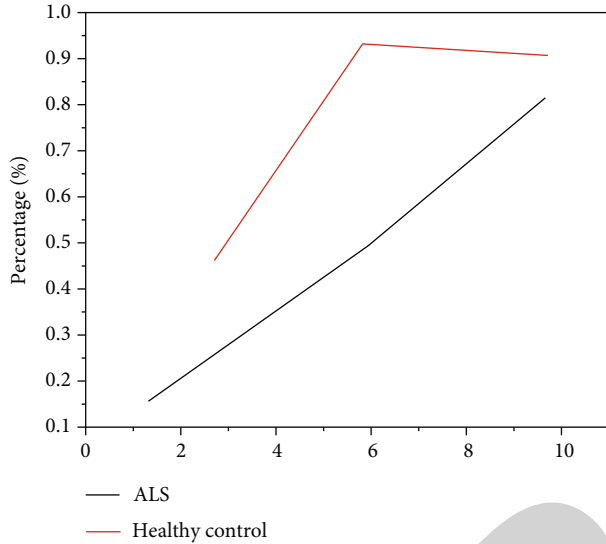


FIGURE 2: Anatomical distribution of three groups of muscle fasciculations.

4.5%, respectively, according to the Kruskal-Wallis  $U$  test. The rate of detection of total muscle fasciculation was significantly different in the three groups ( $H = 24.008$ ,  $P < 0.001$ ), and the detection rate of fasciculation in the ALS group was higher than in the non-ALS group and health management committee. Of the 176 muscles in the ALS group, 103 were diagnosed with fasciculation, with the muscles with the highest scores being the right two-headed (81.3%) and the tongue with the lowest scoring (18.8%) item. The muscle segment we tested, the lumbosacral fasciculation muscle, had the highest detection rate. Fasciculation was found in 12 of the 110 muscles in the non-ALS control group, with the most common in the left biceps (30%) and no fasciculation in the three elongated muscles (0). Of the 110 muscles in the healthy adult group, only 5 had fasciculation, with two left head (10%), two right head (10%), right leg muscle (10%), anterior left tibia (10%), and right tibia anterior muscle (10%) [17].

Table 3 shows that the diagnosis of muscle fasciculation differs from the distribution of muscles in an individual in the ALS group, the disease control group, and the health control group, and the high level of fasciculation detection is usually divided into lower extremities (lumbosacral segment): quadriceps femoris and anterior tibial muscle. With the exception of muscle mass, the detection of fasciculation in each muscle of the ALS group was greater than in the

health control group, and the right biceps, the right pollicis brevis, and the fourth were as follows. The lower limbs are important square test  $P < 0.001$ . The difference is significant. The detection rate of ALS muscle fasciculation is generally higher in the control group, but the detection rate of the following three muscle fasciculations does not differ between the two groups, namely, left biceps and left abductor pollicis brevis [18].

In all groups of ALS patients with upper and lower tubercle onset, the detection rate of fasciculation was 60.84% and 48.49%,  $P = 0.376$ , and the difference was not significant. According to the diagnostic procedure for Awaji ALS, there should be no significant differences in the diagnosis of muscle fasciculation in patients with ALS confirmed and those with ALS outcome and in the study Mann-Whitney  $U$  detector  $P = 0.302$  ( $P > 0.05$ ). He met the medical procedure for Awaji.

Spearman's analysis of the relationship between the speed of diagnosis of fasciitis in the ALS group and two diagnoses of ALS (chronic disease, ALSFRS-R) shows that the value of investigation of muscle fasciculation by muscle ultrasound is associated with acute myocardial infarction (ALSFRS).  $R$  was negative ( $r = 0.501$ ), the results were significant ( $P < 0.05$ ), and the detection rate of ALS fasciculation was independent of infection ( $r = 0.014$ ,  $P = 0.960$ ). The results are shown in Table 4.

**3.4. Accuracy of "Ultrasonic Beam Fibrillation Score" in the Diagnosis of ALS.** To help identify ALS patients in the diagnosis and treatment of non-ALS disease and health control groups, we developed "fasciculation scores," which are defined as muscles with fasciculation detected by muscle ultrasound: 11 bodies. Quantity was as follows. Compared with the control group ( $0.85 \pm 1.531$ ), this score was higher in the ALS group ( $6.44 \pm 2.56$ ),  $P < 0.001$ , and the difference was significant. The area below the ROC curve was used to measure the further diagnosis of ultrasonic radiation fibrillation scores. The results showed that the area under ROC curve (AUC) was 0.96,  $AUC > 0.9$ , with liver biopsy and accuracy.

**3.5. High Frequency Ultrasound Examination.** Closed muscle and tendon injuries are common in clinical practice. For example, the common clinical injuries of fingers, wrist, Achilles tendon, quadriceps tendon, etc. are mostly closed muscle and tendon injuries. Routine ultrasonography fails to identify closed muscles, edema due to muscle, tendon rupture in tendon injuries, hemorrhage, and lymphocytic inflammatory infiltration, hypoechoic images appear due to

TABLE 2: Comparison of the detection rate of muscle fasciculation among the three groups.

	ALS	Disease control group	Healthy control group	<i>P</i> value
Total fibrillation detection rate	58.50%	10.90%	4.50%	<0.001
Fasciculation muscle number	6.44 ± 2.56	1.20 ± 1.87	0.50 ± 1.08	<0.001

TABLE 3: Comparison of the fasciculation detection rate of each muscle by muscle ultrasound in the three groups.

Muscle	Detection rate of fibrillation (%)			<i>P</i> value	<i>P</i> value	<i>P</i> value
	ALS	Disease control group	Healthy control group			
Tongue muscle	18.8	0	0	0.129	0.145	0.145
Trapezius, left	37.5	0	0	0.011	0.026	0.027
Trapezius, right	43.8	0	0	0.004	0.014	0.015
Biceps, left	56.3	30.0	10.0	0.051	0.193	0.018
Biceps, right	81.3	20.0	10.0	<0.001	0.003	<0.001
Abductor pollicis brevis, left	50.0	20.0	0	0.016	0.125	0.007
Abductor pollicis brevis, right	75.0	10.0	10.0	<0.001	0.001	0.001

TABLE 4: The correlation between the detection rate of fascicular fibrillation in patients with ALS and the course of disease and ALSFRS-R.

Variable	Linear correlation coefficient ( <i>r</i> )	<i>P</i>
Disease duration-fasciculation detection rate	-0.501	0.048
ALSFRS score-fasciculation detection rate	0.014	0.960

degeneration and necrosis of damaged tissue or local hypoechoic (calcium deposition) due to disease progression and old lesions, strip hyperechoic (fibrogranular tissue, nodule), etc. or may overlook the scan of the proximal end of the ruptured tendon, resulting in missed diagnosis [19].

Compared with conventional ultrasonography, high frequency ultrasonography can clearly diagnose and evaluate the structural and morphological changes and echoic changes of muscle and tendon injuries, and it can more accurately locate the relationship between the injury site, extent, and surrounding tissues (with or without adhesion), degree (with or without fracture) and whether there is hematoma formation. High-frequency ultrasonography is more sensitive than conventional ultrasonography to detect hidden muscle and tendon lesions. High-frequency ultrasound is better than MRI in resolving the fine structure of muscle and can provide more detailed diagnostic information for clinical practice. Li Jing's study used high-frequency ultrasound (5-10 Hz) to examine 135 patients with calf tendon and muscle injuries, and the results show that high-frequency ultrasonography can detect muscle contusion, tear and tendon injury, and rupture patients and can accurately assess the course (acute, chronic) and degree of disease (partial/complete rupture) [20]. Simple operation, strong repeatability, and high reso-

lution in the diagnosis of lower extremity muscle and tendon injuries and high-frequency ultrasonography can provide clearer and more accurate ultrasonographic images, which can improve the positive rate of clinical diagnosis of lower extremity muscle and tendon injuries. In conclusion, the application of high-frequency ultrasound has advantages in the diagnosis of superficial organ lesions, muscle, and soft tissue damage [21].

Because ultrasonography cannot clearly display the whole picture of blood vessels and the details of anatomical structure, there are certain limitations in the diagnosis of soft tissue tumors. High-frequency ultrasonography was used for the diagnosis of muscular system lesions with high sensitivity (100%). Muscle injury, tumor and inflammatory lesions, tendon rupture, ligamentous fibroma, etc. can show specific changes on high-frequency ultrasonography [22]. Therefore, the author believes that high-frequency ultrasonography can be used for the diagnosis of muscle, tendon injury, hemangioma, and other space-occupying lesions. Because high-frequency ultrasonography can display lesions from multiple sections and orientations, it can dynamically observe hematoma changes, etc., and it can clearly distinguish cystic and solid lesions; so, high-frequency ultrasonography has expanded the application scope of ultrasonography, making ultrasonography more and more widely used in the diagnosis of muscle system injuries and tumors.

#### 4. Result Analysis

This study examined the role of muscle ultrasound in the diagnosis of ALS by studying muscle fasciculation. What we have found is that muscle ultrasound detects more muscle mass in patients with ALS, making it easier to diagnose ALS and more effective in diagnosing it. Muscle ultrasound can provide important information about fasciculation in patients with neurological and musculoskeletal disorders.

Our study showed that there was a significant difference between the prevalence of fasciculation detected by ultrasound examination of patients with ALS and those suspected of having ALS in patients with ALS and older healthy people. We also demonstrated that muscle ultrasound has a higher sensitivity for the detection of muscle fasciculations in ALS patients and developed a more concise and convenient ultrasound fasciculation score to assist in the diagnosis of ALS; that is, 3 of 11 muscles in each patient were detected. Fasciculation, that is, ultrasound fasciculation reaching 3/11, can be used as a diagnostic marker in ALS patients [23].

Under the guidance of ultrasound, local lesions can be located, guided puncture and auxiliary diagnosis, and tendon lengthening surgery, fenestration surgery can be performed for patients with tendinopathy, and injection therapy can be performed for muscle tear injuries and tendinopathy and interventional therapy for bone, muscle, tendinopathy, or nerve damage [24]. By determining the fasciculation and location of tendon rupture injuries by ultrasound examination, the clinic can decide whether to take surgical treatment of the patient. Small Achilles tendon tears only need conservative treatment to avoid developing into complete Achilles tendon rupture. If the fasciculation of the Achilles tendon injury is less than 3/11 after ultrasound evaluation and statistical evaluation, no surgical treatment is required. For those with a complete tear of the Achilles tendon, it is necessary to further measure the distance between the broken ends in the toe flexion state, in order to evaluate surgical treatment. Visible, through ultrasonography, the diagnosis of tendon injury can provide positive guidance for clinical determination of treatment plan. For the diagnosis of muscle and tendon injury, X-ray has no diagnostic specificity; CT, MRI, etc. have high diagnostic rates, but their clinical application is limited. Ultrasound examination is noninvasive, simple to operate, reproducible, and can quickly obtain diagnostic results. It plays an important role in the diagnosis of muscle and tendon injuries. In clinical practice, more application of ultrasonic fusion imaging technology, in order to do a good job of differential diagnosis, improves the accuracy of diagnosis [25].

## 5. Conclusion

The author conducts experiments, induction, and analysis of the relevant contents of ultrasound examination and evaluation, and the data confirms that ultrasound examination can meet the needs of sports injury visualization. Due to time constraints, the programmatic content system proposed by the author has not found enough practical cases to prove it. The rationality and rigor of the content system programming still need to be further verified in future practice. In future research, quantitative research needs to be carried out according to specific cases to determine more quantitative indicators, in order to confirm the effect of the program of rehabilitative physical training under ultrasound examination. In short, the programming of the content system of rehabilitation physical training under ultrasound examination needs to be further verified in future research and makes the program arrangement more reasonable and scientific.

## Data Availability

The data used to support the findings of this study are available from the corresponding author upon request.

## Conflicts of Interest

The authors declare that they have no conflicts of interest.

## References

- [1] S. Jiao, "Biomedical optical imaging technology and applications: from basic research toward clinical diagnosis," *Experimental Biology and Medicine*, vol. 245, no. 4, pp. 269–272, 2020.
- [2] W. Wu, M. Wu, Y. Wang, X. Jiang, and G. Li, "Ultrasonic examination of differences in bone density of chronic obstructive pulmonary disease (COPD) rats constructed by different methods," *Annals of Palliative Medicine*, vol. 9, no. 4, pp. 1872–1878, 2020.
- [3] A. E. Golubev, "Construction of programmed motions of constrained mechanical systems using third-order polynomials," *Journal of Computer and Systems Sciences International*, vol. 60, no. 2, pp. 303–314, 2021.
- [4] A. Deshmukh, E. MCGough, and M. M. Ahmed, "Transaxillary intra-aortic balloon pump promotes physical rehabilitation in patients requiring long-term mechanical circulatory support," *Journal of Cardiothoracic and Vascular Anesthesia*, vol. 35, no. 4, pp. 1255–1256, 2021.
- [5] M. Bertollo, G. Santi, and S. D. Fronso, "Comment on: "development of a revised conceptual framework of physical training for use in research";" *Sports Medicine*, vol. 52, no. 4, pp. 949–951, 2022.
- [6] M. Gr Bovi, S. Markovi, and D. Bogavac, "Teachers' characteristics as factors of the school sport quality in the Republic of Serbia," *Inovacije u Nastavi-Časopis Za Savremenu Nastavu*, vol. 33, no. 4, pp. 79–90, 2020.
- [7] C. Kudo-Saito, Y. Ozaki, H. Imazeki et al., "Targeting oncoimmune drivers of cancer metastasis," *Cancers*, vol. 13, no. 3, p. 554, 2021.
- [8] J. H. Choi, A. R. Kim, and S. W. Choi, "A comparative study on the basic physical fitness, muscle volume, and equivalence of workers in sedentary living by exercise," *Korean Journal of Sports Science*, vol. 30, no. 2, pp. 1097–1102, 2021.
- [9] J. Haller, J. Hillebrecht, and J. Bengel, "The culturally sensitive therapy relationship: a concept for the training and further education of psychotherapists," *Psychotherapie, Psychosomatik, Medizinische Psychologie*, vol. 70, no. 11, pp. 441–448, 2020.
- [10] F. Xun, S. Yapei, W. Ya et al., "A novel manganese coordination polymer based on azobenzene tetracarboxylate and auxiliary pyridine ligand: synthesis, crystal structure and magnetism," *Structural Chemistry*, vol. 40, no. 2, p. 9, 2021.
- [11] C. B. Guo, "Thoughts on the prevention, clinical diagnosis and treatment of osteonecrosis of the jaw and future research directions," *Zhonghua Kou Qiang Yi Xue Za Zhi = Zhonghua Kouqiang Yixue Zazhi = Chinese Journal of Stomatology*, vol. 56, no. 5, pp. 401–403, 2021.
- [12] A. Traylor, D. Dipilla-George, and P. Tirakitsoontorn, "An unusual presentation of chest pain in a patient with cystic fibrosis: a case report," *Pediatric Physical Therapy: The Official*

## Retraction

# Retracted: Effects of Obstructive Sleep Apnea-Hypopnea Syndrome and Cognitive Function in Ischemic Stroke Based on Linear Regression Equation

### Scanning

Received 11 July 2023; Accepted 11 July 2023; Published 12 July 2023

Copyright © 2023 Scanning. This is an open access article distributed under the Creative Commons Attribution License, which permits unrestricted use, distribution, and reproduction in any medium, provided the original work is properly cited.

This article has been retracted by Hindawi following an investigation undertaken by the publisher [1]. This investigation has uncovered evidence of one or more of the following indicators of systematic manipulation of the publication process:

- (1) Discrepancies in scope
- (2) Discrepancies in the description of the research reported
- (3) Discrepancies between the availability of data and the research described
- (4) Inappropriate citations
- (5) Incoherent, meaningless and/or irrelevant content included in the article
- (6) Peer-review manipulation

The presence of these indicators undermines our confidence in the integrity of the article's content and we cannot, therefore, vouch for its reliability. Please note that this notice is intended solely to alert readers that the content of this article is unreliable. We have not investigated whether authors were aware of or involved in the systematic manipulation of the publication process.

In addition, our investigation has also shown that one or more of the following human-subject reporting requirements has not been met in this article: ethical approval by an Institutional Review Board (IRB) committee or equivalent, patient/participant consent to participate, and/or agreement to publish patient/participant details (where relevant).

Wiley and Hindawi regrets that the usual quality checks did not identify these issues before publication and have since put additional measures in place to safeguard research integrity.

We wish to credit our own Research Integrity and Research Publishing teams and anonymous and named external researchers and research integrity experts for contributing to this investigation.

The corresponding author, as the representative of all authors, has been given the opportunity to register their agreement or disagreement to this retraction. We have kept a record of any response received.

### References

- [1] P. Ji, Q. Kou, X. Qu, G. Sun, S. Liu, and J. Zhang, "Effects of Obstructive Sleep Apnea-Hypopnea Syndrome and Cognitive Function in Ischemic Stroke Based on Linear Regression Equation," *Scanning*, vol. 2022, Article ID 4105169, 8 pages, 2022.

## Research Article

# Effects of Obstructive Sleep Apnea-Hypopnea Syndrome and Cognitive Function in Ischemic Stroke Based on Linear Regression Equation

Peng Ji <sup>1</sup>, Qixing Kou <sup>2</sup>, Xueping Qu <sup>2</sup>, Gen Sun <sup>2</sup>, Songcan Liu <sup>2</sup>,  
and Jiewen Zhang <sup>1</sup>

<sup>1</sup>Zhengzhou University People's Hospital, Zhengzhou, Henan 450000, China

<sup>2</sup>The Third People's Hospital of Zhengzhou (Tumor Hospital Affiliated of Henan University), Zhengzhou, Henan 450000, China

Correspondence should be addressed to Jiewen Zhang; 201811111121723@stu.hubu.edu.cn

Received 15 May 2022; Revised 28 May 2022; Accepted 6 June 2022; Published 22 June 2022

Academic Editor: Balakrishnan Nagaraj

Copyright © 2022 Peng Ji et al. This is an open access article distributed under the Creative Commons Attribution License, which permits unrestricted use, distribution, and reproduction in any medium, provided the original work is properly cited.

The objective of this research is to study the effect of obstructive sleep apnea-hypopnea syndrome on cognitive function of stroke. Based on linear regression equation and Montreal Cognitive Assessment Scale, the degree of cognitive impairment in OSAHS patients was evaluated and the influencing factors of OSAHS-induced cognitive impairment and the correlation between the degree of OSAHS and cognitive impairment were explored. The results are as follows: about 68% of OSAHS patients have cognitive dysfunction, and the incidence of cognitive dysfunction is positively correlated with OSAHS; cognitive impairment of OSAHS patients was associated with age, obesity, years of schooling, and intermittent nocturnal hypoxia or hypoventilation; the severity of cognitive dysfunction of OSAHS patients was positively correlated with age and obesity but negatively correlated with education level; Logistic regression analysis results showed that there were three factors that were finally entered into the regression equation, namely, LSaO<sub>2</sub>, BMI, and AHI, and the Logistic regression equation obtained was as follows:  $\text{Logist}P = -0.109X_1 + 0.785X_2 + 1.228X_3$ . This study helps clinical workers to detect and intervene the impaired cognitive ability of patients with OSAHS early, so as to reduce the incidence and mortality of related complications and improve the quality of life of patients.

## 1. Introduction

In recent years, obstructive sleep apnea-hypopnea syndrome (OSAHS) is a kind of sleep disorder with serious harm to human health. Due to the complete or incomplete collapse and obstruction of the upper airway during sleep, apnea or hypopnea occurs repeatedly, causing indirect hypoxia hypercapnia and sleep structure disorder. The main clinical manifestations are snoring during sleep accompanied by recurrent apnea, daytime sleepiness, dry mouth, dizziness, headache, and fatigue, as shown in Figure 1 [1]. The incidence of OSAHS increases with age. For people under 70 years old, the risk of death will increase if risk factors such as obesity, smoking, and drinking are combined with OSAHS. At the same time, the investigation found that the

incidence of OSAHS in males was higher than that in females. The incidence of OSAHS in adult males was 3%-7%, while that in adult females was 2%-5%. Moreover, the incidence of OSAHS in menopausal women was on the rise [2]. The differences in prevalence are due to regional and ethnic differences, age differences, and gender differences in epidemiological investigation methods. Due to the limitations of current epidemiological research methods, it is estimated that the actual prevalence of OSAHS should be higher than the above values. OSAHS is a disease involving multiple systems of the whole body, which can cause damage to multiple target organs of the whole body to a certain extent, such as cardiovascular and cerebrovascular diseases, diabetes, pulmonary heart disease, respiratory failure, and cognitive dysfunction. In recent years, studies have shown that the



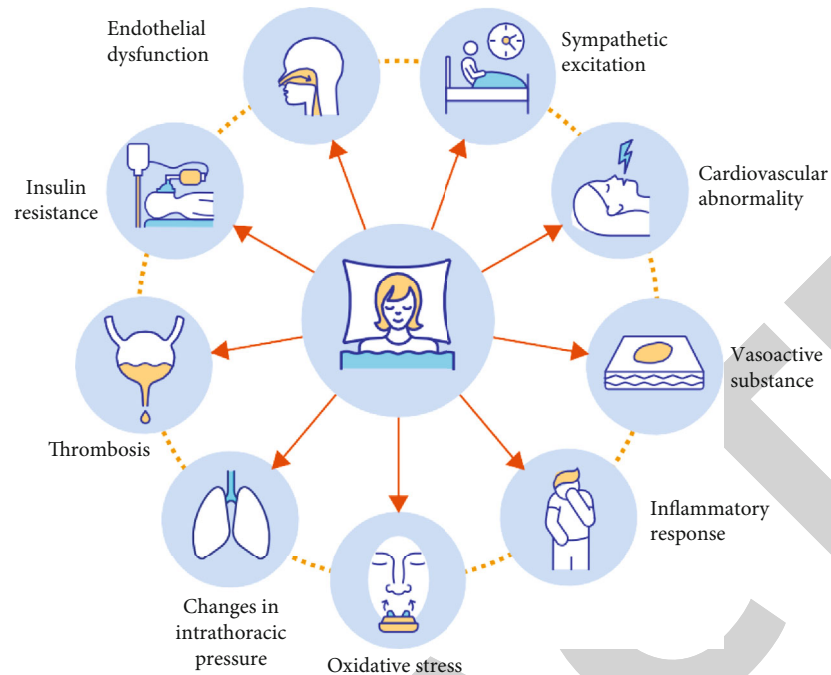


FIGURE 1: Obstructive sleep apnea-hypopnea syndrome.

cognitive dysfunction caused by OSAHS patients is mainly mild cognitive impairment, and with the development of the disease, severe cases may evolve into Alzheimer's disease, among which the incidence of cognitive dysfunction is higher in severe OSAHS patients [3]. Stroke is a kind of cerebral blood circulation disorder with transient or permanent brain dysfunction as the main clinical manifestations. Acute ischemic stroke is a serious threat to patients' life safety due to its rapid onset and often without obvious prodromal symptoms. Studies have pointed out that sleep-disordered breathing is closely related to the prognosis of patients with cerebrovascular diseases, and the incidence of vascular dementia in patients with acute ischemic stroke complicated with OSAHS is significantly higher than that in patients without OSAHS [4]; therefore, it is of great significance to clarify the impact of OSAHS on patients with acute ischemic stroke and take targeted preventive measures to improve the prognosis of patients. Cognition refers to the ability of human brain to process, preserve, and extract information, which involves many fields such as learning, memory, execution, calculation, and understanding [5]. Cognitive dysfunction refers to the impairment of cognitive ability of different degrees caused by different factors. Clinically, it can be manifested as difficulty in concentration, memory decline, executive function decline, reasoning and abstract thinking ability decline, etc. There are more serious disorders such as agnosia and aphasia. At present, the clinical evaluation methods for the cognitive function of patients with OSAHS include the cognitive function assessment scale neuroelectrophysiological imaging. This study explored whether the cognitive function of patients with OSAHS is related to the severity of OSAHS. The objective of this research is to study the correlation between cognitive function and AHI LsO<sub>2</sub> ODI in patients with OSAHS.

## 2. Literature Review

Currently, the commonly used scales for cognitive function testing of OSAHS patients include Montreal Cognitive Assessment Scale (MoCA), Simple Mental State Examination Scale (MMSE), Wechsler Adult Intelligence Scale (WAIS), Extended Dementia Scale (ESD), Lowenstein Cognitive Scale Language Fluency Test (VFT), daily living activity scale, and complete neuropsychological test [6]. Because the assessment scale is relatively simple and time-consuming, it is widely used in the detection of cognitive function. WAIS is mainly aimed at the assessment of intelligence and operational ability, so it is not suitable to evaluate the neurological impairment of OSAHS patients alone. As the scale is complicated, it is also not suitable for large-sample tests. MMSE is widely used in the screening of cognitive dysfunction due to its strong sensitivity, easy operation, and less time-consuming. However, MMSE is relatively simple and easy to miss diagnosis of mild cognitive impairment [7]. ESD is a scale commonly used to assess brain cognitive function at home and abroad in recent years. Its content and items are more detailed, and it can reflect the brain cognitive function comprehensively and completely [8]. Some studies believe that MoCA is more reliable than MMSE in the detection of cognitive dysfunction in patients with OSAHS [9, 10].

Electroencephalography (EEG) and magnetoencephalography (MEG) are widely used in clinical neurophysiological examination [11]. It is believed that event-related potentials (ERPs) extracted from EEG and MEG are closely related to cognitive functions such as memory, judgment, and attention. The concept of event-related potentials was put forward, which provided a more objective and simple method for the study of cognitive function [12]. ERPs are the cognitive processing process of the human brain's

perception of stimulus events and responses to stimulus events recorded on the tester's scalp surface, and the brain potentials are obtained by repeated superposition. It can be understood that it is the evoked potential of cognitive function. P300 is the main indicator for evaluating cognitive functions which are amplitude and latency. A cross-sectional study by Yang and Sun found poor differentiation of ERP waves in patients with cognitive dysfunction, the incubation period of P300 was prolonged, and the amplitude was significantly reduced. It can be used to assess whether a patient's cognitive function is impaired [13]. Compared with imaging, EPRs have the advantages of low cost, high time resolution, and noninvasive multimode assessment. It is a more objective, sensitive, and easy to operate electrophysiological technique for the assessment of cognitive dysfunction.

At present, the clinical evaluation methods for the cognitive function of patients with OSAHS include the Cognitive Function Assessment Scale. The commonly used assessment scale for neuroelectrophysiological imaging is Montreal Cognitive Assessment (MoCA), Mini Mental Status Exam (MMSE), Expansive Scale of Dementia (ESD), etc. MMSE is too simple, insensitive to mild cognitive impairment, and ESD is complex and time-consuming, which is not suitable for the screening of cognitive impairment. Therefore, Montreal Cognitive Assessment Scale is commonly used to evaluate cognitive ability in clinical practice. Therefore, the Montreal Cognitive Assessment Scale (ERPs) is commonly used to evaluate the event-related potentials (ERPs) in neuroelectrophysiology of cognitive ability, in which P300 can be used to evaluate the impairment of cognitive function, which is relatively sensitive. Imaging is an objective and user-friendly assessment method, but it is rarely used in clinical assessment of cognitive function due to its radioactivity and high cost.

In recent years, more and more domestic and foreign scholars began to pay attention to and study the influencing factors and pathogenesis of cognitive dysfunction in OSAHS patients. Most scholars believe that the related factors affecting the cognitive dysfunction of OSAHS patients are as follows: education level, age, education level, obesity, smoking, nocturnal interrupted hypoxia, and sleep structure were considered to be the main factors. OSAHS patients have repeated intermittent hypoxia during sleep, which can lead to abnormal functional metabolism in the hippocampus and cerebellum and other areas of the brain and cause cognitive impairment in learning and memory behaviors. At the same time, hypoxia can produce a large number of oxygen free radicals and lead to oxidative damage, thus inducing neuronal apoptosis [14]. However, sleep fragmentation in OSAHS patients may cause changes in neurotransmitter concentration, resulting in impaired cognitive function. At present, the influencing factors and pathogenesis of cognitive dysfunction in OSAHS patients are still unclear, and there is a lack of large sample data studies, and there are also different literature reports at home and abroad [15].

Some studies believe that OSAHS patients have extensive cognitive dysfunction, which is positively correlated with the severity of OSAHS [16]. The main characteristic of the OSAHS patient is repeated intermittent hypoxia in the pro-

cess of sleep, and hypoxemia can cause systemic dysfunction of many organs, among which the central nervous system is particularly sensitive to hypoxemia [17]. The hippocampal cerebellum and other structures of the brain are very sensitive to hypoxia, which can lead to abnormal brain function and metabolism in this region and cause cognitive impairment such as learning and memory behavior [18]. Morris water maze test was used to investigate the relationship between cognitive function and chronic intermittent hypoxia in rats. The results showed that the progressive decline of cognitive function in chronic intermittent hypoxia rats was associated with pathological injury of prefrontal cortex and hippocampal neurons and progressive reduction of ChAT expression. Studies have shown that the concentration and executive ability of patients with OSAHS are significantly decreased compared with normal people and are correlated with average blood oxygen saturation ( $r = -0.51$ ,  $P = 0.002$ ) and blood oxygen saturation  $< 90\%$  ( $r = 0.56$ ,  $P < 0.001$ ), but not with daytime sleepiness. Recent studies have shown that chronic intermittent hypoxia can affect neuronal proliferation and differentiation, but there is no data to show whether chronic intermittent hypoxia increases or decreases neuronal proliferation [19]. Other studies suggest that chronic intermittent hypoxia may cause learning and memory impairment and increased apoptosis of hippocampal neurons through activation of Wnt/ $\beta$ -catenin, thus leading to cognitive dysfunction in OSAHS patients [20]. OSAHS patients repeatedly have apnea or hypoventilation at night, resulting in hypoxia-reoxygenation damage, resulting in increased oxide production and reduced antioxidant production, resulting in oxidation or antioxidant imbalance, and resulting in oxidative stress reaction [21, 22]. Oxidative stress can cause the release of various vasoactive substances and lead to vascular endothelial cell damage and endothelial dysfunction, resulting in atherosclerosis [23]. At the same time, hypoxemia can stimulate vasoconstriction and increase in red blood cells, which can cause slow blood flow of the body and then aggravate brain tissue ischemia and hypoxia, which in the long run causes extensive damage to brain cells and induces nerve cell apoptosis [24]. Neuronal apoptosis induced by cerebral ischemia and hypoxia is mainly located in the cerebral cortex and hippocampus, which are important parts of information processing, memory, and signal transmission [25]. Based on the current study, the Montreal Cognitive Function Assessment Scale was used to evaluate the cognitive function of the case group and the control group. The incidence of cognitive impairment in the case group with MoCA score of 26 as normal cognitive function (68%) was significantly higher than that in the control group (3%), and moderate to severe OSAHS was higher than that in mild OSAHS patients who are more likely to develop cognitive dysfunction. The detection rate of cognitive dysfunction is also different due to the difference of sample assessment methods and research methods.

### 3. Research Method

*3.1. Research Object.* A retrospective analysis was conducted on patients aged 18-70 years who complained of sleep

TABLE 1: Comparison of general situation between the case group and the control group.

Project	Control group	OSAHS mild	OSAHS moderate	OSAHS severe	F	P
Age (years)	45.78 ± 10.96	51.88 ± 10.59 <sup>b</sup>	51.56 ± 10.99 <sup>a</sup>	43.34 ± 9.63	5.190	0.002
Years of education (years)	14.25 ± 1.76	13.84 ± 1.85	13.72 ± 1.78	14.16 ± 1.74	0.637	0.593
BMI	26.13 ± 3.99 <sup>a</sup>	27.60 ± 4.61	27.40 ± 3.13	29.12 ± 3.66	3.183	0.026

Note: compared with the OSAHS severe group, <sup>a</sup>P < 0.05 and <sup>b</sup>P < 0.01.

TABLE 2: Comparison of the incidence of cognitive dysfunction between the case group and the control group.

Grouping	Cognitive function		$\chi^2$	P
	Normal	Abnormal		
Control group	31	1	62.436	0.000
OSAHS mild	21	11		
OSAHS moderate	7	25		
OSAHS severe	3	29		
Add up	62	66		

snoring and daytime sleepiness in outpatient department of respiratory medicine or ward of a hospital from August 2021 to December 2021. All patients underwent PSG test and MoCA questionnaire for at least 7 hours overnight. During the examination, the subjects were not allowed to drink coffee or take sedative drugs.

**3.2. Inclusion and Exclusion Criteria.** Patients aged between 18 and 70 years old, with junior high school education or above, who could read and write Chinese, were included with the chief complaint of snoring during sleep and daytime sleepiness. The diseases related to cognitive impairment, such as frontotemporal lobe infarction, hypothyroidism, psychiatric diseases, or severe liver insufficiency with a history of psychiatric diseases, were excluded. Patients with history of drug abuse; with serious heart, liver, and kidney insufficiency or malignant tumor; complicated with pneumonia, asthma, chronic obstructive pulmonary disease, and other respiratory diseases; and with diabetes mellitus and vascular complications were excluded.

**3.3. General Data Collection.** A self-made questionnaire was used to collect general information of the subjects, including the following: gender, age, height, weight, occupation, education level, blood pressure, history of smoking and drinking, history of basic diseases such as cardiovascular diseases, history of brain trauma, and history of diabetes. BMI is calculated according to the height and weight. BMI = weight (kg) square (m<sup>2</sup>) of each height, BMI 24.0 is overweight, and BMI 28.0 is obese.

**3.4. Cognitive Function Assessment.** All subjects underwent MoCA to assess cognitive function. The MoCA scale includes the following: executive ability, naming, attention, speech, and other different cognitive areas. The total score of the scale is 30, and the score is 26, which is normal, and the higher the score is, the better the cognitive function is. Meanwhile, for ≤12 years of education, the MoCA score increases by 1 point.

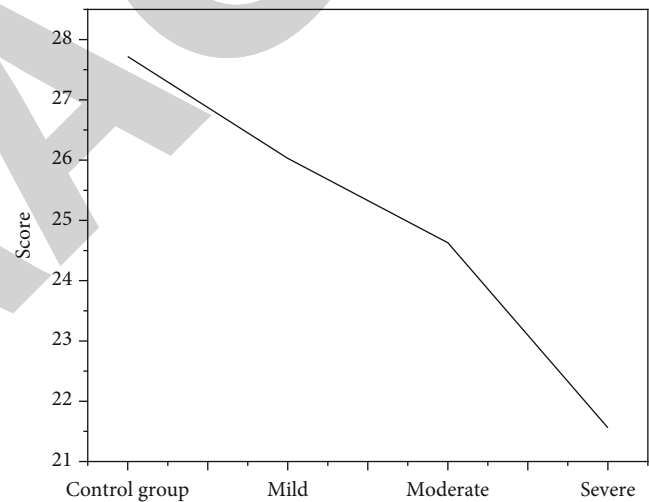


FIGURE 2: MoCA score of the case group and control group. Note: the total score of MoCA was 30, and 26 was normal.

**3.5. Polysomnography (PSG).** All subjects underwent overnight PSG testing in a respiratory and sleep monitoring room of a hospital. Subjects were not allowed to use sedatives, alcohol, coffee, etc., within 24 hours before the examination. The monitoring time was from 22:00 p.m. to 7:00 p.m. the next day, and the monitoring content was mouth and nose airflow, chest respiration, pulse, oxygen, pulse, etc. Monitoring indicators include AHI, LSaO<sub>2</sub>, and ODI. All monitoring data are automatically analyzed by computer, and finally, the results are obtained after manual reading inspection and correction. Each AHI < 5 times was divided into control group, and each AHI < 5 times was divided into case group. The case group was divided into three groups (5 AHI 15 times per mild OSAHS, 15 < AHI 30 times per moderate OSAHS, and AHI 30 times per severe OSAHS).

TABLE 3: Cognitive impairment in case group and control group.

Project	Control group	OSAHS mild	OSAHS moderate	OSAHS severe	F	P
MoCA grade	27.72 ± 1.30	26.03 ± 2.394 <sup>a</sup>	24.63 ± 1.90 <sup>a</sup>	21.56 ± 3.23 <sup>bc</sup>	40.609	0.000
View space	4.75 ± 0.44	4.38 ± 0.98	4.56 ± 0.76	3.72 ± 1.17 <sup>ac</sup>	8.339	0.000
Name	2.91 ± 0.3	2.78 ± 0.55	2.88 ± 0.42	2.94 ± 0.25	0.924	0.431
Notice	5.75 ± 0.44	5.5 ± 0.57	4.81 ± 0.74 <sup>ab</sup>	4.66 ± 1.07 <sup>ab</sup>	16.252	0.000
Language	2.09 ± 0.64	2.06 ± 0.76	1.41 ± 0.5 <sup>ab</sup>	1.5 ± 0.62 <sup>ab</sup>	10.398	0.000
Abstract	1.94 ± 0.25	1.72 ± 0.52	1.78 ± 0.49	1.59 ± 0.67	2.571	0.057
Delayed recall	4.00 ± 0.149	3.28 ± 0.239	3.09 ± 0.231 <sup>a</sup>	1.44 ± 0.25 <sup>abc</sup>	24.119	0.000
Directive force	5.97 ± 0.18	5.81 ± 0.4	5.53 ± 0.72 <sup>a</sup>	5.38 ± 0.71 <sup>ad</sup>	7.650	0.000

Note: compared with the control group, <sup>a</sup> $P \leq 0.01$ ; compared with the mild group, <sup>b</sup> $P < 0.01$ ; compared with the moderate group, <sup>c</sup> $P < 0.01$ ; compared with the mild group, <sup>d</sup> $P < 0.05$ .

**3.6. Data Statistics and Analysis.** A total of 128 patients were included in this study, including 32 in the control group and 32 in the case group with mild, moderate, and severe OSAHS. The SPSS20.0 statistical software was used to process the test data. The measurement data  $\pm$  was expressed as mean standard deviation ( $\bar{x} \pm s$ ), and the counting data was expressed as percentage, and pairwise comparison was used with  $\chi^2$  test. Logistic regression analysis was used to analyze the risk factors, and  $P < 0.05$  was considered statistically significant.

## 4. Interpretation of Result

### 4.1. The General Situation of Case Group and Control Group.

The average age of patients with mild, moderate, and severe OSAHS in the case group was  $51.88 \pm 10.59$ ,  $51.56 \pm 10.99$ , and  $43.34 \pm 9.63$ , respectively; 15 (46.9%), 16 (50%), and 12 (37.5%) had high school education, 17 (53.1%), 16 (50%), and 20 (62.5%) had college education, and the average length of education was  $13.84 \pm 1.85$ ,  $13.72 \pm 1.78$ , and  $14.16 \pm 1.74$ , respectively. Body mass indexes were  $(27.60 \pm 4.61) \text{ kg/m}^2$ ,  $(27.40 \pm 3.13) \text{ kg/m}^2$ , and  $(29.12 \pm 3.66) \text{ kg/m}^2$ , respectively.

The average age of the control group was  $45.78 \pm 10.96$ . 11 (34.4%) have high school education, 21 (65.6%) have college education or above, and the average length of education is  $14.25 \pm 1.76$ . Body mass indexes were  $(26.13 \pm 3.99) \text{ kg/m}^2$ . There was no significant difference in the index of years of education among different groups ( $P = 0.593$ ). The difference in BMI of age was statistically significant, as shown in Table 1.

**4.2. The Incidence of Cognitive Dysfunction in Case Group and Control Group.** In the case group, 65 patients showed cognitive impairment, i.e., MoCA score  $< 26$ , OSAHS with accounting for 68%. There were 11 cases (34 cases) in the mild OSAHS group. There were 25 cases (78%) in the moderate group. There were 29 cases (90%) in the severe group. One of the 32 control group had cognitive dysfunction. Chi-square test showed that the incidence of cognitive dysfunction was statistically different between the control group and the case group ( $\chi^2 = 62.436$ ,  $P = 0.000$ ), and the inci-

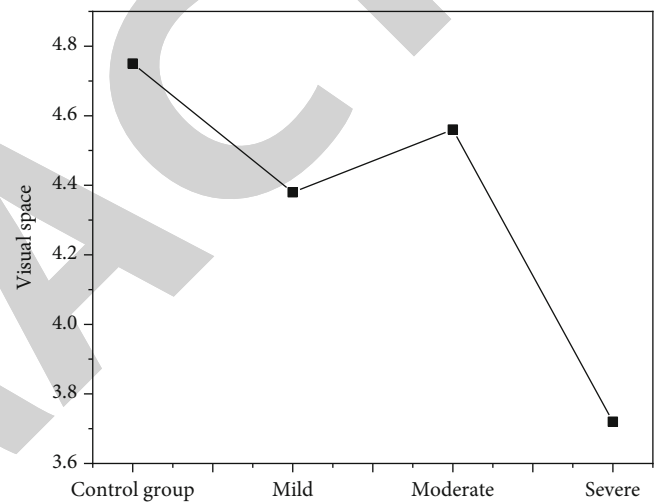


FIGURE 3: Visual spatial score of the case group and control group. Note: the total score of visual space is 5.

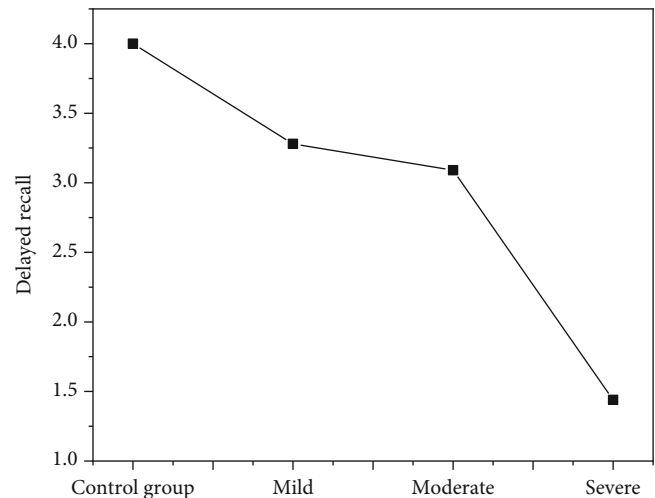


FIGURE 4: Delayed recall scores in the case group and control group. Note: the total score of delayed recall was 5.

TABLE 4: Logistic regression analysis variable meaning and assignment description.

Y (MoCA total marks)	Normal ( $\geq 26$ marks) = 0, abnormal ( $< 26$ marks) = 1
$X_2$ (age)	$< 40$ years = 1 = $X_{21}$ , 40 – 49 years = 2 = $X_{22}$ , 50 – 59 years = 3 = $X_{23}$ , $\geq 60$ years = 4 = $X_{24}$
$X_3$ (education years)	$\leq 9$ years = 1 = $X_{31}$ , 10 – 12 years = 2 = $X_{32}$ , $\geq 13$ years = 3 = $X_{33}$
$X_4$ (BMI)	Normal (18.5-23.9) = 2 = $X_{41}$ , overweight (24.0-27.9) = 2 = $X_{42}$ , obesity ( $\geq 28$ ) = 3 = $X_{43}$
$X_5$ (apnea and hypopnea index)	Normal ( $< 5$ times/h) = 1, mild (5-15 times/h) = 2 Moderate (15 – 30 times/h) = 3, severe ( $> 30$ times/h) = 4
$X_6$ (minimum oxygen saturation at night)	Normal ( $> 90\%$ ) = 1, mild (85%-90%) = 2 Moderate (80% – $< 85\%$ ) = 3, severe ( $< 80\%$ ) = 4

TABLE 5: Logistic regression analysis results.

	Regression coefficient	Standard error	Wald	P	OR	95% CI of OR	
Minimum sATS ( $X_6$ )	-0.109	0.049	4.965	0.026	0.897	0.815	0.987
BMI ( $X_4$ )	0.758	0.363	4.357	0.037	2.133	1.047	4.346
AHI ( $X_5$ )	1.228	0.357	11.806	0.001	3.415	1.695	6.882

dence of cognitive dysfunction in the non-OSAHS group was significantly lower than that in the OSAHS group. Meanwhile, the incidence of cognitive dysfunction in the moderate and severe OSAHS group was significantly higher than that in the mild OSAHS group, as shown in Table 2 and Figure 2.

**4.3. Cognitive Impairment in Case Group and Control Group.** In patients with mild to moderate OSAHS and the control group, MoCA scores from high to low were  $27.72 \pm 1.30$ ,  $26.03 \pm 2.39$ , moderate,  $24.63 \pm 1.90$ , and  $21.56 \pm 3.23$ , respectively. The score difference was statistically significant ( $F = 40.609$ ,  $P = 0.000$ ). The moderate difference between the control group and OSAHS mild OSAHS was statistically significant ( $P \leq 0.01$ ). The moderate difference between the severe OSAHS group and the mild OSAHS group was statistically significant ( $P < 0.01$ ), that is, the more severe the OSAHS patients were, the lower the MoCA score was. The language index of the control group was significantly different from that of the moderate OSAHS group ( $P \leq 0.01$ ). There was statistically significant difference between the mild OSAHS group and the moderate OSAHS group ( $P < 0.01$ ). There was significant difference in delayed recall index between the control group and the moderate OSAHS group ( $P \leq 0.01$ ). There was statistically significant difference between the severe OSAHS group and the moderate OSAHS group ( $P < 0.01$ ). There was significant difference in orientation index between the control group and the moderate OSAHS group ( $P \leq 0.01$ ). The difference between the severe OSAHS group and the mild OSAHS group was statistically significant ( $P < 0.05$ ), as shown in Table 3 and Figures 3 and 4.

**4.4. Logistic Regression Analysis of the Factors Affecting the Cognitive Function of OSAHS Patients.** The cognitive function score of OSAHS patients was divided into a dichotomous variable by MoCA score of 26: (1)  $< 26$ , indicating cognitive dysfunction and (2) a score of 26 indicates normal

cognitive function. The dichotomies of cognitive function scores in the converted OSAHS group were used as dependent variables, and years of education, age, BMI, LSAO<sub>2</sub>, AHI, etc., were used as independent variables. According to the standard of  $A_{in} = 0.05$   $A_{out} = 0.10$ , a progressive binary Logistic regression analysis was performed to explore the age and years of education. The meanings and values of the variables influencing the cognitive function of patients with OSAHS, including BMI, LSAO<sub>2</sub>, and AHI, are shown in Table 4.

**4.5. Multivariate Logistic Regression Analysis of Influence on Cognitive Function of Patients with OSAHS.** The results of Logistic regression analysis showed that there were three factors that were finally entered into the regression equation, namely, LSAO<sub>2</sub>, BMI, and AHI, in which LSAO<sub>2</sub> OR value and 95% CI were all  $< 1$ , which were protective factors for the occurrence of cognitive dysfunction in OSAHS patients. The OR value and 95% CI of BMI and AHI were all  $> 1$ , indicating that OSAHS is a risk factor for cognitive dysfunction in patients. With the increase of LSAO<sub>2</sub>, the risk of cognitive dysfunction in OSAHS patients decreased, and the OR value was 0.897 (95% CI: 0.815, 0.987). The increase of abnormal BMI also increased the risk of cognitive dysfunction in OSAHS patients, with an OR value of 2.133 (95% CI: 1.047, 4.346). Similarly, the increase of AHI anomaly level also increased the risk of cognitive dysfunction in OSAHS patients, and the OR value was 3.415 (95% CI: 1.695, 6.882), and the Logistic regression equation was  $\text{Logist}P = -0.109X_1 + 0.785X_2 + 1.228X_3$ . The results of the multivariate logistic regression analysis are presented in Table 5.

## 5. Conclusion

About 68% of OSAHS patients showed cognitive impairment, and patients with moderate to severe OSAHS were more likely to develop cognitive impairment than those with mild OSAHS. Cognitive dysfunction of OSAHS patients was

associated with age, obesity, education, and intermittent nocturnal hypoxia or hypoventilation. Age, obesity, and education level are risk factors for cognitive dysfunction in OSAHS patients. The severity of cognitive dysfunction of OSAHS patients was positively correlated with age and obesity and negatively correlated with education level. The results of this study showed that the total MoCA score of OSAHS patients was negatively correlated with AHI and positively correlated with the lowest blood oxygen saturation at night. The orientation of visual spatial attention language delay recall was negatively correlated with AHI. Delayed recall of visuospatial attention language was positively correlated with the lowest blood oxygen saturation at night. The results showed that patients with more severe nocturnal hypoxia or hypoventilation had more severe cognitive impairment, especially in visual spatial attention, language delay, recall orientation, and other aspects, confirming that nocturnal hypoxia or hypoventilation is one of the influencing factors of cognitive function in patients with OSAHS. However, whether nocturnal hypoxia or hypoventilation causes cognitive dysfunction in OSAHS patients through oxidative stress inflammatory response or apoptosis induction needs further research and exploration. The older the age, the higher the BMI, and the more severe the cognitive dysfunction. At the same time, the more times of nocturnal apnea and hypopnea in OSAHS patients, the lower the minimum blood oxygen saturation at night, and the more serious the cognitive function impairment, especially in memory, attention, and language.

## Data Availability

The data used to support the findings of this study are available from the corresponding author upon request.

## Conflicts of Interest

The authors declare that they have no conflicts of interest.

## References

- [1] Y. Zhao, H. Li, Y. Chen, K. Li, and S. Yang, "Edaravone mitigates cognitive impairment and hippocampal injury in juvenile rats with obstructive sleep apnea hypopnea syndrome via regulation of cAMP/PKACREB pathway," *Tropical Journal of Pharmaceutical Research*, vol. 20, no. 11, pp. 2299–2304, 2021.
- [2] F. Zhang, X. Wu, W. Duan, F. Wang, and M. Xiang, "Influencing factors of daytime sleepiness in patients with obstructive sleep apnea hypopnea syndrome and its correlation with pulse oxygen decline rate," *Evidence-based Complementary and Alternative Medicine*, vol. 2021, no. 9, 6 pages, 2021.
- [3] D. G. Raptis, O. Sinani, G. G. Rapti, A. Papanikolaou, and G. Xiromerisiou, "Clinically silent small vessel disease of the brain in patients with obstructive sleep apnea hypopnea syndrome," *Diagnostics*, vol. 11, no. 9, p. 1673, 2021.
- [4] J. Zhang, D. Zhao, Z. X. Zhou, Y. Wang, and B. Y. Chen, "Value of night pulse oximetry monitoring in obstructive sleep apnea hypopnea syndrome prediction and classification," *Zhonghua Jie He He Hu Xi Za Zhi= Zhonghua Jiehe He Huxi Zazhi= Chinese Journal of Tuberculosis and Respiratory Diseases*, vol. 44, no. 2, pp. 101–107, 2021.
- [5] M. Y. Pi, L. Y. Xu, J. J. Guo, X. S. Dong, and F. Han, "Feasibility study of telemedicine model for diagnosis and treatment of patients with obstructive sleep apnea hypopnea syndrome in China," *Zhonghua Yi Xue Za Zhi*, vol. 101, no. 22, pp. 1671–1675, 2021.
- [6] Y. Li and Y. Zhang, "To determine pivotal genes driven by methylated DNA in obstructive sleep apnea hypopnea syndrome," *Computational and Mathematical Methods in Medicine*, vol. 2021, no. 15, 9 pages, 2021.
- [7] W. Wang, Y. Zheng, M. Li, S. Lin, and H. Lin, "Recent advances in studies on the role of neuroendocrine disorders in obstructive sleep apnea-hypopnea syndrome-related atherosclerosis," *Nature and Science of Sleep*, vol. 13, pp. 1331–1345, 2021.
- [8] X. Ren, C. Li, X. Ma et al., "Design of multi-information fusion based intelligent electrical fire detection system for green buildings," *Sustainability*, vol. 13, no. 6, p. 3405, 2021.
- [9] Y. Li and Y. Wang, "Obstructive sleep apnea-hypopnea syndrome as a novel potential risk for aging," *Aging and Disease*, vol. 12, no. 2, pp. 586–596, 2021.
- [10] E. Chalkiadaki, K. Andreanos, E. Karmiris, C. Florou, and D. Papaconstantinou, "Ganglion cell layer thickening in patients suffering from obstructive sleep apnea-hypopnea syndrome with long mean apnea-hypopnea duration during sleep," *International Ophthalmology*, vol. 41, no. 3, pp. 923–935, 2021.
- [11] Z. Xiaojun, W. Chan, W. Hao, F. Fang, and X. Wei, "0727 study on the effect of obstructive sleep apnea-hypopnea syndrome on perioperative management in endoscopic sinus surgery patients," *Sleep*, vol. 43, Supplement\_1, p. A277, 2020.
- [12] M. Raj, P. Manimegalai, P. Ajay, and J. Amose, "Lipid data acquisition for devices treatment of coronary diseases health stuff on the internet of medical things," *Journal of Physics: Conference Series*, vol. 1937, article 012038, 2021.
- [13] L. N. Yang and J. Sun, "The change of blood gas and C reactive protein of obstructive sleep apnea-hypopnea syndrome patient with pretherapy and post-treatment of continuous positive airway pressure," *Zhonghua Er Bi Yan Hou Tou Jing Wai Ke Za Zhi= Chinese Journal of Otorhinolaryngology Head and Neck Surgery*, vol. 55, no. 2, pp. 159–162, 2020.
- [14] X. Chen, X. P. Yang, X. Niu, Y. Zhang, and S. Li, "Lingual tonsil hypertrophy as the independent cause of obstructive sleep apnea hypopnea syndrome: a case report," *Zhonghua Er Bi Yan Hou Tou Jing Wai Ke Za Zhi= Chinese journal of otorhinolaryngology head and neck surgery*, vol. 55, no. 4, pp. 403–405, 2020.
- [15] L. Xin, M. Chengyu, and Y. Chongyang, "Power station flue gas desulfurization system based on automatic online monitoring platform," *Journal of Digital Information Management*, vol. 13, no. 6, pp. 480–488, 2015.
- [16] H. J. Zhang and H. G. Liu, "Progress in research on obstructive sleep apnea hypopnea syndrome and nonalcoholic fatty liver disease," *Zhonghua Jie He He Hu Xi Za Zhi= Zhonghua Jiehe He Huxi Zazhi= Chinese Journal of Tuberculosis and Respiratory Diseases*, vol. 43, no. 7, pp. 588–591, 2020.
- [17] A. A. Karpovich, K. V. Shulha, V. I. Shishko, V. V. Inchuk, and D. S. Kaptsiukh, "State of the blood oxygen transport function in obstructive sleep apnea/hypopnea syndrome," *Journal of the Grodno State Medical University*, vol. 18, no. 2, pp. 119–123, 2020.

## *Retraction*

# **Retracted: Effect of Operation Room Nursing Intervention and Ceramic Prosthesis on Total Hip Arthroplasty**

### **Scanning**

Received 5 December 2023; Accepted 5 December 2023; Published 6 December 2023

Copyright © 2023 Scanning. This is an open access article distributed under the Creative Commons Attribution License, which permits unrestricted use, distribution, and reproduction in any medium, provided the original work is properly cited.

This article has been retracted by Hindawi, as publisher, following an investigation undertaken by the publisher [1]. This investigation has uncovered evidence of systematic manipulation of the publication and peer-review process. We cannot, therefore, vouch for the reliability or integrity of this article.

Please note that this notice is intended solely to alert readers that the peer-review process of this article has been compromised.

Wiley and Hindawi regret that the usual quality checks did not identify these issues before publication and have since put additional measures in place to safeguard research integrity.

We wish to credit our Research Integrity and Research Publishing teams and anonymous and named external researchers and research integrity experts for contributing to this investigation.

The corresponding author, as the representative of all authors, has been given the opportunity to register their agreement or disagreement to this retraction. We have kept a record of any response received.

### **References**

- [1] T. Xu and J. Zhang, "Effect of Operation Room Nursing Intervention and Ceramic Prosthesis on Total Hip Arthroplasty," *Scanning*, vol. 2022, Article ID 2421723, 8 pages, 2022.

## Research Article

# Effect of Operation Room Nursing Intervention and Ceramic Prosthesis on Total Hip Arthroplasty

Ting Xu  and Jie Zhang 

Marine Police Hospital of Anesthesiology Department, Jiaxing, Zhejiang 314000, China

Correspondence should be addressed to Jie Zhang; 20120637@stumail.hbu.edu.cn

Received 17 May 2022; Revised 6 June 2022; Accepted 13 June 2022; Published 21 June 2022

Academic Editor: Balakrishnan Nagaraj

Copyright © 2022 Ting Xu and Jie Zhang. This is an open access article distributed under the Creative Commons Attribution License, which permits unrestricted use, distribution, and reproduction in any medium, provided the original work is properly cited.

In order to solve the problems of large trauma, many postoperative complications, and complex operation of artificial hip arthroplasty, a method to analyze the application effect of operating room nursing intervention in artificial hip arthroplasty was proposed. Firstly, 120 patients who underwent hip arthroplasty in our hospital from January to December 2017 were selected; Secondly, they were randomly divided into routine group (60 cases) and intervention group (60 cases); finally, on this basis, the intervention group strengthened the nursing in the operating room and used nanoceramic prosthesis. The Harris score of hip joint, the incidence of postoperative complications, and the satisfaction with nursing services were compared between the two groups. The results showed that the Harris score of hip joint and the satisfaction score of nursing service in the intervention group were significantly higher than those in the routine group ( $P < 0.05$ ); the incidence of postoperative complications in the intervention group was significantly lower than that in the routine group ( $P < 0.05$ ). It is proved that actively carrying out nursing intervention in the operating room and using nanoceramic prosthesis can not only improve the clinical efficacy and nursing service satisfaction of patients undergoing total hip arthroplasty but also reduce the incidence of complications.

## 1. Introduction

With the aggravation of aging and the continuous increase of the elderly population, hip disease is one of the main reasons affecting the healthy life of the elderly. However, with the rapid development of medicine, hip arthroplasty has gradually matured and relieved more pain for patients. At present, the operation has been quite mature. Total hip arthroplasty (THA) uses artificial hip prosthesis to replace the femoral head and acetabulum of the diseased hip joint. Its purpose is to relieve pain, restore joint function, and improve the quality of life of patients. Relevant data show that there are nearly 2 million joint replacement operations in the United States every year, and there is a growing trend year by year. Some researchers have predicted the growth trend of hip arthroplasty. It is speculated that hip arthroplasty will increase to 174% by 2030. Therefore, the

professional and technical requirements of the operation for medical staff are also increasing, and the patients' postoperative effect and life recovery are increasing accordingly. Both doctors and patients hope to experience the least pain and obtain the best postoperative recovery through efficient surgery. The main nursing staff for the rehabilitation of patients after hip arthroplasty will play an important role, as shown in Figure 1.

## 2. Literature Review

Despite the rapid development of hip arthroplasty technology, patients will still leave some unique complications, such as postoperative joint instability and dislocation, bleeding and hematoma, infection, and thrombosis. Among them, the most common is deep venous thrombosis (DVT), which mostly occurs in the lower limb,



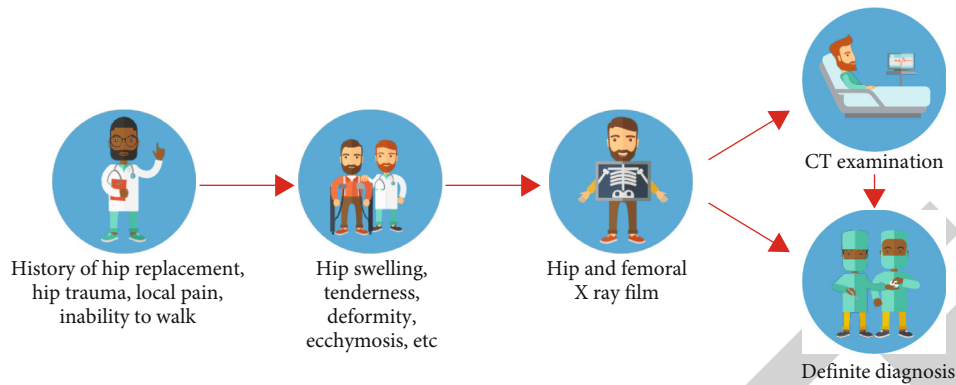


FIGURE 1: HIP arthroplasty.

and the left side is the most common. If the patient does not receive timely and effective treatment and care, the thrombus will affect the whole limb through retrograde expansion, and there will be serious complications—pulmonary embolism (PE), which threatens the life of the patient.

Scholars Wang and others predict that the demand for hip arthroplasty among the elderly in China will be greater, and the growth of hip arthroplasty will be faster [1]. Liu and others reported that the probability of DVT after hip arthroplasty is as high as 75% [2]. Synderm and others synthesized relevant guidelines and literature and found that if corresponding preventive measures were not taken after hip arthroplasty, DVT confirmed by venography occurred in 30% [3]. Li and Zhang also showed that the incidence of DVT after hip arthroplasty was 20% without preventive measures [4]. According to Triantafyllou et al., the probability of DVT after joint replacement is 45% [5]. Garcia-Rey and other studies show that caregivers' mastery of disease-related knowledge will have a positive impact on patients' knowledge and even behavior [6]. Clarkeic and others carried out health education for relatives and caregivers of stroke patients. The results showed that the psychological state and health and safety problems of elderly stroke patients were significantly improved [7]. Liu and others implemented health education for caregivers of patients with pancreatitis at the same time. The results further confirmed that health education participated by caregivers can enhance patients' mastery of relevant disease knowledge and effectively improve patients' psychological status [8]. Lucchini et al. believe that standardized operating room nursing intervention is helpful to improve the clinical treatment effect of total hip arthroplasty [9]. Xiong and Ge believe that surgeons are responsible for the organization and operation of the surgical process, cooperate with assistants, anesthesiologists, and nursing staff, maintain positive communication and exchange with each other, and jointly discuss the treatment methods of various emergency problems [10].

On the basis that patients with hip arthroplasty will still leave some unique complications, this paper puts forward that surgical nursing intervention combined with nanoceramic prosthesis can not only reduce the probability of postoperative complications but also reduce the cost of follow-up treatment and maintenance. Finally, the analysis data under the control test are given to prove the feasibility of this technology. It is

proved that actively carrying out nursing intervention in the operating room and using nanoceramic prosthesis can not only improve the clinical efficacy and nursing service satisfaction of patients undergoing total hip arthroplasty but also reduce the incidence of complications.

### 3. Effect of Nursing Intervention in Operating Room Combined with Nanoceramic Prosthesis on Total Hip Arthroplasty

#### 3.1. Application of Nanoceramic Prosthesis in Hip Arthroplasty

**3.1.1. Application Method.** Inclusion criteria: (1) primary total hip arthroplasty patients with surgical indications; (2) agreed to participate in this study. Exclusion criteria: (1) coinfection; (2) with mental illness; (3) those with insufficient bone mass and unfit for biological fixation; (4) there are other surgical contraindications. The fourth-generation nanoceramic interface hip prosthesis was used in 28 patients. The basic information of the research object is shown in Table 1.

**3.1.2. Prosthesis Materials.** The materials of hip prosthesis are the fourth-generation nanoceramics (Ceramatechag, Plochingen, Germany); the lining and ball joint compatibility interface all adopt biological fixed mortar cup and femoral handle (Corail DePuy, Warsaw, IN).

**3.1.3. Operation Method.** All patients were treated with intravenous inhalation combined with general anesthesia. In the healthy lateral position, take the posterolateral incision of the hip, cut the gluteus maximus muscle membrane, and separate the gluteus maximus muscle. Cut off some external rotation muscles and joint capsule. Osteotomy was performed 1.5 cm on the lesser trochanter, and the femoral head was taken out. Remove the labial margin of acetabulum and femoral round ligament, expand the acetabulum, and test the model in turn. Choose a suitable Pinnacle metal acetabular cup, keep it abducted about 40 degrees and tilted forward about 20 degrees, and fix it with two acetabular screws. Implant corresponding nanoceramic lining. Remove the proliferative osteophyte around the acetabulum. The femoral medullary cavity was found out, and the medullary cavity

TABLE 1: Basic data of research object.

Project	Data	Diagnostic type	Data
Gender (male/female)	15/13	Osteoarthritis	8
Age (years)	52.2	Dislocation of hip joint	4
BMI	24.7	Femoral head necrosis	9
Left/right hip	14/15	Ankylosing spondylitis	1

TABLE 2: Harris score before and after operation.

Project	Preoperative	After operation	<i>t</i>	<i>P</i>
Score	41.7 ± 10.8	92.2 ± 7.0	37.6	0.000

file was expanded in turn. Appropriate femoral head test model was placed and reset. Measure the limb length, and test the hip flexion, adduction, internal rotation, extension, external rotation, and abduction without dislocation. Select suitable Corail femoral stem and nanoceramic femoral head [11]. Reset check is the same as before. Wash repeatedly, stop bleeding thoroughly, and place a drainage tube for drainage. Repair the joint capsule and external rotator brevis muscle, and suture the wound in layers. 1.4 postoperative treatment after operation, cefuroxime was routinely used for 2-3 days to prevent infection, low molecular weight heparin was used for 14 days to prevent venous thrombosis (rivaroxaban was taken if the patient was discharged from the hospital), and celecoxib was used for 3-5 days to relieve pain. The drainage tube was pulled out 24 hours after operation. Two days after operation, they got out of bed with the aid of walking aid for walking function training [12]. After 6 weeks, gradually abandon the turn and walk independently.

**3.1.4. Evaluation Index.** Harris hip score was performed before operation. The patients were followed up at 3 months, 6 months, 12 months, and every other year. Harris score, X-ray implant analysis, and complications were investigated [13]. The last follow-up score was taken as the final result. Harris hip function score grading standard: excellent is 90-100 points, good is 80-89 points, medium is 70-79 points, and poor is 70 points.

**3.1.5. Statistical Analysis.** Spss21.0 software was used to conduct paired *t*-test on the Harris score data before and after operation. The measurement data were expressed in  $\bar{x} \pm s$ , with  $P < 0.05$  as the difference, which was statistically significant, as shown in Table 2.

### 3.2. Characteristics of Nanoceramic Materials

**3.2.1. Advantages of Nanoceramic Materials.** The excellent tribological properties of nanoceramic materials are its main advantages. Alumina nanoceramics are widely used in clinic. Theoretically, the hardness of alumina nanoceramics is 10 times that of cobalt chromium alloy. Alumina with almost 2000VH hardness is the second hard material on earth after diamond. This hardness gives it scratch resistance [14]. The good lubrication brought by the wettability of nanoceramics

is another advantage, especially when a microliquid film is formed on the surface. In addition, the close combination between oxygen and aluminum atoms provides excellent corrosion resistance of nanoceramics, so the biocompatibility is also superior [15]. At the same time, its chemical properties are inert, so there is no need to worry about allergy or rejection. However, the high hardness of alumina nanoceramics is accompanied by low toughness and low bendability [16]. Therefore, it is relatively fragile and cannot be completely deformed.

**3.2.2. Innovation of Nanoceramic Materials.** In order to meet the strict requirements of increasing patient activity and long service life expectation, the material industry has developed a new fourth-generation nanoceramics, namely, alumina-based composite nanoceramics (AMC). This material synthesizes and strengthens the tribological properties of nanoceramics and creates better mechanical resistance. In the friction test, AMC shows excellent wear resistance, especially under the condition of challenging thermal aging, a variety of new technologies have been introduced into the production of AMC, such as the integration of zirconia in alumina matrix, resulting in bio-oxdelta nanoceramics [17]. Nanoytria-reinforced tetragonal zirconia particles prevent the generation and expansion of nanoceramic cracks, improve mechanical properties, and further reduce wear. The flake crystal structure provided by the oxide additive disperses the force leading to the crack. Chromium oxide (0.5%) was added to increase hardness; strontium oxide crystal (0.5%) enhanced toughness and dispersed crack energy. The final AMC consists of 82% alumina, 17% zirconia, and less than 1% chromium oxide and strontium oxide. In vitro experiments, the wear rate of AMC to AMC with 28 mm ball head was reduced from 1.84 mm<sup>3</sup> to 0.16 mm per million cycles compared with the traditional alumina to alumina interface, and the AMC particles were reduced to less than 0.8 μm compared with the size of the third-generation alumina nanoceramic particles (1-5 μm). This is more favorable for the formation of liquid film layer [18], as shown in Figure 2.

**3.2.3. Excellent Wear Resistance.** Due to the high strength and hardness of nanoceramics, nanoceramics can resist the wear of bone tissue, bone cement, and metal debris. In this way, the wear of the weight-bearing surface between prostheses is reduced. Nanoceramics is the compatibility mode with the lowest wear rate in hip arthroplasty. Lusty and others reported that 283 hips (301 hips) underwent the third-generation COC hip arthroplasty, the 7-year in place rate was 99%, the wear rate of nanoceramic head was 0.2 mm<sup>3</sup>, and only one femoral stem had aseptic loosening 2 months after operation.

**3.2.4. Extremely High Hardness.** Nanoceramic materials are very hard, and their hardness is second only to diamond, which is much higher than metal materials such as cobalt chromium alloy and titanium alloy. Therefore, parts made of nanoceramics are not easy to be scratched. It is a kind of brittle material, but its tensile strength is still significantly lower than that of nanoceramic material. The reported incidence of prosthesis fragmentation is 0.015%, and most reports suggest that the incidence of nanoceramic lining is much higher than that

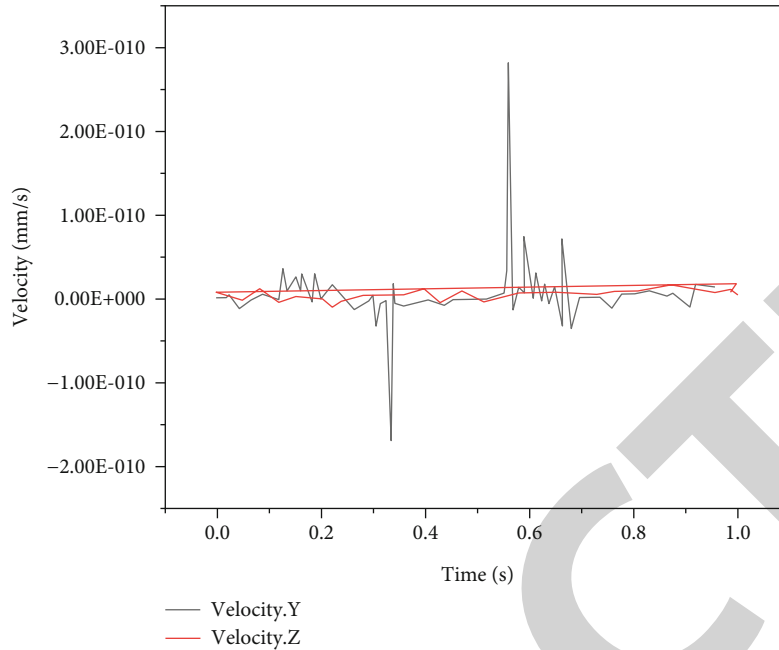


FIGURE 2: Formation curve of AMC particles and liquid film layer.

of nanoceramic femoral head fragmentation [19]. Zirconia nanoceramics have higher hardness and better toughness than alumina, which can reduce the incidence of fragmentation of nanoceramic parts.

**3.2.5. Good Biocompatibility.** The concentration of metal ions in serum of patients with metal prosthesis increases after replacement. The metal particles produced by metal metal prosthesis are not only toxic to macrophages but also affect the growth of osteoblasts. Metal prosthesis can also lead to the hypersensitivity of human tissue to metal ions. Friedman et al. pointed out that the principle to solve osteolysis around the prosthesis is to reduce the wear particles around the prosthesis. Alumina nanoceramics reduce the biological reaction caused by wear and prolong the service life of prosthesis. Nanoceramics can work normally under humid conditions, which overcomes the problem that metal prosthesis is easy to release metal ions in the humid environment in the body. Alumina nanoceramics are biologically inert materials with stable chemical bonds, low histological reaction, and no corrosion. Nanoceramic particles also have less stimulation to the tissue than metal particles. The particles produced during wear are small, and the tissue reaction is small, so the nanoceramic joint can effectively reduce osteolysis [20]. It was found that the wear particles of alumina nanoceramics induced the production of interleukin- (IL-) 6, tumor necrosis factor (TNF), and granulocyte macrophage colony stimulating factor (GM-GSF) lower than polyethylene wear particles. The average diameter of alumina nanoceramics wear particles used in the experiment was  $94\ \mu\text{m}$ . Human peripheral blood monocytes were used to establish the artificial joint model in vitro to make it closer to the actual situation in vivo. The results show that alumina nanoceramic wear particles have lower bioactivity.

These improvements have improved the rupture strength of the material, and each part has been subjected to failure test, which is a standard that cannot be reached by early nanoceramic materials.

## 4. Experimental Results and Discussion

### 4.1. Effect of Operating Room Nursing Intervention Combined with Nanoceramic Prosthesis on the Rehabilitation of Total Hip Replacement

**4.1.1. Technical Route.** Multidisciplinary team usually refers to the clinical treatment mode that experts from multiple disciplines form a relatively fixed expert group to put forward diagnosis and treatment opinions through regular and localized meetings for an organ or system disease. It is widely used in many clinical fields. In this study, it refers to the establishment of a team with researchers as the coordinator, including surgeons, surgical nurses, anesthesiologists, rehabilitators, psychological counselors, nutritionists, and nurses. Under the coordination of caregivers (caregivers are educators of patients' disease related knowledge, transmitters of patients' information, supervisors of patients' compliance with medical orders, and supporters of patients' exercise and medication to prevent DVT), intervention is implemented for elderly patients after hip arthroplasty to effectively prevent DVT [21], as shown in the technical roadmap in Figure 3.

### 4.1.2. Inclusion Criteria

- (1) Age  $\geq 60$  years old
- (2) There are fixed caregivers during the whole hospitalization, and the education level of caregivers is junior middle school or above

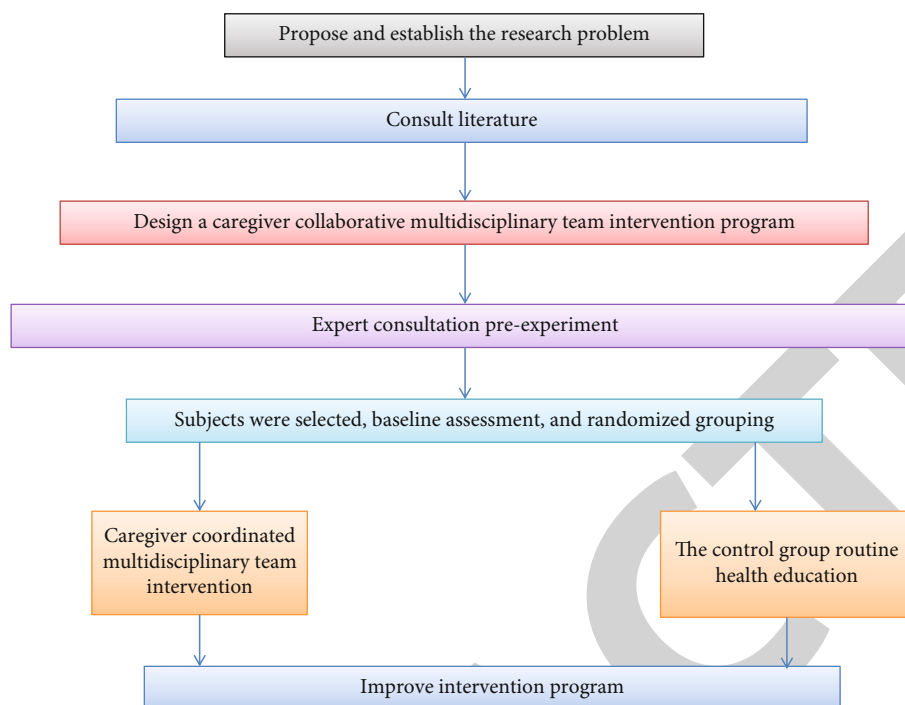


FIGURE 3: Technical roadmap.

- (3) After hip arthroplasty, they can accept intervention measures with the help of caregivers
- (4) No serious diseases such as cardiac and renal dysfunction
- (5) Clear consciousness without obvious impairment of language and cognitive function
- (6) Voluntary participation, informed consent, and researchers

#### 4.1.3. Exclusion Criteria

- (1) Preoperative B-ultrasound examination of patients with lower extremity deep venous thrombosis, thrombophlebitis, or pulmonary embolism
- (2) Abnormal local conditions of lower limbs (such as dermatitis, gangrene, and recent skin transplantation)
- (3) Severe arteriosclerosis or other ischemic vascular diseases and severe deformities of lower limbs
- (4) Congestive cardiac failure and pulmonary edema

#### 4.1.4. Exit Criteria

- (1) The participants were unable to continue the study due to the aggravation of their condition
- (2) Patients asked to withdraw for various reasons during the study

4.1.5. *Sample Size Calculation.* According to the comparison formula of the mean of two samples (1),

$$(x + a)^n = \sum_{k=0}^n \binom{n}{k} x^k a^{n-k}. \quad (1)$$

According to the research results of literature, the difference of health belief score is 4.10, and the standard deviation is 3.6. Finally, it is calculated that 49 patients in each group need hip arthroplasty. Considering the 15% loss of follow-up rate, about 55 samples are needed in each group, and the final total sample size is 110 [22].

#### 4.2. Effectiveness Analysis of Operating Room Nursing Combined with Nanoceramic Prosthesis in Total Hip Arthroplasty

4.2.1. *General Information.* The subjects of this study were 94 patients who underwent total hip arthroplasty in our hospital from March 2017 to February 2019. According to the application of nursing cooperation in the operating room, 48 patients in the observation group (after application: March 2018 to February 2019) and 46 patients in the control group (before application: March 2017 to February 2018) were analyzed. There were 28 males and 20 females in the observation group. The age range was 49-75 years, with an average age of  $61.18 \pm 4.42$  years. There were 29 males and 17 females in the control group. The age range was 48-76 years, with an average of  $62.31 \pm 4.29$  years. The basic data were comparable  $P > 0.05$  [23].

TABLE 3: Physical signs of patients in the two groups before and after nursing.

Group	Time	SBP (mmHg)	DBP (mmHg)	HR (times/min)
Observation group ( $n = 48$ )	Before nursing	123.6 $\pm$ 7.9	79.1 $\pm$ 6.3	73.1 $\pm$ 4.6
	After nursing	127.3 $\pm$ 9.4	83.5 $\pm$ 5.2	74.9 $\pm$ 3.7
Control group ( $n = 46$ )	Before nursing	124.2 $\pm$ 8.3	79.5 $\pm$ 5.9	73.5 $\pm$ 4.4
	After nursing	35.4 $\pm$ 9.6*	89.7 $\pm$ 7.3**	84.6 $\pm$ 5.5*#

TABLE 4: Nursing effect of two groups of patients.

Group	Satisfaction	Postoperative complications
Observation group ( $n = 48$ )	46 (95.83)	1 (2.08)
Control group ( $n = 46$ )	35 (76.09)	8 (17.39)
$\chi^2$	7.686	4.713
$P$	<0.05	

4.2.2. *Method.* Patients in the control group received routine nursing during total hip arthroplasty. During the total hip arthroplasty, the patients in the observation group received nursing cooperation in the operating room. The specific measures are as follows:

- (1) Preoperative preparation: prepare the operating room, and adjust the temperature and humidity to the appropriate range after strict cleaning and disinfection. Check the surgical instruments and various medical items, and check the operation performance of relevant instruments. In the operation guidance, nurses should care about the feelings of patients and ask patients about their thoughts and attitudes towards total hip arthroplasty. According to the patients' cognition of their own diseases and operations, appropriate publicity, and education methods should be applied. Understand the causes of patients' anxiety and tension, and conduct psychological counseling. In order to reduce patients' concern about surgical risk, it is necessary to carry out surgical guidance in combination with successful treatment medical records, improve patients' self-confidence, relax, and accept surgical treatment with a peaceful attitude [24]
- (2) Intraoperative nursing: combined with previous experience, emergency treatment measures should be prepared for common risk events during surgical treatment. When the patient has elevated blood pressure and accelerated heart rate, they need to be vigilant, and the medical staff can respond quickly and deal with it in time. During the operation, the principle of sterility must be strictly followed. Disinfect the skin of the operation field and prepare sterile bandage and operation film. Nurses need to fully master the operation process and actively assist and cooperate with doctors. Deliver surgical instruments timely, accurately, and stably according to the

operation process. According to the patient's hip injury, select the appropriate specification of prosthesis materials. Before installing the prosthesis, it is necessary to prepare the femoral medullary cavity, expand the medullary cavity, correct the osteotomy surface, and reset the femoral head, and then, install the prosthesis correctly after washing and drying with normal saline. At the same time, keep the surgical incision clean and drain and rinse [25]

- (3) Postoperative care: during the postoperative care period, sort out the surgical instruments and related medical articles, and place them in the designated position after checking them, to recycle the medical waste. Strengthen the monitoring of signs, check whether there is loosening and dislocation of artificial acetabulum, and ask the patient's feelings. To properly adjust the patient's posture, we need to consider the patient's comfort and pay attention to protecting the patient's surgical incision. In the hip bone carina, axillary nerve, and other parts, protection should be done to avoid skin damage. Under the guidance and assistance of nursing staff, functional rehabilitation training is carried out, such as hip lifting and turning over

4.2.3. *Results.* The physical signs of the two groups before and after nursing are shown in Table 3.

The nursing effects of the two groups are shown in Table 4.

## 5. Conclusion

During the treatment of total hip arthroplasty, affected by a variety of risk factors, the safety and effectiveness of the operation are reduced, resulting in an unsatisfactory prognosis. The effective development of nursing work in the operating room can provide a good safety guarantee for surgical treatment and postoperative rehabilitation. Strengthening the nursing cooperation in the operating room can effectively manage and control the whole process of surgical treatment, more standardized, and refined implementation of surgical operation, and reduce the occurrence of errors and errors. In the preoperative nursing stage, medical devices, instruments, and various items should be fully prepared and in place. Respect the opinions and ideas of patients, take into account the actual feelings of patients, pay attention to their emotional state, and implement psychological nursing intervention. Through psychological nursing intervention, eliminate patients' negative emotions,

and guide patients to face treatment with a positive and optimistic attitude. In intraoperative nursing, medical staff need to divide their work reasonably and clarify their own responsibilities. The results also showed that the Harris score of hip joint and the satisfaction score of nursing service in the dry group were significantly higher than those in the routine group ( $P < 0.05$ ); the incidence of postoperative complications in the intervention group was significantly lower than that in the routine group ( $P < 0.05$ ). For common risk events, emergency treatment preparations can be made in advance, which can fully ensure the safety of surgery and reduce the harm of risk events. At the same time, good posture management, pain nursing, and complication prevention can actively promote the postoperative rehabilitation of patients. In conclusion, the operating room nursing in total hip arthroplasty combined with nanoceramic prosthesis has a positive impact on improving the safety of surgical treatment and promoting the postoperative rehabilitation of patients.

### Data Availability

The data used to support the findings of this study are available from the corresponding author upon request.

### Conflicts of Interest

The authors declare that they have no conflicts of interest.

### References

- [1] J. Wang, M. Zhang, Y. Xu, X. J. Li, and X. J. Cao, "A rare case of inflammation after total hip arthroplasty due to a malpositioned prosthesis: a case report," *Medicine*, vol. 99, no. 22, article e20468, 2020.
- [2] L. Liu, F. Zhao, G. Zha, X. Zheng, and S. Xu, "Effect of surgeon's handedness on distribution of prosthesis during primary total knee arthroplasty," *Chinese Journal of Reparative and Reconstructive Surgery*, vol. 34, no. 6, pp. 696–701, 2020.
- [3] M. Synder, M. Drobniewski, P. Kozłowski, and A. Grzegorzewski, "Ceramic-ceramic articulation in uncemented total hip arthroplasty," *Wiadomości Lekarskie (Warsaw, Poland: 1960)*, vol. 58, no. 3-4, pp. 193–197, 2005.
- [4] C. Li and H. Zhang, "Early failure for wear after ceramic-on-highly cross-linked polyethylene total hip arthroplasty: a case report," *BMC Musculoskeletal Disorders*, vol. 21, no. 1, 2020.
- [5] A. Triantafyllou, G. Papagiannis, S. Stasi, P. Georgios, and G. C. Babis, "Biomechanical assessment of wear in ceramic on ceramic and ceramic on xlpe thas," *Journal of Mechanics in Medicine and Biology*, vol. 21, no. 2, article 2150023, 2021.
- [6] E. Garcia-Rey, P. Bizot, and E. Garcia-Cimbrelo, "Ceramic-on-ceramic cementless total hip arthroplasty in patients aged 40 years or under: do preoperative conditions affect long-term results?," *Orthopaedics & Traumatology, Surgery & Research*, vol. 107, no. 1, article 102763, 2021.
- [7] I. C. Clarke, V. Good, P. Williams et al., "Ultra-low wear rates for rigid-on-rigid bearings in total hip replacements," *Proceedings of the Institution of Mechanical Engineers, Part H: Journal of Engineering in Medicine*, vol. 214, no. 4, pp. 331–347, 2000.
- [8] Y.-B. Liu, H. Pan, L. Chen et al., "Total hip revision with custom-made spacer and prosthesis: a case report," *World Journal of Clinical Cases*, vol. 9, no. 25, pp. 7605–7613, 2021.
- [9] S. Lucchini, F. Castagnini, F. Giardina, F. Tentoni, and F. Traina, "Cementless ceramic-on-ceramic total hip arthroplasty in post-traumatic osteoarthritis after acetabular fracture: long-term results," *Archives of Orthopaedic and Trauma Surgery*, vol. 141, no. 4, pp. 683–691, 2021.
- [10] D. Xiong and S. Ge, "Friction and wear properties of UHMWPE/Al<sub>2</sub>O<sub>3</sub> ceramic under different lubricating conditions," *Wear*, vol. 250, no. 1-12, pp. 242–245, 2001.
- [11] Q. Zhang, "Relay vibration protection simulation experimental platform based on signal reconstruction of MATLAB software," *Nonlinear Engineering*, vol. 10, no. 1, pp. 461–468, 2021.
- [12] D. Granchi, G. Ciapetti, I. Amato et al., "The influence of alumina and ultra-high molecular weight polyethylene particles on osteoblast-osteoclast cooperation," *Biomaterials*, vol. 25, no. 18, pp. 4037–4045, 2004.
- [13] R. Huang, S. Zhang, W. Zhang, and X. Yang, "Progress of zinc oxide-based nanocomposites in the textile industry," *IET Collaborative Intelligent Manufacturing*, vol. 3, no. 3, pp. 281–289, 2021.
- [14] L. Xin, L. Jianqi, C. Jiayao, Z. Fangchuan, and M. Chengyu, "Study on treatment of printing and dyeing waste gas in the atmosphere with Ce-Mn/GF catalyst," *Arabian Journal of Sciences*, vol. 14, no. 8, 2021.
- [15] D. Dowson, "A comparative study of the performance of metallic and ceramic femoral head components in total replacement hip joints," *Wear*, vol. 190, no. 2, pp. 171–183, 1995.
- [16] M. Bradha, N. Balakrishnan, A. Suvitha et al., "Experimental, computational analysis of Butein and Lanceoletin for natural dye-sensitized solar cells and stabilizing efficiency by IoT," *Environment, Development and Sustainability*, vol. 24, no. 6, pp. 8807–8822, 2022.
- [17] V. O. Saikko, "Wear of the polyethylene acetabular cup: The effect of head material, head diameter, and cup thickness studied with a hip simulator," *Acta Orthopaedica Scandinavica*, vol. 66, no. 6, pp. 501–506, 1995.
- [18] J. D'Antonio, "Bearing surface for young patients: ceramic on ceramic: updated data and why I like it, AR symposia," *Proceeding of the American Academy of Orthopedic Surgeons Annual Meeting, Chicago*, vol. 81, 2006.
- [19] A. Sharma, R. Kumar, M. Talib, S. Srivastava, and R. Iqbal, "Network modelling and computation of quickest path for service-level agreements using bi-objective optimization," *International Journal of Distributed Sensor Networks*, vol. 15, no. 10, 2019.
- [20] S. Williams, A. Schepers, G. Isaac et al., "The 2007 Otto Aufranc AWARD: Ceramic-on-Metal hip Arthroplasties," *Clinical Orthopaedics & Related Research*, vol. 465, pp. 23–32, 2007.
- [21] G. Willmann, H. J. Früh, and H. G. Pfaff, "Wear characteristics of sliding pairs of zirconia (Y-TZP) for hip endoprostheses," *Biomaterials*, vol. 17, no. 22, pp. 2157–2162, 1996.
- [22] J. Garino, M. N. Rahaman, and B. S. Bal, "The Reliability of Modern Alumina Bearings in Total Hip Arthroplasty," *Seminars in Arthroplasty*, vol. 17, no. 3-4, pp. 113–119, 2006.
- [23] K.-H. Koo, Y.-C. Ha, W. H. Jung, S.-R. Kim, J. J. Yoo, and H. J. Kim, "Isolated fracture of the ceramic head after third-generation alumina-on-alumina total hip arthroplasty," *The*

## Retraction

# Retracted: Application of CT Scan in Diagnosis of Iliac-Femoral Vein Thrombosis after Hip Replacement

### Scanning

Received 11 July 2023; Accepted 11 July 2023; Published 12 July 2023

Copyright © 2023 Scanning. This is an open access article distributed under the Creative Commons Attribution License, which permits unrestricted use, distribution, and reproduction in any medium, provided the original work is properly cited.

This article has been retracted by Hindawi following an investigation undertaken by the publisher [1]. This investigation has uncovered evidence of one or more of the following indicators of systematic manipulation of the publication process:

- (1) Discrepancies in scope
- (2) Discrepancies in the description of the research reported
- (3) Discrepancies between the availability of data and the research described
- (4) Inappropriate citations
- (5) Incoherent, meaningless and/or irrelevant content included in the article
- (6) Peer-review manipulation

The presence of these indicators undermines our confidence in the integrity of the article's content and we cannot, therefore, vouch for its reliability. Please note that this notice is intended solely to alert readers that the content of this article is unreliable. We have not investigated whether authors were aware of or involved in the systematic manipulation of the publication process.

In addition, our investigation has also shown that one or more of the following human-subject reporting requirements has not been met in this article: ethical approval by an Institutional Review Board (IRB) committee or equivalent, patient/participant consent to participate, and/or agreement to publish patient/participant details (where relevant).

Wiley and Hindawi regrets that the usual quality checks did not identify these issues before publication and have since put additional measures in place to safeguard research integrity.

We wish to credit our own Research Integrity and Research Publishing teams and anonymous and named external researchers and research integrity experts for contributing to this investigation.

The corresponding author, as the representative of all authors, has been given the opportunity to register their agreement or disagreement to this retraction. We have kept a record of any response received.

### References

- [1] D. Li, L. Wang, Z. Li et al., "Application of CT Scan in Diagnosis of Iliac-Femoral Vein Thrombosis after Hip Replacement," *Scanning*, vol. 2022, Article ID 8428963, 9 pages, 2022.

## Research Article

# Application of CT Scan in Diagnosis of Iliac-Femoral Vein Thrombosis after Hip Replacement

Dong Li <sup>1</sup>, Lishan Wang <sup>1</sup>, Zhanxin Li <sup>1</sup>, Libin Li <sup>2</sup>, Qingwei Wang <sup>1</sup>, Li Zhang <sup>1</sup>, and Zhigang Guo <sup>1</sup>

<sup>1</sup>North China Medical & Health Group Xingtai General Hospital, Xingtai, Hebei 054000, China

<sup>2</sup>Respiratory Department of Hebei General Hospital for Veterans, Xingtai, Hebei 054000, China

Correspondence should be addressed to Zhigang Guo; 18409190@masu.edu.cn

Received 8 May 2022; Revised 20 May 2022; Accepted 26 May 2022; Published 20 June 2022

Academic Editor: Balakrishnan Nagaraj

Copyright © 2022 Dong Li et al. This is an open access article distributed under the Creative Commons Attribution License, which permits unrestricted use, distribution, and reproduction in any medium, provided the original work is properly cited.

Based on the knowledge of the previous film, the CT scan was used to diagnose the disease of women and men after the diagnosis of atherosclerosis by scanning the CT microscope. This article first examines the existing medical procedures in China, highlighting the advantages and disadvantages of various systems in terms of usability and user experience. Combined with the actual needs of hospitals, this paper developed a set of preoperative intelligent measurement system (MIPS) based on pattern recognition for total skeletal joint replacement. It is beneficial for doctors to better observe the lesions of patients before surgery and carry out necessary operations in the PATIENT DR film. In the process, the model is used to identify the patient, and the patient is given a fake score based on the characteristics of the DR film. In nonsymptomatic patients, 13.5% had muscle contraction > 50%, 2.0% had muscle contraction 70%, and the mean pelvic area was 23.48%. The left ventricular muscle has a 45.0% contraction rate, the left ventricle has a 70% contraction, and the median contraction rate is 47.58%. The right muscle, which is inserted between the right artery and the inner lymphatic artery, is the most common type of compression of the right muscle, accounting for 59.26%. In terms of the mean muscle contraction rate on the right side, patients with DVT with right muscles were higher than patients with DVT with left ventricles (48.54% to 22.29%,  $P < 0.001$ ). The mean incidence of left ventricular DVT patients was higher than that of right ventricular DVT patients (71.88% versus 45.83%  $P < 0.0011$ ).

## 1. Introduction

At present, China has a certain theoretical basis for the study of deep vein thrombosis after bone joint replacement and some prevention systems, but most of them are clinical experience, and there is a lack of clinical application standards based on evidence-based theory for the prevention of deep vein thrombosis. Nursing managers and clinical nursing workers in China are focusing on the appropriate prevention measures and effects of DVT, but the viewpoints are outdated and the content is relatively limited. More importantly, current studies lack evidence-based prevention strategies and cluster interventions for DVT, as well as simple, scientific, and effective guiding prevention measures and standardized standards in clinical work, which are not conducive to nursing quality management and process monitoring. In 2008, the

American College of Chest Physicians (ACCP) has developed the 8th edition of its clinical practice guidelines for antithrombotic therapy and thrombotic prophylaxis and issued the 9th edition in 2012. Evidence-based nursing (EBN) is a nursing concept, which is influenced by evidence-based medicine (EBM), also known as evidence-based nursing. The core idea of evidence-based nursing is to use the most reliable scientific evidence to achieve the best nursing effect, which contains three elements: first, use the most appropriate nursing research evidence; second, the clinical experience and personal skills of the nursing staff; and third, the patient's actual situation, values, and subjective will. Combine these three elements together to guide practical work. The implementation of nursing for patients should be patient-centered and should also be combined with the personal experience and rich clinical skills of nursing staff.



## 2. Literature

Gitelzon et al. said that in recent years, with the rapid development of expressways and railways, cars and electric vehicles have increased dramatically, and people's lifestyles have changed. These factors lead to an increase in the incidence of car accidents, joint injury and joint disease, and the deterioration of patients' joint function, leading to the reduction of patients' quality of life [1]. Is et al. said a study shows that joint replacement is on the rise, increasing by 11 percent a year in Europe and the United States and in China, too [2]. Ming et al. said that the patient's damaged limb joints cannot be repaired and replaced with prosthetic limbs, which are usually made of artificial materials to replace the damaged joints, so as to restore and improve the structure and function of the affected joints [3]. At present, total skeletal joint replacement is effective and widely used. Lm et al. said that artificial joint replacement has the advantages of relieving pain, maintaining joint stability, improving joint movement, and preventing shortened and deformed limbs [4]. But artificial joint replacement is not perfect. Dozie et al. said that in addition to the limitation of the stability of the joint itself, venous thromboembolism (VTE) and potentially more harmful secondary pulmonary embolism (PTE) have been widely concerned with the widespread development of such surgeries [5]. One study showed that in patients undergoing joint replacement surgery without effective anticoagulant therapy, many patients developed thrombosis after surgery, and the incidence of deep vein thrombosis reached 88,070. Even with effective interventions, the incidence is high, with approximately 2% to 5% of patients presenting with symptoms of VTE. In the United States, approximately 300,000 people die from DVT each year. Deep vein thrombosis kills about 300,000 people a year in the United States. Zhang et al. said that DVT can cause swelling, pain, and even necrosis of the affected limb, requiring amputation in severe cases, significantly reducing the ability to work and quality of life. More importantly, thromboembolism can be secondary to pulmonary embolism, which can even lead to death due to the urgency and severity of the disease [6]. Therefore, in the diagnosis, treatment and nursing work of joint replacement, prevention, and effective intervention should be strengthened. The patient underwent bone joint replacement surgery and developed deep vein thrombosis after surgery, mainly due to the slow blood flow of the three elements of thrombosis (identified by Virchow in 1856): the main causes of slow blood flow are the weakening of local venous return power caused by the lack of muscle pump in the affected limbs and the weakening of systemic venous return power caused by systemic cardiac function. Popivanov et al. said that due to the need to use anesthesia and sedative muscle relaxation drugs during the operation of the patient, at the same time, the postoperative limb needs a longer time to brake, which better provide local stability for fracture healing, resulting in temporary partial or complete loss of muscle pump function, and local venous return power weakened and slowed down [7]. When the patient's systemic blood flow slowed down and local affected limb blood flow slowed down, local tissues appeared meta-

bolic waste retention, different degrees of tissue hypoxia, and some cell metabolism abnormalities. This can not only lead to decreased fibrinolytic activity and local thrombin aggregation but also lead to varying degrees of vascular endothelial damage, thereby promoting local venous thrombosis. Damage to the blood vessel wall: the normal lining of blood vessels is a barrier to platelet aggregation. Endothelial cells produce prostaglandins, a hormone that dilates blood vessels. In the process of artificial bone arthroplasty, although the adjacent blood vessels are rarely directly damaged, they can still be indirectly damaged. The main possibilities are as follows: indirect injury of bone cement during surgery, thermal injury, infection, and chemical injury. Gitelzon et al. said that the thermal effect of cement can cause blood vessel damage and exogenous clotting when it is filled with cement [1]. In addition, the above mentioned local tissue metabolic waste retention of different degrees of hypoxia and abnormal cell metabolism caused by local and systemic slow blood flow of the affected limb can also lead to intima vein injury. Hypercoagulable state: increased clotting factors can increase blood viscosity. For patients undergoing artificial bone arthroplasty, stimulating cytokines released by local injury and systemic stress response can lead to increased clotting factors, inactivation of fibrinolytic system, and thrombosis. In the process of coagulation fibrinolysis and thrombolysis, D dimer changes and can reflect fibrinolysis activity, so DD can be used as a test indicator for diagnosis and monitoring of thrombolysis. Yadavalli et al. said that there are many factors that can affect the formation of blood clots during bone arthroplasty [8]. These factors include reduced preoperative activity, immobilization, prolonged postoperative bed rest, and the administration of a tourniquet, which may slow venous return. Stress response surgical trauma, thermal injury of local tissue caused by bone cement, and mannitol used to relieve postoperative soft tissue swelling can cause intima injury. At last, perioperative blood loss, fasting, and abstaining from drinking may result in blood concentration and hypercoagulability due to volume factors. Therefore, skeletal joint replacement is a high-risk disease for DVT. Salahuddin and Armstrong said that risk factors for DVT include advanced age, bed rest after trauma, anesthesia, foreign body implantation, and a history of blood clots [9]. In patients with deep vein thrombosis, there are many clinical symptoms. For example, lower limbs can appear pain swelling, skin pigmentation, skin sclerosis, venous ulcer, and so on. Patients even lose the labor force, increasing the pain and economic burden of patients. Therefore, the focus of DVT treatment is prevention. We should do a good job in the assessment of high-risk factors and actively take scientific and reasonable treatment and nursing methods for effective preventive intervention. See Figure 1.

## 3. Method

The UI is also known as the user interface, which is between the system and the user, which knows the internal information and allows people to take the form of the user interface and interact between the user and the device. The related software designed for mutual interaction and communication enables users to operate the hardware conveniently

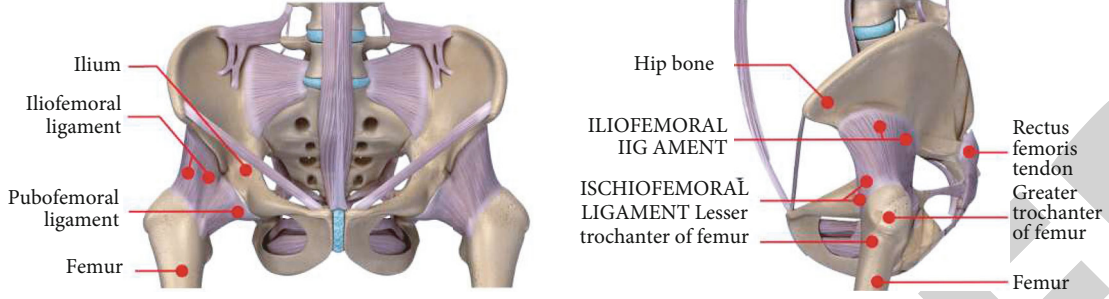


FIGURE 1: CT application of microscope scanning in diagnosis of iliac-femoral vein thrombosis after hip replacement.

and effectively to achieve two-way interaction and complete the desired work. This will make it easier for users to complete the hardware and successfully complete the interface and on-demand tasks. The user interface is broadly defined, including human-computer interaction and graphical user interface. The user interface exists in the field of human and mechanical information exchange [10]. In the long history of interface design and software development, he has been called an artist who does not pay attention to the work of interface design and insults people. In fact, the design of the software interface is similar to the standard design of commercial products, which is the key to purchasing. Interface design is not an easy artwork, it needs to locate the use of the user environment and design for the end user. Therefore, the design of the interface should be combined with user research, which is the process of creating a visual experience for end users [11]. Critically speaking, the interface can be divided into two levels: cognitive (visual, visual, and auditory) and cognitive. The user interface design is an important part of the test equipment [12, 13]. Interface design is a complex task that involves many disciplines such as thinking, reasoning, and speaking, in which everyone plays an important role. The three principles of user interface design are as follows: put the interface under the control of the user; reduce the memory burden of users; keep the interface consistent. Image translation is one of the simplest geometric transformations. Image translation means that all points in the image are blown horizontally and vertically according to the specified translation amount. Let  $(x_0, y_0)$  be a point on the original image, the horizontal translation of the image is  $t_x$ , and the vertical translation is  $t_y$ ; then, the coordinates of the point  $(x_0, y_0)$  after the translation will become  $(x_1, y_1)$ . Obviously, the relationship between  $(x_0, y_0)$  and  $(x_1, y_1)$  is shown in

$$\begin{cases} x_1 = x_0 + t_x, \\ y_1 = y_0 + t_y. \end{cases} \quad (1)$$

The matrix representation is shown in

$$\begin{bmatrix} x_1 \\ y_1 \\ 1 \end{bmatrix} = \begin{bmatrix} 1 & 0 & t_x \\ 0 & 1 & t_y \\ 0 & 0 & 1 \end{bmatrix} \begin{bmatrix} x_0 \\ y_0 \\ 1 \end{bmatrix}. \quad (2)$$

The inverse of the matrix can be obtained as shown in

$$\begin{bmatrix} x_0 \\ y_0 \\ 1 \end{bmatrix} = \begin{bmatrix} 1 & 0 & -t_x \\ 0 & 1 & -t_y \\ 0 & 0 & 1 \end{bmatrix} \begin{bmatrix} x_1 \\ y_1 \\ 1 \end{bmatrix}. \quad (3)$$

It is shown in

$$\begin{cases} x_0 = x_1 - t_x, \\ y_0 = y_1 - t_y. \end{cases} \quad (4)$$

In this way, every point on the translated image can be found in the original image. For example, for the pixel  $(0, 0)$  in the new graph, substitute into the above equations, and the corresponding pixel  $(-t_x, -t_y)$  in the original graph can be obtained. If  $t_x$  or  $t_y$  is greater than 0, then  $(-t_x, -t_y)$  is not in the original image. For points that are not in the original image, you can simply set the pixel value to 0 or 255 (black or white for grayscale images). Similarly, if something is not in the original image, it means that something in the original image has been removed from the display area. If you do not want to lose part of the removed image, you can enlarge the width by  $|t_x|$  and height of the newly generated image by  $|t_y|$ . Changing the image mirror is divided into two types: one is horizontal glass and the other is vertical glass. The operation of the horizontal mirror of the image is to replace the left and right half of the image with the vertical line of the image. Vertical mirror work is the shape of the upper half and half of the image, with the horizontal axis of the image being the center of the mirror. Set the height of the image as height and width as width. After horizontal mirroring, the coordinates of  $(x_0, y_0)$  in the original image will change to  $(\text{Width}-x_0, y_0)$ , and the matrix expression is shown in

$$\begin{bmatrix} x_1 \\ y_1 \\ 1 \end{bmatrix} = \begin{bmatrix} -1 & 0 & \text{Width} \\ 0 & 1 & 0 \\ 0 & 0 & 1 \end{bmatrix} \begin{bmatrix} x_0 \\ y_0 \\ 1 \end{bmatrix}. \quad (5)$$

The expression of inverse operation matrix is shown in

$$\begin{bmatrix} x_0 \\ y_0 \\ 1 \end{bmatrix} = \begin{bmatrix} -1 & 0 & \text{Width} \\ 0 & 1 & 0 \\ 0 & 0 & 1 \end{bmatrix} \begin{bmatrix} x_1 \\ y_1 \\ 1 \end{bmatrix}. \quad (6)$$

It is shown in

$$\begin{cases} x_0 = \text{Width} - x_1, \\ y_0 = y_1. \end{cases} \quad (7)$$

Similarly, the coordinate of  $(x_0, y_0)$  will change to  $(x_0, \text{Height} - y_0)$  after vertical mirror image, and its matrix expression is shown in

$$\begin{bmatrix} x_1 \\ y_1 \\ 1 \end{bmatrix} = \begin{bmatrix} 1 & 0 & 0 \\ 0 & -1 & \text{Height} \\ 0 & 0 & 1 \end{bmatrix} \begin{bmatrix} x_0 \\ y_0 \\ 1 \end{bmatrix}. \quad (8)$$

The expression of inverse operation matrix is shown in

$$\begin{bmatrix} x_0 \\ y_0 \\ 1 \end{bmatrix} = \begin{bmatrix} 1 & 0 & 0 \\ 0 & -1 & \text{Height} \\ 0 & 0 & 1 \end{bmatrix} \begin{bmatrix} x_1 \\ y_1 \\ 1 \end{bmatrix}. \quad (9)$$

It is shown in

$$\begin{cases} x_0 = x_1, \\ y_0 = \text{Height} - y_1. \end{cases} \quad (10)$$

According to the above transformation formula, image horizontal and vertical mirror operation can be very simple. The following is the procedure flow chart of mirror operation, as shown in Figure 2:

The requirements of medical image processing system are analyzed, and the software development tools and development environment are introduced. Then, the whole frame of image processing is designed according to the functional requirements, and the function of each module in the frame is simply introduced. Then, according to the framework structure, the design of software is carried out. First, the user interface is designed according to the system framework. Then, according to the functions involved in the interface, the basic functional principles and program design ideas are described [14]. It focuses on the application and realization of image segmentation and pattern recognition in this software, which can be used as an auxiliary tool for doctor diagnosis.

#### 4. Experiments and Analysis

Among the 90 patients under investigation, all of them completed the treatment without quitting during the course of treatment (the hospital stay of patients undergoing bone

joint replacement is generally about 2 weeks, which is short and patients have good compliance) [15, 16]. There were 27 males and 63 females, with an average age of 20-883 years, with an average age of  $52.45 \pm 12.39$ . There are 32 patients with fractures in the neck, 51 patients with gynecological necrosis and osteoarthritis, and 7 patients with osteoarthritis of the bones and spine. There was no significant difference in the sex, age, and disease history of the patients ( $P > 0.05$ ), as shown in Table 1:

At the end of the experiment, the number of patients with deep atherosclerosis in both groups was low. Diagnosis of atherosclerosis was confirmed by color Doppler ultrasound and was the rate of venous thrombosis in both groups. The control group had 6 patients, the incidence was 13.33070, and the intervention group had 0 patients, with a difference between the two groups ( $P = 0.034$ ). The probability of intervention in the signature group (+) was 28.89%, and the difference was significant compared to the control group ( $X^2 = 4.630, P = 0.031$ ). The Neuhof mark (+) incidence in the intervention group was 22.220%, and the statistical difference was significant compared to the control group ( $X^2 = 5.954, P = 0.015$ ). The incidence of both the human mark (+) and the Neuhof mark (+) in the affected group was lower than that in the control group, with a significant difference ( $P < 0.05$ ) as shown in Table 2.

The body surface temperature of 5 cm above the ankle of the two groups was measured and compared. It was found that there was no difference in the body surface temperature of the two groups before surgery, and the body surface temperature showed an upward trend after surgery and generally decreased gradually on the 7th day after surgery [17, 18]. On days 2, 3, 4, and 7 after surgery, the feet in the affected group had a body height of more than 5 cm lower than that of the body temperature control group ( $P < 0.05$ ). On day 1, one day after surgery, 5 days after surgery, on day 6, day 8, and one day after surgery, the body temperature was 5 cm higher than the ankles of both groups ( $P > 0.05$ ), as shown in Table 3.

The temperature changes of the two groups of patients were depicted by drawing, and it was intuitively found that the temperature of 5 cm above the ankle in both groups increased after surgery. The peak value was reached on the fourth day and then decreased, and the decline rate was consistent from the eighth day. The changes of body temperature at 5 cm above the ankle in the two groups showed that in the early postoperative period, the body temperature at 5 cm above the ankle in the intervention group was lower than that in the control group ( $P < 0.05$ ), as shown in Figure 3.

The peak velocity and average velocity of femoral vein were detected before surgery and the 1st and 7th day after surgery for statistical analysis. The results showed that there was no significant change between the two groups before surgery, and there was no statistical difference ( $P > 0.05$ ). One day after the first surgery, the control group was lower than the surgery, the response group was higher than the surgery, and the highest of the two groups was significantly higher ( $P > 0.05$ ). But no difference was found in mean

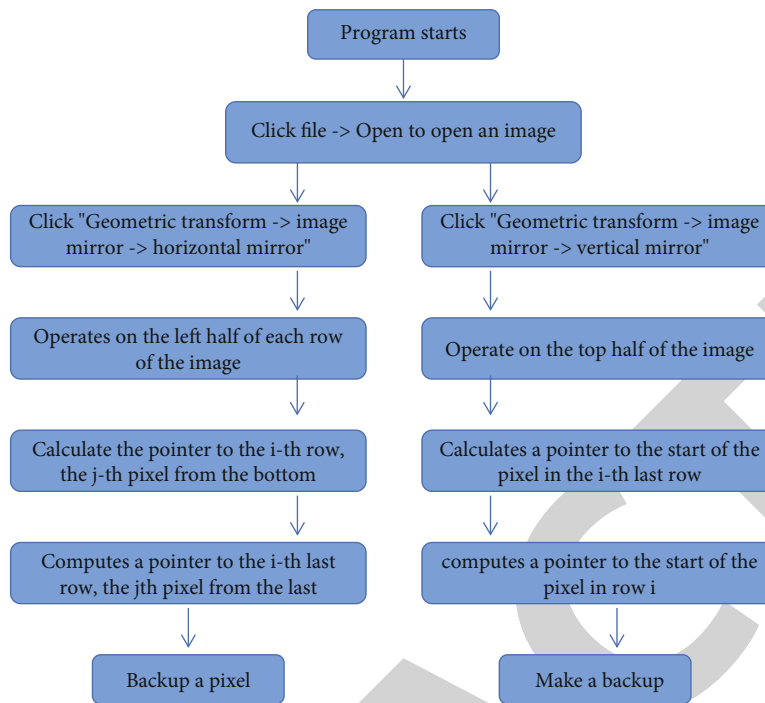


FIGURE 2: Flowchart of image mirroring program.

TABLE 1: General patient information.

Project	Control group (n = 45)	Intervention group (n = 45)	t/X <sup>2</sup>	P	
Number of cases	45 (constituent ratio)	45 (constituent ratio)			
Sex					
	Male	13 (28.98%)	14 (32.33%)	0.053	0.818
	Female	32 (71.11%)	31 (68.89%)		
Education					
	Junior high and below	31 (68.89%)	29 (64.44%)	0.200	0.655
	Junior high and above	14 (31.11%)	16 (35.56%)		
Replacement parts					
	Left	18 (40.00%)	19 (42.22%)	0.118	0.943
	Right	21 (46.67%)	21 (46.67%)		
	Two sides	6 (13.33%)	5 (11.11%)		
Material type					
	Biological type	24 (53.33%)	27 (60.00%)	0.407	0.523
	Bone cement type	21 (46.67%)	18 (40.00%)		
Hypertension					
		17 (37.78%)	15 (33.33%)	0.194	0.660
Diabetes					
		11 (24.44%)	10 (22.22%)	0.062	0.803
Varicosity					
		12 (26.67%)	10 (22.22%)	0.241	0.624
Age					
		6233 ± 6.58	61.12 ± 7.08	0.840*	0.403
BMI (kg/m <sup>2</sup> )					
		24.85 ± 3.08	24.35 ± 3.11	0.766*	0.446
Operation time (min)					
		125 ± 32.05	128.11 ± 30.18	-0.474*	0.637

speed ( $P > 0.05$ ) [19]. On the 7th day after the surgery, the peak and moderate flow rates of the two groups were higher than before the surgery, and the increase was more pronounced in the affected group. The differences between the two groups were significant ( $P < 0.05$ ), as shown in Table 4.

Virchow proposed that the conditions of venous thrombosis need three factors: slow blood flow, damage to the vascular wall, and high blood coagulation state. Venous thrombosis requires a combination of at least two factors,

neither of which alone can lead to thrombosis, and either of which can lead to thrombosis, especially slow blood flow and hypercoagulability. Virchow's theory has been clinically verified for more than half a century and tested by a variety of advanced technologies [20]. Many factors can lead to venous thrombosis after trauma, including pathogenic genes, hypercoagulability, cytokine interactions in inflammatory response, and immobilization [21]. At present, the research on the causes of venous thrombosis after trauma

TABLE 2: Comparison of venous thrombosis and Homan sign (+) and Neuhof sign (+) between the two groups.

Group	<i>n</i>	Homan sign (+)	Neuhof sign (+)	Deep vein thrombosis of the lower extremity (%)
Control group	45	23	21	6 (13.33%)
Intervention group	45	13	10	0 (0.00%)
$\chi^2$		4.630	5.945	4.460
<i>P</i>		0.031 <sup>a</sup>	0.015 <sup>a</sup>	0.034 <sup>b</sup>

is not perfect, and active postoperative prevention is not given, and the problem of venous thrombosis after joint replacement is not sufficiently understood. Major orthopedic surgery, femoral shaft fracture, femoral neck fracture, and other operations, especially bone joint replacement, are prone to thrombosis in lower limb veins due to the long operation time and complicated operation process. During surgery, the body tissue and blood vessels are pulled for a long time, causing tissue damage and then activating the endogenous and exogenous coagulation system [22, 23]. After the coagulation system is started, the coagulation factors in the blood increase, while the operation causes damage to the intima of the blood vessel wall. Platelets attach to the damaged blood vessel wall, release bioactive substances, and promote the formation of thrombosis. During surgery, blood loss can lead to blood concentration, further exacerbating hypercoagulability. Elderly patients often combine with a variety of diseases, such as hyperlipidemia and hypertension. These illnesses can make the body enter the state of hypercoagulability. After surgery, the patient was weak and needed to stay in bed for a long time to slow down the venous return of the lower limbs. Therefore, more attention should be paid to the prevention of DVT in the elderly who undergo bone marrow transplantation. Once the DVT is established, the blood vessels can lead to loss of function, which not only reduces the quality of life of the patient but also worsens the patient, so prevention of DVT should be mentioned. Caring for patients with evidence of drug abuse refers to the process of planning the work of nursing staff in a nursing home, carefully considering and combining research findings with clinical and patient needs according to their needs. Perform the procedures. Evidence-based nursing practice has become a global consensus in nursing, and any professional decision in practice should be based on scientific evidence, not simply on experience. Bundles of care refer to a collection of therapeutic and nursing interventions that are based on evidence. It is aimed at the impact of many factors, difficult to solve the nursing problem. This nursing intervention is supported by evidence-based theory and was first proposed by the Institute for Healthcare Improvement (IHI). Its purpose is to help medical staff to provide better service, as far as possible to provide patients with more perfect and optimized medical and nursing services. This approach significantly reduces the incidence of DVT by combining evidence-based and effective measures for preventing DVT and maximizing the impact of these

measures. Cluster nursing requires nursing staff to constantly sum up experience and lessons and grasp evidence-based evidence when implementing intervention measures. According to the original nursing evidence, give the best nursing plan, and in the nursing process, constantly improve the nursing basis and nursing plan. For patients with deep vein thrombosis, the main local symptoms are limb pain, heavy feeling of limbs, limb swelling, and tenderness (+). Sometimes, it can be accompanied by systemic symptoms, such as increased body temperature and accelerated heart rate; common signs are lower limb edema, skin pigmentation, ulcer, and other signs in severe cases. The larger and the lower limb thrombus, the more blocked blood flow, the slower the reflux, and the larger the swelling range. The faster the clot forms, the more pain the patient feels [24]. Distal venous thrombosis is slow, insidious, and usually undetected, with only mild pain in some patients. Or only the knee below the slight swelling of the limb, the disease further development, can appear Homan sign and Neuhof sign positive. Proximal venous thrombosis is rapid, the onset of acute, can quickly appear lower limb pain, accompanied by high fever and other systemic symptoms, and due to blood reflux disorder, can lead to obvious swelling of the lower limb, the affected side of the skin, subcutaneous weakness and subcutaneous venous expansion. Some blood vessels in the process of thrombosis, because thrombosis stimulates the blood vessel wall, can cause vascular spasm, aggravating the obstruction of blood return of patients with limb ischemia, severe pain, pale limbs, and other symptoms [25]. In clinical work, we found that most patients with venous thrombosis did not have typical symptoms, and the more common symptoms were limb swelling, increased skin temperature, and lower limb pain. Therefore, it is necessary to strengthen the comparison of lower limb swelling degree, temperature, and skin color to improve the early diagnosis rate. In this study, there were 6 cases of thrombosis in the red control group and no cases of thrombosis in the intervention group, and the difference between the two groups was statistically significant. Evidence-based cluster nursing intervention can effectively reduce lower extremity deep vein thrombosis after bone joint replacement. The main symptoms of venous thrombosis are local and systemic reactions. Iliac vein, femoral vein, and popliteal vein thrombosis often caused varying degrees of pain, swelling, and heaviness in the affected limbs. Sometimes, it can be accompanied by systemic symptoms, such as increased body temperature and accelerated heart rate; common signs are lower limb edema, skin pigmentation ulcer, and other signs in severe cases. Clinical common thrombosis is mostly a small range of thrombosis, thrombosis of small venous plexus generally has a small embolization range, the systemic reaction is relatively mild, generally only showing mild pain, and mild swelling of the side of the limb skin temperature slightly increased. This study showed that the postoperative surface temperature of the affected limbs showed an upward trend and generally decreased gradually on the 7th day after surgery. The body surface temperature of 5 cm limb above the ankle in the intervention group was significantly lower than that in the control group on the 2nd, 3rd, 4th, and 7th day

TABLE 3: Comparison of the temperature of 5 cm upper ankle limb between the two groups ( $x \pm s$ , °C).

Group	<i>n</i>	Preoperative	Postoperative day 1	Postoperative day 2	Postoperative day 3	Postoperative day 4
Control group	45	33.49 ± 1.49	33.95 ± 0.82	35.85 ± 1.02	35.48 ± 0.55	35.39 ± 0.75
Intervention group	45	33.46 ± 1.56	33.65 ± 1.01	34.94 ± 0.57	34.70 ± 0.88	34.99 ± 0.96
<i>t</i>		0.093	1.547	5.224	5.042	2.203
<i>P</i>		0.926	0.125	0.000	0.000	0.030

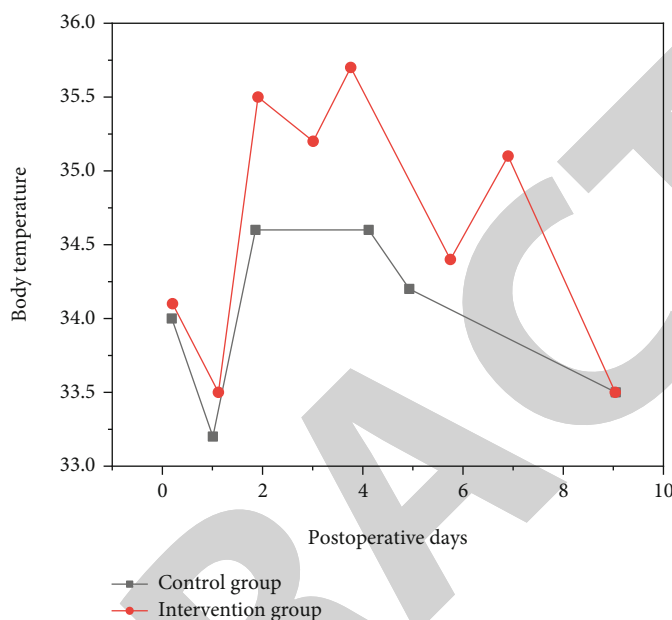


FIGURE 3: Comparison of temperature of 5 cm upper ankle limb between the two groups.

TABLE 4: Comparison of peak and average velocity of femoral vein between two groups.

Group	<i>n</i>	Preoperative		Postoperative day 1		Postoperative day 7	
		Peak systolic velocity	Mean flow rate	Peak systolic velocity	Mean flow rate	Peak systolic velocity	Mean flow rate
Control group	45	17.01 ± 2.78	12.01 ± 3.03	16.32 ± 3.15	11.86 ± 3.71	20.01 ± 3.57	13.91 ± 3.26
Intervention group	45	16.78 ± 3.47	11.68 ± 3.01	17.89 ± 4.01	12.01 ± 4.15	25.10 ± 4.79	15.75 ± 3.02
<i>t</i>		0.347	0.518	-2.065	-0.181	-5.716	-2.778
<i>P</i>		0.729	0.606	0.042	0.857	0.000	0.007

after surgery ( $P < 0.05$ ). The body temperature is 0 cm below the skeleton and 15 cm above the skeleton and is lower than that of the control group on the 1st, 2nd, 3rd, and 4th day after surgery. In this study, it was confirmed that evidence-based cluster nursing intervention could reduce the skin temperature of 5 cm above the ankle, 10 cm below the skeleton, and 15 cm above the skeleton of the affected limb 1–4 days after surgery. After surgery, due to postoperative bed rest, slow venous reflux, and other factors, mild swelling around the incision after surgery can be caused, which is mostly normal. If the patient develops edema of the limb and progresses from the distal to the proximal end of the limb, it is usually caused by venous stasis. When a thrombus

forms in the venous tube, blood return is slowed and the distal venous return is blocked, causing the distal venous pressure to rise. Capillary filter pressure increased, coupled with anoxia and capillary permeability, and increased limb swelling. In venous thrombosis, the arteries spasm and lymphatic return is blocked, causing swelling of the limb in the affected area. Femoral vein thrombosis, resulting in blocked blood flow in the lower limb, blocked capillary flow, and tissue fluid cannot smoothly enter the vein, resulting in swelling of the knee or lower thigh limb. The results of this study showed that cluster nursing intervention could significantly reduce the limb circumference of 15 cm on the affected side of the body bones on the 3rd, 4th, and 5th day after surgery,

but there was no significant difference in the limb circumference of 5 cm on the ankle [26, 27]. Evidence-based cluster nursing interventions can reduce limb swelling. After thrombosis of the muscle vein of the calf, certain physical stimulation can cause pain, especially in dorsiflexion of the ankle joint, the pain is more obvious, and this phenomenon is called Homan sign (+). If the patient has pain when pressing on the fat intestinal muscle, this is called Neuhof sign (+). The main mechanism is that the soleus muscle and fat intestine muscle are passively elongated at the dorsiflexion position of the ankle joint, which stimulates the diseased veins and causes limb pain. When distal deep vein thrombosis occurs in lower limbs, Homan sign and Neuhof sign can show positive signs, so Homan sign and Neuhof sign can be used as the examination to judge whether there is distal vein thrombosis. The results of this study show that compared to the control group, the positive characteristics of Homan and Neuhof in the group were slightly affected, with significant differences between the two groups. Evidence has shown that DVT can reduce the risk of a combination of surveillance services.

## 5. Conclusion

Iliac vein compression syndrome (IVCS) is also known as May-Thurner syndrome or Cockett syndrome. It refers to long-term compression of the right iliac artery in the anterior left iliac vein (LIV) of the lumbar spine with symptoms of deep iliac vein thrombosis (DVT) or venous hypertension such as swollen varicose veins in the left leg. It is associated with symptoms of atherosclerosis, such as deep atherosclerosis (DVT) or atherosclerosis in the left leg. Because of this relationship, many people have varying degrees of muscle contraction on the left side of the CT, but there are no signs of deep atherosclerosis or high blood pressure on the left side. Left lean muscle compression during CT scan is not the same as general lean muscle compression disease. Diagnosing the syndrome of atherosclerosis requires three components. First, the left ventricle is compressed by the right artery. Second, the angiography of the arteries shows that the air sac is thin and narrow and that a large artery can be seen in the abdominal cavity. Third, there is clinical evidence of deep atherosclerosis or intravenous hypertension, such as atherosclerosis or lower limb inflammation. Fourth, treatment occurs at the lower extremities of the arteries, such as at the lower extremities or at the lower extremities, or at the lower right atrium. Complications of pulmonary embolism are very rare. Foreign data has now been reported in right-hand muscle contractions. Fretz reported abnormal contractions of the right muscle due to a split in the pancreas, resulting in a narrowing of the inferior vena cava through most of the pelvic floor muscles and the right artery. Abboud and Burkespierre reported narrowing of the right artery from the right artery due to differences in the veins on the left. All of the above 3 conditions for right-hand muscle contraction have vascular changes. Molloy reports data on right-sided muscle contraction syndrome, in which the right muscle is compressed by the right internal artery, but the lower extremity and CT images are missing. The study

reported that right-sided vascular compression syndrome was reported without modifying the blood vessels and that the patient's treatment of low blood pressure (e.g., lower limb arteries) was suggested. Lower venous arteries indicate severe pain in the arteries and many arteries in the abdomen. CT scan shows that the right atrium is constricted by the right artery. Some studies have shown that compression of the coronary artery disease and deep vein congestion of the lower left leg are more common in women. Malignant neoplasms are more common in men. This is because in the development of lumbar spine in women, the lumbar spine rises forward, increasing the risk of muscle spasms on the left side. This is because in the development of lumbar spine in women, the lumbar spine rises forward, increasing the risk of muscle spasms on the left side. During the three months, lumbar spine disease also increases, so the contraction of the left intestinal muscle becomes more pronounced in the third trimester and after childbirth, which increases the risk of DUT in the lower left. In this study, men had more muscle contraction on the right side than women, and women had more muscle contraction on the left than men. The number of female patients with left ventricular compression is >50% higher than in men. These are anatomical features that describe the different sexes in the DUT that occur on the right and left.

## Data Availability

The data used to support the findings of this study are available from the corresponding author upon request.

## Conflicts of Interest

The authors declared that there is no conflict of interest.

## References

- [1] D. G. Gitelzon, A. G. Faybushevich, D. A. Maximkin, G. I. Veretnik, and K. I. Danishian, "Diagnosis and treatment of iliac vein stenosis," *Journal of Clinical Practice*, vol. 11, no. 4, pp. 64–69, 2020.
- [2] I. Sunayama, T. Yoshimura, T. Sonoura et al., "Usefulness of electron microscopy in the diagnosis of wild-type transthyretin cardiac amyloidosis," *Journal of Cardiology Cases*, vol. 23, no. 4, pp. 166–169, 2021.
- [3] R. T. Ming, K. Damodharan, M. Lim, C. Yap, and T. Y. Tang, "Computed tomography venography versus intravascular ultrasound in the diagnosis of iliofemoral vein stenosis," *Journal of Vascular Surgery Venous and Lymphatic Disorders*, vol. 8, no. 6, pp. 1122–1123, 2020.
- [4] L. Moeri, M. Lichtenberg, S. Gnanapiragasam, S. Barco, and T. Sebastian, "Braided or laser-cut self-expanding nitinol stents for the common femoral vein in patients with post-thrombotic syndrome," *Journal of Vascular Surgery: Venous and Lymphatic Disorders*, vol. 9, no. 3, pp. 760–769, 2021.
- [5] U. W. Dozie, N. A. Ekeh, G. N. Iwuoha, C. J. Nwaokoro, and I. N. S. Dozie, "The efficacy of rapid diagnostic test in the diagnosis of malaria among adults as compared to microscopy in a hospital in Imo state, south eastern Nigeria," *Open Access Library Journal*, vol. 7, no. 7, pp. 1–11, 2020.

## Retraction

# Retracted: Effect Evaluation of Comfort Nursing Materials Assisted Nursing for Patients with Advanced Malignant Tumor

### Scanning

Received 20 June 2023; Accepted 20 June 2023; Published 21 June 2023

Copyright © 2023 Scanning. This is an open access article distributed under the Creative Commons Attribution License, which permits unrestricted use, distribution, and reproduction in any medium, provided the original work is properly cited.

This article has been retracted by Hindawi following an investigation undertaken by the publisher [1]. This investigation has uncovered evidence of one or more of the following indicators of systematic manipulation of the publication process:

- (1) Discrepancies in scope
- (2) Discrepancies in the description of the research reported
- (3) Discrepancies between the availability of data and the research described
- (4) Inappropriate citations
- (5) Incoherent, meaningless and/or irrelevant content included in the article
- (6) Peer-review manipulation

The presence of these indicators undermines our confidence in the integrity of the article's content and we cannot, therefore, vouch for its reliability. Please note that this notice is intended solely to alert readers that the content of this article is unreliable. We have not investigated whether authors were aware of or involved in the systematic manipulation of the publication process.

In addition, our investigation has also shown that one or more of the following human-subject reporting requirements has not been met in this article: ethical approval by an Institutional Review Board (IRB) committee or equivalent, patient/participant consent to participate, and/or agreement to publish patient/participant details (where relevant).

Wiley and Hindawi regrets that the usual quality checks did not identify these issues before publication and have since put additional measures in place to safeguard research integrity.

We wish to credit our own Research Integrity and Research Publishing teams and anonymous and named external researchers and research integrity experts for contributing to this investigation.

The corresponding author, as the representative of all authors, has been given the opportunity to register their agreement or disagreement to this retraction. We have kept a record of any response received.

### References

- [1] M. Zhong, L. He, M. Chen, Z. Lu, R. Li, and L. Li, "Effect Evaluation of Comfort Nursing Materials Assisted Nursing for Patients with Advanced Malignant Tumor," *Scanning*, vol. 2022, Article ID 4766252, 6 pages, 2022.



## Research Article

# Effect Evaluation of Comfort Nursing Materials Assisted Nursing for Patients with Advanced Malignant Tumor

Mei Zhong , Lanying He , Min Chen , Zhongxiang Lu , Ruyu Li , and Ling Li 

Department of Intensive Care Medicine, Sun Yat-sen University Cancer Center, Guangzhou 510060, China

Correspondence should be addressed to Ling Li; 20180052@ayit.edu.cn

Received 17 May 2022; Revised 28 May 2022; Accepted 6 June 2022; Published 17 June 2022

Academic Editor: Balakrishnan Nagaraj

Copyright © 2022 Mei Zhong et al. This is an open access article distributed under the Creative Commons Attribution License, which permits unrestricted use, distribution, and reproduction in any medium, provided the original work is properly cited.

In order to explore the effect of comfort care on patients with advanced malignant tumors assisted by bioceramics, 82 patients with advanced malignant tumors admitted to a cancer hospital were selected as the research object control group: 26 males and 15 females and the observation group: 25 males and 16 females. The control group was given routine care, and the observation group was given comfort care on the basis of the control group. The quality of life (QLQ-C30 functional scale) and nursing satisfaction before and after nursing were compared between the two groups. The results of the study indicate that after care, the physical, role, emotional, cognitive, social, general health, and symptom scores of the observation group were significantly higher than those of the control group, the nursing satisfaction degree of the observation group was 97.56%, which was significantly higher than that of the control group of 82.93%, and the difference was statistically significant ( $P < 0.05$ ). Comfortable care has a definite effect on the care of patients with advanced malignant tumors; it can improve the overall comfort and satisfaction of patients, effectively reduce adverse events, and improve the quality of life of patients.

## 1. Introduction

The body function of patients with advanced malignant tumors is reduced, there are more psychological problems, and the quality of life is significantly reduced; at the same time, the family members of the patients were also affected, and their psychological status was deviated. Therefore, effective interventions for patients and their families can help them alleviate bad psychology and improve the quality of life [1]. Comfort care was first proposed in the 1960s; studies believe that applying it to patients with advanced malignant tumors can play an important role, reflecting the value of his life. Advanced tumors mainly refer to the failure of cancer detection and treatment; once discovered, it is already at an advanced stage, which increases the difficulty of disease treatment. Pain is the most common subjective symptom in patients with advanced cancer, the probability of occurrence is as high as 70%; if timely and effective treatment is not available, it will reduce the quality of life of patients and increase the psychological pressure of patients [2, 3]. With the development of medical care reform, humanized nursing is applied to the treatment of advanced tumors, pro-

vides patients with personalized and creative care, solves the pain on the patient's body, and improves the patient's confidence in disease treatment [4].

Malignant tumors seriously affect the life and health of patients; at present, the clinical treatment of this malignant tumor is to first perform surgical treatment on the patient, complete removal of tumor tissue. And adjuvant chemotherapy and radiation therapy after surgery prevent the residue and metastasis of tumor cells, but the side effects of chemotherapy and radiotherapy are great [5]. For bone tumors, clinical treatment can also cause irreparable bone defects [6]. Therefore, the construction of selenium-doped potassium sodium niobate bioceramics is used to achieve bone defect filling and use the piezoelectric properties of the ceramic sheet and the released Se element to achieve an effective combination of electrotherapy and drug therapy to achieve the purpose of anticancer. For malignant tumors, construction of selenium-doped potassium sodium niobate ceramics, utilizing the photocatalytic performance of ceramic powder and the released Se element, can realize the effective combination of photodynamic therapy and drug therapy to achieve the purpose of anticancer. During the nursing of

patients with advanced malignant tumors assisted by bioceramics, the principle should be to reduce the pain of patients and improve their quality of life. Traditional nursing methods cannot meet the care needs of patients. Th et al. investigated the prognosis of patients with stage I and stage II OSCC, especially the impact of biopsy and operation intervals; research has shown that preoperative interventions for patients with oral malignancies such as tooth extraction, incision, and curettage may be related to poor prognosis. Although biopsy is another preoperative intervention, its impact on the prognosis of patients with oral squamous cell carcinoma (OSCC) is unclear [7].

On the basis of this research, we observe the evaluation of the effect of comfortable nursing on the nursing of patients with advanced malignant tumors assisted by bioceramics. 82 patients with advanced malignant tumors were selected as the research objects. Using a random number table method, they were divided into the control group and observation group with 41 cases each. The control group was given routine care, and the observation group was given comfort care on the basis of the control group. The quality of life and nursing satisfaction of the two groups before and after nursing were compared. The physical, role, mood, cognition, social, general health, and symptom scores of the observation group were significantly higher than those of the control group. Using comfortable care on the basis of routine care can improve the quality of life of patients with advanced malignant tumors and improve nursing satisfaction.

## 2. Research Methods

**2.1. General Information.** 82 patients with advanced malignant tumors admitted to a cancer hospital were selected as the research objects; all met the relevant standards in "Malignant Tumor Interventional Therapy" and signed an informed consent form. Using a random number table method, they were divided into the control group and observation group with 41 cases each. Control group: 26 males and 15 females; age 25-67 years old, average  $45.7 \pm 0.8$  years old. The course of illness is 2-7 years, with an average of  $4.9 \pm 0.6$  years; disease types: 14 cases of gastric cancer, 12 cases of esophageal cancer, 8 cases of liver cancer, 6 cases of cervical cancer, and 1 case of lung cancer. Observation group: 25 males and 16 females; age 25-68 years old, average  $45.8 \pm 0.9$  years old. The course of the disease is 3-7 years, with an average of  $4.8 \pm 0.5$  years; disease types: 13 cases of gastric cancer, 10 cases of esophageal cancer, 9 cases of liver cancer, 6 cases of cervical cancer, and 3 cases of lung cancer. There was no statistically significant difference between the two groups of general information ( $P > 0.05$ ), and they were comparable.

**2.2. Method.** The control group was given routine care: ① provide patients with a quiet and comfortable ward environment; ensure fresh air, suitable temperature, and humidity; and disinfect the ward on time every day and dry the bedding to prevent pressure sores. ② In view of the digestive tract reactions that are prone to chemotherapy, 30 minutes

before chemotherapy, give antiemetic drugs and sedatives as prescribed by the doctor. ③ For patients with mild pain, use cold compresses, physical therapy, and distraction to relieve pain. For patients with moderate to severe pain, use analgesics as directed by your doctor. The observation group was given comfort care on the basis of the control group: ① layout+ward environment according to patients' interests and hobbies, place green potted plants indoors and avoid noise during the nursing process and keep a quiet ward environment; ② pay attention to the psychological changes of patients, when communicating, think about the problem more from the perspective of the patient, pay attention to the use of communication skills, pour in your own emotions and establish a friendly nurse-patient relationship, gain the trust of patients, reduce their psychological pressure, and improve their confidence in treatment; ③ formulate an appropriate diet plan for the patient, focusing on digestible foods with high vitamin content, it is forbidden to eat too sweet and greasy food; instruct patients to drink plenty of water to promote the excretion of metabolites, and prevent constipation; ④ make appropriate exercise programs based on the patient's situation, such as walking, Tai Chi, jogging, etc., the first exercise time is 10-15 min, then gradually increased to 30 min, 2-3 times a week; ⑤ for patients with bone marrow suppression caused by chemotherapy, urge patients to pay attention to oral hygiene and maintain indoor ventilation, wear a mask when going out, and strictly restrict people entering and leaving the ward to prevent cross-infection.

**2.3. Observation Indicators.** The QLQ-C30 functional scale was used to assess the quality of life of the two groups of patients, including physical function, role function, emotional function, cognitive function, the seven dimensions of social function, general health, and symptoms, the full score is 100 points, the higher the score, the better the quality of life. A self-made questionnaire was used to calculate the nursing satisfaction of the two groups, the total score is 100 points,  $>90$  points to satisfaction, 60 to 90 points to basic satisfaction, and  $<60$  is divided into dissatisfaction: satisfaction = (satisfied + basic satisfaction) number of cases / total number of cases  $\times 100\%$ .

**2.4. Potassium Sodium Niobate Bioceramics.** Potassium sodium niobate piezoelectric ceramics have piezoelectric properties similar to those of natural bone tissue; the chemical elements contained in KNN are potassium, sodium, oxygen, and niobium; among them, potassium, sodium, and oxygen are all chemical elements required by the human body; niobium has also been proven to have a bone-promoting effect, and its biological safety has also been recognized. The biocompatibility of potassium sodium niobate piezoelectric ceramics has been confirmed, and its piezoelectric properties are used in antitumor research. At the same time, bioceramics have good photosensitivity; its photosensitivity can also be used for antitumor research. Under visible light, the conduction band and valence band of KNN photosensitive ceramics will generate photo-induced electrons and positively-charged photo-induced holes, respectively, cause a

TABLE 1: Comparison of serum tumor marker levels between the two groups of patients ( $\bar{x} \pm s$ ).

Tumor markers	Observation group ( $n = 913$ )		Control group ( $n = 710$ )	
	Before care	After care	Before care	After care
CA-125	87.91 $\pm$ 4.54	43.66 $\pm$ 2.12	29.11 $\pm$ 3.56	67.15 $\pm$ 2.83
Cyfra21-1	5.92 $\pm$ 0.48	2.05 $\pm$ 0.21	6.26 $\pm$ 0.53	3.87 $\pm$ 0.24
NSE	37.92 $\pm$ 2.05	17.41 $\pm$ 1.93	38.46 $\pm$ 2.41	23.63 $\pm$ 1.88

series of chemical redox reactions to occur in the substances in the solution and generate reactive oxygen species. Therefore, the use of bioceramics as a photocatalyst to achieve photodynamic therapy of cells has become a means of advanced malignant tumors.

**2.5. Statistical Methods.** Use SPSS 18.0 statistical software to process the data, and the measurement data is represented by ( $\bar{x} \pm s$ );  $t$ -test was used for comparison,  $\chi^2$  test was used for count data, and  $P < 0.05$  was considered statistically significant.

### 3. Result Analysis

**3.1. Comparison of Serum Tumor Standard Levels between the Two Groups.** The serum levels of tumor markers such as CA-125, Cyfra21-1, and NSE in the observation group were significantly lower than those in the control group, and the difference was statistically significant ( $P < 0.05$ , Table 1).

**3.2. Comparison of Quality of Life before and after Nursing between the Two Groups.** Before care, two groups of physical function, role function, emotional function, cognitive function, social function, general health, there was no statistically significant difference in symptom scores ( $P > 0.05$ ). After nursing, the observation group's body, role, emotion, cognition, the social, general health status, and symptom scores were significantly higher than those of the control group; the difference was statistically significant ( $P < 0.05$ ), see Table 2.

**3.3. Comparison of Nursing Satisfaction between the Two Groups.** The nursing satisfaction degree of the observation group was 97.56%, which was significantly higher than that of the control group of 82.93%, and the difference was statistically significant ( $P < 0.05$ ), see Table 3.

According to statistics, the treatment compliance of patients in the observation group after nursing was 84.8%, significantly higher than the 65.2% of the control group, and the treatment compliance of the two groups of patients after nursing was statistically different ( $P < 0.05$ ). Comparing the pain relief of the two groups of patients, the pain relief effectiveness of the observation group was higher than that of the control group, and the difference was statistically different ( $P < 0.05$ ), see Figure 1.

### 4. Discussion

Comfortable care is the most pleasant state for patients to obtain physical, psychological, and social functions during

treatment, in order to achieve the above goals, an effective, holistic, creative, and personalized nursing model should be established in clinic and meet the needs of patients to the greatest extent and from multiple angles [8, 9]. For patients with malignant tumors receiving chemotherapy and radiotherapy, comfortable care mode mainly includes basic comfort care, pain care, clinical symptom care, psychosocial care, and adverse reaction care, it can significantly improve the clinical treatment effect, improve the quality of life of patients, and relieve symptoms; it can also reduce the adverse reactions of radiotherapy and chemotherapy and improve patient tolerance, ensuring the smooth progress of clinical treatment [10–12].

At present, with the continuous increase in the incidence of various malignant tumors, cancer pain has become a problem that medical staff cannot ignore. Pain not only affects the patient's body but also puts a huge shackle on the patient's psychology. This requires that the implementation of pain care for patients should start from the "physical, psychological, and social spirit" at the same time to carry out the "trinity" holistic care; this is a challenge to the current role change of medical staff and the level of care [13]. In order to effectively improve the nursing staff's pain nursing service skills, the hospital should regularly arrange nursing staff to participate in pain management lectures, strengthen the pain management awareness of medical staff by organizing various channels such as "teaching, further training, and going out to study" and accurately grasp the assessment method of cancer pain; on the basis of continuous and accurate pain assessment, we strictly abide by the three-step analgesic principle formulated by the WHO and implement corresponding pain care measures [14]. For patients with advanced malignant tumors, comprehensive nursing intervention can play a good role in pain control; nursing staff should not only pay attention to the patient's symptoms and pain, through correct assessment and scientific pain management, at the same time, patients should be given a clean and quiet ward, by strengthening psychological counseling to meet the needs of patients as much as possible, so that patients can maintain a positive attitude to face the disease, so as to effectively alleviate the pain of patients and improve their compliance with treatment, in order to ensure the quality of life in the late stage, so that patients can spend this time comfortably and peacefully [15–17].

Patients with advanced malignant tumors have a short survival time, affected by the disease, patients and their families are under great psychological pressure, and most patients have severe cancer pain, and their quality of life is significantly reduced. We apply comfort care interventions to the treatment of patients with malignant tumors; the

TABLE 2: Comparison of quality of life between the two groups before and after nursing.

Project	Observation group ( <i>n</i> = 41)		Control group ( <i>n</i> = 41)	
	Before care	After care	Before care	After care
Physical function	32.24 ± 5.10	54.20 ± 6.18* <sup>#</sup>	32.20 ± 5.11	45.28 ± 4.62 <sup>#</sup>
Role function	39.51 ± 4.57	53.61 ± 6.43* <sup>#</sup>	39.47 ± 4.41	44.65 ± 4.31 <sup>#</sup>
Emotional function	40.54 ± 4.77	52.50 ± 5.38* <sup>#</sup>	40.62 ± 4.83	46.02 ± 4.91 <sup>#</sup>
Cognitive function	40.10 ± 4.21	55.22 ± 5.64* <sup>#</sup>	40.01 ± 4.16	47.60 ± 4.62 <sup>#</sup>
Social function	38.84 ± 3.45	54.44 ± 5.62* <sup>#</sup>	38.78 ± 3.38	48.05 ± 4.50 <sup>#</sup>
Symptom	41.10 ± 6.13	52.80 ± 5.70* <sup>#</sup>	41.15 ± 6.02	45.12 ± 5.68 <sup>#</sup>
General health	39.24 ± 6.01	59.20 ± 5.73* <sup>#</sup>	39.17 ± 5.95	47.21 ± 5.03 <sup>#</sup>

Note: compared with the control group, \* $P < 0.05$ ; compared with before nursing, <sup>#</sup> $P < 0.05$ .

TABLE 3: Comparison of nursing satisfaction between the two groups (*n* (%)).

Group	Satisfy	Basically satisfied	Dissatisfied	Satisfaction
Observation group ( <i>n</i> = 41)	17 (42.8)	21 (53.65)	1 (2.43)	39 (97.55)
Control group ( <i>n</i> = 41)	13 (34.14)	19 (48.76)	6 (17.06)	343 (82.92)
$\chi^2$ value				3.462
<i>P</i> value				0.025

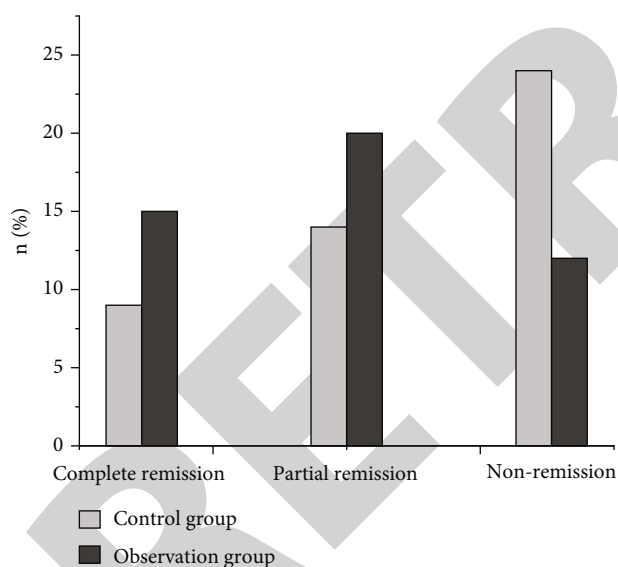


FIGURE 1: Comparison of pain relief between the two groups of patients after nursing.

results showed that the general nursing group performed basic general nursing, and the comfort care group gives comfort care [18]. The results show that the satisfaction of nursing care for advanced malignant tumors in the comfort nursing group was higher than that in the general nursing group,  $P < 0.05$ . Before the intervention, the physical health, mental health, social function, and overall quality of life of the two groups were similar,  $P > 0.05$ . After the intervention, the physical health, mental health, social function, and overall quality of life of the comfortable nursing group were better than those of the ordinary nursing

group,  $P < 0.05$ . The comfort care group nursing operation comfort, speech comfort, and the comfort of the ward environment are  $97.40 \pm 4.57$  points,  $96.61 \pm 2.51$  points, and  $97.40 \pm 2.87$ , which were higher than the score of  $85.51 \pm 2.62$ ,  $85.62 \pm 1.88$ , and  $89.51 \pm 1.21$  of the general nursing group,  $P < 0.05$ . The incidence of adverse nursing events in the comfort care group was 2.50% lower than 20.00% in the general care group,  $P < 0.05$ .

For patients with advanced malignant tumors, chemotherapy is often given clinically; although it can get a certain effect, it is easy to cause vomiting, nausea, and other adverse reactions, coupled with the particularity of the disease, affecting patient comfort. Routine care cannot meet the needs of patients for care [19–21]. Comfort care is a new type of care model that follows the patient-centered concept and meets the psychological and physical needs of patients; the patient can feel the respect and care of the nursing staff, thereby improving the comfort of the patient. The results of this study show that the observation group's body, role, emotion, cognition, society, general health status, symptom score, and nursing satisfaction were significantly higher than those of the control group. This is because it strengthens communication with patients during comfort care and comprehensively evaluates the psychological condition of patients, choosing effective measures to guide can not only meet the physical and psychological needs of patients but also allows patients to feel the care from society and family during their hospitalization, so as to improve its treatment compliance and ensure the treatment and nursing effect [22–24]. At the same time, preaching disease knowledge to patients and guiding them to perform aerobic exercises can improve the patient's health knowledge mastery, self-care awareness, and autonomy. Combining the patient's condition to formulate a scientific

and reasonable diet plan can increase the body's nutrition and improve the quality of life [25].

## 5. Conclusion

In summary, the effect of comfort care on the nursing of patients with advanced malignant tumors assisted by bio-ceramics is definite; it can improve the overall comfort and satisfaction of patients. It can not only reduce the pain and anxiety of patients but also enhance their nursing satisfaction, effectively reduce adverse events, and improve the quality of life of patients.

## Data Availability

The data used to support the findings of this study are available from the corresponding author upon request.

## Conflicts of Interest

The authors declare that they have no conflicts of interest.

## References

- [1] F. Covut, T. Z. Kewan, B. Thapa, A. S. Haddad, and H. Daw, "Feasibility and clinical impact of next-generation sequencing (NGS) in patients with stage IV or recurrent malignancies," *Journal of Clinical Oncology*, vol. 37, article e14697, 15\_supplement, 2019.
- [2] P. N. Mbeje and N. G. Mtshali, "The quality of life of patients with end-stage renal disease on dialysis in South Africa: a grounded theory analysis," *Nursing & Health Sciences Research Journal*, vol. 2, no. 1, pp. 41–48, 2019.
- [3] Y. Iwasa, I. Saito, and M. Suzuki, "Differences in home health nursing care for patients with Parkinson's disease by stage of progress: patients in Hoehn and Yahr stages III, IV, and V," *Parkinson's Disease*, vol. 2021, no. 5, article 8834998, 10 pages, 2021.
- [4] O. Staunton, "Holistic care in advanced pseudomyxoma peritonei: the clinical nurse specialist role in a rare malignancy of the abdomen and pelvis," *Gastrointestinal Nursing*, vol. 18, no. 7, pp. 42–48, 2020.
- [5] A. Hart, Y. S. Ahn, C. Watson, M. Skeans, and V. R. Dharmidharka, "High healthcare resource utilization and cost for PTLD patients following kidney transplants," *Blood*, vol. 136, Supplement 1, pp. 32–33, 2020.
- [6] F. Biello, M. N. Itto, A. Mahmoud et al., "Impact of the G8 score on the outcome of a cohort of elderly patients with solid or hematological malignancies," *Journal of Clinical Oncology*, vol. 39, 15\_supplement, pp. 12038–12038, 2021.
- [7] T. Hemmi, K. Yusa, S. Kasuya et al., "Influence of interval between biopsy and surgery on prognosis of patients with early-stage oral squamous cell carcinoma: a preliminary study," *Journal of Oral and Maxillofacial Surgery, Medicine, and Pathology*, vol. 31, no. 3, pp. 159–162, 2019.
- [8] J. P. Harris, M. Kashyap, J. N. Humphreys, D. T. Chang, and E. L. Pollom, "Longitudinal analysis of mental disorder burden among elderly patients with gastrointestinal malignancies," *Journal of the National Comprehensive Cancer Network: JNCCN*, vol. 19, no. 2, pp. 163–171, 2021.
- [9] M. Fedyanin, U. Boyarskikh, E. Polyanskaya, V. Aliev, and S. Tjulandin, "A prospective study of prognostic role of plasma circulating tumor DNA (ctDNA) in patients (pts) with early-stage malignancies," *Journal of Clinical Oncology*, vol. 38, 15\_supplement, pp. 3559–3559, 2020.
- [10] V. Vukasovi and V. Urainovi, "Nutritional status and quality of life of patients with lymphoma," *Medicinski Podmladak*, vol. 70, no. 2, pp. 14–19, 2019.
- [11] S. G. Ma, J. Hu, and Y. Huang, "The risk factors for perioperative venous thromboembolism in patients with gynecological malignancies: a meta-analysis," *Thrombosis Research*, vol. 196, no. 4, pp. 325–334, 2020.
- [12] M. Uma and H. Sameer, "Assessment of thyroid dysfunction in patients irradiated for head and neck malignancies," *Journal of Evidence Based Medicine and Healthcare*, vol. 7, no. 45, pp. 2626–2630, 2020.
- [13] N. Bacalbasa, C. Diaconu, L. Iliescu, C. Savu, and I. Balescu, "The influence of the metabolic syndrome on early postoperative outcomes of patients with advanced-stage endometrial cancer," *In Vivo*, vol. 34, no. 5, pp. 2913–2917, 2020.
- [14] E. Kalicińska, B. Kuszczak, J. Dbski, U. Szukalski, and T. Wróbel, "Hematological malignancies in polish population: what are the predictors of outcome in patients admitted to intensive care unit?," *Supportive Care in Cancer*, vol. 29, no. 1, pp. 323–330, 2021.
- [15] Z. Y. Lei, T. P. Guan, J. L. Luo, H. S. Tang, and S. Z. Cui, "Rationality of performing hyperthermic intraperitoneal chemotherapy 5-8 weeks after primary tumor resection for patients with locally advanced colorectal cancer-based on COLOPEC," *Zhonghua Wei Chang Wai Ke Za Zhi = Chinese Journal of Gastrointestinal Surgery*, vol. 22, no. 12, pp. 1115–1117, 2019.
- [16] A. Mylonakis, A. Kalfoutzou, K. Siozos, A. Roidou, and D. Voros, "The stage of colorectal cancer in surgical patients in Greece," *Hellenic Journal of Surgery*, vol. 91, no. 3-4, pp. 119–124, 2019.
- [17] A. Ranjan, N. Khanna, and A. Kumar, "Analysis of malignancies in HIV positive patients: observational study in a tertiary care hospital of Jharkhand," *Journal of Evidence Based Medicine and Healthcare*, vol. 7, no. 31, pp. 1526–1530, 2020.
- [18] J. F. Huang, J. Shen, X. Li, R. Rengan, and A. Wu, "Incidence of patients with bone metastases at diagnosis of solid tumors in adults: a large population-based study," *Annals of Translational Medicine*, vol. 8, no. 7, pp. 482–482, 2020.
- [19] M. Marko, P. Leko, D. Jurenová, R. Furda, and M. Gregu, "Importance of PET/CT examination in patients with malignant uveal melanoma," *Ceská a slovenská oftalmologie: casopis České oftalmologické společnosti a Slovenské oftalmologické společnosti*, vol. 76, no. 1, pp. 37–44, 2020.
- [20] A. Sharma and R. Kumar, "Risk-energy aware service level agreement assessment for computing quickest path in computer networks," *International Journal of Reliability and Safety*, vol. 13, no. 1/2, p. 96, 2019.
- [21] A. Hosking, A. A. Hommel, S. Lorenzl et al., "Characteristics of patients with late-stage Parkinsonism who are nursing home residents compared with those living at home," *Journal of the American Medical Directors Association*, vol. 22, no. 2, pp. 440–445, 2021.
- [22] L. Xin, L. Jianqi, C. Jiayao, Z. Fangchuan, and M. Chengyu, "Study on treatment of printing and dyeing waste gas in the atmosphere with Ce-Mn/GF catalyst," *Arabian Journal of Sciences*, vol. 14, no. 8, pp. 1–6, 2021.

## *Retraction*

# **Retracted: Application of Multislice Spiral CT and Three-Dimensional Image Reconstruction Technology in the Observation of Ankle Sports Injury under the Microscope**

### **Scanning**

Received 20 June 2023; Accepted 20 June 2023; Published 21 June 2023

Copyright © 2023 Scanning. This is an open access article distributed under the Creative Commons Attribution License, which permits unrestricted use, distribution, and reproduction in any medium, provided the original work is properly cited.

This article has been retracted by Hindawi following an investigation undertaken by the publisher [1]. This investigation has uncovered evidence of one or more of the following indicators of systematic manipulation of the publication process:

- (1) Discrepancies in scope
- (2) Discrepancies in the description of the research reported
- (3) Discrepancies between the availability of data and the research described
- (4) Inappropriate citations
- (5) Incoherent, meaningless and/or irrelevant content included in the article
- (6) Peer-review manipulation

The presence of these indicators undermines our confidence in the integrity of the article's content and we cannot, therefore, vouch for its reliability. Please note that this notice is intended solely to alert readers that the content of this article is unreliable. We have not investigated whether authors were aware of or involved in the systematic manipulation of the publication process.

In addition, our investigation has also shown that one or more of the following human-subject reporting requirements has not been met in this article: ethical approval by an Institutional Review Board (IRB) committee or equivalent, patient/participant consent to participate, and/or agreement to publish patient/participant details (where relevant).

Wiley and Hindawi regrets that the usual quality checks did not identify these issues before publication and have since put additional measures in place to safeguard research integrity.

We wish to credit our own Research Integrity and Research Publishing teams and anonymous and named external researchers and research integrity experts for contributing to this investigation.

The corresponding author, as the representative of all authors, has been given the opportunity to register their agreement or disagreement to this retraction. We have kept a record of any response received.

### **References**

- [1] D. Zhao, "Application of Multislice Spiral CT and Three-Dimensional Image Reconstruction Technology in the Observation of Ankle Sports Injury Under the Microscope," *Scanning*, vol. 2022, Article ID 8174310, 7 pages, 2022.

## Research Article

# Application of Multislice Spiral CT and Three-Dimensional Image Reconstruction Technology in the Observation of Ankle Sports Injury under the Microscope

Dongxian Zhao 

Medical School, Huainan Union University, Anhui Huainan 232001, China

Correspondence should be addressed to Dongxian Zhao; 1420110222@st.usst.edu.cn

Received 29 April 2022; Revised 25 May 2022; Accepted 1 June 2022; Published 16 June 2022

Academic Editor: Balakrishnan Nagaraj

Copyright © 2022 Dongxian Zhao. This is an open access article distributed under the Creative Commons Attribution License, which permits unrestricted use, distribution, and reproduction in any medium, provided the original work is properly cited.

In order to solve the problem of multislice spiral CT and three-dimensional image reconstruction technology in the observation of ankle sports injuries under the microscope, to meet the needs of the accuracy of the diagnosis of traumatic fractures, to make up for the shortcomings of the traditional treatment cycle, and to improve the recovery speed of patients. The subjects were inpatients in the Orthopedics and Traumatology Department of a hospital from January 2020 to January 2021. The ankle joint belongs to the flexion joint, which is formed by a dense joint at the lower end of the fibula, tibia, and talus. Osteoarthritis is the most common type of bone fracture, accounting for approximately 3.9% of the total skeletal system, and is most likely to occur in adolescents.

## 1. Introduction

Ankle injury is a medical injury that includes an ankle injury and a peripheral ligament injury. In addition to orthopedics, care should be paid to the diagnosis and treatment of concomitant lower tibiofibular syndesmosis and deltoid ligament injury. If the test is missing or incorrect, there will be serious consequences such as traumatic arthritis in the ankle joint in the later stage. The joints are made up of bones and ligaments, and stability is also supported by the bones and ligament system. The skeletal structure consists of the tibia, the end of the fibula, and the talus [1]. The size of the end of the tibia, which functions internally and externally, creates the medial malleolus, the smaller size at the end of the fibula leading to the lateral malleolus, and the posterior margin of the lower end of the tibia protrudes slightly back, which makes the rear malleolus. The lower tibiofibular ligament deepens to the posterior malleolus, thus limiting the posterior transition of the talus at the ankle point. The talus can be divided into three parts: the head of the talus, the neck, and the body. Due to the special shape of the talus, the talus body is wide in the front and narrow in the back, and the difference between the transverse diame-

ters is 2.4 mm on average. It is accommodated in the ankle hole formed by the inner and outer malleolus. The joint formed by the lower end is the main part of the ankle joint. The articular surfaces on both sides and the corresponding inner and outer malleolus form joints. The lateral malleolus is about 1 cm lower than the medial malleolus on the coronal plane, and it is about 1 cm behind the medial malleolus [2]. When the ankle joint is dorsiflexed, the wider part of the external pronation of the talus enters the ankle hole, and the fibula undergoes posterolateral movement and external rotation to adapt to the movement of the talus. When the ankle joint is planted, the internal pronation of the talus is narrower. Part of it enters the ankle point; so no matter where the ankle joint is dorsiflexed or plantar flexed, the talus is in close contact with the articular surfaces in the ankle point. Some people liken the flexion and extension activities of the talus in the ankle cavity to the rolling of a cone with a cut-off point in the ankle joint rotate outside [3].

The ligament structure of the ankle joint mainly includes two ligament complexes, namely, the inferior tibiofibular complex and the internal and external collateral ligament system. Anterior ligament, posterior tibiofibular ligament, tibial interosseous ligament, and tawm in which interosseous

ligament is the strongest, followed by the posterior inferior tibiofibular ligament, and the anterior inferior tibiofibular ligament is the weakest. The medial and lateral ligaments strengthen the joint on both sides, which can prevent the talus from twisting and tilting in the ankle. Inversion of the foot and the anterior talofibular ligament are also important models to prevent anterior displacement of the talus. Ankle sprain is not only the most common injury in athletes but also a high incidence injury in the general population, of which 85% are lateral injuries, which are more common when patients walk on uneven roads, go down stairs, run, jump and land during sports. The ankle joint is plantar-flexed, and the foot is suddenly turned medially, resulting in strong traction on the lateral ligament of the ankle joint, as shown in Figure 1.

## 2. Literature Review

Lu et al. said that ankle ligament injury is the most common sports injury, accounting for approximately 25% of all sports injuries, of which varus sprain leads to injury to the lateral collateral ankle joint in the ankle joint, 85% of ligament injuries. The lateral collateral ligament of the ankle joint is an important structure for maintaining the stability of the ankle joint, especially the anterior talofibular ligament (ATFL) and the calcaneofibular ligament (CFL) play a major role in the stability and their damage can lead to instability of the lateral ankle joint, which severely affects the function of the ankle joint [4]. At the same time, CFL also has the security of subtalar sharing, and damage may also affect the performance of subtalar sharing. The subtalar joint is involved in many movements of the ankle joint. If the subtalar joint is damaged or unstable, it may also affect the function of the joint.

The external ligament, which is prone to injury, and the medial ligament of the ankle alone are rare, and most deltoid ligament injuries are combined with lateral malleolus fractures, or in combination with syndesmosis [5]. Valentini et al. recorded 281 patients with ankle sprains, and the average joint stiffness was only 3% [6]. Almost all medial ligament injuries are partial ligament avulsion. Zhao et al. underwent 42 patients with complete rupture of the deltoid ligament, all with no exceptions combined with other injuries [7]. However, intense valgus violence can still lead to isolated deltoid ligament injury. The three main mechanisms of deltoid ligament injury are pronation-abduction, pronation-external rotation, and supination-external rotation of the foot.

Davydov et al. concluded that although the medial deltoid ligament has a very low incidence of injury and most do not require repair, deltoid ligament injuries often cause significant pain and dysfunction [8]. According to Ishiji et al., patients with deltoid ligament injury experience medial malleolus discomfort and at the same time the ankle joint will exhibit valgus and abduction [9]. Patients often require reconstructive surgery to correct rotational instability, talar tilt, and valgus angulation in the coronal plane. The incidence of adult-acquired flatfoot caused by posterior tibial tendon injury is higher in women than in men, espe-



FIGURE 1: Ankle sprain.

cially in the elderly over 60 years of age. The disease is clinically characterized by insufficiency of the posterior tibial tendon and medial longitudinal arch of the foot, causing external rotation of the heel, abduction of the midfoot, and supination of the forefoot. The X-ray imaging features are that with the development of the deformity, the lateral first metatarsal-crawl angle continues to increase, and the contact area of the talonavicular joint in anterior and posterior view continues to decrease, and other joints will also have similar deformities.

Improving classification for posttibal muscle injury [10]. Wang et al. added step III to the first division, which is associated with deltoid ligament damage, causing the valgus to tilt at the talus of the ankle point. Stage IV flat feet can be divided into two sections, namely, flat feet and flat feet. Flat feet, often accompanied by a slip of the middle ankle, require arthrodesis. When Phase IV flatfoot is associated with a joint, joint or joint replacement requires further treatment of the foot deformity. However, flat feet can be treated with deltoid ligament reconstruction procedures.

Zhou et al. described a technique for reconstructing the deltoid ligament [11]. They cross half of the posterior tibia tendon at the distal end of the tibia and then cut it lengthwise. The distal end of the muscle is still connected to the connective tissue of the body, and the end of the end passes through the middle malleolus hole which has already been drilled. Schwarz and Schwarz describe a new procedure with peroneal longus tendon transplantation [12]. They cut the peroneal longus tendon across the insertion point, passing the peroneal longus tendon through the iliac crest of the talus to the medial malleolus, then through the iliac crest of the medial malleolus to the outside of the tibia, and connect the muscles to the lateral side of the tibia.

## 3. Methods

The subjects were inpatients in the Orthopedics and Traumatology Department of a hospital from January 2020 to January 2021. When the patient falls off, the patient or family member should be contacted as much as possible by visiting the door, making an appointment for follow-up, telephone, etc., asking the reasons, and completing the evaluation items that can be completed. Related research data should be stored securely for record keeping, not only for archiving data but also to complete statistical analysis. Patients do not need to be replenished. Orthopedics and radiologists work together to perform standardized X-ray films and then use spiral CT three-dimensional reconstruction technology to examine fractures, the location of fractures, and fractures of the joint for further examination.



Based on the results of X-ray and CT three-dimensional reconstruction, according to Lauge-Hansen classification, and according to CT and three-dimensional reconstruction examination, self-made CT classification of ankle fractures was obtained[13].

After removal of the surgical contraindications, open reduction and internal healing were performed. The surgery was appropriate and effective. Prevention and daily treatment after surgery were completed, and patients were instructed to achieve optimal function of the legs and feet. The data were processed by SPSS13.0 statistical analysis software, and the values were compared with  $\chi^2$  test,  $P < 0.05$  was considered as significant [14].

This group of 42 patients, 23 males and 19 females, aged 19-887 years, with an average of 51 years. Causes of injury are as follows: 29 cases of bone disease, 5 cases of collision, 6 cases of injury, and 2 cases of other diseases. Internal and external microscopic images of the ankle joint and spiral CT scan of the articular cartilage were affected, and a three-dimensional reconstruction was completed. According to Danis-Weber classification, there were 3 cases of type A, 22 cases of type B, and 11 cases of C (6 cases of noninvasive malleolus rupture). According to the Lauge-Hansen classification, there were 3 cases of supination and adduct, 23 cases of supination-external rotation, 8 cases of pronation-abduction, 3 cases of pronation-external rotation, and 5 cases of vertical compression.

The CT images of all cases showed the course of the fracture line, the position and displacement of the bone fragments, and the involvement of the articular surface. In this group of 42 patients with ankle fractures, CT scan and three-dimensional reconstruction showed 42 cases, including 4 cases of medial malleolus fractures, 8 cases of lateral malleolus fractures, 20 cases of bilateral malleolus fractures, and 10 cases of tri malleolar fractures. Plain X-ray showed 42 cases, including 4 cases of medial malleolus fractures, 3 cases of lateral malleolus fractures, 18 cases of bilateral malleolus fractures, and 17 cases of trimalleolar fractures. 41 cases were confirmed by CT three-dimensional reconstruction, and the diagnostic coincidence rate was 97.6%. Plain films were suspicious in 3 cases, missed diagnosis in 14 cases, and the diagnostic coincidence rate was 59.5%, and the difference was statistically significant, as shown in Figure 2 and Tables 1 and 2.

For the two groups of patients, the sensitivity, specificity, and Youden index of MRI were significantly higher than those of MSCT in sensitivity, specificity, and Youden index, and the difference was statistically significant ( $P < 0.05$ ), as shown in Table 3.

Examination of the unique and sensitive nature of multiple CT 3D reconstruction for joint injuries using surgery and pathology as a standard temperature for diagnostic and specialized testing incidence of multiple CT 3D reconstruction for ankle injuries is 92% and 86%. AUG is 0.954, as shown in Figure 3.

Supplementary diagnosis was made in 14 cases of X-ray missed diagnosis based on CT images. Among them, 9 cases were difficult to display posterior malleolus fractures by conventional X-rays but could be clearly displayed by CT,

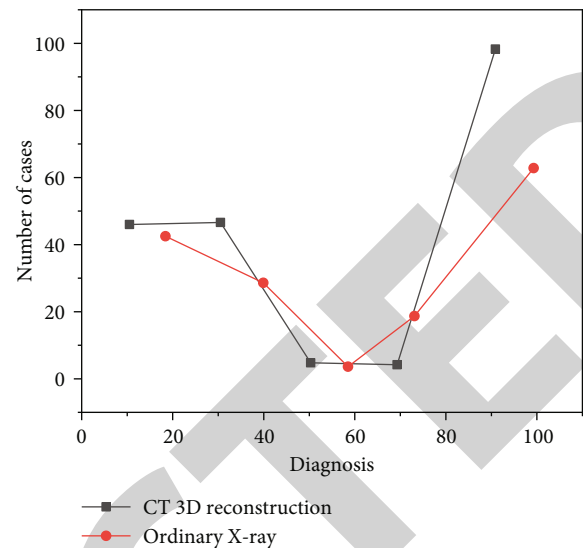


FIGURE 2: Line chart of diagnosis.

and 5 cases were not found medial malleolar fractures by X-rays but could be clearly displayed by CT. 12 cases changed the surgical plan based on X-ray films, and 5 cases of newly discovered medial malleolus fractures were treated with Kirschner wire or cannulated nails. Postoperative plaster fixation was performed in all cases, 2 cases of posterior malleolus were changed from no internal fixation to 2 cases, and 4 cases of surgical approach were changed due to the position of posterior malleolus. All patients achieved or approximated anatomical reduction after operation, and there was no infection, fracture nonunion, and malunion, and the patients basically recovered their original ability to live after operation [15].

Through ankle CT scan and 3D reconstruction, doctors can comprehensively and accurately understand the position and direction of the fracture line, which is conducive to the judgment of fracture classification. Forty-two cases in this group have been completely isolated and classified according to the Lauge-Hansen classification and Danis-Weber classification, and it is important to conduct surgical treatment [16].

CT three-dimensional reconstruction technology is a non-invasive examination. There is no need to change the body position during the examination, and the scanning speed is fast, basically without the cooperation of the patient. It can display the characteristics of fractures three-dimensionally and intuitively, so that clinicians can detect fractures in three-dimensional space comprehensive knowledge. It can accurately display the fracture type and displacement of the medial, lateral, and posterior malleolus and guide clinicians to formulate a careful and detailed surgical plan, so it has great advantages in the diagnosis and treatment of ankle fractures. The X-ray films in this group missed the diagnosis of 5 cases of medial malleolus fractures, and 4 cases were because the medial malleolus fracture line was coronal, and the front and lateral X-ray films were all blocked by the bones on the same plane, so they could not be visualized on the X-ray films. Some of the missed posterior malleolus

TABLE 1: Types of ankle fractures shown by ordinary X-ray films and three-dimensional reconstruction of spiral CT.

Group	Number of cases	Medial malleolus fracture	Lateral malleolus fracture	Fracture of both ankles	Three ankle fractures	Combined dislocation
CT 3D reconstruction	42	4	3	18	17	9
Ordinary X-ray	42	4	8	20	10	9

TABLE 2: Diagnosis of ankle fractures.

Group	Number of cases	Diagnosed	Suspicious	Missed diagnosis	Diagnosis coincidence rate (%)
CT 3D reconstruction	42	41	1	0	97.6
Ordinary X-ray	42	25	3	14	59.5

TABLE 3: Diagnostic sensitivity, specificity, and Youden index of two groups of patients.

Detection method	Sensitivity (%)	Specificity (%)	Youden index (%)
MRI	97.09	90.77	87.89
MSCT	86.47	66.81	53.12
L	7.798	17.580	29.349
P	0.005	0.000	0.000

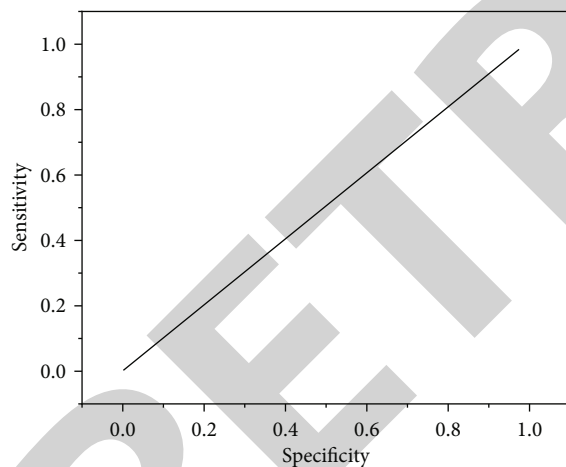


FIGURE 3: Analysis of specificity and sensitivity of three-dimensional reconstruction of multislice spiral CT for acute ankle injury.

fractures were also not shown because the fracture fragments were small and the images overlapped each other on the X-ray films. In addition, CT can clearly display the bone fragments involved in the joint and the soft tissue changes around the bone and joint, which has a high diagnostic value for complex bone and joint injuries. The diagnostic rate of CT three-dimensional reconstruction in this group of cases reached 97.6%, which was significantly better than that of X-ray, thus effectively avoiding missed diagnosis [17].

Spinal CT can not only confirm the presence of bone marrow but also affect the relationship between bone mar-

row and bone marrow bone, providing an important role in the choice of surgery. Because the indication of internal fixation for posterior malleolus fractures is generally determined according to the size of the posterior malleolus fragment, most scholars believe that when a posterior malleolus fracture involves more than a quarter of the distal articular surface of the tibia, the stability of the ankle joint is significantly reduced, and internal reduction should be performed and fixed. When it is less than 1/4, closed reduction and plaster fixation are feasible in most cases [18].

Surgery for the ankle bone depends on the posterior malleolus damage. There are several variations for the ankle to choose from: the path to the outside of the ankle, the path to the inside of the heart malleolus, the path to the back to the medial malleolus and the path posterolateral to the ankle. If the posterior malleolus fragment deviates to the medial side, the medial malleolar approach is optional, and if the posterior malleolus fragment deviates to the lateral side, the posterolateral ankle approach is optional. Because the incision of the medial malleolar posterior pathway can not only rehabilitate and repair the medial malleolus but also resume the posterior malleolus, so it is now widely used in medicine. Yuan Tao et al. publish a case in their publication. X-ray films of one of their patients' affected limbs showed a fracture of the medial malleolus. From the images of spiral CT and three-dimensional reconstruction, only the posterior colliculus of the medial malleolus was fractured, while the anterior colliculus was fractured. The patient was completely intact and free of fractures, and they used the medial malleolus reduction and fixation of the ankle joint through the posteromedial approach. Without the assistance of spiral CT and 3D reconstruction data, the conventional anteromedial approach will inevitably increase the difficulty of intraoperative exposure and internal fixation. In this group of patients with both medial malleolus and posterior malleolus fractures, the posterior malleolus approach was used, and the posterior malleolus were well reduced [19].

For larger bone fragments, according to the fracture line shown on the CT image, compression screws perpendicular to the direction of the fracture line are often used for fixation to obtain a good fixation effect. For ankle fracture fixation, the lateral malleolus usually uses steel plates. For screw fixation, medial malleolus fractures are usually fixed with two cannulated screws. For small bone fragments, compression

screws are not suitable. If the intra-articular free bone fragment is removed, it should be removed first to reduce the possibility of traumatic arthritis; for posterior malleolus fractures, closed reduction and fixation with anterior tibial cannulated screw is a common method, because it is difficult to fully expose the posterior malleolus and the incision is relatively small. Small, reduction and fixation at the same time did not damage the soft tissue on the posterior malleolus fragment, which is conducive to fracture healing. Its indication is that the fracture bones of the posterior malleolus are large and indistinguishable. All posterior malleolus fractures to be fixed in this group were fixed with anterior tibial cannula screws, with stable and good bone quality. For crack repair, compression screw fixation is not necessary [20]. In addition, the rupture of the posterior malleolus does not need to be parallel to the coronal plane at the lower end of the tibia. Therefore, when repairing the posterior malleolus damage, the direction of the nail insertion should be based on data from spiral CT and three-dimensional reconstruction. The direction of the needle is perpendicular to the direction of the fracture line. For minor treatments of posterior cartilage cartilage, it is difficult to develop detailed information and be treated without data by three-dimensional reconstruction of spiral CT and line data alone [21].

#### 4. Results and Analysis

The soft tissue composition around the ankle point was introduced, but the diagnosis and treatment of ligament injury were not described. As explained below, in the absence of fracture of the ankle joint, the soft tissue must bear significant energy. The injury of soft tissue is usually manifested in the injury of the ligaments around the ankle joint. The ankle joint is composed of many bones, and the ligaments of the joint are complex, and the injury is often combined with surrounding ligament injury, and deltoid ligament injury is the most common complicating injury [22]. In the ankle joint, 15% of them injure the deltoid ligament. The deltoid band plays an important role in maintaining the stability of the ankle. When the deltoid ligament is damaged, it will inevitably lead to ankle instability and displacement of the talus, often with lateral malleolus damage and damage to the syndesmotom ligament.

The ligament structure of the ankle joint usually includes two ligament complexes, the tibiofibular complex and the internal and external ligament system. Anterior ligament, posterior lower tibiofibular ligament, and interosseous ligament, of which the interosseous ligament is the strongest, followed by the posterior inferior tibiofibular ligament, and the anterior inferior tibiofibular ligament is the weakest [23]. The medial and lateral collateral ligaments strengthen the joint capsule from both sides, which can prevent the talus from inverting and tilting in the ankle joint. The anterior talofibular ligament is also an important structure to prevent the anterior displacement of the talus. The medial collateral ligament, also known as the deltoid ligament, is mainly composed of the superficial tibiocalcaneal ligament and the deep anterior and posterior tibiotalar ligaments [24]. If the deltoid ligament rupture is not repaired, it can

not be repaired directly due to the separation of the rupture, and the scar is packed and attached, and the tensile strength is not good, so sequelae such as ankle are not stable. Freezing and pain are usually left behind.

The upper layer of the deltoid ligament in the ankle joint starts from the anterior and lower part of the medial malleolus, extending in a fan and in the neck of the talus and calcaneus. It mainly resists valgus stress in the hind foot, can limit the external rotation of the talus, and can withstand the external rotation of the talus. Scientists generally believe that the deep deltoid band has a greater impact on the stability of the ankle than the top layer. Earl M cuts the tibiocalcaneal ligament, reduces the tibial-speech contact area from 26% to 43%, increases tibial pressure from 20% to 30%, and moves the center of gravity to side. The average is 4 mm, when the other end of the deltoid band is removed and the contact characteristics change slightly. Therefore, it is believed that the tibiocalcaneal ligament plays an important role in the stability of the joint. The most important of the joints, and Sharma et al. believe that the most important delta ligaments are the tibiocalcaneal ligament and the deep tibiotalar ligament [25].

Deltoid ligament injury is divided into two types: acute and chronic. Severe injury usually occurs as tenderness and hematoma in the angular ligament of the medial malleolus, while injury occurs as a dull pain in the medial sulcus of the joint. Anterior symptoms [26]. There is a noticeable sensitivity in the front and bottom of the medial malleolus tip, subcutaneous ecchymosis can be seen, and there is depression or nothing on the inside of the ankle. Because of the severity of the injury, the patient has obvious symptoms, so he or she can usually appeal to the patient's heart and use similar measures to protect the ligament. But in long-term injury, the patient's heart is not comfortable because of the symptoms, so the deltoid ligament can. It does not relax, but it can cause instability in the joints in the middle, which often occurs when walking on uneven ground. When going up or down stairs, the performance of "play legs" occurs [27].

The structure of the talus is unique. When the ankle joint is plantar bent, the joint area of the tibia is smaller than the contact area of the tibia. Similarly, the size of the medial area in the ankle will change according to the degree of plantar flexion in the ankle. There are scientists who have suggested that the inaccurate quality of the diagnosis of deltoid ligament damage during X-ray film is high. A simple CT scan can better show the direction of the rupture and damage to the joint, cavity joint and capsule, as well as the location of fractures and fractures and subluxation of the joint. The lower the degree to the MRI, MRI can better describe the edema and blood supply to the soft tissue. Therefore, MRI of ankle joint is an important indication for diagnosing deltoid ligament injury [28].

Arthroscopy technology has gradually become a popular technology because of its unique characteristics of small trauma and strong maneuverability, because it can not only complete the exploration but also can complete the operation under the microscope after reexploration. The 5 mm arthroscope can freely enter and exit the joint cavity, making

it in. Joint injury repair surgery has become the main force. Ankle arthroscopy can intuitively describe the internal structure of the ankle joint and the degree of damage to the soft tissue and can verify the findings of imaging examinations. Surgery is used to diagnose deltoid ligament injuries, because of the large trauma and the difficulty of exposing the tissue, and it is less used in the case of only soft tissue injury. Henari et al. believed that ultrasonography was a simple and accurate way of diagnosis. They performed ultrasonography, X-ray plain film, and arthrography, respectively, for supination and external rotation ankle fractures. Sensitivity and specificity were both 100%.

Ankle deltoid ligament injury usually does not occur alone but is accompanied by lateral malleolus fracture and lower tibiofibular syndesmotic ligament injury. The treatment plan of deltoid ligament is currently divided into two camps. Some scholars believe that as long as the anatomic reduction and displacement can be achieved. Fibula and talus, and strong internal fixation, the deltoid ligament with strong repair function can heal quickly. During the operation, when reducing the medial malleolus fracture, we will find that no matter how the dislocation of the talus is reduced, the anatomical reduction cannot be achieved, and it was found that the broken end of the deltoid ligament entered the joint space and prevented the reduction of the talus. At this time, it is necessary to expand the deltoid ligament and pay attention to the connection and protection of the torn ligament. Whether the deltoid band needs to be repaired depends on the modification of the ankle point. There were no significant differences in the treatment of both surgical and nonsurgical deltoid ligament rupture groups.

For repositioning, the deltoid ligament does not need repair, and some researchers believe that the deltoid ligament plays an important role in maintaining the stability of the ankle. When it is damaged, surgery must be performed. When it comes to the treatment of ankle sprains, there are currently three types: direct suture, suture anchor repair, and deltoid ligament reconstruction. A clinical study of 42 patients was conducted to explore the therapeutic benefits of osteoarthritis with deltoid ligament injury. The results showed that the best was 93.5% in the control group and 67.7% in the control group, with significant differences. They believe that after a hip joint injury with a deltoid ligament injury, cosmetic surgery for the deltoid ligament is critical to the proper functioning of the ankle joint. To monitor the healing of the deltoid ligament damage with suture anchors, suture anchors were screwed into the deltoid ligament at the insertion site of the talus during surgery, and the deep deltoid ligament was repaired and reconstructed. Again simultaneously, the top layer was directly sutured. All care was paid to the repair and reconstruction of the deltoid ligament, and the deltoid ligament was repaired with suture anchors, which not only repaired the extension of the ligament but also the reconstruction of the deltoid ligament. When dealing with a deltoid ligament, first comb the torn ligament, insert two small bone holes with a drill bit at the attachment point to the talus, the tissue, and suture the broken end of the torn ligament, and fix the ligament with

a thin wire from the ankle. The torn body is sewn with silk thread 8. For medial malleolus avulsion, 2 small bone holes were drilled with a bone drill at the medial malleolus, and then, the ligaments were fixed with silk thread through the bone holes. After surgery, the ankle joint is cast in varus position for 4-6 weeks. Compared with the traditional direct suture, the suture anchor to repair the deltoid ligament has less surgical damage and is easy to operate. The anchor is completely embedded in the bone tissue, and the fixation is firm, which is very suitable for the ankle. The joint movement is not affected, and there is no need to resurgery to remove the characteristics.

## 5. Conclusion

It has been proven that the use of multitape spiral CT and three-dimensional imaging reconstruction technology in the examination of ankle sprains in the microscope is possible, which can solve the problem of the fact of diagnosing fractures, causes. There is no natural treatment available, and patients are rehabilitated fast. X-rays are also the easiest way to detect bone damage. It has the advantages of simplicity, convenience, and low cost. It is a commonly used imaging diagnostic method for traumatic fractures, for complex fractures such as the ankle, knee, and shoulder. On the one hand, CT scan and three-dimensional reconstruction are more agile in diagnosis of broken small bone fragments or nondisplaced fractures than X-ray and can also further evaluate the condition of soft tissue at the injury site, which can make up for the insufficiency of X-ray and has a high clinical rate. It has application value, and CT examination has basically been popularized in large and small hospitals at present. It is reasonable to believe that CT examination will definitely play a pivotal role in today's diversification of auxiliary examinations.

## Data Availability

The data used to support the findings of this study are available from the corresponding author upon request.

## Conflicts of Interest

The author declares that he/she has no conflicts of interest.

## Acknowledgments

This work was sponsored in part by the National Natural Science Foundation of Anhui Province ("Clinical observation of low concentration atropine combined with Orthokeratology in the treatment of low Myopia in children and adolescents," KJ2019A0999).

## References

- [1] Y. Zheng, W. Wang, Y. Yang, and Y. Wu, "Single-layer planar wideband rat-race coupler using a shorted parallel-coupled multi-line section," *IEEE Transactions on Circuits and Systems II: Express Briefs*, vol. 67, no. 12, pp. 3053–3057, 2020.

## *Retraction*

# **Retracted: Application of Ultrasonic Intelligent Imaging in L-Selectin Regulating Embryo Implantation in Mongolian Sheep Endometrium**

### **Scanning**

Received 5 December 2023; Accepted 5 December 2023; Published 6 December 2023

Copyright © 2023 Scanning. This is an open access article distributed under the Creative Commons Attribution License, which permits unrestricted use, distribution, and reproduction in any medium, provided the original work is properly cited.

This article has been retracted by Hindawi, as publisher, following an investigation undertaken by the publisher [1]. This investigation has uncovered evidence of systematic manipulation of the publication and peer-review process. We cannot, therefore, vouch for the reliability or integrity of this article.

Please note that this notice is intended solely to alert readers that the peer-review process of this article has been compromised.

Wiley and Hindawi regret that the usual quality checks did not identify these issues before publication and have since put additional measures in place to safeguard research integrity.

We wish to credit our Research Integrity and Research Publishing teams and anonymous and named external researchers and research integrity experts for contributing to this investigation.

The corresponding author, as the representative of all authors, has been given the opportunity to register their agreement or disagreement to this retraction. We have kept a record of any response received.

### **References**

- [1] C. Wang, A. Bao, Q. Hai, Z. Hu, and X. Bai, "Application of Ultrasonic Intelligent Imaging in L-Selectin Regulating Embryo Implantation in Mongolian Sheep Endometrium," *Scanning*, vol. 2022, Article ID 3323768, 9 pages, 2022.

## Research Article

# Application of Ultrasonic Intelligent Imaging in L-Selectin Regulating Embryo Implantation in Mongolian Sheep Endometrium

Changshou Wang <sup>1</sup>, Adong Bao <sup>1</sup>, Qing Hai <sup>1</sup>, Zhengxiang Hu <sup>2</sup>, and Xiaoying Bai <sup>3</sup>

<sup>1</sup>Department of Agronomy, Hetao College, Bayannur, Inner Mongolia 015000, China

<sup>2</sup>Bayannur Forestry and Grassland Bureau, Bayannur Inner Mongolia 015000, China

<sup>3</sup>Animal Disease Prevention and Control Center, Kezuo Middle Banner, Tongliao, Inner Mongolia 029300, China

Correspondence should be addressed to Changshou Wang; 201904012202@stu.zjsru.edu.cn

Received 15 May 2022; Revised 28 May 2022; Accepted 6 June 2022; Published 15 June 2022

Academic Editor: Balakrishnan Nagaraj

Copyright © 2022 Changshou Wang et al. This is an open access article distributed under the Creative Commons Attribution License, which permits unrestricted use, distribution, and reproduction in any medium, provided the original work is properly cited.

In order to explore the practical application of ultrasonic imaging in the pregnancy stage of Mongolian sheep and the role of L-selectin in the embryo implantation process of Mongolian sheep, this paper systematically observed the early embryonic development by B-mode ultrasonic imaging wave diagnostic instrument with 5 MHz rectal probe and detected the expression of sLex and L-selectin in embryonic cells (jar cells) and endometrial cells (RL95-2 cells) by immunoassay to show the role of L-selectin in embryonic adhesion. The results were as follows: the correct rate of fetal sex determination by ultrasound imaging increased with the increase of pregnancy days and reached 93% at 84 days; sLex/L-selectin on the surface of Jar/RL95-2 cells is involved in the adhesion between embryo and endometrium; and when the concentration of L-selectin was 30  $\mu\text{g/ml}$ , the implantation success rate of fertilized eggs and embryos was the highest, reaching 95%. It is proved that ultrasonic intelligent imaging exploration can summarize the imaging characteristics of the early development law of sheep fetus, which provides a basis for B-ultrasound to monitor fetal growth and predict fetal age. While discussing the molecular mechanism of implantation, it provides a new idea and means for the clinical intervention of contraception and pregnancy assistance with oligosaccharide as the target.

## 1. Introduction

Livestock embryo transfer technology has developed from the experimental stage after the 1980s to 1990s to the application of livestock production, which has become a major revolution in livestock breeding and improvement technology. Sheep embryo transfer technology refers to the use of improved breeds or excellent individual ewes as donors for superovulation, so that they can produce more embryos and take the varieties or individual ewes with poor production performance as recipients. The embryos produced by the donor are transferred into the recipient's uterus by surgical method, and the fetus of excellent individuals is conceived by the belly of poor ewes, so as to achieve the purpose of rapidly expanding the offspring of good breeding

sheep. The reproduction speed of purebred sheep can be greatly accelerated by carrying out sheep embryo transfer technology [1]. Due to the current shortage of purebred sheep in China, the market price of each purebred sheep is tens of thousands of Yuan. Embryo transfer technology can improve the reproduction efficiency of purebred sheep several times or more than ten times. As an effective way to speed up the reproduction speed of improved sheep, embryo transfer technology can obtain good economic and social benefits, and its application prospect is very broad. Among the factors affecting the production efficiency of raising sheep, variety is the primary factor. The application of excellent sheep breeds is the basis for improving the production level of sheep and promoting the development of sheep industry [2]. The growth performance and meat production

performance of some excellent foreign sheep breeds are better than those of domestic local breeds. However, due to the expensive introduction of breeding sheep, low reproductive rate and, long reproductive cycle, they cannot be popularized rapidly. Young sheep aged 2-5 years old with good phenotype, high production level, stable heredity, healthy physique, normal estrous cycle, no reproductive tract diseases, and normal reproductive history of 1-2 fetuses were selected as donors [3]. The donor and recipient sheep must be selected and kept in place 3~4 months before the operation, and the epidemic disease vaccination, necessary epidemic disease monitoring, and insect repellent shall be done well, and the feeding shall be strengthened from 2 months before the operation. Especially in the treatment of donor sheep, if the feeding management is not in place, it will cause nonovulation or corpus luteum to form white body and affect embryo quality and nonfertilization of embryos [4]. It is suggested to eliminate the donor sheep that are too thin and avoid the waste of hormones and human and material resources. The sheep also suffer from poor embryo production effect and slow surgical recovery. Select an excellent donor and acceptor. Empty ewes with large size, no reproductive tract diseases, high milk yield, and strong lactation ability are selected as the acceptor. The acceptor sheep are 2~5 years old and have a history of normal reproduction of 1~2 fetuses. It is suggested to eliminate too thin recipients. The embryo transfer rate of too thin recipients is low, resulting in the waste of hormones, manpower, and material resources. In addition, before and after embryo transfer, how to promote the success rate of transfer and judge whether embryo implantation has become a key issue [5].

## 2. Literature Review

Sui et al. believed that after embryo transfer, pregnancy diagnosis should be made as soon as possible to determine the sheep without pregnancy, and timely measures should be taken to make them pregnant, which is of great significance for protecting the fetus, reducing empty pregnancy, shortening the litter interval of ewes, and improving the reproductive rate of sheep [6]. Pillarisetti et al. believe that in practice, the most commonly used pregnancy identification method is to test the estrus of rams to observe whether the transplanted sheep return to estrus. If they do not return to estrus, they are pregnant, and if they return to estrus, they are not pregnant. Generally, they test estrus continuously for 2-3 estrus cycles. This method has a good effect on ewes with normal estrus, and the accuracy is more than 90%. It is not applicable to false pregnant sheep without pregnancy and estrus and those who have estrus after pregnancy, but this phenomenon occurs less in sheep production [7]. Labuda et al. believe that after pregnancy, ewes have vigorous metabolism, increased appetite, and improved digestive function, which are manifested in weight gain, glossy coat, docile temperament, cautious and stable action, etc. these phenomena can be used as important indicators for external observation. In actual production, the number of no return cases is often higher than the actual number of conceived babies. To solve

this problem, the following methods can be adopted for further inspection [8]. Zhang et al. believed that ultrasonic detection method is to use the reflection of ultrasonic wave for pregnancy examination. This method is generally used at 6 weeks of estrus, and the accuracy rate is about 98%. Ultrasonic diagnosis is a physical examination method that closely combines the physical characteristics of ultrasound with the acoustic characteristics of animal tissue structure. The specific method is to keep the ewe standing in the semi-inferous frame, fix the neck with a rope, and examine it in two ways: rectum and in vitro. First from the rectum, when the rectum cannot be accurately examined, use in vitro examination. During rectal examination, first take out the resident feces in the rectum, apply the coupling agent on the probe, bring it into the rectum by fingers, send it to the front and back of the pelvic entrance, and scan it at 45°-90° downward. In in vitro examination, it is mainly in the hairless area on the inner side of the roots of the two strands or on both sides of the breast without shearing. After the probe is coated with coupling agent, it is scanned by sticking the skin to the direction of the uterus at the entrance of the pelvic cavity, and typical images are selected for photography and video recording [9]. Mohammadkhani et al. believed that the content of progesterone in the blood of ewes increased significantly after pregnancy. According to this characteristic, the ewes were diagnosed for early pregnancy, that is, measured by fluorescence spectrophotometry 20 days after transplantation. The progesterone content per milliliter of plasma in sheep was more than 1.5  $\mu\text{g}$ , the accuracy of infertility was 100%, and the accuracy of pregnancy was 93%. The progesterone content per milliliter of milk of dairy goats is greater than or equal to 8.3  $\mu\text{g}$ , the accuracy of infertility is 100%, and the accuracy of pregnancy is 90%. The accuracy of infertility and pregnancy was 100% and 98.6% in sheep when the content of progesterone in plasma per milliliter was greater than or equal to 3  $\mu\text{g}$ . The plasma progesterone content of goats per milliliter is greater than 3  $\mu\text{g}$ , and the pregnancy accuracy is 86% [10]. Luo et al. believe that after ewe pregnancy, the embryo, placenta, and maternal tissue produce prolactin or enzyme chemicals, respectively, and their content increases significantly in a certain period after pregnancy. Some substances have strong antigenicity and can stimulate the immune response of ewe body. Pregnancy can be identified through some physical and chemical properties of antigen antibody binding reaction, such as agglutination reaction and precipitation reaction. Generally, the specially prepared anti pregnancy serum can be used to check whether the ewes 10-15 days after mating are pregnant [11]. After Fan et al. first used the ultrasound imaging technology to diagnose sheep pregnancy, many scholars used it to predict gestational age and gestational period [12]. For example, Zhong and others used it to measure placental diameter to predict gestational age. They believed that there was a positive correlation between gestational age and placental growth, but they found that the placental diameter had developed to the maximum by 80 d of pregnancy [13]. Tenorio-Chávez and others used it to measure the biparietal diameter (BPD) of the fetal skull to predict fetal age [14]. In addition, Reichert and others

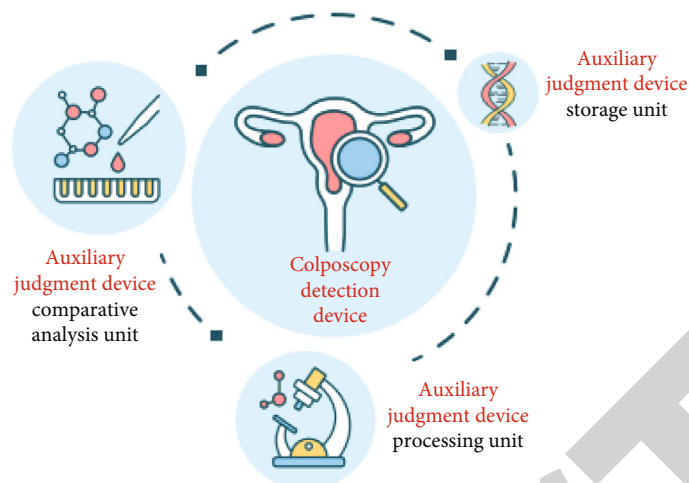


FIGURE 1: Ultrasonic imaging method.

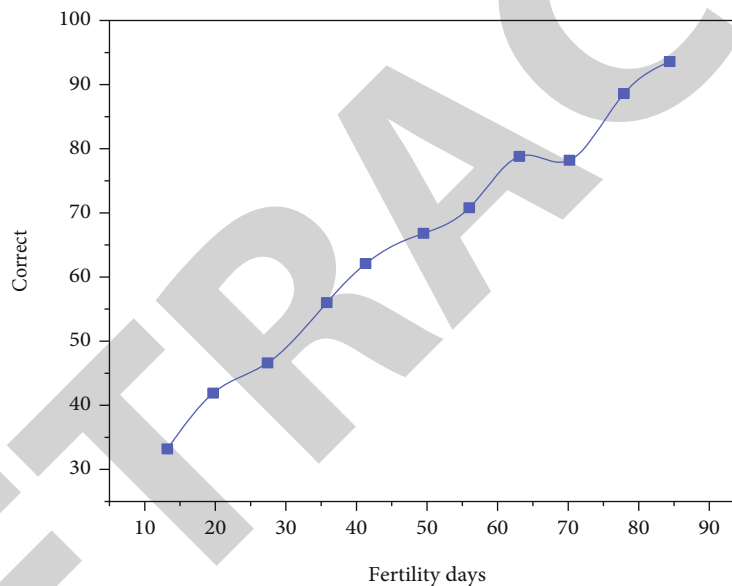


FIGURE 2: Success rate of ultrasound imaging in detecting gender.

also used it to monitor the effects of forage poisoning on sheep fetal development, such as abortion and teratogenesis. Although the above prediction has gone deep into the study of fetus itself, there is no report on the observation of sheep fetal development system [15].

Based on this, this experiment is to observe the early development law of sheep fetus through systematic tracking and exploration on the basis of ultrasonic imaging in the diagnosis of early pregnancy of sheep, in order to provide useful data for the feeding and management of sheep during pregnancy, the monitoring of embryo growth, and development and the diagnosis of related diseases (Figure 1).

### 3. Research Methods

**3.1. Ultrasonic Imaging Exploration.** The Alokassd210dx-ii ultrasonic diagnostic device (referred to as B-ultrasound,

with rectal probe), frequency 5 MHz, with photographic and video equipment, was used

9 Mongolian and hybrid pregnant ewes of 1~2 generations, 4 at 15~18 days after mating, and 5 at 30~38 days of pregnancy were included. Ewes stand or lie on their sides, exclude feces stored in the rectum, take the probe into the rectum by fingers after applying coupling agent, and scan it to the front of the bladder, down and at 45 on both sides, observe the fetal body, fetal heart, fetal viscera, fetal movement, placenta, etc., and select typical images for photography and video recording [15].

#### 3.2. Effect of L-Selectin on Embryonic Cells

**3.2.1. Cell Culture.** RL95-2 cells were cultured in the DMEM/F12 (1:1) medium (containing 10% fetal bovine serum, 5 g/ml insulin, 100 IU/ml penicillin, and 100 g/ml streptomycin), and jar cells were cultured in the RPMI1640 medium. Culture



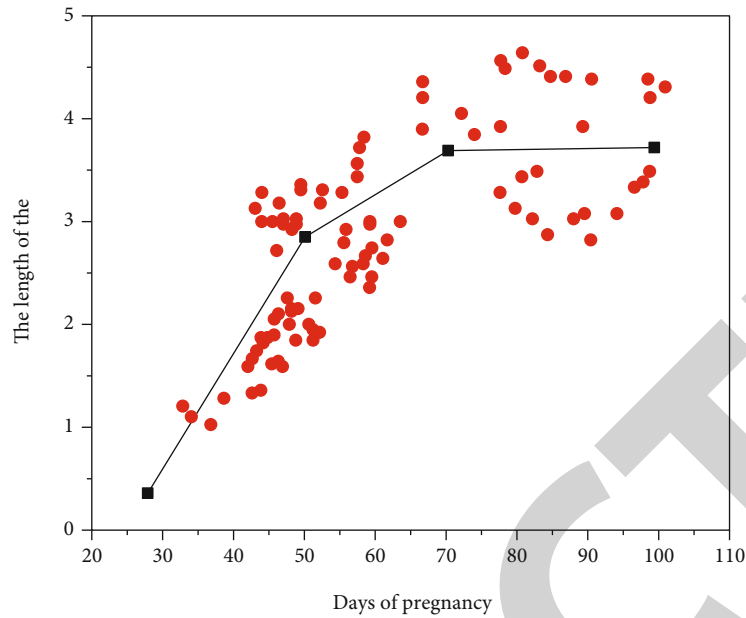


FIGURE 3: Changes in placental growth.

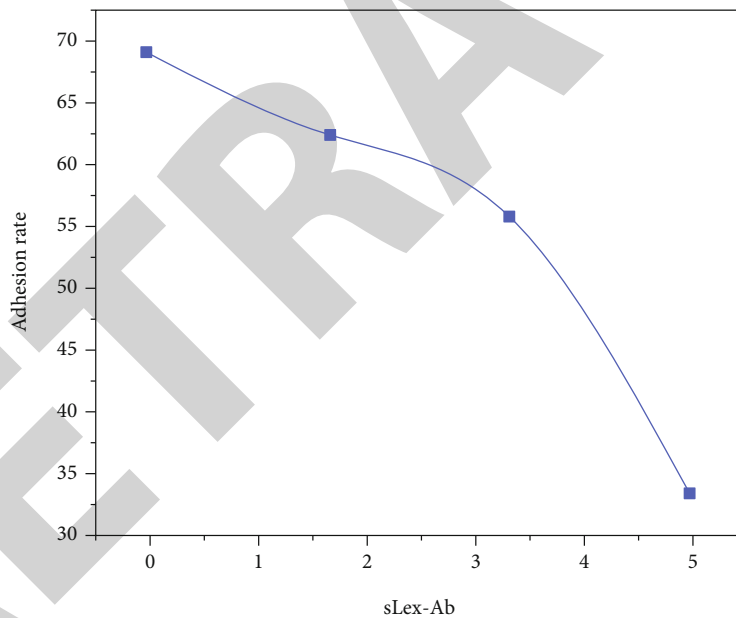


FIGURE 4: Effect of L-selectin on adhesion of jar cells to RL95-2 cells (sLex Ab).

conditions are as follows: 37°C, volume fraction 5% CO<sub>2</sub>, and 90% saturated humidity.

**3.2.2. Cell Transfection.** The cells were spread on 6-well plates and transfected with liposome 2000 when they grew to 70%-80% fusion. Take 4.0 μg FUT7 overexpression vector and gently mix it with 250 μl medium (no serum, no double antibody); 10 μl liposomes were gently mixed with 250 μl DMEM/F12 medium (serum-free, double antibody free) and incubated at room temperature for 5 min. Mix the above two liquids evenly and incubate them at room temperature (25°C) for 20 minutes to form DNA and liposome complex.

Add the cell pores to be transfected, culture for 4 hours under the conditions of 37°C, volume fraction of 5% CO<sub>2</sub> and 90% humidity, and add 1 ml of DMEM (containing volume fraction of 20% fetal bovine serum) to each well. After transfection, the cells were cultured for 48 hours under the same conditions [16].

**3.2.3. Cell Adhesion Test.** Endometrial cells (RL95-2) are laid in the culture hole with cover glass in advance, and the cells climb and grow. After the cells grew to 90% fusion, jar cells were collected, counted, and added to RL95-2 cells for coculture for 1 h. Take out the cover glass containing RL95-2 and

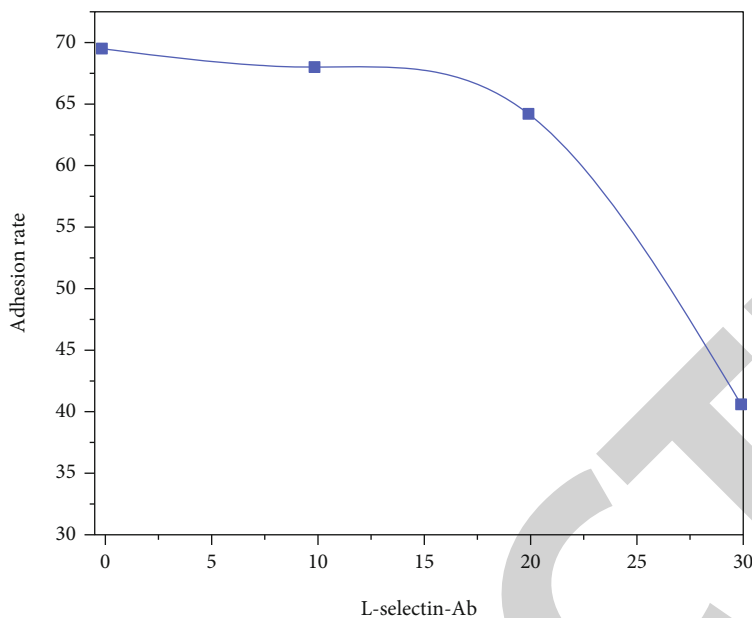


FIGURE 5: Effect of L-selectin on adhesion of JAR cells to RL95-2 cells (L-selectin Ab).

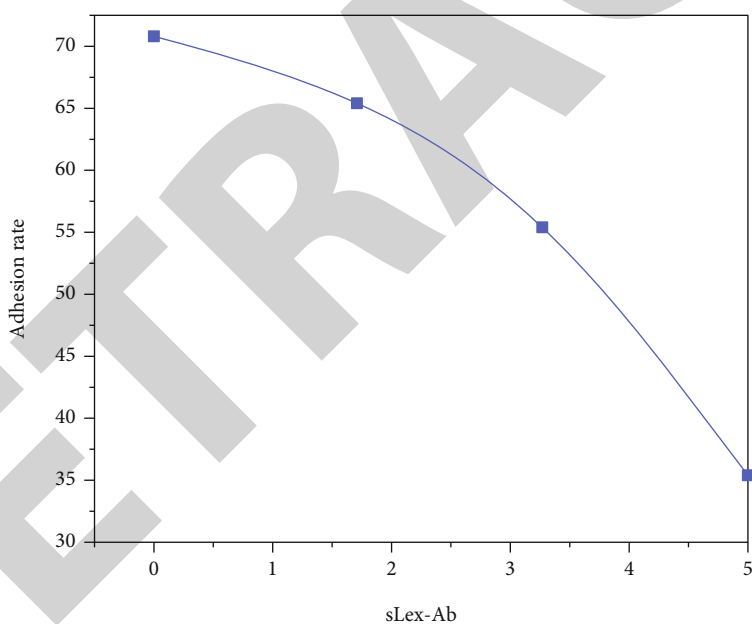


FIGURE 6: Effect of L-selectin on the adhesion of RL95-2 cells to jar cells (sLex Ab).

jar cells, invert it into a centrifuge tube containing PBS, and centrifuge at 1000 r/m for 5 min. Take out the cover glass and collect and count the nonadherent jar cells. Calculate the adhesion rate of embryonic cells. The adhesion rate = (number of jar cells adhered/number of jar cells added) × 100%.

**3.3. Role of L-Selectin in Embryo Transfer.** Different concentrations of L-selectin were incubated with Mongolian sheep fertilized eggs and then transferred to the uterus of healthy age recipient ewes, and then the embryo implantation was detected by ultrasonic imaging to analyze the effect of L-selectin on Mongolian sheep embryo implantation [17].

## 4. Result Analysis

**4.1. Results of Ultrasonic Imaging Detection of Pregnant Ewes.** The fetal body reflex is an oval light mass with weak reflection in the dark area of the uterine horn. The body length is about 0.6 cm at the first 19 days after mating and increases to 1 cm at 21 days. The measurement was carried out until the 43rd day of pregnancy, and then the measurement was stopped because the full length of the fetus could not be displayed. The fetal body increases with the increase of pregnancy days. It takes about 7 days for the fetal body to grow by about 1 cm from 28 to 41 days. It seems to grow faster after 40 days of pregnancy.

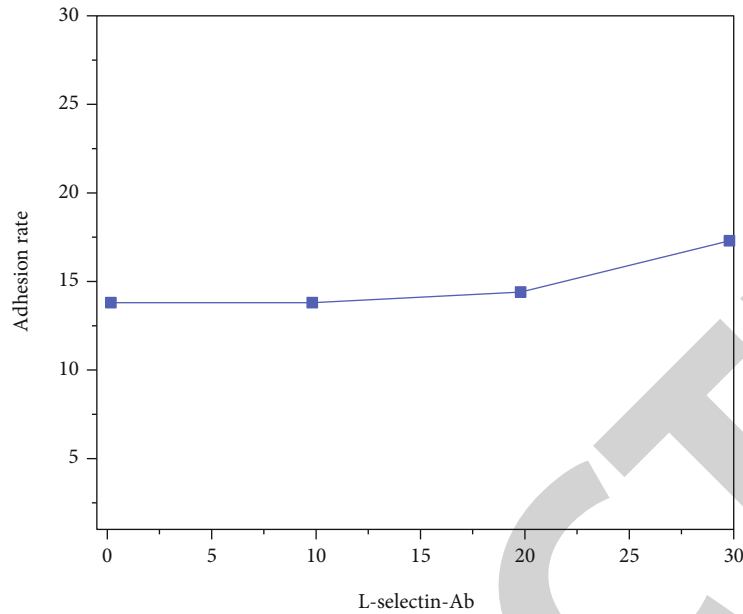


FIGURE 7: Effect of L-selectin on the adhesion of RL95-2 cells to JAR cells (L-selectin Ab).

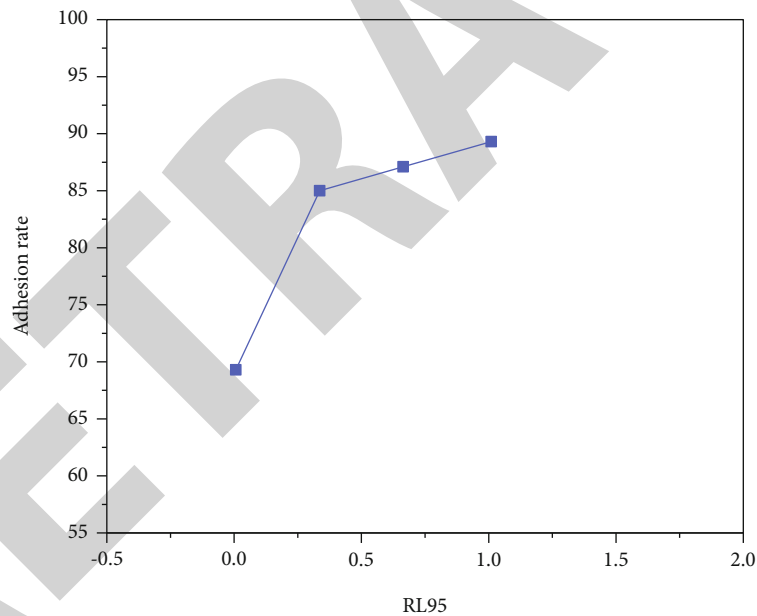


FIGURE 8: Effect of FUT7 on the adhesion rate between jar and RL95-2 cells.

Fetal heart beat can be observed on the 20th day of pregnancy. After 43 days of pregnancy, due to fetal growth, fetal heart beat can be seen only when fetal chest is scanned. Fetal chest depth was 2.7 cm at 58 d and 4.6 cm at 83 d. Fetal heart area is 1.8 cm × 1.5 cm at 68 d 2 cm, 2.1 cm × 1.2 cm on 76 d, and 2.5 cm wide on 83 d [18].

According to whether there is scrotal reflex, due to fetal movement, fetal position is difficult to fix, and it is difficult to judge the gender. Three cases were randomly judged in the test, one case on the 47th and 61th days of pregnancy. A convex weak reflex was observed between the roots of two hind limbs, which was considered the scrotum. It was

judged as a male lamb, and the postmortem examination was in accordance with [19]. One case was judged as a male lamb according to the convex reflection at 52 d, and the sheep scanned the part at 89 d, but no convex weak reflection was found, so it was judged as a female lamb, and it was confirmed as a female lamb after autopsy. The specific results are shown in Figure 2. The correct rate of fetal sex determination by ultrasound imaging increased with the increase of pregnancy days and reached 93% at 84 days.

The placenta was first detected on the 30th day of pregnancy. There was a small flat oval bulge on the uterine wall, about 0.3 cm long. From the first detection of the placenta on

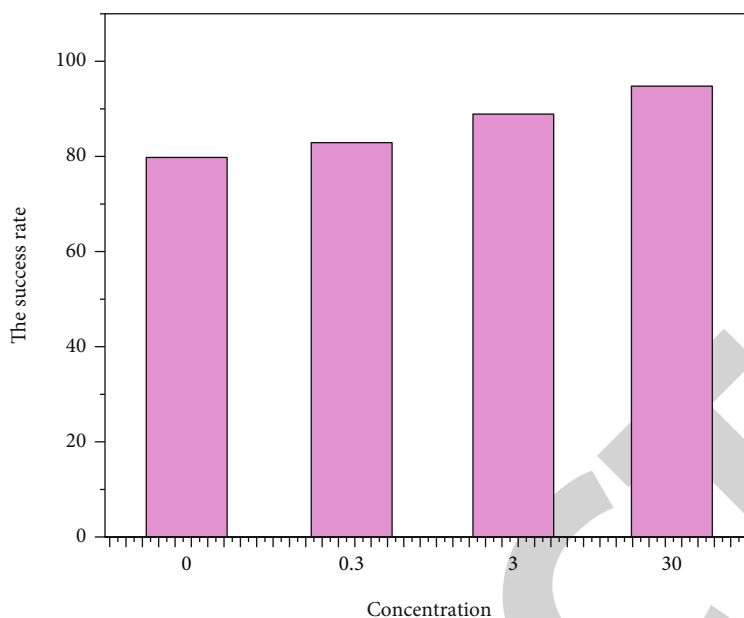


FIGURE 9: Effect of L-selectin on embryo implantation.

the 30th day of pregnancy to the 77th day of pregnancy, it increases with the increase of the number of days of pregnancy, as shown in Figure 3. The size of placenta detected after 77 d did not increase with the increase of gestational days. The umbilical cord reflex and umbilical artery pulsation were found at 33 d of pregnancy. The umbilical cord diameter increased with the increase of pregnancy days. On 89 d, four lumen umbilicuses were detected, that is, the cross-section of umbilical cord showing the lumen of four vessels of umbilical cord at the same time, which is  $1.5\text{ cm} \times 1.3\text{ cm}$ . The fetal urachal tube and bladder connected to it were observed [20].

**4.2. The Role of L-Selectin in the Adhesion between the Embryo and Endometrium.** Under normal conditions, the adhesion rate between jar cells and RL95-2 cells is  $69.7 \pm 2.6\%$ . When jar cells are blocked with sLex antibodies of  $0.05\ \mu\text{g/ml}$ ,  $0.5\ \mu\text{g/ml}$ , and  $5\ \mu\text{g/ml}$ , respectively, the adhesion rates between JAR cells and RL95-2 cells are  $64.9 \pm 1.1\%$ ,  $53.8 \pm 4.4\%$ , and  $35.3 \pm 1.5\%$ , respectively, that is, after sLex antibody treatment, the adhesion rate between jar cells and RL95-2 cells decreases in a dose-dependent manner [21]. When the antibody concentration was  $30\ \mu\text{g/ml}$ , the adhesion rate was  $40.3 \pm 3.68\%$  ( $P < 0.01$ ), as shown in Figures 4 and 5.

After blocking RL95-2 cells with the sLex antibody, the adhesion rate between jar cells and RL95-2 cells decreased. When the concentration of sLex antibody was  $5\ \mu\text{g/ml}$ , the inhibition degree was the most obvious ( $35.3 \pm 1.5\%$ ). The difference was statistically significant ( $P < 0.01$ ) [22]. RL95-2 was blocked with the L-selectin antibody. When the concentration of L-selectin antibody was  $30\ \mu\text{g/ml}$ , the adhesion rate was  $42.6 \pm 2.4\%$  ( $P < 0.01$ ). Compared with the untreated group ( $68.9 \pm 1.4\%$ ), the adhesion rate decreased significantly, as shown in Figures 6 and 7.

In order to further explore the role of sLex/selectin adhesion system in embryo implantation, the role of sLex in embryo implantation was studied by regulating the synthesis level of sLex [23]. Both in vivo and in vitro studies show that FUT7 is the key enzyme for sLex synthesis. After transfection of FUT7 overexpression vector into jar cells or RL95-2 cells, the expression of FUT7 increased, and the synthesis of sLex oligosaccharide antigen on the cell surface increased. Cell adhesion experiment showed that after jar or RL95-2 cells were transfected with FUT7 overexpression vector, compared with the nontransfected group ( $68.9 \pm 1.4\%$ ), the adhesion rate between jar and RL95-2 cells increased ( $86.6 \pm 3.0\%$ ,  $84.3 \pm 1.9\%$ ). After two kinds of cells were transfected with the FUT7 overexpression vector at the same time, the adhesion rate between jar and RL95-2 cells increased most significantly ( $89.4 \pm 1.2\%$ ) ( $P < 0.01$ ), as shown in Figure 8.

In conclusion, sLex/L-selectin on the surface of JAR/RL95-2 cells is involved in the adhesion between embryo and endometrium.

**4.3. Effect of L-Selectin on Embryo Implantation.** After incubation with Mongolian sheep fertilized eggs with different concentrations of L-selectin, they were, respectively, transplanted into the uterus of healthy age recipient ewes, and then the implantation of embryos was detected by ultrasonic imaging. The results are shown in Figure 9.

When the concentration of L-selectin is  $30\ \mu\text{g/ml}$ , the implantation success rate of fertilized eggs and embryos is the highest, reaching 95% [24].

## 5. Conclusion

The results of this experiment have a preliminary understanding of some regularity of the early development of sheep fetus. Although there are few data and need to be

further studied in the future, it has been explained that ultrasound imaging is a good method to visually study the fetus and its physiological activities. This paper preliminarily summarizes the imaging characteristics of the early development law of sheep fetus, which provides a basis for monitoring fetal growth by B-ultrasound and predicting fetal age. For the prediction of gestational age and gestational period, it is more scientific to make a comprehensive judgment when measuring the fetal body length, head length, and placental size, combined with the characteristic changes of fetal development in different stages of pregnancy. During the implantation window, embryonic jar cells express sLex oligosaccharide antigen, and endometrial RL95-2 cells express L-selectin. The mutual recognition of sLex and L-selectin mediates the adhesion between mother and fetus. At the same time, jar cells express L-selectin, and RL95-2 cells express sLex. The combination of the two also plays a biological function in the process of embryo implantation, that is, sLex/L-selectin adhesion system plays a role in the two-way recognition of sLex and L-selectin between the mother and fetus. While exploring the molecular mechanism of implantation, this study provides a new idea and means for the clinical intervention of contraception and pregnancy assistance targeting oligosaccharides.

## Data Availability

The data used to support the findings of this study are available from the corresponding author upon request.

## Conflicts of Interest

The authors declare that they have no conflicts of interest.

## Acknowledgments

This article was financially supported by the Inner Mongolia Autonomous Region Higher Education Institutions Scientific Research Natural Science Key Project (NJZZ19242).

## References

- [1] C. Chen, S. Liu, C. Zhao et al., "Activity of keloids evaluated by multimodal photoacoustic/ultrasonic imaging system," *Photoacoustics*, vol. 24, no. 11, article 100302, 2021.
- [2] Z. Li, F. Guo, C. Fei et al., "Liquid lens with adjustable focus for ultrasonic imaging," *Applied Acoustics*, vol. 175, no. 4, article 107787, 2021.
- [3] J. P. Leo-Neto, G. S. Cardoso, A. S. Marques, M. Andrade, and J. H. Lopes, "Subwavelength focusing beam and superresolution ultrasonic imaging using a core-shell lens," *Physical Review Applied*, vol. 13, no. 1, article 14062, 2020.
- [4] Y. Li, L. Li, L. Zhu, K. Maslov, and L. V. Wang, "Snapshot photoacoustic topography through an ergodic relay for high-throughput imaging of optical absorption," *Nature Photonics*, vol. 14, no. 3, pp. 164–170, 2020.
- [5] S. Chatillon, A. Waguët, V. Brulon, E. Iakovleva, and J. L. Gennisson, "Aberration correction in transcranial ultrasonic imaging using ct data and simulation-based focusing algorithms," *The Journal of the Acoustical Society of America*, vol. 148, no. 4, pp. 2485–2485, 2020.
- [6] H. Sui, P. Xu, J. Huang, and H. Zhu, "Space optimized plane wave imaging for fast ultrasonic inspection with small active aperture: simulation and experiment," *Sensors*, vol. 21, no. 1, 2021.
- [7] L. Pillarisetti, G. Raju, and A. Subramanian, "Sectorial plane wave imaging for ultrasonic array-based angle beam inspection," *Journal of Nondestructive Evaluation*, vol. 40, no. 3, pp. 1–16, 2021.
- [8] C. Labuda, W. R. Newman, and B. K. Hoffmeister, "Parametric imaging of ultrasonic backscatter of fixed sheep brain," *The Journal of the Acoustical Society of America*, vol. 148, no. 4, pp. 2774–2774, 2020.
- [9] Z. Zhuang, J. Zhang, G. Lian, and B. W. Drinkwater, "Comparison of time domain and frequency-wavenumber domain ultrasonic array imaging algorithms for non-destructive evaluation," *Sensors*, vol. 20, no. 17, p. 4951, 2020.
- [10] R. Mohammadkhani, L. Z. Fragonara, J. Padiyar, I. Petrunin, A. Tsourdos, and I. Gray, "Improving depth resolution of ultrasonic phased array imaging to inspect aerospace composite structures," *Sensors*, vol. 20, no. 2, 2020.
- [11] J. Luo, K. Lu, Y. Chen, and B. Zhang, "Automatic identification of cashmere and wool fibers based on microscopic visual features and residual network model," *Micron*, vol. 143, no. 21, article 103023, 2021.
- [12] R. Fan, W. Zhang, L. Li, L. Jia, and Y. Chen, "Individual and synergistic toxic effects of carbendazim and chlorpyrifos on zebrafish embryonic development," *Chemosphere*, vol. 280, article 130769, Supplement 1, 2021.
- [13] K. Zhong, Y. Meng, J. Wu, Y. Wei, and H. Lu, "Effect of flupyradifurone on zebrafish embryonic development," *Environmental Pollution*, vol. 285, no. 6, article 117323, 2021.
- [14] P. Tenorio-Chávez, M. Cerro-López, L. I. Castro-Pastrana, M. M. Ramírez-Rodríguez, and L. M. Gómez-Oliván, "Effects of effluent from a hospital in Mexico on the embryonic development of zebrafish, *Danio rerio*," *Science of The Total Environment*, vol. 727, no. 2, article 138716, 2020.
- [15] D. Kumar, A. Sharma, R. Kumar, and N. Sharma, "Restoration of the network for next generation (5G) optical communication network," in *2019 International Conference on Signal Processing and Communication (ICSC)*, IEEE, 2019.
- [16] L. Xin, L. Jianqi, C. Jiayao, and Z. Fangchuan, "Degradation of benzene, toluene, and xylene with high gaseous hourly space velocity by double dielectric barrier discharge combined with Mn3O4/activated carbon fibers," *Journal of Physics D: Applied Physics*, vol. 55, no. 12, article 125206, 2022.
- [17] Z. Duan, X. Duan, S. Zhao et al., "Barrier function of zebrafish embryonic chorions against microplastics and nanoplastics and its impact on embryo development," *Journal of Hazardous Materials*, vol. 395, no. 4, article 122621, 2020.
- [18] R. Huang, P. Yan, and X. Yang, "Knowledge map visualization of technology hotspots and development trends in China's textile manufacturing industry," *IET Collaborative Intelligent Manufacturing*, vol. 3, no. 3, pp. 243–251, 2021.
- [19] N. Schwab, T. Schneider-Hohendorf, B. Pignolet, D. Brassat, and H. Wiendl, "Author response: prospective validation of the PML risk biomarker l-selectin and influence of natalizumab extended intervals," *Neurology*, vol. 95, no. 11, 2020.
- [20] B. Tugemann, "Reader response: prospective validation of the pml risk biomarker l-selectin and influence of natalizumab

## Retraction

# Retracted: Magnetic Resonance Imaging Assessment of Fatigue Injury during Exercise

### Scanning

Received 18 July 2023; Accepted 18 July 2023; Published 19 July 2023

Copyright © 2023 Scanning. This is an open access article distributed under the Creative Commons Attribution License, which permits unrestricted use, distribution, and reproduction in any medium, provided the original work is properly cited.

This article has been retracted by Hindawi following an investigation undertaken by the publisher [1]. This investigation has uncovered evidence of one or more of the following indicators of systematic manipulation of the publication process:

- (1) Discrepancies in scope
- (2) Discrepancies in the description of the research reported
- (3) Discrepancies between the availability of data and the research described
- (4) Inappropriate citations
- (5) Incoherent, meaningless and/or irrelevant content included in the article
- (6) Peer-review manipulation

The presence of these indicators undermines our confidence in the integrity of the article's content and we cannot, therefore, vouch for its reliability. Please note that this notice is intended solely to alert readers that the content of this article is unreliable. We have not investigated whether authors were aware of or involved in the systematic manipulation of the publication process.

In addition, our investigation has also shown that one or more of the following human-subject reporting requirements has not been met in this article: ethical approval by an Institutional Review Board (IRB) committee or equivalent, patient/participant consent to participate, and/or agreement to publish patient/participant details (where relevant).

Wiley and Hindawi regrets that the usual quality checks did not identify these issues before publication and have since put additional measures in place to safeguard research integrity.

We wish to credit our own Research Integrity and Research Publishing teams and anonymous and named external researchers and research integrity experts for contributing to this investigation.

The corresponding author, as the representative of all authors, has been given the opportunity to register their agreement or disagreement to this retraction. We have kept a record of any response received.

### References

- [1] Z. Ai, N. Li, J. An, and L. Zhang, "Magnetic Resonance Imaging Assessment of Fatigue Injury during Exercise," *Scanning*, vol. 2022, Article ID 9971966, 7 pages, 2022.

## Research Article

# Magnetic Resonance Imaging Assessment of Fatigue Injury during Exercise

Zhengguo Ai <sup>1,2</sup>, Na Li <sup>3</sup>, Jing An <sup>4</sup> and Lei Zhang <sup>5</sup>

<sup>1</sup>School of Sport Economics and Management, Tianjin University of Sport, Tianjin 301617, China

<sup>2</sup>School of Sport, Daqing Normal University, Daqing, Heilongjiang 163712, China

<sup>3</sup>Daqing Oilfield General Hospital, Daqing, Heilongjiang 163700, China

<sup>4</sup>Section of Recruitment and Employment, Harbin Sport University, Harbin, Heilongjiang 150008, China

<sup>5</sup>Department of Physical Education, Heilongjiang Institute of Technology, Harbin, Heilongjiang 150050, China

Correspondence should be addressed to Lei Zhang; 2009020138@st.tbu.edu.cn

Received 15 May 2022; Revised 28 May 2022; Accepted 6 June 2022; Published 16 June 2022

Academic Editor: Balakrishnan Nagaraj

Copyright © 2022 Zhengguo Ai et al. This is an open access article distributed under the Creative Commons Attribution License, which permits unrestricted use, distribution, and reproduction in any medium, provided the original work is properly cited.

In order to investigate the changes of temporal function metabolism of lumbar and back muscles after exercise, a magnetic resonance imaging- (MRI-) based assessment of fatigue injury during exercise was proposed. A total of 100 healthy adult volunteers were selected, including 48 males and 52 females, aged from 19 to 30 years, with an average age of 24.8 + 2.3 years. They were divided into four groups according to the different time points of 0, 15, 30, and 45 minutes after exercise, with 25 persons in each group. PHILIPS Achieva 3.0 T Tx MRI scanner was used to perform BOLD and T2-mapping before and after exercise in four groups of healthy volunteers. All data were analyzed by statistical software. The results showed that the total CSA of the dorsi extensor muscle group and the CSA value of the dorsi extensor muscle group at different levels at different time points before and after exercise increased slowly in exercise period and decreased rapidly in recovery period. It was verified that BOLD MRI and T2-mapping imaging can indirectly evaluate the trend of CSA water metabolism and blood oxygen level in healthy adults after exercise.

## 1. Introduction

The lumbar dorsiflexors, including the multifidus longissimus and iliocostus muscles, are the most important part of the core muscles of the human body. Its main role is to participate in the bearing of the spine to maintain human standing posture to maintain the shape of the spine and participate in human walking and other activities. The extensor dorsi muscle group is the largest at the lumbar level, but it is also the most vulnerable part [1]. Long-term poor posture or bending weight can make the low back muscle group (mainly multifidus erector longissimus) in passive stretch or contraction state for a long time. This can lead to insufficient oxygen supply to local muscle tissue, accumulation of metabolites, and stimulate local formation of injurious aseptic inflammation. Severe cases can cause local soft tissue hyperplasia, adhesion, and even degeneration. Patients show recurrent lumbar pain or discomfort, which is often clinically

diagnosed as lumbar muscle strain or chronic lower backpain (LBP) [2]. At present, the diagnosis of psoas muscle strain or LBP patients mainly depends on the signs and symptoms, and its treatment is mostly rehabilitation training or massage acupuncture laser irradiation. At present, imaging evaluation of the paralumbar muscles in these patients is only limited to morphological evaluation, including measurement of muscle CSA and CT value of lumbar and back muscles to evaluate the degree of muscle atrophy and fat infiltration.

## 2. Literature Review

Wouters et al. found that long-term poor posture or bending and loading can keep the low back muscles (mainly the multifidus erector longissimus) in a passive stretch or contraction state for a long time. This will lead to insufficient oxygen supply to local muscle tissue, accumulation of

metabolites, and stimulate local formation of injurious aseptic inflammation. Severe cases can cause local soft tissue hyperplasia, adhesion, and even degeneration. Patients show recurrent lumbar pain or discomfort, which is often clinically diagnosed as lumbar muscle strain or chronic lower backpain (LBP). At present, the diagnosis of psoas muscle strain or LBP patients mainly depends on the signs and symptoms, and its treatment is mostly rehabilitation training or massage acupuncture laser irradiation [3]. Zhang et al. found that imaging assessment of the paralumbar muscles in these patients is currently limited to morphological assessment, including measurement of muscle CSA and lumbar back muscle CT values to assess muscle atrophy and fat infiltration [4]. Zhu et al. believed that BOLD MRI could achieve noninvasive detection of microdeoxygenated hemoglobin changes in tissues and could be superimposed with high-resolution anatomical images. Therefore, BOLD MRI could not only achieve accurate spatial positioning but also noninvasive reaction of microblood perfusion in tissues. T2-mapping is a magnetic resonance examination technology that uses T2 relaxation time as a measurement index to quantitatively analyze changes in tissue components. It can also achieve accurate spatial positioning and detect changes in microwater content in soft tissues [5]. Studies have proved that BOLD MRI and T2-mapping can be applied to muscle functional magnetic resonance imaging. Therefore, this study intends to use functional magnetic resonance BOLD MRI and T2-mapping to scan the lumbar extensor muscle group before and after exercise in healthy young people, as shown in Figure 1. Observe the changes of  $R2^*$  and T2 values of the lumbar dorsiflexor muscle group before and after exercise. Tantawy et al. analyzed the characteristics of blood perfusion changes of the lumbar dorsi muscle group and water molecule changes in muscle space before and after exercise and compared with the changes of muscle cross-sectional area before and after exercise, to further explore the feasibility of functional magnetic resonance assessment of lumbar and back muscle function [6].

### 3. Methods

In order to further clarify its curative effect and therapeutic advantage, medical records were retrospectively analyzed to explore the clinical effect of magnetic resonance imaging on fatigue injury caused by exercise. A total of 100 healthy volunteers were selected, including 48 males and 52 females, aged from 20 to 28 years, with an average age of  $(24.8 \pm 2.3)$  years. The average body weight was  $(57.52 \text{ kg} \pm 9.20 \text{ kg})$ . The average height is  $(164.28 \pm 7.26)$  cm. The body mass index is  $17.78 \sim 23.65 \text{ kg/m}^2$ , and average body mass index is  $(20.77 \pm 2.26) \text{ kg/m}^2$ . All volunteers were scanned before exercise and divided into four groups with 25 participants in each group, including 12 males and 13 females, according to different time points of 0, 15, 30, and 45 minutes after exercise.

If skeletal muscle's own blood perfusion and water molecular content are affected, the results of the study will produce errors [7]. The content of muscle fiber in the skeletal muscle and the activity of the target muscle before the

experiment will affect the experimental results. Muscle degeneration caused by any disease through special muscle resistance training or heavy manual labor will lead to changes in the content of muscle fibers in the skeletal muscle compared to normal people, as well as changes in the amount of blood perfusion in the skeletal muscle. However, the intense activity of the target muscle group before the examination will increase the content of water molecules in the intracellular and intercellular space of the skeletal muscle, thus interfering with the experimental results [8]. Therefore, the selection criteria for volunteers are listed below:

- (1) Normal serial MRI scans of healthy adult volunteers showed no abnormalities in lumbar and paravertebral muscles
- (2) Light manual workers, such as student civil servants
- (3) Within 48 hours before the scanning, the volunteers had not done strenuous exercise such as running, playing ball, fitness, and swimming
- (4) Fasting within 2 hours prior to scanning and coffee drinking within 24 hours prior to scanning

The exclusion criteria for volunteers are as follows:

- (1) Routine magnetic resonance sequence lumbar degenerative changes: bulging of lumbar intervertebral disc or atrophy of lumbar muscle and fat infiltration
- (2) People who have undergone special resistance training of lumbar and back muscles and heavy manual workers, such as athletes and fitness coaches
- (3) Low back pain, long-term bed rest, low back surgery, history of scoliosis deformity, neuromuscular diseases, etc.
- (4) Unable to complete the lumbar muscle training program
- (5) The volunteers could not undergo MRI tests for claustrophobia or carrying metal objects

A Dutch PHILIPS Achieva 3.0T superconducting magnetic resonance scanner (maximum gradient field intensity  $> 80 \text{ Mtm}$ , maximum gradient switching rate  $220 \text{ mT (m)}$ ) was used. The acquisition coil was an orthogonal 15-channel spinal coil. The scanning flow chart is shown in Figure 2. Then, with the lumbar spine as the axis, sagittal T2WI scan was performed with 9 layers and a thickness of 0.4 mm.

Axial T1WI scanning was performed with sagittal T2WI as the reference plane and the upper edge of L3 and L4 as the center. The scanning layers were 32, and the interval was 0.4 mm. All volunteers underwent preexercise scanning and were divided into 4 subgroups according to time points: 0 min, 15 min, 30 min, and 45 min. Each subgroup underwent scanning at corresponding time points. Scan sequence and parameters are shown in Table 1 [9].

The whole exercise process was guided by a special person and lasted for about 10 minutes. After 15, 30, and 45



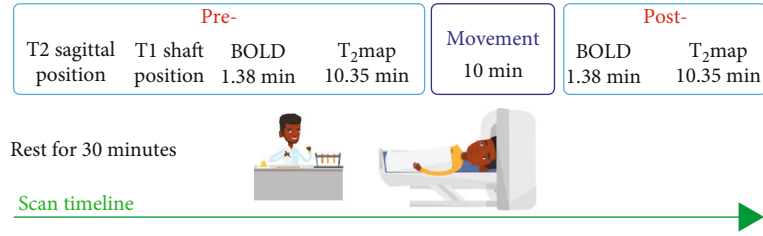


FIGURE 1: Flow chart of muscle functional magnetic resonance scan.

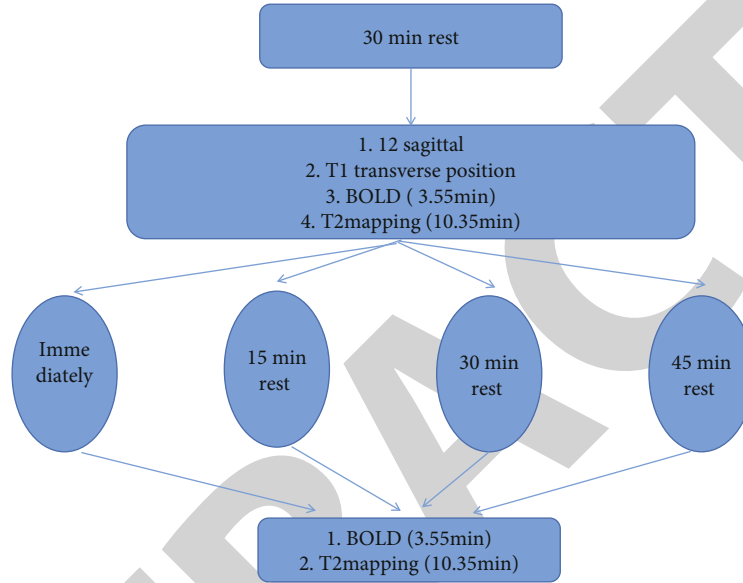


FIGURE 2: Magnetic resonance scanning flow chart.

TABLE 1: MRI scanning sequence and scanning parameters.

Scan sequence	Sweeping solid (mm)	Echo time (ms)	Repeat time (ms)	NEX	Thickness of layer (mm)	Interlamellar spacing (mm)	The layer number of scanning	
T2WI sagittal view	PSE	$0.91 \times 1.32 \times 4.00$	120	2000	2	4	0.4	9
TIWI cross-sectional place	FSE	$0.71 \times 0.90 \times 4.00$	7.6	344	3	4	0.4	32
BOLD cross-sectional place	EPI	$1.5U \times 1.50 \times 4.00$	3.7/10.3/15.9/ 21.5/27.1/32.7	466	6	3	0.7	24
T2-napping cross-sectional place	FSE	$0.76 \times 0.76 \times 0.30$	7/13/19/25/31/37	1974	1	3	0.7	24

minutes of exercise, the volunteers lay flat on a simple folding bed and rested until the scan to avoid the influence of paravertebral muscle tension caused by standing or sitting position.

Precautions before scanning were as follows: the volunteers rested for 30 minutes before scanning, lying flat on a simple folding bed. Before scanning, the volunteers used a double abdominal band to compress the abdomen to avoid artifacts caused by excessive breathing. The volunteers lay flat on the scanning bed with their heads fixed. In order to prevent discomfort caused by the noise during the scanning, they wore earphones to reduce the noise. Foam boards were

placed below the waist, and foam pads were placed on both lower limbs to raise the legs, so as to reduce the gap between the waist and the scanning bed. At the same time, volunteers were asked to adopt chest breathing as far as possible during the scanning process, so as to reduce the generation of respiratory motion artifacts [10]. During the scan, place your hands in front of your chest, but avoid crossing them. Keep your elbows out of your body and as far away from your waist as possible to minimize artifacts. If the volunteers were female, they should remove their underwear to avoid metal artifacts. They were asked to keep their bodies still during

the scanning and avoid motion artifacts [11]. The exercise method is as follows: adopt simple Roman stool to do goat stand up movement, namely, the upper body antigravity flexion and extension movement. In the past, dorsiflexion was a movement, the whole movement process was divided into three groups, each group did 15 movements, and the interval between groups rested for 30 seconds. The main points of action are as follows: the feet are fixed, the body lies on the bench, the upper body slides to the lower abdomen and sticks to the side of the stool, the hands are crossed in front of the chest when the action is carried out, the upper body is quite upward as far as possible, when the highest point stops for three seconds, and then the body overcomes the gravity effect and slowly goes down [12]. The whole movement should be maintained in the way of fast rise and slow fall, not relying on gravity or inertia to complete the action quickly.

After scanning, GE ADW4.4 postprocessing workstation was used for image processing and analysis. Taking the upper edge of L3 and L4 vertebrae as the level of interest, the boundary of longissimus multifidus and iliocostus muscle was delineated in the cross-section of the corresponding level, and the CSA and corresponding T2 values of each muscle were recorded. The R2\* values of each muscle were measured by the same method. During the measurement of muscle values, the range of the region of interest should avoid tendon and intramuscular fat components. The post-processing threshold of BOLD MRI is 71~201, the confidence is 0.05, and the color level is 20~100. The postprocessing threshold of T2-mapping was 10, the confidence was 0.05, the value of color levels ranging from 33 to 71 was measured by two attending physicians who had been engaged in bone and muscle imaging diagnosis for a long time by the double-blind method, and the average value was calculated [13].

SPSS 24.0 software was used for statistical analysis of the general condition of the volunteers (height, weight, age, BMI) and independent sample *t*-test. One-way ANOVA was used for the CSA, T2 values, and R2\* of all muscles of different genders (longissimus multifidus and iliocostal muscle) on the left and right sides at multiple time points before and after exercise. The LSD method was used for pairwise comparison of CSA, T2 values, and R2\* values of all muscles. Pearson correlation analysis was used for correlation analysis.

The general information of male and female healthy volunteers is shown in Table 2. After statistical analysis, the average height and weight of male were higher than that of female ( $P < 0.05$ ), while there were no significant differences in age and body mass index (BMI) between male and female ( $P > 0.05$ ).

The general situation of volunteers in each group was shown in Table 3. After statistical analysis, there was no significant difference in the height, weight, age, and BMI of volunteers in each group ( $P > 0.05$ ).

The comparison of the total CSA of the dorsi extensor muscle group at different time points before and after exercise showed that the changes of the total CSA of the dorsi extensor muscle group at different time points before

and after exercise were statistically significant ( $P < 0.05$ ). CSA increased 15 minutes after exercise compared with 0 minutes before exercise and decreased 30 and 45 minutes after exercise compared with 15 minutes after exercise. There is a comparison of CSA of dorsi extensor muscle groups at different levels at different time points before and after exercise by statistical analysis, L3 upper margin layer, and L4. The changes of CSA of the dorsi extensor muscle group at the upper margin were statistically significant at different time points before and after exercise ( $P < 0.05$ ). CSA increased 15, 30, and 45 minutes after exercise compared with that before exercise, and CSA increased 15, 30, and 45 minutes after exercise compared with that at 0 minutes after exercise [14].

The comparison of CSA of muscles at different levels at different time points before and after exercise was shown in Figure 3. After statistical analysis, THE CSA of multifidus muscle at L4 level increased 15 and 45 minutes after exercise compared with before exercise and decreased 30 minutes after exercise compared with 15 minutes after exercise, with statistical significance ( $P < 0.05$ ). The CSA of multifidus muscle at L3 increased 15 minutes after exercise compared with before exercise and decreased 30 minutes after exercise compared with 15 minutes after exercise, with statistical significance ( $P < 0.05$ ). The CSA of the longissimus muscle at L4 increased 15, 30, and 45 minutes after exercise compared with that before exercise, and the CSA increased 15, 30, and 45 minutes after exercise compared with that at 0 minutes after exercise with statistical significance ( $P < 0.05$ ). L3 level of longissimus muscle increased 15 minutes after exercise compared with 0 minutes before exercise and decreased 30 and 45 minutes after exercise compared with 15 minutes after exercise, with statistical significance ( $P < 0.05$ ).

CSA changes of iliocostal muscle at L3 and L4 levels at different time points before and after exercise were not statistically significant ( $P > 0.05$ ).

The comparison of the CSA of the left and right muscles at different levels at different time points before and after exercise showed that the CSA at L4 level increased 15 and 45 minutes after exercise compared with before exercise and decreased 30 minutes after exercise compared with 15 minutes after exercise, with statistical significance ( $P < 0.05$ ). At L3 level, the CSA of the left multifidus muscle increased 15 and 45 minutes after exercise compared with before exercise, decreased 30 minutes after exercise compared with 15 minutes after exercise and increased 45 minutes after exercise compared with 30 minutes after exercise, with statistical significance ( $P < 0.05$ ). The CSA of the right longissimus muscle at L4 level increased 15, 30, and 45 minutes after exercise compared with that before exercise, the CSA at L4 level increased 15, 30 and 45 minutes after exercise compared with that at 0 minutes after exercise, and the difference was statistically significant ( $P < 0.05$ ). CSA increased in 45 minutes compared with 0 minutes after exercise, and the difference was statistically significant ( $P < 0.05$ ). At L3 level, the CSA of bilateral longissimus muscle increased 15 minutes after exercise compared with 0 minutes before exercise and decreased 30 and 45 minutes after exercise compared with 15 minutes after exercise, and the differences were statistically significant

TABLE 2: Male and female volunteers were generally compared.

	Cases	Height (cm)	Weight (kg)	Age (year)	BMI (kg/m <sup>2</sup> )
Male	48	170.75 ± 5.43	63.28 ± 8.31	24.48 ± 2.56	21.72 ± 2.42
Female	52	160.05 ± 4.95	53.17 ± 6.56	23.39 ± 2.06	20.28 ± 2.26
<i>T</i> value		11.06	8.45	2.53	3.37
<i>P</i> value		<0.001	<0.001	0.054	0.131

TABLE 3: Analysis of general situation among each group.

	First group	Second group	Time		<i>F</i>	<i>P</i>
			Third group	Fourth group		
Height (cm)	165.34 ± 7.25	164.41 ± 8.37	164.72 ± 7.18	165.92 ± 8.14	0.180	0.963
Weight (kg)	56.83 ± 7.54	57.54 ± 7.53	56.38 ± 8.31	57.13 ± 6.89	0.653	0.349
Age (year)	23.3 ± 3.1	23.8 ± 2.0	22.8 ± 1.7	22.7 ± 0.6	0.543	0.197
BMI (kg/m <sup>2</sup> )	21.3 ± 1.9	21.7 ± 2.9	20.7 ± 2.2	20.4 ± 2.5	1.326	0.078

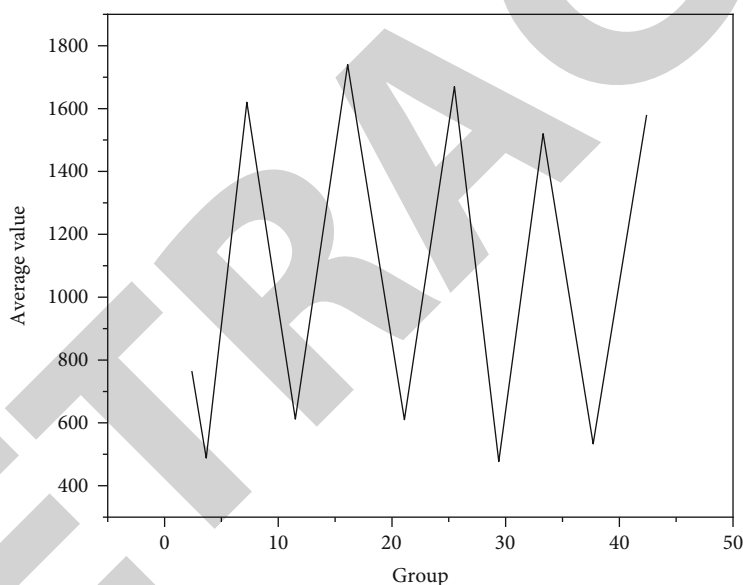


FIGURE 3: Comparison of CSA of muscles at different levels at different time points before and after exercise.

( $P < 0.05$ ). There was no significant difference in CSA at L3 and L4 levels at different time points before and after exercise of bilateral iliocostal muscles ( $P > 0.05$ ).

The comparison of CSA of left and right muscles at different levels and different genders at different time points before and after exercise was statistically analyzed. In male volunteers, the CSA at L4 level increased 15 minutes after exercise compared with before exercise, CSA decreased 30 minutes after exercise compared with 15 minutes after exercise, and CSA increased 45 minutes after exercise compared with 30 minutes after exercise, with statistical significance ( $P < 0.05$ ). At L3 level, the CSA of right multifidus muscle increased 15 minutes after exercise compared with before exercise, increased 15 minutes after exercise compared with 0 minutes after exercise, and decreased 30 minutes after exercise compared with 15 minutes after exercise, with sta-

tistical significance ( $P < 0.05$ ). The CSA of right multifidus muscle of female volunteers increased 15, 30, and 45 minutes after exercise compared with that before exercise and 45 minutes after exercise compared with that 0 minutes after exercise, with statistical significance ( $P < 0.05$ ). The CSA of left multifidus muscle at L4 level increased 30 and 45 minutes after exercise compared with that before exercise, and the difference was statistically significant ( $P < 0.05$ ). L3 level CSA of right multifidus muscle increased at 0 min after exercise compared with before exercise and decreased at 15, 30, and 45 min after exercise compared with 0 min after exercise, and the difference was statistically significant ( $P < 0.05$ ). L3 level CSA of left multifidus muscle increased 15 minutes after exercise compared with before exercise and decreased 30 minutes after exercise compared with 15 after exercise, with statistical significance ( $P < 0.05$ ) [15, 16].

#### 4. Discussion

The lower part of the human dorsi extensor muscle group starts from the posterior edge of the dorsal iliac ridge of the sacrum and passes up to the level of the L4 vertebra to the longissimus multifidus and iliocostus muscles. The iliocostal muscle is located in the inner side of the posterior edge of each costal arch, and its main function is to participate in spinal dorsi extension and assist the rotation of the upper body. The longissimus is attached upward to the mastoid process, and the multifidus arises laterally in the form of a short tendon of lumbar vertebrae's nipple. At the top, the spinous process of the upper vertebral body, the longissimus muscle, and the multifidus muscle are mainly involved in spinal dorsi extension [17, 18]. The dorsiflexor muscle group is the most important part of the core muscle group of the human body, and its role is to maintain the normal shape of the spine and participate in the maintenance of walking and posture. The dorsi extensor muscle group is the largest at the level of lumbar vertebrae, its morphology and structure are relatively complex, and it is also the most vulnerable to injury. It is closely related to LBP strain of psoas muscle or disc herniation, and it is the most important muscle group to be paid attention to in clinical rehabilitation training. MRI has a high resolution of soft tissue, and its display of the lumbar extensor muscle group is superior to CT and ultrasound and with the advent of functional MRI. In particular, magnetic resonance phosphorus spectrum analysis can not only observe the changes of CSA before and after muscle exercise but also dynamically monitor the mutual transformation process between phosphocreatine and ATP before and after muscle exercise. However, phosphorus spectrum analysis requires special magnetic resonance detection equipment and is difficult to be popularized in clinical use. Bold MRI is widely used in the study of nervous system function, usually to detect changes in local blood M flow in the brain under a certain disease state or a certain task state, so as to reflect the range of lesions or functional areas in the brain. With the development of fMRI, BOLD MRI has also been gradually applied to the research outside the nervous system, including kidney, liver, and skin tissue. However, BOLD MRI is rarely reported in the study of the skeletal muscle system, especially in the study of the lumbar dorsi muscle group [19, 20]. In the 1990s, Ogawa et al. discovered that deoxygenated hemoglobin changed the signal of blood vessels and surrounding water molecules, and this changed signal could be detected by gradient echo sequence of high-field MRI, thus discovering BOLD enhancement effect. Deoxyhemoglobin in the human body is a paramagnetic material, and its iron ions contain four unpaired electrons; so, it can affect the relaxation time of neighboring protons. When the amount of deoxygenated hemoglobin in a single blood vessel increases, decreased T2 or T2\* signaling of water molecules in and around blood vessels, that is, the transverse relaxation rate of adjacent water molecules  $R2$  ( $1/T2$ ) and  $R2^*$  ( $1/T2^*$ ) is increased. The decrease of  $R2^*$  signal in tissues can indirectly reflect the decrease of deoxygenated hemoglobin content in small blood vessels in tissues, thus reflecting the changes of blood perfusion volume in tissues in the resting task state.

There were significant differences in  $R2^*$  values of the left and right iliocostal muscles at the L3 upper margin of normal healthy volunteers before and after exercise, and the difference was more significant in the female group (left change > right) but not in the male group. Comparison of the CSA of the left and right iliocostal muscles at the L3 upper margin before and after exercise showed that the CSA changes of the left iliocostal muscles before and after exercise were more obvious in the female group than in the right side, while the difference between the left and right sides was not obvious in the normal male group. However, there was no significant difference in the changes of CSA or  $R2^*$  before and after muscle exercise at the upper edge of L4 in both male and female groups. After analysis, the  $R2^*$  values and CSA changes of the left and right iliocostal muscles before and after exercise at the upper margin of L3 in the female group were more obvious than those on the right. The two showed corresponding consistency, and the difference existed in the female group, while there was no difference in the male group. The reason may be that during the whole dorsiflexion movement, the longissimus muscle of the female multifidus is not strong enough to contralateral iliocostal muscle contraction, and corresponding blood flow is reduced due to the compensatory assistance of one side (left) iliocostal muscle contraction. In L4, there was no significant difference in CSA and  $R2^*$  between the left and right sides before and after the exercise of each muscle in the upper margin layer, but L3. There are significant differences between the left and right iliocostal muscles at the upper margin, which may be due to the fact that the dorsal extensor muscle group at L4 and L3 is mainly involved in the dorsal extension movement, while the iliocostal muscles at L3 are not only involved in the dorsal extension movement but also have the function of assisting lateral rotation.

#### 5. Conclusion

BOLD MRI and T2-mapping's imaging can indirectly assess the trend of CSA water metabolism and blood oxygen level in the back muscle of healthy adults after exercise. After exercise, the CSA and T2 values of lumbar and back muscles showed slow movement: rising and rapid downward trend in the recovery period;  $R2^*$  showed a rapid decrease in the exercise period and a rapid increase in the recovery period. The T2 value of the longissimus muscle at level 3 increased earlier than that at L4, and the change rate of T2 value of the longissimus muscle at the right level of L3 increased earlier than that at the left level of L3 and L4. The T2 value of the horizontal left iliocostal muscle increased later than the right side of L4. The left and right sides of the muscle could affect the change rate of T2 value of the longissimus muscle and iliocostal muscle after exercise. The CSA of longissimus multifidus of different genders increased slowly during the exercise period and maintained a trend during recovery period in females, while decreased slowly during the recovery period in males. The changes of CSA after exercise of multifidus muscle and longissimus muscle were influenced by different genders.

## Retraction

# Retracted: Analysis of Infertility Factors Caused by Gynecological Chronic Pelvic Inflammation Disease Based on Multivariate Regression Analysis of Logistic

### Scanning

Received 20 June 2023; Accepted 20 June 2023; Published 21 June 2023

Copyright © 2023 Scanning. This is an open access article distributed under the Creative Commons Attribution License, which permits unrestricted use, distribution, and reproduction in any medium, provided the original work is properly cited.

This article has been retracted by Hindawi following an investigation undertaken by the publisher [1]. This investigation has uncovered evidence of one or more of the following indicators of systematic manipulation of the publication process:

- (1) Discrepancies in scope
- (2) Discrepancies in the description of the research reported
- (3) Discrepancies between the availability of data and the research described
- (4) Inappropriate citations
- (5) Incoherent, meaningless and/or irrelevant content included in the article
- (6) Peer-review manipulation

The presence of these indicators undermines our confidence in the integrity of the article's content and we cannot, therefore, vouch for its reliability. Please note that this notice is intended solely to alert readers that the content of this article is unreliable. We have not investigated whether authors were aware of or involved in the systematic manipulation of the publication process.

In addition, our investigation has also shown that one or more of the following human-subject reporting requirements has not been met in this article: ethical approval by an Institutional Review Board (IRB) committee or equivalent, patient/participant consent to participate, and/or agreement to publish patient/participant details (where relevant).

Wiley and Hindawi regrets that the usual quality checks did not identify these issues before publication and have since put additional measures in place to safeguard research integrity.

We wish to credit our own Research Integrity and Research Publishing teams and anonymous and named external researchers and research integrity experts for contributing to this investigation.

The corresponding author, as the representative of all authors, has been given the opportunity to register their agreement or disagreement to this retraction. We have kept a record of any response received.

### References

- [1] L. Liu, G. Yang, J. Ren, L. Zhang, T. Wu, and Q. Zheng, "Analysis of Infertility Factors Caused by Gynecological Chronic Pelvic Inflammation Disease Based on Multivariate Regression Analysis of Logistic," *Scanning*, vol. 2022, Article ID 7531190, 7 pages, 2022.

## Research Article

# Analysis of Infertility Factors Caused by Gynecological Chronic Pelvic Inflammation Disease Based on Multivariate Regression Analysis of Logistic

Linmei Liu <sup>1</sup>, Gang Yang <sup>2</sup>, Jigang Ren <sup>1</sup>, Limei Zhang <sup>1</sup>, Ting Wu <sup>1</sup>,  
and Qiao Zheng <sup>1</sup>

<sup>1</sup>Department of Traditional Chinese Medicine, Affiliated Hospital of North Sichuan Medical College, Nanchong, Jiangxi 637000, China

<sup>2</sup>Department of Hepatobiliary Surgery, Affiliated Hospital of North Sichuan Medical College, Nanchong, Jiangxi 637000, China

Correspondence should be addressed to Linmei Liu; 194630112@smail.cczu.edu.cn

Received 8 May 2022; Revised 20 May 2022; Accepted 3 June 2022; Published 16 June 2022

Academic Editor: Balakrishnan Nagaraj

Copyright © 2022 Linmei Liu et al. This is an open access article distributed under the Creative Commons Attribution License, which permits unrestricted use, distribution, and reproduction in any medium, provided the original work is properly cited.

In order to solve the complex and recurrent problem of chronic pelvic inflammation disease (CPID) in the process of the clinical treatment, a method of understanding the influencing factors of CPID by investigating the actual situation of clinical cases and using logistics regression analysis was proposed in this study. A total of 204 outpatients were selected from a certain hospital. The ratio of the cases in the experimental group to those in the control group stands at 1:1. The results were obtained as follows. According to the data of CPID patients collected in the paper, the majority of patients had a high school education background or below technical secondary school education background, accounting for 66.7%. And the majority of patients were manual workers, accounting for 69.1%. All the exp (B) values of the frequency of sex life per month  $\geq 9$  times, frequent sex life during menstruation, IUD contraception, no contraception, abortion  $\geq 3$  times, vaginal irrigation per week  $\geq 1$  time, and intrauterine surgery  $\geq 3$  times were more than 1. These seven factors were the risk factors for chronic pelvic inflammation. Oral contraceptives were a weak protective factor of chronic pelvic inflammation. These factors including early drug withdrawal (53.1%), without understanding the condition of the disease (35.7%), no time to review the disease (24.5%), and irregular medication (21.4%) accounted for a large proportion. They were associated with the recurrence of CPID. This method is aimed at providing some foundations for establishing effective prevention and control measures for chronic pelvic inflammation and providing a recognized clinical diagnosis and efficacy evaluation criteria for the treatment of chronic pelvic inflammation.

## 1. Introduction

Pelvic inflammatory disease (PID) refers to the inflammation of the female upper genital tract and its surrounding tissues, mainly including endometritis, salpingitis, fallopian tube and ovarian abscess, and pelvic peritonitis. Inflammation can be limited to one site or involve several sites simultaneously. Pelvic inflammation is divided into two categories, namely, acute and chronic. The deterioration of acute pelvic inflammation can cause diffuse peritonitis, sepsis, and septic shock. And it is life-threatening for severe cases. If it is not completely cured

in the acute phase, it will become chronic pelvic inflammatory disease (CPID), which often lasts for a long time and occurs repeatedly. It can cause the diseases including infertility, tubal pregnancy, and chronic pelvic pain, seriously affecting women's health and increasing the economic burden of the family and society, as shown in Figure 1. Pelvic inflammation is a common gynecological disease. The main pathogens are staphylococcal, streptococcus, Escherichia coli, anaerobic bacteria, and so on [1]. In recent years, due to the wide prevalence of sexually transmitted diseases, the pathogen type of pelvic inflammatory disease has changed. And because of the change

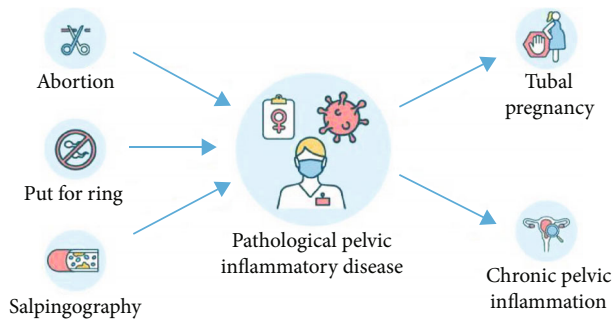


FIGURE 1: Influencing factors of pelvic inflammation.

of modern human life patterns, the pathogenic factors of pelvic inflammatory disease have also become more complicated. At present, the incidence of pelvic inflammation has an upward trend, which has become the focus of domestic and foreign researches and has attracted the attention of experts from different countries. Because of the long disease course of PID that lasts for several months or years, or even decades, which has a great impact on women's health and fertility, the disease can lead to chronic pelvic pain (CPP), infertility, tubal pregnancy, and so on, seriously affecting women's health and increasing the economic burden of the family and society. Chronic pelvic pain caused by the long-term inflammation can cause a negative influence on women's daily life, work, and sexual life. It is because some viruses can threaten mother and child simultaneously through vertical infection that the treatment of PID is getting more and more attention and has become a highly anticipated topic in the medical community [2]. Over the years, professional workers have explored the etiology, pathogenesis, and treatment of pelvic inflammation unremittingly. Many drugs and methods have been used in the treatment of pelvic inflammation, but its curative effect is not very satisfactory. In order to explore the related factors of chronic pelvic inflammation and provide a scientific basis for further preventing the disease, the investigation of chronic pelvic inflammation still needs to be studied. This paper is aimed at investigating the related factors and relapse factors affecting the incidence of chronic pelvic inflammatory disease and at providing a reference for the prevention and treatment of this disease. At the same time, through the diagnosis of chronic pelvic inflammation patients and the exploration of the syndrome characteristics, it is aimed at providing new ideas for chronic pelvic inflammation syndrome and at providing clinical basis for scientific treatment [3]. Based on the above, logistic multivariate regression analysis was used to analyze the effect of chronic pelvic inflammation on infertility in women.

## 2. Literature Review

Pelvic inflammatory disease (PID) refers to a group of infectious diseases in the female upper genital tract, mainly including endometritis, salpingitis, fallopian tube and ovarian abscess (cyst), and pelvic peritonitis. Liu et al. believed that inflammation could be limited to one site and could also involve several parts at the same time. It could spread to the

whole pelvic organs and peritoneum. The most common were salpingitis and salpingoophoritis, and simple endometritis and ovaritis were less common [4]. Reyftmann et al. believed that these symptoms including lower abdominal pain and discomfort, lumbosacral pain, low heat fluctuations, fatigue-prone, menstruation disorder, increased menstrual volume, and infertility were common. Even neurasthenia symptoms appeared, such as depression, fatigue and weakness, body discomfort, and insomnia [5]. Balla et al. believed that PID was the name of western medicine, and the name of pelvic inflammation did not appear in the ancient books of traditional Chinese medicine. According to the symptoms, signs, and clinical manifestations, it could be attributed to "female abdominal pain," "leukorrhoea disease," "heat into blood room," and "dysmenorrhea" [6]. Dabis considered that PID was one of the most frequent and important inflammation in pregestational women. PID was characterized by stubborn and recurrent disease, which seriously affects women's physical and mental health [7]. Chen et al. believed that its incidence rate remained high in recent years, and it was prone to recurrence, which seriously affected women's health. About 1 million women in the United States each year developed PID from a variety of pathogenic bacteria. The infection rate was highest among teenagers. Every year, more than 100,000 women were infertile due to pelvic inflammatory disease, and about 70,000 women have tubal pregnancy caused by PID [8]. According to Kaplan and Kirici, a woman spent 1060-3180 to treat PID in her lifetime on average. If the diagnosis and treatment were not timely, there would be a variety of sequelae, such as ectopic pregnancy, tubal ovarian abscess, infertility, dyspareunia, and chronic pelvic pain [9]. Siegenthaler et al. noted that chlamydial pelvic inflammatory disease had been reported as a risk factor for ovarian cancer. About 33.74% of PID patients were infected with HPV virus, so they were more prone to cervical cancer than the general population [10]. Yang et al. believed that the transmission route of pelvic inflammation usually included the following four forms: lymphatic system, blood circulation, spread along the genital mucosa, and direct spread. At present, it was believed that PID episodes were mostly related to the following factors: infection after intrauterine operation, sexual activity and age, lower reproductive tract infection, poor sexual hygiene, and inflammation of adjacent organs [11]. Lemly and Gupta summarized the following 10 inducing factors of PID: female genital anatomy characteristics, female genital natural defense function vulnerable, female life period of physiological characteristics, sexual activity, sexually transmitted diseases, contraception, abortion or vaginitis, vaginal flushing, iatrogenic infection, and other diseases such as tuberculosis and appendicitis [12]. Perhar et al. believed that the pathogens causing pelvic inflammatory disease had two sources, including aerobic and anaerobic pathogens from the original living in the vagina and pathogens from the outside, such as *Neisseria gonorrhoeae*, *Chlamydia trachomatis*, *Mycobacterium tuberculosis*, and *Pseudomonas aeruginosa*. The main pathogen was pyogenic bacteria, such as pathogens of streptococcus PID can be simple aerobic, simple anaerobic bacteria, or aerobic bacteria and anaerobic bacteria mixed infection, which may or may not be associated with sexually transmitted diseases. In order to prevent PID from attacking recurrently, in addition to the

comprehensive treatment, attention must be paid to its nursing, so as to obtain better treatment effect and prevent its recurrence [13].

### 3. Research Methods

*3.1. Diagnostic Criteria.* Diagnostic criteria are formulated with reference to the relevant contents of the Guiding Principles for Clinical Research of New Chinese Medicine issued by the Ministry of Health.

- (1) Medical history: having a history of acute pelvic inflammation
- (2) Symptoms
  - (i) Low fever and fatigue: systemic symptoms are not obvious. Sometimes the patients are prone to fatigue, with only low fever. Neurasthenia symptoms can appear for some patients with a long disease course, such as depression, physical discomfort, insomnia, and other diseases
  - (ii) Lower abdominal swelling pain or low lumbar swelling pain: this is the main clinical symptom. The pain is caused by the chronic inflammation of the uterus, tubal adhesion, or pelvic blood stasis. The pain may aggravate before and after fatigue, sexual intercourse, and menstruation [14]
  - (iii) Increased leucorrhea: leucorrhea is star-yellow or light yellow in form of water, or yellow green, sometimes with a bad smell
  - (iv) Menstrual imbalance: the symptom is with more menstruation volume or prolonged menstruation, due to pelvic blood stasis caused by chronic inflammation or affecting ovarian function
  - (v) Infertility: the symptom appears due to tubal adhesion obstruction caused by chronic inflammation
- (3) Signs: the uterus is often in a backward flexion position, with limited activity or fixed adhesion. When it is uterine myositis, the uterus can have tenderness. If it is salpingitis, the cord to phase the fallopian tube on one side or both sides of the uterus will be touched, with tenderness. If it is the fallopian tube water or fallopian tube ovarian cyst, cystic mass on pelvic side or both sides can be touched, with limited activity and tenderness. If it is pelvic connective tissue inflammation, the plate thickening can be touched on one or both sides of the uterus with tenderness. Or low ligament in the uterus is thickening and hardening, with tenderness [15].

For the above signs, the following two items should appear at the same time at least. The one is uterine movement being limited or adhesion fixation with tenderness. The other is tenderness in attachment area (corticate thickening or sheet thickening or packing).

#### (4) Auxiliary examination

- (i) Blood routine: the total number of leukocyte or neutrophils slightly increases
- (ii) Blood sedimentation rate examination: if inflammatory mass forms, the blood sedimentation rate increases slightly faster
- (iii) B ultrasound examination: thickening fallopian tube, effusion, or pelvic inflammatory mass can be explored
- (iv) Vaginal or cervical canal discharge smear examination: it is abnormal or pathogens can be detected
- (v) C reaction protein determination: if there is an inflammatory mass formation, examine whether C reaction protein increases or not
- (vi) Serum CA-125 measurement: if there is an inflammatory mass formation, examine whether serum CA-125 increases or not
- (vii) Laparoscopy: the formation of uterine and tubal adhesion lesions or pelvic inflammatory mass can be seen. It can be diagnosed according to the above main symptoms and necessary signs, combined with the medical history and auxiliary examination [16]

*3.2. Data of the Experiment Subjects.* A total of 204 outpatients were selected from a certain hospital. The ratio of the cases in the experimental group to those in the control group stands at 1 : 1. The control group was mainly selected from family members, relatives, friends, colleagues, or classmates of the selected cases. And healthy people aged no more than 3 years compared with the selected cases were randomly selected, with a total of 204 cases [17] (note: all research subjects had a sexual history).

The average age of the experimental group was  $29.16 \pm 7.63$  years old. The average age of the control group was  $30.08 \pm 7.54$  years old. There was no statistical difference in age between the two groups. Age distribution is shown in Table 1.

## 4. Results Analysis

*4.1. Clinical Data of the Experimental Group.* The minimum age was 19 years old, and the maximum age was 46 years old in the experimental group. And the patients were graded at 5 years as an age group. The specific information is shown in Figure 2.

As shown in Figure 2, in the collected data of CPID patients, the high incidence age of chronic pelvic inflammation was 25-34 years old, and the number of cases in this age group accounted for 55.9% of the total number of cases in the experimental group.

In the collected data of CPID patients, education and occupation are distributed in Figure 3.



TABLE 1: The distribution of CPID cases and age of the control group.

Age (years old)	Case load (case)	The control group (case)
Below 20 (not including 20)	3	2
20-24	32	35
25-29	62	61
30-34	52	55
35-39	39	36
Above 40 (including 40)	16	15
Total	204	204

Note: the age distribution of the two groups was tested by  $\chi^2$ .  $P > 0.05$ . It is not significant.

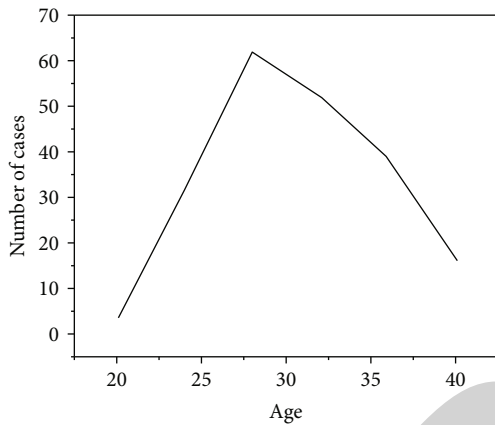


FIGURE 2: Age distribution of the CPID cases.

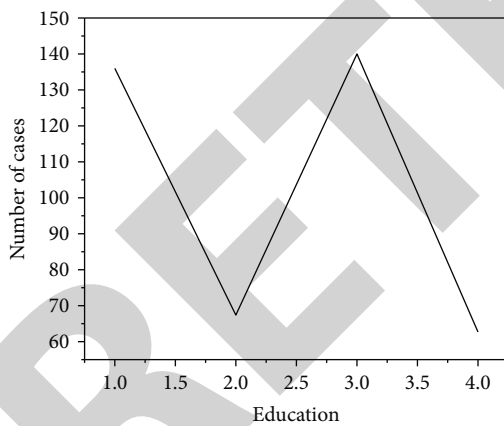


FIGURE 3: The distribution of education and occupation of the CPID cases.

As shown in Figure 3, in the collected data of the CPID patients, the majority of patients had a high school education background or below technical secondary school education background, accounting for 66.7%. And the majority of patients were manual workers, accounting for 69.1%.

#### 4.2. Analysis of the Factors Associated with CPID Pathogenesis.

By using the logistic regression analysis, the dependent variable  $Y$  is whether to suffer from chronic pelvic inflammation ( $0 =$  not suffer from CPID,  $1 =$  suffer from CPID). The factors

with the significant differences between the experimental group and the control group were obtained, including education, occupation, frequency of sex, menstrual sex, contraception (no contraception, IUD contraception, oral contraceptives), number of abortions, vaginal irrigation, intrauterine surgical operation, degree of work fatigue, and life pressure, which were regarded as independent variables. By using the backward deletion method, the binary logistic regression model was adopted. Logistic regression analysis was performed [18]. Results are shown in Table 2.

According to Table 2, the Sig. values of the eight factors listed were all less than 0.05, which were statistically significant. All the exp ( $B$ ) values of the frequency of sex life per month  $\geq 9$  times, frequent sex life during menstruation, IUD contraception, no contraception, abortion  $\geq 3$  times, vaginal irrigation per week  $\geq 1$  time, and intrauterine surgery  $\geq 3$  times were more than 1. These seven factors were the risk factors for chronic pelvic inflammation. Combined with the regression factor  $B$  (positive correlation), it could be known that those with the above 7 factors were prone to chronic pelvic inflammation [19]. The exp ( $B$ ) value of oral contraceptives was less than 1. Combined with the regression coefficient  $B$  (negative correlation), it indicated that it was a protective factor of chronic pelvic inflammatory disease. But its exp ( $B$ ) value was close to 1, indicating that it was a weak protective factor.

The logistic regression equation was obtained from Table 2, as shown as follows:

$$P = \frac{e^{-1.194+0.691A+0.754B+0.311C+0.415D-0.023E+1.564F+0.761G+2.045H}}{1 + e^{-1.194+0.691A+0.754B+0.311C+0.415D-0.023E+1.564F+0.761G+2.045H}} \quad (1)$$

where  $A$  is the frequency of sex life per month  $\geq 9$  times,  $B$  is the frequent sex life during menstruation,  $C$  is the IUD contraception,  $D$  is the no contraception,  $E$  is the oral contraceptives,  $P$  is the abortion  $\geq 3$  times,  $G$  is the vaginal irrigation per week  $\geq 1$  time, and  $H$  is the intrauterine surgery  $\geq 3$  times.

The positive probability of CPID can be calculated in the regression equation.

4.3. Analysis of the Factors Associated with the Recurrence of CPID. Among the 204 CPID cases investigated, 98 were patients with CPID recurrence. The recurrence patients filled in the

TABLE 2: Results of the logistic regression analysis of the factors associated with CPID.

Correlative factors	B	S.E.	Wald	df	Sig.	Exp (B)	95.0% C.I. for exp (B)	
							Lower	Upper
The frequency of sex life per month $\geq 9$ times	0.691	0.297	5.430	1	0.020	1.996	1.116	3.570
Frequent sex life during menstruation	0.754	0.259	8.510	1	0.004	2.126	1.281	3.528
IUD contraception	0.311	0.140	4.914	1	0.027	1.365	1.037	1.796
No contraception	0.415	0.146	8.061	1	0.005	1.514	1.137	2.016
Oral contraceptives	-0.023	0.006	13.027	1	0.000	0.977	0.965	0.989
Abortion $\geq 3$ times	1.564	0.774	4.084	1	0.043	4.778	1.048	21.783
Vaginal irrigation per week $\geq 1$ time	0.761	0.771	0.976	1	0.032	2.141	0.473	9.700
Intrauterine surgery $\geq 3$ times	2.045	0.807	6.421	1	0.011	7.732	1.589	37.675
Constant	-1.194	0.338	12.450	1	0.000	0.303		

TABLE 3: Table of correlative factors related with recurrence of CPID.

Correlative factors	Number	Percentage (%)
No time to review the disease	24	24.5
Underestimating the disease	12	12.2
Without understanding the condition of the disease	35	35.7
Irregular medication	21	21.4
Early drug withdrawal	52	53.1
Other	8	8.2

Note: patients should fill in two or more related factors at the same time when filling in the form.

TABLE 4: Reasons for drug withdrawal.

Reasons	Number	Percentage (%)
Forgetting to take medicine	8	8.2
Stopping the medication after the symptoms decrease by yourself	54	55.1
Poor effect	16	16.3
The side effect of drug	9	9.2
High prices	11	11.2

TABLE 5: Table of the doctor's advice.

	Regular medication	Paying attention to hygiene	Regular review	Forbidding sex life during menstrual period
Yes	61.2	66.3	80.6	51.2
No	38.8	33.7	19.4	48.8

recurrence-related factor table and the recurrence-related factors were investigated [20]. The results are shown in Table 3.

As can be seen from Table 3, according to the collected data in this survey, these factors including early drug withdrawal (53.1%), without understanding the condition of the disease (35.7%), no time to review the disease (24.5%), and irregular medication (21.4%) accounted for a large proportion. They were associated with the recurrence of CPID.

As shown in Table 4, in the collected data in this paper, the factor stopping the medication after the symptoms decrease by yourself (55.1%) accounted for a large proportion.

As can be seen from Table 5 that in the collected data in this survey, patients have a good compliance with doctors' advice on

paying attention to hygiene and forbidding sex life during menstrual period, but poor compliance with regular review [21].

**4.4. Discussions.** As for patient care, patients suffering from CPID should follow the following five pieces of advice. First, one should pay attention to rest, avoid sex life being too frequent, and arrange the work and rest time. Second, one should adjust the mood to have a happy and optimistic spirit. Third, one should protect the spleen and stomach, pay attention to the diet and nutrition, and avoid spicy and stimulating foods. Fourth, one should beware of the invasion of wind, cold, and humid heat. Fifth, one should do appropriate exercises and strengthen the resistance ability

of the body. Logistic regression is a multivariate analysis method to study the relationship between dichotomous or multicategorical dependent variables and multiple influencing factors. Logistic regression belongs to probabilistic regression, which is applicable to data with categorical variables (including ordered classification and disordered classification) [22]. According to the study design, it can be divided into nonconditional logistic regression and conditional logistic regression. According to the type of dependent variable, it can be divided into binary logistic regression, multiclassified disordered logistic regression, and multiclassified ordered regression. In dichotomy logistic regression, if the effect of an event (such as disease or not)  $Y$  (dependent variable) is affected by a group of independent variables  $X_1, X_2, X_3, \dots, X_m$  that is dichotomized, the value of  $Y = 1$  indicates an event (such as disease and positive reaction), and  $Y = 0$  means an event does not occur (such as disease does not occur and negative reaction). Logistic regression analysis is widely used in the epidemiological study of disease risk factors and can also be used to screen the meaningful symptoms of syndrome differentiation. The syndrome is composed of a group of symptoms of different influences on the syndrome, which should distinguish between the primary and secondary symptoms. A logistic regression model of the syndrome can be established if the symptoms of the syndrome are used as the dependent variable  $Y$  and the symptoms appear in the syndrome are used as the independent variable  $X$ . The different contribution rates of these independent variables (symptoms) to the dependent variables (syndrome) can be analyzed by logistic regression. And the independent variables with too small or more scattered contribution rates can be excluded.

## 5. Conclusion

Chronic pelvic inflammation disease (CPID) is a common disease clinically in gynecology, which frequently occurs. The treatment of chronic pelvic inflammation is a more complex process. In this study, CPID was investigated with the help of the case-by-case method, and the related factors and recurrence characteristics of CPID were preliminarily understood.

The results of this study are shown as follows.

- (1) By the means of  $X$  and  $X^2$  test, the correlation factors of the difference with statistical significance between the experiment group and the control group were found. By using logistic regression analysis, the high risk factors of chronic pelvic inflammation were obtained including the frequency of sex life per month  $\geq 9$  times, frequent sex life during menstruation, IUD contraception, no contraception, abortion  $\geq 3$  times, vaginal irrigation per week  $\geq 1$  time, and intrauterine surgery  $\geq 3$  times. And the weak protective factor was oral contraceptives
- (2) According to the collected data in this survey, these factors including early drug withdrawal (53.1%), without understanding the condition of the disease (35.7%), no time to review the disease (24.5%), and irregular medication (21.4%) accounted for a large proportion. They were associated with the recurrence of CPID

## Data Availability

The data used to support the findings of this study are available from the corresponding author upon request.

## Conflicts of Interest

The authors declare that there is no conflict of interest.

## References

- [1] Z. Liang, X. Wang, Y. H. Liu, D. M. Zhang, and L. Shi, "Analgesic effect of electroacupuncture on chronic pelvic pain in patients with sequelae of pelvic inflammatory disease," *Zhongguo zhen jiu = Chinese acupuncture & moxibustion*, vol. 41, no. 4, pp. 395–399, 2021.
- [2] R. K. Chaudhary, N. Doggalli, and N. Subedi, "Univariate and multivariate sex dimorphism in the diverse age group of the South Indian dentition using the polyvinyl siloxane elastomeric impression material," *Egyptian Journal of Forensic Sciences*, vol. 11, no. 1, pp. 1–12, 2021.
- [3] P. A. Kale, K. G. Jangale, and A. Kakade, "Comparison of antibiotics and prebiotics in treatment of pelvic inflammatory disease," *Journal of SAFOMS*, vol. 8, no. 1, pp. 24–26, 2020.
- [4] Y. H. Liu, X. Wang, Z. Liang, H. Li, and L. Shi, "Acupuncture combined with western medication on chronic pelvic pain after pelvic inflammatory disease: a multi-center randomized controlled trial," *Zhongguo zhen jiu = Chinese Acupuncture & Moxibustion*, vol. 41, no. 1, pp. 31–35, 2021.
- [5] L. Reyftmann, P. Lowenstein, and C. Bura, "Residual peritoneal lipiodol after hycosy can mimic pelvic inflammatory disease or endometriosis," *Journal of Minimally Invasive Gynecology*, vol. 29, no. 2, pp. 181–182, 2022.
- [6] F. Balla, B. Ismaili, E. Demaliaj, and A. Elmasllari, "The incidence and prevalence of pelvic inflammatory disease and its impact in infertility, pelvicgia and surgical interventions," *Romanian Journal of Medical Practice*, vol. 15, no. 3, pp. 307–312, 2020.
- [7] R. Dabis, "Clinical cure rate of pelvic inflammatory disease. Should ceftriaxone be part of the first line regimen?," *International Journal of STD & AIDS*, vol. 31, no. 14, pp. 1432–1433, 2020.
- [8] Y. Chen, S. Wei, L. Huang, M. Luo, and C. Yin, "Fuhe qianjin combined with antibiotic therapy for pelvic inflammatory disease: a systematic review and meta-analysis," *Evidence-based Complementary and Alternative Medicine*, vol. 2020, Article ID 5372839, 10 pages, 2020.
- [9] S. Kaplan and P. Kirici, "Pelvic inflammatory disease and contraception: a cross-sectional study in tertiary center," *Journal of Health Sciences and Medicine*, vol. 3, no. 4, pp. 454–459, 2020.
- [10] F. Siegenthaler, E. Krause, and M. D. Mueller, "Diagnostik und therapie der adnexitis (pelvic inflammatory disease)," *Therapeutische Umschau*, vol. 77, no. 4, pp. 164–170, 2020.
- [11] Z. Yang, Q. Hu, Z. Feng, and Y. Sun, "Development and validation of a nomogram for predicting severity in patients with hemorrhagic fever with renal syndrome: a retrospective study," *Open Medicine*, vol. 16, no. 1, pp. 944–954, 2021.
- [12] D. Lemly and N. Gupta, "Sexually transmitted infections part 2: discharge syndromes and pelvic inflammatory disease," *Pediatrics in Review*, vol. 41, no. 10, pp. 522–537, 2020.

## Retraction

# Retracted: Effect of Nursing Intervention on Coronary CT Angiography in Elderly Patients

### Scanning

Received 20 June 2023; Accepted 20 June 2023; Published 21 June 2023

Copyright © 2023 Scanning. This is an open access article distributed under the Creative Commons Attribution License, which permits unrestricted use, distribution, and reproduction in any medium, provided the original work is properly cited.

This article has been retracted by Hindawi following an investigation undertaken by the publisher [1]. This investigation has uncovered evidence of one or more of the following indicators of systematic manipulation of the publication process:

- (1) Discrepancies in scope
- (2) Discrepancies in the description of the research reported
- (3) Discrepancies between the availability of data and the research described
- (4) Inappropriate citations
- (5) Incoherent, meaningless and/or irrelevant content included in the article
- (6) Peer-review manipulation

The presence of these indicators undermines our confidence in the integrity of the article's content and we cannot, therefore, vouch for its reliability. Please note that this notice is intended solely to alert readers that the content of this article is unreliable. We have not investigated whether authors were aware of or involved in the systematic manipulation of the publication process.

In addition, our investigation has also shown that one or more of the following human-subject reporting requirements has not been met in this article: ethical approval by an Institutional Review Board (IRB) committee or equivalent, patient/participant consent to participate, and/or agreement to publish patient/participant details (where relevant).

Wiley and Hindawi regrets that the usual quality checks did not identify these issues before publication and have since put additional measures in place to safeguard research integrity.

We wish to credit our own Research Integrity and Research Publishing teams and anonymous and named external researchers and research integrity experts for contributing to this investigation.

The corresponding author, as the representative of all authors, has been given the opportunity to register their agreement or disagreement to this retraction. We have kept a record of any response received.

### References

- [1] Y. Yin and Z. Wei, "Effect of Nursing Intervention on Coronary CT Angiography in Elderly Patients," *Scanning*, vol. 2022, Article ID 3663285, 7 pages, 2022.

## Research Article

# Effect of Nursing Intervention on Coronary CT Angiography in Elderly Patients

Yajuan Yin <sup>1,2</sup> and Zhongting Wei <sup>1,2</sup>

<sup>1</sup>School of Nursing Science, Guangxi University of Science and Technology, Liuzhou, Guangxi 545006, China

<sup>2</sup>Guangxi University of Science and Technology Second Hospital, Liuzhou, Guangxi 545006, China

Correspondence should be addressed to Yajuan Yin; 202009000324@hceb.edu.cn

Received 5 May 2022; Revised 20 May 2022; Accepted 27 May 2022; Published 15 June 2022

Academic Editor: Balakrishnan Nagaraj

Copyright © 2022 Yajuan Yin and Zhongting Wei. This is an open access article distributed under the Creative Commons Attribution License, which permits unrestricted use, distribution, and reproduction in any medium, provided the original work is properly cited.

To investigate the clinical benefits of coronary CT angiography in older adults. The results of this trial were 110 patients who underwent CT angiography (selected from 20 March 2016 to 20 March 2017). Use computer group mode. The control group received health care, including 50 patients, and the control group received usual care, including 60 patients. Then, the best and best image quality, time-consuming analysis, and satisfaction were compared between the two groups. The experimental results showed that the best and best image quality (83.00%), examination time ( $5.72 \pm 1.81$ ) minutes, and patient satisfaction (100.00%) of the experimental group were better than those of the control group ( $P < 0.05$ ). Targeted healthcare for patients undergoing coronary CT angiography can improve the patient's ability to receive a diagnosis with a consistent attitude, reduce work hours, reduce adverse factors, and improve patient satisfaction with care.

## 1. Introduction

Coronary heart disease is a fatal heart disease that kills many people. The literature shows that heart disease accounts for about 15% of all deaths and has a significant impact on the life and health of patients [1]. Early diagnosis and early treatment are important ways to reduce cardiovascular mortality and improve prognosis. Conventional coronary angiography (CAG) is the gold standard for diagnosing coronary heart disease, but treatment is limited by high costs. CT coronary angiography (CTCA) is widely used for the diagnosis of coronary heart disease because of the physical improvement and resolution of a large number of CT films. However, how to reduce patient discomfort, complete screening, and good imaging has become an important part of electrical research [2]. Multislice spiral CT coronary angiography (MSCTCA) is a new, concealed, and safe device that has been widely used in hospitals. MSCTCA can be used as a first-line diagnosis and clinical examination of vascular stenosis. The sensitivity, specificity, and accuracy of its measurements have been recognized, leading to better and more accurate treatments for hospitals [3].

Coronary CT angiography (Figure 1) is an important basis for screening and preliminary diagnosis of coronary intervention at present. It belongs to a new diagnostic mode. It has the advantages of safety, noninvasive, high-diagnostic accuracy, and simple operation. It has high sensitivity and specificity for coronary artery and can accurately evaluate the degree of lesions, so as to provide basis for the formulation of treatment plan. However, with the deepening of relevant reports, it can be found that the CT angiography of coronary artery can be affected by factors such as environment, psychology, respiratory coordination, and heart rate. In this regard, it is also necessary to strengthen nursing intervention and guidance, so as to ensure image quality and improve the success rate of examination. Routine nursing is more passive and one-sided, which is not conducive to wide promotion. Therefore, targeted nursing intervention should be selected to improve the imaging quality by standardizing the nursing before, during, and after the examination. This paper is aimed at exploring the value of different nursing methods in patients undergoing coronary CT angiography, as described below [4].

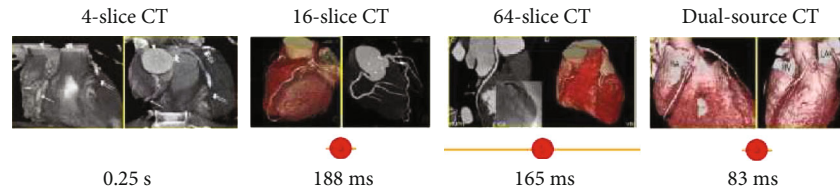


FIGURE 1: Coronary CT angiography.

## 2. Literature Review

Liu and others think that coronary heart disease is the abbreviation of coronary heart disease, and it is often found in the middle and old age population. With the increase of age, the incidence rate of disease is gradually increasing. CAG is the gold standard for judging the degree of coronary artery stenosis, but the examination price is high and invasive, causing serious damage to the patient's body [5]. Smeets and others believe that CTCA is a new noninvasive and safe technology with high sensitivity and specificity. How to maintain the best state of patients during examination and improve the imaging quality of CTCA has become the most concerned issue of Radiology Department [6]. Faan and others believe that CTCA is an important screening method for evaluating coronary artery disease in patients with coronary heart disease. 64 slice spiral CT has the characteristics of fast scanning, high image quality, and high diagnostic accuracy, but good nursing cooperation is an important part of successful examination, especially heart rate and psychological regulation [7]. Yang and others found that the change of heart rate plays an important role in the imaging quality of CTCA. When the heart rate is slow, CTCA can get the best imaging quality. Therefore, a stable heart rate should be maintained during the examination [8]. Msosa and others believe that the factors affecting heart rate include basic heart rate, mood fluctuation, and severity of disease. Before the examination, nurses actively communicate with patients, listen to their voices, find the source of patients' anxiety factors, explain the pathogenesis of coronary heart disease and the importance of CTCA examination through professional knowledge, patiently answer patients' questions, improve patients' understanding of CTCA examination of coronary heart disease, alleviate patients' tension, enhance their self-confidence to overcome the disease, reduce patients' psychological burden, and stabilize their heart rate [9]. Zima and others since the wide application of multislice spiral CT, the CT scanning speed have been significantly improved. The imaging mode has entered the era of three-dimensional volume scanning from two-dimensional image acquisition. Moreover, the postprocessing methods of multislice spiral CT images are diverse, which increases the application range of spiral CT [10]. Sole and others believe that CT angiography (CTA) refers to rapid spiral CT scanning while rapidly injecting contrast agent into vein, and the obtained data is processed by advanced computer to form the image of blood vessel. Cti1 examination has the advantages of small trauma, rapid examination, convenient imaging, and accurate diagnosis. This imaging examination method provides a reliable anatomical basis for surgical operation planning

and plays an extremely important role in the evaluation of blood vessels before and after liver operation [11]. Alperovitch-Najenson and others believe that powerful CT postprocessing function, after scanning, dual source CT can automatically select the best phase of coronary artery development for reconstruction through prospective ECG gating equipment. When the automatic selection is wrong, manual reconstruction can also be further selected [12].

## 3. Experimental Analysis

**3.1. Subjects.** A total of 100 subjects were accepted from March 20, 2016, to March 20, 2017. The researchers divided the patients who underwent CT angiography into two groups of 40 before and after admission. The procedure includes (1) when the patient is resting, the heart rate is less than 100 beats per minute, and the breath is less than 30; (2) after the ECG examination, the patient can see the clear vision of the nasal cavity, as well as the sound quality; (3) all patients have coronary artery CT angiography indications; (4) all patients have signed the written consent [13].

Exclusion procedure: (1) exclude patients with severe arrhythmia; (2) exclude patients with congestive heart failure; (3) exclude patients with liver and kidney insufficiency and hyperthyroidism; (4) exclude patients who are allergic to iodine concentration. The mean age of the research group was  $(52.86 \pm 3.22)$  years, including 26 males and 24 females [14].

**3.2. Experimental Method.** Scanning method: the CT scanner used this time adopts the light speed 61 row model provided by GE company to assist the patient in the supine position, and 350 mg/ml iohexol is injected through elbow vein. The coronary artery and intracardiac and extracardiac structures of the observation group are observed, and the patient images are processed after surface reconstruction, multiplanar reconstruction, volume reproduction, and maximum density projection. The control group was given routine nursing guidance and informed of relevant knowledge and precautions before the examination [15]. The observation group adopted targeted nursing intervention, mainly including

- (1) *Nursing before Examination.* ① Psychological nursing: in order to reduce the image artifacts caused by arrhythmia or rapid heart rate and maintain a stable heart rate, it is also necessary to do a good job of psychological counseling to help patients eliminate their inner tension and patiently explain the function, purpose, and relevant matters of concern of this

examination. In order to prevent accidents, it is also necessary to ask the patients whether they have organ diseases and drug allergy history before examination; ① in order to ensure the accurate and smooth pushing of the contrast medium, it is also necessary to select the blood vessel puncture without puncture, phlebitis, and thick and straight on the same day and select the corresponding needle model according to the injection flow rate and blood vessel conditions. At the same time, the venous trocar has unique elasticity and flexibility, safe and simple operation, little stimulation to blood vessels, and will not lead to leakage or trocar prolapse due to high pressure or too fast injection speed [16]. After successful puncture, 1 ml of contrast medium needs to be injected and observed for 15 minutes. The examination can be continued only after it is confirmed that there is no allergic reaction; ① respiratory training: respiratory artifact is the main factor leading to the failure of the examination. For this, it is also necessary to teach the patients the correct nursing methods before the examination and reasonably adjust the respiratory rate according to the instructions of the CT machine, so as to improve the image quality. During the examination, the respiratory rate should be kept in a uniform state, the chest and abdominal wall should not move up and down, and the lips should be closed tightly. Breathe only after hearing the breath holding display light goes out or the instructions, and the breath holding time should not be pushed back. Train several times according to the method until the patients fully master and understand it. For patients with poor hypoxia tolerance or lung diseases, oxygen inhalation intervention is also needed to maintain body braking, and the patients are instructed not to sneeze, swallow, cough, and other actions; ① therefore, it is also necessary to take  $\beta$  receptor blocker before the examination, so as to control the heart rate, and so as to avoid arrhythmia and artifacts. Before the examination, ask the patient to lie down and rest for 15 minutes, and then continue the examination after the mood fluctuation is stable [17]

- (2) In order to avoid the failure of breath holding, breath holding training should be carried out again, and the smoothness of the indwelling needle should be checked. When injecting contrast agent, maintain the speed of 5 ml per second. In the process of examination, once the patient has abnormal phenomena, it is necessary to stop the examination immediately and give corresponding symptom intervention [18]
- (3) *Postexamination Care.* After the scanning is completed, separate the puncture needle and high-pressure syringe, and keep the needle for observation for 30 minutes. After the patient has no abnormalities, it can be removed. For patients with vomiting symptoms, they need to be treated with correspond-

TABLE 1: Excellent and good rate of comparative image quality (cases (%)).

Group	Number of cases	Excellent	Good	Poor
Observation group	50	42	8	0
Control group	60	31	12	7
$\chi^2$	—		7.623	
$P$	—		<0.05	

TABLE 2: Comparison of nursing effects.

Group	Number of cases	Inspection time	Nursing satisfaction
Observation group	50	$5.54 \pm 1.75$	50
Control group	60	$8.14 \pm 1.34$	41
$t$	—	7.356	9.836
$P$	—	<0.05	<0.05

ing antiemetic drugs and encourage patients to drink more water to promote the discharge of contrast agent

3.3. *Observation Indicators.* The nursing satisfaction of patients was evaluated by nursing evaluation scale. The total score was 100, 80~100 was very satisfied, 60~79 was satisfied, and <59 was dissatisfied. The nursing satisfaction was (very satisfied + satisfied)/total person  $\times$  100%. Excellent rate of image quality: excellent rate = excellent rate + good rate; excellent: the vessel contour is clear, and there is no artifact in the coronary artery; good: the contour of local blood vessels is blurred or there are artifacts in local coronary arteries; poor: vessel contour is blurred or vessel display is interrupted, and artifacts appear in all or most of the coronary arteries.

3.4. *Statistical Treatment.* The statistical software SPSS 22.0 was used for data processing. The inspection time was represented by  $(x \pm s)$ , and the  $t$ -test was used; the excellent rate of image quality and nursing satisfaction of counting data are expressed in (%), and  $\chi^2$  test is adopted. If the final comparison result shows that  $P < 0.05$ , it indicates that the data difference is statistically significant [19].

3.5. *Result Analysis.* The image quality of the control group was higher than that of the control group, and the difference was statistically significant ( $P < 0.05$ ), as shown in Table 1.

The nursing rate in the control group was higher than that in the control group, and the monitoring period was shorter than that in the control group ( $P < 0.05$ ), as shown in Table 2.

The comparison of baseline heart rate and postoperative heart rate after the health study between the two groups is shown in Table 3. As can be seen from Table 3, there was no difference in heart rate between the two groups; after a healthy workout (waiting for a 15-minute rest), heart rate increased faster than heart rate in both groups. Compared with the group, the difference was statistically significant;

TABLE 3: Comparison of basic heart rate and heart rate after health education between the two groups.

Group $n$	Basal heart rate	Heart rate after health education	$t$	$P$
Observation group 50	62.38 ± 3.58	94.26 ± 8.06	10.31	<0.001
Control group 60	63.49 ± 3.48	93.16 ± 6.23	8.87	<0.001
$t$	1.13	7.16		
$P$	>0.05	<0.001		

TABLE 4: Comparison of heart rate control time and breathing coordination training time between the two groups.

Group $n$	Heart rate control time (min)	Breathing coordination training time (min)
Observation group 50	52.37 ± 12.62	62.34 ± 11.24
Control group 60	31.63 ± 12.56	34.21 ± 6.37
$t$	6.91	10.35
$P$	<0.001	<0.001

after the health study, the heart rate of the control group was faster than that of the affected group. There were significant differences between the two groups.

The comparison of cardiac control time and breathing time in the combined breathing group between the two groups is shown in Table 4. As can be seen from Table 4, after oral administration of metoprolol hydrochloride, the heart rate was below 70 BPM and the time it took for the joint to breathe. Training time in both groups was shorter in the group intervention than in the control group. The difference between the two groups was significant [20].

The incidence and efficacy of heart rate > 10 bpm between the two groups are shown in Figure 2. As can be seen from Figure 2, the effect of the heart rate change > 10 bpm control group was lower than that of the control group, and the success rate was higher than that of the control group. Differences between the two groups were significantly identified.

#### 4. Discussion

It can be seen from the experiment that the heart rate of the examiners in both the intervention group and the control group is faster than the basic heart rate after entering the waiting room and resting quietly for 15 minutes, which is related to the examiners' tension in the specific environment of the hospital, fear of the examination process, and strangeness to the medical staff [21]. Nervous and fearful emotions can cause the examiner's sympathetic nerve to be excited and his heart rate to increase. The faster heart rate coronary angiography, in addition to the higher chance of image artifacts, the time of image postprocessing is also significantly prolonged. Therefore, the examiner's emotional tension will increase the examiner's dose of heart rate control and prolong the time of heart rate control, resulting in the prolongation of the workflow. Its center rate is an important factor that directly affects the image quality. At present, some studies believe that when the heart rate of patients is ≤65 BPM during coronary artery imaging, relatively good image quality can be obtained. Some scholars also observed that the

greater the fluctuation range of heart rate during the examination, the more obvious the decline of image quality, especially when the fluctuation range of heart rate is ≥0.5 bpm. Therefore, we routinely require that the examiner's heart rate be controlled below 70 BPM before examination. When the heart rate fluctuation amplitude is 10 bpm during the examination, it has little impact on the quality of coronary artery imaging. Some authors suggest using a receptor blocker to control heart rate. When the subject is in the routine examination room, it may be related to the increase of heart rate fluctuation when we are in the examination room or lying in the examination room. When the subject is nervous, it may be found that the heart rate of some subjects will increase when we are lying in the examination room. Some subjects need to wait for  $\beta$  long time after taking metoprolol orally for many times, and the heart rate is still difficult to control, resulting in failure of examination and prolongation of workflow, resulting in waste of personnel and equipment resources [22].

It can be seen from the experimental data that there was no significant difference in the basal heart rate between the two groups of examiners. After 15 minutes of rest in the waiting room, the heart rate in the control group was significantly higher than that in the intervention group ( $P < 0.001$ ), and the difference was statistically significant. By fully communicating with the inspectors in the intervention group before the inspection, the inspectors have a full understanding of the entire inspection process, actively cooperate with the inspection, and reduce tension and fear [23]. At the same time, combined with oral metoprolol hydrochloride, it can quickly control the examiner's heart rate and reduce the fluctuation range of heart rate during the examination. The results showed that the heart rate control time of the examiners in the intervention group was significantly shorter than that in the control group, the incidence of heart rate fluctuations > 10 bpm during the inspection process was significantly lower than that in the control group, and the inspection success rate was significantly higher than that in the control group. It shows that effective health education and psychological nursing measures can



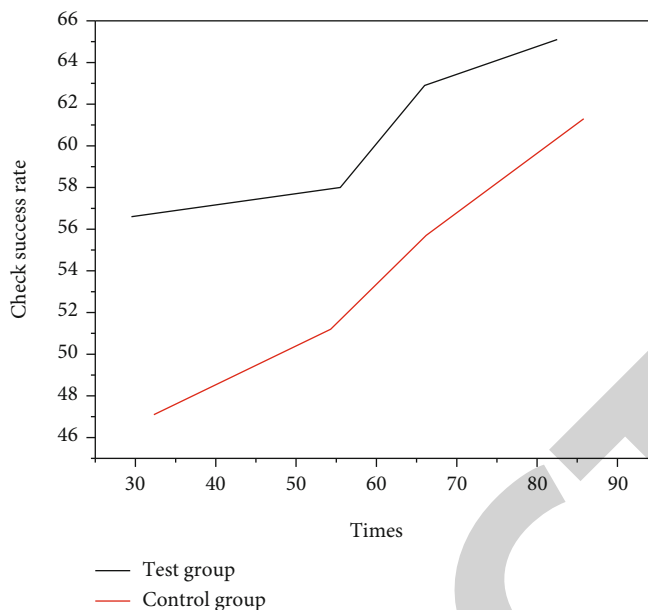


FIGURE 2: Comparison of incidence and examination success rate of heart rate fluctuation amplitude > 10 BPM between the two groups.

ensure the success rate of examination while optimizing the workflow.

In the process of coronary artery imaging, it is generally necessary for the subject to hold his breath for 5~10 s, but some subjects cannot hold their breath due to tension and other reasons, resulting in respiratory motion artifacts. In order to reduce the impact of breathing on coronary artery imaging, train the examiner to hold his breath after inhaling evenly and repeat it many times until the examiner can successfully complete the inhaling and holding action within the estimated scanning time after hearing the instruction. In addition, the respiratory movement of some examiners is uneven, resulting in the selection of trigger points sometimes low and resulting in shear artifacts. Therefore, it is necessary to emphasize the importance of uniform breathing to the examiners [24]. In the control group, the technician only instructed the examiner to follow the instructions of the machine, inhale deeply first, and then hold his breath, but the examiner often breathed involuntarily, so that the technician needed to repeatedly train the examiner's breathing cooperation. In the intervention group, the nurses trained the examiners to inhale evenly before the examination and then hold their nose while holding their breath. This has a better effect, controlling the examiners' involuntary spontaneous breathing and reducing the generation of respiratory artifacts.

Coronary CTA examination should obtain excellent images. As a nursing staff, every patient can achieve the best state before the examination. Let patients actively cooperate during the examination and actively communicate with patients after the examination, which is not only to ensure clear image quality but also the main purpose of nursing work.

In terms of psychological nursing, targeted psychological intervention should be implemented before the examination to overcome the tension of patients, such as eliminating the

fear of large-scale instrument examination, the harm of ionizing radiation to the body and the safety of contrast agent, so as to reduce the psychological burden of patients, and so as to stabilize the heart rate. Some studies have shown that the relaxation training of behavior and scientific comforting language can significantly reduce the impact of patients' bad emotions on their physical state, restore the homeostasis of internal environment, and successfully check.

In terms of heart rate control, the intervention group gave 25 mg Betaloc sublingual with a heart rate of more than 70 beats/min, with a maximum of no more than 100 mg. When necessary, oxygen inhalation was given to reduce the heart rate and stabilize the heart rate. The heart rate was controlled below 70 beats/min, which achieved good results and obtained the best image quality. In terms of breath control, good breath holding is a necessary and key factor for the successful completion of cardiac coronary artery examination. If the patient cannot hold his breath during the scanning process, the respiratory artifact is large, resulting in tomography and displacement of cardiac vascular image, which has a great impact on the image quality and has an impact on the diagnosis, which must be avoided [25].

## 5. Conclusion

In addition to the direct impact on heart rate and respiration, the quality of multislice spiral CT coronary imaging has a direct impact on its scanning technology, the amount of contrast medium, and the injection rate. Any improper operation may lead to the failure of the examination. Therefore, before apricot examination, giving patients careful and scientific nursing and controlling interference factors will help patients complete the examination better and faster and improve the image quality of coronary CTA. All patients in the intervention group obtained satisfactory images,

which is inseparable from the careful nursing work before and during the examination. Careful nursing is an important guarantee for the success of the examination. To sum up, the nursing staff should fully communicate with the examinee before the contrast examination, and the appropriate combined application of metoprolol hydrochloride tablets can effectively control the examinee's tension, slow down the examinee's heart rate, and narrow the range of heart rate fluctuation during the examination. In addition, simple and easy breathing cooperation training can ensure better image quality, improve the success rate of examination and diagnosis accuracy, optimize the workflow, and give full play to the equipment and human resources. In a word, targeted nursing intervention can provide patients with high-quality, comprehensive, and scientific nursing service guidance. When used in patients undergoing coronary CT angiography, it can not only improve the examination quality but also reduce the artifacts caused by various influencing factors on the imaging image, meet the needs of diagnosis, promote the smooth progress of the examination, and improve the image quality.

### Data Availability

The data used to support the findings of this study are available from the corresponding author upon request.

### Conflicts of Interest

The author declared that there is no conflicts of interest.

### References

- [1] Y. Wang, D. Zhang, and S. Wei, "Effect of nursing intervention in the operating room based on simple virtual reality augmented technology on preventing gastrointestinal surgical incision infection," *Journal of Healthcare Engineering*, vol. 2021, no. 6, 10 pages, 2021.
- [2] J. Yang, M. Xu, Y. Wang, and Z. Gao, "Analysis of the effect of intensive care based on lean nursing intervention," *Engineering*, vol. 2021, no. 3, pp. 1–9, 2021.
- [3] A. P. Manal, E. Fareed, and H. Elsayad, "Effect of selected nursing intervention on clinical outcomes among patients with nasogastric tube in intensive care units," *Japan Journal of Nursing Science*, vol. 6, no. 6, pp. 21–32, 2021.
- [4] A. K. Johnson, M. A. L. Sherry Razo, J. Smith, A. Cain, and B. Detaranto, "A person centered nursing care intervention on a medical surgical unit," *Geriatric Nursing*, vol. 42, no. 5, pp. 1125–1128, 2021.
- [5] H. Liu, D. Zhu, J. Cao, J. Jiao, and X. Wu, "The effects of a standardized nursing intervention model on immobile patients with stroke: a multicenter study in China," *European Journal of Cardiovascular Nursing*, vol. 18, no. 8, pp. 753–763, 2019.
- [6] C. Smeets, M. Smalbrugge, R. Koopmans, M. Nelissen-Vrancken, and S. U. Zuidema, "Can the proper intervention reduce psychotropic drug prescription in nursing home residents with dementia? Results of a cluster-randomized controlled trial," *International Psychogeriatrics*, vol. 33, no. 6, pp. 1–10, 2020.
- [7] A. B. Faan, B. S. Cauvin, A. C. Msn, K. Pretorius, and K. Johnson, "Application of project management tools and techniques to support nursing intervention research," *Nursing Outlook*, vol. 68, no. 4, pp. 396–405, 2020.
- [8] J. Yang, H. Hu, and Y. Li, "Effect of dual-track interactive nursing intervention model on anxiety and depression in patients with coronary heart disease," *Psychiatry Danubina*, vol. 32, no. 2, pp. 197–204, 2020.
- [9] A. Msosa, J. Bruce, and R. Crouch, "Effect of a formative assessment intervention on nursing skills laboratory learning in a resource-constrained country," *Nurse Education Today*, vol. 97, no. 1–2, p. 104677, 2020.
- [10] M. Zimansky, L. Stasielowicz, I. Franke, H. Remmers, H. Friedel, and J. Atzpodien, "Effects of implementing a brief family nursing intervention with hospitalized oncology patients and their families in Germany: a quasi-experimental study," *Journal of Family Nursing*, vol. 26, no. 4, pp. 346–357, 2020.
- [11] M. L. Sole, S. Talbert, X. Yan et al., "Nursing oral suction intervention to reduce aspiration and ventilator events (no-aspirate): a randomized clinical trial," *Journal of Advanced Nursing*, vol. 75, no. 5, pp. 1108–1118, 2019.
- [12] D. Alperovitch-Najenson, C. Weiner, J. Ribak, and L. Kalichman, "Sliding sheet use in nursing practice: an intervention study," *Workplace Health & Safety*, vol. 68, no. 4, pp. 171–181, 2020.
- [13] R. Spratling, M. S. Faulkner, I. Feinberg, and M. J. Hayat, "Creating opportunities for personal empowerment: symptom and technology management resources (cope-star) for caregivers of children who require medical technology," *Journal of Advanced Nursing*, vol. 76, no. 1, pp. 347–355, 2020.
- [14] L. A. Mcinnis and A. Morehead, "Exercise as a therapeutic intervention," *Nursing Clinics of North America*, vol. 55, no. 4, pp. 543–556, 2020.
- [15] H. S. Kim and J. S. Kang, "Effect of a group music intervention on cognitive function and mental health outcomes among nursing home residents: a randomized controlled pilot study," *Geriatric Nursing*, vol. 42, no. 3, pp. 650–656, 2021.
- [16] L. Brown, G. Gardner, and A. Bonner, "A randomized controlled trial testing a decision support intervention for older patients with advanced kidney disease," *Journal of Advanced Nursing*, vol. 75, no. 11, pp. 3032–3044, 2019.
- [17] C. Baab, A. C. Bakker, M. E. de Vugt et al., "Effects of a Multidisciplinary Intervention on the Presence of Neuropsychiatric Symptoms and Psychotropic Drug Use in Nursing Home Residents With Young-Onset Dementia: Behavior and Evolution of Young-Onset Dementia Part 2 (BEYOND-II) Study," *The American Journal of Geriatric Psychiatry*, vol. 27, no. 6, pp. 581–589, 2019.
- [18] D. Cheung, S. K. Tang, K. Ho, C. Jones, and V. Chiang, "Strategies to engage people with dementia and their informal caregivers in dyadic intervention: a scoping review," *Geriatric Nursing*, vol. 42, no. 2, pp. 412–420, 2021.
- [19] K. A. Williams, E. J. Lee, M. Wilmoth, C. Selwyn, and K. Bydalek, "Screening, brief intervention, and referral to treatment/motivational interviewing school-based therapy pilot study," *Journal of Addictions Nursing*, vol. 32, no. 1, pp. 14–19, 2021.
- [20] B. Margaret, A. George, T. Phagdol, B. S. Nayak, and L. E. Lewis, "Designing a mobile health intervention for preterm home care: application of conceptual framework," *Public Health Nursing*, vol. 39, no. 1, pp. 296–302, 2022.

## Retraction

# Retracted: Analysis of Pathogen Characteristics and Nursing Factors of Tonsil Infection Based on Regression Equation

### Scanning

Received 26 September 2023; Accepted 26 September 2023; Published 27 September 2023

Copyright © 2023 Scanning. This is an open access article distributed under the Creative Commons Attribution License, which permits unrestricted use, distribution, and reproduction in any medium, provided the original work is properly cited.

This article has been retracted by Hindawi following an investigation undertaken by the publisher [1]. This investigation has uncovered evidence of one or more of the following indicators of systematic manipulation of the publication process:

- (1) Discrepancies in scope
- (2) Discrepancies in the description of the research reported
- (3) Discrepancies between the availability of data and the research described
- (4) Inappropriate citations
- (5) Incoherent, meaningless and/or irrelevant content included in the article
- (6) Peer-review manipulation

The presence of these indicators undermines our confidence in the integrity of the article's content and we cannot, therefore, vouch for its reliability. Please note that this notice is intended solely to alert readers that the content of this article is unreliable. We have not investigated whether authors were aware of or involved in the systematic manipulation of the publication process.

In addition, our investigation has also shown that one or more of the following human-subject reporting requirements has not been met in this article: ethical approval by an Institutional Review Board (IRB) committee or equivalent, patient/participant consent to participate, and/or agreement to publish patient/participant details (where relevant).

Wiley and Hindawi regrets that the usual quality checks did not identify these issues before publication and have since put additional measures in place to safeguard research integrity.

We wish to credit our own Research Integrity and Research Publishing teams and anonymous and named external researchers and research integrity experts for contributing to this investigation.

The corresponding author, as the representative of all authors, has been given the opportunity to register their agreement or disagreement to this retraction. We have kept a record of any response received.

### References

- [1] L. Zhang and Y. Yang, "Analysis of Pathogen Characteristics and Nursing Factors of Tonsil Infection Based on Regression Equation," *Scanning*, vol. 2022, Article ID 3149619, 7 pages, 2022.

## Research Article

# Analysis of Pathogen Characteristics and Nursing Factors of Tonsil Infection Based on Regression Equation

Longfang Zhang  and Yuanyuan Yang 

Department of Otorhinolaryngology and Stomatology, The First Affiliated Hospital of Soochow University, Suzhou, Jiangsu 215008, China

Correspondence should be addressed to Yuanyuan Yang; 14095110220050@hainanu.edu.cn

Received 6 May 2022; Revised 26 May 2022; Accepted 1 June 2022; Published 11 June 2022

Academic Editor: Balakrishnan Nagaraj

Copyright © 2022 Longfang Zhang and Yuanyuan Yang. This is an open access article distributed under the Creative Commons Attribution License, which permits unrestricted use, distribution, and reproduction in any medium, provided the original work is properly cited.

In order to meet the needs of the analysis and application of regression equation in clinical medicine of tonsil infection, this paper focuses on the semiparametric regression model method, cross-validation method, empirical method, and multiple regression equation analysis of atypical data using regression equation. The general method of analyzing this kind of data is given, and the parameter estimation and hypothesis testing of the model are systematically studied. The experimental results showed that among the 90 paraffin-embedded tissue specimens of chronic tonsillitis and adenoid hypertrophy in this study, 26 out of 49 male children were EBERs positive, accounting for 53.06% of male children (26/49 cases). 28 of the 41 female children were positive, accounting for 68.29 of the female children (28/41 cases). There were 14 cases in infant group, 20 cases in preschool age group, 25 cases in school-age group, and 31 cases in adolescence group; the EBERs-positive rate was 42.86% (6/14 cases) in early childhood and 55.00% in early school-age (11/20 cases), and the EBERs-positive rate was 60.00% in school-age group (15/20 cases) and 70.97% in adolescent group. The results showed that the latent infection rate of adenoid hypertrophy EBV in children with chronic tonsillitis showed no significant difference between genders. It is proved that the regression equation method can meet the needs of clinical analysis and application of tonsil infection.

## 1. Introduction

Tonsillitis is a very common disease that is rarely considered an important risk factor for oropharyngeal cancer, but the relationship between inflammation and carcinogenesis has been well documented. Foreign scholars have also confirmed that there is a correlation between the development of nasopharyngeal carcinoma and surrounding inflammation [1]. Although inflammatory processes are known to increase the risk of cancer, the relationship between chronic tonsillitis and cancer remains unknown. High-risk HPV and EBV infection play an important role in tumor transformation of human oral epithelial cells, and viral infection does play a role in inducing cancer mechanism, but the potential role of viral infection leading to virus-induced carcinogenesis has not been verified [2]. As a simple and effective method

to find the regression equation, the least square method has been mastered and widely used. Recent studies on the robustness of mathematical statistics have found that when there are out varies, the robustness of the regression equation obtained by the least square method is often affected [3]. In this regard, some methods of robust regression are proposed to overcome this defect. For example, a more robust regression equation can be obtained by using the absolute sum of residuals as the objective function of minimization, that is, the least one method; see Figure 1 [4]. In this paper, by using the robustness of median over mean, and with the aid of residual analysis, a new robust regression equation is presented to analyze the characteristics of tonsillar infection pathogens and nursing factors that can resist the interference of abnormal data by several iterations of the initial regression equation.

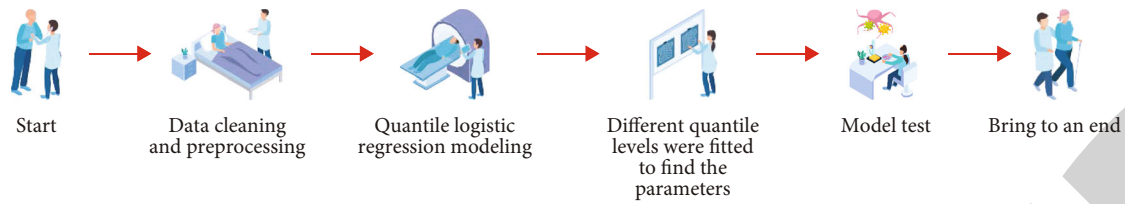


FIGURE 1: Regression equation flow.

## 2. Literature Review

Wang and Zhang believed that the parameter estimation of multiple regression models in previous studies usually adopts the least square parameter estimation method, but the least square regression model requires no collinearity between independent variables. When there is serious collinearity between independent variables, the parameter estimation will be seriously harmed, the model error will be increased, and the robustness of the model will be destroyed. In addition, multiple linear regression often requires the sample content to be 10~20 times of the number of variables. In practical problems, it is sometimes difficult to expand the sample content [5]. To solve this problem, Undiyaundeye proposed a new multivariate statistical analysis method partial least squares (PLS) regression in 1983 [6]. Grauso et al. has studied and pointed out that in the regression modeling of dependent variable to multiple independent variables, when there is a high degree of correlation within each variable set, the partial least squares regression modeling analysis is more effective than the general multiple regression, and its conclusion is more reliable [7]. By analyzing the function of partial least squares regression on the synthesis and screening of multivariate information, Attafuah et al. revealed the modeling mechanism of partial least squares regression under multiple correlation conditions and also demonstrated the extensive application scope of this new multivariate analysis method [8]. Yu et al. used specific examples to compare and analyze the least squares regression (MLR) principal component regression (PCR) and partial least squares regression (PLS), revealing that PLS can provide a more reasonable. In addition to the robust regression model, some research contents similar to principal component analysis and canonical correlation analysis can be completed at the same time to provide more rich and in-depth information [9]. Lu et al. believes that partial least squares regression analysis provides a many-to-many linear regression modeling method to establish linear or even nonlinear regression prediction equations of dependent variables with respect to independent variables. It is especially suitable for the case where two groups of variables have a large number of multiple correlations and the amount of observed data is small [10]. Bazan et al. believed that the least square regression analysis was initially applied in the field of metrology and achieved success. In recent years, it has been rapidly extended to other fields, such as bioinformatics and social sciences, and achieved good results. However, it is seldomly applied in the field of medicine and health, which explains the application analysis of partial least square regression of tonsil infection pathogen characteristics

and nursing influencing factors [11]. Tarr et al. noted that with the deepening understanding of disease and its influencing factors and various indicators, multifactor analysis method has been widely used. Multivariate analysis, also known as multivariate statistical analysis, is a series of statistical methods to study the relationship between multiple factors (variables) and the relationship between samples (individuals) with these factors, such as discriminant analysis, cluster analysis, and principal component analysis [12]. In this series of methods, multivariate linear regression is the basis of multivariate statistical methods to study the linear relationship between multiple independent variables and one dependent variable.

On the basis of the current research, this paper focuses on the semiparametric regression model method, cross-validation method, empirical method, and multiple regression equation analysis of atypical data by using regression equation; gives the general method of analyzing this kind of data; and systematically studies the parameter estimation and hypothesis testing of the model, to prove the effect of regression equation method on clinical analysis and application of tonsil infection.

## 3. Research Method

**3.1. Semiparametric Regression Model Method.** In practical problems, people often encounter other situations where the assumptions of the classical statistical model cannot be fully satisfied. For example, the specific dependency relationship between response variables and explanatory variables is not clear or linear; that is, the model formal assumption does not meet the distribution of response variables, is not easy to judge, or does not meet the required distribution, that is, the data source assumption does not meet. At this point, the classical regression analysis method cannot guarantee good results, parameter estimates are unreliable, and it is even difficult to give a reasonable explanation for the selling problem. Therefore, classical statistical methods have their limitations; it is difficult to conduct regression analysis on atypical data, while nonparametric regression, one of the exploratory analysis methods, can effectively analyze atypical data.

At this point, the classical regression analysis method cannot guarantee good results. Parameter estimates are not reliable, and it is even difficult to give a reasonable explanation of the sellability problem. Therefore, classical statistical methods have their limitations. It is difficult to perform regression analysis on atypical data, but nonparametric regression, one of the exploratory analysis methods, can effectively analyze atypical data [13].

According to the different assumptions of regression function, regression models can be divided into two types: parametric regression model and nonparametric regression

model. If the regression function belongs to a class of functions determined by a finite number of parameters, the function form is known, and the parameters are unknown, that is, the model form is known, and it is called parametric regression model. If the regression function is restricted to a certain class of smooth functions, such as continuously differentiable functions with square integrable second derivatives, that is, a set of functions belonging to an infinite dimension, it is called a nonparametric regression model. Like classical regression, nonparametric regression also has two main purposes: one is to explore and describe the relationship between variables, and the other is to predict and estimate, that is, regression is regarded as a model-based data induction method [14].

The model studies the dependence between the response variable and the single explanatory variable  $t$ , and it can solve many important problems. However, in practical work, many things or phenomena are affected by multiple variables, so it is necessary to study the relationship between multiple variables. Multiple regressions are often used in statistical analysis to study the dependence relationship affected by multiple explanatory variables, and the more general model of multiple regressions is the linear model:  $y_i = x_i' \beta + \varepsilon_i$ .  $x_i$  is the vector composed of the  $i$ th observed explanatory variable, which can be a continuous variable or a categorical variable.  $\beta$  is the unknown regression coefficient vector. In general,  $x_i$  contains a constant  $L$  corresponding to the intercept [15]. In order to relax the linearity assumption of one of the explanatory variables in the linear model, a semiparametric regression model can be considered.

**3.1.1. Model Description.** Assume that for each observation  $y_i$ , there is a  $p+1$  explanatory variable, in which the  $p$ -dimensional vector  $x_i$  and the quantitative variable  $t$ , and if the reaction variable  $y$  is linearly related to the explanatory variable  $x$ , there is the following model, as

$$y_i = x_i' \beta + g(t_i) + \varepsilon_i \quad (1)$$

is an unknown  $p$ -dimensional regression coefficient vector  $\beta$ ,  $g(t)$  is an unknown smooth function,  $x$  is a linear variable, and  $t$  is a spline variable.  $\varepsilon$  is independent of delta  $(x, y)$ .  $E(\varepsilon) = 0$ , and  $V(\varepsilon) = \sigma^2$  (unknown). Obviously,  $x_i$  does not contain constant  $1$ , and the constant term can be included in  $g(t)$ , so the above model is called semiparametric regression model or partial spline.

The semiparametric regression model is more adaptable than the parametric linear model. In practical work, the semiparametric regression model is an extension of the linear model because some variable often has an influence on the performance of the unknown function. In the actual application of Model Formula (1), response variables are linearly correlated, and most explanatory variables should be based on professional theoretical knowledge or previous experience. The processing of spline  $T$  variable is different from other linear variables in that it is processed in a nonparametric form.

The semiparametric regression model is solved by the penalty least squares method, where the estimation of  $\beta$

and  $g(t)$  minimizes the following weighted sum of penalty squares.

$$S_w(\beta, g) = \sum_{i=1}^n w_i \{y_i - x_i' \beta - g(t_i)\}^2 + \alpha \int g''(t)^2 dt. \quad (2)$$

Smooth parameter  $\alpha > 0$ ,  $w_i > 0$ , and  $w_i = 1$  without weighting [16].

Set  $Y = (y_1 \cdots y_n)'$ ,  $W = \text{diag}(w_1, \cdots, w_n)$ ,  $X$  is  $n \times p$  matrix, the  $i$ th is  $x_i$ ; to consider the stalemate, suppose  $t_1, t_2, \cdots, t_n$  by  $s_1, s_2, \cdots, s_q$ ; and the matrix that shows the relationship between them is called the incidence matrix, which is denoted by  $N$ .  $N$  is an  $n \times q$  matrix whose elements are  $N_{ij}$ , if  $t_i = s_j$ , and  $N_{ij} = 1$ ; otherwise,  $N_{ij} = 0$ . If  $t_i$  is not identical, then  $q \geq 2$ . Make  $a_j = g(s_j)$ ,  $j = 1, 2, \cdots, q$ . Then the vector  $g$  to be estimated is  $(a_1, a_2, \cdots, a_q)'$ . Similarly, if  $s_1 < s_2 < \cdots < s_q$ , and  $a_j = g(s_j)$ , then two matrices  $Q$  and  $R$  can be defined, except that  $t_1, t_2, \cdots, t_n$  should be replaced by  $s_1, s_2, \cdots, s_q$  and  $K = OR^{-1}Q'$ , and then  $\int g''(s)^2 ds = g'Kg$ .

Use matrix notation to represent  $S_w(\beta, g)$ , then:

$$S_w(\beta, g) = (Y - X\beta - Ng)'W(Y - X\beta - Ng) + \alpha g'Kg. \quad (3)$$

When  $\beta$  and  $g$  are solutions to the following partitioned matrix equation, the above formula takes a minimum.

$$\begin{bmatrix} X'WX & X'WN \\ N'WX & N'WX + \alpha K \end{bmatrix} \begin{pmatrix} \beta \\ g \end{pmatrix} = \begin{bmatrix} X' \\ N' \end{bmatrix} WY. \quad (4)$$

**3.2. Cross-Validation.** Cross-validation is a method in which each observed value participates in both model establishment and model evaluation, in order to obtain the sum of squares of residuals (Prediction Residual Error Sum of Squares, PRESS), which reflects the disturbance error caused by the change of observation points. Finally, the total sum of squares of all residuals is obtained as the total sum of squares of residuals [17, 18]. The cross-validation method can be divided into

- (1) leave-one-out (LOO)
- (2) two batch cross-validation method
- (3) split-sample cross-validation method
- (4) random sample cross-validation method. For example, the batch cross-validation method, that is,  $q$  consecutive observations are determined as test data set each time, and the remaining observations are used to establish the model. When  $Q = 1$ , it is the truncated cross-validation method [19]. The larger the PRESS value is, the more unstable the model is. Finally, the number of extracted components is determined according to the principle of minimizing the sum of squares of predicted residuals

**3.3. Experience Method.** It is determined according to the cumulative contribution rate of components. Generally, extracted components explain most of the variation

TABLE 1: Data list 1.

$t$	$x_1$	$x_2$	$\varepsilon$	$y$	$\hat{y}$
1	13.7573	9.0395	3.75143	117.821	113.7
2	15.052	7.3279	1.14067	122.813	122.411
3	8.6033	7.3862	0.23542	94.179	92.477
4	8.6597	8.5354	-7.34831	75.51	81.595
5	15.2607	4.0964	3.86252	127.148	124.918
6	12.7431	7.4814	-3.4369	88.786	92.752
7	16.268	6.4557	9.27355	114.115	106.738
8	10.168	5.2876	-3.75255	81.923	85.032
9	13.2466	5.3008	0.40266	92.177	92.14
10	11.5926	5.5634	1.03347	81.719	80.133
11	6.7552	12.4906	-0.30367	24.013	21.325
12	12.956	8.818	-3.99901	56.798	60.147
13	11.1053	3.6854	-6.52679	71.167	76.288
14	7.7996	6.2757	-1.49224	48.193	46.746
15	16.1694	6.3666	0.46688	75.036	74.903
16	12.5233	4.4313	1.40592	70.742	68.307
17	16.213	9.0616	-7.86257	47.241	55.469
18	12.7037	6.6083	4.72638	58.156	52.658
19	11.1916	6.9559	-0.50045	43.68	43.025
20	9.0719	10.1228	-2.09744	16.307	16.571
21	13.2374	8.2352	-2.20841	38.275	40.706
22	14.1714	6.0503	1.91203	55.233	54.373
23	12.148	5.0736	-5.52984	44.491	50.723
24	11.029	10.0753	3.65699	22.564	19.43
25	10.8887	8.3597	3.08169	29.333	27.203
26	15.014	5.5422	3.69035	57.719	57.095
27	14.0647	6.6078	2.63609	47.195	47.519
28	10.9326	6.8775	0.81989	32.828	33.939
29	12.3795	6.8564	3.39402	40.131	39.377
30	15.2033	11.4076	9.15392	31.726	26.192
31	12.7406	4.4082	3.07456	53.77	53.48
32	14.3541	4.9055	-2.34343	51.552	57.089
33	7.2211	7.3388	4.36714	21.857	17.452
34	12.2964	7.379	-0.13148	35.106	36.812
35	7.5594	5.2159	6.15973	37.439	30.556
36	13.783	6.797	0.10761	45.426	46.447
37	11.7396	6.5214	2.97025	44.074	40.832
38	9.2977	5.9949	-4.85962	32.179	35.232
39	8.6071	6.3306	-5.48525	29.16	32.042
40	11.2352	9.6646	-4.16542	23.979	26.075
41	13.8607	7.6723	-4.27133	45.259	48.329
42	13.6616	8.4751	-0.61364	46.365	45.577
43	14.8575	10.0036	-0.35908	45.238	44.672
44	11.3236	5.1932	-4.19473	57.101	59.337

TABLE 2: Data list 2.

$t$	$x_1$	$x_2$	$\varepsilon$	$y$	$\hat{y}$
45	13.0163	4.9998	-9.97231	60.984	70.019
46	11.2934	3.7157	0.90965	75.786	73.759
47	12.3691	4.0188	5.37863	85.636	80.071
48	13.1409	8.0467	9.53689	74.973	65.923
49	11.8286	7.1126	-8.29482	61.239	70.013
50	12.0206	5.9175	6.27481	86.574	81.372
51	9.9082	7.023	-3.72382	67.744	72.118
52	11.4828	8.8829	1.1973	72.648	73.099
53	7.1578	5.1667	-3.58128	76.989	81.040
54	16.1750	4.2811	6.46804	127.001	124.974
55	8.0296	3.9454	8.23395	107.718	100.957
56	12.2365	7.2613	-1.83271	99.812	104.805
57	14.5338	9.3725	2.89922	106.677	107.781
58	12.2149	8.6182	2.84722	108.163	108.284
59	14.1007	4.9623	8.82781	145.267	139.972
60	13.6661	48874	2.12864	143.379	144.101

convenient but not accurate, and the accuracy of regression equation is not high [20].

### 3.4. Determination Method of Multiple Regression Equation

**3.4.1. Forward Selection Method.** The forward selection method is to investigate the relationship between variables outside the equation and dependent variables and introduce the variables with the closest relationship into the equation one by one until there are no variables with significant relationship outside the equation to be introduced [21].

**3.4.2. Backward Elimination.** That is, each variable is first included in the equation, and then the significance of the linear relationship between  $X'$  and  $Y$  is judged, and the independent variables with no significant significance are removed from the equation one by one until all the independent variables contained in the formula have significant significance for  $Y$ .

**3.4.3. Stepwise Regression.** This is a more reasonable and convenient method established on the basis of the previous two methods; that is, from the selected  $m$  independent variables, according to the size of the corresponding variable contribution of each variable, two-way cross is introduced and removed one by one for screening. Before and after an independent variable is selected or removed, a hypothesis test is performed to ensure that each time a new variable is introduced, only the independent variable that has a significant effect on  $Y$  is included in the equation. This is repeated until no independent variable with no significant effect can be removed from the equation, and no independent variable with significant effect can be selected outside the equation to achieve the optimal standard.

**3.4.4. Optimal Subset Regression Method.** That is, from the subset regression equation of all possible combinations of all independent variables, the best one is selected according to

information of independent variables and dependent variables, such as 65%, 75%, and 80%. This method is similar to the determination of the number of principal components in principal component analysis. This method is simple and

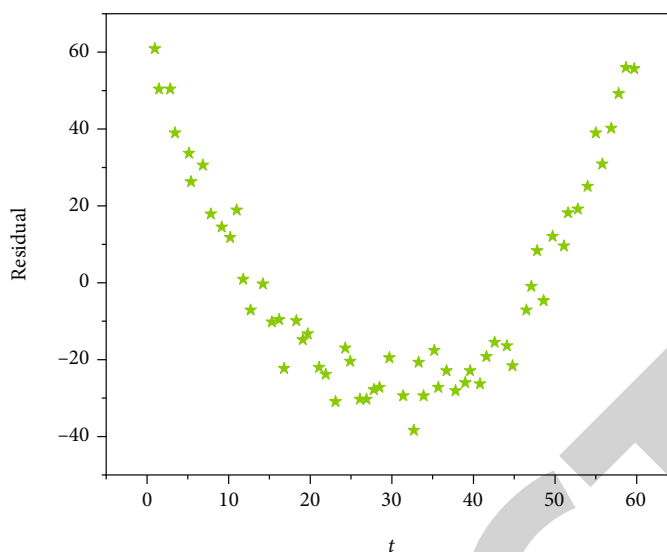


FIGURE 2: Residuals of linear model fitting.

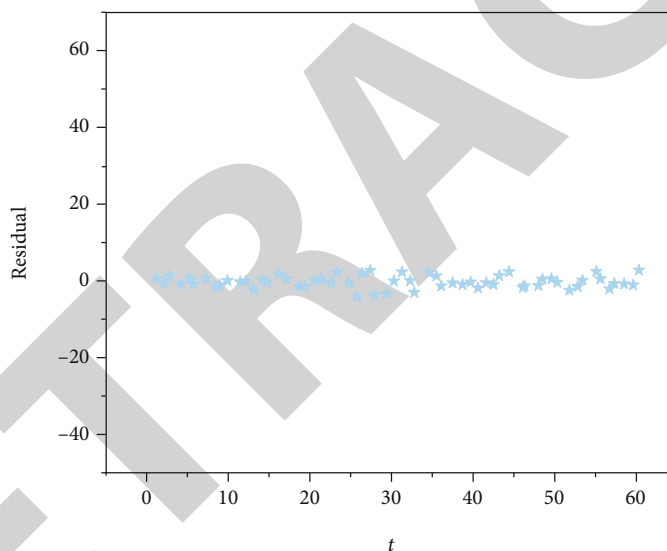


FIGURE 3: Residuals of semiparametric model fitting.

TABLE 3: Expression rates of EBERs in children of different genders.

Sex	Cases	EBERs expression rates	
		Positive	Negative
Male	49	26 (53.06%)	23 (46.94%)
Female	41	28 (68.29%)	13 (31.71%)

(note:  $\chi^2 = 2.16; P > 0.05$ ).

some index (such as  $R^2$ , modified  $R^2$ , and  $C_p$ ). This method is foolproof, but when there are many independent variables, the calculation amount is very large (for example, there can be  $2^m - 1$  subset equation with  $m$  independent variables).

#### 4. Outcome Analysis

##### 4.1. Simulated Example Calculation

TABLE 4: EBERs expression in different age groups.

Group	Cases	EBERs expression	
		Negative	Positive
Children's group	14	6 (42.86%)	8 (57.14%)
Preschool age group	20	11 (55.00%)	9 (45.00%)
School-age	25	15 (60.00%)	10 (40%)
Adolescence group	31	22 (70.97%)	9 (29.03%)

(Note:  $\chi^2 = 3.48; P > 0.05$ ).

4.1.1. *The Research Group.* All study samples were divided into age groups according to the age staging standard of pediatrics of the third edition of the eight-year program published by People's Medical Publishing House. It is divided into early childhood: 1- <3 years old; preschool age: 3- <6



TABLE 5: Analysis of T lymphocyte subsets in children with EB-positive and negative Epstein-Barr virus chronic tonsillitis.

	CD3 + T(%)	CD4 + T(%)	CD8 + T(%)	CD4+/CD8+
EB virus positive	68.83 ± 394	31.23 ± 479	3054 ± 5.54	102 ± 0.25
EB virus negative	68.62 ± 390	32.82 ± 6.29	2993 ± 6.28	1 09 ± 0.27
P value	>0.05	>0.05	>0.05	>0.05

years old; school-age: 6- <10 years old; and adolescence: 10 to 20 years old; there are four groups.

Forty pathological specimens of children with chronic tonsillitis were assigned to the tonsil group, and 50 pathological specimens were selected from 191 children with adenoid hypertrophy to the adenoid group by simple random sampling method. Ninety tonsil and adenoid specimens were divided into male group ( $n = 49$ ) and female group ( $n = 41$ ) according to sex. According to age grouping criteria, 90 cases of tonsil and adenoid pathological specimens were divided into infant group ( $n = 14$ ), preschool age group ( $n = 20$ ), school-age group ( $n = 25$ ), and adolescence ( $n = 31$ ). Ninety tissue specimens were divided into 1, 2, 3, ... 90. After numbering, immunohistochemistry and in situ hybridization were performed [22].

**4.1.2. Simulation Example Calculation.** A simulation example is given to illustrate the fitting effect of semiparametric model. In this example,  $P = 2$ ,  $n = 60$ ,  $t$  changes from 1 to 60,  $x_1 \sim N(12.66, 2.57^2)$ ,  $x_2 \sim N(6.7, 1.87^2)$ , error terms  $\varepsilon$  are independent and distributed  $N(0, 5^2)$ , and  $y = 3.4x_1 + 5.2x_2 + 0.1(t - 30)^2 + 30.2 + \varepsilon$ . A sample simulation data can be generated by SAS program, as shown in Tables 1 and 2.

Assuming that  $y$  is linearly dependent on  $x_1$  and  $x_2$ , if the data is artificially fitted with a parametric linear model, the regression equation can be obtained:  $\hat{y} = 49.0545 + 0.1282t + 4.4925x_1 - 6.0078x_2$ . Although the regression equation is meaningful ( $P \approx 0.0005$ ), the fitting effect is poor,  $SSE = 45494.6025$ ,  $R^2 = 0.2692$ , and the mean square error is 812.4037. It can be seen from Figure 2 that there is a conic trend between residual and  $T$ ; that is, residual still contains useful regression information. If the semiparametric regression model is used for fitting, the calculated  $\alpha$  value is 148.75, and the regression coefficients of  $x_1$  and  $x_2$  are 3.7976 and -5.2356, respectively. The test results were significant ( $P < 0.01$ ),  $SSE = 980.6252$ ,  $MSE = 19.2357$ , and  $R^2 = 0.9842$ . The residual error of model fitting is shown in Figure 3. As can be seen from the above calculation results and Figure 3, the fitting effect of the semiparametric model has been greatly improved, and the relationship between  $Y$  and  $T$  has been correctly reflected [23, 24].

## 4.2. Comparison of EBER-Positive Rate in Different Tissues, Sex, and Age Groups

**4.2.1. Comparison of EBERs-Positive Expression Rate between Different Genders.** In this study, paraffin-embedded tissue sections of 90 patients with chronic tonsillitis and adenoid hypertrophy were collected. EBERs were positive in 26 of the 49 male children, accounting for 53.06 of male children (26/49 cases); among 41 female children, 28 were EBERs pos-

itive, accounting for 68.29 of the female children (28/41 cases). Set  $\chi^2$  test,  $\chi^2 = 2.16$ , and  $P = 0.14 > 0.05$  (see Table 3).

**4.2.2. Comparison of EBERs-Positive Rate in Different Age Groups.** In 90 cases of chronic tonsillitis and adenoid hypertrophy of tonsils, there were 14 cases in the infant group, 20 cases in the preschool age group, 25 cases in the school-age group, and 31 cases in the adolescent group. The positive rate of EBERs was 42.86% (6/14 cases) in early childhood and 55.00 in preschool age (11/20 cases). The EBERs-positive rate was 60.00% in school-age group (15/20 cases) and 70.97 in adolescent group (22/31 cases). Set  $\chi^2$  test,  $\chi^2 = 3.48$ , and  $P = 0.32 > 0.05$  (see Table 4).

**4.3. Analysis of T Lymphocyte Subsets in Children with Chronic Tonsillitis.** The CD3 + T lymphocytes of 19 children with chronic tonsillitis in Epstein-Barr virus-positive group were  $68.83 \pm 3.941$ , CD4 + T cell were  $31.23 \pm 4.79$ , CD8 + T cell were  $30.54 \pm 5.54$ , and the ratio of CD4+/CD8+ was  $1.02 \pm 0.25$ . There was no statistical significance between these cells and the lymphoid subsets of children with chronic tonsillitis in the Epstein-Barr virus-negative group [25]. See Table 5 for details.

## 5. Conclusion

In this study, 40 cases of chronic tonsillitis in children and 50 cases of adenoid hypertrophy in children were examined for LMP1 and EBER. Based on regression equation, this paper focuses on semiparametric regression model method, cross validation method, empirical method, and multiple regression equation analysis of atypical data and gives the general method of analyzing this kind of data. The parameter estimation and hypothesis testing of the model were systematically studied. The T lymphocyte subsets in peripheral blood of 40 children with chronic tonsillitis were detected by flow cytometry, and the following conclusions were drawn:

The latent infection rate of adenoid hypertrophy EBV in children was higher than that of chronic tonsillitis in children.

The latent infection rate of adenoid hypertrophy EBV in children with chronic tonsillitis showed no significant difference between genders.

This study involves a relatively new field of statistics, many analytical methods are not perfect, and there is a lack of ready-made statistical software. In order to be convenient and practical, the obtained analysis methods need to be programmed in the future and then analyzed by examples to obtain satisfactory results through the program and verify their practicability.

## Retraction

# Retracted: Comparative Study of Macular Vascular Density and Retinal Thickness in Myopia Children with Different Microscope Diopters Based on OCTA

### Scanning

Received 11 July 2023; Accepted 11 July 2023; Published 12 July 2023

Copyright © 2023 Scanning. This is an open access article distributed under the Creative Commons Attribution License, which permits unrestricted use, distribution, and reproduction in any medium, provided the original work is properly cited.

This article has been retracted by Hindawi following an investigation undertaken by the publisher [1]. This investigation has uncovered evidence of one or more of the following indicators of systematic manipulation of the publication process:

- (1) Discrepancies in scope
- (2) Discrepancies in the description of the research reported
- (3) Discrepancies between the availability of data and the research described
- (4) Inappropriate citations
- (5) Incoherent, meaningless and/or irrelevant content included in the article
- (6) Peer-review manipulation

The presence of these indicators undermines our confidence in the integrity of the article's content and we cannot, therefore, vouch for its reliability. Please note that this notice is intended solely to alert readers that the content of this article is unreliable. We have not investigated whether authors were aware of or involved in the systematic manipulation of the publication process.

In addition, our investigation has also shown that one or more of the following human-subject reporting requirements has not been met in this article: ethical approval by an Institutional Review Board (IRB) committee or equivalent, patient/participant consent to participate, and/or agreement to publish patient/participant details (where relevant).

Wiley and Hindawi regrets that the usual quality checks did not identify these issues before publication and have since put additional measures in place to safeguard research integrity.

We wish to credit our own Research Integrity and Research Publishing teams and anonymous and named external researchers and research integrity experts for contributing to this investigation.

The corresponding author, as the representative of all authors, has been given the opportunity to register their agreement or disagreement to this retraction. We have kept a record of any response received.

### References

- [1] M. Chen and F. Zhao, "Comparative Study of Macular Vascular Density and Retinal Thickness in Myopia Children with Different Microscope Diopters Based on OCTA," *Scanning*, vol. 2022, Article ID 5038918, 6 pages, 2022.

## Research Article

# Comparative Study of Macular Vascular Density and Retinal Thickness in Myopia Children with Different Microscope Diopters Based on OCTA

Meiling Chen  and Fanning Zhao 

The First Hospital of Yulin, Yulin, Shaanxi 719000, China

Correspondence should be addressed to Fanning Zhao; 1423020221@st.usst.edu.cn

Received 6 May 2022; Revised 26 May 2022; Accepted 1 June 2022; Published 11 June 2022

Academic Editor: Balakrishnan Nagaraj

Copyright © 2022 Meiling Chen and Fanning Zhao. This is an open access article distributed under the Creative Commons Attribution License, which permits unrestricted use, distribution, and reproduction in any medium, provided the original work is properly cited.

In order to study the vascular density and retinal thickness of myopic children, a depth study was carried out on the basis of OCTA microscope. Through the methods of prospective cross-sectional research, statistical analysis, and basic data comparison, the research examination of myopia children under OCTA was successfully analyzed. There were significant differences in the density of superficial capillaries in the whole macular region, inner ring, temporal side of inner ring, and nasal side ( $P = 0.033, 0.024, 0.018, 0.032$ ), and there was no significant difference in other ranges ( $P > 0.05$ ). Macular fovea, as the most sensitive part of the retina, has pathological changes, which will also lead to serious negative effects on vision. The limitations of cross-sectional studies include the results of a relatively small sample size. After the study of OCTA in the macular region of children with myopia, it is related to the progressive atrophy of the retina and choroid in the macular region. When there are obvious pathological changes in the macular region, the thickness of the macular region becomes significantly thinner. We found that there was a positive correlation between retinal vascular density and retinal thickness in the fovea and above of myopia. The retinal thickness of the whole macular region, the inner ring and its four quadrants, and the outer ring and its four quadrants were positively correlated with SE (standard error) (all  $P < 0.05$ ); Foveal ring retinal thickness was not associated with SE.

## 1. Introduction

The changes of retinal vascular density and thickness in the macular region of adolescents with different degrees of myopia and their correlation were studied by optical coherence tomography and vascular OCTA imaging. Relevant reports show that ametropia has become the second general disability disease in the world, which will seriously affect the health and visual function of patients. Myopia is the highest incidence of refractive errors in the world. With the continuous changes of people's lifestyle in recent years, the incidence rate of myopia is increasing year by year, and it is beginning to become younger. Relevant data show that the number of myopia in China accounts for about 33% worldwide, which is 10% higher than the world average. It has become an important public health problem. Juvenile myopia has become a major public health problem

in the world. It is estimated that 13% of children will become highly myopia by 2050. Lutein, also known as "eye gold," is the most important nutrient in the human retina. Lutein is contained in the macula (center of vision) and lens of the retina of the eye, especially in the macula. Lutein is an important antioxidant and a member of the carotenoid family, also known as "phytolutein." It coexists with zeaxanthin in nature. Scientific research has shown that lutein is the only carotenoid found in the retina and lens of the eye. This element cannot be manufactured by the human body and must be supplemented by external intake. Without this element, the eyes will be blinded. Ultraviolet and blue light from sunlight entering the eyes will produce a large number of free radicals, leading to cataracts, macular degeneration, and even cancer. Lutein can filter blue light, decompose the damage of strong light and ultraviolet rays to the human eye, so as to avoid the damage of blue light to the

eye, and prevent vision deterioration and blindness caused by the lack of lutein, so lutein is also called the eye's guardian. High myopia has a high probability of vascular related fundus complications. Due to the limitations of previous detection techniques, we can rarely observe the subtle changes of fundus blood vessels in healthy adolescents with myopia. In recent years, the emerging optical coherence tomography angiography (OCTA) can obtain the blood flow and structural information of retinal vessels and choroidal microvessels in a noninvasive, high-resolution, and three-dimensional way, which provides a new method for clinical observation of fundus vessels and structures in myopia children. In patient groups with different diopters, the application of the same OCTA can show obvious differences in retinal vascular density and thickness in macular area. There is a positive correlation between density increase and thickness thickening in relevant patients. The close relationship between them can be found through relevant examination and control, as shown in Figure 1. The superficial retinal vascular density and retinal thickness in the fovea and parafovea of four groups of myopia were collected and analyzed by OCTA. Results the superficial vessel density and retinal thickness of macular fovea were not correlated with equivalent spherical lens ( $r = 0.119, 0.221; P > 0.05$ ) and ocular axis length ( $r = -0.026, -0.119; P > 0.05$ ). There was a positive correlation between superficial vascular density and retinal thickness ( $r = 0.674$ ). The vascular density and retinal thickness of the superficial layer near the fovea were positively correlated with the equivalent spherical mirror ( $r = 0.429, 0.379; P < 0.05$ ) and negatively correlated with the length of the ocular axis ( $r = -0.297, -0.274; P < 0.05$ ). There was no correlation between superficial vascular density and retinal thickness ( $r = 0.199, P > 0.05$ ).

## 2. Literature Review

Gus and others said whether there will be changes in retinal choroidal microvessels and blood flow with the elongation of ocular axis in the process of progressive myopia in children. To study the application of the emerging OCTA technology to detect the retinal choroidal blood flow and structure in the macular region of myopia children [1], Xiu and others believe that theoretically, the perfusion of central retinal artery may be related to the thickness of inner retina, and the perfusion of ciliary artery may be related to the thickness of outer retina and choroid. The superficial and deep retinal vessels are located in the inner retinal tissue. There is no significant difference in the inner retinal thickness among the three groups in the study, and there is no correlation between the superficial and deep retinal vessel density and the inner retinal thickness [2]. Chan and others believe that the pathological changes of fundus macula caused by myopia are an important reason affecting visual function. Therefore, studying the changes of retinal tissue structure in patients with myopia is helpful to early detect macular lesions, so as to provide guidance for early diagnosis and clinical treatment of the disease [3]. Nambudiri and others said that the macula, as the most sensitive part of vision on the retina, plays an extremely important role in visual function. Once the macular retina has abnormal deformation, hole, or bleeding, it will seriously damage the patient's visual function and

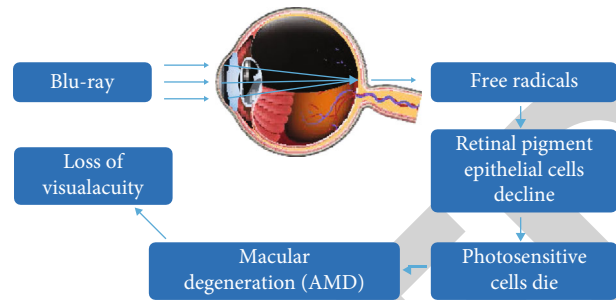


FIGURE 1: Process of retinopathy.

reduce the patient's quality of life [4]. Therefore, Li and others believe that due to the limitations of detection methods, it is impossible to carry out accurate morphological quantitative examination and functional measurement of myopia macular retina in clinic. With the gradual development of imaging technology, optical coherence tomography angiography (OCTA) began to be applied in clinic and achieved ideal results [5]. Rahmati and others believed that the equivalent spherical lens in the mild myopia group, moderate myopia group, high myopia group, and ultrahigh myopia group showed a gradual decreasing trend, while the axial length showed a gradual increasing trend. There were statistically significant differences in indexes between groups (all  $P < 0.05$ ) [6]. Therefore, Doubi and others studied that the retinal vascular density and retinal thickness of fovea, parafovea, temporal side, upper, nasal side, and lower in the ultrahigh myopia group were significantly lower than those in the mild myopia group, moderate myopia group, and high myopia group [7]. Yamada and others said that myopia is the most common eye disease in the world. The prevalence of myopia among children in East Asia and Southeast Asia, especially Singapore, Japan, Korea, Taiwan, Hongkong, and Chinese mainland, has reached 80% to 90%. The prevalence of myopia in Sydney, Europe, the United States, and Israel is also increasing by [8]. Hashemi and others believe that at this stage, myopia will lead to degenerative changes in the retina, such as thinning of the retina, reduction of the thickness of nerve fiber layer, and atrophy around the optic disc. Retinal degenerative changes in myopia are related to the decrease of retinal blood flow and vascular changes [9]. Li believes that the increase of myopia degree and the lengthening of ocular axis will cause a series of fundus complications. Among them, high myopia macular disease is the main cause affecting visual function. Its pathological changes are closely related to the thickness and density of macular retina. Early structural examination can be carried out for early diagnosis and treatment [10].

## 3. Research Methods

**3.1. Prospective Cross-Sectional Research Methods.** After admission, all patients underwent routine examinations, including vision, intraocular pressure, axial length, and slit lamp, and the basic data of all patients were counted and recorded by using a self-made patient basic data questionnaire, mainly including age, gender, contact information, home address, equivalent spherical mirror, and axial length [11]. All patients underwent OCTA test. The specific methods are

as follows: help patients take their seats and adjust their eyeballs to a reasonable position. The frequency domain system RTVue XR Avanti was purchased from an American company. Collect the microvessel density and retinal thickness in the macular region. The relevant scanning parameters are set as follows: the scanning frequency is 70 kHz, the light source is 840 nm, and the bandwidth is 45 nm. All patients are required to complete the examination scan of both eyes in the same examination [12]. The microvascular maps of the surface and deep layers of the retina were obtained by automatic stratification. The retinal thickness pattern was collected, and the scanning range was 5 mm × 5 mm, the retinal thickness in the central area of macula, above the inner ring, below the inner ring, nasal side of the inner ring, temporal side of the inner ring, and nasal side of the outer ring was calculated by automatic stratification. Outdoor activities can inhibit myopia by secreting dopamine. Wearing antiblue light glasses at night can improve sleep quality and reduce the incidence of myopia. Lutein eye patch can supplement various nutrients to protect photoreceptor cells to prevent vision decline. Atropine, photobiological goggles, and breastfeeding light instrument to thicken the choroid to improve myopia, and eye training to enhance the ability of the ciliary muscle to adjust, these methods are useful for myopia improvement. In the strategy of prevention and control of myopia, we should combine these methods to treat together, wear antiblue light glasses when facing the computer at work and apply lutein eye patch after get off work to supplement the nutrients consumed by the eyes, or photobiomodulation Repair damaged cells and thicken the choroid, participate in outdoor activities to stimulate dopamine secretion, etc., in order to maximize the deterioration of myopia, and to protect young children who have not developed high myopia more quickly. Figure 2 shows the average of children's ocular axis development, and Figure 3 shows the trend of myopia and high myopia in recent years and in the future. All patients were examined routinely, and their visual acuity, intraocular pressure, and optometry were checked. Then, the same OCTA (Cai Si OCT5000) examination was performed. The patient took the seat and adjusted the eyeball to a reasonable position. Then, the device frequency was set to 70 kHz, the wavelength was controlled at 840 nm, and then, the bandwidth was further set to 35 nm. The microvessel density pattern was controlled within 3 mm × 3 mm, scan the center of the concave sitting position in the form of a fence, scan both horizontally and vertically, and then remove the motion artifact. The time is controlled at about 2.9 s [13].

**3.2. Statistical Analysis.** SPSS 20.0 software was used to analyze all the data. The equivalent sphericity and axial level of patients with different degrees of myopia were also different. It is considered that with the continuous increase of myopia, the ocular axis expands, and the retina of myopia without fundus disease has changed accordingly, resulting in obvious changes in the above indicators. High myopia is prone to retinal detachment, hydrops, floaters, etc., and even lead to permanent blindness. Supplementing enough lutein can make the eyes have enough nutrition, which can reduce the occurrence of lesions. Tests have shown that lutein can help patients with age-related macular degeneration to improve vision. Pos-

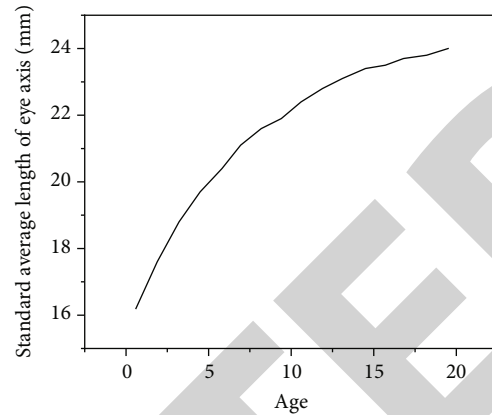


FIGURE 2: Average development of children's ocular axis.

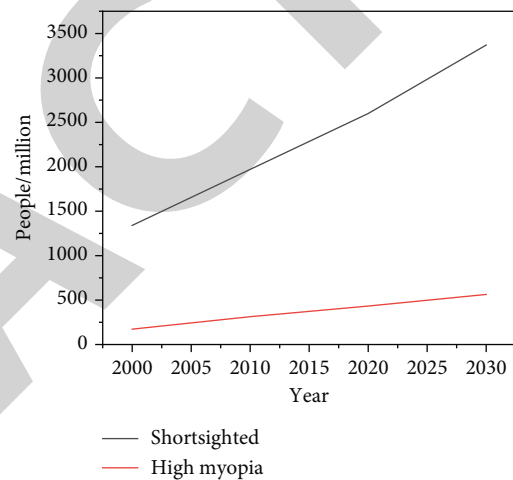


FIGURE 3: Trends of myopia and high myopia in recent years and in the future.

sibly related to altered fluid transport in the social and development jump. There is a project phone of ions and water between the social and the retinal verse equipment. The study found that in the case of recovery of emmetropia after form deprivation myopia, with thickening of the choroid, there is an area of high osmotic pressure that is in the retina during form it, but moves to the outside after vision recovery. For the choroid, shifting the location of high osmotic pressure changes the flow of them, allowing fluid from the rest to flow to the choroid, thereby thickening the choroid. Studies have explored ways of choroidal thickening and found not just one, but as many as five. Choroidal thickening can improve myopia to a certain extent, that is to say, we can improve myopia in five ways from the choroidal thickening alone. And choroidal thickening is only one of the ways to improve myopia. Myopia is a multifactor eye disease, and there are many ways to improve it. In addition to the abovementioned choroidal thickening, outdoor activities secrete dopamine, sufficient sleep every night, and high-density macular pigment, etc. have also been found to have the effect of improving myopia. There are five ways of choroidal thickening. Studies have found that atropine, OK mirror, and myopia defocusing methods may

regulate choroidal thickening in different ways, but they can all make choroidal thickening. If we use the combination therapy method, when using atropine eye drops, and also use OK lens or myopia defocus treatment, the choroidal thickening will be greater, and the effect of myopia improvement will be more obvious. In addition, the levels of microvessel density in the surface and deep layers of macula in the three groups were gradually increased [14]. This suggests that myopia is closely related to the change of microvessel density in macula, that is, with the increasing degree of myopia, the microvessel density in macula also shows a corresponding change. The author believes that the increase of myopia degree will lead to more obvious extension of ocular axis, then promote the reduction of retinal thickness, further reduce oxygen demand and blood circulation, and finally change the microvessel density in macula. Therefore, the ocular axis and retinal thickness may be important factors leading to the change of microvessel density, which should be paid attention to [15]. Figure 4 shows the decline curve of children's hyperopia reserve age. The detection of vascular parameters in the macular region of myopia by OCTA is also gradually rising, but most studies know little about the peripheral vessels in the macular region, and few studies analyze the macular blood flow parameters separately. In this study, we used a high-resolution system to quantitatively compare the density of shallow and deep capillaries and retinal thickness in the macular region of adolescents and children with different diopters and explore their correlation with diopters, in order to find the thickness in myopia adolescents and children with different diopters, and provide more clinical evidence for myopia prevention and control [16]. Figure 5 shows the effect of ocular axis extension.

**3.3. Basic Data Comparison Method.** A total of 115 adolescents and children were included. There was no significant difference in age and gender among the four groups ( $P > 0.05$ ). The SE of the four groups were  $0 \pm 0.3$ ,  $-1.7 \pm 0.6$ ,  $-4.2 \pm 0.9$ , and  $-7.7 \pm 1.5D$ , respectively ( $P < 0.001$ ). We believe that the lengthening of ocular axis may lead to the thinning of retina and the reduction of oxygen demand, resulting in the reduction of blood circulation and the decrease of vascular density. However, this study shows that with the increase of myopia, only the macular vascular density of ultrahigh myopia decreases significantly, which may be related to the small sample size of this study or the individual differences of the subjects [17]. For myopia, an eye disease with a high incidence and incurable, you may not know that it is also related to changes in choroidal thickness. The choroid is also involved in the refraction adjustment of the eyes. By increasing its own thickness, it pushes the position of the retina forward and shortens the distance between the focal plane and the retina, thereby improving the blurred image of myopia to a certain extent. Although no excellent prove in its thickness was seen in mild and moderate myopia, there was a significant difference in choroidal thickness between mild and high or very high myopia groups. The choroidal thickness was thinner in subjects with high myopia and thicker in those with low. This is consistent with previous knowledge that choroidal thickness was significantly negatively correlated with diopter. Choroidal thickening is an important indicator of myopia improvement,

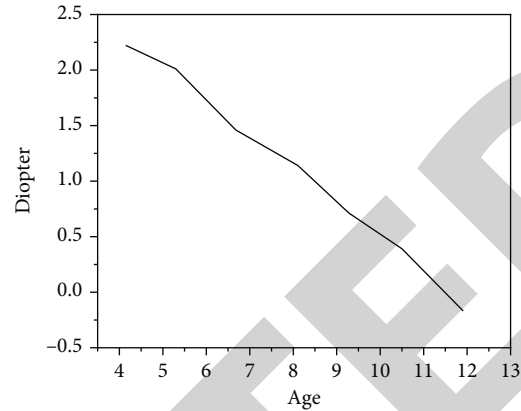


FIGURE 4: Age decline curve of hyperopia reserve in children.

so it is necessary to explore the possible causes of changes in choroidal thickness. In this study, we also found that the retinal vascular density of fovea was not correlated with the equivalent spherical mirror and the length of ocular axis, while the parafoveal vascular density was positively correlated with things. We believe that the degree of myopia increases and the eyeball gradually extends, which causes the mechanical expansion and thinning of the retina, the straightening of retinal blood vessels and the narrowing of blood vessel diameter, resulting in the reduction of blood vessel density [18]. Figure 6 shows the prevalence of myopia at different ages. Because the fovea is closely connected with the vitreous, the influence of fovea on vascular density is small. It was found that there was no proof of difference in social vascular density in different degrees of myopia. Figure 7 shows the factors that reduce retinal vascular density. It may be related to the younger age and myopia of the subjects, and the fundus changes are mainly located in the peripheral retina. Therefore, the mechanism of the effect of different myopia diopters on macular vascular density needs to be further studied [19].

## 4. Results and Analysis

In the correlation analysis of macular vascular density, retinal thickness, and diopter in adolescents and children with different myopia diopters, this study found that in general, shallow capillary density, deep capillary density, and retinal thickness were negatively correlated with myopia diopter. That is, the detection values of these three indicators decrease with the increase of myopia diopter, which is consistent. It may be due to the increase of myopia diopter, the growth of ocular axis, and the stretching of retina, so that the diameter of blood vessels decreases and the density of blood vessels decreases [20]. Choroidal thickening may be associated with increased size and number of capillary openings. The capillaries of the choroid come down to Bruch's membrane, then to the retinal pigment epithelium, and then to the photoreceptor area. When the oxygen and nutrients of the capillaries and the fluid flow out through the orifices of the blood vessels, they will be screened and passed by the blood-retinal barrier formed by Bruch's membrane and the retinal pigment epithelium, and the fluid that cannot pass through the barrier will stay in the

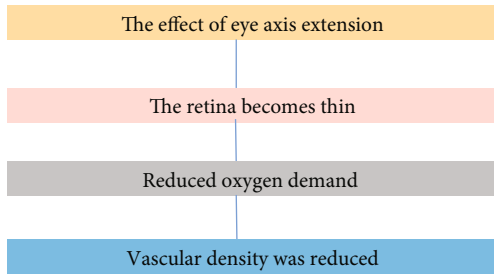


FIGURE 5: Effect of ocular axis extension.

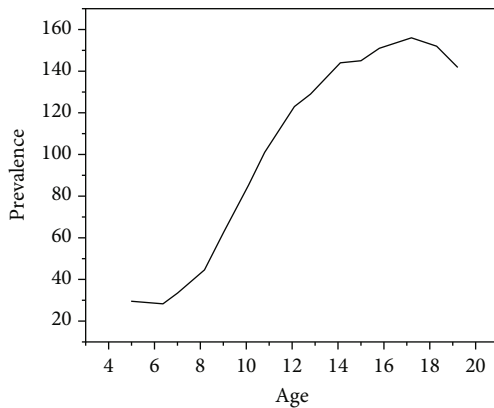


FIGURE 6: Prevalence of myopia at different ages.

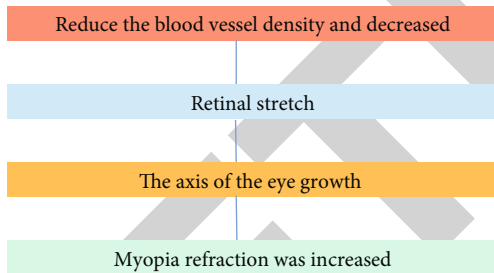


FIGURE 7: Factors reducing retinal vascular density.

lumen of the choroid. The size and number of capillaries open to determine the flow of fluid into the choroid. When the orifice is enlarged and the number of openings increases, it means that the fluid flow of the choroid will also increase, and the natural choroid will thicken. With the increase of myopia, the thickness of retina and choroid becomes thinner, while the thickness of nerve fiber layer decreases and the area of peripheral atrophy increases. To a certain extent, it can increase the risk of a series of pathological changes such as macular hemorrhage, retinal hole, retinal split, and retinal detachment, which will lead to visual loss and seriously threaten the physical and mental health of patients and their existing visual function. There were significant differences in the density of superficial capillaries in the whole macular region, inner ring, temporal side of inner ring, and nasal side ( $P = 0.033, 0.024, 0.018, 0.032$ ), and there was no significant difference in other ranges ( $P > 0.05$ ). The mechanism of this

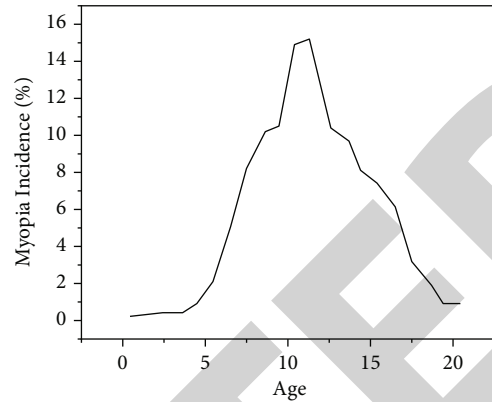


FIGURE 8: Relationship between age and incidence rate of myopia.

pathological change is not completely clear, but it is mainly closely related to the blood supply of retina and choroid. Figure 8 is a curve of the relationship between age and myopia incidence rate. As the sharpest part of vision on the retina, the macular fovea produces pathological changes, which will also lead to serious negative effects on vision [21]. Due to the limitation of cross-sectional study, the included sample size is relatively small, so it is difficult to rule out the impact of individual differences on the measurement results. It is urgent to further increase the sample size to further confirm the research results. In addition, children's eyeballs are in the period of development and growth, and the influence of age can not be ignored. Due to the limitation of sample size, there is no stratified study on age in this group. In conclusion, OCTA can be used as a noninvasive and practical imaging technology to quantitatively evaluate and find various early pathological changes related to ametropia. The discovery of these early changes provides key evidence for the prevention of early complications of the disease.

## 5. Conclusion

It should be noted that most of the previous research reports focus on the macular retinopathy of the elderly, while there are few studies on similar lesions in juvenile myopia, which is also the frontier and innovation of this study. From the results of this study, it can be seen that juvenile myopia may also affect the macular microvessel density and retinal thickness of patients. In the process of clinical diagnosis and treatment in the future, we should pay full attention to the ocular examination data of such patients, so as to prevent myopia and related complications more scientifically and objectively. With the gradual increase of myopia, a series of pathological changes will occur in the eyeball, such as the elongation of the ocular axis, the weakening of mechanical properties and the stretching and thinning of the sclera. The capillary density of the whole macular region, the inner ring and its temporal and nasal superficial layer is positively correlated with SE ( $r = 0.201, 0.201, 0.221, 0.219; P = 0.002, 0.002, 0.001, 0.001$ ), which may lead to the stretching and thinning of the retinal thickness. It is also considered that it may be related to the progressive atrophy of the retina and choroid in the macular region. When there are obvious pathological changes in the

## *Retraction*

# **Retracted: Evaluation of the Effect of Refined Nursing Intervention on Coronary CT Imaging Microscopy**

### **Scanning**

Received 20 June 2023; Accepted 20 June 2023; Published 21 June 2023

Copyright © 2023 Scanning. This is an open access article distributed under the Creative Commons Attribution License, which permits unrestricted use, distribution, and reproduction in any medium, provided the original work is properly cited.

This article has been retracted by Hindawi following an investigation undertaken by the publisher [1]. This investigation has uncovered evidence of one or more of the following indicators of systematic manipulation of the publication process:

- (1) Discrepancies in scope
- (2) Discrepancies in the description of the research reported
- (3) Discrepancies between the availability of data and the research described
- (4) Inappropriate citations
- (5) Incoherent, meaningless and/or irrelevant content included in the article
- (6) Peer-review manipulation

The presence of these indicators undermines our confidence in the integrity of the article's content and we cannot, therefore, vouch for its reliability. Please note that this notice is intended solely to alert readers that the content of this article is unreliable. We have not investigated whether authors were aware of or involved in the systematic manipulation of the publication process.

Wiley and Hindawi regrets that the usual quality checks did not identify these issues before publication and have since put additional measures in place to safeguard research integrity.

We wish to credit our own Research Integrity and Research Publishing teams and anonymous and named external researchers and research integrity experts for contributing to this investigation.

The corresponding author, as the representative of all authors, has been given the opportunity to register their

agreement or disagreement to this retraction. We have kept a record of any response received.

### **References**

- [1] T. Qian, "Evaluation of the Effect of Refined Nursing Intervention on Coronary CT Imaging Microscopy," *Scanning*, vol. 2022, Article ID 4870548, 6 pages, 2022.



## Research Article

# Evaluation of the Effect of Refined Nursing Intervention on Coronary CT Imaging Microscopy

Tao Qian 

Huashan Hospital, Fudan University, Shanghai 201100, China

Correspondence should be addressed to Tao Qian; [jsxy000139@m.fafu.edu.cn](mailto:jsxy000139@m.fafu.edu.cn)

Received 28 April 2022; Revised 20 May 2022; Accepted 26 May 2022; Published 9 June 2022

Academic Editor: Balakrishnan Nagaraj

Copyright © 2022 Tao Qian. This is an open access article distributed under the Creative Commons Attribution License, which permits unrestricted use, distribution, and reproduction in any medium, provided the original work is properly cited.

The aim is to study the benefits of using advanced medical services for coronary CT angiography. From August 2019 to August 2020, 50 patients who underwent CT angiography were selected and divided into control groups and study groups, with 25 patients in each group. The monitoring team provides basic support, and the training team provides maximum support. Experimental results showed that the positive microscopic image of the study group after the intervention was better than that of the control group, and the stress score was lower than that of the control group ( $P < 0.05$  and  $30.73 \pm 9.57$  min) and short ( $58.32 \pm 13.15$  seconds and  $53.17 \pm 11.84$  minutes) between control groups, with significant differences. The significance is ( $P < 0.05$ ). Patient care is relevant to patients with coronary CT angiography, which has been shown to improve heart rate, reduce stress, improve microscopic imaging, and provide relevant liver function tests. It is recommended to promote the show.

## 1. Introduction

With the advancement of science and technology, imaging technology has also advanced in medicine, and CT has become the most widely used form of computed tomography. The sensitivity of CT scans to medical scans from both scanner and cardiology clinics is 99%. Today, it is an important method in the diagnosis of heart disease and can be used to reduce the risk of heart disease due to its unique properties, such as reducing heart disease, changes in heart rate, differences in heart rate, changes in heart rate, and pulmonary edema. Some effective measures are needed to control the patient's breathing, and a decrease in heart rate is the most important factor in reducing the diagnosis [1]. The process of examining CT images when comparing tomography is complex and difficult, and many factors need to be determined during the scanning process, which can lead to major complications if there is an error during testing. The results of the patient's diagnosis affect the effectiveness of the patient's treatment; in most cases, the patient does not affect the timing of the disease; some procedures are difficult to access. Mind and know the concept of CT scanner, and some simple ideas are forgotten. Physicians should be available to assist and guide the patient in a CT

scan, to minimize the incidence of errors during patient examination and to improve the patient's microscopic performance pictures. Nursing staff should make preparations in advance in the process of patient inspection and cooperate with doctors to provide safety guidance for patients, and refined nursing can effectively guide patients to conduct inspections [2].

## 2. Literature Review

Kelion believes that coronary CT examination is a way of checking whether various indicators of arterial blood vessels are normal. The CT equipment in coronary CT examination generally consists of 3 parts. The first part is the scanning part, which is composed of a scanning frame, a detector, and an X-ray tube. The second part is a computer system, which systematically processes the scanned information and data and stores and calculates data. The third part is the storage system and the microscope image display system. After the data in the storage system is processed by the computer, the irradiated microscope image can be displayed on the TV screen, or the microscope image can be photographed with an organ camera and multiple cameras [3]. Henein et al. believe that, with the development of science

and technology, the number of detectors has gradually changed from the original 1 to 4800, and the capacity of the computer has become larger and the calculation speed has been accelerated, so that the imaging of the injected contrast agent in angiography is clearer and then displays, according to the microscope image, information to more clearly identify the underlying condition [4]. Christian and Loewe believe that, in coronary CT examination, the examination process is very tedious and complicated, and there are many things that patients should pay attention to before examination, and there are still many patients who are not suitable for CT examination. During the examination, the doctor should not only instruct the patient to carry out the precautions for the examination, but also the patient should perform breathing training before the examination, so that the examination results obtained are more accurate, and the examination cannot be arbitrarily moved to avoid artifacts and affect microscope image quality, so patients need a refined mode of care [5]. Schermund et al. believe that, through the detection of coronary CT images, the degree of lesions and blockages in the coronary arteries can be clearly seen [6]. Wang et al. believe that CT imaging of coronary arteries is a way to review the recovery status after treatment, and it is also a diagnostic method to check the condition of cardiovascular disease, which can provide a basis for doctors' clinical diagnosis; the refined nursing mode is based on the different conditions of each patient, in order to provide patients with a refined nursing model and formulate reasonable management plans for patients [7]. Pontone et al. believe that, in the nursing process, nursing staff must formulate a detailed nursing plan and integrate it into their daily work, do the best in every nursing link, continuously improve the quality of their work, and bring more comfortable nursing services to patients [8]. Rossi and Ferrante believe that the patient receives a sophisticated nursing mode before the examination, which can enable the patient to understand the characteristics of his disease in detail after admission, help the patient to reduce anxiety and tension, and at the same time cooperate with the treatment method to control the heart rate to ensure that the heart rate can be in a stable state. Nursing staff should also observe the patient's psychological mood, so that the patient can actively cooperate with the treatment [9]. In coronary CT angiography, the results are easily interfered by various factors, thereby reducing the accuracy. In order to this end, Zhonghua and Sun believe that it is proposed to conduct simple training on patients before the examination to make their heart rate and breathing match; in addition, medical staff provide refined nursing care to patients, such as health education and psychological guidance, which also relieves the patient's nervousness and achieves better inspection results [10]. Kay believes that, with the rapid development of modern medical devices, many CT spiral machines have been widely used in medicine. Dual-source CT is a very important, specialized, and proven method of screening patients with cardiovascular disease and is the preferred method of cardiology. Coronary CT angiography reveals changes in the function of various organs, pulmonary motility, and heart rate [11].

In the current study, the authors selected 50 patients who underwent CT angiography between August 2019 and August 2020 and selected 25 patients from the control panel and study group. Participate in patient care on the management team and learn more about patient care on the research team. X-ray performance, stress scores, duration of cardiac output, and heart rate monitoring time were compared between the two groups. The experiments showed that the microscopic image quality of the postreflection study group was better than that of the control group and that the stress was lower than that of the control group ( $P < 0.05$  and  $30.73 \pm 9.57$  min), the control panel is shorter than  $58.32 \pm 13.15$  and  $53.17 \pm 11.84$  minutes, and the difference is significant. The significance is  $P < 0.05$ .

### 3. Materials and Methods

**3.1. General Information.** In our hospital, 50 patients with diabetes were included in the study, and according to the admission criteria, 25 patients were included in the study and control group. The group consisted of 12 men and 8 women, with an average age of 36–772 ( $54.32 \pm 1.05$ ). There were 11 males and 14 females on the dashboard, with an average age of 35–773 ( $55.02 \pm 1.05$ ). The coronary arteries are shown in Figure 1. There were no significant differences in the total data of the two groups ( $P > 0.05$ ). Outcome: all patients with multiple sclerosis with symptoms of cardiovascular disease such as pain, chest pain, and palpitations [12]. All patients were physically and mentally healthy. Procedure: patients over 80 years of age, patients with heart failure, patients with arrhythmias, and patients with impaired liver function. The study was approved by the Health Council, and all patients agreed on the purpose and procedures of the study and provided information to all patients' families. It is a pleasure to participate in this study.

**3.2. Methods.** The test method is as follows: CT scan using a dual-section CT machine and two high-pressure vessels, injecting 85 ml of nonionic medium, and controlling the injection rate to 5 ml/s. After injecting another substance, 20 ml of saline solution is usually injected in the same amount. Patients were examined transversely, posteriorly, and anteriorly, with a control level of 1 cm through the trachea and main thoracic vein. The start of the stimulus was 100HU, the delay time was set to 5 s, and the scanning range was up to 2 cm from the diaphragm below the tube. The board provided general care to the patient, the radiologists helped prepare the patients for the examination, and the patients explained the diagnostic procedures and concepts [13]. The research group was given refined nursing intervention, and the main measures were as follows: (1) nursing before examination. Before the examination, the medical staff should learn about the patient's past medical history, the results of echocardiography, and the results of the electrocardiogram, closely observe the patient's breathing and heart rate, understand the contraindications of the examination, assess the risk issues that may arise during the patient examination, including drug risk, heart failure, and arrhythmia. The psychological state of the patient and whether he is

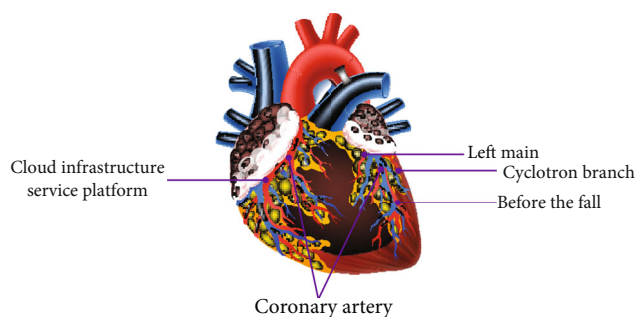


FIGURE 1: Coronary artery image.

allergic to the contrast medium should also be clarified. (2) Psychological care. Because most patients do not understand the content of coronary CT angiography, they are prone to negative emotions such as fear and tension. Nursing staff should evaluate the patient's psychological state, inform the patient in detail the examination process and precautions, and ensure that the patient understands the noninvasiveness and safety of coronary CT angiography, so as to relieve their negative psychological emotions. Nursing staff should also inform patients about the impact of respiratory rate and heart rate on test results and make sure he is at peace of mind throughout the inspection [14]. (3) Heart rate control measures. When the patient's basal heart rate is about 75 beats/min, betaloc 25 mg is given orally; for patients whose basal heart rate exceeds 85 beats/min, the dosage of betaloc is increased. During the administration period, the blood pressure changes of the patients were closely observed. If the patient's basal heart rate still did not reach the standard range, oral atenolol was given. (4) Breathing training. In the waiting area, the nursing staff instructed the patient to perform breathing exercises, the inspiratory volume was 80% of the maximum air volume, and instructed the patient to practice breathing repeatedly until the prescribed breathing frequency was mastered. During breath-holding, the patient was instructed to keep the abdomen in a stable state to prevent artifacts in the microscope image. (5) Observe the occurrence of adverse reactions. There may be a certain burning sensation after the injection of contrast agent, which is a normal physiological phenomenon [15]. Inform the patient not to worry too much, so as to ensure that the heart rate after the injection of the drug is stable. In addition, patients should be closely observed for the occurrence of adverse reactions. During the specific scan, the nursing staff observes whether the patient has abnormal reactions, and if there is an adverse reaction, the scan should be stopped immediately. (6) After the examination care. After the inspection, the nursing staff should ask the patient whether there is any discomfort and instruct the patient to observe it in the observation room for 30 minutes. If there is no adverse reaction during the period, the venous branch can be pulled out. Instruct the patient to drink plenty of water within 24 hours after the examination; in this way, the contrast agent is excreted to avoid the absorption of the contrast agent by the kidneys, causing discomfort [16].

3.3. *Evaluation Indicators.* The quality of microscope images, waiting time for examination, examination time, and radiation dose were compared between the two groups. (1) Microscope image quality evaluation criteria. The quality of microscope images was evaluated by 2 radiologists with more than 5 years of experience. Grade I: the outline of coronary vessels is clear and free of artifacts. Grade II: the outline of local blood vessels is unclear, and there are artifacts in the coronary arteries. Grade III: the contours of blood vessels are blurred or show terminals, and most of the coronary arteries are artifacts. Grades I and II are diagnostic success. (2) Waiting time for inspection: the time the patient entered the examination room from the lounge, accurate to the minute. Inspection time: the time from entering the inspection room to the completion of the inspection, accurate to minutes. Radiated dose = dose length product  $\times$  chest conversion coefficient (0.017). Comparing the excellent and good rate of imaging in patients: excellent: the trunk is clear, the diagnosis is comprehensive, and there is no artifact; good: the entire length of individual trunks is blurred, and the microscope image is slightly artifact; and poor: the diagnosis is limited, the artifact is moderate, and it cannot be used for clinical diagnosis. In addition, the SAS stress assessment and SDS stress assessment were used to measure patients' mood swings, a score of 0-100 or higher, and higher than the patient's mental health [17].

3.4. *Statistical Methods.* Data analysis was performed using SPSS22.0 statistical data, census data were analyzed by chi-square test, and measurement data were analyzed by *t* test.  $P < 0.05$  indicates the size difference [18].

## 4. Results and Discussion

4.1. *Microscope Image Quality Levels.* After intervention, the quality of microscope images in the study group was significantly better than that in the control group ( $P < 0.05$ ). See Figures 2 and 3.

4.2. *Anxiety Score.* Prior to the intervention, there was no significant difference in anxiety scores between the two groups ( $P > 0.05$ ) [19]. See Figures 4 and 5.

4.3. *Breathing Coordination Training and Heart Rate Control Time.* Respiration time and heart rate control time in the study group were  $32.14 \pm 8.22$  seconds and  $30.73 \pm 9.57$  minutes, while in the control group,  $58.32 \pm 13.15$  seconds and  $53.17 \pm 11.84$  minutes were shorter, and the difference is statistically significant ( $P < 0.05$ ) [20].

4.4. *Comparison of SAS and SDS Scores of Patients before and after Nursing.* Prior to intervention, there was no difference between SAS and SDS in patients ( $P > 0.05$ ). After intervention, the control panel and the control panel SAS and SDS were lower than the control panel ( $P < 0.05$ ). See Figures 6 and 7.

4.5. *Discussion.* Coronary CT angiography can comprehensively reflect the status of coronary obstructive lesions and malformed lesions and clarify the specific location and scope

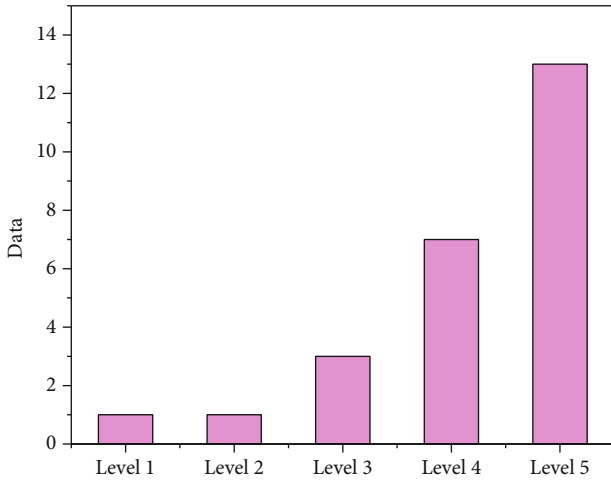


FIGURE 2: Comparison of image quality levels in the study group.

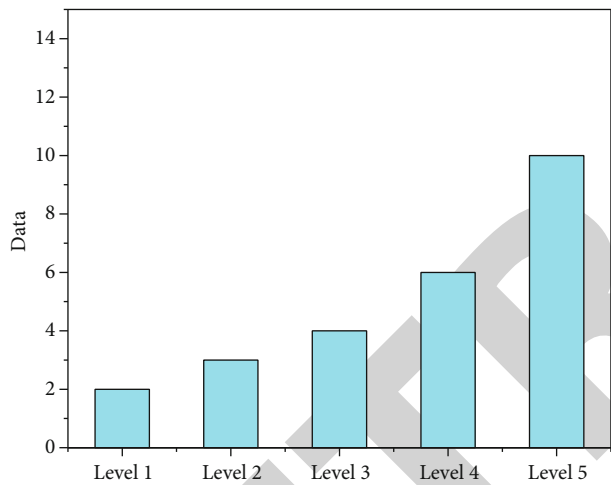


FIGURE 3: Comparison of image quality levels in the control group.

of lesions. Coronary CT angiography must be done when giving patients cardiovascular perfusion and interventional therapy, which can provide an important reference for clinical diagnosis and treatment. Coronary CT angiography has become the preferred method for diagnosing patients with coronary heart disease [21]. Refinement nursing intervention is an individualized management plan for different patients, which continuously improves and optimizes the quality of nursing, comprehensively applies the management concept to nursing intervention work, comprehensively improves the quality of nursing services, and provides high-quality nursing services for patients. Numerous studies have shown that early diagnosis and early treatment can reduce mortality from heart disease. Coronary heart disease occurs in areas with more than 70% stenosis [22]. Coronary CT angiography has been shown in many studies to be used in the early diagnosis of coronary heart disease and in some cases is recommended for use in avoidable cardiovascular ventilation in patients with abnormal or inappropriate blood vessels. CT angiography of coronary arteries has been

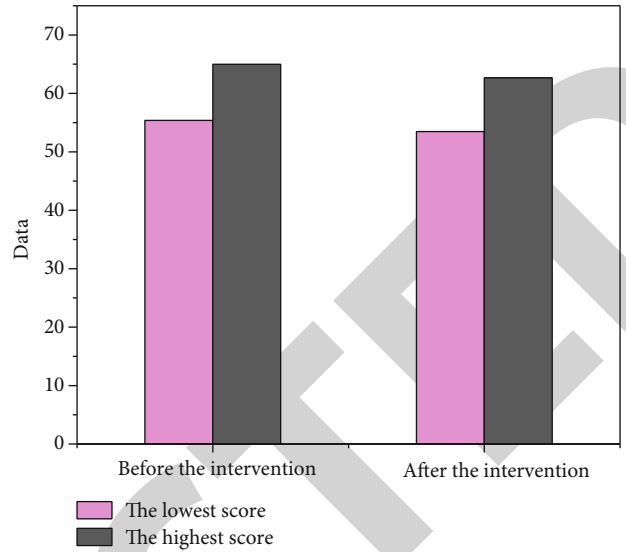


FIGURE 5: Anxiety scores in the control group before and after the intervention.

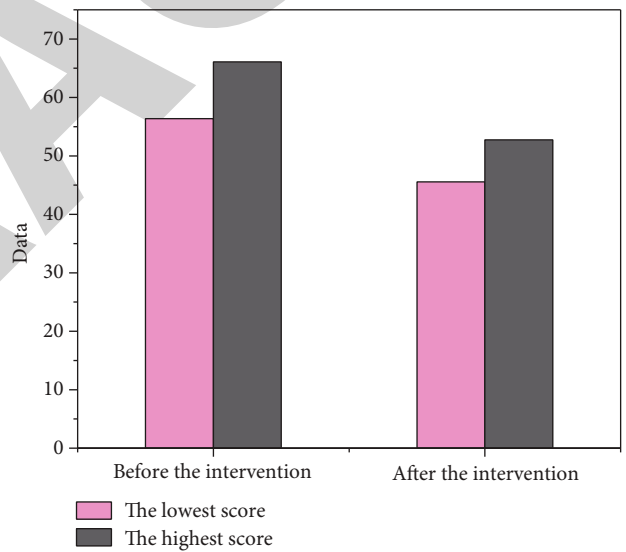


FIGURE 4: Anxiety scores of the study group before and after the intervention.

proved by a number of studies to be applicable for the preliminary diagnosis of coronary heart disease and has a high positive predictive value for moderate and severe coronary artery stenosis, which can avoid invasive angiography for some patients with normal coronary arteries or those who do not need interventional therapy [23]. The development of coronary angiography affects not only the visual and structural features but also the patient's breathing, heart rate, and heart rate during the experiment. Therefore, care should be taken when examining the patient to minimize image distortion and distortion. The results of this study showed that the performance of the emergency group was 96.36%, which was higher than that of the normal group (85.45%) ( $P < 0.05$ ), and the experiment was due to the following reasons: (1)

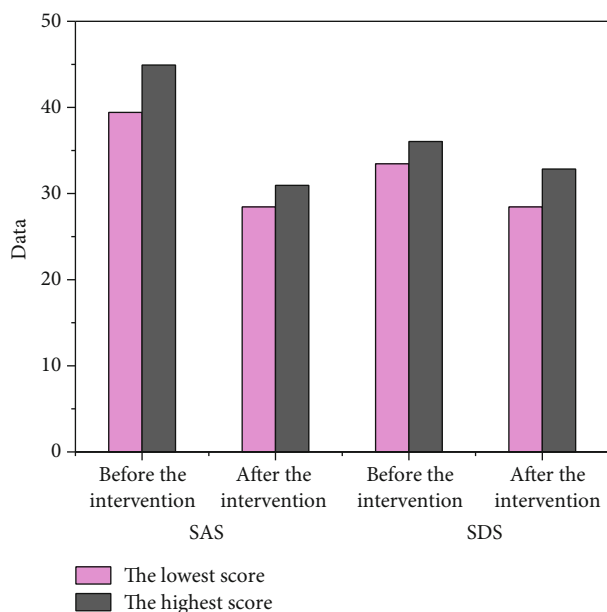


FIGURE 6: SAS and SDS score results of patients in the control group.

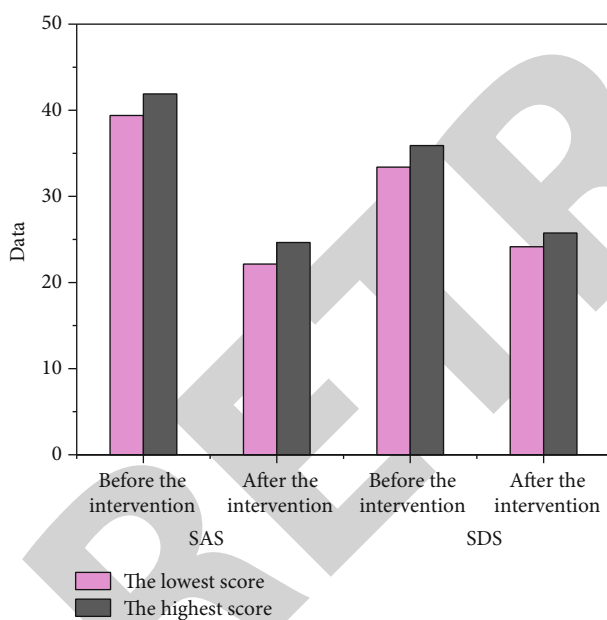


FIGURE 7: SAS and SDS score results of patients in the study group.

Before the examination, the patients in the intensive nursing group received more careful and meticulous nursing intervention, and the patients could receive detailed health education services after admission; in addition, the nurses also provide psychological care to the patients according to their different ages and personality characteristics, so as to control their nervous emotions, so that the patients' anxiety, depression, and other negative emotions can be significantly relieved, so that the patients can stay in the hours; you can quickly control your emotions during the test, maintain a more stable mental state, and shorten the waiting time

[24]. (2) Before injecting the contrast agent into the patient, store it in a 37°C incubator, which can significantly relieve the irritation to the patient during the contrast agent injection process and further shorten the waiting time for examination. (3) The patients in the intensive care group also received breathing training before the examination, which can effectively reduce the breathing range of the patients and keep their breathing stable, reduce the artifacts caused by excessive breathing amplitude, improve the success rate of microscope image diagnosis, effectively shorten the inspection time, reduce the exposure of patients to rays, and reduce the radiation dose. (4) The patient's heart rate can also be effectively controlled through refined nursing; some studies have shown that heart rate is negatively correlated with coronary imaging quality, and low heart rate is conducive to improving the quality of coronary imaging, further shortening the exposure time of patients under the radiation, and reducing the dose of X-ray radiation [25].

Coronary CT angiography can better reveal the anatomical malformation of coronary confluence in patients, which is of great significance for clinical diagnosis and treatment. The accuracy of the test results is affected by many subjective and objective factors, especially the patient's own emotions, psychology, breathing, heart rate, etc. Therefore, nursing intervention for patients, improving the patient's cooperation ability, and changing the patient's cognition have an important impact on ensuring the accuracy of the inspection results. True management is about improving the management of everyone, from the actual needs of the patient to the continuous improvement of care, with the focus on solving all aspects of the patient's problem and providing the best service. For patients, take good care. The results of this study showed that the negative attitudes of the patients in the study group were more stressful and the patient outcomes were very positive. Intensive care begins with patient care, seeks to improve and model their work, continues to improve communication between patient care and staff, and provides care to the patient [26].

## 5. Conclusion

In this study, advanced nursing measures were taken in the study group, and general nursing measures were taken in the control group. The cardiac study group was much better than the control group. This difference is statistically significant ( $P < 0.05$ ) and suggests that the use of advanced nursing interventions had a significant effect on coronary CT angiography. In conclusion, careful nursing treatment has a significant healing effect in patients with coronary CT angiography and helps to stabilize the heartbeat, relieve the patient's anxiety, and improve the quality of the microscopic image. The accuracy of clinical diagnostic results is high. It is recommended to seek advice and advertise program.

## Data Availability

The data used to support the findings of this study are available from the corresponding author upon request.

## *Retraction*

# **Retracted: The Application Value of CT Three-Dimensional Microscope Reconstruction Technology in the Diagnosis of Cervical Cancer**

### **Scanning**

Received 5 December 2023; Accepted 5 December 2023; Published 6 December 2023

Copyright © 2023 Scanning. This is an open access article distributed under the Creative Commons Attribution License, which permits unrestricted use, distribution, and reproduction in any medium, provided the original work is properly cited.

This article has been retracted by Hindawi, as publisher, following an investigation undertaken by the publisher [1]. This investigation has uncovered evidence of systematic manipulation of the publication and peer-review process. We cannot, therefore, vouch for the reliability or integrity of this article.

Please note that this notice is intended solely to alert readers that the peer-review process of this article has been compromised.

Wiley and Hindawi regret that the usual quality checks did not identify these issues before publication and have since put additional measures in place to safeguard research integrity.

We wish to credit our Research Integrity and Research Publishing teams and anonymous and named external researchers and research integrity experts for contributing to this investigation.

The corresponding author, as the representative of all authors, has been given the opportunity to register their agreement or disagreement to this retraction. We have kept a record of any response received.

### **References**

- [1] S. Sun, X. Wang, and Y. Chen, "The Application Value of CT Three-Dimensional Microscope Reconstruction Technology in the Diagnosis of Cervical Cancer," *Scanning*, vol. 2022, Article ID 5648195, 6 pages, 2022.

## Research Article

# The Application Value of CT Three-Dimensional Microscope Reconstruction Technology in the Diagnosis of Cervical Cancer

Shaoliang Sun <sup>1</sup>, Xiye Wang <sup>2</sup>, and Yanjia Chen <sup>1</sup>

<sup>1</sup>Department of Radiology, Shengzhou People's Hospital, Zhejiang 312400, China

<sup>2</sup>Department of Obstetrics and Gynecology, Shengzhou People's Hospital, Zhejiang 312400, China

Correspondence should be addressed to Shaoliang Sun; 31115213@njau.edu.cn

Received 6 May 2022; Revised 20 May 2022; Accepted 26 May 2022; Published 6 June 2022

Academic Editor: Balakrishnan Nagaraj

Copyright © 2022 Shaoliang Sun et al. This is an open access article distributed under the Creative Commons Attribution License, which permits unrestricted use, distribution, and reproduction in any medium, provided the original work is properly cited.

In order to study the application value of CT three-dimensional microscope reconstruction technology in the diagnosis of cervical cancer. In this paper, 232 patients with newly diagnosed stage IA-II A2 and some stage III C: cervical cancer (stage IB1-IIA2 of stage f go in 2009) were selected, and 204 patients with stage IB1-IIA2 of stage 2009 fig 0 were selected. The original data of DICOM were obtained by CT scanning and imported into mics10.01 software to complete lymph node reconstruction. The short diameter value > 10 mm is used as the standard to judge whether the lymph node is metastatic. Referring to the 2018fig 0 staging standard, if it indicates that the lymph node is positive, it is IIICr stage. The gold standard is the diagnosis of III CP according to the surgical and pathological results, and then the diagnostic efficiency of III C stage is evaluated. The experimental results showed that 65 cases were diagnosed as IIIC stage, and 70 cases were diagnosed as IIICp stage. There was consistency between IIICr and IIICp stage, and the kappa value was 0.340. Using CT multiphase enhanced scanning and three-dimensional reconstruction technology to diagnose cervical cancer has high detection rate and high accuracy of staging diagnosis, which is worthy of clinical application.

## 1. Introduction

Every year, there are more than 490000 new cervical cancer patients worldwide, of which the number of new cervical cancer patients in China accounts for about 30% of the total number of patients in the world. In recent years, the society has been developing continuously, people's life rhythm is quickening, the pressure of women is increasing, and the degree of sexual openness is increasing, making the incidence rate of cervical cancer increasing year by year, and the group of patients is becoming younger. Studies have shown that since 2001, the incidence of cervical cancer in my country has increased by 13.5% every year, and the mortality rate has increased by 8.1% every year. Accurately diagnosing the stage of a patient's condition can improve treatment outcomes and reduce mortality. Traditional gynecological examinations are not very effective in diagnosing cervical cancer staging [1]. Spiral CT has high accuracy and short scanning time. After three-dimensional reconstruction, the images are more vivid

and clear, and the diagnostic accuracy of various diseases is higher.

Imaging suggests that lymph node metastasis is classified as IIICr for these patients, 2021nccn guidelines do not recommend stratified treatment, and all recommend radiotherapy. Different scholars have different opinions [2]. Some scholars believe that direct surgical treatment can also be selected for young patients with lymph node metastasis (III CR) indicated by the imaging of go stage a-iiia2 in 2009. On the one hand, the purpose of the operation is to evaluate and remove the pelvic and paraaortic lymph nodes more accurately, play a role in staging and reducing the tumor load, and avoid the damage of ovarian function caused by direct radiotherapy and chemotherapy. On the other hand, through postoperative pathology, we can understand whether there are high-risk factors affecting the prognosis of patients, such as lymph node metastasis and parauterine infiltration, so as to further determine whether radiotherapy and chemotherapy and radiotherapy irradiation field are needed for individualized treatment [3]. Of course, the

difference in the prognostic effect between the two treatment regimens needs to be verified by further clinical prospective research data. Therefore, we should be cautious in the clinical diagnosis and treatment of stage III C. Considering that patients with positive lymph nodes need supplementary radiotherapy after operation, resulting in significantly increased total complications and decreased quality of life, it is very important for the treatment strategy decision and prognosis of patients with cervical cancer to further clarify the existence of lymph node metastasis through imaging before operation.

Imaging examination has important clinical significance in evaluating the accuracy of stage III C and studying the high-risk factors of lymph node metastasis. According to the clinical data of cervical cancer patients treated in O1, the application value of 3D reconstruction technology based on CT original data (Figure 1) in the MCR stage of cervical cancer was discussed, and the risk factors of cervical cancer lymph node metastasis were further analyzed. The second part of this study mainly constructs the digital three-dimensional model of in vivo lymph nodes through three-dimensional reconstruction technology, measures the short diameter and long diameter of their lymph nodes and calculates their ratio, discusses the value of different indicators to judge lymph node metastasis, and looks for a more suitable diagnostic standard for metastatic lymph nodes of cervical cancer [4].

## 2. Literature Review

Zhang et al. improved computed tomography (CT) equipment and improved image processing techniques, showing that CT can not only accurately reflect the morphological characteristics of primary cervical cancer and distant lymph node metastasis, but also reflect the pathophysiological characteristics of cervical cancer. [5]. Xiao et al. believed that the spectral CT imaging technology uses kV fast conversion technology to obtain monochromatic images of various energy units and weakens the iodine contrast through material separation technology, so that the iodine concentration can be calculated [6]. Li et al. expand the use of traditional CT scans to provide hospitals with more metrics and diagnostic tools. However, few studies have reported the application of spectral imaging in cervical cancer. The 640-line CT three-dimensional energy spectrum imaging can be completed in only two times [7]. Zhang and others found that sure exposure smart Ma technology can automatically match different kV, maintain consistent noise level, and obtain the best image quality [8]. Konarev and others believe that the combination of 3D adaptive iterative dose reduction (aidr-3d) reconstruction technology can effectively reduce the radiation dose of CT energy spectrum imaging of cervical cancer [9]. Zhang and Zhu believe that compared with conventional pelvic extraperitoneal radiotherapy, 3D-CRT and intensity-modulated radiotherapy developed in recent years can obtain the image information of lesions and adjacent normal tissues under the enhanced CT simulator and formulate the radiotherapy plan in combination with MRI, PET-CT, and other image diagnosis images [10]. Ali and

others reported that during radiotherapy for cervical cancer, before cervical and uterine body displacement, the anterior and posterior directions of cervical and uterine body displacement are the largest [11]. Zhang and others performed imaging examination under different conditions on patients with radical cervical squamous cell carcinoma through multiple CT scans. The three-dimensional spatial coordinates of the reference center point in the CT image were compared with the bone reference point, and the influencing factors of the bladder skin on the positioning of target areas such as the cervix under different bladder skin filling degrees were analyzed. It was confirmed that the deviation of cervical lesions and uterine body in the  $x$ -axis direction was the smallest, and the mobility of cervical lesions and uterine body increased with the increase of bladder skin filling [12].

## 3. Experimental Analysis

**3.1. Subjects.** Patients with cervical cancer initially diagnosed as stage ia-ii<sub>a</sub>2 and some stage III Cr (stage b1-ii<sub>a</sub>2 of FIGO staging in 2009) from January 2018 to January 2019 were selected.

### 3.1.1. Inclusion Criteria

- (1) Cervical cancer was diagnosed by pathological examination before operation. According to gynecological examination and imaging examination, the included cases were staged according to the FIGO staging standard in 2018
- (2) The initial treatment of all cases was radical hysterectomy + pelvic lymphadenectomy and abdominal paraaortic lymphadenectomy
- (3) All patients underwent whole abdominal enhanced CT scanning before operation
- (4) There was no preoperative infection and no other malignant tumor
- (5) Complete clinical and pathological data
- (6) This study obtained the consent of patients and their families and passed the review of the ethics committee of the hospital

### 3.1.2. Exclusion Criteria

- (1) Preoperative radiotherapy or chemical therapy
- (2) Vaginal cancer and other primary tumors
- (3) Incomplete clinical or pathological data
- (4) The stage was late and there was no indication of operation

**3.2. Research Methods.** In this study, the new version of FIGO staging of uterine barium cancer in 2018 was used to revise the results of gynecological examination and imaging examination of cases of uterine barium cancer in Yili in 2018. IIICr patients included in the study were cervical



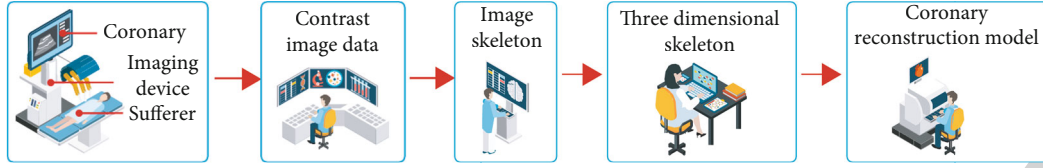


FIGURE 1: 3D reconstruction technology.

TABLE 1: Determination of IIICr and IIICp in different clinical stages.

Clinical stages	Phase III C was determined by CT examination		Stage III C was determined by operation and pathology	
	Number of cases	Percentage	Number of cases	Percentage
IB ( $n = 158$ )	54	26.8%	46	28.7%
IIA ( $n = 56$ )	20	26.5%	21	40.1%
( $n = 214$ )	56	29.4%	69	31.7%

TABLE 2: Diagnostic efficacy of CT in stage IIC at different clinical stages.

Clinical stages	Susceptibility	Specificity	Positive predictive value	Negative predictive value
IB	46.94%	7.08%	49.27%	78.95%
IIA	60.87%	75.83%	45.67%	74.29%
Total	52.87%	80.41%	73.92%	85.65%

cancer cases with the original clinical stage of I b1-II A2 [13, 14]. According to the size of lymph nodes measured by CT three-dimensional reconstruction technology, if the short diameter value is  $\geq 10$  mm, it is regarded as positive imaging lymph nodes, and the stage is IIICr stage. Because only a small number of cases have undergone abdominal paraaortic lymph node resection, IIIC stage in this study refers to the cases with positive pelvic lymph nodes. Then, according to the pathological results, whether lymph node metastasis is determined. If it is positive, it is defined as IIICp stage. In the process of clinical staging, two doctors above the level of deputy chief physician shall conduct gynecological examination to understand the general situation of cervical vagina and organs and tissues around the cervix, and then judge the focus and lymph node metastasis in combination with imaging examination to obtain the final staging.

The selection of diagnosis and treatment plan for patients with cervical cancer is based on FIGO staging and NCCN guidelines. Surgical treatment (radical hysterectomy + bilateral pelvic lymphadenectomy and abdominal paraaortic lymphadenectomy) is the main treatment. The operation shall be completed by doctors at or above the level of deputy chief physician. For stage IIICr, NCCN guidelines recommend concurrent radiotherapy and chemotherapy. However, since most of these patients are stage I A2-II A2 with or without lymph node metastasis

according to the 2009 FIGO stage, most of the previous treatment will choose surgery. Therefore, for stage III C: patients with cervical cancer (stage I B1-II A2 in 2009 FIGO stage), surgery pathological staging (- pelvic lymphadenectomy + paraaortic lymphadenectomy and sampling) can be performed before concurrent radiotherapy and chemotherapy [15].

**3.2.1. Data Import and Processing.** The DICOM raw data obtained from CT scanning is directly imported into mimics 10.01 3D reconstruction software developed by Belgian materialise company to automatically complete image (tissue) positioning, obtain different cross-sectional data required for 3D reconstruction, and realize gray value insertion according to signal strength [16].

**3.2.2. Pelvic Lymph Nodes In Vivo.** In two-dimensional CT images, pelvic lymph nodes usually show medium density circular or oval soft tissue shadow, which can be compared with surrounding fat. Anatomically, lymph nodes are mostly distributed along blood vessels and need to be distinguished from continuous arteriovenous. Import the obtained DICOM data of delay period into Mimics software; conduct operation through automatic positioning, interpolation processing, and other methods; and set the best reconstruction wide value (4-130 hu). After segmentation by using the threshold tool in the software editing tool (edit masks), draw the lymph nodes with the help of the sketching tool, and finally, calculate the reconstruction to obtain the corresponding three-dimensional model [17].

**3.3. Statistical Methods.** In this study, SPSS 18.0 software was used as the information processing tool. Measurement data should be presented as mean  $\pm$  standard deviation and count data as frequency and percentage. For age as a continuous variable, the one-sample K-S test was used to test for normality; to compare ratios between groups, the chi-square test, univariate analysis, and Mann-Whitney  $U$  test were used to analyze differences in degree data.  $P < 0.05$  indicates a statistically significant difference. Multivariate analysis ROC curves were drawn using logistic regression analysis, and the best predictors of blood SCC Ag and PLR were calculated. Using the results of lymph node analysis as the gold standard for evaluating lymph node metastasis, the sensitivity, specificity, positive predictive value, and negative predictive value of CT 3D reconstruction were calculated [18].

**3.4. Result Analysis.** 204 patients with FIGO stage b1-II A2 in 2009 were selected. The diagnosis efficiency of MC stage was evaluated by CT three-dimensional reconstruction

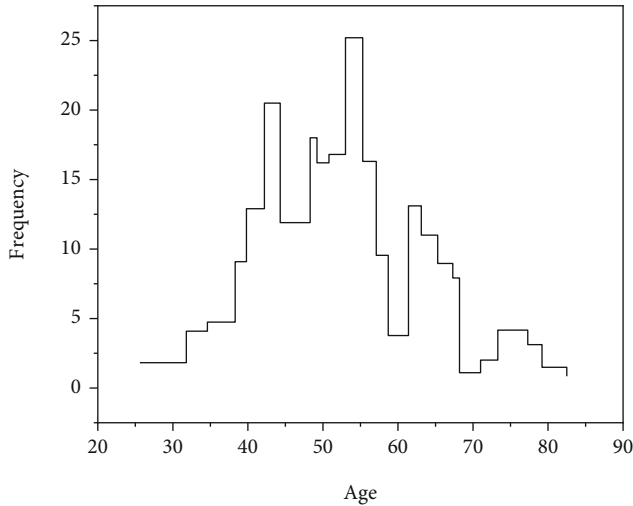


FIGURE 2: Age distribution of patients.

technology with the diagnosis of MCP as the gold standard. As shown in Table 1, 204 patients with cervical cancer underwent the construction of digital three-dimensional models of pelvic lymph nodes before treatment. It was found that 56 patients were diagnosed as stage III Cr; 60 cases of positive lymph nodes were found after operation, that is, 60 cases of stage III CP. At the same time, it is also concluded that with the increase of stage, the detection of lymph nodes by CT and pathology shows an upward trend [19].

The diagnostic effect of CT on lymph node metastasis in different clinical stages is further calculated as shown in Table 2. The CT diagnosis results of stage IIA lymph node metastasis are higher than those of stage IB, but the overall diagnostic accuracy of stage IIC is not high. The sensitivity and specificity were 52.86% and 80.56%, respectively, and the positive and negative predictive values were 56.92% and 77.85%, respectively. The results of IIICr and III CP stability studies showed that there was a correlation between CT and pathology in the diagnosis of lymph nodes, with a kappa value of 0.340. Insensitivity leads to an increased risk of misdiagnosis, i.e., stage III C indicates that a large proportion of postoperative disease is lymphadenopathy (IIICp), even if it was not diagnosed before surgery [20].

From January 2017 to January 2021, a total of 242 patients were diagnosed with cervical cancer for the first time in the Affiliated Hospital of the Third Medical University. Of these, 71 cases of pelvic lymphadenopathy were diagnosed as metastases in 29.3% (71/242). Their age distribution was 25-80 years [21], which was inconsistent with a normal distribution. As shown in Figure 2, the mean age was  $50.86 \pm 11.20$  years, and the mean age was 51 years. The Mann-Whitney  $U$  test showed that there was no significant difference in age between patients with nonmetastatic lymph nodes and those with nonmetastatic lymph nodes ( $P = 0.139$ ).

The age, FIGO stage, tumor diameter, tumor growth scheme, disease type, degree of differentiation, lymphatic invasion, interstitial invasion depth, uterine invasion, vaginal resection margin, and lymph node metastasis of 242 cervical cancer patients were statistically analyzed. Table 3 shows that FIGO stage, tumor diameter, tumor growth pro-

TABLE 3: Variable test results for pelvic lymph node metastases in cervical cancer patients.

Clinicopathological factors	Negative lymph node metastasis	Positive lymph node metastasis	$X^2/z$ value	$P$ value
Age				
≤45	52	26	2.126	0.15
>45	118	35		
Stage				
IA	25	1	-5.740	<0.001
IB	78	19		
IIA	21	14		
IIICr	26	34		

tol, disease type, degree of differentiation, lymphatic invasion, interstitial penetration depth, uterine cavity, and vaginal margin were statistically different between positive and negative lymph nodes. That is, pelvic lymph node metastasis is related to the above factors, and the  $P$  value is less than 0.05. Age was not associated with lymph node metastasis ( $P > 0.05$ ).

Statistically significant risk factors examined by univariate analysis were analyzed using multivariate logistic regression methods. The results are shown in Table 4. Finally, differentiation, lymphatic invasion, depth of interstitial invasion, and uterine invasion were independent factors affecting lymph node metastasis ( $P < 0.05$ ). Among them, parathyroid attack significantly affected lymph node metastasis (OR = 35.649, 95% confidence interval CI 4.356-291.739,  $P = 0.001$ ); the incidence of pelvic lymph node metastasis was 5.806 times higher in patients with positive vascular invasion (OR = 5.806, 95% CI: 1.373-24.557; 0.017). The risk of lymph node metastasis was 3612 times higher in patients with incomplete cervical stromal invasion than in patients with invasive stroma  $< 1/2$ ; 95% CI: 1.442-9.049; OR = 3.042, 95%, CI: 1.0-8.992. The greater the tissue difference, the lower the risk of pelvic lymph node metastasis [22, 23].

#### 4. Discussion

The status of pelvic lymph nodes is closely related to the prognosis of cervical cancer and is an important factor in the choice of treatment for cervical cancer. The 2021nccn guidelines highlight node positivity as one of the risk factors for additional postoperative radiotherapy. Therefore, in clinical practice, it is clinically important to carefully evaluate whether cervical cancer patients develop pelvic metastases before treatment, that is, the following two conditions, mainly stage IIIC. First, imaging examination showed that lymph node enlargement was diagnosed as stage IIICr, but postoperative pathology confirmed that lymph nodes were negative, because not all enlarged lymph nodes in imaging examination were true metastasis. Because the latest guidelines did not recommend stratified treatment for stage III C patients, synchronous radiotherapy and chemotherapy were recommended for all these patients, which would make

TABLE 4: Multivariate logistic regression analysis of high-risk factors for lymph node metastasis.

Factor	Partial regression coefficient	Standard error	Wald	P	OR	95% CI
Degree of differentiation						
Low differentiation	—	—	10.952	0.004	—	—
Medium differentiation	-2.168	0.918	6.225	0.006	0.082	0.014-0.456
High differentiation	-2.280	1.029	11.842	0.001	0.043	0.005-0.254

them miss the best time of surgical treatment and delay their condition; on the other hand, radiotherapy will make women of childbearing age lose ovarian function and thus lose reproductive function [24]. Second, imaging examination failed to find lymph node metastasis, but the operation showed positive lymph nodes (stage III CP). At this time, the patient needs to receive supplementary radiotherapy. This unnecessary lymph node dissection and radiotherapy will increase the total complications, such as lower limb lymphedema and pelvic lymph cyst with infection, and reduce the quality of life. Therefore, if we can judge whether lymph node metastasis is more accurate through imaging examination before treatment and improve the accuracy of stage III CX diagnosis, the prognosis of cervical cancer patients will be greatly improved.

At present, the conventional imaging methods used to predict cervical cancer lymph node metastasis include CT and MRI, which mainly rely on the short axis diameter of lymph nodes > lomm as the diagnostic standard. However, considering that cancer cell infiltration and reactive proliferation can lead to, the traditional imaging methods can not make accurate judgment, and their diagnostic value is medium. Therefore, some studies have confirmed that the size of lymph nodes combined with some imaging features, such as irregular shape or adhesion with surrounding tissues, ring enhancement after enhancement.

Cervical cancer is the second-largest female reproductive system malignancy after breast cancer. Patients with this disease account for 1/8 of all women with malignant tumors. Early determination of the condition of patients with cervical cancer and FIGO staging will help doctors to formulate an appropriate treatment plan as soon as possible and improve the effect of treatment. In the past, FIGO staging mainly depended on the subjective judgment of doctors, which required doctors to have solid theoretical knowledge and rich clinical experience. With the wide application of spiral CT in clinic, the results of multiphase enhanced spiral CT scanning and three-dimensional reconstruction technology have become an important basis for staging diagnosis of cervical cancer. The coincidence rate between the results of CT examination and pathological examination in these patients is high. When using spiral CT to examine patients with cervical cancer, the diameter of their lymph nodes can be measured on the cross-section, and then, the shape and location of lymph nodes can be reconstructed [25]. However, when this method is used to examine patients with cervical cancer, it has poor ability to distinguish the internal structure of lymph nodes and low sensitivity to lymph nodes with metastasis but small volume, especially lymph nodes with a diameter of less than 10 mm. This will make the diag-

nosis false positive or false negative. The detection rate and staging accuracy of these patients using spiral CT multiphase enhanced scanning and three-dimensional reconstruction technology are significantly higher than those using B-ultrasound. This is consistent with the results of relevant studies. It can be seen that the detection rate of cervical cancer diagnosed by spiral CT multiphase enhanced scanning and three-dimensional reconstruction technology is high, which is worthy of clinical application.

## 5. Conclusion

This study measured and analyzed the diameter of the three-dimensional model of pelvic lymph nodes. It was found that if the shortest diameter of lymph nodes  $\geq 6.47$  mm was used as the standard to judge the lymph node metastasis of cervical cancer, the diagnostic efficiency was improved, the sensitivity was 0.892, the specificity was 0.686, and the yoden index was 0.578. In order to make up for the deficiency of judging whether the lymph node is metastatic only by the short diameter value in clinical work, this study also combined the morphological standard of short length diameter ratio to comprehensively judge the metastatic lymph node. The normal lymph nodes without metastasis are long oval, and their short/long diameter ratio will be less than 0.5. The difference is that the abnormal positive lymph nodes tend to be spherical or irregular, and their short long diameter ratio is more than 0.5. With the help of digital three-dimensional reconstruction technology to reconstruct the three-dimensional model of pelvic lymph nodes, and accurately measure the relevant anatomical parameters, it is preliminarily concluded that taking the shortest diameter of lymph nodes  $\geq 6.47$  mm and the ratio of short to long diameter  $\geq 0.57$  as the diagnostic criteria, it has a certain reference value to judge lymph node metastasis.

This study selects the case study of our unit, which has selective bias on the selection of research objects. The small sample size has certain limitations on the research results. In this study, the diagnostic efficiency of three-dimensional reconstruction technology is moderate. The reason may be that the research department is retrospective study, the imaging equipment lacks advanced nature, and only the lymph node short diameter > 10 mm is the diagnostic standard. It cannot make correct judgment for normal size lymph nodes and lead to an increase in missed diagnosis rate. In addition, it is necessary to further combine other imaging features of lymph nodes, such as edge and enhancement, to improve the accuracy of diagnosis.

## Retraction

# Retracted: Application of CT Ultrasonography Combined with Microscopic Intraperitoneal Hyperthermic Perfusion Chemotherapy in Postoperative Treatment of Oocyst Carcinoma

### Scanning

Received 20 June 2023; Accepted 20 June 2023; Published 21 June 2023

Copyright © 2023 Scanning. This is an open access article distributed under the Creative Commons Attribution License, which permits unrestricted use, distribution, and reproduction in any medium, provided the original work is properly cited.

This article has been retracted by Hindawi following an investigation undertaken by the publisher [1]. This investigation has uncovered evidence of one or more of the following indicators of systematic manipulation of the publication process:

- (1) Discrepancies in scope
- (2) Discrepancies in the description of the research reported
- (3) Discrepancies between the availability of data and the research described
- (4) Inappropriate citations
- (5) Incoherent, meaningless and/or irrelevant content included in the article
- (6) Peer-review manipulation

The presence of these indicators undermines our confidence in the integrity of the article's content and we cannot, therefore, vouch for its reliability. Please note that this notice is intended solely to alert readers that the content of this article is unreliable. We have not investigated whether authors were aware of or involved in the systematic manipulation of the publication process.

In addition, our investigation has also shown that one or more of the following human-subject reporting requirements has not been met in this article: ethical approval by an Institutional Review Board (IRB) committee or equivalent, patient/participant consent to participate, and/or agreement to publish patient/participant details (where relevant).

Wiley and Hindawi regrets that the usual quality checks did not identify these issues before publication and have since put additional measures in place to safeguard research integrity.

We wish to credit our own Research Integrity and Research Publishing teams and anonymous and named external researchers and research integrity experts for contributing to this investigation.

The corresponding author, as the representative of all authors, has been given the opportunity to register their agreement or disagreement to this retraction. We have kept a record of any response received.

### References

- [1] Z. Xia and H. Jin, "Application of CT Ultrasonography Combined with Microscopic Intraperitoneal Hyperthermic Perfusion Chemotherapy in Postoperative Treatment of Oocyst Carcinoma," *Scanning*, vol. 2022, Article ID 5444552, 6 pages, 2022.

## Research Article

# Application of CT Ultrasonography Combined with Microscopic Intraperitoneal Hyperthermic Perfusion Chemotherapy in Postoperative Treatment of Oocyst Carcinoma

Zongbao Xia <sup>1</sup> and Hong Jin <sup>2</sup>

<sup>1</sup>Department of Gynecology, Jingmen First people's Hospital, Jingmen, Hubei 448000, China

<sup>2</sup>Department of Ultrasound, Jingmen First people's Hospital, Jingmen, Hubei 448000, China

Correspondence should be addressed to Hong Jin; 18291050228@stu.suse.edu.cn

Received 28 April 2022; Revised 14 May 2022; Accepted 23 May 2022; Published 6 June 2022

Academic Editor: Balakrishnan Nagaraj

Copyright © 2022 Zongbao Xia and Hong Jin. This is an open access article distributed under the Creative Commons Attribution License, which permits unrestricted use, distribution, and reproduction in any medium, provided the original work is properly cited.

For the postoperative treatment of oocyte carcinoma, CT and CT ultrasonography combined with microscopic intraperitoneal should be combined with peritoneal heat perfusion chemotherapy. The authors selected 50 patients who received treatment for ovarian cancer from 2017 to 2018 and divided them into two groups (observation group, 30 cases, control group, 20 cases). Cisplatin, associated with peritoneal hyperthermia, led the control group, and we monitored all patients for 1 year and provided clinical trials, lifestyle, and results for both disease group. The experimental results showed that the target reduction rate of the control group was 70%, while that of the control group was only 40%, lower than that of the control group  $P < 0.05$ . The life expectancy of the control group was higher than that of the control group,  $P < 0.05$ . Nausea, vomiting, diarrhea, bone marrow compression, and constipation in the study group were slightly higher than those in the control group (35%), but there was no significant difference between the two groups ( $P > 0.05$ ). Chemotherapy combined with intraperitoneal infusion of loplatin has no side effects, helps improve survival, and can be used in a variety of clinical trials.

## 1. Introduction

Disease and mortality rates were higher than and lower than for uterine and endometrial cancers. The disease poses a serious threat to the physical and mental health of countless women. According to statistics, 295,000 new cases of ovarian cancer are reported worldwide each year, and about 185,000 people die from ovarian cancer. In 2018, the American journal CA published statistics on ovarian cancer. In 2019, 23,000 new cases and 15,000 deaths are expected nationwide. Over the past 10 years, the incidence of ovarian cancer in Mongolia has increased by 30 percent and the death rate by 18 percent. Recent statistics show that the incidence of ovarian cancer is high, and monitoring the development of ovarian cancer and improving treatment is of great significance to support women's lives, physical health, and social development [1]. There are many types of ovarian cancer, of which above skin cancer is the most common, accounting

for more than 70 percent of all ovarian cancers. Ovarian cancer is unique in that there are no specific symptoms in the early stages of the disease, and 70-80% of patients miss the best time to seek treatment to advance to a higher level. Ovarian cancer is associated with chronic metastasis. There is no good treatment. The 5-year survival rate is 20%~30%. Ovarian death is the leading cause of death in women. Therapy has become a hot topic in the research community, especially when it comes to ovarian cancer [2].

The main feature of advanced ovarian cancer is tumor metastasis, and the main route of metastasis is in the pelvis and abdomen, which makes the cancer cells difficult to control, and the survival rate of patients is low. Many researchers seek to study ways to control disease progression and prolong patients' lives. With the development of medical devices, CRS has become an important part of the treatment of ovarian cancer, eliminating as much pelvic and abdominal cancer as possible, reducing the residual tumor

diameter to less than 1 cm, and even eliminating macroscopic cancer cell damage. Although CRS can maximize the increased risk of injury in ovarian cancer patients, the combination of CRS-based systemic chemotherapy in ovarian cancer patients can improve the treatment effect of ovarian cancer patients [3]. However, due to the limited penetration of chemotherapy drugs into the meridians of the whole body, the ability to kill cancer cells in the peritoneal cavity is not strong, so after systemic chemotherapy, tumor lesions and cancer cells may remain in the peritoneal cavity. Patients with severe ascites associated with an increased risk of postoperative cancer recurrence are affected by combined treatment outcomes, and long-term survival remains suboptimal. The effectiveness of local abdominal therapy (Figure 1) is closely related to the prognosis of advanced ovarian cancer. Therefore, optimizing local peritoneal therapy and controlling ascites is an effective way to improve the therapeutic effect of ovarian cancer [4].

## 2. Literature Review

Lee et al.'s study, ovarian cancer is considered one of the three most common cancers in pregnant women. Ovarian cancer cannot be diagnosed early and often develops because of the location of the ovaries and the absence of specific symptoms early on. In the absence of effective treatment for heart disease, death can affect a woman's quality of life and well-being [5]. In Kim et al.'s study, CRS and systemic platinum and paclitaxel chemotherapy improve prognosis and survival in ovarian cancer patients but are currently accepted as adjuvant therapy for advanced ovarian cancer surgery. Despite the use of paclitaxel-based intravenous chemotherapy, the long-term survival of ovarian cancer patients after this procedure remains poor, and most ovarian cancer patients eventually die of recurrence [6]. In Alberti et al.'s study, the main approach to ovarian cancer metastasis is considered to be the removal of implants on various organ surfaces in the abdominal cavity, wide-abdominal implants, residual disease at the site of metastatic implantation, and free cancer cells, which focuses on improving the treatment outcomes of advanced ovarian cancer [7]. In Hu et al.'s study, drugs are not considered to be fully effective because sunlight and peritoneal occlusion inhibit the spread of anti-cancer chemotherapeutic drugs to the cancer, resulting in reduced effective concentrations of chemotherapeutic drugs reaching tumor tissue. The remnants of the metastatic implantation site help repair damage and destroy cancer-free cells [8]. Intraperitoneal hyperthermia, studied by Gray and Haworth, has been shown to improve ascites control and quality of life in patients with epithelial ovarian cancer [9]. In Yiu et al.'s study, intravenous chemotherapy with paclitaxel has been shown to combine cisplatin with peritoneal hyperthermia, and the treatment of ovarian cancer may extend disease-free life. Therefore, it can be concluded that intraperitoneal hyperthermic perfusion therapy for ovarian cancer helps control ascites, destroys pelvic peritoneal cancer cells, and significantly improves the effect of destroying cancer cells [10]. Therefore, Matrone et al. suggest that localized cancers are more accessible to chemother-

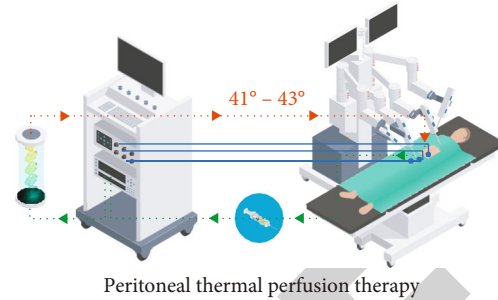


FIGURE 1: Intraperitoneal hyperthermic perfusion chemotherapy.

TABLE 1: Comparison of treatment between the two groups ( $n = 20$ , cases/%).

Group	CR	PR	SD	PD	Objective response rate
Observation group	2	11	6	1	69.0
Control group	0	7	7	4	3.0

apeutic drugs if the drugs can be injected directly into the abdomen, which is an effective treatment to improve the effect of advanced peritoneal therapy and cancer metastasis [11]. In Wang's study, CRS combined with intraperitoneal hyperthermic perfusion therapy is more serious after 7 to 10 days, the main reason is that the body temperature changes greatly when the body's stress response is severe due to intraperitoneal perfusion therapy. This increases the incidence of adverse reactions and their complications [12]. Horry et al. have shown that peritoneal hyperthermia is effective in the treatment of peritoneal hyperthermia because it effectively eliminates symptoms of ovarian cancer, prolongs patient survival, improves patient quality of life, and reduces complications and adverse reactions. This is considered the best treatment for ovarian cancer [13].

## 3. Experimental Analysis

**3.1. Experimental Subjects.** There were 50 inpatients with ovarian cancer in our hospital from 2017 to 2018, and 20-30 patients were randomly examined. In the control group, there were 11 cases of cystadenocarcinoma, 6 cases of mucositis, and 4 cases of lymphoma. According to FIGO staging procedure, there were 3 cases of endometrial leukemia, 10 cases of stage III, and 10 cases of stage IV [14]. The age group was 45-669 years old, and the mean age was  $53.5 \pm 38$  years old. The pathological group included plasma cystadenocarcinoma, mucous membrane carcinoma, lymphocytic carcinoma, and endometrioid carcinoma 8, 6, 5, and 3. Under the Fi-Go programme, 10 cases were registered in phase III and 8 in phase IV. There were no differences in age, type of disease, or level of treatment between the control groups.  $P > 0.05$  can be compared [15, 16].

### 3.2. Experimental Method

**3.2.1. Included and Excluded Procedures.** Selection criteria were as follows: (1) All patients were diagnosed with ovarian cancer by postoperative pathology, imaging, and gynecological

TABLE 2: The adverse reactions between the two groups were compared ( $n = 30, \%$ ).

Group	Feel sick and vomit	Diarrhea	Constipate	Myelosuppression	Incidence
Observation group	3	1	3	2	34.0
Control group	2	2	1	1	31.0

examination; (2) the age of the patients was over 45 years old; and (3) the patients should voluntarily cooperate with the research activities and sign the informed consent. Inclusion criteria were as follows: (1) Patients with severe heart, brain, liver, renal failure, or other cancers; (2) patients with contraindications to surgery; (3) patients with mental illness or cognitive impairment; (4) not signed patients who do not cooperate with the consent form for research activities specified in this guideline; and (5) patients diagnosed with stage I and II ovarian cancer [17].

**3.2.2. Treatment.** Patients in the control group were given carboplatin AUC (100 mg) and combined injection of 135 mg/m<sup>2</sup> paclitaxel (30 mg), once every three days. Patients were treated once a week for up to six hours. The control group was provided with chemotherapy and carboplatin AUC administration (100 mg) combined with 135 mg/m<sup>2</sup> paclitaxel (30 mg) intravenous infusion. Patients were treated once for 3 weeks and continued for 6 times as a course of treatment. Patients were directly assisted with chemotherapy (same below). On this basis, patients in the observation group were treated with cisplatin intraperitoneal thermal perfusion. On the first day of intraperitoneal perfusion chemotherapy, paclitaxel was intravenously injected, and 75 mg/m<sup>2</sup> cisplatin (20 mg) was intraperitoneally injected on the second day for continuous treatment [18]. Paclitaxel was reapplied on day 8. If the patient had ascites, abdominal heat infusion should be started only after ascites had been drained.

**3.2.3. Observation Indicators.** The clinical effects of the two groups of patients were compared: complete remission in CR means that the patient's injury has disappeared for more than 1 month; PR partial remission means that the patient's injury has been significantly eliminated; stable SD injury indicates that the patient's injury still exists; and PD lesions indicate that these conditions are in treatment and were not satisfied. The staff of our hospital followed up the patients for one year, accurately recorded the survival time and side effects of the two groups of patients, and used the Karnofsky scale to evaluate patients' higher quality of life [19, 20].

**3.3. Statistical Methods.** Statistical analysis was performed by SPSS 20.0 software. The number of data was expressed as  $n$  and %, and the measured data was expressed as the mean standard deviation of brothers, based on which  $T$  tests were performed.  $P < 0.01$  indicated statistically significant difference.

**3.4. Analysis of Results.** As shown in Table 1, the target response rate was 70% higher in the control group,  $\chi^2 = 4.8$ , and  $P < 0.05$ .

TABLE 3: Comparison of survival between the two groups [ $n(\%)$ ].

Group	Example number	Survival in 1 year	2 years of survival
The research group	34	31	28
Anchoring group	34	24	19
$\chi^2$		4.660	5.581
$P$		0.031	0.018

As shown in Table 2, the mean values of negative results were similar between the two groups, there was no significant difference between the two groups,  $\chi^2 = 0.265$ , and  $P > 0.05$ .

The mean 1-year and 2-year life expectancy of the experimental group was 91.18% and 82.35%, respectively, higher than that of the control group (70.59% and 55.88%,  $P < 0.05$ ) (see Table 3).

The incidence of adverse events in the study group was 28.57%. Negative cases accounted for 25% in the user group, and there was no significant difference ( $P > 0.05$ ) (see Table 4).

The PFS of control group and control group were  $(9.59 \pm 6.50)$  months and  $(9.30 \pm 4.38)$  months, respectively. As shown in Figure 2, there was no significant difference between the control panels in terms of PFS and operating system ( $P > 0.05$ ).

## 4. Discussion

Surgical resection is very common in the treatment of ovarian cancer and has also been found in long-term clinical practice. However, in ovarian cancer patients, surgery may achieve some therapeutic effect, but it is not possible to completely eliminate the cancer. There are still many patients with tissue, lymph nodes, and postoperative recurrence [21]. Therefore, ovarian cancer patients should undergo surgical removal of the ovaries with appropriate chemical and physical methods as adjuvant therapy. In the past, clinicians administered intravenous chemotherapy to patients, but this treatment is prone to adverse consequences, resulting in patient intolerance, serious decline in patient compliance, and many patients abandoning treatment. With the continuous development and application of medical technology, more and more doctors are researching and using peritoneal chemotherapy, making full use of long-term care and high-concentration local drugs to chemotherapy patients. Direct contact with the injured part of the patient reduces the risk of adverse patient reactions and

TABLE 4: Comparison of the incidence of adverse events between the two groups [ $n(\%)$ ].

Group	Diarrhea	Bone marrow transplant	Nausea and vomiting	Astriction	Total incidence
The research group	1	3	3	2	27.56%
Anchoring group	2	2	1	2	24.00%

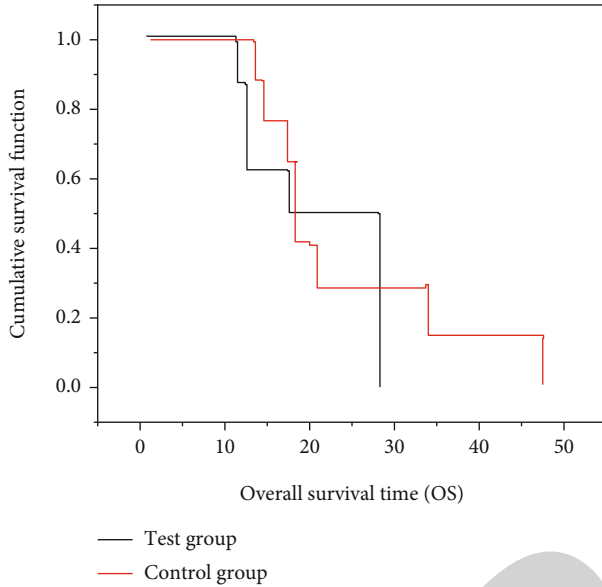


FIGURE 2: Kaplan-Meier survival curve was used to compare the overall survival rates between the two groups.

ensures high safety. Some scholars have shown in the results of their research reports the use of hyperthermia that can kill tumor cells in patients, so the combined application of hyperthermia and chemotherapy for tumor patients can help to enhance the effect of treatment, control the patient's lesions, and further reduce the volume of the lesions, it has a very important application value for the treatment and recovery of patients [22, 23].

The incidence of ovarian cancer has hidden characteristics, and the disease will spread and metastasize to the abdominal cavity in the early stage, and at the time of diagnosis, it has generally developed to the middle and late stages, and most of them are treated with chemotherapy. Ovarian cancer is highly malignant and has a low cure rate, and in clinical practice, comprehensive surgical treatment is mainly used, but surgery cannot completely stop the seeding and dissemination of intra-abdominal cancer cells, so the postoperative recurrence rate is high. Chemotherapy cannot have a good inhibitory effect on tumor proliferation and implantation and cannot reduce ascites [24]. The main spread of ovarian cancer is to spread to adjacent organs or implant in the parietal and visceral peritoneal surfaces. Therefore, the direct infusion of chemotherapeutic drugs can effectively increase the local drug concentration and improve the ability to kill tumors. Paclitaxel and cisplatin are the most commonly used chemotherapy regimens in clinical practice, and paclitaxel is a cell cycle-specific drug that can effectively accelerate the polymerization of tubulin

and inhibit its depolymerization, thereby affecting tumor proliferation. Cisplatin is the first-generation platinum preparation and is the most widely used drug in intraperitoneal hyperthermia. Through intraperitoneal hyperthermic perfusion of cisplatin, free cancer cells in the abdominal cavity can be killed and eliminated, and the rate of liver metastasis and postoperative recurrence can be reduced. At the same time, because the drug does not directly enter the body's circulation, there is less damage to the kidneys and a lower incidence of adverse reactions in the digestive tract. Since the new blood vessels in the tumor do not respond to heat, when the temperature reaches  $>40^{\circ}\text{C}$ , the cancer cells will gradually die, and the critical temperature of general tissues is about  $45.7\text{-}47.0^{\circ}\text{C}$ . Therefore, hyperthermic perfusion therapy can effectively stimulate the body's immunity and achieve the effect of antitumor. Hyperthermic perfusion chemotherapy can improve the internal blood supply of the body and accelerates the accumulation and response of chemotherapy drugs and reversal of drug resistance in ovarian cancer cells. Elevated temperature can also make cancer cells generate nitric oxide (NO), increase cytotoxicity, and enhance the expression of some genes under the action of cisplatin [25].

## 5. Conclusion

Ovarian cancer is the most common cause of the disease, but it spreads early without any symptoms and is usually diagnosed in the secondary and later stages of the cancer. Currently, cancer treatment is relatively low, surgery is an important choice, but does not affect the spread of breast cancer, and surgery cure rate is very high. Postoperative chemotherapy is therapeutic, but inhibition is unclear. Increasing the local concentration of loplatin is more effective in stopping the spread of cancer because loplatin penetrates the abdominal cavity, circulates directly into the gastrointestinal tract, and improves the ability to fight cancer. In this study, patients in the user group received the same treatment and patients in the study group received abdominal hyperthermia. The incidence of adverse events and subsequent survival was compared between the two groups. The results showed that the incidence of adverse events was 28.57%. The incidence of adverse events in control group was 25%, and there was no significant difference ( $P > 0.05$ ) and ( $P < 0.05$ ). In conclusion, loplatin combined with peritoneal hyperthermia in the treatment of ovarian cancer will not cause adverse reactions compared with physicians but also play an important role in improving the quality of life and survival rate of patients and general treatment.

At present, studies have found that the application of intraperitoneal hyperthermic perfusion and basic chemotherapy



has application advantages, but there are few relevant research data, and there is a lack of application research on tumor cytoreduction combined with intraperitoneal hyperthermic perfusion chemotherapy. Ovarian cancer treatment is feasible. Based on the current research status analysis, cytoreductive surgery combined with intraperitoneal hyperthermic perfusion chemotherapy will become a hot topic in future research. Research and analysis on this can achieve breakthrough research results and provide a reference for the clinical treatment of advanced ovarian cancer.

## Data Availability

The data used to support the findings of this study are available from the corresponding author upon request.

## Conflicts of Interest

The authors declare that they have no conflicts of interest.

## Acknowledgments

This study was supported by the Clinical Application of Ovarian Cancer in Intraperitoneal Thermal Perfusion Chemotherapy Jingmen General Science and Technology Project 2019yfyb034.

## References

- [1] N. Laplace, V. Kepenekian, A. Friggeri, O. Vassal, and N. Bakrin, "Sodium thiosulfate protects from renal impairment following hyperthermic intraperitoneal chemotherapy (hipec) with cisplatin," *International Journal of Hyperthermia*, vol. 37, no. 1, pp. 897–902, 2020.
- [2] W. Zhang, J. Li, and S. Yang, "Real-time interleaved photoacoustic and ultrasound imaging for guiding interventional procedures," *Applied Acoustics*, vol. 156, pp. 1–6, 2019.
- [3] L. Demi, M. Demi, R. Prediletto, and G. Soldati, "Real-time multi-frequency ultrasound imaging for quantitative lung ultrasound - first clinical results," *The Journal of the Acoustical Society of America*, vol. 148, no. 2, pp. 998–1006, 2020.
- [4] H. Yoon and S. Y. Emelianov, "Combined multiwavelength photoacoustic and plane-wave ultrasound imaging for probing dynamic phase-change contrast agents," *IEEE Transactions on Biomedical Engineering*, vol. 66, no. 2, pp. 595–598, 2019.
- [5] S. Li, S. Mi, R. Guo, X. Ma, and M. Han, "Application of ultrasound fusion imaging technique for unilateral percutaneous vertebroplasty in treatment of osteoporotic thoracolumbar compression fracture," *Journal of X-Ray Science and Technology*, vol. 28, no. 5, pp. 171–183, 2020.
- [6] B. H. Kim, V. Kumar, A. Alizad, and M. Fatemi, "Gap-filling method for suppressing grating lobes in ultrasound imaging: theory and simulation results," *The Journal of the Acoustical Society of America*, vol. 145, no. 3, pp. EL236–EL242, 2019.
- [7] G. S. Alberti, H. Ammari, F. Romero, and T. Wintz, "Dynamic spike superresolution and applications to ultrafast ultrasound imaging," *SIAM Journal on Imaging Sciences*, vol. 12, no. 3, pp. 1501–1527, 2019.
- [8] R. Hu, Q. Zeng, X. Su, W. Feng, and H. Xiang, "The correlation between targeted contrast-enhanced ultrasound imaging and tumor neovascularization of ovarian cancer xenografts in nude mice," *Journal of Healthcare Engineering*, vol. 2021, no. 1, Article ID 5553649, 13 pages, 2021.
- [9] M. Gray and K. J. Haworth, "Advances in ultrasound imaging: passive cavitation imaging/mapping," *The Journal of the Acoustical Society of America*, vol. 149, no. 4, pp. A91–A91, 2021.
- [10] B. Y. Yiu, A. J. Chee, and A. C. Yu, "GPU technology in the high frame rate ultrasound imaging era," *The Journal of the Acoustical Society of America*, vol. 146, no. 4, pp. 2860–2860, 2019.
- [11] G. Matrone and A. Ramalli, "Filtered delay multiply and sum beamforming in high frame-rate ultrasound imaging," *The Journal of the Acoustical Society of America*, vol. 146, no. 4, pp. 2860–2860, 2019.
- [12] B. Wang, "Diagnosis of waist muscle injury after exercise based on high-frequency ultrasound image," *Journal of Healthcare Engineering*, vol. 2021, no. 8, Article ID 5528309, 10 pages, 2021.
- [13] M. J. Horry, S. Chakraborty, M. Paul, A. Ulhaq, and N. Shukla, "Covid-19 detection through transfer learning using multimodal imaging data," *IEEE Access*, vol. 8, pp. 149808–149824, 2020.
- [14] L. Deng, A. Hughes, and K. Hynynen, "A noninvasive ultrasound resonance method for detecting skull induced Phase Shifts may provide a signal for adaptive focusing," *IEEE Transactions on Biomedical Engineering*, vol. 67, no. 9, pp. 2628–2637, 2020.
- [15] J. Liu, T. Lei, and F. Wu, "Evaluation of severity of infectious pneumonia for newborn using ultrasound image under adaptive image denoising algorithm," *Scientific Programming*, vol. 2021, no. 11, Article ID 6191448, 7 pages, 2021.
- [16] M. C. Ba, H. Long, X. L. Zhang, Y. F. Gong, and S. Z. Cui, "Laparoscopic hyperthermic intraperitoneal perfusion chemotherapy for patients with malignant ascites secondary to unresectable gastric cancer," *Surgical Laparoscopy, Endoscopy & Percutaneous Techniques*, vol. 30, no. 1, pp. 55–61, 2020.
- [17] W. Graf and H. Birgisson, "ASO author reflections: can patient selection for cytoreductive surgery and hyperthermic intraperitoneal chemotherapy be improved?," *Annals of Surgical Oncology*, vol. 27, no. 1, pp. 301–302, 2020.
- [18] M. E. Pletcher, B. E. Gleeson, and C. DL, "Peritoneal cancers and hyperthermic intraperitoneal chemotherapy," *Surgical Clinics of North America*, vol. 100, no. 3, pp. 589–613, 2020.
- [19] C. W. Mangieri, O. Moaven, C. D. Valenzuela et al., "Utility of hyperthermic intraperitoneal chemotherapy in cases of incomplete cytoreductive surgery," *Journal of Surgical Oncology*, vol. 125, no. 4, pp. 703–711, 2022.
- [20] B. Badgwell, N. Ikoma, M. B. Murphy et al., "A phase ii trial of cytoreduction, gastrectomy, and hyperthermic intraperitoneal perfusion with chemotherapy for patients with gastric cancer and stage iv peritoneal disease," *Journal of Clinical Oncology*, vol. 38, 4\_supplement, pp. 361–361, 2020.
- [21] L. Xin, L. Jianqi, C. Jiayao, and Z. Fangchuan, "Degradation of benzene, toluene, and xylene with high gaseous hourly space velocity by double dielectric barrier discharge combined with Mn<sub>3</sub>O<sub>4</sub>/activated carbon fibers," *Journal of Physics D: Applied Physics*, vol. 55, no. 12, article 125206, 2022.
- [22] M. Bradha, N. Balakrishnan, and S. Suvi, "Experimental, computational analysis of Butein and Lanceoletin for natural